ANTENNA THEORY
ANALYSIS AND DESIGN

THIRD EDITION

Constantine A. Balanis



A JOHN WILEY & SONS, INC., PUBLICATION

EX2042
Page 1 of 1072

Copyright © 2005 by John Wiley & Sons, Inc. All rights reserved.

Published by John Wiley & Sons, Inc., Hoboken, New Jersey.
Published simultaneously in Canada.

No part of this publication may be reproduced, stored in a retrieval system, or transmitted in any form or by any means, electronic, mechanical, photocopying, recording, scanning, or otherwise, except as permitted under Section 107 or 108 of the 1976 United States Copyright Act, without either the prior written permission of the Publisher, or authorization through payment of the appropriate per-copy fee to the Copyright Clearance Center, Inc., 222 Rosewood Drive, Danvers, MA 01923, 978-750-8400, fax 978-646-8600, or on the web at www.copyright.com. Requests to the Publisher for permission should be addressed to the Permissions Department, John Wiley & Sons, Inc., 111 River Street, Hoboken, NJ 07030, (201) 748-6011, fax (201) 748-6008.

Limit of Liability/Disclaimer of Warranty: While the publisher and author have used their best efforts in preparing this book, they make no representations or warranties with respect to the accuracy or completeness of the contents of this book and specifically disclaim any implied warranties of merchantability or fitness for a particular purpose. No warranty may be created or extended by sales representatives or written sales materials. The advice and strategies contained herein may not be suitable for your situation. You should consult with a professional where appropriate. Neither the publisher nor author shall be liable for any loss of profit or any other commercial damages, including but not limited to special, incidental, consequential, or other damages.

For general information on our other products and services please contact our Customer Care Department within the U.S. at 877-762-2974, outside the U.S. at 317-572-3993 or fax 317-572-4002.

Wiley also publishes its books in a variety of electronic formats. Some content that appears in print, however, may not be available in electronic format.

Library of Congress Cataloging-in-Publication Data is available.

ISBN: 0-471-66782-X

Printed in the United States of America.

10 9 8 7 6 5 4 3 2 1

Preface

The third edition of *Antenna Theory* is designed to meet the needs of electrical engineering and physics students at the senior undergraduate and beginning graduate levels, and those of practicing engineers. The text presumes that the students have knowledge of basic undergraduate electromagnetic theory, including Maxwell's equations and the wave equation, introductory physics, and differential and integral calculus. Mathematical techniques required for understanding some advanced topics in the later chapters are incorporated in the individual chapters or are included as appendices.

The third edition has maintained all of the attractive features of the first two editions, including the three-dimensional graphs to display the radiation characteristics of antennas, especially the amplitude patterns. This feature was hailed as an innovative and first of its kind addition in a textbook on antennas. Additional graphs have been added to illustrate features of the radiation characteristics of some antennas. However, there have been many new features added to this edition. In particular,

- A new chapter on *Smart Antennas* (Chapter 16)
- A section on *Fractal Antennas* (Section 11.6)
- Summary tables of important equations in the respective chapters (Chapters 2, 4, 5, 6, 12–14)
- New figures, photos, and tables
- Additional end-of-the-chapter problems
- CD with the following *Multimedia Material:*
  - *Power Point* view graphs of lecture notes for each chapter, in multicolor
  - End-of-the-chapter *Interactive Questionnaires* for review (40–65 for each chapter) based on *Java*
  - *Animations* based on *Java*
  - *Applets* based on *Java*
  - *MATLAB* programs translated from the *FORTRAN* programs of the second edition
  - A number of new *MATLAB* programs
  - *FORTRAN* programs from the second edition.

  The CD is attached to the book, and it will open automatically once inserted in the computer. *It is highly recommended that the reader uses the Internet Explorer (IE) to open the Multimedia Material; other browsers may not perform well.* For additional instructions on how to open and use the material in the CD, there is a HELP file in the CD.

EX2042
Page 3 of 1072

The book's main objective is to introduce, in a unified manner, the fundamental principles of antenna theory and to apply them to the analysis, design, and measurements of antennas. Because there are so many methods of analysis and design and a plethora of antenna structures, applications are made to some of the most basic and practical configurations, such as linear dipoles; loops; arrays; broadband, and frequency-independent antennas; aperture antennas; horn antennas; microstrip antennas; and reflector antennas.

A tutorial chapter on Smart Antennas has been included to introduce the student in a technology that will advance antenna theory and design, and revolutionize wireless communications. It is based on antenna theory, digital signal processing, networks and communications. MATLAB simulation software has also been included, as well as a plethora of references for additional reading.

Introductory material on analytical methods, such as the Moment Method and Fourier transform (spectral) technique, is also included. These techniques, together with the fundamental principles of antenna theory, can be used to analyze and design almost any antenna configuration. A chapter on antenna measurements introduces state-of-the-art methods used in the measurements of the most basic antenna characteristics (pattern, gain, directivity, radiation efficiency, impedance, current, and polarization) and updates progress made in antenna instrumentation, antenna range design, and scale modeling. Techniques and systems used in near- to far-field measurements and transformations are also discussed.

A sufficient number of topics have been covered, some for the first time in an undergraduate text, so that the book will serve not only as a text but also as a reference for the practicing and design engineer and even the amateur radio buff. These include design procedures, and associated computer programs, for Yagi–Uda and log-periodic arrays, horns, and microstrip patches; synthesis techniques using the Schelkunoff, Fourier transform, Woodward–Lawson, Tschebyscheff, and Taylor methods; radiation characteristics of corrugated, aperture-matched, and multimode horns; analysis and design of rectangular and circular microstrip patches; and matching techniques such as the binomial, Tschebyscheff, T-, gamma, and omega matches.

The text contains sufficient mathematical detail to enable the average undergraduate electrical engineering and physics students to follow, without too much difficulty, the flow of analysis and design. A certain amount of analytical detail, rigor, and thoroughness allows many of the topics to be traced to their origin. My experiences as a student, engineer, and teacher have shown that a text for this course must not be a book of unrelated formulas, and it must not resemble a "cookbook." This book begins with the most elementary material, develops underlying concepts needed for sequential topics, and progresses to more advanced methods and system configurations. Each chapter is subdivided into sections or subsections whose individual headings clearly identify the antenna characteristic(s) discussed, examined, or illustrated.

A distinguished feature of this book is its three-dimensional graphical illustrations from the first edition, which have been expanded and supplemented in the second and third editions. In the past, antenna texts have displayed the three-dimensional energy radiated by an antenna by a number of separate two-dimensional patterns. With the advent and revolutionary advances in digital computations and graphical displays, an additional dimension has been introduced for the first time in an undergraduate antenna text by displaying the radiated energy of a given radiator by a single three-dimensional graphical illustration. Such an image, formed by the graphical capabilities of the computer and available at most computational facilities, gives a clear view of

the energy radiated in all space surrounding the antenna. It is hoped that this will lead to a better understanding of the underlying principles of radiation and provide a clearer visualization of the pattern formation in all space.

In addition, there is an abundance of general graphical illustrations, design data, references, and an expanded list of end-of-the chapter problems. Many of the principles are illustrated with examples, graphical illustrations, and physical arguments. Although students are often convinced that they understand the principles, difficulties arise when they attempt to use them. An example, especially a graphical illustration, can often better illuminate those principles. As they say, "a picture is worth a thousand words."

Numerical techniques and computer solutions are illustrated and encouraged. A number of MATLAB computer programs are included in the CD attached to the book. Each program is interactive and prompts the user to enter the data in a sequential manner. Some of these programs are translations of the FORTRAN ones that were included in the first and second editions. However, many new ones have been developed. Every chapter, other than Chapters 3 and 17, have at least one MATLAB computer program; some have as many as four. The outputs of the MATLAB programs include graphical illustrations and tabulated results. For completeness, the FORTRAN computer programs are also included, although there is not as much interest in them. The computer programs can be used for analysis and design. Some of them are more of the design type while some of the others are of the analysis type. Associated with each program there is a READ ME file, which summarizes the respective program.

The purpose of the Lecture Notes is to provide the instructors a copy of the text figures and some of the most important equations of each chapter. They can be used by the instructors in their lectures but need to be supplemented with additional narratives. The students can use them to listen to the instructors' lectures, without having to take detailed notes, but can supplement them in the margins with annotations from the lectures. Each instructor will use the notes in a different way.

The Interactive Questionnaires are intended as reviews of the material in each chapter. The student can use them to review for tests, exams, and so on. For each question, there are three possible answers, but only one is correct. If the reader chooses one of them and it the correct answer, it will so indicate. However, if the chosen answer is the wrong one, the program will automatically indicate the correct answer. An explanation button is provided, which gives a short narrative on the correct answer or indicates where in the book the correct answer can be found.

The Animations can be used to illustrate some of the radiation characteristics, such as amplitude patterns, of some antenna types, like line sources, dipoles, loops, arrays, and horns. The Applets cover more chapters and can be used to examine some of the radiation characteristics (such as amplitude patterns, impedance, bandwidth, etc.) of some of the antennas. This can be accomplished very rapidly without having to resort to the MATLAB programs, which are more detailed.

For course use, the text is intended primarily for a two-semester (or two- or three-quarter) sequence in antenna theory. The first course should be given at the senior undergraduate level, and should cover most of the material in Chapters 1 through 7, and Chapters 16 and 17. The material in Chapters 8 through 16 should be covered in a beginning graduate-level course. Selected chapters and sections from the book can be covered in a single semester, without loss of continuity. However, it is almost essential that most of the material in Chapters 2 through 6 be covered in the first course and before proceeding to any more advanced topics. To cover all the material of the text

in the proposed time frame would be, in some cases, a very ambitious task. Sufficient topics have been included, however, to make the text complete and to give the teacher the flexibility to emphasize, deemphasize, or omit sections or chapters. Some of the chapters and sections can be omitted without loss of continuity.

In the entire book, an $e^{j\omega t}$ time variation is assumed, and it is suppressed. The International System of Units, which is an expanded form of the rationalized MKS system, is used in the text. In some cases, the units of length are in meters (or centimeters) and in feet (or inches). Numbers in parentheses () refer to equations, whereas those in brackets [] refer to references. For emphasis, the most important equations, once they are derived, are boxed. In some of the basic chapters, the most important equations are summarized in tables.

I would like to acknowledge the invaluable suggestions from all those that contributed to the first and second editions, too numerous to mention here. Their names and contributions are stated in the respective editions. It is a pleasure to acknowledge the invaluable suggestions and constructive criticisms of the reviewers of the third edition: Dr. Stuart A. Long of University of Houston, Dr. Christos Christodoulou of University of New Mexico, Dr. Leo Kempel of Michigan State, and Dr. Sergey N. Makarov of Worcester Polytechnic University. There have been many other contributors to this edition, and their contributions are valued and acknowledged. Many graduate and undergraduate students from Arizona State University who have written many of the MATLAB computer programs. Some of these programs were translated from the FORTRAN ones, which appeared in the first and second editions. However a number of entirely new MATLAB programs have been created, which are included for the first time, and do not have a FORTRAN counterpart. The name(s) of the individual contributors to each program is included in the respective program. The author acknowledges Dr. Sava V. Savov of Technical University of Varna, Bulgaria, for the valuable discussions, contributions and figures related to the integration of equation (5-59) in closed form in terms of Bessel functions; Dr. Yahya Rahmat-Samii and Dr. John P. Gianvittorio of UCLA for the figures on Fractal antennas. I would like to thank Craig R. Birtcher of Arizona State University for proofreading part of the manuscript; Bo Yang of Arizona State University for proofreading part of the manuscript, revising a number of the MATLAB programs, and developing the flow chart for accessing the CD Multimedia material; and Razib S. Shishir of Arizona State University for developing all of the Java-based software, including the Interactive Questionnaires, Applets, and Animations. Special thanks to the many companies (Motorola, Inc., Northrop Grumman Corporation, March Microwave Systems, B.V., Ball Aerospace & Technologies Corporation, Samsung, Midland Radio Corporation, Winegard Company, Antenna Research Associates, Inc., Seavey Engineering Associates, Inc., and TCI, A Dielectric Company) for providing photos, illustrations, and copyright permissions. The author acknowledges the long-term friendship and support from Dennis DeCarlo, George C. Barber, Dr. Karl Moeller, Dr. Brian McCabe, Dr. W. Dev Palmer, Michael C. Miller, Frank A. Cansler, and the entire AHE Program membership, too long to be included here. The friendship and collaborative arrangements with Prof. Thodoros D. Tsiboukis and Prof. John N. Sahalos, both from the Aristotle University of Thessaloniki, Greece, are recognized and appreciated. The loyalty and friendship of my graduate students is acknowledged and valued. To all my teachers, thank you. You have been my role models and inspiration.

I am also grateful to the staff of John Wiley & Sons, Inc., especially George Telecki, Associate Publisher, Wiley-Interscience, for his interest, support, cooperation, and production of the third edition; Danielle Lacourciere, Associate Managing Editor, for the production of the book; and Rachel Witmer, Editorial Assistant, for managing the production of the cover. Finally, I must pay tribute to my family (Helen, Renie, and Stephanie) for their support, patience, sacrifice, and understanding for the many hours of neglect during the completion of the first, second, and third editions of this book. It has been a pleasant but daunting task.

Constantine A. Balanis
Arizona State University
Tempe, AZ

Contents

Preface **xiii**

1 Antennas **1**

1.1 Introduction 1
1.2 Types of Antennas 4
1.3 Radiation Mechanism 7
1.4 Current Distribution on a Thin Wire Antenna 17
1.5 Historical Advancement 20
1.6 Multimedia 24
References 24

2 Fundamental Parameters of Antennas **27**

2.1 Introduction 27
2.2 Radiation Pattern 27
2.3 Radiation Power Density 38
2.4 Radiation Intensity 40
2.5 Beamwidth 42
2.6 Directivity 44
2.7 Numerical Techniques 58
2.8 Antenna Efficiency 64
2.9 Gain 65
2.10 Beam Efficiency 69
2.11 Bandwidth 70
2.12 Polarization 70
2.13 Input Impedance 80
2.14 Antenna Radiation Efficiency 85
2.15 Antenna Vector Effective Length and Equivalent Areas 87
2.16 Maximum Directivity and Maximum Effective Area 92
2.17 Friis Transmission Equation and Radar Range Equation 94
2.18 Antenna Temperature 104
2.19 Multimedia 108
References 112
Problems 114

EX2042
Page 8 of 1072

3 Radiation Integrals and Auxiliary Potential Functions 133

3.1 Introduction 133
3.2 The Vector Potential A for an Electric Current Source J 135
3.3 The Vector Potential F for a Magnetic Current Source M 137
3.4 Electric and Magnetic Fields for Electric (J) and Magnetic (M) Current Sources 138
3.5 Solution of the Inhomogeneous Vector Potential Wave Equation 139
3.6 Far-Field Radiation 142
3.7 Duality Theorem 144
3.8 Reciprocity and Reaction Theorems 144
References 150
Problems 150

4 Linear Wire Antennas 151

4.1 Introduction 151
4.2 Infinitesimal Dipole 151
4.3 Small Dipole 162
4.4 Region Separation 165
4.5 Finite Length Dipole 170
4.6 Half-Wavelength Dipole 182
4.7 Linear Elements Near or on Infinite Perfect Conductors 184
4.8 Ground Effects 205
4.9 Computer Codes 214
4.10 Multimedia 217
References 218
Problems 219

5 Loop Antennas 231

5.1 Introduction 231
5.2 Small Circular Loop 232
5.3 Circular Loop of Constant Current 246
5.4 Circular Loop with Nonuniform Current 255
5.5 Ground and Earth Curvature Effects for Circular Loops 261
5.6 Polygonal Loop Antennas 263
5.7 Ferrite Loop 266
5.8 Mobile Communication Systems Applications 268
5.9 Multimedia 269
References 273
Problems 275

6 Arrays: Linear, Planar, and Circular 283

6.1 Introduction 283
6.2 Two-Element Array 284
6.3 *N*-Element Linear Array: Uniform Amplitude and Spacing 290
6.4 *N*-Element Linear Array: Directivity 313

EX2042
Page 9 of 1072

6.5 Design Procedure 318
6.6 N-Element Linear Array: Three-Dimensional Characteristics 320
6.7 Rectangular-to-Polar Graphical Solution 322
6.8 N-Element Linear Array: Uniform Spacing, Nonuniform Amplitude 324
6.9 Superdirectivity 345
6.10 Planar Array 349
6.11 Design Considerations 362
6.12 Circular Array 365
6.13 Multimedia 369
References 370
Problems 371

7 Antenna Synthesis and Continuous Sources 385

7.1 Introduction 385
7.2 Continuous Sources 386
7.3 Schelkunoff Polynomial Method 388
7.4 Fourier Transform Method 393
7.5 Woodward-Lawson Method 399
7.6 Taylor Line-Source (Tschebyscheff-Error) 406
7.7 Taylor Line-Source (One-Parameter) 410
7.8 Triangular, Cosine, and Cosine-Squared Amplitude Distributions 417
7.9 Line-Source Phase Distributions 418
7.10 Continuous Aperture Sources 419
7.11 Multimedia 423
References 423
Problems 424

8 Integral Equations, Moment Method, and Self and Mutual Impedances 433

8.1 Introduction 433
8.2 Integral Equation Method 434
8.3 Finite Diameter Wires 442
8.4 Moment Method Solution 450
8.5 Self-Impedance 458
8.6 Mutual Impedance Between Linear Elements 468
8.7 Mutual Coupling in Arrays 478
8.8 Multimedia 491
References 491
Problems 494

9 Broadband Dipoles and Matching Techniques 497

9.1 Introduction 497
9.2 Biconical Antenna 500
9.3 Triangular Sheet, Bow-Tie, and Wire Simulation 506
9.4 Cylindrical Dipole 508

9.5 Folded Dipole 515
9.6 Discone and Conical Skirt Monopole 521
9.7 Matching Techniques 523
9.8 Multimedia 541
References 542
Problems 543

10 Traveling Wave and Broadband Antennas 549

10.1 Introduction 549
10.2 Traveling Wave Antennas 549
10.3 Broadband Antennas 566
10.4 Multimedia 600
References 600
Problems 602

11 Frequency Independent Antennas, Antenna Miniaturization, and Fractal Antennas 611

11.1 Introduction 611
11.2 Theory 612
11.3 Equiangular Spiral Antennas 614
11.4 Log-Periodic Antennas 619
11.5 Fundamental Limits of Electrically Small Antennas 637
11.6 Fractal Antennas 641
11.7 Multimedia 648
References 648
Problems 650

12 Aperture Antennas 653

12.1 Introduction 653
12.2 Field Equivalence Principle: Huygens' Principle 653
12.3 Radiation Equations 660
12.4 Directivity 662
12.5 Rectangular Apertures 663
12.6 Circular Apertures 683
12.7 Design Considerations 692
12.8 Babinet's Principle 697
12.9 Fourier Transforms in Aperture Antenna Theory 701
12.10 Ground Plane Edge Effects: The Geometrical Theory of Diffraction 721
12.11 Multimedia 726
References 726
Problems 728

13 Horn Antennas 739

13.1 Introduction 739
13.2 *E*-Plane Sectoral Horn 739

13.3 H-Plane Sectoral Horn 755
13.4 Pyramidal Horn 769
13.5 Conical Horn 783
13.6 Corrugated Horn 785
13.7 Aperture-Matched Horns 792
13.8 Multimode Horns 794
13.9 Dielectric-Loaded Horns 797
13.10 Phase Center 799
13.11 Multimedia 802
References 802
Problems 805

14 Microstrip Antennas 811

14.1 Introduction 811
14.2 Rectangular Patch 816
14.3 Circular Patch 843
14.4 Quality Factor, Bandwidth, and Efficiency 852
14.5 Input Impedance 855
14.6 Coupling 856
14.7 Circular Polarization 859
14.8 Arrays and Feed Networks 865
14.9 Multimedia 872
References 872
Problems 876

15 Reflector Antennas 883

15.1 Introduction 883
15.2 Plane Reflector 883
15.3 Corner Reflector 884
15.4 Parabolic Reflector 893
15.5 Spherical Reflector 934
15.6 Multimedia 936
References 937
Problems 939

16 Smart Antennas 945

16.1 Introduction 945
16.2 Smart-Antenna Analogy 946
16.3 Cellular Radio Systems Evolution 947
16.4 Signal Propagation 954
16.5 Smart Antennas' Benefits 957
16.6 Smart Antennas' Drawbacks 958
16.7 Antenna 958
16.8 Antenna Beamforming 962
16.9 Mobile Ad hoc Networks (MANETs) 977
16.10 Smart-Antenna System Design, Simulation, and Results 982

16.11 Beamforming, Diversity Combining, Rayleigh-Fading, and Trellis-Coded Modulation 990
16.12 Other Geometries 993
16.13 Multimedia 994
References 995
Problems 999

17 Antenna Measurements **1001**

17.1 Introduction 1001
17.2 Antenna Ranges 1003
17.3 Radiation Patterns 1021
17.4 Gain Measurements 1028
17.5 Directivity Measurements 1034
17.6 Radiation Efficiency 1036
17.7 Impedance Measurements 1036
17.8 Current Measurements 1038
17.9 Polarization Measurements 1038
17.10 Scale Model Measurements 1044
References 1045

Appendix I: $f(x) = \dfrac{\sin(x)}{x}$ **1049**

Appendix II: $f_N(x) = \left|\dfrac{\sin(Nx)}{N\sin(x)}\right| N = 1, 3, 5, 10, 20$ **1051**

Appendix III: Cosine and Sine Integrals **1053**

Appendix IV: Fresnel Integrals **1057**

Appendix V: Bessel Functions **1063**

Appendix VI: Identities **1075**

Appendix VII: Vector Analysis **1079**

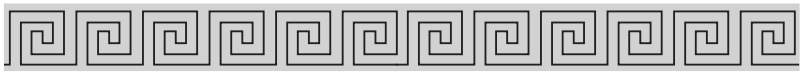
Appendix VIII: Method of Stationary Phase **1089**

Appendix IX: Television, Radio, Telephone, and Radar Frequency Spectrums **1095**

Index **1099**

EX2042
Page 13 of 1072

CHAPTER 1



Antennas

1.1 INTRODUCTION

An antenna is defined by Webster's Dictionary as "a usually metallic device (as a rod or wire) for radiating or receiving radio waves." The *IEEE Standard Definitions of Terms for Antennas* (IEEE Std 145–1983)* defines the antenna or aerial as "a means for radiating or receiving radio waves." In other words the antenna is the transitional structure between free-space and a guiding device, as shown in Figure 1.1. The guiding device or transmission line may take the form of a coaxial line or a hollow pipe (waveguide), and it is used to transport electromagnetic energy from the transmitting source to the antenna, or from the antenna to the receiver. In the former case, we have a transmitting antenna and in the latter a receiving antenna.

A transmission-line Thevenin equivalent of the antenna system of Figure 1.1 in the transmitting mode is shown in Figure 1.2 where the source is represented by an ideal generator, the transmission line is represented by a line with characteristic impedance Z_c, and the antenna is represented by a load Z_A $[Z_A = (R_L + R_r) + jX_A]$ connected to the transmission line. The Thevenin and Norton circuit equivalents of the antenna are also shown in Figure 2.27. The load resistance R_L is used to represent the conduction and dielectric losses associated with the antenna structure while R_r, referred to as the *radiation resistance*, is used to represent radiation by the antenna. The reactance X_A is used to represent the imaginary part of the impedance associated with radiation by the antenna. This is discussed more in detail in Sections 2.13 and 2.14. Under ideal conditions, energy generated by the source should be totally transferred to the radiation resistance R_r, which is used to represent radiation by the antenna. However, in a practical system there are conduction-dielectric losses due to the lossy nature of the transmission line and the antenna, as well as those due to reflections (mismatch) losses at the interface between the line and the antenna. Taking into account the internal impedance of the source and neglecting line and reflection (mismatch) losses, maximum

IEEE Transactions on Antennas and Propagation, vols. AP-17, No. 3, May 1969; AP-22, No. 1, January 1974; and AP-31, No. 6, Part II, November 1983.

Antenna Theory: Analysis Design, Third Edition, by Constantine A. Balanis
ISBN 0-471-66782-X Copyright © 2005 John Wiley & Sons, Inc.

EX2042
Page 14 of 1072

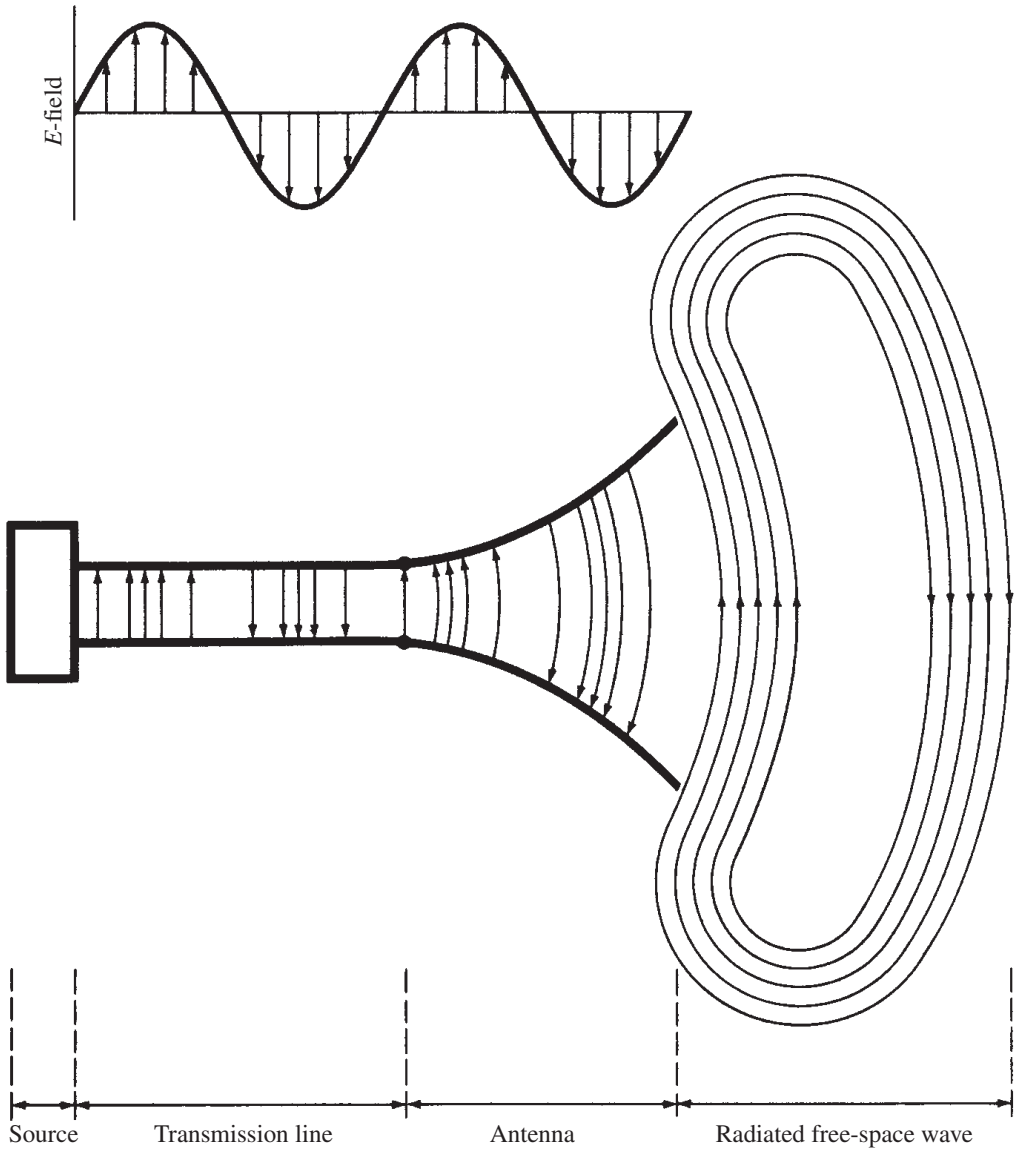


Figure 1.1 Antenna as a transition device.

power is delivered to the antenna under *conjugate matching*. This is discussed in Section 2.13.

The reflected waves from the interface create, along with the traveling waves from the source toward the antenna, constructive and destructive interference patterns, referred to as *standing waves*, inside the transmission line which represent pockets of energy concentrations and storage, typical of resonant devices. A typical standing wave pattern is shown dashed in Figure 1.2, while another is exhibited in Figure 1.15. If the antenna system is not properly designed, the transmission line could act to a large degree as an energy storage element instead of as a wave guiding and energy transporting device. If the maximum field intensities of the standing wave are sufficiently large, they can cause arching inside the transmission lines.

The losses due to the line, antenna, and the standing waves are undesirable. The losses due to the line can be minimized by selecting low-loss lines while those of

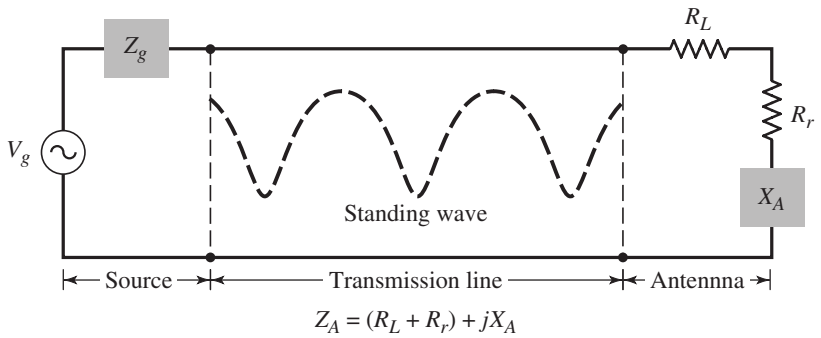


Figure 1.2 Transmission-line Thevenin equivalent of antenna in transmitting mode.

the antenna can be decreased by reducing the loss resistance represented by R_L in Figure 1.2. The standing waves can be reduced, and the energy storage capacity of the line minimized, by matching the impedance of the antenna (load) to the characteristic impedance of the line. This is the same as matching loads to transmission lines, where the load here is the antenna, and is discussed more in detail in Section 9.7. An equivalent similar to that of Figure 1.2 is used to represent the antenna system in the receiving mode where the source is replaced by a receiver. All other parts of the transmission-line equivalent remain the same. The radiation resistance R_r is used to represent in the receiving mode the transfer of energy from the free-space wave to the antenna. This is discussed in Section 2.13 and represented by the Thevenin and Norton circuit equivalents of Figure 2.27.

In addition to receiving or transmitting energy, an antenna in an advanced wireless system is usually required to *optimize* or *accentuate* the radiation energy in some directions and suppress it in others. *Thus the antenna must also serve as a directional device in addition to a probing device*. It must then take various forms to meet the particular need at hand, and it may be a piece of conducting wire, an aperture, a patch, an assembly of elements (array), a reflector, a lens, and so forth.

For wireless communication systems, the antenna is one of the most critical components. A good design of the antenna can relax system requirements and improve overall system performance. A typical example is TV for which the overall broadcast reception can be improved by utilizing a high-performance antenna. The antenna serves to a communication system the same purpose that eyes and eyeglasses serve to a human.

The field of antennas is vigorous and dynamic, and over the last 60 years antenna technology has been an indispensable partner of the communications revolution. Many major advances that occurred during this period are in common use today; however, many more issues and challenges are facing us today, especially since the demands for system performances are even greater. Many of the major advances in antenna technology that have been completed in the 1970s through the early 1990s, those that were under way in the early 1990s, and signals of future discoveries and breakthroughs were captured in a special issue of the *Proceedings of the IEEE* (Vol. 80, No. 1, January 1992) devoted to Antennas. The introductory paper of this special issue [1] provides a carefully structured, elegant discussion of the fundamental principles of radiating elements and has been written as an introduction for the nonspecialist and a review for the expert.

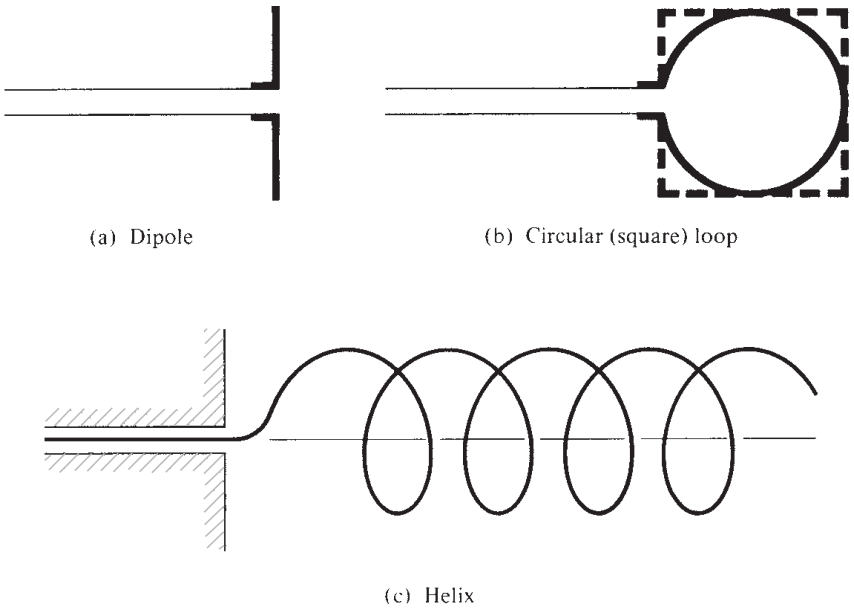


Figure 1.3 Wire antenna configurations.

1.2 TYPES OF ANTENNAS

We will now introduce and briefly discuss some forms of the various antenna types in order to get a glance as to what will be encountered in the remainder of the book.

1.2.1 Wire Antennas

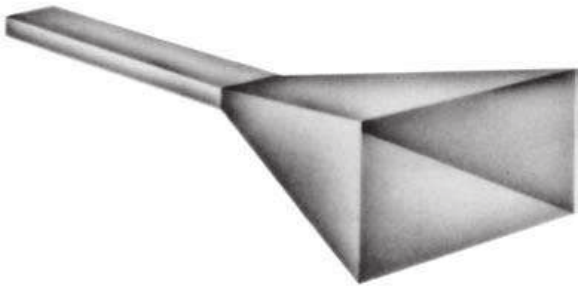
Wire antennas are familiar to the layman because they are seen virtually everywhere—on automobiles, buildings, ships, aircraft, spacecraft, and so on. There are various shapes of wire antennas such as a straight wire (dipole), loop, and helix which are shown in Figure 1.3. Loop antennas need not only be circular. They may take the form of a rectangle, square, ellipse, or any other configuration. The circular loop is the most common because of its simplicity in construction. Dipoles are discussed in more detail in Chapter 4, loops in Chapter 5, and helices in Chapter 10.

1.2.2 Aperture Antennas

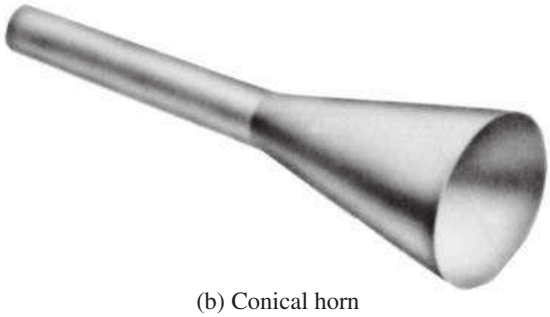
Aperture antennas may be more familiar to the layman today than in the past because of the increasing demand for more sophisticated forms of antennas and the utilization of higher frequencies. Some forms of aperture antennas are shown in Figure 1.4. Antennas of this type are very useful for aircraft and spacecraft applications, because they can be very conveniently flush-mounted on the skin of the aircraft or spacecraft. In addition, they can be covered with a dielectric material to protect them from hazardous conditions of the environment. Waveguide apertures are discussed in more detail in Chapter 12 while horns are examined in Chapter 13.

1.2.3 Microstrip Antennas

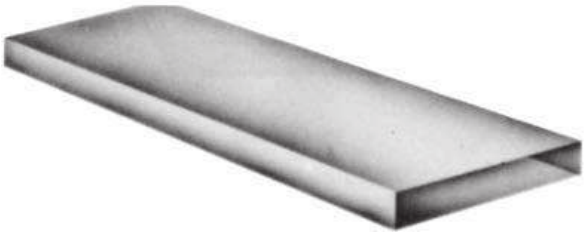
Microstrip antennas became very popular in the 1970s primarily for spaceborne applications. Today they are used for government and commercial applications. These antennas



(a) Pyramidal horn



(b) Conical horn



(c) Rectangular waveguide

Figure 1.4 Aperture antenna configurations.

consist of a metallic patch on a grounded substrate. The metallic patch can take many different configurations, as shown in Figure 14.2. However, the rectangular and circular patches, shown in Figure 1.5, are the most popular because of ease of analysis and fabrication, and their attractive radiation characteristics, especially low cross-polarization radiation. The microstrip antennas are low profile, comformable to planar and nonplanar surfaces, simple and inexpensive to fabricate using modern printed-circuit technology, mechanically robust when mounted on rigid surfaces, compatible with MMIC designs, and very versatile in terms of resonant frequency, polarization, pattern, and impedance. These antennas can be mounted on the surface of high-performance aircraft, spacecraft, satellites, missiles, cars, and even handheld mobile telephones. They are discussed in more detail in Chapter 14.

1.2.4 Array Antennas

Many applications require radiation characteristics that may not be achievable by a single element. It may, however, be possible that an aggregate of radiating elements in an electrical and geometrical arrangement (*an array*) will result in the desired

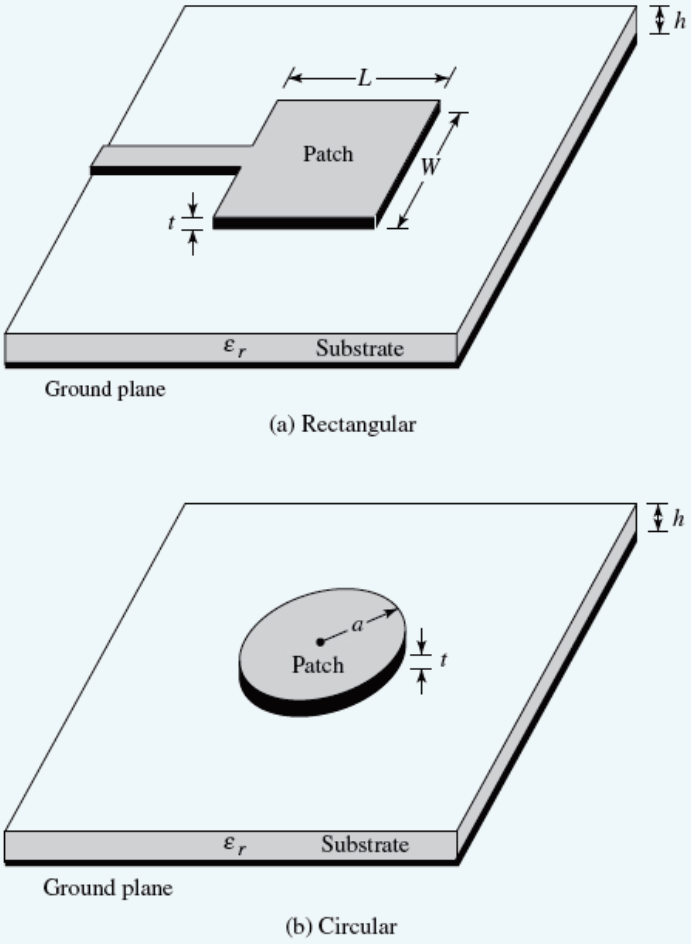


Figure 1.5 Rectangular and circular microstrip (patch) antennas.

radiation characteristics. The arrangement of the array may be such that the radiation from the elements adds up to give a radiation maximum in a particular direction or directions, minimum in others, or otherwise as desired. Typical examples of arrays are shown in Figure 1.6. Usually the term *array* is reserved for an arrangement in which the individual radiators are separate as shown in Figures 1.6(a–c). However the same term is also used to describe an assembly of radiators mounted on a continuous structure, shown in Figure 1.6(d).

1.2.5 Reflector Antennas

The success in the exploration of outer space has resulted in the advancement of antenna theory. Because of the need to communicate over great distances, sophisticated forms of antennas had to be used in order to transmit and receive signals that had to travel millions of miles. A very common antenna form for such an application is a parabolic reflector shown in Figures 1.7(a) and (b). Antennas of this type have been built with diameters as large as 305 m. Such large dimensions are needed to achieve the high gain required to transmit or receive signals after millions of miles of travel. Another form of a reflector, although not as common as the parabolic, is the corner reflector, shown in Figure 1.7(c). These antennas are examined in detail in Chapter 15.

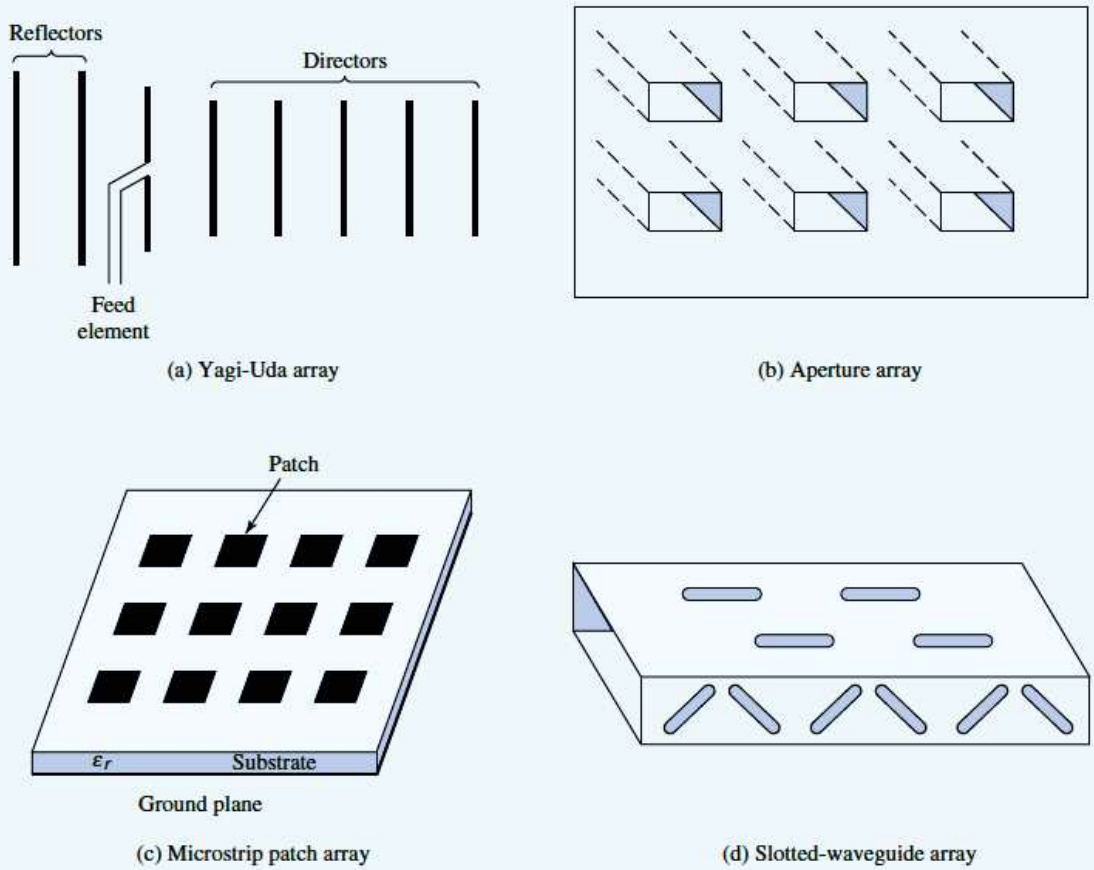


Figure 1.6 Typical wire, aperture, and microstrip array configurations.

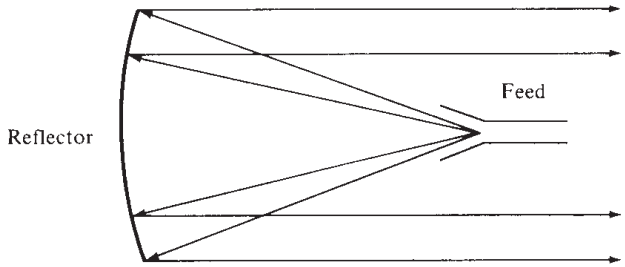
1.2.6 Lens Antennas

Lenses are primarily used to collimate incident divergent energy to prevent it from spreading in undesired directions. By properly shaping the geometrical configuration and choosing the appropriate material of the lenses, they can transform various forms of divergent energy into plane waves. They can be used in most of the same applications as are the parabolic reflectors, especially at higher frequencies. Their dimensions and weight become exceedingly large at lower frequencies. Lens antennas are classified according to the material from which they are constructed, or according to their geometrical shape. Some forms are shown in Figure 1.8 [2].

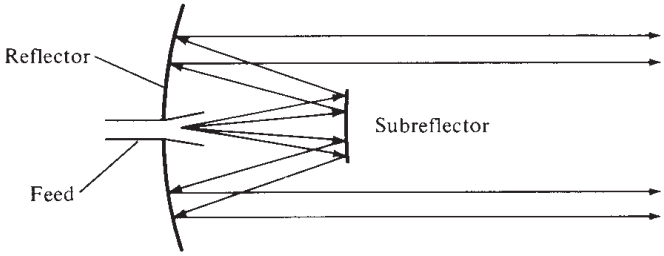
In summary, an ideal antenna is one that will radiate all the power delivered to it from the transmitter in a desired direction or directions. In practice, however, such ideal performances cannot be achieved but may be closely approached. Various types of antennas are available and each type can take different forms in order to achieve the desired radiation characteristics for the particular application. Throughout the book, the radiation characteristics of most of these antennas are discussed in detail.

1.3 RADIATION MECHANISM

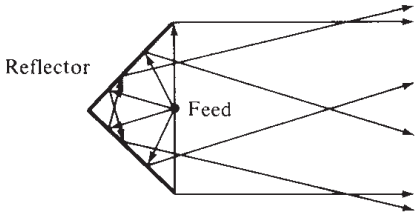
One of the first questions that may be asked concerning antennas would be "how is radiation accomplished?" In other words, how are the electromagnetic fields generated



(a) Parabolic reflector with front feed

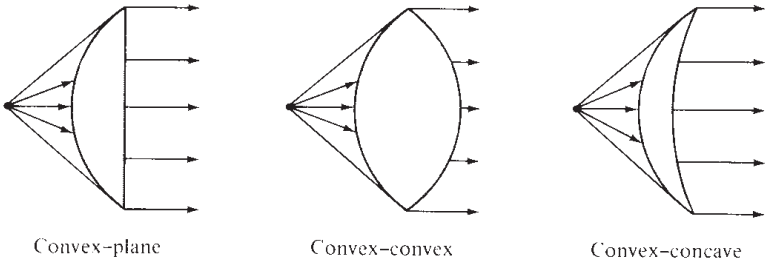


(b) Parabolic reflector with Cassegrain feed

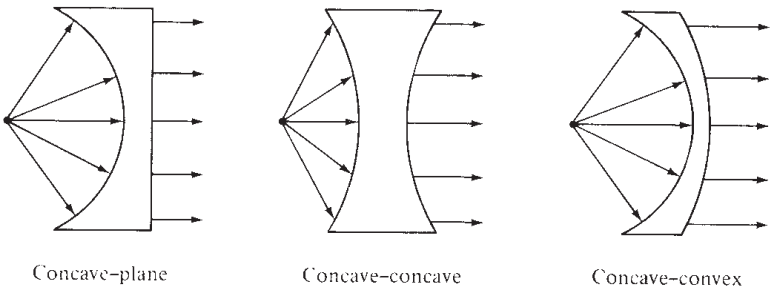


(c) Corner reflector

Figure 1.7 Typical reflector configurations.



(a) Lens antennas with index of refraction $n > 1$



(b) Lens antennas with index of refraction $n < 1$

Figure 1.8 Typical lens antenna configurations. (SOURCE: L. V. Blake, *Antennas*, Wiley, New York, 1966).

EX2042
Page 21 of 1072

by the source, contained and guided within the transmission line and antenna, and finally "detached" from the antenna to form a free-space wave? The best explanation may be given by an illustration. However, let us first examine some basic sources of radiation.

1.3.1 Single Wire

Conducting wires are material whose prominent characteristic is the motion of electric charges and the creation of current flow. Let us assume that an electric volume charge density, represented by q_v (coulombs/m^3), is distributed uniformly in a circular wire of cross-sectional area A and volume V, as shown in Figure 1.9. The total charge Q within volume V is moving in the z direction with a uniform velocity v_z (meters/sec). It can be shown that the current density J_z (amperes/m^2) over the cross section of the wire is given by [3]

$$J_z = q_v v_z \tag{1-1a}$$

If the wire is made of an ideal electric conductor, the current density J_s (amperes/m) resides on the surface of the wire and it is given by

$$J_s = q_s v_z \tag{1-1b}$$

where q_s (coulombs/m^2) is the surface charge density. If the wire is very thin (ideally zero radius), then the current in the wire can be represented by

$$I_z = q_l v_z \tag{1-1c}$$

where q_l (coulombs/m) is the charge per unit length.

Instead of examining all three current densities, we will primarily concentrate on the very thin wire. The conclusions apply to all three. If the current is time varying, then the derivative of the current of (1-1c) can be written as

$$\frac{dI_z}{dt} = q_l \frac{dv_z}{dt} = q_l a_z \tag{1-2}$$

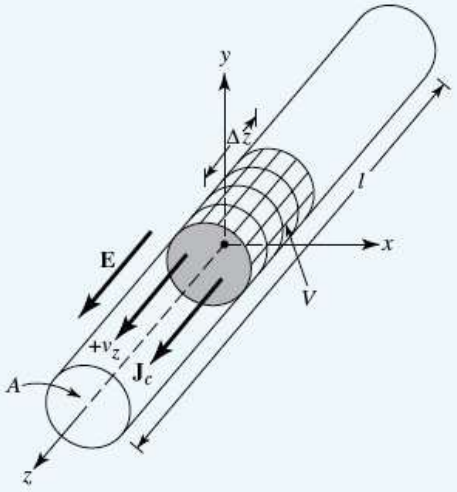


Figure 1.9 Charge uniformly distributed in a circular cross section cylinder wire.

where $dv_z/dt = a_z$ (meters/sec^2) is the acceleration. If the wire is of length l, then (1-2) can be written as

$$\boxed{l\frac{dI_z}{dt} = lq_l\frac{dv_z}{dt} = lq_l a_z} \tag{1-3}$$

Equation (1-3) is the basic relation between current and charge, and it also serves as the fundamental relation of electromagnetic radiation [4], [5]. It simply states that *to create radiation, there must be a time-varying current or an acceleration (or deceleration) of charge*. We usually refer to currents in time-harmonic applications while charge is most often mentioned in transients. To create charge acceleration (or deceleration) the wire must be curved, bent, discontinuous, or terminated [1], [4]. Periodic charge acceleration (or deceleration) or time-varying current is also created when charge is oscillating in a time-harmonic motion, as shown in Figure 1.17 for a $\lambda/2$ dipole. Therefore:

1. If a charge is not moving, current is not created and there is no radiation.
2. If charge is moving with a uniform velocity:
   a. There is no radiation if the wire is straight, and infinite in extent.
   b. There is radiation if the wire is curved, bent, discontinuous, terminated, or truncated, as shown in Figure 1.10.
3. If charge is oscillating in a time-motion, it radiates even if the wire is straight.

A qualitative understanding of the radiation mechanism may be obtained by considering a pulse source attached to an open-ended conducting wire, which may be connected to the ground through a discrete load at its open end, as shown in Figure 1.10(d). When the wire is initially energized, the charges (free electrons) in the wire are set in motion by the electrical lines of force created by the source. When charges are accelerated in the source-end of the wire and decelerated (negative acceleration with respect to original motion) during reflection from its end, it is suggested that radiated fields are produced at each end and along the remaining part of the wire, [1], [4]. *Stronger radiation with a more broad frequency spectrum occurs if the pulses are of shorter or more compact duration while continuous time-harmonic oscillating charge produces, ideally, radiation of single frequency determined by the frequency of oscillation.* The acceleration of the charges is accomplished by the external source in which forces set the charges in motion and produce the associated field radiated. The deceleration of the charges at the end of the wire is accomplished by the internal (self) forces associated with the induced field due to the buildup of charge concentration at the ends of the wire. The internal forces receive energy from the charge buildup as its velocity is reduced to zero at the ends of the wire. Therefore, charge acceleration due to an exciting electric field and deceleration due to impedance discontinuities or smooth curves of the wire are mechanisms responsible for electromagnetic radiation. While both current density ($\mathbf{J}_c$) and charge density (q_v) appear as source terms in Maxwell's equation, charge is viewed as a more fundamental quantity, especially for transient fields. Even though this interpretation of radiation is primarily used for transients, it can be used to explain steady state radiation [4].

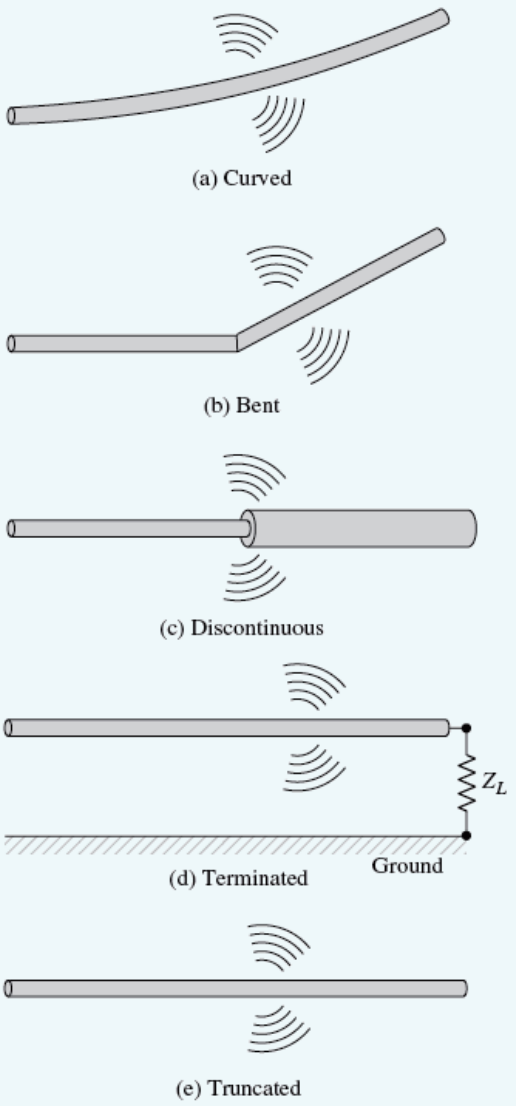


Figure 1.10 Wire configurations for radiation.

1.3.2 Two-Wires

Let us consider a voltage source connected to a two-conductor transmission line which is connected to an antenna. This is shown in Figure 1.11(a). Applying a voltage across the two-conductor transmission line creates an electric field between the conductors. The electric field has associated with it electric lines of force which are tangent to the electric field at each point and their strength is proportional to the electric field intensity. The electric lines of force have a tendency to act on the free electrons (easily detachable from the atoms) associated with each conductor and force them to be displaced. The movement of the charges creates a current that in turn creates a magnetic field intensity. Associated with the magnetic field intensity are magnetic lines of force which are tangent to the magnetic field.

We have accepted that electric field lines start on positive charges and end on negative charges. They also can start on a positive charge and end at infinity, start at infinity and end on a negative charge, or form closed loops neither starting or ending on any charge. Magnetic field lines always form closed loops encircling current-carrying

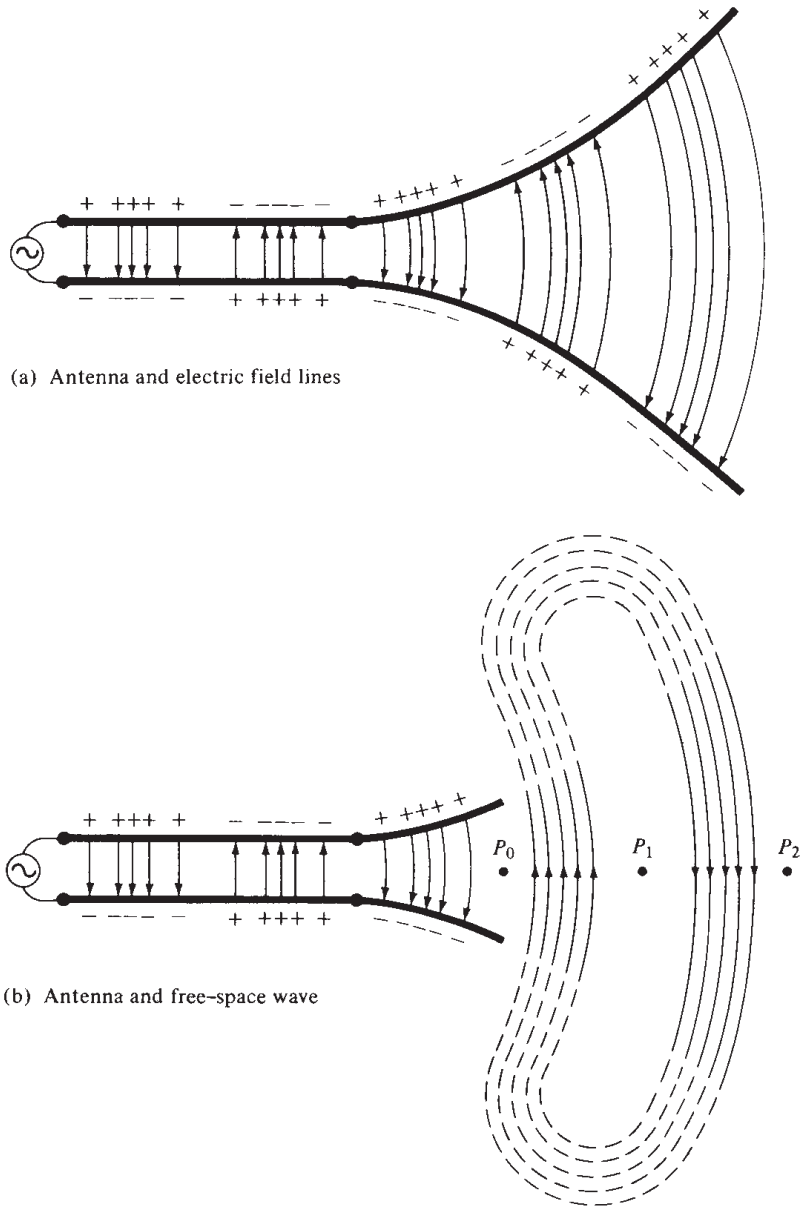


Figure 1.11 Source, transmission line, antenna, and detachment of electric field lines.

conductors because physically there are no magnetic charges. In some mathematical formulations, it is often convenient to introduce equivalent magnetic charges and magnetic currents to draw a parallel between solutions involving electric and magnetic sources.

The electric field lines drawn between the two conductors help to exhibit the distribution of charge. If we assume that the voltage source is sinusoidal, we expect the electric field between the conductors to also be sinusoidal with a period equal to that of the applied source. The relative magnitude of the electric field intensity is indicated by the density (bunching) of the lines of force with the arrows showing the relative direction (positive or negative). The creation of time-varying electric and magnetic fields between the conductors forms electromagnetic waves which travel along the transmission line, as shown in Figure 1.11(a). The electromagnetic waves enter the antenna and have associated with them electric charges and corresponding currents. If

we remove part of the antenna structure, as shown in Figure 1.11(b), free-space waves can be formed by "connecting" the open ends of the electric lines (shown dashed). The free-space waves are also periodic but a constant phase point P_0 moves outwardly with the speed of light and travels a distance of $\lambda/2$ (to P_1) in the time of one-half of a period. It has been shown [6] that close to the antenna the constant phase point P_0 moves faster than the speed of light but approaches the speed of light at points far away from the antenna (analogous to phase velocity inside a rectangular waveguide). Figure 1.12 displays the creation and travel of free-space waves by a prolate spheroid with $\lambda/2$ interfocal distance where λ is the wavelength. The free-space waves of a center-fed $\lambda/2$ dipole, except in the immediate vicinity of the antenna, are essentially the same as those of the prolate spheroid.

The question still unanswered is how the guided waves are detached from the antenna to create the free-space waves that are indicated as closed loops in Figures 1.11 and 1.12. Before we attempt to explain that, let us draw a parallel between the guided and free-space waves, and water waves [7] created by the dropping of a pebble in a calm body of water or initiated in some other manner. Once the disturbance in the water has been initiated, water waves are created which begin to travel outwardly. If the disturbance has been removed, the waves do not stop or extinguish themselves but continue their course of travel. If the disturbance persists, new waves are continuously created which lag in their travel behind the others. The same is true with the electromagnetic waves created by an electric disturbance. If the initial electric disturbance by the source is of a short duration, the created electromagnetic waves travel inside the

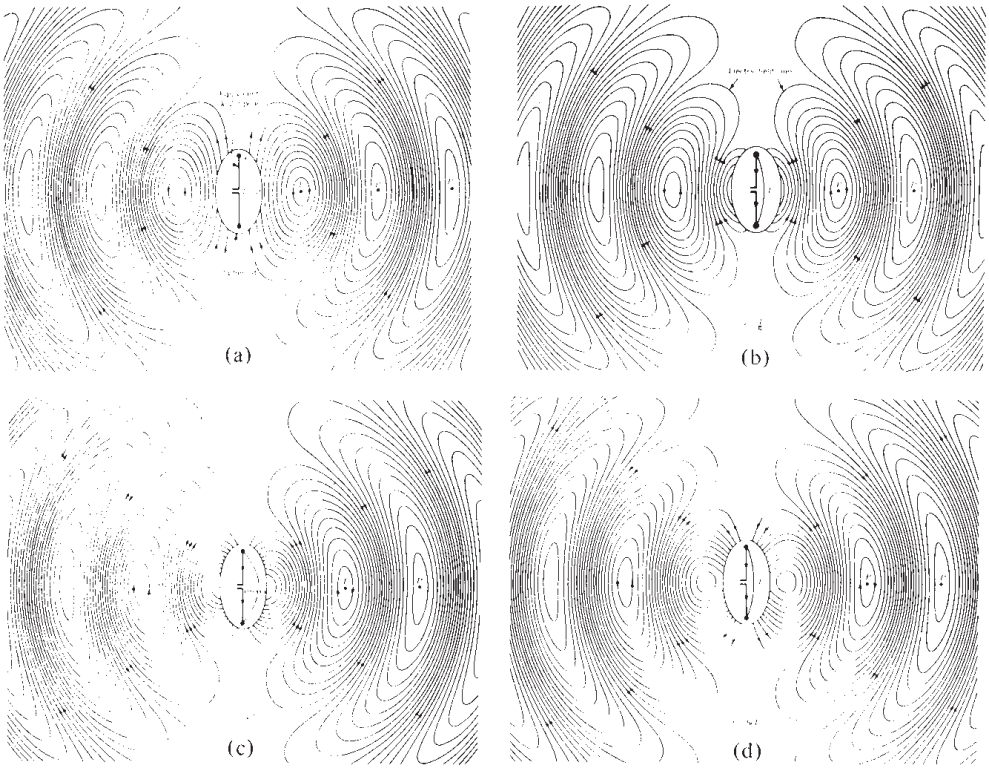


Figure 1.12 Electric field lines of free-space wave for a $\lambda/2$ antenna at $t = 0$, $T/8$, $T/4$, and $3T/8$. (SOURCE: J. D. Kraus, *Electromagnetics*, 4th ed., McGraw-Hill, New York, 1992. Reprinted with permission of J. D. Kraus and John D. Cowan, Jr.).

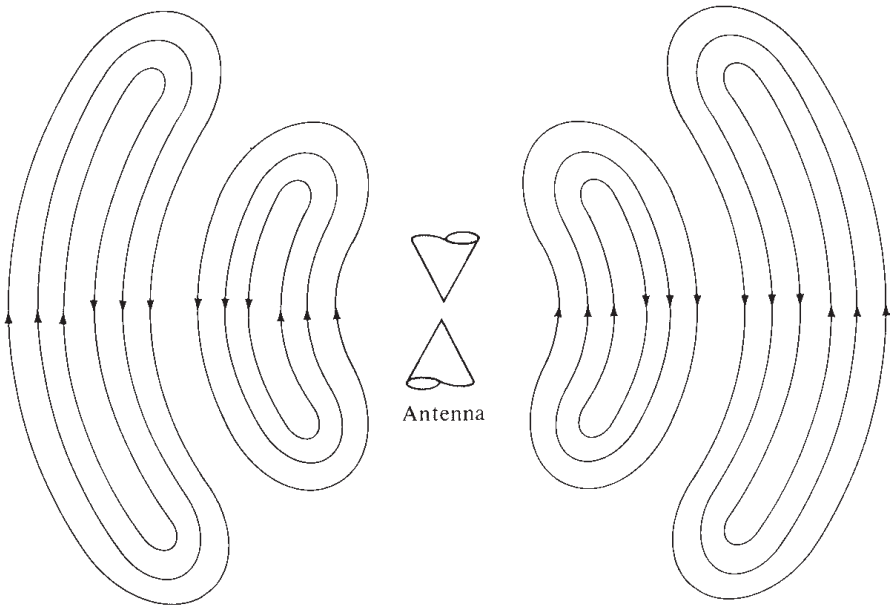


Figure 1.13 Electric field lines of free-space wave for biconical antenna.

transmission line, then into the antenna, and finally are radiated as free-space waves, even if the electric source has ceased to exist (as was with the water waves and their generating disturbance). If the electric disturbance is of a continuous nature, electromagnetic waves exist continuously and follow in their travel behind the others. This is shown in Figure 1.13 for a biconical antenna. When the electromagnetic waves are within the transmission line and antenna, their existence is associated with the presence of the charges inside the conductors. However, when the waves are radiated, they form closed loops and there are no charges to sustain their existence. *This leads us to conclude that electric charges are required to excite the fields but are not needed to sustain them and may exist in their absence. This is in direct analogy with water waves*.

1.3.3 Dipole

Now let us attempt to explain the mechanism by which the electric lines of force are detached from the antenna to form the free-space waves. This will again be illustrated by an example of a small dipole antenna where the time of travel is negligible. This is only necessary to give a better physical interpretation of the detachment of the lines of force. Although a somewhat simplified mechanism, it does allow one to visualize the creation of the free-space waves. Figure 1.14(a) displays the lines of force created between the arms of a small center-fed dipole in the first quarter of the period during which time the charge has reached its maximum value (assuming a sinusoidal time variation) and the lines have traveled outwardly a radial distance $\lambda/4$. For this example, let us assume that the number of lines formed are three. During the next quarter of the period, the original three lines travel an additional $\lambda/4$ (a total of $\lambda/2$ from the initial point) and the charge density on the conductors begins to diminish. This can be thought of as being accomplished by introducing opposite charges which at the end of the first half of the period have neutralized the charges on the conductors. The lines of force created by the opposite charges are three and travel a distance $\lambda/4$ during

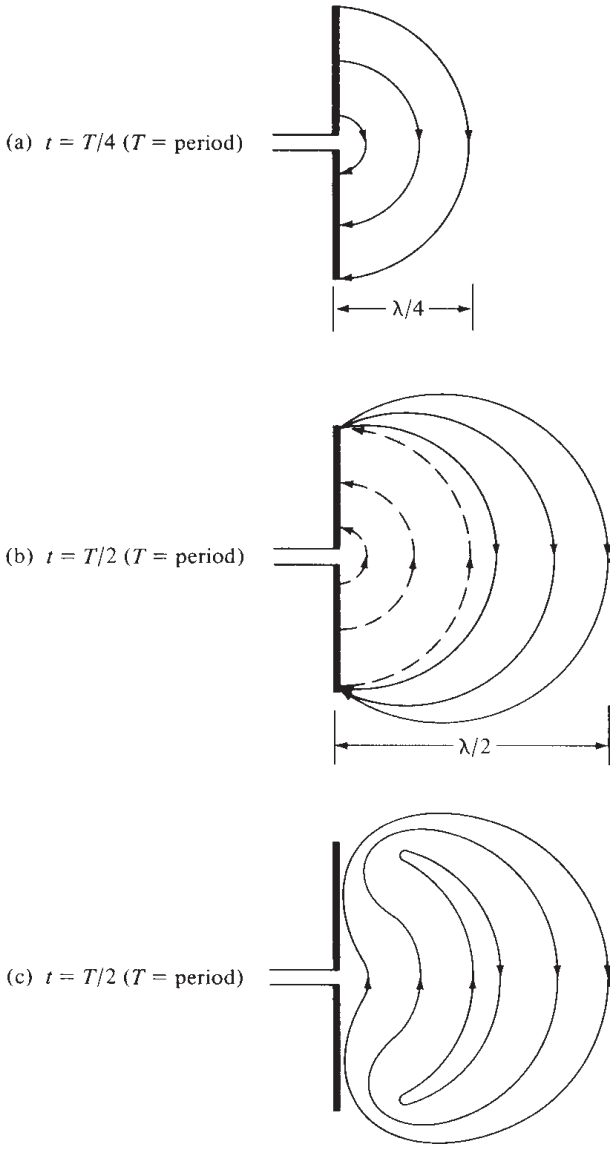


Figure 1.14 Formation and detachment of electric field lines for short dipole.

the second quarter of the first half, and they are shown dashed in Figure 1.14(b). The end result is that there are three lines of force pointed upward in the first $\lambda/4$ distance and the same number of lines directed downward in the second $\lambda/4$. Since there is no net charge on the antenna, then the lines of force must have been forced to detach themselves from the conductors and to unite together to form closed loops. This is shown in Figure 1.14(c). In the remaining second half of the period, the same procedure is followed but in the opposite direction. After that, the process is repeated and continues indefinitely and electric field patterns, similar to those of Figure 1.12, are formed.

1.3.4 Computer Animation-Visualization of Radiation Problems

A difficulty that students usually confront is that the subject of electromagnetics is rather abstract, and it is hard to visualize electromagnetic wave propagation and

interaction. With today's advanced numerical and computational methods, and animation and visualization software and hardware, this dilemma can, to a large extent, be minimized. To address this problem, we have developed and included in this chapter computer programs to animate and visualize three radiation problems. Descriptions of the computer programs are found in the computer disc included in this book. Each problem is solved using the Finite-Difference Time-Domain (FD-TD) method [8]–[10], a method which solves Maxwell's equations as a function of time in discrete time steps at discrete points in space. A picture of the fields can then be taken at each time step to create a movie which can be viewed as a function of time. Other animation and visualization software, referred to as *applets*, are included in the attached CD.

The three radiation problems that are animated and can be visualized using the computer program of this chapter and included in the computer disc are:

a. *Infinite length line source (two-dimensional) excited by a single Gaussian pulse and radiating in an unbounded medium.*
b. *Infinite length line source (two-dimensional) excited by a single Gaussian pulse and radiating inside a perfectly electric conducting (PEC) square cylinder.*
c. *E-plane sectoral horn (two-dimensional form of Figure 13.2) excited by a continuous cosinusoidal voltage source and radiating in an unbounded medium.*

In order to animate and then visualize each of the three radiation problems, the user needs *MATLAB* [11] and the *MATLAB M-file*, found in the computer disc included in the book, to produce the corresponding FD-TD solution of each radiation problem. For each radiation problem, the *M-File* executed in *MATLAB* produces a movie by taking a picture of the computational domain every third time step. The movie is viewed as a function of time as the wave travels in the computational space.

A. Infinite Line Source in an Unbounded Medium (***tm_open***)
The first FD-TD solution is that of an infinite length line source excited by a single time-derivative Gaussian pulse, with a duration of approximately 0.4 nanoseconds, in a two-dimensional TM^z-computational domain. The unbounded medium is simulated using a six-layer Berenger Perfectly Matched Layer (PML) Absorbing Boundary Condition (ABC) [9], [10] to truncate the computational space at a finite distance without, in principle, creating any reflections. Thus, the pulse travels radially outward creating a *traveling* type of a wavefront. The outward moving wavefronts are easily identified using the coloring scheme for the intensity (or gray scale for black and white monitors) when viewing the movie. The movie is created by the *MATLAB M-File* which produces the FD-TD solution by taking a picture of the computational domain every third time step. Each time step is 5 picoseconds while each FD-TD cell is 3 mm on a side. The movie is 37 frames long covering 185 picoseconds of elapsed time. The entire computational space is 15.3 cm by 15.3 cm and is modeled by 2500 square FD-TD cells (50×50), including 6 cells to implement the PML ABC.

B. Infinite Line Source in a PEC Square Cylinder (***tm_box***)
This problem is simulated similarly as that of the line source in an unbounded medium, including the characteristics of the pulse. The major difference is that the computational domain of this problem is truncated by PEC walls; *therefore there is no need for*

PML ABC. For this problem the pulse travels in an outward direction and is reflected when it reaches the walls of the cylinder. The reflected pulse along with the radially outward traveling pulse interfere constructively and destructively with each other and create a *standing* type of a wavefront. The peaks and valleys of the modified wavefront can be easily identified when viewing the movie, using the colored or gray scale intensity schemes. Sufficient time is allowed in the movie to permit the pulse to travel from the source to the walls of the cylinder, return back to the source, and then return back to the walls of the cylinder. Each time step is 5 picoseconds and each FD-TD cell is 3 mm on a side. The movie is 70 frames long covering 350 picoseconds of elapsed time. The square cylinder, and thus the computational space, has a cross section of 15.3 cm by 15.3 cm and is modeled using an area 50 by 50 FD-TD cells.

C. E-Plane Sectoral Horn in an Unbounded Medium (***te_horn***)
The E-plane sectoral horn is excited by a cosinusoidal voltage (CW) of 9.84 GHz in a TE^Z computational domain, instead of the Gaussian pulse excitation of the previous two problems. The unbounded medium is implemented using an eight-layer Berenger PML ABC. The computational space is 25.4 cm by 25.4 cm and is modeled using 100 by 100 FD-TD cells (each square cell being 2.54 mm on a side). The movie is 70 frames long covering 296 picoseconds of elapsed time and is created by taking a picture every third frame. Each time step is 4.23 picoseconds in duration. The horn has a total flare angle of 52° and its flared section is 2.62 cm long, is fed by a parallel plate 1 cm wide and 4.06 cm long, and has an aperture of 3.56 cm.

1.4 CURRENT DISTRIBUTION ON A THIN WIRE ANTENNA

In the preceding section we discussed the movement of the free electrons on the conductors representing the transmission line and the antenna. In order to illustrate the creation of the current distribution on a linear dipole, and its subsequent radiation, let us first begin with the geometry of a lossless two-wire transmission line, as shown in Figure 1.15(a). The movement of the charges creates a traveling wave current, of magnitude $I_0/2$, along each of the wires. When the current arrives at the end of each of the wires, it undergoes a complete reflection (equal magnitude and 180° phase reversal). The reflected traveling wave, when combined with the incident traveling wave, forms in each wire a pure standing wave pattern of sinusoidal form as shown in Figure 1.15(a). The current in each wire undergoes a 180° phase reversal between adjoining half-cycles. This is indicated in Figure 1.15(a) by the reversal of the arrow direction. Radiation from each wire individually occurs because of the time-varying nature of the current and the termination of the wire.

For the two-wire balanced (symmetrical) transmission line, the current in a half-cycle of one wire is of the same magnitude but 180° out-of-phase from that in the corresponding half-cycle of the other wire. If in addition the spacing between the two wires is very small ($s \ll \lambda$), the fields radiated by the current of each wire are essentially cancelled by those of the other. The net result is an almost ideal (and desired) nonradiating transmission line.

As the section of the transmission line between $0 \leq z \leq l/2$ begins to flare, as shown in Figure 1.15(b), it can be assumed that the current distribution is essentially unaltered

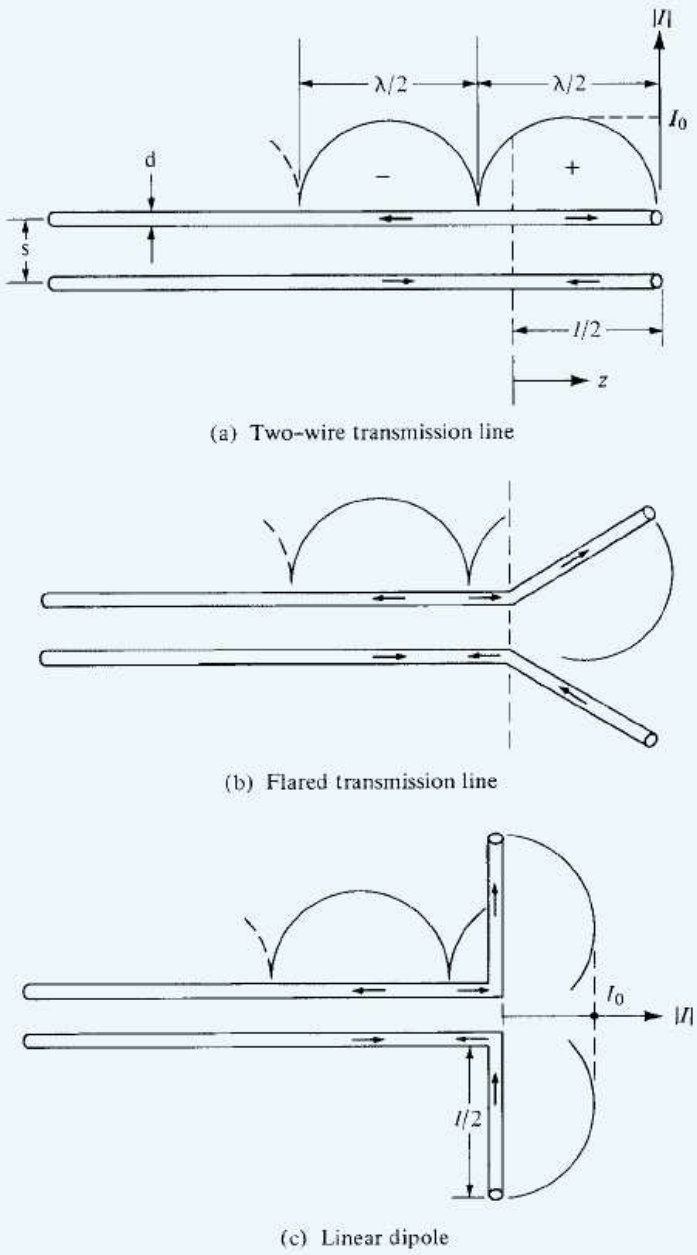


Figure 1.15 Current distribution on a lossless two-wire transmission line, flared transmission line, and linear dipole.

in form in each of the wires. However, because the two wires of the flared section are not necessarily close to each other, the fields radiated by one do not necessarily cancel those of the other. Therefore ideally there is a net radiation by the transmission-line system.

Ultimately the flared section of the transmission line can take the form shown in Figure 1.15(c). This is the geometry of the widely used dipole antenna. Because of the standing wave current pattern, it is also classified as a standing wave antenna (as contrasted to the traveling wave antennas which will be discussed in detail in Chapter 10). If $l < \lambda$, the phase of the current standing wave pattern in each arm is the same throughout its length. In addition, spatially it is oriented in the same direction as

that of the other arm as shown in Figure 1.15(c). Thus the fields radiated by the two arms of the dipole (vertical parts of a flared transmission line) will primarily reinforce each other toward most directions of observation (the phase due to the relative position of each small part of each arm must also be included for a complete description of the radiation pattern formation).

If the diameter of each wire is very small ($d \ll \lambda$), the ideal standing wave pattern of the current along the arms of the dipole is sinusoidal with a null at the end. However, its overall form depends on the length of each arm. For center-fed dipoles with $l \ll \lambda, l = \lambda/2, \lambda/2 < l < \lambda$ and $\lambda < l < 3\lambda/2$, the current patterns are illustrated in Figures 1.16(a–d). The current pattern of a very small dipole (usually $\lambda/50 < l \leq \lambda/10$) can be approximated by a triangular distribution since $\sin(kl/2) \simeq kl/2$ when $kl/2$ is very small. This is illustrated in Figure 1.16(a).

Because of its cyclical spatial variations, the current standing wave pattern of a dipole longer than $\lambda(l > \lambda)$ undergoes 180° phase reversals between adjoining half-cycles. Therefore the current in all parts of the dipole does not have the same phase. This is demonstrated graphically in Figure 1.16(d) for $\lambda < l < 3\lambda/2$. In turn, the fields radiated by some parts of the dipole will not reinforce those of the others. As a result,

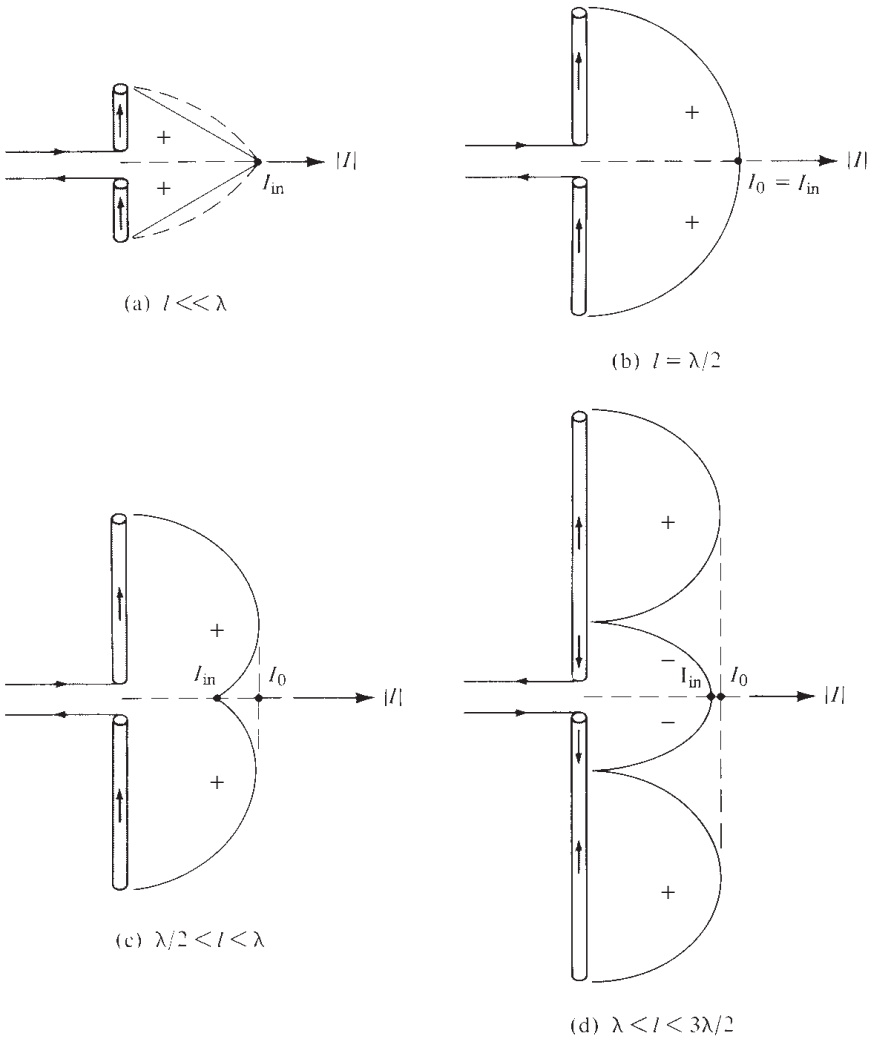


Figure 1.16 Current distribution on linear dipoles.

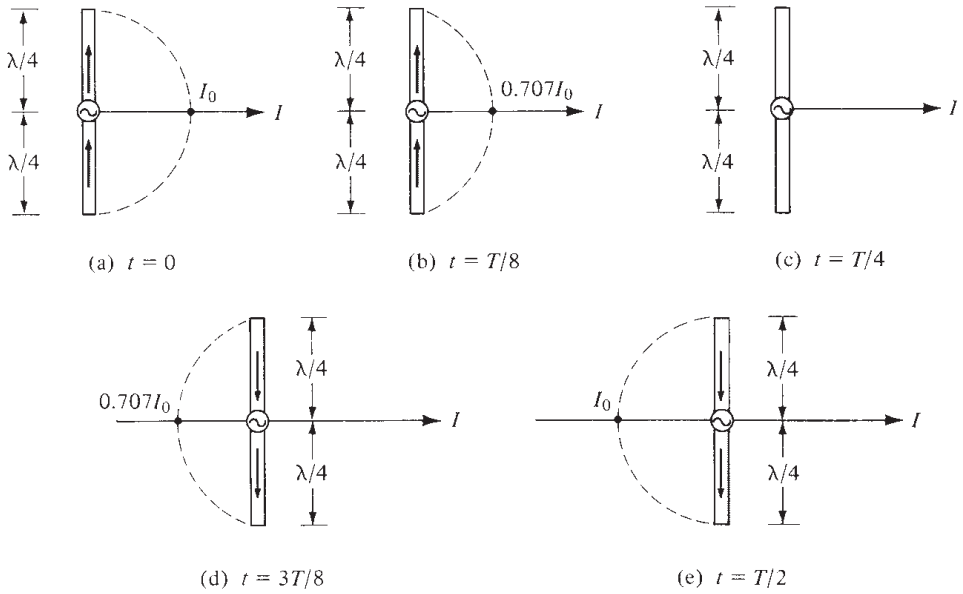


Figure 1.17 Current distribution on a $\lambda/2$ wire antenna for different times.

significant interference and cancelling effects will be noted in the formation of the total radiation pattern. See Figure 4.11 for the pattern of a $\lambda/2$ dipole and Figure 4.7 for that of a 1.25λ dipole.

For a time-harmonic varying system of radian frequency $\omega = 2\pi f$, the current standing wave patterns of Figure 1.16 represent the maximum current excitation for any time. The current variations, as a function of time, on a $\lambda/2$ center-fed dipole are shown in Figure 1.17 for $0 \leq t \leq T/2$ where T is the period. These variations can be obtained by multiplying the current standing wave pattern of Figure 1.16(b) by $\cos(\omega t)$.

1.5 HISTORICAL ADVANCEMENT

The history of antennas [12] dates back to James Clerk Maxwell who unified the theories of electricity and magnetism, and eloquently represented their relations through a set of profound equations best known as *Maxwell's Equations*. His work was first published in 1873 [13]. He also showed that light was electromagnetic and that both light and electromagnetic waves travel by wave disturbances of the same speed. In 1886, Professor Heinrich Rudolph Hertz demonstrated the first wireless electromagnetic system. He was able to produce in his laboratory at a wavelength of 4 m a spark in the gap of a transmitting $\lambda/2$ dipole which was then detected as a spark in the gap of a nearby loop. It was not until 1901 that Guglielmo Marconi was able to send signals over large distances. He performed, in 1901, the first transatlantic transmission from Poldhu in Cornwall, England, to St. John's Newfoundland. His transmitting antenna consisted of 50 vertical wires in the form of a fan connected to ground through a spark transmitter. The wires were supported horizontally by a guyed wire between two 60-m wooden poles. The receiving antenna at St. John's was a 200-m wire pulled and supported by a kite. This was the dawn of the antenna era.

From Marconi's inception through the 1940s, antenna technology was primarily centered on wire related radiating elements and frequencies up to about UHF. It was

not until World War II that modern antenna technology was launched and new elements (such as waveguide apertures, horns, reflectors) were primarily introduced. Much of this work is captured in the book by Silver [14]. A contributing factor to this new era was the invention of microwave sources (such as the klystron and magnetron) with frequencies of 1 GHz and above.

While World War II launched a new era in antennas, advances made in computer architecture and technology during the 1960s through the 1990s have had a major impact on the advance of modern antenna technology, and they are expected to have an even greater influence on antenna engineering into the twenty-first century. Beginning primarily in the early 1960s, numerical methods were introduced that allowed previously intractable complex antenna system configurations to be analyzed and designed very accurately. In addition, asymptotic methods for both low frequencies (e.g., Moment Method (MM), Finite-Difference, Finite-Element) and high frequencies (e.g., Geometrical and Physical Theories of Diffraction) were introduced, contributing significantly to the maturity of the antenna field. While in the past antenna design may have been considered a secondary issue in overall system design, today it plays a critical role. In fact, many system successes rely on the design and performance of the antenna. Also, while in the first half of this century antenna technology may have been considered almost a "cut and try" operation, today it is truly an engineering art. Analysis and design methods are such that antenna system performance can be predicted with remarkable accuracy. In fact, many antenna designs proceed directly from the initial design stage to the prototype without intermediate testing. The level of confidence has increased tremendously.

The widespread interest in antennas is reflected by the large number of books written on the subject [15]. These have been classified under four categories: Fundamental, Handbooks, Measurements, and Specialized. This is an outstanding collection of books, and it reflects the popularity of the antenna subject, especially since the 1950s. Because of space limitations, only a partial list is included here [2], [5], [7], [16]–[39], including the first and second editions of this book in 1982, 1997. Some of these books are now out of print.

1.5.1 Antenna Elements

Prior to World War II most antenna elements were of the wire type (long wires, dipoles, helices, rhombuses, fans, etc.), and they were used either as single elements or in arrays. During and after World War II, many other radiators, some of which may have been known for some and others of which were relatively new, were put into service. This created a need for better understanding and optimization of their radiation characteristics. Many of these antennas were of the aperture type (such as open-ended waveguides, slots, horns, reflectors, lenses), and they have been used for communication, radar, remote sensing, and deep space applications both on airborne and earth-based platforms. Many of these operate in the microwave region and are discussed in Chapters 12, 13, 15 and in [40].

Prior to the 1950s, antennas with broadband pattern and impedance characteristics had bandwidths not much greater than about 2:1. In the 1950s, a breakthrough in antenna evolution was created which extended the maximum bandwidth to as great as 40:1 or more. Because the geometries of these antennas are specified by angles instead of linear dimensions, they have ideally an infinite bandwidth. Therefore, they are referred to as *frequency independent*. These antennas are primarily used in the

10–10,000 MHz region in a variety of applications including TV, point-to-point communications, feeds for reflectors and lenses, and many others. This class of antennas is discussed in more detail in Chapter 11 and in [41].

It was not until almost 20 years later that a fundamental new radiating element, which has received a lot of attention and many applications since its inception, was introduced. This occurred in the early 1970s when the microstrip or patch antennas was reported. This element is simple, lightweight, inexpensive, low profile, and conformal to the surface. These antennas are discussed in more detail in Chapter 14 and in [42].

Major advances in millimeter wave antennas have been made in recent years, including integrated antennas where active and passive circuits are combined with the radiating elements in one compact unit (monolithic form). These antennas are discussed in [43].

Specific radiation pattern requirements usually cannot be achieved by single antenna elements, because single elements usually have relatively wide radiation patterns and low values of directivity. To design antennas with very large directivities, it is usually necessary to increase the electrical size of the antenna. This can be accomplished by enlarging the electrical dimensions of the chosen single element. However, mechanical problems are usually associated with very large elements. An alternative way to achieve large directivities, without increasing the size of the individual elements, is to use multiple single elements to form an *array*. An array is a sampled version of a very large single element. In an array, the mechanical problems of large single elements are traded for the electrical problems associated with the feed networks of arrays. However, with today's solid-state technology, very efficient and low-cost feed networks can be designed.

Arrays are the most versatile of antenna systems. They find wide applications not only in many spaceborne systems, but in many earthbound missions as well. In most cases, the elements of an array are identical; this is not necessary, but it is often more convenient, simpler, and more practical. With arrays, it is practical not only to synthesize almost any desired amplitude radiation pattern, but the main lobe can be scanned by controlling the relative phase excitation between the elements. This is most convenient for applications where the antenna system is not readily accessible, especially for spaceborne missions. The beamwidth of the main lobe along with the side lobe level can be controlled by the relative amplitude excitation (distribution) between the elements of the array. In fact, there is a trade-off between the beamwidth and the side lobe level based on the amplitude distribution. Analysis, design, and synthesis of arrays are discussed in Chapters 6 and 7. However, advances in array technology are reported in [44]–[48].

A new antenna array design referred to as *smart antenna*, based on basic technology of the 1970s and 1980s, is sparking interest especially for wireless applications. This antenna design, which combines antenna technology with that of digital signal processing (DSP), is discussed in some detail in Chapter 16.

1.5.2 Methods of Analysis

There is plethora of antenna elements, many of which exhibit intricate configurations. To analyze each as a boundary-value problem and obtain solutions in closed form, the antenna structure must be described by an orthogonal curvilinear coordinate system. This places severe restrictions on the type and number of antenna systems that can be analyzed using such a procedure. Therefore, other exact or approximate methods are often pursued. Two methods that in the last three decades have been preeminent in the analysis of many previously intractable antenna problems are the *Integral Equation* (IE) method and the *Geometrical Theory of Diffraction* (GTD).

The Integral Equation method casts the solution to the antenna problem in the form of an integral (hence its name) where the unknown, usually the induced current density, is part of the integrand. Numerical techniques, such as the Moment Method (MM), are then used to solve for the unknown. Once the current density is found, the radiation integrals of Chapter 3 are used to find the fields radiated and other systems parameters. This method is most convenient for wire-type antennas and more efficient for structures that are small electrically. One of the first objectives of this method is to formulate the IE for the problem at hand. In general, there are two type of IE's. One is the *Electric Field Integral Equation (EFIE)*, and it is based on the boundary condition of the total tangential electric field. The other is the *Magnetic Field Integral Equation (MFIE)*, and it is based on the boundary condition that expresses the total electric current density induced on the surface in terms of the incident magnetic field. The MFIE is only valid for closed surfaces. For some problems, it is more convenient to formulate an EFIE, while for others it is more appropriate to use an MFIE. Advances, applications, and numerical issues of these methods are addressed in Chapter 8 and in [3] and [49].

When the dimensions of the radiating system are many wavelengths, low-frequency methods are not as computationally efficient. However, high-frequency asymptotic techniques can be used to analyze many problems that are otherwise mathematically intractable. One such method that has received considerable attention and application over the years is the GTD, which is an extension of geometrical optics (GO), and it overcomes some of the limitations of GO by introducing a diffraction mechanism. The Geometrical Theory of Diffraction is briefly discussed in Section 12.10. However, a detailed treatment is found in Chapter 13 of [3] while recent advances and applications are found in [50] and [51].

For structures that are not convenient to analyze by either of the two methods, a combination of the two is often used. Such a technique is referred to as a *hybrid method*, and it is described in detail in [52]. Another method, which has received a lot of attention in scattering, is the Finite-Difference Time-Domain (FDTD). This method has also been applied to antenna radiation problems [53]–[56]. A method that is beginning to gain momentum in its application to antenna problems is the Finite Element Method [57]–[61].

1.5.3 Some Future Challenges

Antenna engineering has enjoyed a very successful period during the 1940s–1990s. Responsible for its success have been the introduction and technological advances of some new elements of radiation, such as aperture antennas, reflectors, frequency independent antennas, and microstrip antennas. Excitement has been created by the advancement of the low-frequency and high-frequency asymptotic methods, which has been instrumental in analyzing many previously intractable problems. A major factor in the success of antenna technology has been the advances in computer architecture and numerical computation methods. Today antenna engineering is considered a truly fine engineering art.

Although a certain level of maturity has been attained, there are many challenging opportunities and problems to be solved. Phased array architecture integrating monolithic MIC technology is still a most challenging problem. Integration of new materials, such as *metamaterials* [62], *artificial magnetic conductors* and *soft/hard surfaces* [63], into antenna technology offers many opportunities, and asymptotic methods will play key roles in their incorporation and system performance. Computational electromagnetics using supercomputing and parallel computing capabilities will model complex electromagnetic wave interactions, in both the frequency and time domains. Innovative antenna designs,

such as those using *smart antennas* [64], and *multifunction, reconfigurable antennas and antenna systems* [65], to perform complex and demanding system functions remain a challenge. New basic elements are always welcome and offer refreshing opportunities. New applications include, but are not limited to wireless communications, direct broadcast satellite systems, global positioning satellites (GPS), high-accuracy airborne navigation, global weather, earth resource systems, and others. Because of the many new applications, the lower portion of the EM spectrum has been saturated and the designs have been pushed to higher frequencies, including the millimeter wave frequency bands.

1.6 MULTIMEDIA

In the CD that is part of this book, the following multimedia resources related to this chapter are included:

a. **Java**-based **interactive** questionnaire with answers.
b. Three **Matlab**-based **animation-visualization** programs designated
   - ***tm_open***
   - ***tm_box***
   - ***te_horn***

   which are described in detail in Section 1.3.4 and the corresponding READ ME file of the attached CD.
c. **Power Point (PPT)** viewgraphs.

REFERENCES

1. C. A. Balanis, "Antenna Theory: A Review," *Proc. IEEE*, Vol. 80, No. 1, pp. 7–23, January 1992.
2. L. V. Blake, *Antennas*, Wiley, New York, 1966, p. 289.
3. C. A. Balanis, *Advanced Engineering Electromagnetics*, Wiley, New York, 1989.
4. E. K. Miller and J. A. Landt, "Direct Time-Domain Techniques for Transient Radiation and Scattering from Wires," *Proc. IEEE*, Vol. 68, No. 11, pp. 1396–1423, November 1980.
5. J. D. Kraus, *Antennas*, McGraw-Hill, New York, 1988.
6. J. D. Kraus, *Electromagnetics*, McGraw-Hill, New York, 1992, pp. 761–763.
7. S. A. Schelkunoff and H. T. Friis, *Antenna Theory and Practice*, Wiley, New York, 1952.
8. K. S. Yee, "Numerical Solution of Initial Boundary Value Problems Involving Maxwell's Equations in Isotropic Media," *IEEE Trans. Antennas Propagat.*, Vol. AP-14, No. 3, pp. 302–307, May 1966.
9. J. P. Berenger, "A Perfectly Matched Layer for the Absorption of Electromagnetic Waves," *J. Comput. Phys.*, Vol. 114, pp. 185–200, October 1994.
10. W. V. Andrew, C. A. Balanis, and P. A. Tirkas, "A Comparison of the Berenger Perfectly Matched Layer and the Lindman Higher-Order ABC's for the FDTD Method," *IEEE Microwave Guided Wave Lett.*, Vol. 5, No. 6, pp. 192–194, June 1995.
11. *The Student Edition of MATLAB*: Version 4: User's Guide, The MATH WORKS, Inc., Prentice-Hall, Inc., Englewood Cliffs, NJ, 1995.
12. J. D. Kraus, "Antennas since Hertz and Marconi," *IEEE Trans. Antennas Propagat.*, Vol. AP-33, No. 2, pp. 131–137, February 1985.
13. J. C. Maxwell, *A Treatise on Electricity and Magnetism*, Oxford University Press, London, UK, 1873, 1904.

14. S. Silver (Ed.), *Microwave Antenna Theory and Design*, MIT Radiation Lab. Series, Vol. 12, McGraw-Hill, New York, 1949.
15. S. Stutzman, "Bibliography for Antennas," *IEEE Antennas Propagat. Mag.*, Vol. 32, pp. 54–57, August 1990.
16. J. Aharoni, *Antennae*, Oxford University Press, London, UK, 1946.
17. S. A. Schelkunoff, *Advanced Antenna Theory*, Wiley, New York, 1952.
18. E. A. Laport, *Radio Antenna Engineering*, McGraw-Hill, New York, 1952.
19. C. H. Walter, *Traveling Wave Antennas*, McGraw-Hill, New York, 1968.
20. E. Wolff, *Antenna Analysis*, Wiley, New York, 1966 (first edition), Artech House, Norwood, MA, 1988 (second edition).
21. W. L. Weeks, *Antenna Engineering*, McGraw-Hill, New York, 1968.
22. E. Jordan and K. Balmain, *Electromagnetic Waves and Radiating Systems*, Prentice-Hall, New York, 1968.
23. R. E. Collin and F. J. Zucker (Eds.), *Antenna Theory*, Parts 1 and 2, McGraw-Hill, New York, 1969.
24. W. V. T. Rusch and P. D. Potter, *Analysis of Reflector Antennas*, Academic Press, New York, 1970.
25. W. L. Stutzman and G. A. Thiele, *Antenna Theory and Design*, Wiley, New York, 1998.
26. R. S. Elliot, *Antenna Theory and Design*, Prentice-Hall, New York, 1981.
27. K. F. Lee, *Principles of Antenna Theory*, Wiley, New York, 1984.
28. R. E. Collin, *Antennas and Radiowave Propagation*, McGraw-Hill, New York, 1985.
29. T. A. Milligan, *Modern Antenna Design*, McGraw-Hill, New York, 1985.
30. J. R. Wait, *Introduction to Antennas and Propagation*, IEE, Hithin Herts, UK, 1966.
31. F. R. Connor, *Antennas*, Edward Arnold, London, 1989.
32. K. Chang (Ed.), *Handbook of Microwave and Optical Components*, Vol. I, Wiley-Interscience, New York, 1989, Chapters 10–13.
33. R. C. Johnson and H. Jasik, *Antenna Engineering Handbook*, McGraw-Hill, New York, 1984.
34. R. C. Hansen (Ed.), *Microwave Scanning Antennas*, Vols. I–III, Academic Press, New York, 1964 (reprinted by Peninsula Publishing, Los Altos, CA).
35. A. W. Rudge, K. Milne, A. D. Olver, and P. Knight (Eds.), *The Handbook of Antenna Design*, Vols. 1 and 2, Peter Peregrinus, London, 1982.
36. Y. T. Lo and S. W. Lee (Eds.), *Antenna Handbook: Theory, Applications, and Design*, Van Nostrand Reinhold, New York, 1988.
37. I. J. Bahl and P. Bhartia, *Microstrip Antennas*, Artech House, Norwood, MA, 1980.
38. J. R. James and P. S. Hall (Eds.), *Handbook of Microstrip Antennas*, Vols. I and II, Peter Peregrinus, 1989.
39. D. M. Pozar, *Antenna Design Using Personal Computers*, Artech House, Norwood, MA, 1985.
40. W. V. T. Rusch, "The Current State of the Reflector Antenna Art-Entering the 1990s," *Proc. IEEE*, Vol. 80, No. 1, pp. 113–126, January 1992.
41. P. E. Mayes, "Frequency-Independent Antennas and Broad-Band Derivatives Thereof," *Proc. IEEE*, Vol. 80, No. 1, pp. 103–112, January 1992.
42. D. M. Pozar, "Microstrip Antennas," *Proc. IEEE*, Vol. 80, No. 1, pp. 79–91, January 1992.
43. F. K. Schwering, "Millimeter Wave Antennas," *Proc. IEEE*, Vol. 80, No. 1, pp. 92–102, January 1992.

44. W. H. Kummer, "Basic Array Theory," *Proc. IEEE*, Vol. 80, No. 1, pp. 127–140, January 1992.
45. R. C. Hansen, "Array Pattern Control and Synthesis," *Proc. IEEE*, Vol. 80, No. 1, pp. 141–151, January 1992.
46. W. F. Gabriel, "Adaptive Processing Array Systems," *Proc. IEEE*, Vol. 80, No. 1, pp. 152–162, January 1992.
47. R. J. Mailloux, "Antenna Array Architecture," *Proc. IEEE*, Vol. 80, No. 1, pp. 163–172, January 1992.
48. R. Tang and R. W. Burns, "Array Technology," *Proc. IEEE*, Vol. 80, No. 1, pp. 173–182, January 1992.
49. E. K. Miller and G. J. Burke, "Low-Frequency Computational Electromagnetics for Antenna Analysis," *Proc. IEEE*, Vol. 80, No. 1, pp. 24–43, January 1992.
50. P. H. Pathak, "High-Frequency Techniques for Antenna Analysis," *Proc. IEEE*, Vol. 80, No. 1, pp. 44–65, January 1992.
51. R. J. Marhefka and W. D. Burnside, "Antennas on Complex Platforms," *Proc. IEEE*, Vol. 80, No. 1, pp. 204–208, January 1992.
52. G. A. Thiele, "Overview of Selected Hybrid Methods in Radiating System Analysis," *Proc. IEEE*, Vol. 80, No. 1, pp. 66–78, January 1992.
53. J. C. Maloney, G. S. Smith, and W. R. Scott Jr., "Accurate Computation of the Radiation from Simple Antennas using the Finite-Difference Time-Domain Method," *IEEE Trans. Antennas Propagat.*, Vol. 38, No. 7, pp. 1059–1068, July 1990.
54. D. S. Katz, M. J. Piket-May, A. Taflove, and K. R. Umashankar, "FDTD Analysis of Electromagnetic Wave Radiation from Systems Containing Horn Antennas," *IEEE Trans. Antennas Propagat.*, Vol. 39, No. 8, pp. 1203–1212, August 1991.
55. P. A. Tirkas and C. A. Balanis, "Finite-Difference Time-Domain Techniques for Antenna Radiation," *IEEE Trans. Antennas Propagat.*, Vol. 40, No. 3, pp. 334–340, March 1992.
56. P. A. Tirkas and C. A. Balanis, "Contour Path FDTD Method for Analysis of Pyramidal Horns With Composite Inner E-Plane Walls," *IEEE Trans. Antennas Propagat.*, Vol. 42, No. 11, pp. 1476–1483, November 1994.
57. J. Jin, *The Finite Element Method in Electromagnetics*, Wiley, New York, 1993.
58. J. M. Jin and J. L. Volakis, "Scattering and Radiation Analysis of Three-Dimensional Cavity Arrays Via a Hybrid Finite-Element Method," *IEEE Trans. Antennas Propagat.*, Vol. 41, No. 11, pp. 1580–1586, November 1993.
59. D. T. McGrath and V. P. Pyati, "Phased Array Antenna Analysis with Hybrid Finite Element Method," *IEEE Trans. Antennas Propagat.*, Vol. 42, No. 12, pp. 1625–1630, December 1994.
60. W. Sun and C. A. Balanis, "Vector One-Way Wave Absorbing Boundary Condition for FEM Applications," *IEEE Trans. Antennas Propagat.*, Vol. 42, No. 6, pp. 872–878, June 1994.
61. E. W. Lucas and T. P. Fontana, "A 3-D Hybrid Finite Element/Boundary Element Method for the Unified Radiation and Scattering Analysis of General Infinite Periodic Arrays," *IEEE Trans. Antennas Propagat.*, Vol. 43, No. 2, pp. 145–153, February 1995.
62. *IEEE Trans. Antennas Propagat.*, Special Issue on *Metamaterials*, Vol. 51, No. 10, October 2003.
63. *IEEE Trans. Antennas Propagat.*, Special Issue on *Artificial Magnetic Conductors, Soft/Hard Surfaces and Other Complex Surfaces*, Vol. 53, No. 1, Jan. 2005.
64. *IEEE Trans. Antennas Propagat.*, Special Issue on *Wireless Information Technology and Networks*, Vol. 50, No. 5, May 2002.
65. *IEEE Trans. Antennas Propagat.*, Special Issue on *Multifunction Antennas and Antenna Systems*, Vol. 54, No. 1, Jan. 2006.

CHAPTER 2

Fundamental Parameters of Antennas

2.1 INTRODUCTION

To describe the performance of an antenna, definitions of various parameters are necessary. Some of the parameters are interrelated and not all of them need be specified for complete description of the antenna performance. Parameter definitions will be given in this chapter. Many of those in quotation marks are from the *IEEE Standard Definitions of Terms for Antennas* (IEEE Std 145-1983).* This is a revision of the IEEE Std 145-1973.

2.2 RADIATION PATTERN

An antenna *radiation pattern* or *antenna pattern* is defined as "a mathematical function or a graphical representation of the radiation properties of the antenna as a function of space coordinates. In most cases, the radiation pattern is determined in the far-field region and is represented as a function of the directional coordinates. Radiation properties include power flux density, radiation intensity, field strength, directivity, phase or polarization." The radiation property of most concern is the two- or three-dimensional spatial distribution of radiated energy as a function of the observer's position along a path or surface of constant radius. A convenient set of coordinates is shown in Figure 2.1. A trace of the received electric (magnetic) field at a constant radius is called the amplitude field *pattern*. On the other hand, a graph of the spatial variation of the power density along a constant radius is called an amplitude *power pattern*.

Often the *field* and *power* patterns are normalized with respect to their maximum value, yielding *normalized field* and *power patterns*. Also, the power pattern is usually plotted on a logarithmic scale or more commonly in decibels (dB). This scale is usually desirable because a logarithmic scale can accentuate in more details those parts of the

IEEE Transactions on Antennas and Propagation, Vols. AP-17, No. 3, May 1969; Vol. AP-22, No. 1, January 1974; and Vol. AP-31, No. 6, Part II, November 1983.

Antenna Theory: Analysis Design, Third Edition, by Constantine A. Balanis
ISBN 0-471-66782-X Copyright © 2005 John Wiley & Sons, Inc.

EX2042
Page 40 of 1072

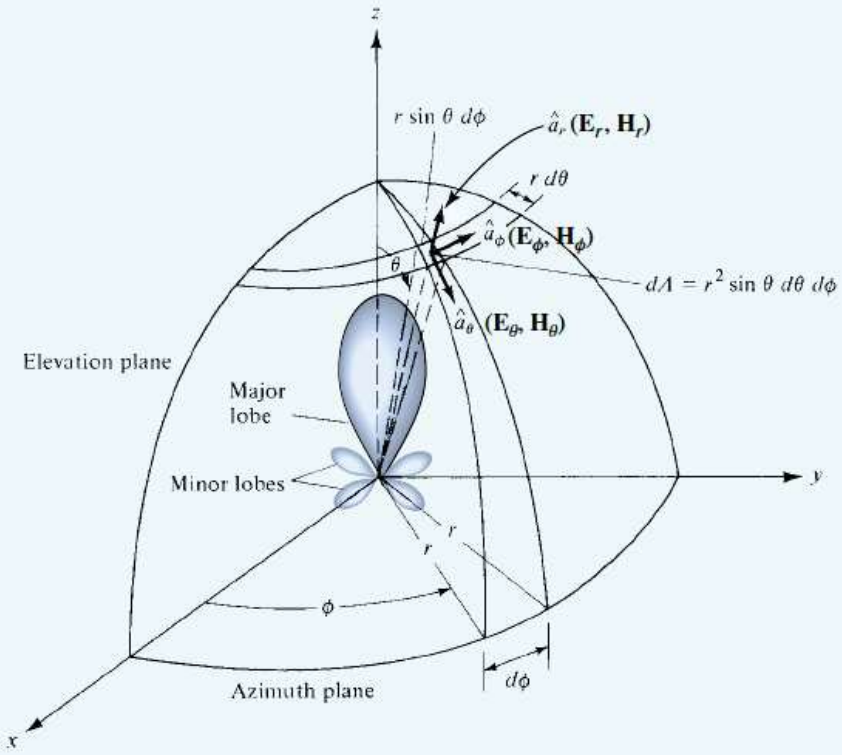


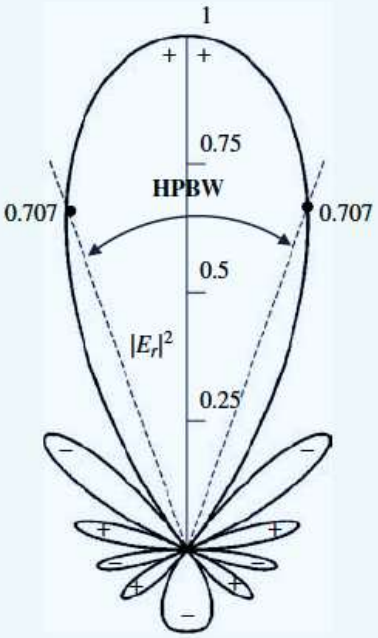
Figure 2.1 Coordinate system for antenna analysis.

pattern that have very low values, which later we will refer to as minor lobes. For an antenna, the

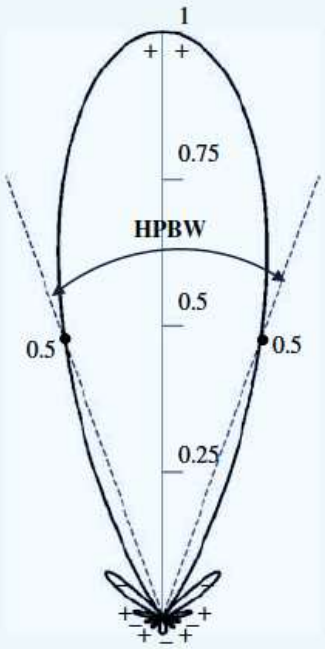
a. *field* pattern (*in linear scale*) typically represents a plot of the magnitude of the electric or magnetic field as a function of the angular space.
b. *power* pattern (*in linear scale*) typically represents a plot of the square of the magnitude of the electric or magnetic field as a function of the angular space.
c. *power* pattern (*in dB*) represents the magnitude of the electric or magnetic field, in decibels, as a function of the angular space.

To demonstrate this, the two-dimensional normalized field pattern (*plotted in linear scale*), power pattern (*plotted in linear scale*), and power pattern (*plotted on a logarithmic dB scale*) of a 10-element linear antenna array of isotropic sources, with a spacing of $d = 0.25\lambda$ between the elements, are shown in Figure 2.2. *In this and subsequent patterns, the plus* (+) *and minus* (−) *signs in the lobes indicate the relative polarization of the amplitude between the various lobes, which changes (alternates) as the nulls are crossed.* To find the points where the pattern achieves its half-power (−3 dB points), relative to the maximum value of the pattern, you set the value of the

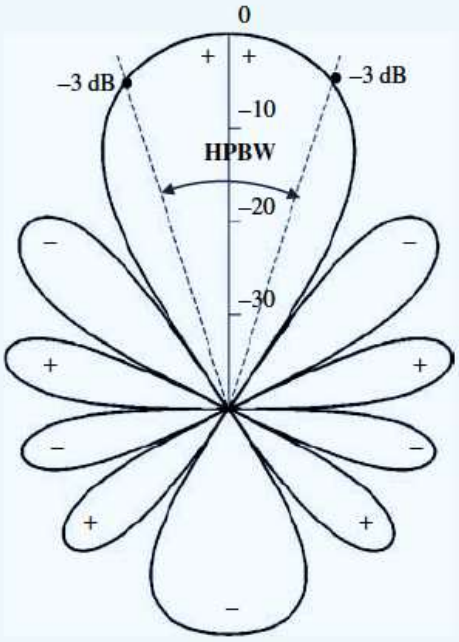
a. field pattern at 0.707 value of its maximum, as shown in Figure 2.2(a)
b. power pattern (in a linear scale) at its 0.5 value of its maximum, as shown in Figure 2.2(b)
c. power pattern (in dB) at −3 dB value of its maximum, as shown in Figure 2.2(c).



(a) Field pattern (in linear scale)



(b) Power pattern (in linear scale)



(c) Power pattern (in dB)

Figure 2.2 Two-dimensional normalized *field* pattern (*linear scale*), *power* pattern (*linear scale*), and *power* pattern (*in dB*) of a 10-element linear array with a spacing of $d = 0.25\lambda$.

All three patterns yield the same angular separation between the two half-power points, 38.64°, on their respective patterns, *referred to as HPBW* and illustrated in Figure 2.2. This is discussed in detail in Section 2.5.

In practice, the three-dimensional pattern is measured and recorded in a series of two-dimensional patterns. However, for most practical applications, a few plots of the

pattern as a function of θ for some particular values of ϕ, plus a few plots as a function of ϕ for some particular values of θ, give most of the useful and needed information.

2.2.1 Radiation Pattern Lobes

Various parts of a radiation pattern are referred to as *lobes*, which may be subclassified into *major* or *main, minor, side*, and *back* lobes.

A *radiation lobe* is a "portion of the radiation pattern bounded by regions of relatively weak radiation intensity." Figure 2.3(a) demonstrates a symmetrical three-dimensional polar pattern with a number of radiation lobes. Some are of greater radiation intensity than others, but all are classified as lobes. Figure 2.3(b) illustrates

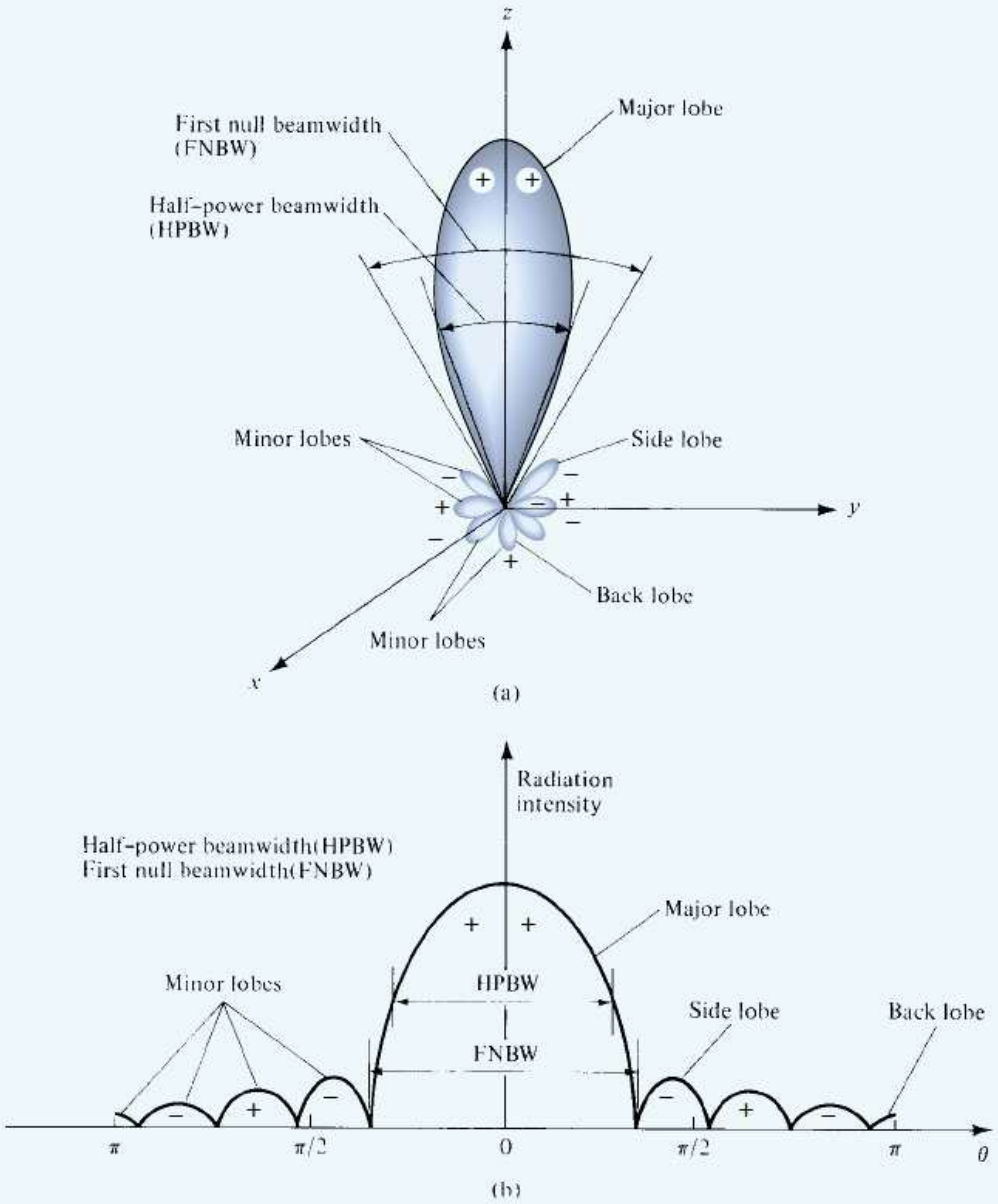


Figure 2.3 (a) Radiation lobes and beamwidths of an antenna pattern. (b) Linear plot of power pattern and its associated lobes and beamwidths.

EX2042
Page 43 of 1072

a linear two-dimensional pattern [one plane of Figure 2.3(a)] where the same pattern characteristics are indicated.

MATLAB-based computer programs, designated as ***polar*** and ***spherical***, have been developed and are included in the CD of this book. These programs can be used to plot the two-dimensional patterns, both polar and semipolar (*in linear* and *dB scales*), in polar form and spherical three-dimensional patterns (*in linear* and *dB scales*). A description of these programs is found in the attached CD. Other programs that have been developed for plotting rectangular and polar plots are those of [1]–[3].

A *major lobe* (also called main beam) is defined as "the radiation lobe containing the direction of maximum radiation." In Figure 2.3 the major lobe is pointing in the $\theta = 0$ direction. In some antennas, such as split-beam antennas, there may exist more than one major lobe. A *minor lobe* is any lobe except a major lobe. In Figures 2.3(a) and (b) all the lobes with the exception of the major can be classified as minor lobes. A *side lobe* is "a radiation lobe in any direction other than the intended lobe." (Usually a side lobe is adjacent to the main lobe and occupies the hemisphere in the direction of the main beam.) A *back lobe* is "a radiation lobe whose axis makes an angle of approximately 180° with respect to the beam of an antenna." Usually it refers to a minor lobe that occupies the hemisphere in a direction opposite to that of the major (main) lobe.

Minor lobes usually represent radiation in undesired directions, and they should be minimized. Side lobes are normally the largest of the minor lobes. The level of minor lobes is usually expressed as a ratio of the power density in the lobe in question to that of the major lobe. This ratio is often termed the side lobe ratio or side lobe level. Side lobe levels of −20 dB or smaller are usually not desirable in most applications.

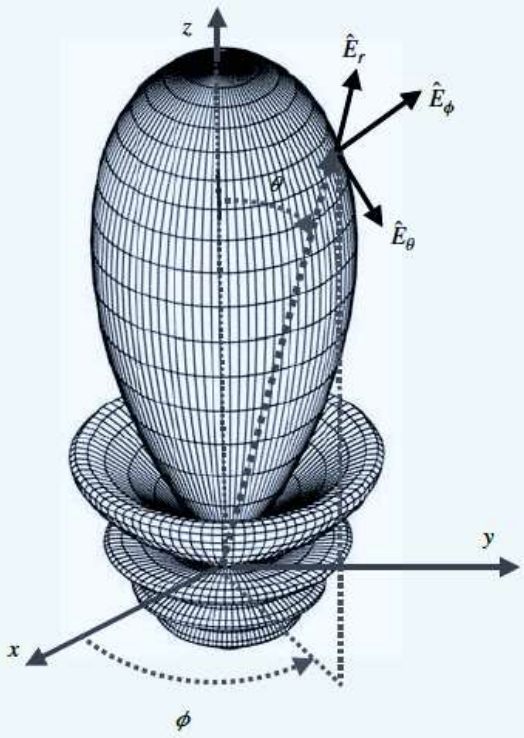


Figure 2.4 Normalized three-dimensional amplitude *field* pattern (*in linear scale*) of a 10-element linear array antenna with a uniform spacing of $d = 0.25\lambda$ and progressive phase shift $\beta = -0.6\pi$ between the elements.

Attainment of a side lobe level smaller than -30 dB usually requires very careful design and construction. In most radar systems, low side lobe ratios are very important to minimize false target indications through the side lobes.

A normalized three-dimensional far-field amplitude pattern, plotted on a linear scale, of a 10-element linear antenna array of isotropic sources with a spacing of $d = 0.25\lambda$ and progressive phase shift $\beta = -0.6\pi$, between the elements is shown in Figure 2.4. It is evident that this pattern has one major lobe, five minor lobes and one back lobe. The level of the side lobe is about -9 dB relative to the maximum. A detailed presentation of arrays is found in Chapter 6. For an amplitude pattern of an antenna, there would be, in general, three electric-field components (E_r, E_θ, E_ϕ) at each observation point on the surface of a sphere of constant radius $r = r_c$, as shown in Figure 2.1. In the far field, the radial E_r component for all antennas is zero or vanishingly small compared to either one, or both, of the other two components (see Section 3.6 of Chapter 3). Some antennas, depending on their geometry and also observation distance, may have only one, two, or all three components. In general, the magnitude of the total electric field would be $|\mathbf{E}| = \sqrt{|E_r|^2 + |E_\theta|^2 + |E_\phi|^2}$. The radial distance in Figure 2.4, and similar ones, represents the magnitude of $|\mathbf{E}|$.

2.2.2 Isotropic, Directional, and Omnidirectional Patterns

An *isotropic* radiator is defined as "a hypothetical lossless antenna having equal radiation in all directions." Although it is ideal and not physically realizable, it is often

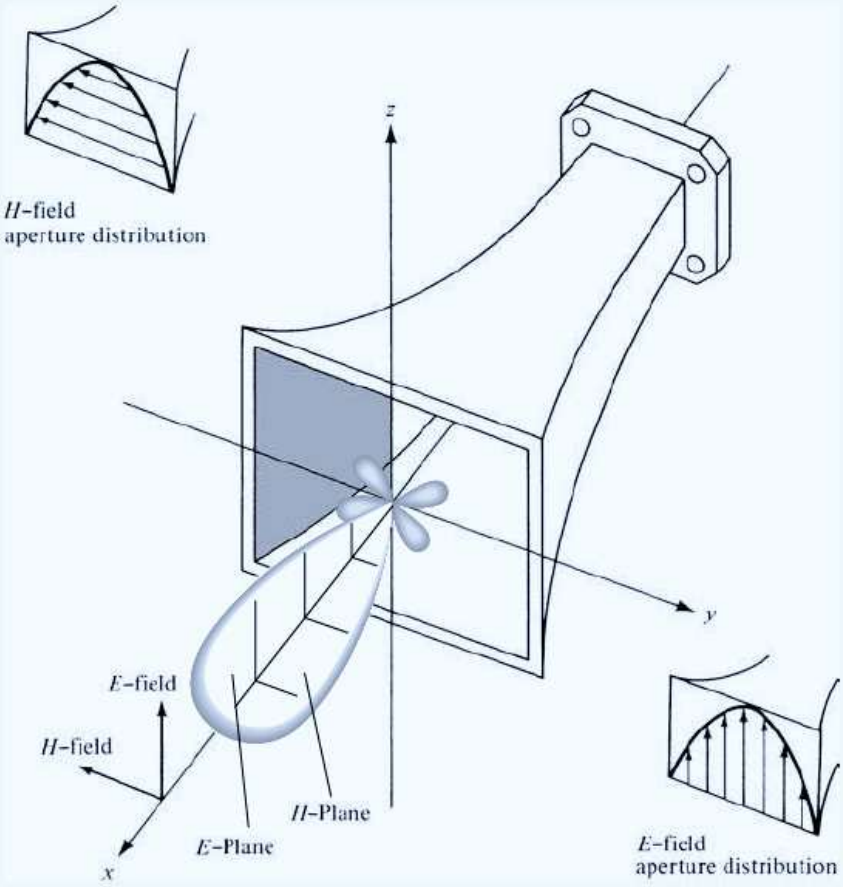


Figure 2.5 Principal E- and H-plane patterns for a pyramidal horn antenna.

EX2042
Page 45 of 1072

taken as a reference for expressing the directive properties of actual antennas. A *directional* antenna is one "having the property of radiating or receiving electromagnetic waves more effectively in some directions than in others. This term is usually applied to an antenna whose maximum directivity is significantly greater than that of a half-wave dipole." Examples of antennas with directional radiation patterns are shown in Figures 2.5 and 2.6. It is seen that the pattern in Figure 2.6 is nondirectional in the azimuth plane $[f(\phi), \theta = \pi/2]$ and directional in the elevation plane $[g(\theta), \phi = \text{constant}]$. This type of a pattern is designated as *omnidirectional*, and it is defined as one "having an essentially nondirectional pattern in a given plane (in this case in azimuth) and a directional pattern in any orthogonal plane (in this case in elevation)." An *omnidirectional* pattern is then a special type of a *directional* pattern.

2.2.3 Principal Patterns

For a linearly polarized antenna, performance is often described in terms of its principal E- and H-plane patterns. The *E-plane* is defined as "the plane containing the electric-field vector and the direction of maximum radiation," and the *H-plane* as "the plane containing the magnetic-field vector and the direction of maximum radiation." Although it is very difficult to illustrate the principal patterns without considering a specific example, it is the usual practice to orient most antennas so that at least one of the principal plane patterns coincide with one of the geometrical principal planes. An illustration is shown in Figure 2.5. For this example, the x-z plane (elevation plane; $\phi = 0$) is the principal E-plane and the x-y plane (azimuthal plane; $\theta = \pi/2$) is the principal H-plane. Other coordinate orientations can be selected.

The omnidirectional pattern of Figure 2.6 has an infinite number of principal E-planes (elevation planes; $\phi = \phi_c$) and one principal H-plane (azimuthal plane; $\theta = 90°$).

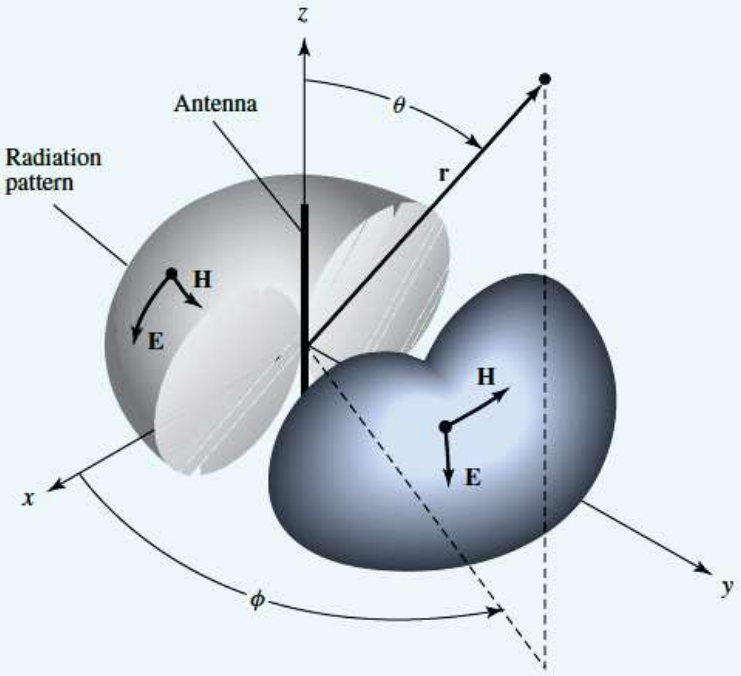


Figure 2.6 Omnidirectional antenna pattern.

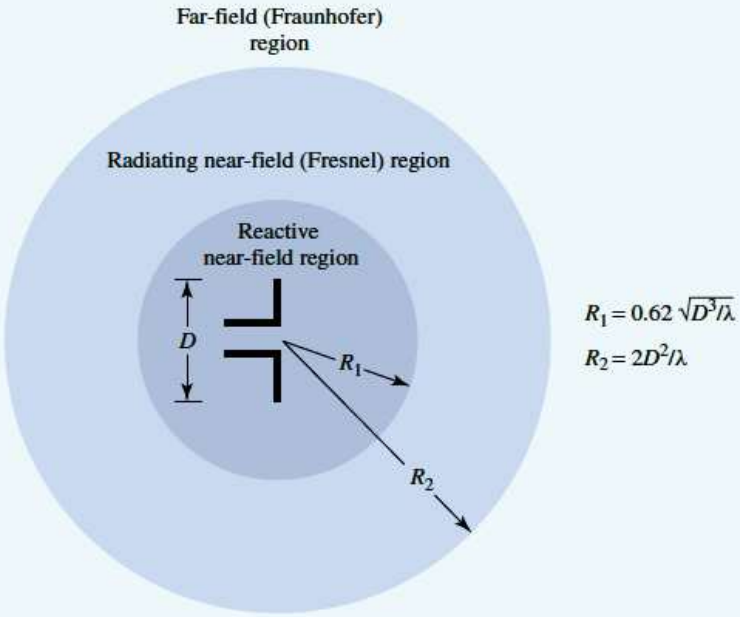


Figure 2.7 Field regions of an antenna.

2.2.4 Field Regions

The space surrounding an antenna is usually subdivided into three regions: (a) reactive near-field, (b) radiating near-field (Fresnel) and (c) far-field (Fraunhofer) regions as shown in Figure 2.7. These regions are so designated to identify the field structure in each. Although no abrupt changes in the field configurations are noted as the boundaries are crossed, there are distinct differences among them. The boundaries separating these regions are not unique, although various criteria have been established and are commonly used to identify the regions.

Reactive near-field region is defined as "that portion of the near-field region immediately surrounding the antenna wherein the reactive field predominates." For most antennas, the outer boundary of this region is commonly taken to exist at a distance $R < 0.62\sqrt{D^3/\lambda}$ from the antenna surface, where λ is the wavelength and D is the largest dimension of the antenna. "For a very short dipole, or equivalent radiator, the outer boundary is commonly taken to exist at a distance $\lambda/2\pi$ from the antenna surface."

Radiating near-field (Fresnel) region is defined as "that region of the field of an antenna between the reactive near-field region and the far-field region wherein radiation fields predominate and wherein the angular field distribution is dependent upon the distance from the antenna. If the antenna has a maximum dimension that is not large compared to the wavelength, this region may not exist. For an antenna focused at infinity, the radiating near-field region is sometimes referred to as the Fresnel region on the basis of analogy to optical terminology. If the antenna has a maximum overall dimension which is very small compared to the wavelength, this field region may not exist." The inner boundary is taken to be the distance $R \geq 0.62\sqrt{D^3/\lambda}$ and the outer boundary the distance $R < 2D^2/\lambda$ where D is the largest* dimension of the antenna. This criterion is based on a maximum phase error of $\pi/8$. In this region the field pattern is, in general, a function of the radial distance and the radial field component may be appreciable.

*To be valid, D must also be large compared to the wavelength ($D > \lambda$).

Far-field (Fraunhofer) region is defined as "that region of the field of an antenna where the angular field distribution is essentially independent of the distance from the antenna. If the antenna has a maximum* overall dimension D, the far-field region is commonly taken to exist at distances greater than $2D^2/\lambda$ from the antenna, λ being the wavelength. The far-field patterns of certain antennas, such as multibeam reflector antennas, are sensitive to variations in phase over their apertures. For these antennas $2D^2/\lambda$ may be inadequate. In physical media, if the antenna has a maximum overall dimension, D, which is large compared to $\pi/|\gamma|$, the far-field region can be taken to begin approximately at a distance equal to $|\gamma|D^2/\pi$ from the antenna, γ being the propagation constant in the medium. For an antenna focused at infinity, the far-field region is sometimes referred to as the Fraunhofer region on the basis of analogy to optical terminology." In this region, the field components are essentially transverse and the angular distribution is independent of the radial distance where the measurements are made. The inner boundary is taken to be the radial distance $R = 2D^2/\lambda$ and the outer one at infinity.

The amplitude pattern of an antenna, as the observation distance is varied from the reactive near field to the far field, changes in shape because of variations of the fields, both magnitude and phase. A typical progression of the shape of an antenna, with the largest dimension D, is shown in Figure 2.8. It is apparent that in the reactive near-field region the pattern is more spread out and nearly uniform, with slight variations. As the observation is moved to the radiating near-field region (Fresnel), the pattern begins to smooth and form lobes. In the far-field region (Fraunhofer), the pattern is well formed, usually consisting of few minor lobes and one, or more, major lobes.

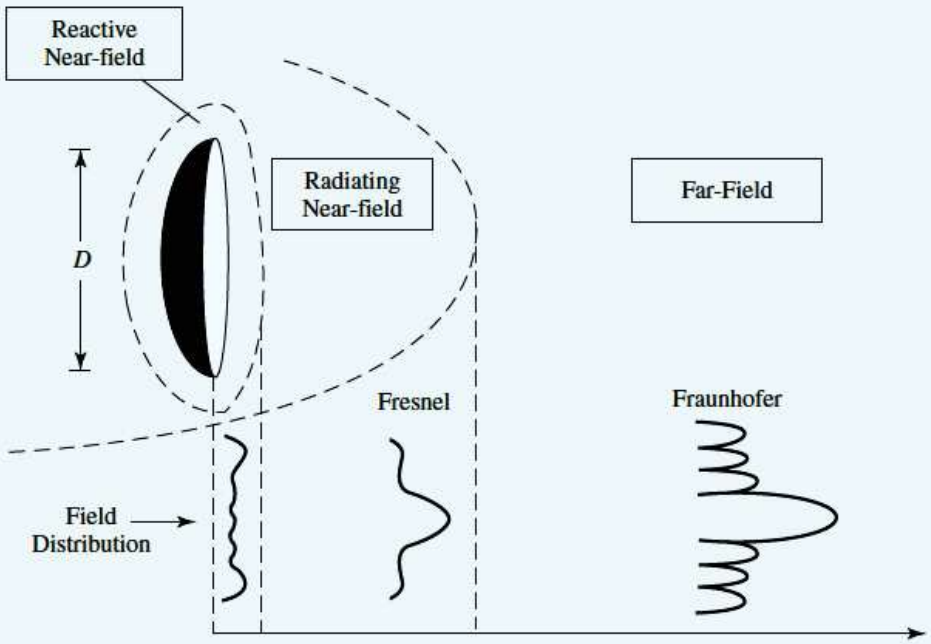


Figure 2.8 Typical changes of antenna amplitude pattern shape from reactive near field toward the far field. (SOURCE: Y. Rahmat-Samii, L. I. Williams, and R. G. Yoccarino, The UCLA Bi-polar Planar-Near-Field Antenna Measurement and Diagnostics Range," *IEEE Antennas & Propagation Magazine*, Vol. 37, No. 6, December 1995 © 1995 IEEE).

*To be valid, D must also be large compared to the wavelength ($D > \lambda$).

To illustrate the pattern variation as a function of radial distance beyond the minimum $2D^2/\lambda$ far-field distance, in Figure 2.9 we have included three patterns of a parabolic reflector calculated at distances of $R = 2D^2/\lambda, 4D^2/\lambda$, and infinity [4]. It is observed that the patterns are almost identical, except for some differences in the pattern structure around the first null and at a level below 25 dB. Because infinite distances are not realizable in practice, the most commonly used criterion for minimum distance of far-field observations is $2D^2/\lambda$.

2.2.5 Radian and Steradian

The measure of a plane angle is a radian. One *radian* is defined as the plane angle with its vertex at the center of a circle of radius r that is subtended by an arc whose length is r. A graphical illustration is shown in Figure 2.10(a). Since the circumference of a circle of radius r is $C = 2\pi r$, there are 2π rad $(2\pi r/r)$ in a full circle.

The measure of a solid angle is a steradian. One *steradian* is defined as the solid angle with its vertex at the center of a sphere of radius r that is subtended by a spherical surface area equal to that of a square with each side of length r. A graphical illustration is shown in Figure 2.10(b). Since the area of a sphere of radius r is $A = 4\pi r^2$, there are 4π sr $(4\pi r^2/r^2)$ in a closed sphere.

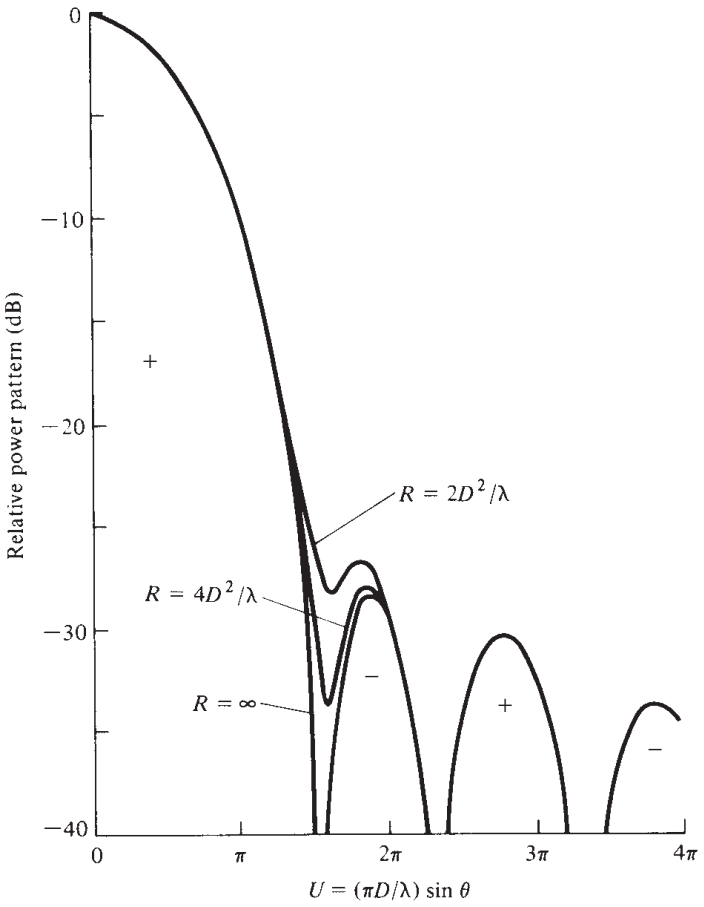


Figure 2.9 Calculated radiation patterns of a paraboloid antenna for different distances from the antenna. (SOURCE: J. S. Hollis, T. J. Lyon, and L. Clayton, Jr. (eds.), *Microwave Antenna Measurements*, Scientific-Atlanta, Inc., July 1970).

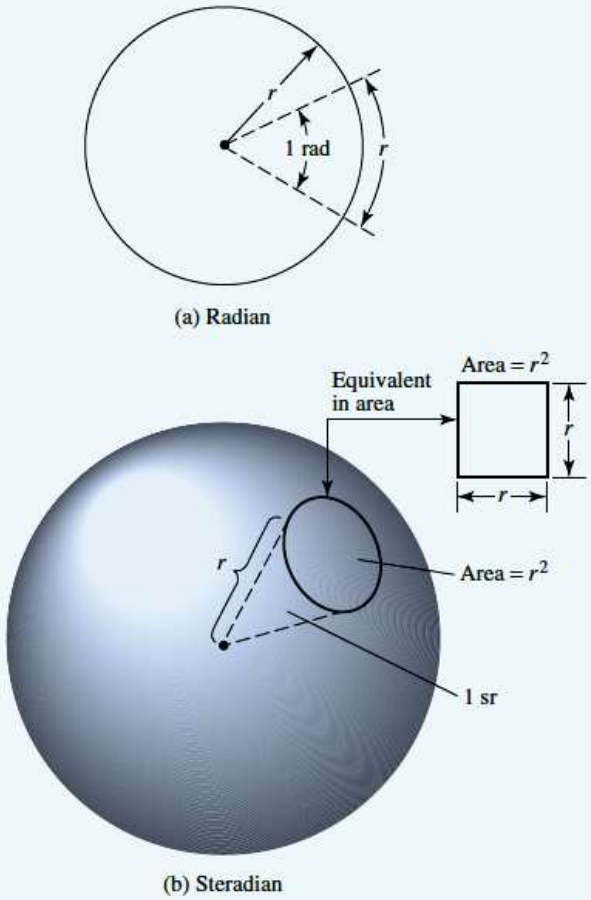


Figure 2.10 Geometrical arrangements for defining a radian and a steradian.

The infinitesimal area dA on the surface of a sphere of radius r, shown in Figure 2.1, is given by

$$dA = r^2 \sin\theta \, d\theta \, d\phi \quad (\text{m}^2) \tag{2-1}$$

Therefore, the element of solid angle $d\Omega$ of a sphere can be written as

$$d\Omega = \frac{dA}{r^2} = \sin\theta \, d\theta \, d\phi \quad (\text{sr}) \tag{2-2}$$

Example 2.1

For a sphere of radius r, find the solid angle Ω_A (in square radians or steradians) of a spherical cap on the surface of the sphere over the north-pole region defined by spherical angles of $0 \le \theta \le 30^\circ, 0 \le \phi \le 180^\circ$. Refer to Figures 2.1 and 2.10. Do this

a. exactly.
b. using $\Omega_A \approx \Delta\Theta_1 \cdot \Delta\Theta_2$, where $\Delta\Theta_1$ and $\Delta\Theta_2$ are two perpendicular angular separations of the spherical cap passing through the north pole.

Compare the two.

Solution:

a. Using (2-2), we can write that

$$\Omega_A = \int_0^{360^\circ}\int_0^{30^\circ} d\Omega = \int_0^{2\pi}\int_0^{\pi/6} \sin\theta\, d\theta\, d\phi = \int_0^{2\pi} d\phi \int_0^{\pi/6} \sin\theta\, d\theta$$
$$= 2\pi[-\cos\theta]\Big|_0^{\pi/6} = 2\pi[-0.867 + 1] = 2\pi(0.133) = 0.83566$$

b. $\Omega_A \approx \Delta\Theta_1 \cdot \Delta\Theta_2 \overbrace{=}^{\Delta\Theta_1=\Delta\Theta_2} (\Delta\Theta_1)^2 = \dfrac{\pi}{3}\left(\dfrac{\pi}{3}\right) = \dfrac{\pi^2}{9} = 1.09662$

It is apparent that the approximate beam solid angle is about 31.23% in error.

2.3 RADIATION POWER DENSITY

Electromagnetic waves are used to transport information through a wireless medium or a guiding structure, from one point to the other. It is then natural to assume that power and energy are associated with electromagnetic fields. The quantity used to describe the power associated with an electromagnetic wave is the instantaneous Poynting vector defined as

$$\mathcal{W} = \mathcal{E} \times \mathcal{H} \tag{2-3}$$

$\mathcal{W}$ = instantaneous Poynting vector (W/m^2)
$\mathcal{E}$ = instantaneous electric-field intensity (V/m)
$\mathcal{H}$ = instantaneous magnetic-field intensity (A/m)

Note that script letters are used to denote instantaneous fields and quantities, while roman letters are used to represent their complex counterparts.

Since the Poynting vector is a power density, the total power crossing a closed surface can be obtained by integrating the normal component of the Poynting vector over the entire surface. In equation form

$$\mathcal{P} = \oiint_S \boldsymbol{\mathcal{W}} \cdot d\mathbf{s} = \oiint_S \mathcal{W} \cdot \hat{\mathbf{n}}\, da \tag{2-4}$$

$\mathcal{P}$ = instantaneous total power (W)
$\hat{\mathbf{n}}$ = unit vector normal to the surface
da = infinitesimal area of the closed surface (m^2)

For applications of time-varying fields, it is often more desirable to find the average power density which is obtained by integrating the instantaneous Poynting vector over one period and dividing by the period. For time-harmonic variations of the form

$e^{j\omega t}$, we define the complex fields $\mathbf{E}$ and $\mathbf{H}$ which are related to their instantaneous counterparts $\mathscr{E}$ and $\mathscr{H}$ by

$$\mathscr{E}(x, y, z; t) = \text{Re}[\mathbf{E}(x, y, z)e^{j\omega t}] \tag{2-5}$$

$$\mathscr{H}(x, y, z; t) = \text{Re}[\mathbf{H}(x, y, z)e^{j\omega t}] \tag{2-6}$$

Using the definitions of (2-5) and (2-6) and the identity $\text{Re}[\mathbf{E}e^{j\omega t}] = \frac{1}{2}[\mathbf{E}e^{j\omega t} + \mathbf{E}^* e^{-j\omega t}]$, (2-3) can be written as

$$\mathscr{W} = \mathscr{E} \times \mathscr{H} = \tfrac{1}{2}\text{Re}[\mathbf{E} \times \mathbf{H}^*] + \tfrac{1}{2}\text{Re}[\mathbf{E} \times \mathbf{H}e^{j2\omega t}] \tag{2-7}$$

The first term of (2-7) is not a function of time, and the time variations of the second are twice the given frequency. The time average Poynting vector (average power density) can be written as

$$\boxed{\mathbf{W}_{\text{av}}(x, y, z) = [\mathscr{W}(x, y, z; t)]_{\text{av}} = \tfrac{1}{2}\text{Re}[\mathbf{E} \times \mathbf{H}^*]} \quad (\text{W/m}^2) \tag{2-8}$$

The $\frac{1}{2}$ factor appears in (2-7) and (2-8) because the $\mathbf{E}$ and $\mathbf{H}$ fields represent peak values, and it should be omitted for RMS values.

A close observation of (2-8) may raise a question. If the real part of $(\mathbf{E} \times \mathbf{H}^*)/2$ represents the average (real) power density, what does the imaginary part of the same quantity represent? At this point it will be very natural to assume that the imaginary part must represent the reactive (stored) power density associated with the electromagnetic fields. In later chapters, it will be shown that the power density associated with the electromagnetic fields of an antenna in its far-field region is predominately real and will be referred to as *radiation density*.

Based upon the definition of (2-8), the average power radiated by an antenna (radiated power) can be written as

$$\boxed{\begin{aligned} P_{\text{rad}} = P_{\text{av}} &= \oiint_S \mathbf{W}_{\text{rad}} \cdot d\mathbf{s} = \oiint_S \mathbf{W}_{\text{av}} \cdot \hat{\mathbf{n}}\, da \\ &= \frac{1}{2}\oiint_S \text{Re}(\mathbf{E} \times \mathbf{H}^*) \cdot d\mathbf{s} \end{aligned}} \tag{2-9}$$

The power pattern of the antenna, whose definition was discussed in Section 2.2, is just a measure, as a function of direction, of the average power density radiated by the antenna. The observations are usually made on a large sphere of constant radius extending into the far field. In practice, absolute power patterns are usually not desired. However, the performance of the antenna is measured in terms of the gain (to be discussed in a subsequent section) and in terms of relative power patterns. Three-dimensional patterns cannot be measured, but they can be constructed with a number of two-dimensional cuts.

Example 2.2

The radial component of the radiated power density of an antenna is given by

$$\mathbf{W}_{\text{rad}} = \hat{\mathbf{a}}_r W_r = \hat{\mathbf{a}}_r A_0 \frac{\sin\theta}{r^2} \quad (\text{W/m}^2)$$

where A_0 is the peak value of the power density, θ is the usual spherical coordinate, and $\hat{\mathbf{a}}_r$ is the radial unit vector. Determine the total radiated power.

Solution: For a closed surface, a sphere of radius r is chosen. To find the total radiated power, the radial component of the power density is integrated over its surface. Thus

$$P_{\text{rad}} = \oiint_S \mathbf{W}_{\text{rad}} \cdot \hat{\mathbf{n}}\, da$$

$$= \int_0^{2\pi} \int_0^{\pi} \left(\hat{\mathbf{a}}_r A_0 \frac{\sin\theta}{r^2}\right) \cdot (\hat{\mathbf{a}}_r r^2 \sin\theta\, d\theta\, d\phi) = \pi^2 A_0 \quad (\text{W})$$

A three-dimensional normalized plot of the average power density at a distance of $r = 1$ m is shown in Figure 2.6.

An isotropic radiator is an ideal source that radiates equally in all directions. Although it does not exist in practice, it provides a convenient isotropic reference with which to compare other antennas. Because of its symmetric radiation, its Poynting vector will not be a function of the spherical coordinate angles θ and ϕ. In addition, it will have only a radial component. Thus the total power radiated by it is given by

$$P_{\text{rad}} = \oiint_S \mathbf{W}_0 \cdot d\mathbf{s} = \int_0^{2\pi} \int_0^{\pi} [\hat{\mathbf{a}}_r W_0(r)] \cdot [\hat{\mathbf{a}}_r r^2 \sin\theta\, d\theta\, d\phi] = 4\pi r^2 W_0 \tag{2-10}$$

and the power density by

$$\mathbf{W}_0 = \hat{\mathbf{a}}_r W_0 = \hat{\mathbf{a}}_r \left(\frac{P_{\text{rad}}}{4\pi r^2}\right) \quad (\text{W/m}^2) \tag{2-11}$$

which is uniformly distributed over the surface of a sphere of radius r.

2.4 RADIATION INTENSITY

Radiation intensity in a given direction is defined as "the power radiated from an antenna per unit solid angle." The radiation intensity is a far-field parameter, and it can be obtained by simply multiplying the radiation density by the square of the distance. In mathematical form it is expressed as

$$\boxed{U = r^2 W_{\text{rad}}} \tag{2-12}$$

where

U = radiation intensity (W/unit solid angle)
W_{rad} = radiation density (W/m^2)

The radiation intensity is also related to the far-zone electric field of an antenna, referring to Figure 2.4, by

$$U(\theta,\phi) = \frac{r^2}{2\eta}|\mathbf{E}(r,\theta,\phi)|^2 \simeq \frac{r^2}{2\eta}\left[|E_\theta(r,\theta,\phi)|^2 + |E_\phi(r,\theta,\phi)|^2\right] \simeq \frac{1}{2\eta}\left[|E_\theta^\circ(\theta,\phi)|^2 + |E_\phi^\circ(\theta,\phi)|^2\right] \tag{2-12a}$$

where

$\mathbf{E}(r,\theta,\phi)$ = far-zone electric-field intensity of the antenna $= \mathbf{E}^\circ(\theta,\phi)\dfrac{e^{-jkr}}{r}$
E_θ, E_ϕ = far-zone electric-field components of the antenna
η = intrinsic impedance of the medium

The radial electric-field component (E_r) is assumed, if present, to be small in the far zone. Thus the power pattern is also a measure of the radiation intensity.

The total power is obtained by integrating the radiation intensity, as given by (2-12), over the entire solid angle of 4π. Thus

$$P_{\text{rad}} = \oiint_\Omega U\, d\Omega = \int_0^{2\pi}\int_0^{\pi} U \sin\theta\, d\theta\, d\phi \tag{2-13}$$

where $d\Omega$ = element of solid angle $= \sin\theta\, d\theta\, d\phi$.

Example 2.3

For the problem of Example 2.2, find the total radiated power using (2-13).

Solution: Using (2-12)

$$U = r^2 W_{\text{rad}} = A_0 \sin\theta$$

and by (2-13)

$$P_{\text{rad}} = \int_0^{2\pi}\int_0^{\pi} U \sin\theta\, d\theta\, d\phi = A_0 \int_0^{2\pi}\int_0^{\pi} \sin^2\theta\, d\theta\, d\phi = \pi^2 A_0$$

which is the same as that obtained in Example 2.2. A three-dimensional plot of the relative radiation intensity is also represented by Figure 2.6.

For an isotropic source U will be independent of the angles θ and ϕ, as was the case for W_{rad}. Thus (2-13) can be written as

$$P_{\text{rad}} = \oiint_\Omega U_0\, d\Omega = U_0 \oiint_\Omega d\Omega = 4\pi U_0 \tag{2-14}$$

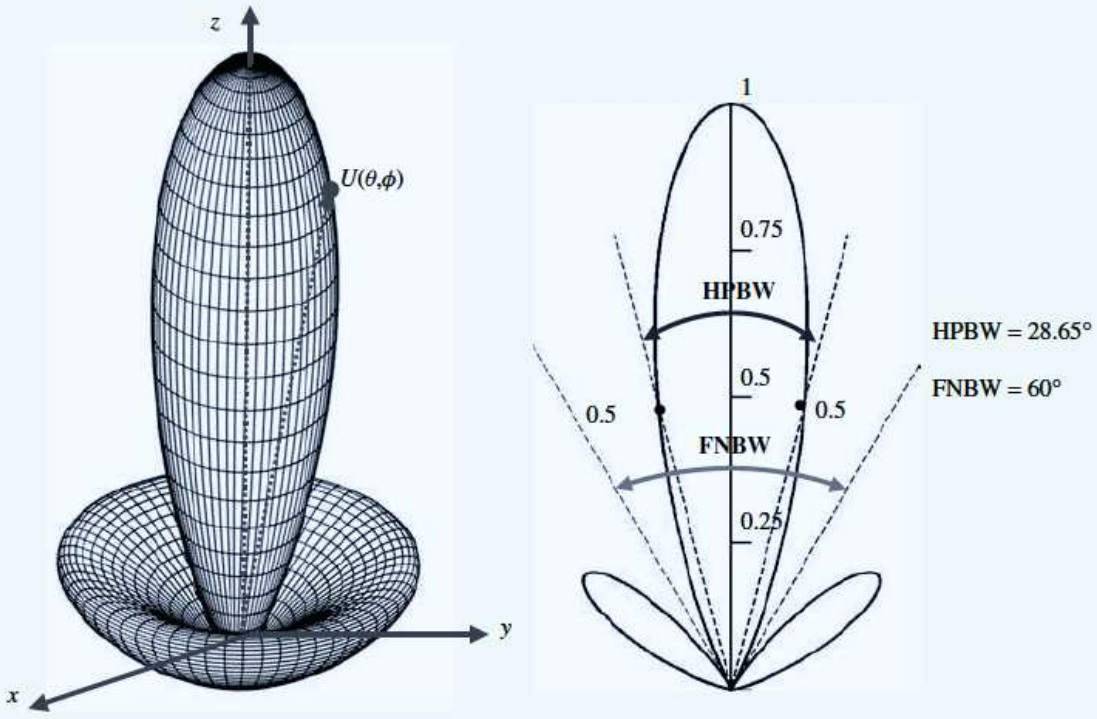
or the radiation intensity of an isotropic source as

$$U_0 = \frac{P_{\text{rad}}}{4\pi} \tag{2-15}$$

2.5 BEAMWIDTH

Associated with the pattern of an antenna is a parameter designated as *beamwidth*. The *beamwidth* of a pattern is defined as the angular separation between two identical points on opposite side of the pattern maximum. In an antenna pattern, there are a number of beamwidths. One of the most widely used beamwidths is the *Half-Power Beamwidth* (*HPBW*), which is defined by IEEE as: "In a plane containing the direction of the maximum of a beam, the angle between the two directions in which the radiation intensity is one-half value of the beam." This is demonstrated in Figure 2.2. Another important beamwidth is the angular separation between the first nulls of the pattern, and it is referred to as the *First-Null Beamwidth* (*FNBW*). Both the *HPBW* and *FNBW* are demonstrated for the pattern in Figure 2.11 for the pattern of Example 2.4. Other beamwidths are those where the pattern is −10 dB from the maximum, or any other value. However, in practice, the term *beamwidth*, with no other identification, usually refers to *HPBW*.

The beamwidth of an antenna is a very important figure of merit and often is used as a trade-off between it and the side lobe level; that is, as the beamwidth decreases, the side lobe increases and vice versa. In addition, the beamwidth of the antenna is also



(a) Three dimensional (b) Two-dimensional

Figure 2.11 Three- and two-dimensional power patterns (in linear scale) of $U(\theta) = \cos^2(\theta)\cos^2(3\theta)$.

EX2042
Page 55 of 1072

used to describe the resolution capabilities of the antenna to distinguish between two adjacent radiating sources or radar targets. The most common resolution criterion states that *the resolution capability of an antenna to distinguish between two sources is equal to half the first-null beamwidth (FNBW/2), which is usually used to approximate the half-power beamwidth (HPBW)* [5], [6]. That is, two sources separated by angular distances equal or greater than FNBW/2 $\approx$ HPBW of an antenna with a uniform distribution can be resolved. If the separation is smaller, then the antenna will tend to smooth the angular separation distance.

Example 2.4

The normalized radiation intensity of an antenna is represented by

$$U(\theta) = \cos^2(\theta)\cos^2(3\theta), \quad (0 \le \theta \le 90^\circ, \quad 0^\circ \le \phi \le 360^\circ)$$

The three- and two-dimensional plots of this, plotted in a linear scale, are shown in Figure 2.11. Find the

a. half-power beamwidth HPBW (*in radians and degrees*)
b. first-null beamwidth FNBW (*in radians and degrees*)

Solution:

a. Since the $U(\theta)$ represents the *power* pattern, to find the half-power beamwidth you set the function equal to half of its maximum, or

$$U(\theta)|_{\theta=\theta_h} = \cos^2(\theta)\cos^2(3\theta)|_{\theta=\theta_h} = 0.5 \Rightarrow \cos\theta_h \cos 3\theta_h = 0.707$$

$$\theta_h = \cos^{-1}\left(\frac{0.707}{\cos 3\theta_h}\right)$$

Since this is an equation with transcendental functions, it can be solved iteratively. After a few iterations, it is found that

$$\theta_h \approx 0.25 \ radians = 14.325^\circ$$

Since the function $U(\theta)$ is symmetrical about the maximum at $\theta = 0$, then the HPBW is

$$\text{HPBW} = 2\theta_h \approx 0.50 \ radians = 28.65^\circ$$

b. To find the first-null beamwidth (FNBW), you set the $U(\theta)$ equal to zero, or

$$U(\theta)|_{\theta=\theta_n} = \cos^2(\theta)\cos^2(3\theta)|_{\theta=\theta_n} = 0$$

This leads to two solutions for θ_n.

$$\cos\theta_n = 0 \Rightarrow \theta_n = \cos^{-1}(0) = \frac{\pi}{2}\ radians = 90^\circ$$

$$\cos 3\theta_n = 0 \Rightarrow \theta_n = \frac{1}{3}\cos^{-1}(0) = \frac{\pi}{6}\ radians = 30^\circ$$

The one with the smallest value leads to the FNBW. Again, because of the symmetry of the pattern, the FNBW is

$$\text{FNBW} = 2\theta_n = \frac{\pi}{3}\ radians = 60^\circ$$

2.6 DIRECTIVITY

In the 1983 version of the *IEEE Standard Definitions of Terms for Antennas*, there has been a substantive change in the definition of *directivity*, compared to the definition of the 1973 version. Basically the term *directivity* in the new 1983 version has been used to replace the term *directive gain* of the old 1973 version. In the new 1983 version the term *directive gain* has been deprecated. According to the authors of the new 1983 standards, "this change brings this standard in line with common usage among antenna engineers and with other international standards, notably those of the International Electrotechnical Commission (IEC)." Therefore *directivity of an antenna* defined as "the ratio of the radiation intensity in a given direction from the antenna to the radiation intensity averaged over all directions. The average radiation intensity is equal to the total power radiated by the antenna divided by 4π. If the direction is not specified, the direction of maximum radiation intensity is implied." Stated more simply, the directivity of a nonisotropic source is equal to the ratio of its radiation intensity in a given direction over that of an isotropic source. In mathematical form, using (2-15), it can be written as

$$\boxed{D = \frac{U}{U_0} = \frac{4\pi U}{P_{\text{rad}}}} \tag{2-16}$$

If the direction is not specified, it implies the direction of maximum radiation intensity (maximum directivity) expressed as

$$\boxed{D_{\max} = D_0 = \frac{U|_{\max}}{U_0} = \frac{U_{\max}}{U_0} = \frac{4\pi U_{\max}}{P_{\text{rad}}}} \tag{2-16a}$$

D = directivity (dimensionless)
D_0 = maximum directivity (dimensionless)

U = radiation intensity (W/unit solid angle)
$U_{\max}$ = maximum radiation intensity (W/unit solid angle)
U_0 = radiation intensity of isotropic source (W/unit solid angle)
P_{rad} = total radiated power (W)

For an isotropic source, it is very obvious from (2-16) or (2-16a) that the directivity is unity since U, $U_{\max}$, and U_0 are all equal to each other.

For antennas with orthogonal polarization components, we define the *partial directivity of an antenna for a given polarization in a given direction* as "that part of the radiation intensity corresponding to a given polarization divided by the total radiation intensity averaged over all directions." With this definition for the partial directivity, then in a given direction "the total directivity is the sum of the partial directivities for any two orthogonal polarizations." For a spherical coordinate system, the total maximum directivity D_0 for the orthogonal θ and ϕ components of an antenna can be written as

$$D_0 = D_\theta + D_\phi \tag{2-17}$$

while the partial directivities D_θ and D_ϕ are expressed as

$$D_\theta = \frac{4\pi U_\theta}{(P_{\text{rad}})_\theta + (P_{\text{rad}})_\phi} \tag{2-17a}$$

$$D_\phi = \frac{4\pi U_\phi}{(P_{\text{rad}})_\theta + (P_{\text{rad}})_\phi} \tag{2-17b}$$

where

U_θ = radiation intensity in a given direction contained in θ field component
U_ϕ = radiation intensity in a given direction contained in ϕ field component
$(P_{\text{rad}})_\theta$ = radiated power in all directions contained in θ field component
$(P_{\text{rad}})_\phi$ = radiated power in all directions contained in ϕ field component

Example 2.5

As an illustration, find the maximum directivity of the antenna whose radiation intensity is that of Example 2.2. Write an expression for the directivity as a function of the directional angles θ and ϕ.

Solution: The radiation intensity is given by

$$U = r^2 W_{\text{rad}} = A_0 \sin\theta$$

The maximum radiation is directed along $\theta = \pi/2$. Thus

$$U_{\max} = A_0$$

In Example 2.2 it was found that

$$P_{\text{rad}} = \pi^2 A_0$$

Using (2-16a), we find that the maximum directivity is equal to

$$D_0 = \frac{4\pi U_{\max}}{P_{\text{rad}}} = \frac{4}{\pi} = 1.27$$

Since the radiation intensity is only a function of θ, the directivity as a function of the directional angles is represented by

$$D = D_0 \sin\theta = 1.27 \sin\theta$$

Before proceeding with a more general discussion of directivity, it may be proper at this time to consider another example, compute its directivity, compare it with that of the previous example, and comment on what it actually represents. This may give the reader a better understanding and appreciation of the directivity.

Example 2.6

The radial component of the radiated power density of an infinitesimal linear dipole of length $l \ll \lambda$ is given by

$$\mathbf{W}_{\text{av}} = \hat{\mathbf{a}}_r W_r = \hat{\mathbf{a}}_r A_0 \frac{\sin^2\theta}{r^2} \quad (\text{W/m}^2)$$

where A_0 is the peak value of the power density, θ is the usual spherical coordinate, and $\hat{\mathbf{a}}_r$ is the radial unit vector. Determine the maximum directivity of the antenna and express the directivity as a function of the directional angles θ and ϕ.

Solution: The radiation intensity is given by

$$U = r^2 W_r = A_0 \sin^2\theta$$

The maximum radiation is directed along $\theta = \pi/2$. Thus

$$U_{\max} = A_0$$

The total radiated power is given by

$$P_{\text{rad}} = \oiint_{\Omega} U \, d\Omega = A_0 \int_0^{2\pi} \int_0^{\pi} \sin^2\theta \sin\theta \, d\theta \, d\phi = A_0 \left(\frac{8\pi}{3}\right)$$

Using (2-16a), we find that the maximum directivity is equal to

$$D_0 = \frac{4\pi U_{\max}}{P_{\text{rad}}} = \frac{4\pi A_0}{\frac{8\pi}{3}(A_0)} = \frac{3}{2}$$

which is greater than 1.27 found in Example 2.5. Thus the directivity is represented by

$$D = D_0 \sin^2\theta = 1.5 \sin^2\theta$$

At this time it will be proper to comment on the results of Examples 2.5 and 2.6. To better understand the discussion, we have plotted in Figure 2.12 the relative radiation intensities of Example 2.5 ($U = A_0 \sin\theta$) and Example 2.6 ($U = A_0 \sin^2\theta$) where A_0 was set equal to unity. We see that both patterns are omnidirectional but that of Example 2.6 has more directional characteristics (is narrower) in the elevation plane. Since the directivity is a "figure of merit" describing how well the radiator directs energy in a certain direction, it should be convincing from Figure 2.12 that the directivity of Example 2.6 should be higher than that of Example 2.5.

To demonstrate the significance of directivity, let us consider another example; in particular let us examine the directivity of a half-wavelength dipole ($l = \lambda/2$), which is derived in Section 4.6 of Chapter 4 and can be approximated by

$$D = D_0 \sin^3\theta = 1.67 \sin^3\theta \tag{2-18}$$

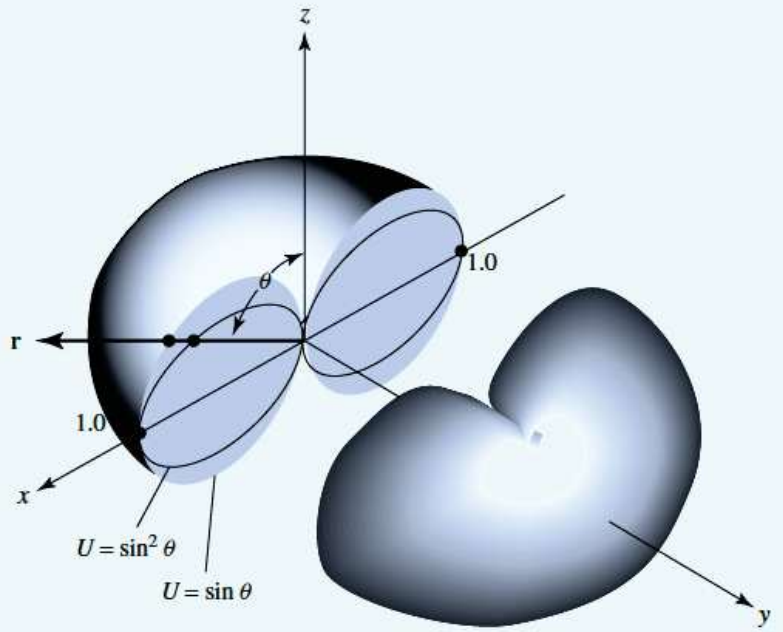


Figure 2.12 Three-dimensional radiation intensity patterns. (SOURCE: P. Lorrain and D. R. Corson, *Electromagnetic Fields and Waves*, 2nd ed., W. H. Freeman and Co. Copyright © 1970).

since it can be shown that

$$\sin^3\theta \simeq \left[\frac{\cos\left(\frac{\pi}{2}\cos\theta\right)}{\sin\theta}\right]^2 \tag{2-18a}$$

where θ is measured from the axis along the length of the dipole. The values represented by (2-18) and those of an isotropic source ($D = 1$) are plotted two- and three-dimensionally in Figure 2.13(a,b). For the three-dimensional graphical representation of Figure 2.13(b), at each observation point only the largest value of the two directivities is plotted. It is apparent that when $\sin^{-1}(1/1.67)^{1/3} = 57.44^\circ < \theta < 122.56^\circ$, the dipole radiator has greater directivity (greater intensity concentration) in those directions than that of an isotropic source. Outside this range of angles, the isotropic radiator has higher directivity (more intense radiation). The maximum directivity of the dipole (relative to the isotropic radiator) occurs when $\theta = \pi/2$, and it is 1.67 (or 2.23 dB) more intense than that of the isotropic radiator (with the same radiated power).

The three-dimensional pattern of Figure 2.13(b), and similar ones, are included throughout the book to represent the three-dimensional radiation characteristics of antennas. These patterns are plotted using software developed in [2] and [3], and can be used to visualize the three-dimensional radiation pattern of the antenna. These three-dimensional programs, along with the others, can be used effectively toward the design and synthesis of antennas, especially arrays, as demonstrated in [7] and [8]. A MATLAB-based program, designated as 3-D ***Spherical***, is also included in the attached CD to produce similar plots.

The directivity of an isotropic source is unity since its power is radiated equally well in all directions. *For all other sources, the maximum directivity will always be greater than unity, and it is a relative "figure of merit" which gives an indication of the directional properties of the antenna as compared with those of an isotropic source*. In equation form, this is indicated in (2-16a). The directivity can be smaller than unity; in fact it can be equal to zero. For Examples 2.5 and 2.6, the directivity is equal to zero in the $\theta = 0$ direction. *The values of directivity will be equal to or greater than zero and equal to or less than the maximum directivity* $(0 \le D \le D_0)$.

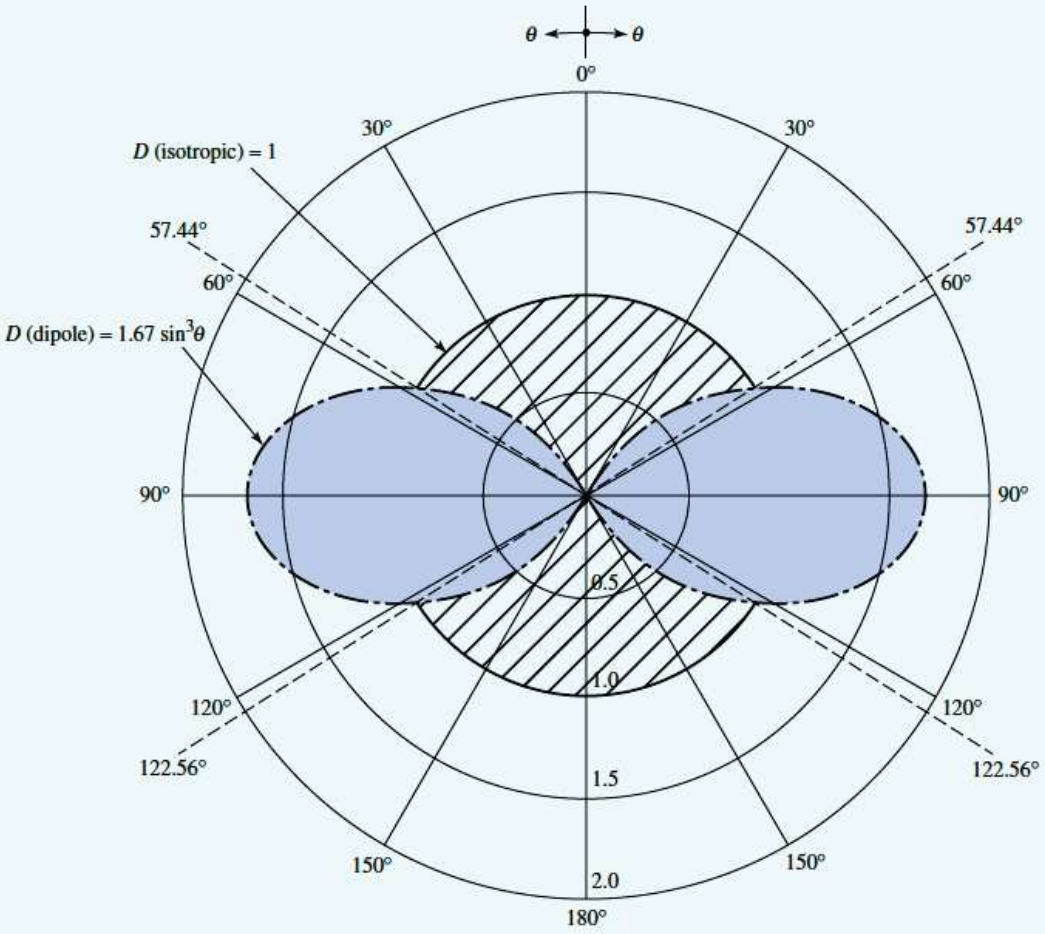
A more general expression for the directivity can be developed to include sources with radiation patterns that may be functions of both spherical coordinate angles θ and ϕ. In the previous examples we considered intensities that were represented by only one coordinate angle θ, in order not to obscure the fundamental concepts by the mathematical details. So it may now be proper, since the basic definitions have been illustrated by simple examples, to formulate the more general expressions.

Let the radiation intensity of an antenna be of the form

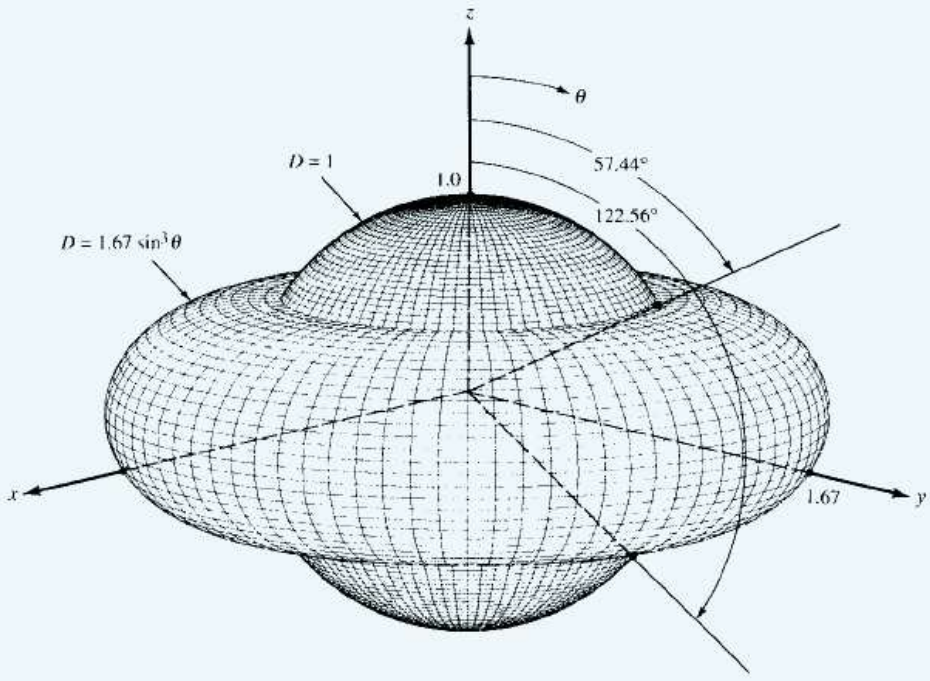
$$U = B_0 F(\theta,\phi) \simeq \frac{1}{2\eta}\left[|E_\theta^0(\theta,\phi)|^2 + |E_\phi^0(\theta,\phi)|^2\right] \tag{2-19}$$

where B_0 is a constant, and E_θ^0 and E_ϕ^0 are the antenna's far-zone electric-field components. The maximum value of (2-19) is given by

$$U_{\max} = B_0 F(\theta,\phi)|_{\max} = B_0 F_{\max}(\theta,\phi) \tag{2-19a}$$



(a) Two-dimensional



(b) Three-dimensional

Figure 2.13 Two- and three-dimensional directivity patterns of a $\lambda/2$ dipole. (SOURCE: C. A. Balanis, "Antenna Theory: A Review." *Proc. IEEE*, Vol. 80, No. 1. January 1992. © 1992 IEEE).

EX2042
Page 62 of 1072

The total radiated power is found using

$$P_{\text{rad}} = \oiint_{\Omega} U(\theta, \phi)\, d\Omega = B_0 \int_0^{2\pi} \int_0^{\pi} F(\theta, \phi) \sin\theta\, d\theta\, d\phi \tag{2-20}$$

We now write the general expression for the directivity and maximum directivity using (2-16) and (2-16a), respectively, as

$$\boxed{D(\theta, \phi) = 4\pi \frac{F(\theta, \phi)}{\displaystyle\int_0^{2\pi} \int_0^{\pi} F(\theta, \phi) \sin\theta\, d\theta\, d\phi}} \tag{2-21}$$

$$\boxed{D_0 = 4\pi \frac{F(\theta, \phi)|_{\max}}{\displaystyle\int_0^{2\pi} \int_0^{\pi} F(\theta, \phi) \sin\theta\, d\theta\, d\phi}} \tag{2-22}$$

Equation (2-22) can also be written as

$$\boxed{D_0 = \frac{4\pi}{\left[\displaystyle\int_0^{2\pi} \int_0^{\pi} F(\theta, \phi) \sin\theta\, d\theta\, d\phi\right] \Big/ F(\theta, \phi)|_{\max}} = \frac{4\pi}{\Omega_A}} \tag{2-23}$$

where Ω_A is the beam solid angle, and it is given by

$$\Omega_A = \frac{1}{F(\theta, \phi)|_{\max}} \int_0^{2\pi} \int_0^{\pi} F(\theta, \phi) \sin\theta\, d\theta\, d\phi = \int_0^{2\pi} \int_0^{\pi} F_n(\theta, \phi) \sin\theta\, d\theta\, d\phi \tag{2-24}$$

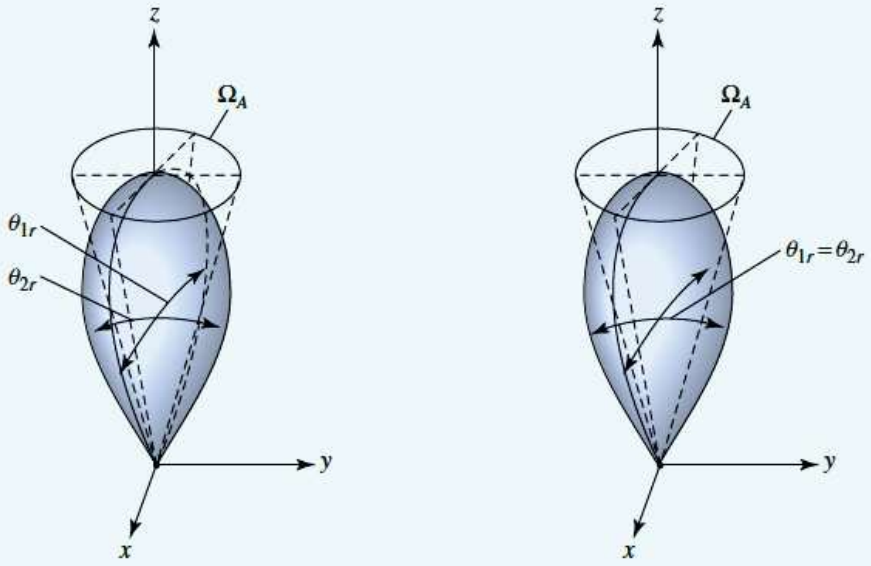
$$F_n(\theta, \phi) = \frac{F(\theta, \phi)}{F(\theta, \phi)|_{\max}} \tag{2-25}$$

Dividing by $F(\theta, \phi)|_{\max}$ merely normalizes the radiation intensity $F(\theta, \phi)$, and it makes its maximum value unity.

The beam solid angle Ω_A is defined as the solid angle through which all the power of the antenna would flow if its radiation intensity is constant (and equal to the maximum value of U) for all angles within Ω_A.

2.6.1 Directional Patterns

Instead of using the exact expression of (2-23) to compute the directivity, it is often convenient to derive simpler expressions, even if they are approximate, to compute the directivity. These can also be used for design purposes. For antennas with one narrow major lobe and very negligible minor lobes, the beam solid angle is approximately equal to the product of the half-power beamwidths in two perpendicular planes [5] shown



(a) Nonsymmetrical pattern (b) Symmetrical pattern

Figure 2.14 Beam solid angles for nonsymmetrical and symmetrical radiation patterns.

in Figure 2.14(a). For a rotationally symmetric pattern, the half-power beamwidths in any two perpendicular planes are the same, as illustrated in Figure 2.14(b).

With this approximation, (2-23) can be approximated by

$$D_0 = \frac{4\pi}{\Omega_A} \simeq \frac{4\pi}{\Theta_{1r}\Theta_{2r}} \tag{2-26}$$

The beam solid angle Ω_A has been approximated by

$$\Omega_A \simeq \Theta_{1r}\Theta_{2r} \tag{2-26a}$$

where

Θ_{1r} = half-power beamwidth in one plane (rad)
Θ_{2r} = half-power beamwidth in a plane at a right angle to the other (rad)

If the beamwidths are known in degrees, (2-26) can be written as

$$D_0 \simeq \frac{4\pi(180/\pi)^2}{\Theta_{1d}\Theta_{2d}} = \frac{41{,}253}{\Theta_{1d}\Theta_{2d}} \tag{2-27}$$

where

Θ_{1d} = half-power beamwidth in one plane (degrees)
Θ_{2d} = half-power beamwidth in a plane at a right angle to the other (degrees)

For planar arrays, a better approximation to (2-27) is [9]

$$D_0 \simeq \frac{32{,}400}{\Omega_A(\text{degrees})^2} = \frac{32{,}400}{\Theta_{1d}\Theta_{2d}} \tag{2-27a}$$

The validity of (2-26) and (2-27) is based on a pattern that has only one major lobe and any minor lobes, if present, should be of very low intensity. For a pattern with two identical major lobes, the value of the maximum directivity using (2-26) or (2-27) will be twice its actual value. For patterns with significant minor lobes, the values of maximum directivity obtained using (2-26) or (2-27), which neglect any minor lobes, will usually be too high.

Example 2.7

The radiation intensity of the major lobe of many antennas can be adequately represented by

$$U = B_0 \cos\theta$$

where B_0 is the maximum radiation intensity. The radiation intensity exists only in the upper hemisphere ($0 \le \theta \le \pi/2$, $0 \le \phi \le 2\pi$), and it is shown in Figure 2.15.

Find the

a. beam solid angle; exact and approximate.
b. maximum directivity; exact using (2-23) and approximate using (2-26).

Solution: The half-power point of the pattern occurs at $\theta = 60°$. Thus the beamwidth in the θ direction is 120° or

$$\Theta_{1r} = \frac{2\pi}{3}$$

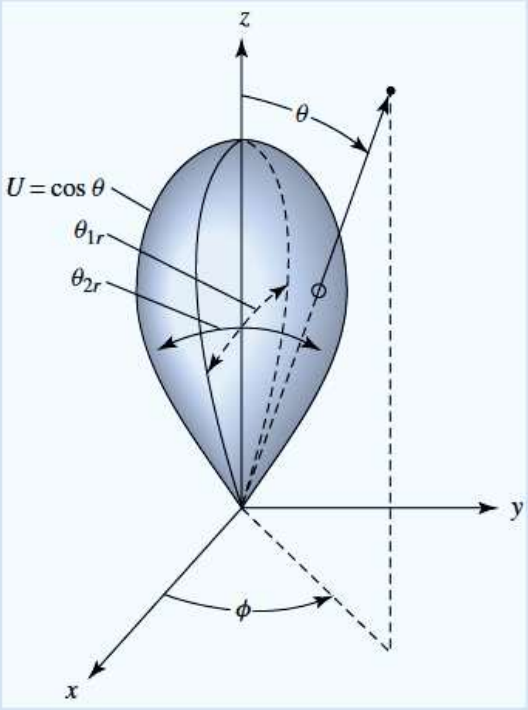


Figure 2.15 Radiation intensity pattern of the form $U = \cos\theta$ in the upper hemisphere.

Since the pattern is independent of the ϕ coordinate, the beamwidth in the other plane is also equal to

$$\Theta_{2r} = \frac{2\pi}{3}$$

a. *Beam solid angle* Ω_A:
Exact: Using (2-24), (2-25)

$$\Omega_A = \int_0^{360^\circ} \int_0^{90^\circ} \cos\theta \, d\Omega = \int_0^{2\pi} \int_0^{\pi/2} \cos\theta \sin\theta \, d\theta \, d\phi$$
$$= \int_0^{2\pi} d\phi \int_0^{\pi/2} \cos\theta \sin\theta \, d\theta$$
$$= 2\pi \int_0^{\pi/2} \cos\theta \sin\theta \, d\theta = \pi \int_0^{\pi/2} \sin(2\theta) \, d\theta = \pi \text{ steradians}$$

Approximate: Using (2-26a)

$$\Omega_A \approx \Theta_{1r}\Theta_{2r} = \frac{2\pi}{3}\left(\frac{2\pi}{3}\right) = \left(\frac{2\pi}{3}\right)^2 = 4.386 \text{ steradians}$$

b. *Directivity* D_0:
Exact: $D_0 = \dfrac{4\pi}{\Omega_A} = \dfrac{4\pi}{\pi} = 4$ (dimensionless) $= 6.02$ dB
The same exact answer is obtained using (2-16a).
Approximate: $D_0 \approx \dfrac{4\pi}{\Omega_A} = \dfrac{4\pi}{4.386} = 2.865$ (dimensionless) $= 4.57$ dB

The exact maximum directivity is 4 and its approximate value, using (2-26), is 2.865. Better approximations can be obtained if the patterns have much narrower beamwidths, which will be demonstrated later in this section.

Many times it is desirable to express the directivity in decibels (dB) instead of dimensionless quantities. The expressions for converting the dimensionless quantities of directivity and maximum directivity to decibels (dB) are

$$D(\text{dB}) = 10\log_{10}[D(\text{dimensionless})] \tag{2-28a}$$
$$D_0(\text{dB}) = 10\log_{10}[D_0(\text{dimensionless})] \tag{2-28b}$$

It has also been proposed [10] that the maximum directivity of an antenna can also be obtained approximately by using the formula

$$\frac{1}{D_0} = \frac{1}{2}\left(\frac{1}{D_1} + \frac{1}{D_2}\right) \tag{2-29}$$

where

$$D_1 \simeq \frac{1}{\left[\dfrac{1}{2\ln 2}\displaystyle\int_0^{\Theta_{1r}/2} \sin\theta\, d\theta\right]} \simeq \frac{16\ln 2}{\Theta_{1r}^2} \tag{2-29a}$$

$$D_2 \simeq \frac{1}{\left[\dfrac{1}{2\ln 2}\displaystyle\int_0^{\Theta_{2r}/2} \sin\theta\, d\theta\right]} \simeq \frac{16\ln 2}{\Theta_{2r}^2} \tag{2-29b}$$

Θ_{1r} and Θ_{2r} are the half-power beamwidths (in radians) of the E- and H-planes, respectively. The formula of (2-29) will be referred to as the arithmetic mean of the maximum directivity. Using (2-29a) and (2-29b) we can write (2-29) as

$$\frac{1}{D_0} \simeq \frac{1}{2\ln 2}\left(\frac{\Theta_{1r}^2}{16} + \frac{\Theta_{2r}^2}{16}\right) = \frac{\Theta_{1r}^2 + \Theta_{2r}^2}{32\ln 2} \tag{2-30}$$

or

$$\boxed{D_0 \simeq \frac{32\ln 2}{\Theta_{1r}^2 + \Theta_{2r}^2} = \frac{22.181}{\Theta_{1r}^2 + \Theta_{2r}^2}} \tag{2-30a}$$

$$D_0 \simeq \frac{22.181(180/\pi)^2}{\Theta_{1d}^2 + \Theta_{2d}^2} = \frac{72{,}815}{\Theta_{1d}^2 + \Theta_{2d}^2} \tag{2-30b}$$

where Θ_{1d} and Θ_{2d} are the half-power beamwidths in degrees. Equation (2-30a) is to be contrasted with (2-26) while (2-30b) should be compared with (2-27).

In order to make an evaluation and comparison of the accuracies of (2-26) and (2-30a), examples whose radiation intensities (power patterns) can be represented by

$$U(\theta,\phi) = \begin{cases} B_0\cos^n(\theta) & 0 \le \theta \le \pi/2, \quad 0 \le \phi \le 2\pi \\ 0 & \text{elsewhere} \end{cases} \tag{2-31}$$

where $n = 1 - 10$, 11.28, 15, and 20 are considered. The maximum directivities were computed using (2-26) and (2-30a) and compared with the exact values as obtained using (2-23). The results are shown in Table 2.1. From the comparisons it is evident that the error due to Tai & Pereira's formula is always negative (i.e., it predicts lower values of maximum directivity than the exact ones) and monotonically decreases as n increases (the pattern becomes more narrow). However, the error due to Kraus' formula is negative for small values of n and positive for large values of n. For small values of n the error due to Kraus' formula is negative and positive for large values of n; the error is zero when $n = 5.497 \simeq 5.5$ (half-power beamwidth of 56.35°). In addition, for symmetrically rotational patterns the absolute error due to the two approximate formulas is identical when $n = 11.28$, which corresponds to a half-power beamwidth of 39.77°. From these observations we conclude that, Kraus' formula is more accurate for small values of n (broader patterns) while Tai & Pereira's is more accurate for large values of n (narrower patterns). Based on absolute error and symmetrically rotational

TABLE 2.1 Comparison of Exact and Approximate Values of Maximum Directivity for $U = \cos^n \theta$ Power Patterns

n	Exact Equation (2-22)	Kraus Equation (2-26)	Kraus % Error	Tai and Pereira Equation (2-30a)	Tai and Pereira % Error
1	4	2.86	−28.50	2.53	−36.75
2	6	5.09	−15.27	4.49	−25.17
3	8	7.35	−8.12	6.48	−19.00
4	10	9.61	−3.90	8.48	−15.20
5	12	11.87	−1.08	10.47	−12.75
6	14	14.13	+0.93	12.46	−11.00
7	16	16.39	+2.48	14.47	−9.56
8	18	18.66	+3.68	16.47	−8.50
9	20	20.93	+4.64	18.47	−7.65
10	22	23.19	+5.41	20.47	−6.96
11.28	24.56	26.08	+6.24	23.02	−6.24
15	32	34.52	+7.88	30.46	−4.81
20	42	45.89	+9.26	40.46	−3.67

patterns, Kraus' formula leads to smaller error for $n < 11.28$ (half-power beamwidth greater than 39.77°) while Tai & Pereira's leads to smaller error for $n > 11.28$ (half-power beamwidth smaller than 39.77°). The results are shown plotted in Figure 2.16 for $0 < n \leq 450$.

2.6.2 Omnidirectional Patterns

Some antennas (such as dipoles, loops, broadside arrays) exhibit omnidirectional patterns, as illustrated by the three-dimensional patterns in Figure 2.17 (a,b). As single-lobe directional patterns can be approximated by (2-31), omnidirectional patterns can often be approximated by

$$U = |\sin^n(\theta)| \qquad 0 \leq \theta \leq \pi, \quad 0 \leq \phi \leq 2\pi \tag{2-32}$$

where n represents both integer and noninteger values. The directivity of antennas with patterns represented by (2-32) can be determined in closed from using the definition of (2-16a). However, as was done for the single-lobe patterns of Figure 2.14, approximate directivity formulas have been derived [11], [12] for antennas with omnidirectional patterns similar to the ones shown in Figure 2.17 whose main lobe is approximated by (2-32). The approximate directivity formula for an omnidirectional pattern as a function of the pattern half-power beamwidth (in degrees), which is reported by McDonald in [11], was derived based on the array factor of a broadside collinear array [see Section 6.4.1 and (6-38a)] and is given by

$$D_0 \simeq \frac{101}{\text{HPBW (degrees)} - 0.0027\ [\text{HPBW (degrees)}]^2} \tag{2-33a}$$

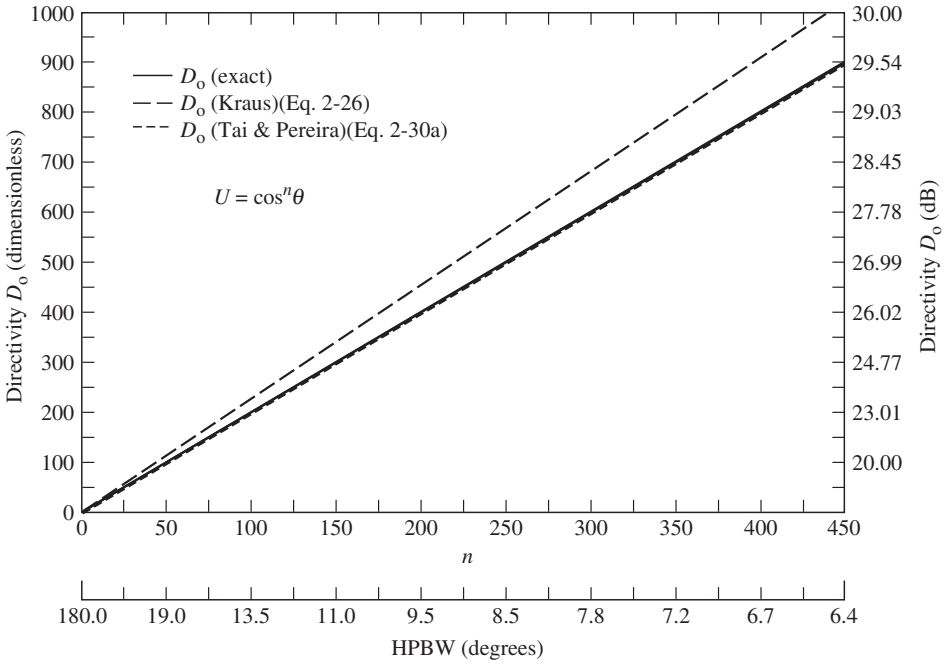


Figure 2.16 Comparison of exact and approximate values of directivity for directional $U = \cos^n \theta$ power patterns.

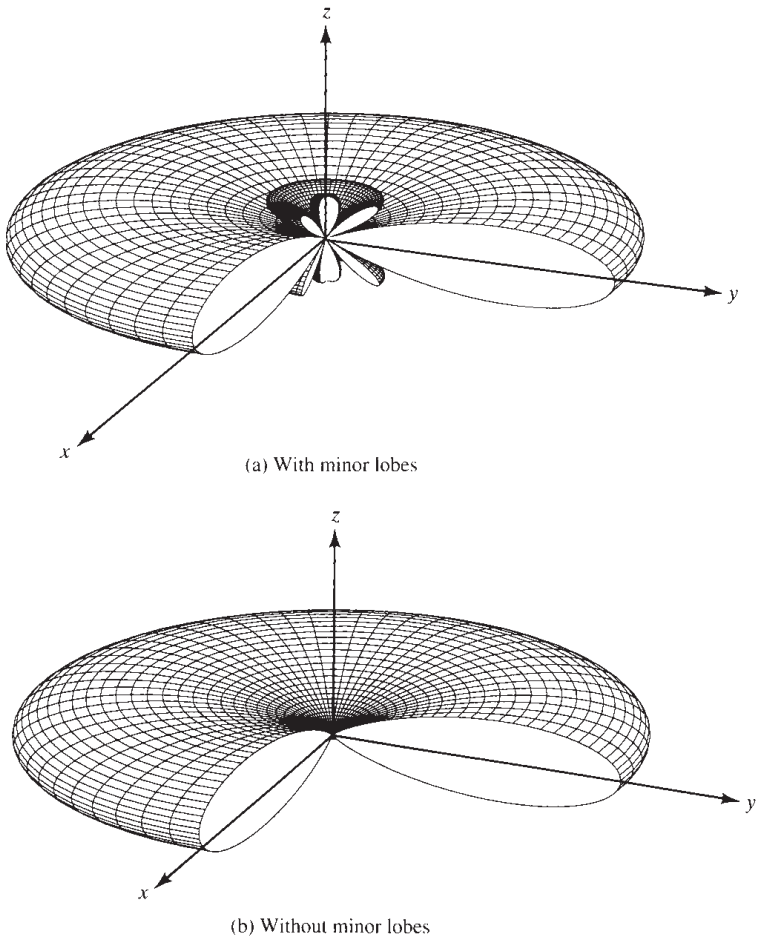


Figure 2.17 Omnidirectional patterns with and without minor lobes.

However, that reported by Pozar in [12] is derived based on the exact values obtained using (2-32) and then representing the data in closed-form using curve-fitting, and it is given by

$$D_0 \simeq -172.4 + 191\sqrt{0.818 + 1/\text{HPBW (degrees)}} \tag{2-33b}$$

The approximate formula of (2-33a) should, in general, be more accurate for omnidirectional patterns with minor lobes, as shown in Figure 2.17(a), while (2-33b) should be more accurate for omnidirectional patterns with minor lobes of very low intensity (ideally no minor lobes), as shown in Figure 2.17(b).

The approximate formulas of (2-33a) and (2-33b) can be used to design omnidirectional antennas with specified radiation pattern characteristics. To facilitate this procedure, the directivity of antennas with omnidirectional patterns approximated by (2-32) is plotted in Figure 2.18 versus n and the half-power beamwidth (in degrees). Three curves are plotted in Figure 2.18; one using (2-16a) and referred as *exact*, one using (2-33a) and denoted as *McDonald*, and the third using (2-33b) and denoted as *Pozar*. Thus, the curves of Figure 2.18 can be used for design purposes, as follows:

a. Specify the desired directivity and determine the value of n and half-power beamwidth of the omnidirectional antenna pattern, or
b. Specify the desired value of n or half-power beamwidth and determine the directivity of the omnidirectional antenna pattern.

To demonstrate the procedure, an example is taken.

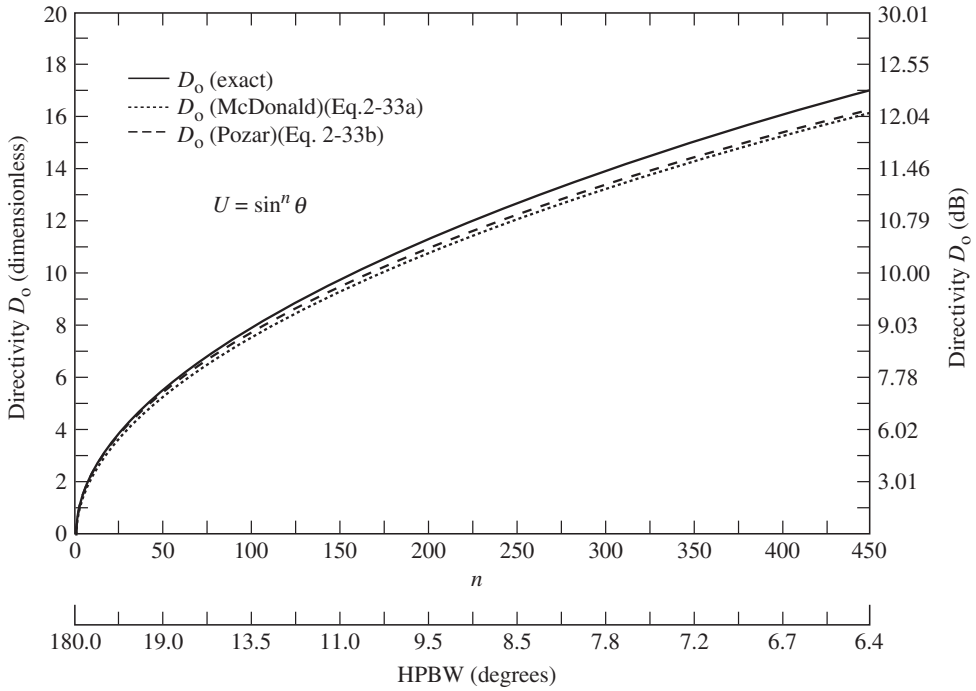


Figure 2.18 Comparison of exact and approximate values of directivity for omnidirectional $U = \sin^n \theta$ power patterns.

Example 2.8

Design an antenna with omnidirectional amplitude pattern with a half-power beamwidth of 90°. Express its radiation intensity by $U = \sin^n \theta$. Determine the value of n and attempt to identify elements that exhibit such a pattern. Determine the directivity of the antenna using (2-16a), (2-33a), and (2-33b).

Solution: Since the half-power beamwidth is 90°, the angle at which the half-power point occurs is $\theta = 45°$. Thus

$$U(\theta = 45°) = 0.5 = \sin^n(45°) = (0.707)^n$$

or

$$n = 2$$

Therefore, the radiation intensity of the omnidirectional antenna is represented by $U = \sin^2 \theta$. An infinitesimal dipole (see Chapter 4) or a small circular loop (see Chapter 5) are two antennas which possess such a pattern.

Using the definition of (2-16a), the exact directivity is

$$U_{\max} = 1$$

$$P_{\text{rad}} = \int_0^{2\pi} \int_0^{\pi} \sin^2 \theta \, \sin\theta \, d\theta \, d\phi = \frac{8\pi}{3}$$

$$D_0 = \frac{4\pi}{8\pi/3} = \frac{3}{2} = 1.761 \text{ dB}$$

Since the half-power beamwidth is equal to 90°, then the directivity based on (2-33a) is equal to

$$D_0 = \frac{101}{90 - 0.0027(90)^2} = 1.4825 = 1.71 \text{ dB}$$

while that based on (2-33b) is equal to

$$D_0 = -172.4 + 191\sqrt{0.818 + 1/90} = 1.516 = 1.807 \text{ dB}$$

The value of n and the three values of the directivity can also be obtained using Figure 2.18, although they may not be as accurate as those given above because they have to be taken off the graph. However, the curves can be used for other problems.

2.7 NUMERICAL TECHNIQUES

For most practical antennas, their radiation patterns are so complex that closed-form mathematical expressions are not available. Even in those cases where expressions are available, their form is so complex that integration to find the radiated power, required to compute the maximum directivity, cannot be performed. Instead of using the approximate expressions of Kraus, Tai and Pereira, McDonald, or Pozar alternate and more accurate techniques may be desirable. With the high-speed computer systems now available, the answer may be to apply numerical methods.

EX2042
Page 71 of 1072

Let us assume that the radiation intensity of a given antenna is separable, and it is given by

$$U = B_0 f(\theta) g(\phi) \tag{2-34}$$

where B_0 is a constant. The directivity for such a system is given by

$$D_0 = \frac{4\pi U_{\max}}{P_{\text{rad}}} \tag{2-35}$$

where

$$P_{\text{rad}} = B_0 \int_0^{2\pi} \left\{ \int_0^{\pi} f(\theta) g(\phi) \sin\theta \, d\theta \right\} d\phi \tag{2-36}$$

which can also be written as

$$P_{\text{rad}} = B_0 \int_0^{2\pi} g(\phi) \left\{ \int_0^{\pi} f(\theta) \sin\theta \, d\theta \right\} d\phi \tag{2-37}$$

If the integrations in (2-37) cannot be performed analytically, then from integral calculus we can write a series approximation

$$\int_0^{\pi} f(\theta) \sin\theta \, d\theta = \sum_{i=1}^{N} [f(\theta_i) \sin\theta_i] \Delta\theta_i \tag{2-38}$$

For N uniform divisions over the π interval,

$$\Delta\theta_i = \frac{\pi}{N} \tag{2-38a}$$

Referring to Figure 2.19, θ_i can take many different forms. Two schemes are shown in Figure 2.19 such that

$$\theta_i = i\left(\frac{\pi}{N}\right), \quad i = 1, 2, 3, \ldots, N \tag{2-38b}$$

or

$$\theta_i = \frac{\pi}{2N} + (i-1)\frac{\pi}{N}, \quad i = 1, 2, 3, \ldots, N \tag{2-38c}$$

In the former case, θ_i is taken at the trailing edge of each division; in the latter case, θ_i is selected at the middle of each division. The scheme that is more desirable will depend upon the problem under investigation. Many other schemes are available.

In a similar manner, we can write for the ϕ variations that

$$\int_0^{2\pi} g(\phi) \, d\phi = \sum_{j=1}^{M} g(\phi_j) \Delta\phi_j \tag{2-39}$$

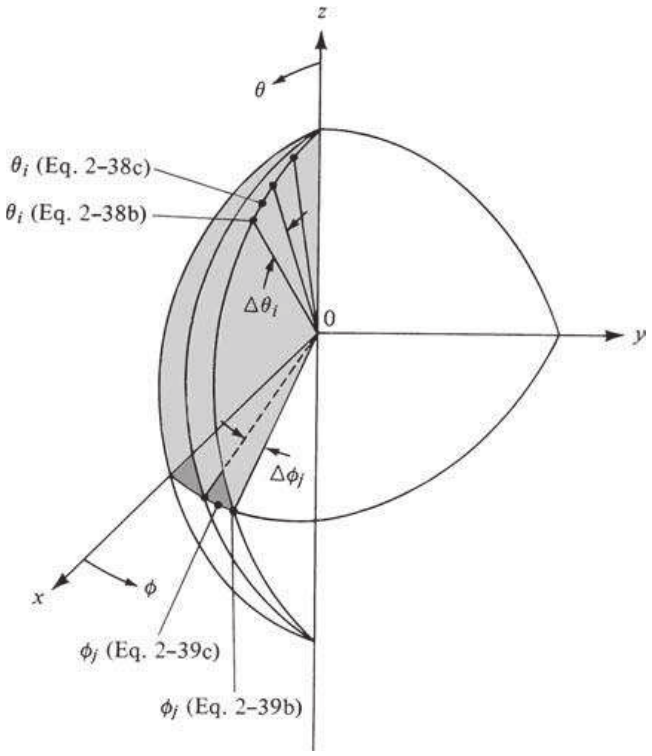


Figure 2.19 Digitization scheme of pattern in spherical coordinates.

where for M uniform divisions

$$\Delta\phi_j = \frac{2\pi}{M} \tag{2-39a}$$

Again referring to Figure 2.19

$$\phi_j = j\left(\frac{2\pi}{M}\right), \quad j = 1, 2, 3, \ldots, M \tag{2-39b}$$

or

$$\phi_j = \frac{2\pi}{2M} + (j-1)\frac{2\pi}{M}, \quad j = 1, 2, 3, \ldots, M \tag{2-39c}$$

Combining (2-38), (2-38a), (2-39), and (2-39a) we can write (2-37) as

$$P_{\text{rad}} = B_0\left(\frac{\pi}{N}\right)\left(\frac{2\pi}{M}\right)\sum_{j=1}^{M}\left\{g(\phi_j)\left[\sum_{i=1}^{N} f(\theta_i)\sin\theta_i\right]\right\} \tag{2-40}$$

The double summation of (2-40) is performed by adding for each value of $j\,(j = 1, 2, 3, \ldots, M)$ all values of $i\,(i = 1, 2, 3, \ldots, N)$. In a computer program flowchart, this can be performed by a loop within a loop. Physically, (2-40) can be interpreted by referring to Figure 2.19. It simply states that for each value of $g(\phi)$ at the azimuthal angle $\phi = \phi_j$, the values of $f(\theta)\sin\theta$ are added for all values of $\theta = \theta_i (i = 1, 2, 3, \ldots, N)$. The values of θ_i and ϕ_j can be determined by using either of the forms as given by (2-38b) or (2-38c) and (2-39b) or (2-39c).

EX2042
Page 73 of 1072

Since the θ and ϕ variations are separable, (2-40) can also be written as

$$P_{\text{rad}} = B_0 \left(\frac{\pi}{N}\right)\left(\frac{2\pi}{M}\right)\left[\sum_{j=1}^{M} g(\phi_j)\right]\left[\sum_{i=1}^{N} f(\theta_i)\sin\theta_i\right] \tag{2-41}$$

in which case each summation can be performed separately.

If the θ and ϕ variations are not separable, and the radiation intensity is given by

$$U = B_0 F(\theta, \phi) \tag{2-42}$$

the digital form of the radiated power can be written as

$$\boxed{P_{\text{rad}} = B_0 \left(\frac{\pi}{N}\right)\left(\frac{2\pi}{M}\right)\sum_{j=1}^{M}\left[\sum_{i=1}^{N} F(\theta_i, \phi_j)\sin\theta_i\right]} \tag{2-43}$$

θ_i and ϕ_j take different forms, two of which were introduced and are shown pictorially in Figure 2.19. The evaluation and physical interpretation of (2-43) is similar to that of (2-40).

To examine the accuracy of the technique, two examples will be considered.

Example 2.9(a)

The radiation intensity of an antenna is given by

$$U(\theta, \phi) = \begin{cases} B_0 \sin\theta \sin^2\phi, & 0 \le \theta \le \pi, \quad 0 \le \phi \le \pi \\ 0 & \text{elsewhere} \end{cases}$$

The three-dimensional pattern of $U(\theta, \phi)$ is shown in Figure 2.20.

Determine the maximum directivity numerically by using (2-41) with θ_i and ϕ_j of (2-38b) and (2-39b), respectively. Compare it with the exact value.

Solution: Let us divide the θ and ϕ intervals each into 18 equals segments ($N = M = 18$). Since $0 \le \phi \le \pi$, then $\Delta\phi_j = \pi/M$ and (2-41) reduces to

$$P_{\text{rad}} = B_0 \left(\frac{\pi}{18}\right)^2 \left[\sum_{j=1}^{18} \sin^2\phi_j\right]\left[\sum_{i=1}^{18} \sin^2\theta_i\right]$$

with

$$\theta_i = i\left(\frac{\pi}{18}\right) = i(10^\circ), \quad i = 1, 2, 3, \ldots, 18$$

$$\phi_j = j\left(\frac{\pi}{18}\right) = j(10^\circ), \quad j = 1, 2, 3, \ldots, 18$$

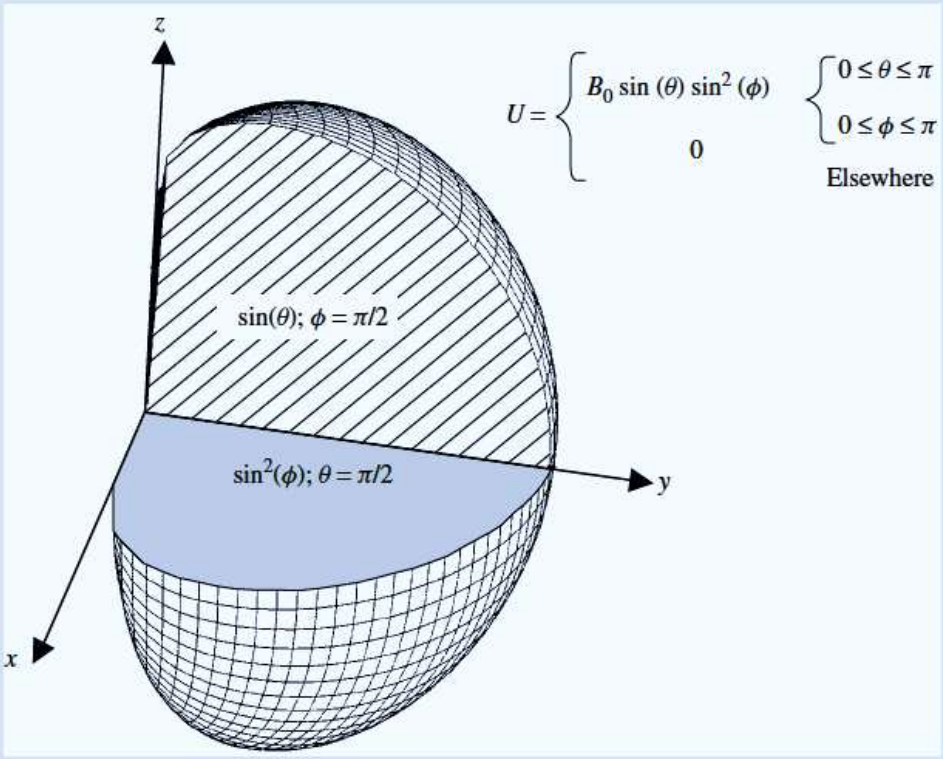


Figure 2.20 Three-dimensional pattern of the radiation of Examples 2.9(a,b).

Thus

$$P_{\text{rad}} = B_0 \left(\frac{\pi}{18}\right)^2 [\sin^2(10^\circ) + \sin^2(20^\circ) + \cdots + \sin^2(180^\circ)]^2$$

$$P_{\text{rad}} = B_0 \left(\frac{\pi}{18}\right)^2 (9)^2 = B_0 \left(\frac{\pi^2}{4}\right)$$

and

$$D_0 = \frac{4\pi U_{\max}}{P_{\text{rad}}} = \frac{4\pi}{\pi^2/4} = \frac{16}{\pi} = 5.0929$$

The exact value is given by

$$P_{\text{rad}} = B_0 \int_0^{\pi} \sin^2\phi \, d\phi \int_0^{\pi} \sin^2\theta \, d\theta = \frac{\pi}{2}\left(\frac{\pi}{2}\right) B_0 = \frac{\pi^2}{4} B_0$$

and

$$D_0 = \frac{4\pi U_{\max}}{P_{\text{rad}}} = \frac{4\pi}{\pi^2/4} = \frac{16}{\pi} = 5.0929$$

which is the same as the value obtained numerically!

Example 2.9(b)

Given the same radiation intensity as that in Example 2.9(a), determine the directivity using (2-41) with θ_i and ϕ_j of (2-38c) and (2-39c).

Solution: Again using 18 divisions in each interval, we can write (2-41) as

$$P_{\text{rad}} = B_0 \left(\frac{\pi}{18}\right)^2 \left[\sum_{j=1}^{18} \sin^2 \phi_j\right] \left[\sum_{i=1}^{18} \sin^2 \theta_i\right]$$

with

$$\theta_i = \frac{\pi}{36} + (i-1)\frac{\pi}{18} = 5^\circ + (i-1)10^\circ, \quad i = 1, 2, 3, \ldots, 18$$
$$\phi_j = \frac{\pi}{36} + (j-1)\frac{\pi}{18} = 5^\circ + (j-1)10^\circ, \quad j = 1, 2, 3, \ldots, 18$$

Because of the symmetry of the divisions about the $\theta = \pi/2$ and $\phi = \pi/2$ angles, we can write

$$P_{\text{rad}} = B_0 \left(\frac{\pi}{18}\right)^2 \left[2\sum_{j=1}^{9} \sin^2 \phi_j\right] \left[2\sum_{i=1}^{9} \sin^2 \theta_i\right]$$

$$P_{\text{rad}} = B_0 \left(\frac{\pi}{18}\right)^2 4[\sin^2(5^\circ) + \sin^2(15^\circ) + \cdots + \sin^2(85^\circ)]^2$$

$$P_{\text{rad}} = B_0 \left(\frac{\pi}{18}\right)^2 4(4.5)^2 = B_0 \left(\frac{\pi}{18}\right)^2 (81) = B_0 \left(\frac{\pi^2}{4}\right)$$

which is identical to that of the previous example. Thus

$$D_0 = \frac{4\pi U_{\max}}{P_{\text{rad}}} = \frac{4\pi}{\pi^2/4} = \frac{16}{\pi} = 5.0929$$

which again is equal to the exact value!

It is interesting to note that decreasing the number of divisions (M and/or N) to 9, 6, 4, and even 2 leads to the same answer, which also happens to be the exact value! To demonstrate as to why the number of divisions does not affect the answer for this pattern, let us refer to Figure 2.21 where we have plotted the $\sin^2 \phi$ function and divided the $0^\circ \leq \phi \leq 180^\circ$ interval into six divisions. The exact value of the directivity uses the area under the solid curve. Doing the problem numerically, we find the area under the rectangles, which is shown shaded. Because of the symmetrical nature of the function, it can be shown that the shaded area in section #1 (included in the numerical evaluation) is equal to the blank area in section #1′ (left out by the numerical method). The same is true for the areas in sections #2 and #2′, and #3 and #3′. Thus, there is a one-to-one compensation. Similar justification is applicable for the other number of divisions.

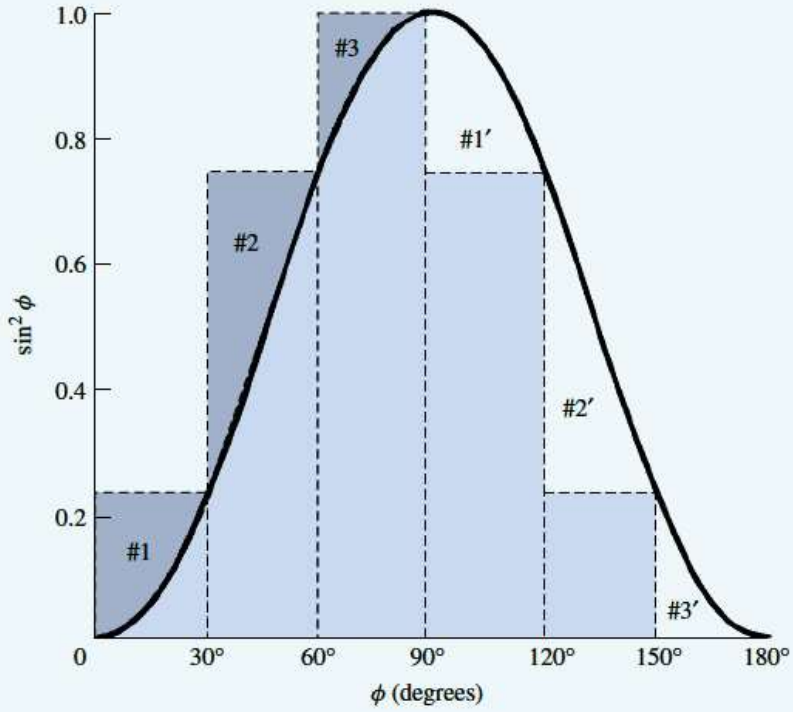


Figure 2.21 Digitized form of $\sin^2\phi$ function.

It should be emphasized that all functions, even though they may contain some symmetry, do not give the same answers independent of the number of divisions. As a matter of fact, in most cases the answer only approaches the exact value as the number of divisions is increased to a large number.

A MATLAB and FORTRAN computer program called ***Directivity*** has been developed to compute the maximum directivity of any antenna whose radiation intensity is $U = F(\theta, \phi)$ based on the formulation of (2-43). The intensity function F does not have to be a function of both θ and ϕ. The numerical evaluations are made at the trailing edge, as defined by (2-38b) and (2-39b). The program is included in the attached CD. It contains a *subroutine* for which the intensity factor $U = F(\theta, \phi)$ for the required application must be specified by the user. As an illustration, the antenna intensity $U = \sin\theta \sin^2\phi$ has been inserted in the subroutine. In addition, the upper and lower limits of θ and ϕ must be specified for each application of the same pattern.

2.8 ANTENNA EFFICIENCY

Associated with an antenna are a number of efficiencies and can be defined using Figure 2.22. The total antenna efficiency e_0 is used to take into account losses at the input terminals and within the structure of the antenna. Such losses may be due, referring to Figure 2.22(b), to

1. reflections because of the mismatch between the transmission line and the antenna
2. I^2R losses (conduction and dielectric)

EX2042
Page 77 of 1072

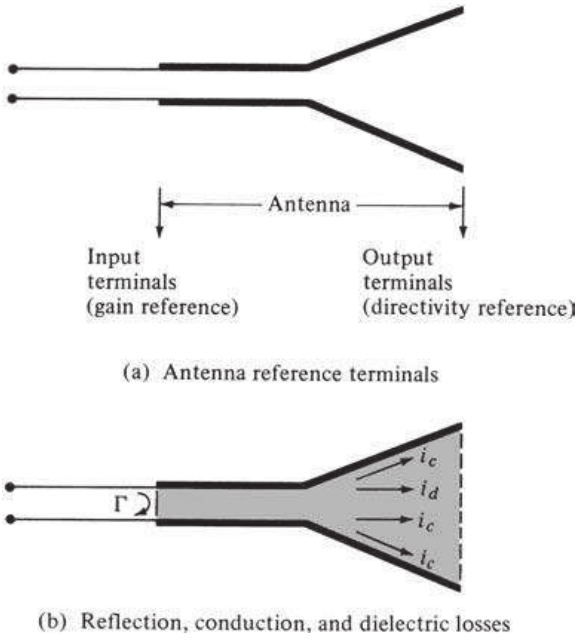


Figure 2.22 Reference terminals and losses of an antenna.

In general, the overall efficiency can be written as

$$\boxed{e_0 = e_r e_c e_d} \tag{2-44}$$

where

e_0 = total efficiency (dimensionless)
e_r = reflection (mismatch) efficiency $= (1 - |\Gamma|^2)$ (dimensionless)
e_c = conduction efficiency (dimensionless)
e_d = dielectric efficiency (dimensionless)
Γ = voltage reflection coefficient at the input terminals of the antenna [$\Gamma = (Z_{in} - Z_0)/(Z_{in} + Z_0)$ where Z_{in} = antenna input impedance, Z_0 = characteristic impedance of the transmission line]
VSWR = voltage standing wave ratio $= \dfrac{1 + |\Gamma|}{1 - |\Gamma|}$

Usually e_c and e_d are very difficult to compute, but they can be determined experimentally. Even by measurements they cannot be separated, and it is usually more convenient to write (2-44) as

$$e_0 = e_r e_{cd} = e_{cd}(1 - |\Gamma|^2) \tag{2-45}$$

where $e_{cd} = e_c e_d$ = antenna radiation efficiency, which is used to relate the gain and directivity.

2.9 GAIN

Another useful measure describing the performance of an antenna is the *gain*. Although the gain of the antenna is closely related to the directivity, it is a measure that takes into

account the efficiency of the antenna as well as its directional capabilities. Remember that directivity is a measure that describes only the directional properties of the antenna, and it is therefore controlled only by the pattern.

Gain of an antenna (in a given direction) is defined as "the ratio of the intensity, in a given direction, to the radiation intensity that would be obtained if the power accepted by the antenna were radiated isotropically. The radiation intensity corresponding to the isotropically radiated power is equal to the power accepted (input) by the antenna divided by 4π." In equation form this can be expressed as

$$\text{Gain} = 4\pi \frac{\text{radiation intensity}}{\text{total input (accepted) power}} = 4\pi \frac{U(\theta, \phi)}{P_{in}} \quad \text{(dimensionless)} \tag{2-46}$$

In most cases we deal with *relative gain*, which is defined as "the ratio of the power gain in a given direction to the power gain of a reference antenna in its referenced direction." The power input must be the same for both antennas. The reference antenna is usually a dipole, horn, or any other antenna whose gain can be calculated or it is known. In most cases, however, the reference antenna is a *lossless isotropic source*. Thus

$$G = \frac{4\pi U(\theta, \phi)}{P_{in}(\text{lossless isotropic source})} \quad \text{(dimensionless)} \tag{2-46a}$$

When the direction is not stated, the power gain is usually taken in the direction of maximum radiation.

Referring to Figure 2.22(a), we can write that the total radiated power (P_{rad}) is related to the total input power (P_{in}) by

$$P_{\text{rad}} = e_{cd} P_{in} \tag{2-47}$$

where e_{cd} is the antenna radiation efficiency (dimensionless) which is defined in (2-44), (2-45) and Section 2.14 by (2-90). According to the IEEE Standards, "gain does not include losses arising from impedance mismatches (reflection losses) and polarization mismatches (losses)."

In this edition of the book we define two gains; one, referred to as *gain* (G), and the other, referred to as *absolute gain* (G_{abs}), that also takes into account the reflection/mismatch losses represented in both (2-44) and (2-45).

Using (2-47) reduces (2-46a) to

$$G(\theta, \phi) = e_{cd} \left[4\pi \frac{U(\theta, \phi)}{P_{\text{rad}}} \right] \tag{2-48}$$

which is related to the directivity of (2-16) and (2-21) by

$$\boxed{G(\theta, \phi) = e_{cd} D(\theta, \phi)} \tag{2-49}$$

In a similar manner, the maximum value of the gain is related to the maximum directivity of (2-16a) and (2-23) by

$$\boxed{G_0 = G(\theta, \phi)|_{\max} = e_{cd} D(\theta, \phi)|_{\max} = e_{cd} D_0} \tag{2-49a}$$

While (2-47) does take into account the losses of the antenna element itself, *it does not take into account the losses when the antenna element is connected to a transmission line*, as shown in Figure 2.22. These connection losses are usually referred to as *reflections (mismatch) losses*, and they are taken into account by introducing a reflection (mismatch) efficiency e_r, which is related to the reflection coefficient as shown in (2-45) or $e_r = (1 - |\Gamma|^2)$. Thus, we can introduce an *absolute gain* G_{abs} that takes into account the reflection/mismatch losses (due to the connection of the antenna element to the transmission line), and it can be written as

$$\boxed{\begin{aligned} G_{abs}(\theta, \phi) &= e_r G(\theta, \phi) = (1 - |\Gamma|^2) G(\theta, \phi) \\ &= e_r e_{cd} D(\theta, \phi) = e_o D(\theta, \phi) \end{aligned}} \tag{2-49b}$$

where e_o is the overall efficiency as defined in (2-44), (2-45). Similarly, the *maximum absolute* gain G_{0abs} of (2-49a) is related to the maximum directivity D_0 by

$$\boxed{\begin{aligned} G_{0abs} &= G_{abs}(\theta, \phi)|_{\max} = e_r G(\theta, \phi)|_{\max} = (1 - |\Gamma|^2) G(\theta, \phi)|_{\max} \\ &= e_r e_{cd} D(\theta, \phi)|_{\max} = e_o D(\theta, \phi)|_{\max} = e_o D_0 \end{aligned}} \tag{2-49c}$$

If the antenna is matched to the transmission line, that is, the antenna input impedance Z_{in} *is equal to the characteristic impedance* Z_c *of the line* ($|\Gamma| = 0$)*, then the two gains are equal* ($G_{abs} = G$).

As was done with the directivity, we can define the *partial gain of an antenna for a given polarization in a given direction* as "that part of the radiation intensity corresponding to a given polarization divided by the total radiation intensity that would be obtained if the power accepted by the antenna were radiated isotropically." With this definition for the partial gain, then, in a given direction, "the total gain is the sum of the partial gains for any two orthogonal polarizations." For a spherical coordinate system, the total maximum gain G_0 for the orthogonal θ and ϕ components of an antenna can be written, in a similar form as was the maximum directivity in (2-17)–(2-17b), as

$$G_0 = G_\theta + G_\phi \tag{2-50}$$

while the partial gains G_θ and G_ϕ are expressed as

$$G_\theta = \frac{4\pi U_\theta}{P_{in}} \tag{2-50a}$$

$$G_\phi = \frac{4\pi U_\phi}{P_{in}} \tag{2-50b}$$

where

U_θ = radiation intensity in a given direction contained in E_θ field component
U_ϕ = radiation intensity in a given direction contained in E_ϕ field component
P_{in} = total input (accepted) power

For many practical antennas an approximate formula for the gain, corresponding to (2-27) or (2-27a) for the directivity, is

$$\boxed{G_0 \simeq \frac{30{,}000}{\Theta_{1d}\Theta_{2d}}} \tag{2-51}$$

In practice, whenever the term "gain" is used, it usually refers to the *maximum gain* as defined by (2-49a) or (2-49c).

Usually the gain is given in terms of decibels instead of the dimensionless quantity of (2-49a). The conversion formula is given by

$$G_0(\text{dB}) = 10\log_{10}[e_{cd}D_0 \text{ (dimensionless)}] \tag{2-52}$$

Example 2.10

A lossless resonant half-wavelength dipole antenna, with input impedance of 73 ohms, is connected to a transmission line whose characteristic impedance is 50 ohms. Assuming that the pattern of the antenna is given approximately by

$$U = B_0 \sin^3\theta$$

find the maximum absolute gain of this antenna.

Solution: Let us first compute the maximum directivity of the antenna. For this

$$U|_{\max} = U_{\max} = B_0$$

$$P_{\text{rad}} = \int_0^{2\pi}\int_0^{\pi} U(\theta,\phi)\sin\theta\, d\theta\, d\phi = 2\pi B_0 \int_0^{\pi} \sin^4\theta\, d\theta = B_0\left(\frac{3\pi^2}{4}\right)$$

$$D_0 = 4\pi\frac{U_{\max}}{P_{\text{rad}}} = \frac{16}{3\pi} = 1.697$$

Since the antenna was stated to be lossless, then the radiation efficiency $e_{cd} = 1$.

Thus, the total maximum gain is equal to

$$G_0 = e_{cd}D_0 = 1(1.697) = 1.697$$

$$G_0(\text{dB}) = 10\log_{10}(1.697) = 2.297$$

which is identical to the directivity because the antenna is lossless.

There is another loss factor which is not taken into account in the gain. That is the loss due to reflection or mismatch losses between the antenna (load) and the transmission line. This loss is accounted for by the reflection efficiency of (2-44) or (2-45), and it is equal to

$$e_r = (1 - |\Gamma|^2) = \left(1 - \left|\frac{73-50}{73+50}\right|^2\right) = 0.965$$

$$e_r(\text{dB}) = 10\log_{10}(0.965) = -0.155$$

Therefore the overall efficiency is

$$e_0 = e_r e_{cd} = 0.965$$
$$e_0(\text{dB}) = -0.155$$

Thus, the overall losses are equal to 0.155 dB. The absolute gain is equal to

$$G_{0abs} = e_0 D_0 = 0.965(1.697) = 1.6376$$
$$G_{0abs}(\text{dB}) = 10\log_{10}(1.6376) = 2.142$$

The gain in dB can also be obtained by converting the directivity and radiation efficiency in dB and then adding them. Thus,

$$e_{cd}(\text{dB}) = 10\log_{10}(1.0) = 0$$
$$D_0(\text{dB}) = 10\log_{10}(1.697) = 2.297$$
$$G_0(\text{dB}) = e_{cd}(\text{dB}) + D_0(\text{dB}) = 2.297$$

which is the same as obtained previously. The same procedure can be used for the absolute gain.

2.10 BEAM EFFICIENCY

Another parameter that is frequently used to judge the quality of transmitting and receiving antennas is the *beam efficiency*. For an antenna with its major lobe directed along the z-axis ($\theta = 0$), as shown in Figure 2.1(a), the beam efficiency (BE) is defined by

$$\text{BE} = \frac{\text{power transmitted (received) within cone angle } \theta_1}{\text{power transmitted (received) by the antenna}}(\text{dimensionless}) \qquad (2\text{-}53)$$

where θ_1 is the half-angle of the cone within which the percentage of the total power is to be found. Equation (2-53) can be written as

$$\text{BE} = \frac{\displaystyle\int_0^{2\pi}\int_0^{\theta_1} U(\theta,\phi)\sin\theta\, d\theta\, d\phi}{\displaystyle\int_0^{2\pi}\int_0^{\pi} U(\theta,\phi)\sin\theta\, d\theta\, d\phi} \qquad (2\text{-}54)$$

If θ_1 is chosen as the angle where the first null or minimum occurs (see Figure 2.1), then the beam efficiency will indicate the amount of power in the major lobe compared to the total power. A very high beam efficiency (between the nulls or minimums), usually in the high 90s, is necessary for antennas used in radiometry, astronomy, radar, and other applications where received signals through the minor lobes must be minimized. The beam efficiencies of some typical rectangular and circular aperture antennas will be discussed in Chapter 12.

2.11 BANDWIDTH

The *bandwidth* of an antenna is defined as "the range of frequencies within which the performance of the antenna, with respect to some characteristic, conforms to a specified standard." The bandwidth can be considered to be the range of frequencies, on either side of a center frequency (usually the resonance frequency for a dipole), where the antenna characteristics (such as input impedance, pattern, beamwidth, polarization, side lobe level, gain, beam direction, radiation efficiency) are within an acceptable value of those at the center frequency. For broadband antennas, the bandwidth is usually expressed as the ratio of the upper-to-lower frequencies of acceptable operation. For example, a 10:1 bandwidth indicates that the upper frequency is 10 times greater than the lower. For narrowband antennas, the bandwidth is expressed as a percentage of the frequency difference (upper minus lower) over the center frequency of the bandwidth. For example, a 5% bandwidth indicates that the frequency difference of acceptable operation is 5% of the center frequency of the bandwidth.

Because the characteristics (input impedance, pattern, gain, polarization, etc.) of an antenna do not necessarily vary in the same manner or are even critically affected by the frequency, there is no unique characterization of the bandwidth. The specifications are set in each case to meet the needs of the particular application. Usually there is a distinction made between pattern and input impedance variations. Accordingly *pattern bandwidth* and *impedance bandwidth* are used to emphasize this distinction. Associated with pattern bandwidth are gain, side lobe level, beamwidth, polarization, and beam direction while input impedance and radiation efficiency are related to impedance bandwidth. For example, the pattern of a linear dipole with overall length less than a half-wavelength ($l < \lambda/2$) is insensitive to frequency. The limiting factor for this antenna is its impedance, and its bandwidth can be formulated in terms of the Q. The Q of antennas or arrays with dimensions large compared to the wavelength, excluding superdirective designs, is near unity. Therefore the bandwidth is usually formulated in terms of beamwidth, side lobe level, and pattern characteristics. For intermediate length antennas, the bandwidth may be limited by either pattern or impedance variations, depending upon the particular application. For these antennas, a 2:1 bandwidth indicates a good design. For others, large bandwidths are needed. Antennas with very large bandwidths (like 40:1 or greater) have been designed in recent years. These are known as *frequency independent* antennas, and they are discussed in Chapter 11.

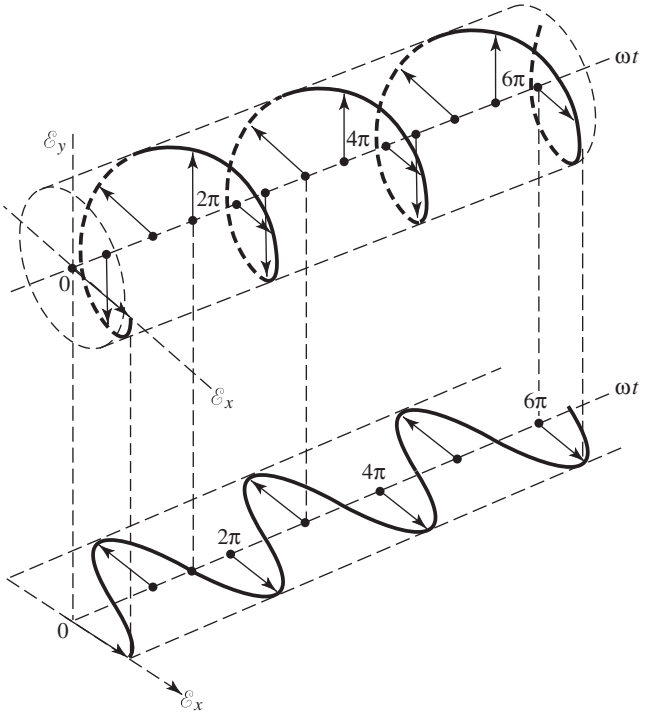
The above discussion presumes that the coupling networks (transformers, baluns, etc.) and/or the dimensions of the antenna are not altered in any manner as the frequency is changed. It is possible to increase the acceptable frequency range of a narrowband antenna if proper adjustments can be made on the critical dimensions of the antenna and/or on the coupling networks as the frequency is changed. Although not an easy or possible task in general, there are applications where this can be accomplished. The most common examples are the antenna of a car radio and the "rabbit ears" of a television. Both usually have adjustable lengths which can be used to tune the antenna for better reception.

2.12 POLARIZATION

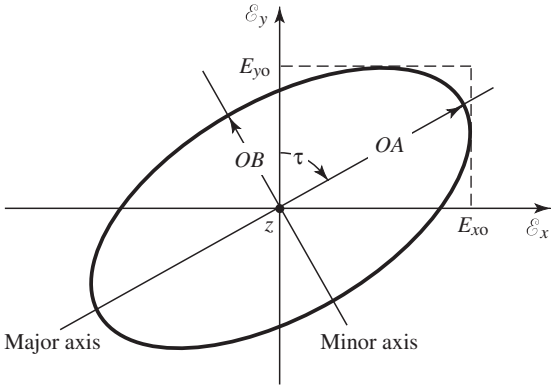
Polarization of an antenna in a given direction is defined as "the polarization of the wave transmitted (radiated) by the antenna. *Note:* When the direction is not stated,

the polarization is taken to be the polarization in the direction of maximum gain." In practice, polarization of the radiated energy varies with the direction from the center of the antenna, so that different parts of the pattern may have different polarizations.

Polarization of a radiated wave is defined as "that property of an electromagnetic wave describing the time-varying direction and relative magnitude of the electric-field vector; specifically, the figure traced as a function of time by the extremity of the vector at a fixed location in space, and the sense in which it is traced, *as observed along the direction of propagation*." Polarization then is the curve traced by the end point of the arrow (vector) representing the instantaneous electric field. The field must be observed along the direction of propagation. A typical trace as a function of time is shown in Figures 2.23(a) and (b).



(a) Rotation of wave



(b) Polarization ellipse

Figure 2.23 Rotation of a plane electromagnetic wave and its polarization ellipse at $z = 0$ as a function of time.

The polarization of a wave can be defined in terms of a wave *radiated (transmitted)* or *received* by an antenna in a given direction. The polarization of a wave *radiated* by an antenna in a specified direction at a point in the far field is defined as "the polarization of the (locally) plane wave which is used to represent the radiated wave at that point. At any point in the far field of an antenna the radiated wave can be represented by a plane wave whose electric-field strength is the same as that of the wave and whose direction of propagation is in the radial direction from the antenna. As the radial distance approaches infinity, the radius of curvature of the radiated wave's phase front also approaches infinity and thus in any specified direction the wave appears locally as a plane wave." This is a far-field characteristic of waves radiated by all practical antennas, and it is illustrated analytically in Section 3.6 of Chapter 3. The polarization of a wave *received* by an antenna is defined as the "polarization of a plane wave, incident from a given direction and having a given power flux density, which results in maximum available power at the antenna terminals."

Polarization may be classified as linear, circular, or elliptical. If the vector that describes the electric field at a point in space as a function of time is always directed along a line, the field is said to be *linearly* polarized. In general, however, the figure that the electric field traces is an ellipse, and the field is said to be elliptically polarized. Linear and circular polarizations are special cases of elliptical, and they can be obtained when the ellipse becomes a straight line or a circle, respectively. The figure of the electric field is traced in a *clockwise* (CW) or *counterclockwise* (CCW) sense. *Clockwise* rotation of the electric-field vector is also designated as *right-hand polarization* and *counterclockwise* as *left-hand polarization*.

In general, the polarization characteristics of an antenna can be represented by its *polarization pattern* whose one definition is "the spatial distribution of the polarizations of a field vector excited (radiated) by an antenna taken over its radiation sphere. When describing the polarizations over the radiation sphere, or portion of it, reference lines shall be specified over the sphere, in order to measure the tilt angles (see tilt angle) of the polarization ellipses and the direction of polarization for linear polarizations. An obvious choice, though by no means the only one, is a family of lines tangent at each point on the sphere to either the θ or ϕ coordinate line associated with a spherical coordinate system of the radiation sphere. At each point on the radiation sphere the polarization is usually resolved into a pair of orthogonal polarizations, the *co-polarization* and *cross polarization*. To accomplish this, the co-polarization must be specified at each point on the radiation sphere." "*Co-polarization* represents the polarization the antenna is intended to radiate (receive) while *cross-polarization* represents the polarization orthogonal to a specified polarization, which is usually the co-polarization."

"For certain linearly polarized antennas, it is common practice to define the co-polarization in the following manner: First specify the orientation of the co-polar electric-field vector at a pole of the radiation sphere. Then, for all other directions of interest (points on the radiation sphere), require that the angle that the co-polar electric-field vector makes with each great circle line through the pole remain constant over that circle, the angle being that at the pole."

"In practice, the axis of the antenna's main beam should be directed along the polar axis of the radiation sphere. The antenna is then appropriately oriented about this axis to align the direction of its polarization with that of the defined co-polarization at the pole." "This manner of defining co-polarization can be extended to the case of elliptical polarization by defining the constant angles using the major axes of the polarization ellipses rather

than the co-polar electric-field vector. The sense of polarization (rotation) must also be specified."

The polarization of the wave radiated by the antenna can also be represented on the Poincaré sphere [13]–[16]. Each point on the Poincaré sphere represents a unique polarization. The north pole represents left circular polarization, the south pole represents right circular, and points along the equator represent linear polarization of different tilt angles. All other points on the Poincaré sphere represent elliptical polarization. For details, see Figure 17.24 of Chapter 17.

The polarization of an antenna is measured using techniques described in Chapter 17.

2.12.1 Linear, Circular, and Elliptical Polarizations

The instantaneous field of a plane wave, traveling in the negative z direction, can be written as

$$\mathscr{E}(z;t) = \hat{\mathbf{a}}_x \mathscr{E}_x(z;t) + \hat{\mathbf{a}}_y \mathscr{E}_y(z;t) \tag{2-55}$$

According to (2-5), the instantaneous components are related to their complex counterparts by

$$\begin{aligned} \mathscr{E}_x(z;t) &= \mathrm{Re}[E_x{}^- e^{j(\omega t+kz)}] = \mathrm{Re}[E_{xo} e^{j(\omega t+kz+\phi_x)}] \\ &= E_{xo}\cos(\omega t + kz + \phi_x) \end{aligned} \tag{2-56}$$

$$\begin{aligned} \mathscr{E}_y(z;t) &= \mathrm{Re}[E_y{}^- e^{j(\omega t+kz)}] = \mathrm{Re}[E_{yo} e^{j(\omega t+kz+\phi_y)}] \\ &= E_{yo}\cos(\omega t + kz + \phi_y) \end{aligned} \tag{2-57}$$

where E_{xo} and E_{yo} are, respectively, the maximum magnitudes of the x and y components.

A. Linear Polarization

For the wave to have linear polarization, the time-phase difference between the two components must be

$$\Delta\phi = \phi_y - \phi_x = n\pi, \quad n = 0, 1, 2, 3, \ldots \tag{2-58}$$

B. Circular Polarization

Circular polarization can be achieved *only* when the magnitudes of the two components are the same *and* the time-phase difference between them is odd multiples of $\pi/2$. That is,

$$|\mathscr{E}_x| = |\mathscr{E}_y| \Rightarrow E_{xo} = E_{yo} \tag{2-59}$$

$$\Delta\phi = \phi_y - \phi_x = \begin{cases} +(\frac{1}{2} + 2n)\pi, n = 0, 1, 2, \ldots & \text{for CW} \quad (2\text{-}60) \\ -(\frac{1}{2} + 2n)\pi, n = 0, 1, 2, \ldots & \text{for CCW} \quad (2\text{-}61) \end{cases}$$

If the direction of wave propagation is reversed (i.e., $+z$ direction), the phases in (2-60) and (2-61) for CW and CCW rotation must be interchanged.

C. Elliptical Polarization

Elliptical polarization can be attained *only* when the time-phase difference between the two components is odd multiples of $\pi/2$ *and* their magnitudes are not the same *or*

when the time-phase difference between the two components is not equal to multiples of $\pi/2$ (irrespective of their magnitudes). That is,

$$|\mathscr{E}_x| \neq |\mathscr{E}_y| \Rightarrow E_{xo} \neq E_{yo}$$

$$\text{when } \Delta\phi = \phi_y - \phi_x = \begin{cases} +(\frac{1}{2} + 2n)\pi & \text{for CW} \quad (2\text{-}62a) \\ -(\frac{1}{2} + 2n)\pi & \text{for CCW} \quad (2\text{-}62b) \end{cases}$$

$$n = 0, 1, 2, \ldots$$

or

$$\Delta\phi = \phi_y - \phi_x \neq \pm\frac{n}{2}\pi = \begin{cases} > 0 & \text{for CW} \quad (2\text{-}63) \\ < 0 & \text{for CCW} \quad (2\text{-}64) \end{cases}$$

$$n = 0, 1, 2, 3, \ldots$$

For elliptical polarization, the curve traced at a given position as a function of time is, in general, a tilted ellipse, as shown in Figure 2.23(b). The ratio of the major axis to the minor axis is referred to as the axial ratio (AR), and it is equal to

$$\text{AR} = \frac{\text{major axis}}{\text{minor axis}} = \frac{OA}{OB}, \quad 1 \leq \text{AR} \leq \infty \tag{2-65}$$

where

$$OA = \left[\tfrac{1}{2}\{E_{xo}^2 + E_{yo}^2 + [E_{xo}^4 + E_{yo}^4 + 2E_{xo}^2 E_{yo}^2 \cos(2\Delta\phi)]^{1/2}\}\right]^{1/2} \tag{2-66}$$

$$OB = \left[\tfrac{1}{2}\{E_{xo}^2 + E_{yo}^2 - [E_{xo}^4 + E_{yo}^4 + 2E_{xo}^2 E_{yo}^2 \cos(2\Delta\phi)]^{1/2}\}\right]^{1/2} \tag{2-67}$$

The tilt of the ellipse, *relative to the y axis*, is represented by the angle τ given by

$$\tau = \frac{\pi}{2} - \frac{1}{2}\tan^{-1}\left[\frac{2E_{xo}E_{yo}}{E_{xo}^2 - E_{yo}^2}\cos(\Delta\phi)\right] \tag{2-68}$$

When the ellipse is aligned with the principal axes [$\tau = n\pi/2, n = 0, 1, 2, \ldots$], the major (minor) axis is equal to $E_{xo}(E_{yo})$ or $E_{yo}(E_{xo})$ and the axial ratio is equal to E_{xo}/E_{yo} or E_{yo}/E_{xo}.

SUMMARY

We will summarize the preceding discussion on polarization by stating the general characteristics, and the *necessary and sufficient* conditions that the wave must have in order to possess *linear, circular* or *elliptical* polarization.

Linear Polarization A *time-harmonic wave is linearly polarized at a given point in space if the electric-field (or magnetic-field) vector at that point is always oriented along the same straight line at every instant of time*. This is accomplished if the field vector (electric or magnetic) possesses:

a. Only one component, or
b. Two orthogonal linear components that are in time phase or 180° (or multiples of 180°) out-of-phase.

Circular Polarization *A time-harmonic wave is circularly polarized at a given point in space if the electric (or magnetic) field vector at that point traces a circle as a function of time*.

The *necessary and sufficient* conditions to accomplish this are if the field vector (electric or magnetic) possesses *all* of the following:

a. The field must have two orthogonal linear components, and
b. The two components must have the same magnitude, and
c. The two components must have a time-phase difference of odd multiples of 90°.

The sense of rotation is always determined by rotating the phase-leading component toward the phase-lagging component and observing the field rotation as the wave is viewed as it travels away from the observer. If the rotation is clockwise, the wave is right-hand (or clockwise) circularly polarized; if the rotation is counterclockwise, the wave is left-hand (or counterclockwise) circularly polarized. The rotation of the phase-leading component toward the phase-lagging component should be done along the angular separation between the two components that is less than 180°. *Phases equal to or greater than* 0° *and less than* 180° *should be considered leading whereas those equal to or greater than* 180° *and less than* 360° *should be considered lagging*.

Elliptical Polarization *A time-harmonic wave is elliptically polarized if the tip of the field vector (electric or magnetic) traces an elliptical locus in space. At various instants of time the field vector changes continuously with time at such a manner as to describe an elliptical locus. It is right-hand (clockwise) elliptically polarized if the field vector rotates clockwise, and it is left-hand (counterclockwise) elliptically polarized if the field vector of the ellipse rotates counterclockwise* [13]. The sense of rotation is determined using the same rules as for the circular polarization. In addition to the sense of rotation, elliptically polarized waves are also specified by their axial ratio whose magnitude is the ratio of the major to the minor axis.

A wave is elliptically polarized if it is not linearly or circularly polarized. Although linear and circular polarizations are special cases of elliptical, usually in practice elliptical polarization refers to other than linear or circular. The *necessary and sufficient* conditions to accomplish this are if the field vector (electric or magnetic) possesses *all* of the following:

a. The field must have two orthogonal linear components, and
b. The two components can be of the same or different magnitude.
c. (1) If the two components are not of the same magnitude, the time-phase difference between the two components must not be 0° or multiples of 180° (because it will then be linear). (2) If the two components are of the same magnitude, the time-phase difference between the two components must not be odd multiples of 90° (because it will then be circular).

If the wave is elliptically polarized with two components not of the same magnitude but with odd multiples of 90° time-phase difference, the polarization ellipse will not be tilted but it will be aligned with the principal axes of the field components. The major axis of the ellipse will align with the axis of the field component which is larger of the

two, while the minor axis of the ellipse will align with the axis of the field component which is smaller of the two.

2.12.2 Polarization Loss Factor and Efficiency

In general, the polarization of the receiving antenna will not be the same as the polarization of the incoming (incident) wave. This is commonly stated as "polarization mismatch." The amount of power extracted by the antenna from the incoming signal will not be maximum because of the polarization loss. Assuming that the electric field of the incoming wave can be written as

$$\mathbf{E}_i = \hat{\boldsymbol{\rho}}_w E_i \tag{2-69}$$

where $\hat{\boldsymbol{\rho}}_w$ is the unit vector of the wave, and the polarization of the electric field of the receiving antenna can be expressed as

$$\mathbf{E}_a = \hat{\boldsymbol{\rho}}_a E_a \tag{2-70}$$

where $\hat{\boldsymbol{\rho}}_a$ is its unit vector (polarization vector), the polarization loss can be taken into account by introducing a *polarization loss factor* (PLF). It is defined, based on the polarization of the antenna in its transmitting mode, as

$$\text{PLF} = |\hat{\boldsymbol{\rho}}_w \cdot \hat{\boldsymbol{\rho}}_a|^2 = |\cos \psi_p|^2 \text{ (dimensionless)} \tag{2-71}$$

where ψ_p is the angle between the two unit vectors. The relative alignment of the polarization of the incoming wave and of the antenna is shown in Figure 2.24. If the antenna is polarization matched, its PLF will be unity and the antenna will extract maximum power from the incoming wave.

Another figure of merit that is used to describe the polarization characteristics of a wave and that of an antenna is the *polarization efficiency* (*polarization mismatch* or *loss factor*) which is defined as "the ratio of the power received by an antenna from a given plane wave of arbitrary polarization to the power that would be received by the same antenna from a plane wave of the same power flux density and direction of

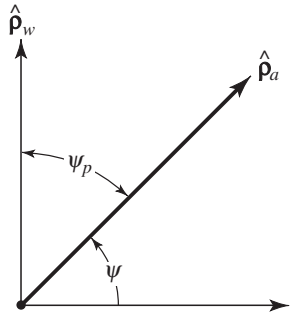


Figure 2.24 Polarization unit vectors of incident wave ($\hat{\boldsymbol{\rho}}_w$) and antenna ($\hat{\boldsymbol{\rho}}_a$), and polarization loss factor (PLF).

propagation, whose state of polarization has been adjusted for a maximum received power." This is similar to the PLF and it is expressed as

$$p_e = \frac{|\boldsymbol{\ell}_\mathbf{e} \cdot \mathbf{E}^{\text{inc}}|^2}{|\boldsymbol{\ell}_\mathbf{e}|^2 |\mathbf{E}^{\text{inc}}|^2} \tag{2-71a}$$

where

$\boldsymbol{\ell}_e$ = vector effective length of the antenna
$\mathbf{E}^{\text{inc}}$ = incident electric field

The vector effective length ℓ_e of the antenna has not yet been defined, and it is introduced in Section 2.15. It is a vector that describes the polarization characteristics of the antenna. Both the PLF and p_e lead to the same answers.

The conjugate (*) is not used in (2-71) or (2-71a) so that a right-hand circularly polarized incident wave (when viewed in its direction of propagation) is matched to right-hand circularly polarized receiving antenna (when its polarization is determined in the transmitting mode). Similarly, a left-hand circularly polarized wave will be matched to a left-hand circularly polarized antenna.

To illustrate the principle of polarization mismatch, two examples are considered.

Example 2.11

The electric field of a linearly polarized electromagnetic wave given by

$$\mathbf{E}_i = \hat{\mathbf{a}}_x E_0(x, y) e^{-jkz}$$

is incident upon a linearly polarized antenna whose electric-field polarization is expressed as

$$\mathbf{E}_a \simeq (\hat{\mathbf{a}}_x + \hat{\mathbf{a}}_y) E(r, \theta, \phi)$$

Find the polarization loss factor (PLF).

Solution: For the incident wave

$$\hat{\boldsymbol{\rho}}_w = \hat{\mathbf{a}}_x$$

and for the antenna

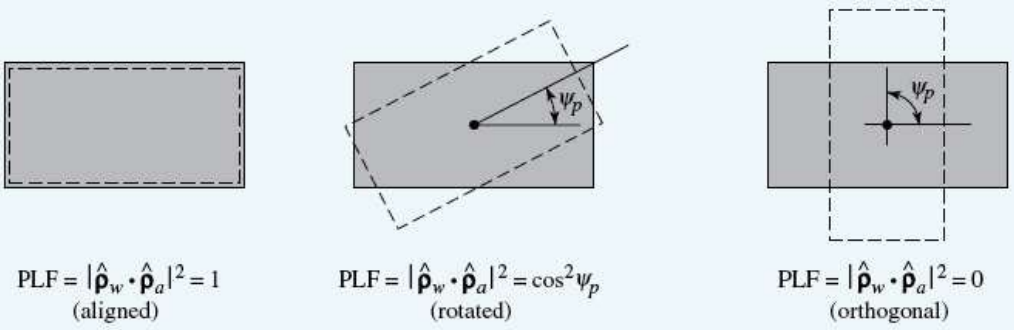
$$\hat{\boldsymbol{\rho}}_a = \frac{1}{\sqrt{2}}(\hat{\mathbf{a}}_x + \hat{\mathbf{a}}_y)$$

The PLF is then equal to

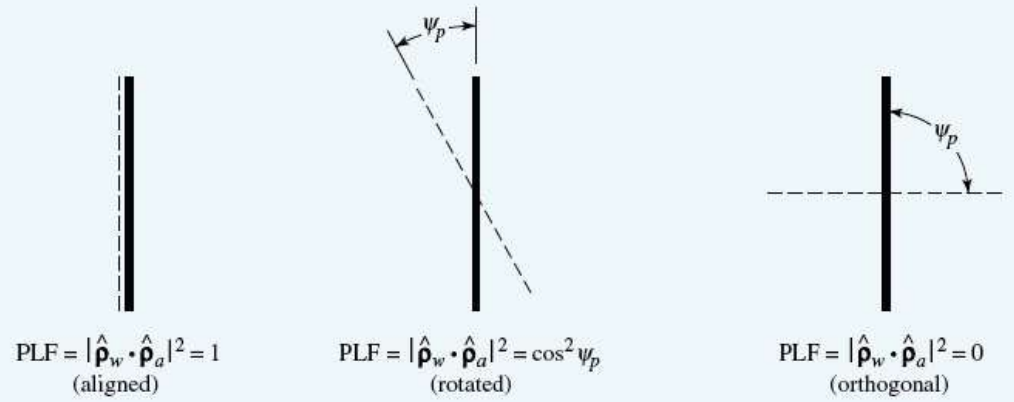
$$\text{PLF} = |\hat{\boldsymbol{\rho}}_w \cdot \hat{\boldsymbol{\rho}}_a|^2 = |\hat{\mathbf{a}}_x \cdot \frac{1}{\sqrt{2}}(\hat{\mathbf{a}}_x + \hat{\mathbf{a}}_y)|^2 = \tfrac{1}{2}$$

which in dB is equal to

$$\text{PLF (dB)} = 10 \log_{10} \text{PLF (dimensionless)} = 10 \log_{10}(0.5) = -3$$



(a) PLF for transmitting and receiving aperture antennas



(b) PLF for transmitting and receiving linear wire antennas

Figure 2.25 Polarization loss factors (PLF) for aperture and linear wire antennas.

Even though in Example 2.11 both the incoming wave and the antenna are linearly polarized, there is a 3-dB loss in extracted power because the polarization of the incoming wave is not aligned with the polarization of the antenna. If the polarization of the incoming wave is orthogonal to the polarization of the antenna, then there will be no power extracted by the antenna from the incoming wave and the PLF will be zero or $-\infty$ dB. In Figures 2.25(a,b) we illustrate the polarization loss factors (PLF) of two types of antennas: wires and apertures.

We now want to consider an example where the polarization of the antenna and the incoming wave are described in terms of complex polarization vectors.

Example 2.12

A right-hand (clockwise) circularly polarized wave radiated by an antenna, placed at some distance away from the origin of a spherical coordinate system, is traveling in the inward radial direction at an angle (θ, ϕ) and it is impinging upon a right-hand circularly polarized receiving antenna placed at the origin (see Figures 2.1 and 17.23 for the geometry of the coordinate system). The polarization of the receiving antenna is defined in the transmitting

mode, as desired by the definition of the IEEE. Assuming the polarization of the incident wave is represented by

$$\mathbf{E}_w = (\hat{\mathbf{a}}_\theta + j\hat{\mathbf{a}}_\phi)E(r, \theta, \phi)$$

Determine the polarization loss factor (PLF).

Solution: The polarization of the incident right-hand circularly polarized wave traveling along the $-r$ radial direction is described by the unit vector

$$\hat{\boldsymbol{\rho}}_w = \left(\frac{\hat{\mathbf{a}}_\theta + j\hat{\mathbf{a}}_\phi}{\sqrt{2}}\right)$$

while that of the receiving antenna, in the transmitting mode, is represented by the unit vector

$$\hat{\boldsymbol{\rho}}_a = \left(\frac{\hat{\mathbf{a}}_\theta - j\hat{\mathbf{a}}_\phi}{\sqrt{2}}\right)$$

Therefore the polarization loss factor is

$$\text{PLF} = |\hat{\boldsymbol{\rho}}_w \cdot \hat{\boldsymbol{\rho}}_a|^2 = \frac{1}{4}|1 + 1|^2 = 1 = 0 \text{ dB}$$

Since the polarization of the incoming wave matches (including the sense of rotation) the polarization of the receiving antenna, there should not be any losses. Obviously the answer matches the expectation.

Based upon the definitions of the wave transmitted and received by an antenna, the polarization of an antenna in the *receiving* mode is related to that in the *transmitting* mode as follows:

1. "In the same plane of polarization, the polarization ellipses have the same axial ratio, the same sense of polarization (rotation) and the same spatial orientation.
2. "Since their senses of polarization and spatial orientation are specified by viewing their polarization ellipses in the respective directions in which they are propagating, one should note that:
   a. Although their senses of polarization are the same, they would appear to be opposite if both waves were viewed in the same direction.
   b. Their tilt angles are such that they are the negative of one another with respect to a common reference."

Since the polarization of an antenna will almost always be defined in its transmitting mode, according to the IEEE Std 145-1983, "the receiving polarization may be used to specify the polarization characteristic of a nonreciprocal antenna which may transmit and receive arbitrarily different polarizations."

The polarization loss must always be taken into account in the link calculations design of a communication system because in some cases it may be a very critical factor. Link calculations of communication systems for outer space explorations are very stringent because of limitations in spacecraft weight. In such cases, power is a

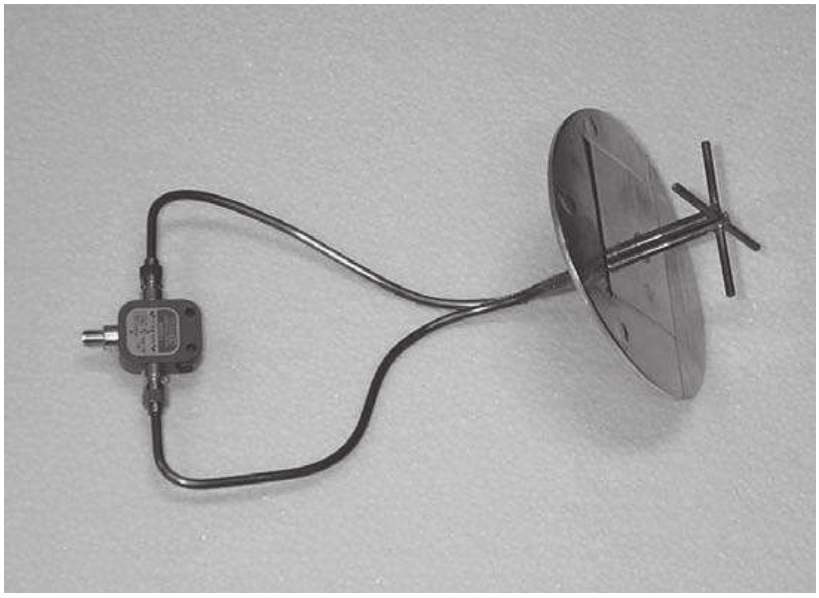


Figure 2.26 Geometry of elliptically polarized cross-dipole antenna.

limiting consideration. The design must properly take into account all loss factors to ensure a successful operation of the system.

An antenna that is elliptically polarized is that composed of two crossed dipoles, as shown in Figure 2.26. The two crossed dipoles provide the two orthogonal field components that are not necessarily of the same field intensity toward all observation angles. If the two dipoles are identical, the field intensity of each along zenith (perpendicular to the plane of the two dipoles) would be of the same intensity. Also, if the two dipoles were fed with a 90° degree time-phase difference (phase quadrature), the polarization along zenith would be circular and elliptical toward other directions. One way to obtain the 90° time-phase difference $\Delta\phi$ between the two orthogonal field components, radiated respectively by the two dipoles, is by feeding one of the two dipoles with a transmission line which is $\lambda/4$ longer or shorter than that of the other $[\Delta\phi = k\Delta\ell = (2\pi/\lambda)(\lambda/4) = \pi/2]$. One of the lengths (longer or shorter) will provide right-hand (CW) rotation while the other will provide left-hand (CCW) rotation.

2.13 INPUT IMPEDANCE

Input impedance is defined as "the impedance presented by an antenna at its terminals or the ratio of the voltage to current at a pair of terminals or the ratio of the appropriate components of the electric to magnetic fields at a point." In this section we are primarily interested in the input impedance at a pair of terminals which are the input terminals of the antenna. In Figure 2.27(a) these terminals are designated as $a - b$. The ratio of the voltage to current at these terminals, with no load attached, defines the impedance of the antenna as

$$\boxed{Z_A = R_A + jX_A} \tag{2-72}$$

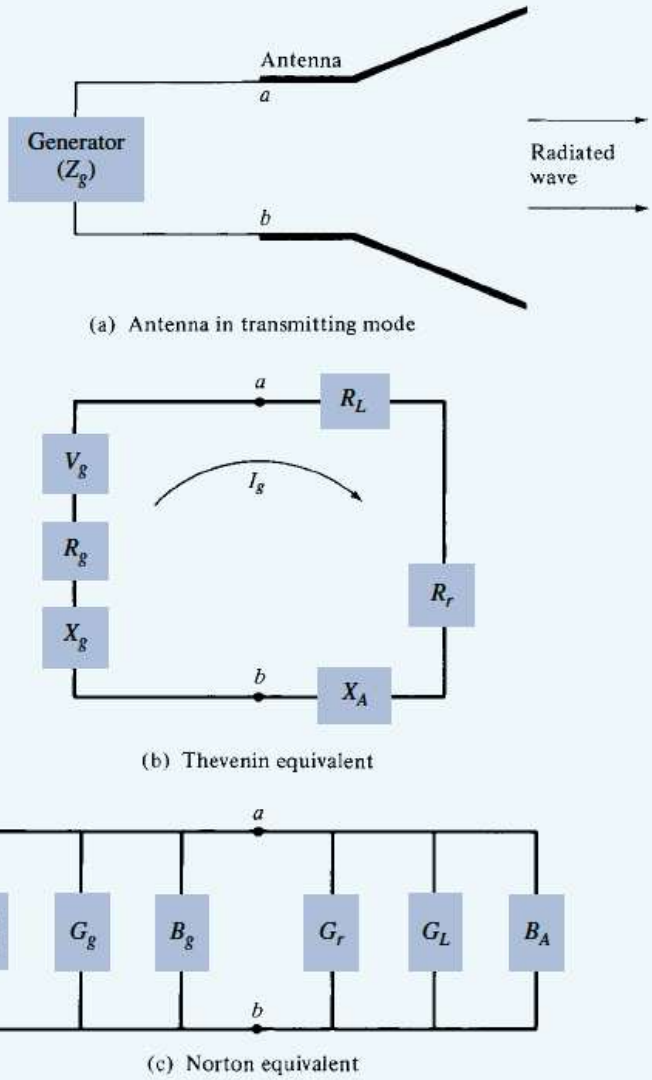


Figure 2.27 Transmitting antenna and its equivalent circuits.

where

Z_A = antenna impedance at terminals a–b (ohms)
R_A = antenna resistance at terminals a–b (ohms)
X_A = antenna reactance at terminals a–b (ohms)

In general the resistive part of (2-72) consists of two components; that is

$$\boxed{R_A = R_r + R_L} \tag{2-73}$$

where

R_r = radiation resistance of the antenna
R_L = loss resistance of the antenna

The radiation resistance will be considered in more detail in later chapters, and it will be illustrated with examples.

If we assume that the antenna is attached to a generator with internal impedance

$$Z_g = R_g + jX_g \tag{2-74}$$

where

R_g = resistance of generator impedance (ohms)
X_g = reactance of generator impedance (ohms)

and the antenna is used in the transmitting mode, we can represent the antenna and generator by an equivalent circuit* shown in Figure 2.27(b). To find the amount of power delivered to R_r for radiation and the amount dissipated in R_L as heat ($I^2R_L/2$), we first find the current developed within the loop which is given by

$$I_g = \frac{V_g}{Z_t} = \frac{V_g}{Z_A + Z_g} = \frac{V_g}{(R_r + R_L + R_g) + j(X_A + X_g)} \quad (A) \tag{2-75}$$

and its magnitude by

$$|I_g| = \frac{|V_g|}{[(R_r + R_L + R_g)^2 + (X_A + X_g)^2]^{1/2}} \tag{2-75a}$$

where V_g is the peak generator voltage. The power delivered to the antenna for radiation is given by

$$P_r = \frac{1}{2}|I_g|^2 R_r = \frac{|V_g|^2}{2}\left[\frac{R_r}{(R_r + R_L + R_g)^2 + (X_A + X_g)^2}\right] \quad (W) \tag{2-76}$$

and that dissipated as heat by

$$P_L = \frac{1}{2}|I_g|^2 R_L = \frac{|V_g|^2}{2}\left[\frac{R_L}{(R_r + R_L + R_g)^2 + (X_A + X_g)^2}\right] \quad (W) \tag{2-77}$$

The remaining power is dissipated as heat on the internal resistance R_g of the generator, and it is given by

$$P_g = \frac{|V_g|^2}{2}\left[\frac{R_g}{(R_r + R_L + R_g)^2 + (X_A + X_g)^2}\right] \quad (W) \tag{2-78}$$

The maximum power delivered to the antenna occurs when we have conjugate matching; that is when

$$R_r + R_L = R_g \tag{2-79}$$

$$X_A = -X_g \tag{2-80}$$

*This circuit can be used to represent small and simple antennas. It cannot be used for antennas with lossy dielectric or antennas over lossy ground because their loss resistance cannot be represented in series with the radiation resistance.

For this case

$$P_r = \frac{|V_g|^2}{2}\left[\frac{R_r}{4(R_r+R_L)^2}\right] = \frac{|V_g|^2}{8}\left[\frac{R_r}{(R_r+R_L)^2}\right] \tag{2-81}$$

$$P_L = \frac{|V_g|^2}{8}\left[\frac{R_L}{(R_r+R_L)^2}\right] \tag{2-82}$$

$$P_g = \frac{|V_g|^2}{8}\left[\frac{R_g}{(R_r+R_L)^2}\right] = \frac{|V_g|^2}{8}\left[\frac{1}{R_r+R_L}\right] = \frac{|V_g|^2}{8R_g} \tag{2-83}$$

From (2-81)–(2-83), it is clear that

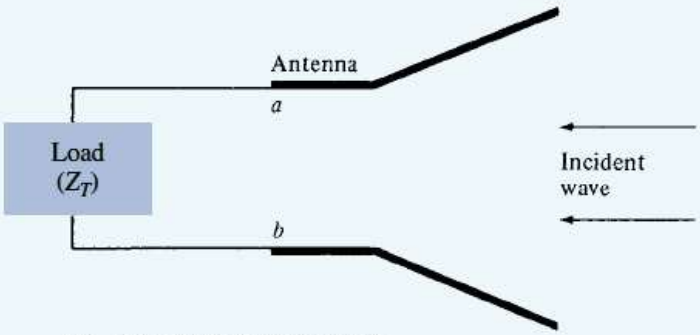
$$P_g = P_r + P_L = \frac{|V_g|^2}{8}\left[\frac{R_g}{(R_r+R_L)^2}\right] = \frac{|V_g|^2}{8}\left[\frac{R_r+R_L}{(R_r+R_L)^2}\right] \tag{2-84}$$

The power supplied by the generator during conjugate matching is

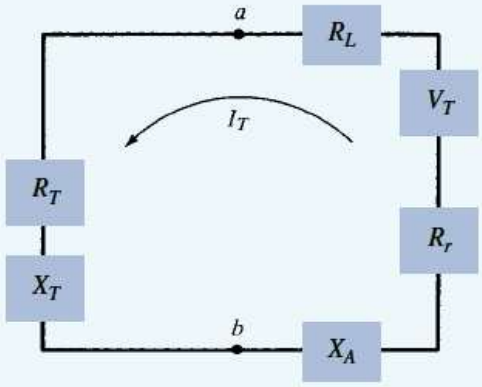
$$P_s = \frac{1}{2}V_g I_g^* = \frac{1}{2}V_g\left[\frac{V_g^*}{2(R_r+R_L)}\right] = \frac{|V_g|^2}{4}\left[\frac{1}{R_r+R_L}\right] \quad (W) \tag{2-85}$$

Of the power that is provided by the generator, half is dissipated as heat in the internal resistance (R_g) of the generator and the other half is delivered to the antenna. This only happens when we have *conjugate matching*. Of the power that is delivered to the antenna, part is radiated through the mechanism provided by the radiation resistance and the other is dissipated as heat which influences part of the overall efficiency of the antenna. If the antenna is lossless and matched to the transmission line ($e_o = 1$), then half of the total power supplied by the generator is radiated by the antenna during conjugate matching, and the other half is dissipated as heat in the generator. Thus, to radiate half of the available power through R_r you must dissipate the other half as heat in the generator through R_g. These two powers are, respectively, analogous to the power transferred to the load and the power scattered by the antenna in the receiving mode. In Figure 2.27 it is assumed that the generator is directly connected to the antenna. If there is a transmission line between the two, which is usually the case, then Z_g represents the equivalent impedance of the generator transferred to the input terminals of the antenna using the impedance transfer equation. If, in addition, the transmission line is lossy, then the available power to be radiated by the antenna will be reduced by the losses of the transmission line. Figure 2.27(c) illustrates the Norton equivalent of the antenna and its source in the transmitting mode.

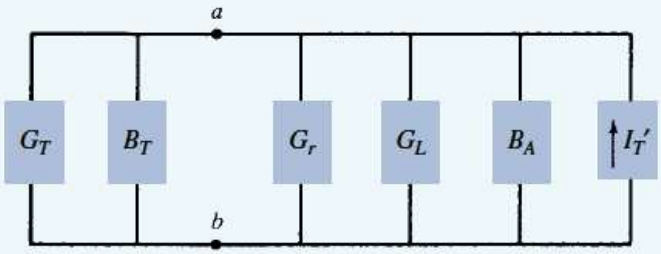
The use of the antenna in the receiving mode is shown in Figure 2.28(a). The incident wave impinges upon the antenna, and it induces a voltage V_T which is analogous to V_g of the transmitting mode. The Thevenin equivalent circuit of the antenna and its load is shown in Figure 2.28(b) and the Norton equivalent in Figure 2.28(c). The discussion for the antenna and its load in the receiving mode parallels that for the transmitting mode, and it will not be repeated here in detail. Some of the results will



(a) Antenna in receiving mode



(b) Thevenin equivalent



(c) Norton equivalent

Figure 2.28 Antenna and its equivalent circuits in the receiving mode.

be summarized in order to discuss some subtle points. Following a procedure similar to that for the antenna in the transmitting mode, it can be shown using Figure 2.28 that in the receiving mode under conjugate matching ($R_r + R_L = R_T$ and $X_A = -X_T$) the powers delivered to R_T, R_r, and R_L are given, respectively, by

$$P_T = \frac{|V_T|^2}{8}\left[\frac{R_T}{(R_r + R_L)^2}\right] = \frac{|V_T|^2}{8}\left(\frac{1}{R_r + R_L}\right) = \frac{|V_T|^2}{8R_T} \tag{2-86}$$

$$P_r = \frac{|V_T|^2}{2}\left[\frac{R_r}{4(R_r + R_L)^2}\right] = \frac{|V_T|^2}{8}\left[\frac{R_r}{(R_r + R_L)^2}\right] \tag{2-87}$$

$$P_L = \frac{|V_T|^2}{8}\left[\frac{R_L}{(R_r + R_L)^2}\right] \tag{2-88}$$

while the *induced* (*collected* or *captured*) is

$$P_c = \frac{1}{2} V_T I_T^* = \frac{1}{2} V_T \left[\frac{V_T^*}{2(R_r + R_L)} \right] = \frac{|V_T|^2}{4} \left(\frac{1}{R_r + R_L} \right) \tag{2-89}$$

These are analogous, respectively, to (2-81)–(2-83) and (2-85). The power P_r of (2-87) delivered to R_r is referred to as *scattered* (or *reradiated*) power. It is clear through (2-86)–(2-89) that under conjugate matching of the total power collected or captured [P_c of (2-89)] half is delivered to the load R_T [P_T of (2-86)] and the other half is scattered or reradiated through R_r [P_r of (2-87)] and dissipated as heat through R_L [P_L of (2-88)]. If the losses are zero ($R_L = 0$), then half of the captured power is delivered to the load and the other half is scattered. This indicates that in order to deliver half of the power to the load you must scatter the other half. This becomes important when discussing effective equivalent areas and aperture efficiencies, especially for high directivity aperture antennas such as waveguides, horns, and reflectors with aperture efficiencies as high as 80 to 90%. Aperture efficiency (ϵ_{ap}) is defined by (2-100) and is the ratio of the maximum effective area to the physical area. The effective area is used to determine the power delivered to the load, which under conjugate matching is only one-half of that intercepted; the other half is scattered and dissipated as heat. For a lossless antenna ($R_L = 0$) under conjugate matching, the maximum value of the effective area is equal to the physical area ($\epsilon_{ap} = 1$) and the scattering area is also equal to the physical area. Thus half of the power is delivered to the load and the other half is scattered. Using (2-86) to (2-89) we conclude that even though the aperture efficiencies are higher than 50% (they can be as large as 100%) all of the power that is captured by the antenna is not delivered to the load but it includes that which is scattered plus dissipated as heat by the antenna. The most that can be delivered to the load is only half of that captured and that is only under conjugate matching and lossless transmission line.

The input impedance of an antenna is generally a function of frequency. Thus the antenna will be matched to the interconnecting transmission line and other associated equipment only within a bandwidth. In addition, the input impedance of the antenna depends on many factors including its geometry, its method of excitation, and its proximity to surrounding objects. Because of their complex geometries, only a limited number of practical antennas have been investigated analytically. For many others, the input impedance has been determined experimentally.

2.14 ANTENNA RADIATION EFFICIENCY

The antenna efficiency that takes into account the reflection, conduction, and dielectric losses was discussed in Section 2.8. The conduction and dielectric losses of an antenna are very difficult to compute and in most cases they are measured. Even with measurements, they are difficult to separate and they are usually lumped together to form the e_{cd} efficiency. The resistance R_L is used to represent the conduction-dielectric losses.

The *conduction-dielectric efficiency* e_{cd} is defined as *the ratio of the power delivered to the radiation resistance* R_r *to the power delivered to* R_r *and* R_L. Using (2-76) and

(2-77), the radiation efficiency can be written as

$$\boxed{e_{cd} = \left[\frac{R_r}{R_L + R_r}\right]} \quad \text{(dimensionless)} \tag{2-90}$$

For a metal rod of length l and uniform cross-sectional area A, the dc resistance is given by

$$R_{dc} = \frac{1}{\sigma}\frac{l}{A} \quad \text{(ohms)} \tag{2-90a}$$

If the skin depth $\delta[\delta = \sqrt{2/(\omega\mu_0\sigma)}]$ of the metal is very small compared to the smallest diagonal of the cross section of the rod, the current is confined to a thin layer near the conductor surface. Therefore the high-frequency resistance can be written, based on a *uniform current distribution*, as

$$R_{hf} = \frac{l}{P}R_s = \frac{l}{P}\sqrt{\frac{\omega\mu_0}{2\sigma}} \quad \text{(ohms)} \tag{2-90b}$$

where P is the perimeter of the cross section of the rod ($P = C = 2\pi b$ for a circular wire of radius b), R_s is the conductor surface resistance, ω is the angular frequency, μ_0 is the permeability of free-space, and σ is the conductivity of the metal.

Example 2.13

A resonant half-wavelength dipole is made out of copper ($\sigma = 5.7 \times 10^7$S/m) wire. Determine the conduction-dielectric (radiation) efficiency of the dipole antenna at $f = 100$ MHz if the radius of the wire b is $3 \times 10^{-4}\lambda$, and the radiation resistance of the $\lambda/2$ dipole is 73 ohms.

Solution: At $f = 10^8$ Hz

$$\lambda = \frac{v}{f} = \frac{3 \times 10^8}{10^8} = 3 \text{ m}$$

$$l = \frac{\lambda}{2} = \frac{3}{2}\text{m}$$

$$C = 2\pi b = 2\pi(3 \times 10^{-4})\lambda = 6\pi \times 10^{-4}\lambda$$

For a $\lambda/2$ dipole with a sinusoidal current distribution $R_L = \frac{1}{2}R_{hf}$ where R_{hf} is given by (2-90b). See Problem 2.52. Therefore,

$$R_L = \frac{1}{2}R_{hf} = \frac{0.25}{6\pi \times 10^{-4}}\sqrt{\frac{\pi(10^8)(4\pi \times 10^{-7})}{5.7 \times 10^7}} = 0.349 \text{ ohms}$$

Thus,

$$e_{cd}(\text{dimensionless}) = \frac{73}{73 + 0.349} = 0.9952 = 99.52\%$$

$$e_{cd}(\text{dB}) = 10\log_{10}(0.9905) = -0.02$$

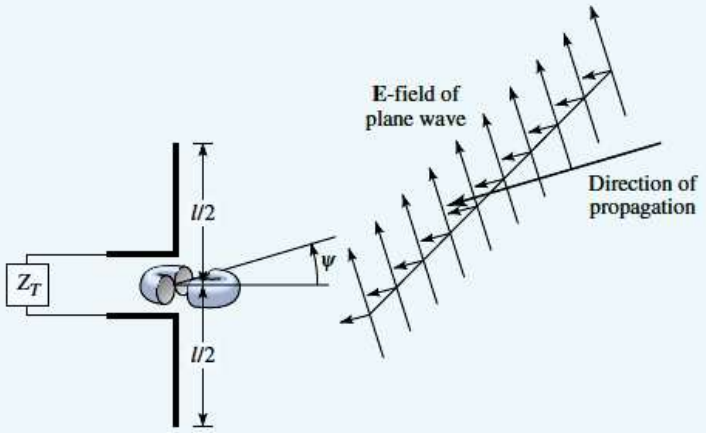
2.15 ANTENNA VECTOR EFFECTIVE LENGTH AND EQUIVALENT AREAS

An antenna in the receiving mode, whether it is in the form of a wire, horn, aperture, array, dielectric rod, etc., is used to capture (collect) electromagnetic waves and to extract power from them, as shown in Figures 2.29(a) and (b). For each antenna, an equivalent length and a number of equivalent areas can then be defined.

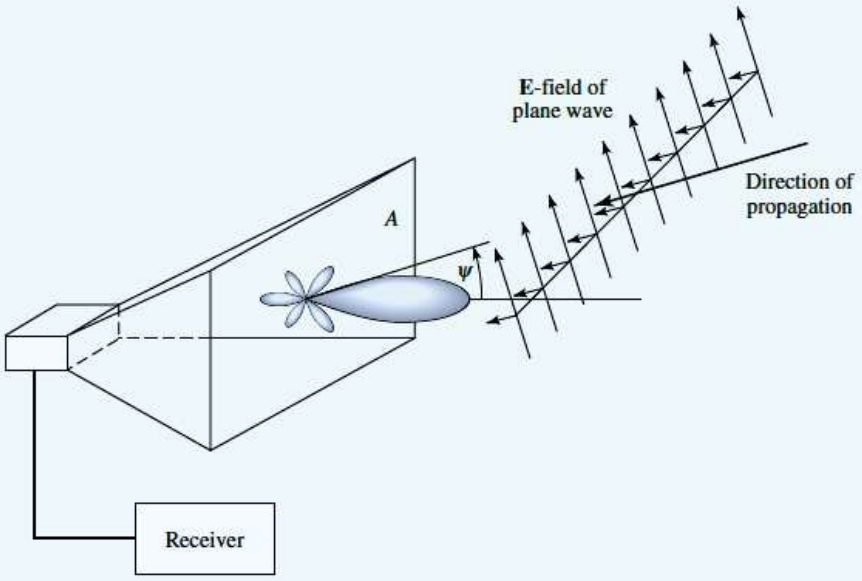
These equivalent quantities are used to describe the receiving characteristics of an antenna, whether it be a linear or an aperture type, when a wave is incident upon the antenna.

2.15.1 Vector Effective Length

The effective length of an antenna, whether it be a linear or an aperture antenna, is a quantity that is used to determine the voltage induced on the open-circuit terminals



(a) Dipole antenna in receiving mode



(b) Aperture antenna in receiving mode

Figure 2.29 Uniform plane wave incident upon dipole and aperture antennas.

of the antenna when a wave impinges upon it. The vector effective length $\boldsymbol{\ell}_e$ for an antenna is usually a complex vector quantity represented by

$$\boldsymbol{\ell}_e(\theta, \phi) = \hat{\mathbf{a}}_\theta l_\theta(\theta, \phi) + \hat{\mathbf{a}}_\phi l_\phi(\theta, \phi) \tag{2-91}$$

It should be noted that it is also referred to as the *effective height*. It is a far-field quantity and it is related to the *far-zone* field $\mathbf{E}_a$ radiated by the antenna, with current I_{in} in its terminals, by [13]–[18]

$$\mathbf{E}_a = \hat{\mathbf{a}}_\theta E_\theta + \hat{\mathbf{a}}_\phi E_\phi = -j\eta \frac{kI_{in}}{4\pi r} \boldsymbol{\ell}_e e^{-jkr} \tag{2-92}$$

The effective length represents the antenna in its transmitting and receiving modes, and it is particularly useful in relating the open-circuit voltage V_{oc} of receiving antennas. This relation can be expressed as

$$V_{oc} = \mathbf{E}^i \cdot \boldsymbol{\ell}_e \tag{2-93}$$

where

V_{oc} = open-circuit voltage at antenna terminals
$\mathbf{E}^i$ = incident electric field
$\boldsymbol{\ell}_e$ = vector effective length

In (2-93) V_{oc} can be thought of as the voltage induced in a linear antenna of length ℓ_e when $\boldsymbol{\ell}_e$ and $\mathbf{E}^i$ are linearly polarized [19], [20]. From the relation of (2-93) the *effective length of a linearly polarized antenna receiving a plane wave in a given direction* is defined as "the ratio of the magnitude of the open-circuit voltage developed at the terminals of the antenna to the magnitude of the electric-field strength in the direction of the antenna polarization. Alternatively, the effective length is the length of a thin straight conductor oriented perpendicular to the given direction and parallel to the antenna polarization, having a uniform current equal to that at the antenna terminals and producing the same far-field strength as the antenna in that direction."

In addition, as shown in Section 2.12.2, the antenna vector effective length is used to determine the polarization efficiency of the antenna. To illustrate the usefulness of the vector effective length, let us consider an example.

Example 2.14

The far-zone field radiated by a small dipole of length $l < \lambda/10$ and with a triangular current distribution, as shown in Figure 4.4, is derived in Section 4.3 of Chapter 4 and it is given by (4-36a), or

$$\mathbf{E}_a = \hat{\mathbf{a}}_\theta j\eta \frac{kI_{in} l e^{-jkr}}{8\pi r} \sin\theta$$

Determine the vector effective length of the antenna.

Solution: According to (2-92), the vector effective length is

$$\boldsymbol{\ell}_e = -\hat{\mathbf{a}}_\theta \frac{l}{2} \sin\theta$$

This indicates, as it should, that the effective length is a function of the direction angle θ, and its maximum occurs when $\theta = 90^\circ$. This tells us that the maximum open-circuit voltage at the dipole terminals occurs when the incident direction of the wave of Figure 2.29(a) impinging upon the small dipole antenna is normal to the axis (length) of the dipole ($\theta = 90^\circ$). This is expected since the dipole has a radiation pattern whose maximum is in the $\theta = 90^\circ$. In addition, the effective length of the dipole to produce the same output open-circuit voltage is only half (50%) of its physical length if it were replaced by a thin conductor having a uniform current distribution (it can be shown that the maximum effective length of an element with an ideal uniform current distribution is equal to its physical length).

2.15.2 Antenna Equivalent Areas

With each antenna, we can associate a number of equivalent areas. These are used to describe the power capturing characteristics of the antenna when a wave impinges on it. One of these equivalent areas is the *effective area (aperture)*, which in a given direction is defined as "the ratio of the available power at the terminals of a receiving antenna to the power flux density of a plane wave incident on the antenna from that direction, the wave being polarization-matched to the antenna. If the direction is not specified, the direction of maximum radiation intensity is implied." In equation form it is written as

$$A_e = \frac{P_T}{W_i} = \frac{|I_T|^2 R_T/2}{W_i} \tag{2-94}$$

where

A_e = effective area (effective aperture) (m^2)
P_T = power delivered to the load (W)
W_i = power density of incident wave (W/m^2)

The effective aperture is the area which when multiplied by the incident power density gives the power delivered to the load. Using the equivalent of Figure 2.28, we can write (2-94) as

$$A_e = \frac{|V_T|^2}{2W_i}\left[\frac{R_T}{(R_r + R_L + R_T)^2 + (X_A + X_T)^2}\right] \tag{2-95}$$

Under conditions of maximum power transfer (*conjugate matching*), $R_r + R_L = R_T$ and $X_A = -X_T$, the effective area of (2-95) reduces to the maximum effective aperture given by

$$A_{em} = \frac{|V_T|^2}{8W_i}\left[\frac{R_T}{(R_L + R_r)^2}\right] = \frac{|V_T|^2}{8W_i}\left[\frac{1}{R_r + R_L}\right] \tag{2-96}$$

When (2-96) is multiplied by the incident power density, it leads to the maximum power delivered to the load of (2-86).

All of the power that is intercepted, collected, or captured by an antenna is not delivered to the load, as we have seen using the equivalent circuit of Figure 2.28. In fact, under conjugate matching only half of the captured power is delivered to the load; the other half is scattered and dissipated as heat. Therefore to account for the

scattered and dissipated power we need to define, in addition to the effective area, the *scattering, loss* and *capture* equivalent areas. In equation form these can be defined similarly to (2-94)–(2-96) for the effective area.

The *scattering area* is defined as the equivalent area when multiplied by the incident power density is equal to the scattered or reradiated power. Under conjugate matching this is written, similar to (2-96), as

$$A_s = \frac{|V_T|^2}{8W_i}\left[\frac{R_r}{(R_L + R_r)^2}\right] \tag{2-97}$$

which when multiplied by the incident power density gives the scattering power of (2-87).

The *loss area* is defined as the equivalent area, which when multiplied by the incident power density leads to the power dissipated as heat through R_L. Under conjugate matching this is written, similar to (2-96), as

$$A_L = \frac{|V_T|^2}{8W_i}\left[\frac{R_L}{(R_L + R_r)^2}\right] \tag{2-98}$$

which when multiplied by the incident power density gives the dissipated power of (2-88).

Finally the *capture area* is defined as the equivalent area, which when multiplied by the incident power density leads to the total power captured, collected, or intercepted by the antenna. Under conjugate matching this is written, similar to (2-96), as

$$A_c = \frac{|V_T|^2}{8W_i}\left[\frac{R_T + R_r + R_L}{(R_L + R_r)^2}\right] \tag{2-99}$$

When (2-99) is multiplied by the incident power density, it leads to the captured power of (2-89). In general, the total capture area is equal to the sum of the other three, or

$$\textit{Capture Area} = \textit{Effective Area} + \textit{Scattering Area} + \textit{Loss Area}$$

This is apparent under conjugate matching using (2-96)–(2-99). However, it holds even under nonconjugate matching conditions.

Now that the equivalent areas have been defined, let us introduce the *aperture efficiency* ϵ_{ap} of an antenna, which is defined as the ratio of the maximum effective area A_{em} of the antenna to its physical area A_p, or

$$\epsilon_{ap} = \frac{A_{em}}{A_p} = \frac{\text{maximum effective area}}{\text{physical area}} \tag{2-100}$$

For aperture type antennas, such as waveguides, horns, and reflectors, the maximum effective area cannot exceed the physical area but it can equal it ($A_{em} \leq A_p$ or $0 \leq \epsilon_{ap} \leq 1$). Therefore the maximum value of the aperture efficiency cannot exceed unity (100%). For a lossless antenna ($R_L = 0$) the maximum value of the scattering area is also equal to the physical area. Therefore even though the aperture efficiency is greater than 50%, for a lossless antenna under conjugate matching only half of the captured power is delivered to the load and the other half is scattered.

We can also introduce a *partial effective area* of an antenna *for a given polarization* in a given direction, which is defined as "the ratio of the available power at the terminals of a receiving antenna to the power flux density of a plane wave incident on the antenna from that direction and with a specified polarization differing from the receiving polarization of the antenna."

The effective area of an antenna is not necessarily the same as the physical aperture. It will be shown in later chapters that aperture antennas with uniform amplitude and phase field distributions have maximum effective areas equal to the physical areas; they are smaller for nonuniform field distributions. In addition, the maximum effective area of wire antennas is greater than the physical area (if taken as the area of a cross section of the wire when split lengthwise along its diameter). Thus the wire antenna can capture much more power than is intercepted by its physical size! This should not come as a surprise. If the wire antenna would only capture the power incident on its physical size, it would be almost useless. So electrically, the wire antenna looks much bigger than its physical stature.

To illustrate the concept of effective area, especially as applied to a wire antenna, let us consider an example. In later chapters, we will consider examples of aperture antennas.

Example 2.15

A uniform plane wave is incident upon a very short lossless dipole ($l \ll \lambda$), as shown in Figure 2.29(a). Find the maximum effective area assuming that the radiation resistance of the dipole is $R_r = 80(\pi l/\lambda)^2$, and the incident field is linearly polarized along the axis of the dipole.

Solution: For $R_L = 0$, the maximum effective area of (2-96) reduces to

$$A_{em} = \frac{|V_T|^2}{8W_i}\left[\frac{1}{R_r}\right]$$

Since the dipole is very short, the induced current can be assumed to be constant and of uniform phase. The induced voltage is

$$V_T = El$$

where

$V_T =$ induced voltage on the dipole
$E =$ electric field of incident wave
$l =$ length of dipole

For a uniform plane wave, the incident power density can be written as

$$W_i = \frac{E^2}{2\eta}$$

where η is the intrinsic impedance of the medium ($\simeq 120\pi$ ohms for a free-space medium). Thus

$$A_{em} = \frac{(El)^2}{8(E^2/2\eta)(80\pi^2 l^2/\lambda^2)} = \frac{3\lambda^2}{8\pi} = 0.119\lambda^2$$

The above value is only valid for a lossless antenna (the losses of a short dipole are usually significant). If the loss resistance is equal to the radiation resistance ($R_L = R_r$) and the sum of the two is equal to the load (receiver) resistance ($R_T = R_r + R_L = 2R_r$), then the effective area is only one-half of the maximum effective area given above.

Let us now examine the significance of the effective area. From Example 2.15, the maximum effective area of a short dipole with $l \ll \lambda$ was equal to $A_{em} = 0.119\lambda^2$. Typical antennas that fall under this category are dipoles whose lengths are $l \leq \lambda/50$. For the purpose of demonstration, let us assume that $l = \lambda/50$. Because $A_{em} = 0.119\lambda^2 = lw_e = (\lambda/50)w_e$, the maximum effective electrical width of this dipole is $w_e = 5.95\lambda$. Typical physical diameters (widths) of wires used for dipoles may be about $w_p = \lambda/300$. Thus the maximum effective width w_e is about 1,785 times larger than its physical width.

2.16 MAXIMUM DIRECTIVITY AND MAXIMUM EFFECTIVE AREA

To derive the relationship between directivity and maximum effective area, the geometrical arrangement of Figure 2.30 is chosen. Antenna 1 is used as a transmitter and 2 as a receiver. The effective areas and directivities of each are designated as A_t, A_r and D_t, D_r. If antenna 1 were isotropic, its radiated power density at a distance R would be

$$W_0 = \frac{P_t}{4\pi R^2} \tag{2-101}$$

where P_t is the total radiated power. Because of the directive properties of the antenna, its actual density is

$$W_t = W_0 D_t = \frac{P_t D_t}{4\pi R^2} \tag{2-102}$$

The power collected (received) by the antenna and transferred to the load would be

$$P_r = W_t A_r = \frac{P_t D_t A_r}{4\pi R^2} \tag{2-103}$$

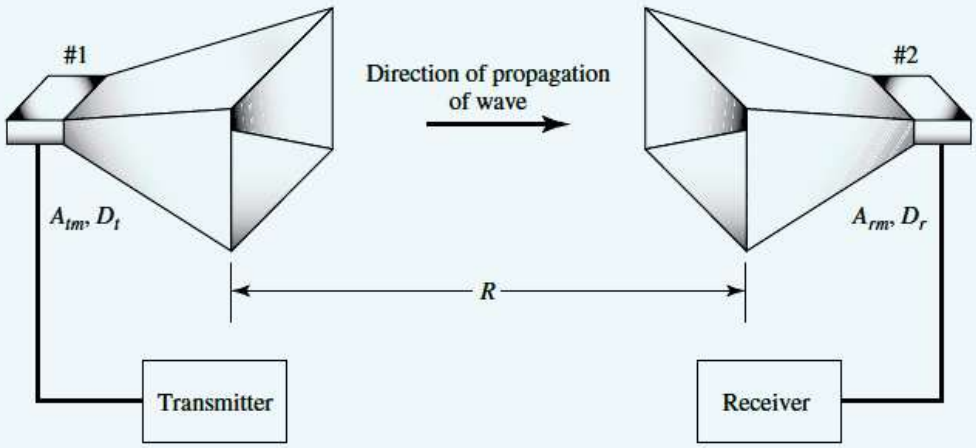


Figure 2.30 Two antennas separated by a distance R.

EX2042
Page 105 of 1072

or

$$D_t A_r = \frac{P_r}{P_t}(4\pi R^2) \tag{2-103a}$$

If antenna 2 is used as a transmitter, 1 as a receiver, and the intervening medium is linear, passive, and isotropic, we can write that

$$D_r A_t = \frac{P_r}{P_t}(4\pi R^2) \tag{2-104}$$

Equating (2-103a) and (2-104) reduces to

$$\frac{D_t}{A_t} = \frac{D_r}{A_r} \tag{2-105}$$

Increasing the directivity of an antenna increases its effective area in direct proportion. Thus, (2-105) can be written as

$$\frac{D_{0t}}{A_{tm}} = \frac{D_{0r}}{A_{rm}} \tag{2-106}$$

where A_{tm} and A_{rm} (D_{0t} and D_{0r}) are the *maximum* effective areas (directivities) of antennas 1 and 2, respectively.

If antenna 1 is isotropic, then $D_{0t} = 1$ and its maximum effective area can be expressed as

$$A_{tm} = \frac{A_{rm}}{D_{0r}} \tag{2-107}$$

Equation (2-107) states that the maximum effective area of an isotropic source is equal to the ratio of the maximum effective area to the maximum directivity of any other source. For example, let the other antenna be a very short ($l \ll \lambda$) dipole whose effective area ($0.119\lambda^2$ from Example 2.15) and maximum directivity (1.5) are known.

The maximum effective area of the isotropic source is then equal to

$$A_{tm} = \frac{A_{rm}}{D_{0r}} = \frac{0.119\lambda^2}{1.5} = \frac{\lambda^2}{4\pi} \tag{2-108}$$

Using (2-108), we can write (2-107) as

$$A_{rm} = D_{0r} A_{tm} = D_{0r}\left(\frac{\lambda^2}{4\pi}\right) \tag{2-109}$$

In general then, the *maximum effective aperture* (A_{em}) *of any antenna is related to its maximum directivity* (D_0) *by*

$$\boxed{A_{em} = \frac{\lambda^2}{4\pi} D_0} \tag{2-110}$$

Thus, when (2-110) is multiplied by the power density of the incident wave it leads to the maximum power that can be delivered to the load. This assumes that there are no

conduction-dielectric losses (radiation efficiency e_{cd} is unity), the antenna is matched to the load (reflection efficiency e_r is unity), and the polarization of the impinging wave matches that of the antenna (polarization loss factor PLF and polarization efficiency p_e are unity). If there are losses associated with an antenna, its maximum effective aperture of (2-110) must be modified to account for conduction-dielectric losses (radiation efficiency). Thus,

$$A_{em} = e_{cd}\left(\frac{\lambda^2}{4\pi}\right) D_0 \tag{2-111}$$

The maximum value of (2-111) assumes that the antenna is matched to the load and the incoming wave is polarization-matched to the antenna. If reflection and polarization losses are also included, then the maximum effective area of (2-111) is represented by

$$\begin{aligned} A_{em} &= e_0\left(\frac{\lambda^2}{4\pi}\right) D_0 |\hat{\boldsymbol{\rho}}_w \cdot \hat{\boldsymbol{\rho}}_a|^2 \\ &= e_{cd}(1 - |\Gamma|^2)\left(\frac{\lambda^2}{4\pi}\right) D_0 |\hat{\boldsymbol{\rho}}_w \cdot \hat{\boldsymbol{\rho}}_a|^2 \end{aligned} \tag{2-112}$$

2.17 FRIIS TRANSMISSION EQUATION AND RADAR RANGE EQUATION

The analysis and design of radar and communications systems often require the use of the *Friis Transmission Equation* and the *Radar Range Equation*. Because of the importance [21] of the two equations, a few pages will be devoted for their derivation.

2.17.1 Friis Transmission Equation

The Friis Transmission Equation relates the power received to the power transmitted between two antennas separated by a distance $R > 2D^2/\lambda$, where D is the largest dimension of either antenna. Referring to Figure 2.31, let us assume that the transmitting antenna is initially isotropic. If the input power at the terminals of the transmitting antenna is P_t, then its isotropic power density W_0 at distance R from the antenna is

$$W_0 = e_t \frac{P_t}{4\pi R^2} \tag{2-113}$$

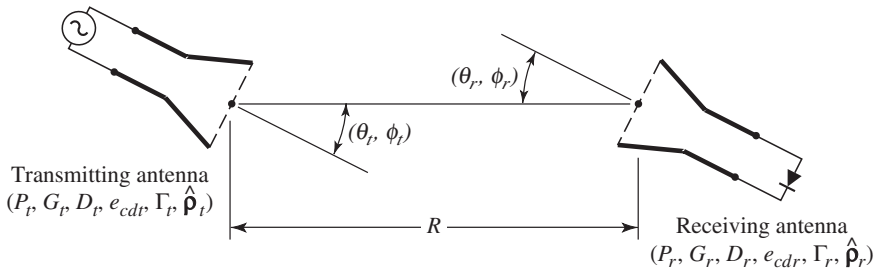


Figure 2.31 Geometrical orientation of transmitting and receiving antennas for Friis transmission equation.

where e_t is the radiation efficiency of the transmitting antenna. For a nonisotropic transmitting antenna, the power density of (2-113) in the direction θ_t, ϕ_t can be written as

$$W_t = \frac{P_t G_t(\theta_t, \phi_t)}{4\pi R^2} = e_t \frac{P_t D_t(\theta_t, \phi_t)}{4\pi R^2} \tag{2-114}$$

where $G_t(\theta_t, \phi_t)$ is the gain and $D_t(\theta_t, \phi_t)$ is the directivity of the transmitting antenna in the direction θ_t, ϕ_t. Since the effective area A_r of the receiving antenna is related to its efficiency e_r and directivity D_r by

$$A_r = e_r D_r(\theta_r, \phi_r) \left(\frac{\lambda^2}{4\pi}\right) \tag{2-115}$$

the amount of power P_r collected by the receiving antenna can be written, using (2-114) and (2-115), as

$$P_r = e_r D_r(\theta_r, \phi_r) \frac{\lambda^2}{4\pi} W_t = e_t e_r \frac{\lambda^2 D_t(\theta_t, \phi_t) D_r(\theta_r, \phi_r) P_t}{(4\pi R)^2} |\hat{\boldsymbol{\rho}}_t \cdot \hat{\boldsymbol{\rho}}_r|^2 \tag{2-116}$$

or the ratio of the received to the input power as

$$\boxed{\frac{P_r}{P_t} = e_t e_r \frac{\lambda^2 D_t(\theta_t, \phi_t) D_r(\theta_r, \phi_r)}{(4\pi R)^2}} \tag{2-117}$$

The power received based on (2-117) assumes that the transmitting and receiving antennas are matched to their respective lines or loads (reflection efficiencies are unity) and the polarization of the receiving antenna is polarization-matched to the impinging wave (polarization loss factor and polarization efficiency are unity). If these two factors are also included, then the ratio of the received to the input power of (2-117) is represented by

$$\boxed{\frac{P_r}{P_t} = e_{cdt} e_{cdr} (1 - |\Gamma_t|^2)(1 - |\Gamma_r|^2) \left(\frac{\lambda}{4\pi R}\right)^2 D_t(\theta_t, \phi_t) D_r(\theta_r, \phi_r) |\hat{\boldsymbol{\rho}}_t \cdot \hat{\boldsymbol{\rho}}_r|^2} \tag{2-118}$$

For reflection and polarization-matched antennas aligned for maximum directional radiation and reception, (2-118) reduces to

$$\boxed{\frac{P_r}{P_t} = \left(\frac{\lambda}{4\pi R}\right)^2 G_{0t} G_{0r}} \tag{2-119}$$

Equations (2-117), (2-118), or (2-119) are known as the *Friis Transmission Equation*, and it relates the power P_r (delivered to the receiver load) to the input power of the

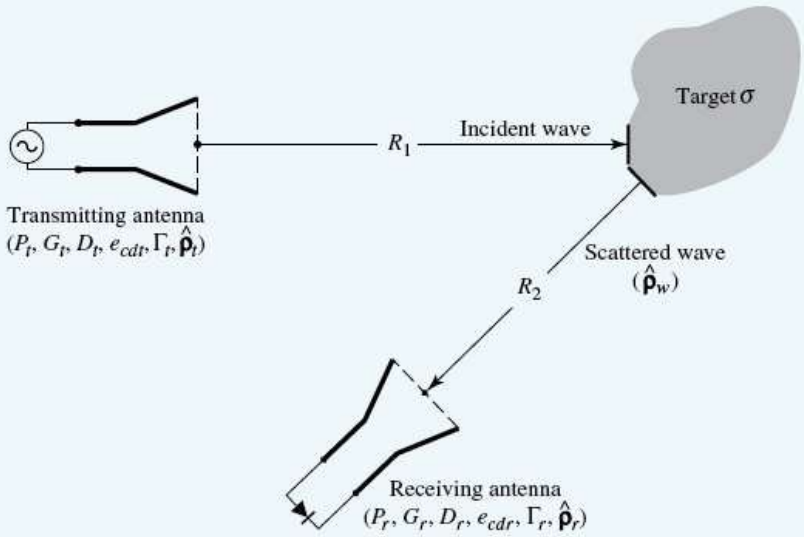


Figure 2.32 Geometrical arrangement of transmitter, target, and receiver for radar range equation.

transmitting antenna P_t. The term $(\lambda/4\pi R)^2$ is called the *free-space loss factor*, and it takes into account the losses due to the spherical spreading of the energy by the antenna.

2.17.2 Radar Range Equation

Now let us assume that the transmitted power is incident upon a target, as shown in Figure 2.32. We now introduce a quantity known as the *radar cross section* or *echo area* (σ) of a target which is defined as *the area intercepting that amount of power which, when scattered isotropically, produces at the receiver a density which is equal to that scattered by the actual target* [13]. In equation form

$$\lim_{R\to\infty}\left[\frac{\sigma W_i}{4\pi R^2}\right] = W_s \tag{2-120}$$

or

$$\boxed{\begin{aligned}\sigma &= \lim_{R\to\infty}\left[4\pi R^2\frac{W_s}{W_i}\right] = \lim_{R\to\infty}\left[4\pi R^2\frac{|\mathbf{E}^s|^2}{|\mathbf{E}^i|^2}\right]\\ &= \lim_{R\to\infty}\left[4\pi R^2\frac{|\mathbf{H}^s|^2}{|\mathbf{H}^i|^2}\right]\end{aligned}} \tag{2-120a}$$

where

σ = radar cross section or echo area (m^2)
R = observation distance from target (m)
W_i = incident power density (W/m^2)
W_s = scattered power density (W/m^2)
$\mathbf{E}^i$ ($\mathbf{E}^s$) = incident (scattered) electric field (V/m)
$\mathbf{H}^i$ ($\mathbf{H}^s$) = incident (scattered) magnetic field (A/m)

EX2042
Page 109 of 1072

Any of the definitions in (2-120a) can be used to derive the radar cross section of any antenna or target. For some polarization one of the definitions based either on the power density, electric field, or magnetic field may simplify the derivation, although all should give the same answers [13].

Using the definition of radar cross section, we can consider that the transmitted power incident upon the target is initially captured and then it is reradiated isotropically, insofar as the receiver is concerned. The amount of captured power P_c is obtained by multiplying the incident power density of (2-114) by the radar cross section σ, or

$$P_c = \sigma W_t = \sigma \frac{P_t G_t(\theta_t, \phi_t)}{4\pi R_1^2} = e_t \sigma \frac{P_t D_t(\theta_t, \phi_t)}{4\pi R_1^2} \tag{2-121}$$

The power captured by the target is reradiated isotropically, and the scattered power density can be written as

$$W_s = \frac{P_c}{4\pi R_2^2} = e_{cdt} \sigma \frac{P_t D_t(\theta_t, \phi_t)}{(4\pi R_1 R_2)^2} \tag{2-122}$$

The amount of power delivered to the receiver load is given by

$$P_r = A_r W_s = e_{cdt} e_{cdr} \sigma \frac{P_t D_t(\theta_t, \phi_t) D_r(\theta_r, \phi_r)}{4\pi} \left(\frac{\lambda}{4\pi R_1 R_2} \right)^2 \tag{2-123}$$

where A_r is the effective area of the receiving antenna as defined by (2-115).

Equation (2-123) can be written as the ratio of the received power to the input power, or

$$\boxed{\frac{P_r}{P_t} = e_{cdt} e_{cdr} \sigma \frac{D_t(\theta_t, \phi_t) D_r(\theta_r, \phi_r)}{4\pi} \left(\frac{\lambda}{4\pi R_1 R_2} \right)^2} \tag{2-124}$$

Expression (2-124) is used to relate the received power to the input power, and it takes into account only conduction-dielectric losses (radiation efficiency) of the transmitting and receiving antennas. It does not include reflection losses (reflection efficiency) and polarization losses (polarization loss factor or polarization efficiency). If these two losses are also included, then (2-124) must be expressed as

$$\boxed{\begin{aligned} \frac{P_r}{P_t} = e_{cdt} e_{cdr} (1 - |\Gamma_t|^2)(1 - |\Gamma_r|^2) \sigma \frac{D_t(\theta_t, \phi_t) D_r(\theta_r, \phi_r)}{4\pi} \\ \times \left(\frac{\lambda}{4\pi R_1 R_2} \right)^2 |\hat{\boldsymbol{\rho}}_w \cdot \hat{\boldsymbol{\rho}}_r|^2 \end{aligned}} \tag{2-125}$$

where

$\hat{\boldsymbol{\rho}}_w$ = polarization unit vector of the scattered waves
$\hat{\boldsymbol{\rho}}_r$ = polarization unit vector of the receiving antenna

For polarization-matched antennas aligned for maximum directional radiation and reception, (2-125) reduces to

$$\boxed{\frac{P_r}{P_t} = \sigma \frac{G_{0t} G_{0r}}{4\pi} \left[\frac{\lambda}{4\pi R_1 R_2}\right]^2} \tag{2-126}$$

Equation (2-124), or (2-125) or (2-126) is known as the *Radar Range Equation*. It relates the power P_r (delivered to the receiver load) to the input power P_t transmitted by an antenna, after it has been scattered by a target with a radar cross section (echo area) of σ.

Example 2.16

Two *lossless X*-band (8.2–12.4 GHz) horn antennas are separated by a distance of 100λ. The reflection coefficients at the terminals of the transmitting and receiving antennas are 0.1 and 0.2, respectively. The maximum directivities of the transmitting and receiving antennas (over isotropic) are 16 dB and 20 dB, respectively. Assuming that the input power in the lossless transmission line connected to the transmitting antenna is 2W, and the antennas are aligned for maximum radiation between them and are polarization-matched, find the power delivered to the load of the receiver.

Solution: For this problem

$$\begin{aligned}
e_{cdt} &= e_{cdr} = 1 \text{ because antennas are lossless.} \\
|\hat{\boldsymbol{\rho}}_t \cdot \hat{\boldsymbol{\rho}}_r|^2 &= 1 \text{ because antennas are polarization-matched} \\
\left.\begin{aligned} D_t &= D_{0t} \\ D_r &= D_{0r} \end{aligned}\right\} &\text{ because antennas are aligned for maximum radiation between them} \\
D_{0t} &= 16 \text{ dB} \Rightarrow 39.81 \text{ (dimensionless)} \\
D_{0r} &= 20 \text{ dB} \Rightarrow 100 \text{ (dimensionless)}
\end{aligned}$$

Using (2-118), we can write

$$\begin{aligned}
P_r &= [1 - (0.1)^2][1 - (0.2)^2][\lambda/4\pi(100\lambda)]^2(39.81)(100)(2) \\
&= 4.777 \text{ mW}
\end{aligned}$$

2.17.3 Antenna Radar Cross Section

The radar cross section, usually referred to as RCS, is a far-field parameter, which is used to characterize the scattering properties of a radar target. For a target, there is *monostatic* or *backscattering RCS* when the transmitter and receiver of Figure 2.32 are at the same location, and a *bistatic RCS* when the transmitter and receiver are not at the same location. In designing low-observable or low-profile (stealth) targets,

TABLE 2.2 RCS of Some Typical Targets

	Typical RCSs [22]	
Object	**RCS** (m^2)	**RCS** (dBsm)
Pickup truck	200	23
Automobile	100	20
Jumbo jet airliner	100	20
Large bomber *or* commercial jet	40	16
Cabin cruiser boat	10	10
Large fighter aircraft	6	7.78
Small fighter aircraft *or* four-passenger jet	2	3
Adult male	1	0
Conventional winged missile	0.5	−3
Bird	0.01	−20
Insect	0.00001	−50
Advanced tactical fighter	0.000001	−60

it is the parameter that you attempt to minimize. For complex targets (such as aircraft, spacecraft, missiles, ships, tanks, automobiles) it is a complex parameter to derive. In general, the RCS of a target is a function of the polarization of the incident wave, the angle of incidence, the angle of observation, the geometry of the target, the electrical properties of the target, and the frequency of operation. The units of RCS of three-dimensional targets are meters squared (m^2) or for normalized values decibels per squared meter (dBsm) or RCS per squared wavelength in decibels (RCS/λ^2 in dB). Representative values of some typical targets are shown in Table 2.2 [22]. Although the frequency was not stated [22], these numbers could be representative at X-band.

The RCS of a target can be controlled using primarily two basic methods: *shaping* and the use of *materials*. Shaping is used to attempt to direct the scattered energy toward directions other than the desired. However, for many targets shaping has to be compromised in order to meet other requirements, such as aerodynamic specifications for flying targets. Materials is used to trap the incident energy within the target and to dissipate part of the energy as heat or to direct it toward directions other than the desired. Usually both methods, shaping and materials, are used together in order to optimize the performance of a radar target. One of the "golden rules" to observe in order to achieve low RCS is to "*round corners, avoid flat and concave surfaces, and use material treatment in flare spots*."

There are many methods of analysis to predict the RCS of a target [13], [22]–[33]. Some of them are full-wave methods, others are designated as asymptotic methods, either low-frequency or high-frequency, and some are considered as numerical methods. The methods of analysis are often contingent upon the shape, size, and material composition of the target. Some targets, because of their geometrical complexity, are often simplified and are decomposed into a number of basic shapes (such as strips, plates, cylinders, cones, wedges) which when put together represent a very good replica

of the actual target. This has been used extensively and proved to be a very good approach. The topic is very extensive to be treated here in any detail, and the reader is referred to the literature [13], [22]–[33]. There is a plethora of references but because of space limitations, only a limited number is included here to get the reader started on the subject.

Antennas individually are radar targets which many exhibit large radar cross section. In many applications, antennas are mounted on the surface of other complex targets (such as aircraft, spacecraft, satellites, missiles, automobiles), and become part of the overall radar target. In such configurations, many antennas, especially aperture types (such as waveguides, horns) become large contributors to the total RCS, monostatic or bistatic, of the target. Therefore in designing low-observable targets, the antenna type, location and contributions become an important consideration of the overall design.

The scattering and transmitting (radiation) characteristics of an antenna are related [34]–[36]. There are various methods which can be used to analyze the fields scattered by an antenna. The presentation here parallels that in [23], [37]–[40]. In general the electric field scattered by an antenna with a load impedance Z_L can be expressed by

$$\mathbf{E}^s(Z_L) = \mathbf{E}^s(0) - \frac{I_s}{I_t}\frac{Z_L}{Z_L + Z_A}\mathbf{E}^t \tag{2-127}$$

where

$\mathbf{E}^s(Z_L)$ = electric field scattered by antenna with a load Z_L
$\mathbf{E}^s(0)$ = electric field scattered by short-circuited antenna ($Z_L = 0$)
I_s = short-circuited current induced by the incident field on the antenna with $Z_L = 0$
I_t = antenna current in transmitting mode
$Z_A = R_A + jX_A =$ antenna input impedance
$\mathbf{E}^t$ = electric field radiated by the antenna in transmitting mode

By defining an antenna reflection coefficient of

$$\Gamma_A = \frac{Z_L - Z_A}{Z_L + Z_A} \tag{2-128}$$

the scattered field of (2-127) can be written as

$$\mathbf{E}^s(Z_L) = \mathbf{E}^s(0) - \frac{I_s}{I_t}\frac{1}{2}(1 + \mathbf{\Gamma}_A)\mathbf{E}^t \tag{2-129}$$

Therefore according to (2-129) the scattered field by an antenna with a load Z_L is equal to the scattered field when the antenna is short-circuited ($Z_L = 0$) minus a term related to the reflection coefficient and the field transmitted by the antenna.

Green has expressed the field scattered by an antenna terminated with a load Z_L in a more convenient form which allows it to be separated into the *structural* and *antenna mode* scattering terms [23], [37]–[40]. This is accomplished by assuming that the antenna is loaded with a conjugate-matched impedance ($Z_L = Z_A^*$). Doing this generates using

(2-127) another equation for the field scattered by the antenna with a load $Z_L = Z_A^*$. When this new equation is subtracted from (2-127) it eliminates the short-circuited scattered field, and we can write that the field scattered by the antenna with a load Z_L is

$$\mathbf{E}^s(Z_L) = \mathbf{E}^s(Z_A^*) - \frac{I_s}{I_t}\frac{\mathbf{\Gamma}^* Z_A}{2R_A}\mathbf{E}^t \tag{2-130}$$

$$\mathbf{\Gamma}^* = \frac{Z_L - Z_A^*}{Z_L + Z_A^*} \tag{2-130a}$$

where

$\mathbf{E}^s(Z_L)$ = electric field scattered by the antenna with load Z_L
$\mathbf{E}^s(Z_A^*)$ = electric field scattered by the antenna with a conjugate-matched load
$I(Z_A^*)$ = current induced by the incident wave at the terminals matched with a conjugate impedance load
Γ^* = conjugate-matched reflection coefficient
Z_L = load impedance attached to antenna terminals

For the short-circuited case and the conjugate-matched transmitting (radiating) case, the product of their currents and antenna impedance are related by [34]

$$I_s Z_A = I_m^*(Z_A + Z_A^*) = 2R_A I_m^* \tag{2-131}$$

where I_m^* is the scattering current when the antenna is conjugate-matched ($Z_L = Z_A^*$). Substituting (2-131) into (2-130) for I_s reduces (2-130) to

$$\mathbf{E}^s(Z_L) = \mathbf{E}^s(Z_A^*) - \frac{I_m^*}{I_t}\Gamma^*\mathbf{E}^t \tag{2-132}$$

It can also be shown that if the antenna is matched with a load Z_A (instead of Z_A^*), then (2-132) can be written as

$$\mathbf{E}^s(Z_L) = \mathbf{E}^s(Z_A) - \frac{I_m}{I_t}\Gamma_A\mathbf{E}^t \tag{2-133}$$

Therefore the field scattered by an antenna loaded with an impedance Z_L is related to the field radiated by the antenna in the transmitting mode in three different ways, as shown by (2-129), (2-132), and (2-133). According to (2-129) the field scattered by an antenna when it is loaded with an impedance Z_L is equal to the field scattered by the antenna when it is short-circuited ($Z_L = 0$) minus a term related to the antenna reflection coefficient and the field transmitted by the antenna. In addition, according to (2-132), the field scattered by an antenna when it is terminated with an impedance Z_L is equal to the field scattered by the antenna when it is conjugate-matched with an impedance Z_A^* minus the field transmitted (radiated) times the conjugate reflection coefficient. The second term is weighted by the two currents. Alternatively, according to (2-133), the field scattered by the antenna when it is terminated with an impedance Z_L is equal to the field scattered by the antenna when it is matched with an impedance Z_A minus the field transmitted (radiated) times the reflection coefficient weighted by the two currents.

In (2-132) the first term consists of the *structural* scattering term and the second of the *antenna mode* scattering term. The *structural* scattering term is introduced by the currents induced on the surface of the antenna by the incident field when the antenna is conjugate-matched, and it is independent of the load impedance. The *antenna mode* scattering term is only a function of the radiation characteristics of the antenna, and its scattering pattern is the square of the antenna radiation pattern. The antenna mode depends on the power absorbed in the load of a lossless antenna and the power which is radiated by the antenna due to a load mismatch. This term vanishes when the antenna is conjugate-matched.

From the scattered field expression of (2-129), it can be shown that the total radar cross section of the antenna terminated with a load Z_L can be written as [40]

$$\sigma = |\sqrt{\sigma^s} - (1 + \Gamma_A)\sqrt{\sigma^a} e^{j\phi_r}|^2 \tag{2-134}$$

where

σ = total RCS with antenna terminated with Z_L
σ^s = RCS due to structural term
σ^a = RCS due to antenna mode term
ϕ_r = relative phase between the structural and antenna mode terms

If the antenna is short-circuited ($\Gamma_A = -1$), then according to (2-134)

$$\sigma_{\text{short}} = \sigma^s \tag{2-135}$$

If the antenna is open-circuited ($\Gamma_A = +1$), then according to (2-134)

$$\sigma_{\text{open}} = |\sqrt{\sigma^s} - 2\sqrt{\sigma^a} e^{j\phi_r}|^2 = \sigma_{\text{residual}} \tag{2-136}$$

Lastly, if the antenna is matched $Z_L = Z_A (\Gamma_A = 0)$, then according to (2-134)

$$\sigma_{\text{match}} = |\sqrt{\sigma^s} - \sqrt{\sigma^a} e^{j\phi_r}|^2 \tag{2-137}$$

Therefore under matched conditions, according to (2-137), the range of values (minimum to maximum) of the radar cross section is

$$|\sigma^s - \sigma^a| \leq \sigma \leq |\sigma^s + \sigma^a| \tag{2-138}$$

The minimum value occurring when the two RCSs are in phase while the maximum occurs when they are out of phase.

Example 2.17

The structural RCS of a resonant wire dipole is in phase and in magnitude slightly greater than four times that of the antenna mode. Relate the short-circuited, open-circuited, and matched RCSs to that of the antenna mode.

Solution: Using (2-135)

$$\sigma_{\text{short}} = 4\sigma_{\text{antenna}}$$

Using (2-136)

$$\sigma_{\text{open}} = 2\sigma_{\text{antenna}}(0) = 0 \text{ or very small}$$

The matched value is obtained using (2-137), or

$$\sigma_{\text{match}} = \sigma_{\text{antenna}}$$

To produce a zero RCS, (2-134) must vanish. This is accomplished if

$$Re(\Gamma_A) = -1 + \cos\phi_r\sqrt{\sigma^s/\sigma^a} \tag{2-139a}$$

$$Im(\Gamma_A) = -\sin\phi_r\sqrt{\sigma^s/\sigma^a} \tag{2-139b}$$

Assuming positive values of resistances, the real value of Γ_A cannot be greater than unity. Therefore there are some cases where the RCS cannot be reduced to zero by choosing Z_L. Because Z_A can be complex, there is no limit on the imaginary part of Γ_A.

In general, the structural and antenna mode scattering terms are very difficult to predict and usually require that the antenna is solved as a boundary-value problem. However, these two terms have been obtained experimentally utilizing the Smith chart [37]–[39].

For a monostatic system the receiving and transmitting antennas are collocated. In addition, if the antennas are identical ($G_{0r} = G_{0t} = G_0$) and are polarization-matched ($P_r = P_t = 1$), the total radar cross section of the antenna for backscattering can be written as

$$\sigma = \frac{\lambda_0^2}{4\pi}G_0^2|A - \Gamma^*|^2 \tag{2-140}$$

where A is a complex parameter independent of the load.

If the antenna is a thin dipole, then $A \simeq 1$ and (2-140) reduces to

$$\begin{aligned}\sigma &\simeq \frac{\lambda_0^2}{4\pi}G_0^2|1 - \Gamma^*|^2 = \frac{\lambda_0^2}{4\pi}G_0^2\left|1 - \frac{Z_L - Z_A^*}{Z_L + Z_A}\right| \\ &= \frac{\lambda_0^2}{4\pi}G_0^2\left|\frac{2R_A}{Z_L + Z_A}\right|^2\end{aligned} \tag{2-141}$$

If in addition we assume that the dipole length is $l = \lambda_0/2$ and is short-circuited ($Z_L = 0$), then the normalized radar cross section of (2-141) is equal to

$$\frac{\sigma}{\lambda_0^2} \simeq \frac{G_0^2}{\pi} = \frac{(1.643)^2}{\pi} = 0.8593 \simeq 0.86 \tag{2-142}$$

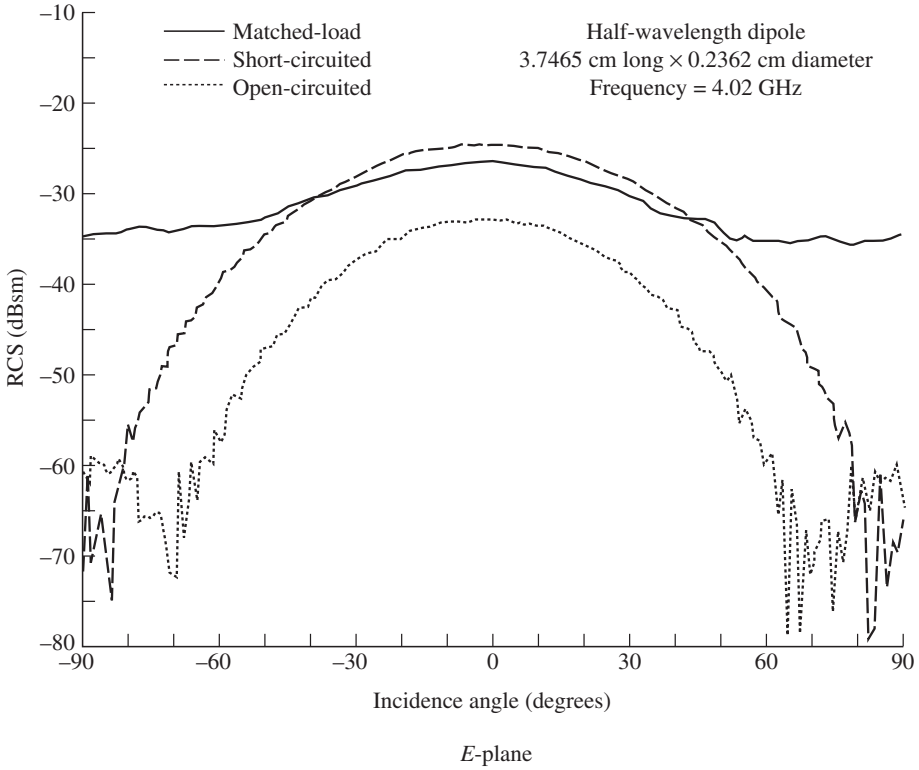


Figure 2.33 E-plane monostatic RCS ($\sigma_{\theta\theta}$) versus incidence angle for a half-wavelength dipole.

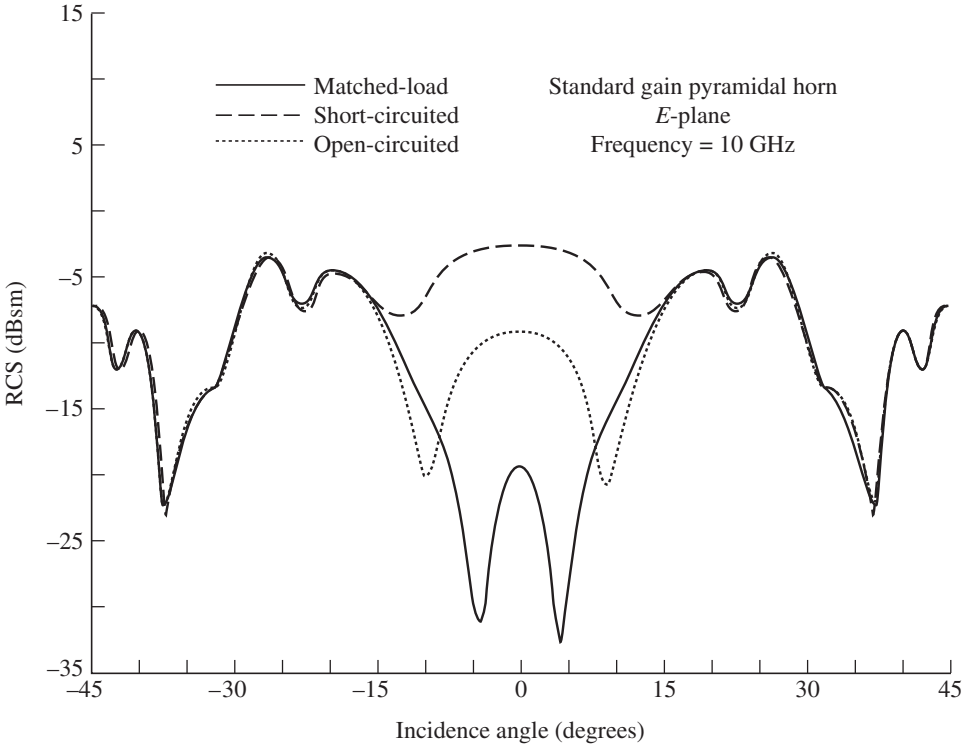
which agrees with experimental corresponding maximum monostatic value of Figure 2.33 and those reported in the literature [41], [42].

Shown in Figure 2.33 is the measured E-plane monostatic RCS of a half-wavelength dipole when it is matched to a load, short-circuited (straight wire) and open-circuited (gap at the feed). The aspect angle is measured from the normal to the wire. As expected, the RCS is a function of the observation (aspect) angle. Also it is apparent that there are appreciable differences between the three responses. For the short-circuited case, the maximum value is approximately -24 dBsm which closely agrees with the computed value of -22.5 dBsm using (2-142). Similar responses for the monostatic RCS of a pyramidal horn are shown in Figure 2.34(a) for the E-plane and in Figure 2.34(b) for the H-plane. The antenna is a commercial X-band (8.2-12.4 GHz) 20-dB standard gain horn with aperture dimension of 9.2 cm by 12.4 cm. The length of the horn is 25.6 cm. As for the dipole, there are differences between the three responses for each plane. It is seen that the short-circuited response exhibits the largest return.

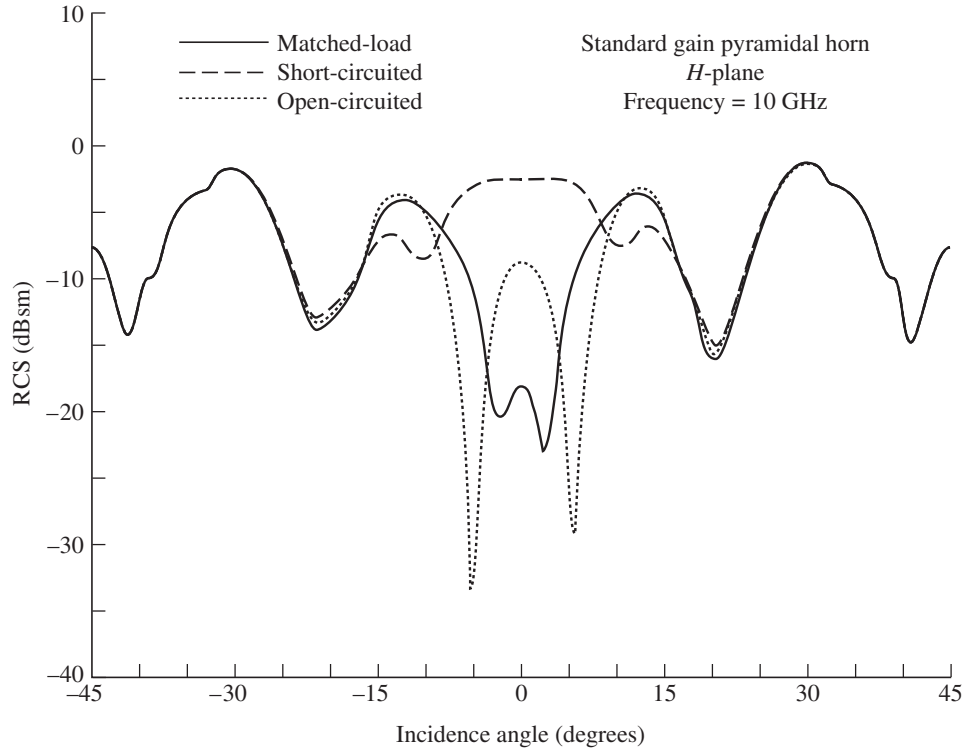
Antenna RCS from model measurements [43] and microstrip patches [44], [45] have been reported.

2.18 ANTENNA TEMPERATURE

Every object with a physical temperature above absolute zero (0 K $= -273^{\circ}$C) radiates energy [6]. The amount of energy radiated is usually represented by an equivalent



(a) E-plane ($\sigma_{\theta\theta}$)



(b) H-plane ($\sigma_{\phi\phi}$)

Figure 2.34 E- and H-plane monostatic RCS versus incidence angle for a pyramidal horn antenna.

EX2042
Page 118 of 1072

temperature T_B, better known as brightness temperature, and it is defined as

$$T_B(\theta, \phi) = \epsilon(\theta, \phi)T_m = (1 - |\Gamma|^2)T_m \tag{2-143}$$

where

T_B = brightness temperature (equivalent temperature; K)
ϵ = emissivity (dimensionless)
T_m = molecular (physical) temperature (K)
$\Gamma(\theta, \phi)$ = reflection coefficient of the surface for the polarization of the wave

Since the values of emissivity are $0 \leq \epsilon \leq 1$, the maximum value the brightness temperature can achieve is equal to the molecular temperature. Usually the emissivity is a function of the frequency of operation, polarization of the emitted energy, and molecular structure of the object. Some of the better natural emitters of energy at microwave frequencies are (a) the ground with equivalent temperature of about 300 K and (b) the sky with equivalent temperature of about 5 K when looking toward zenith and about 100–150 K toward the horizon.

The brightness temperature emitted by the different sources is intercepted by antennas, and it appears at their terminals as an antenna temperature. The temperature appearing at the terminals of an antenna is that given by (2-143), after it is weighted by the gain pattern of the antenna. In equation form, this can be written as

$$T_A = \frac{\displaystyle\int_0^{2\pi}\int_0^{\pi} T_B(\theta, \phi)G(\theta, \phi)\sin\theta\, d\theta\, d\phi}{\displaystyle\int_0^{2\pi}\int_0^{\pi} G(\theta, \phi)\sin\theta\, d\theta\, d\phi} \tag{2-144}$$

where

T_A = antenna temperature (effective noise temperature of the antenna radiation resistance; K)
$G(\theta, \phi)$ = gain (power) pattern of the antenna

Assuming no losses or other contributions between the antenna and the receiver, the noise power transferred to the receiver is given by

$$P_r = kT_A\Delta f \tag{2-145}$$

where

P_r = antenna noise power (W)
k = Boltzmann's constant (1.38×10^{-23} J/K)
T_A = antenna temperature (K)
Δf = bandwidth (Hz)

If the antenna and transmission line are maintained at certain physical temperatures, and the transmission line between the antenna and receiver is lossy, the antenna temperature T_A as seen by the receiver through (2-145) must be modified to include the other contributions and the line losses. If the antenna itself is maintained at a certain

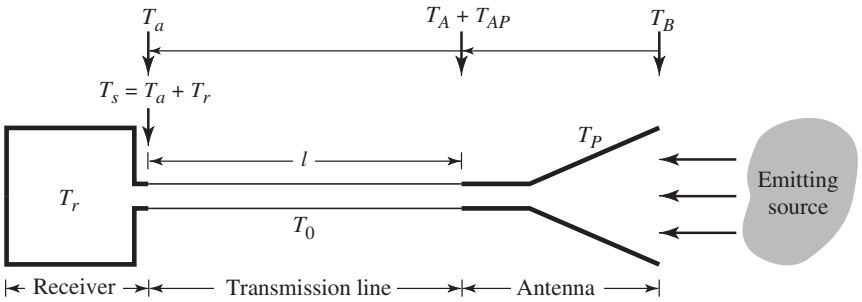


Figure 2.35 Antenna, transmission line, and receiver arrangement for system noise power calculation.

physical temperature T_p and a transmission line of length l, constant physical temperature T_0 throughout its length, and uniform attenuation of α (Np/unit length) is used to connect an antenna to a receiver, as shown in Figure 2.35, the effective antenna temperature at the receiver terminals is given by

$$T_a = T_A e^{-2\alpha l} + T_{AP} e^{-2\alpha l} + T_0(1 - e^{-2\alpha l}) \tag{2-146}$$

where

$$T_{AP} = \left(\frac{1}{e_A} - 1\right) T_p \tag{2-146a}$$

T_a = antenna temperature at the receiver terminals (K)
T_A = antenna noise temperature at the antenna terminals (2-144) (K)
T_{AP} = antenna temperature at the antenna terminals due to physical temperature (2-146a) (K)
T_p = antenna physical temperature (K)
α = attenuation coefficient of transmission line (Np/m)
e_A = thermal efficiency of antenna (dimensionless)
l = length of transmission line (m)
T_0 = physical temperature of the transmission line (K)

The antenna noise power of (2-145) must also be modified and written as

$$P_r = kT_a \Delta f \tag{2-147}$$

where T_a is the antenna temperature at the receiver input as given by (2-146).

If the receiver itself has a certain noise temperature T_r (due to thermal noise in the receiver components), the *system noise power at the receiver terminals* is given by

$$P_s = k(T_a + T_r)\Delta f = kT_s \Delta f \tag{2-148}$$

where

P_s = system noise power (at receiver terminals)
T_a = antenna noise temperature (at receiver terminals)
T_r = receiver noise temperature (at receiver terminals)
$T_s = T_a + T_r =$ effective system noise temperature (at receiver terminals)

EX2042
Page 120 of 1072

A graphical relation of all the parameters is shown in Figure 2.35. The effective system noise temperature T_s of radio astronomy antennas and receivers varies from very few degrees (typically $\simeq$ 10 K) to thousands of Kelvins depending upon the type of antenna, receiver, and frequency of operation. Antenna temperature changes at the antenna terminals, due to variations in the target emissions, may be as small as a fraction of one degree. To detect such changes, the receiver must be very sensitive and be able to differentiate changes of a fraction of a degree.

Example 2.18

The effective antenna temperature of a target at the input terminals of the antenna is 150 K. Assuming that the antenna is maintained at a thermal temperature of 300 K and has a thermal efficiency of 99% and it is connected to a receiver through an X-band (8.2–12.4 GHz) rectangular waveguide of 10 m (loss of waveguide = 0.13 dB/m) and at a temperature of 300 K, find the effective antenna temperature at the receiver terminals.

Solution: We first convert the attenuation coefficient from dB to Np by $\alpha(\text{dB/m}) = 20(\log_{10} \text{e})\alpha(\text{Np/m}) = 20(0.434)\alpha(\text{Np/m}) = 8.68\alpha(\text{Np/m})$. Thus $\alpha(\text{Np/m}) = \alpha(\text{dB/m})/8.68 = 0.13/8.68 = 0.0149$. The effective antenna temperature at the receiver terminals can be written, using (2-146a) and (2-146), as

$$T_{AP} = 300\left(\frac{1}{0.99} - 1\right) = 3.03$$

$$T_a = 150e^{-0.149(2)} + 3.03e^{-0.149(2)} + 300[1 - e^{-0.149(2)}]$$

$$= 111.345 + 2.249 + 77.31 = 190.904 \text{ K}$$

The results of the above example illustrate that the antenna temperature at the input terminals of the antenna and at the terminals of the receiver can differ by quite a few degrees. For a smaller transmission line or a transmission line with much smaller losses, the difference can be reduced appreciably and can be as small as a fraction of a degree.

A summary of the pertinent parameters and associated formulas and equation numbers for this chapter are listed in Table 2.3.

2.19 MULTIMEDIA

In the CD that is part of the book, the following multimedia resources are included for the review, understanding, and visualization of the material of this chapter:

a. **Java**-based **interactive questionnaire**, with answers.
b. **Java**-based **applet** for computing and displaying graphically the directivity of an antenna.
c. **Matlab** and **Fortran** computer program, designated ***Directivity***, for computing the directivity of an antenna. A description of this program is in the READ ME file of the attached CD.

EX2042
Page 121 of 1072

d. **Matlab** plotting computer programs:
   - **2-D Polar** (designated as ***Polar***). This program can be used to plot the two-dimensional patterns, in both polar and semipolar form (*in linear or dB scale*), of an antenna.
   - **3-D Spherical**. This program (designated as ***Spherical***) can be used to plot the three-dimensional pattern (*in linear or dB scale*) of an antenna in spherical form.

   A description of these programs is in the corresponding READ ME files of the attached CD.

e. **Power Point (PPT)** viewgraphs, in multicolor.

TABLE 2.3 Summary of Important Parameters and Associated Formulas and Equation Numbers

Parameter	Formula	Equation Number
Infinitesimal area of sphere	$dA = r^2 \sin\theta \, d\theta \, d\phi$	(2-1)
Elemental solid angle of sphere	$d\Omega = \sin\theta \, d\theta \, d\phi$	(2-2)
Average power density	$\mathbf{W}_{av} = \frac{1}{2}\text{Re}[\mathbf{E} \times \mathbf{H}^*]$	(2-8)
Radiated power/average radiated power	$P_{rad} = P_{av} = \oiint_S \mathbf{W}_{av} \cdot d\mathbf{s} = \frac{1}{2} \oiint_S \text{Re}[\mathbf{E} \times \mathbf{H}^*] \cdot d\mathbf{s}$	(2-9)
Radiation density of isotropic radiator	$W_0 = \frac{P_{rad}}{4\pi r^2}$	(2-11)
Radiation intensity (far field)	$U = r^2 W_{rad} = B_0 F(\theta, \phi) \simeq \frac{r^2}{2\eta} \times \left[\lvert E_\theta(r, \theta, \phi)\rvert^2 + \lvert E_\phi(r, \theta, \phi)\rvert^2\right]$	(2-12), (2-12a)
Directivity $D(\theta, \phi)$	$D = \frac{U}{U_0} = \frac{4\pi U}{P_{rad}} = \frac{4\pi}{\Omega_A}$	(2-16), (2-23)
Beam solid angle Ω_A	$\Omega_A = \int_0^{2\pi} \int_0^{\pi} F_n(\theta, \phi) \sin\theta \, d\theta \, d\phi$ $F_n(\theta, \phi) = \frac{F(\theta, \phi)}{\lvert F(\theta, \phi)\rvert_{\max}}$	(2-24) (2-25)

(*continued overleaf*)

TABLE 2.3 (*continued*)

Parameter	Formula	Equation Number
Maximum directivity D_0	$D_{\max} = D_0 = \dfrac{U_{\max}}{U_0} = \dfrac{4\pi U_{\max}}{P_{rad}}$	(2-16a)
Partial directivities D_θ, D_ϕ	$D_0 = D_\theta + D_\phi$ $D_\theta = \dfrac{4\pi U_\theta}{P_{rad}} = \dfrac{4\pi U_\theta}{(P_{rad})_\theta + (P_{rad})_\phi}$ $D_\phi = \dfrac{4\pi U_\phi}{P_{rad}} = \dfrac{4\pi U_\phi}{(P_{rad})_\theta + (P_{rad})_\phi}$	(2-17) (2-17a) (2-17b)
Approximate maximum directivity (*one main lobe pattern*)	$D_0 \simeq \dfrac{4\pi}{\Theta_{1r}\Theta_{2r}} = \dfrac{41{,}253}{\Theta_{1d}\Theta_{2d}}$ (Kraus) $D_0 \simeq \dfrac{32\ln 2}{\Theta_{1r}^2 + \Theta_{2r}^2} = \dfrac{22.181}{\Theta_{1r}^2 + \Theta_{2r}^2} = \dfrac{72{,}815}{\Theta_{1d}^2 + \Theta_{2d}^2}$ (Tai-Pereira)	(2-26), (2-27) (2-30), (2-30a), (2-30b)
Approximate maximum directivity (*omnidirectional pattern*)	$D_0 \simeq \dfrac{101}{\text{HPBW(degrees)} - 0.0027[\text{HPBW(degrees)}]^2}$ (McDonald) $D_0 \simeq -172.4 + 191\sqrt{0.818 + \dfrac{1}{\text{HPBW(degrees)}}}$ (Pozar)	(2-33a) (2-33b)
Gain $G(\theta, \phi)$	$G = \dfrac{4\pi U(\theta,\phi)}{P_{in}} = e_{cd}\left[\dfrac{4\pi U(\theta,\phi)}{P_{rad}}\right] = e_{cd} D(\theta,\phi)$ $P_{rad} = e_{cd} P_{in}$	(2-46), (2-47), (2-49)
Antenna radiation efficiency e_{cd}	$e_{cd} = \dfrac{R_r}{R_r + R_L}$	(2-90)
Loss resistance R_L (*straight wire/uniform current*)	$R_L = R_{hf} = \dfrac{l}{P}\sqrt{\dfrac{\omega\mu_0}{2\sigma}}$	(2-90b)
Loss resistance R_L (*straight wire/*$\lambda/2$ *dipole*)	$R_L = \dfrac{l}{2P}\sqrt{\dfrac{\omega\mu_0}{2\sigma}}$	

TABLE 2.3 (*continued*)

Parameter	Formula	Equation Number
Maximum gain G_0	$G_0 = e_{cd} D_{\max} = e_{cd} D_0$	(2-49a)
Partial gains G_θ, G_ϕ	$G_0 = G_\theta + G_\phi$ $G_\theta = \dfrac{4\pi U_\theta}{P_{in}}, \quad G_\phi = \dfrac{4\pi U_\phi}{P_{in}}$	(2-50) (2-50a), (2-50b)
Absolute gain G_{abs}	$G_{abs} = e_r G(\theta,\phi) = e_r e_{cd} D(\theta,\phi) = (1 - \lvert\Gamma\rvert^2) e_{cd} D(\theta,\phi)$ $= e_0 D(\theta,\phi)$	(2-49a) (2-49b)
Total antenna efficiency e_0	$e_0 = e_r e_c e_d = e_r e_{cd} = (1 - \lvert\Gamma\rvert^2) e_{cd}$	(2-52)
Reflection efficiency e_r	$e_r = (1 - \lvert\Gamma\rvert^2)$	(2-45)
Beam efficiency BE	$\text{BE} = \dfrac{\int_0^{2\pi}\int_0^{\theta_1} U(\theta,\phi)\sin\theta\, d\theta\, d\phi}{\int_0^{2\pi}\int_0^{\pi} U(\theta,\phi)\sin\theta\, d\theta\, d\phi}$	(2-54)
Polarization loss factor (PLF)	$\text{PLF} = \lvert\hat{\boldsymbol{\rho}}_w \cdot \hat{\boldsymbol{\rho}}_a\rvert^2$	(2-71)
Vector effective length $\boldsymbol{\ell}_e(\theta,\phi)$	$\boldsymbol{\ell}_e(\theta,\phi) = \hat{\mathbf{a}}_\theta l_\theta(\theta,\phi) + \hat{\mathbf{a}}_\phi l_\phi(\theta,\phi)$	(2-91)
Polarization efficiency p_e	$p_e = \dfrac{\lvert\boldsymbol{\ell}_e \cdot \mathbf{E}^{inc}\rvert^2}{\lvert\boldsymbol{\ell}_e\rvert^2 \lvert\mathbf{E}^{inc}\rvert^2}$	(2-71a)
Antenna impedance Z_A	$Z_A = R_A + jX_A = (R_r + R_L) + jX_A$	(2-72), (2-73)
Maximum effective area A_{em}	$A_{em} = \dfrac{\lvert V_T\rvert^2}{8W_i}\left[\dfrac{1}{R_r + R_L}\right] = e_{cd}\left(\dfrac{\lambda^2}{4\pi}\right) D_0 \lvert\hat{\boldsymbol{\rho}}_w \cdot \hat{\boldsymbol{\rho}}_a\rvert^2$ $= \left(\dfrac{\lambda^2}{4\pi}\right) G_0 \lvert\hat{\boldsymbol{\rho}}_w \cdot \hat{\boldsymbol{\rho}}_a\rvert^2$	(2-96), (2-111), (2-112)
Aperture efficiency ε_{ap}	$\varepsilon_{ap} = \dfrac{A_{em}}{A_p} = \dfrac{\text{maximum effective area}}{\text{physical area}}$	(2-100)

(*continued overleaf*)

TABLE 2.3 (*continued*)

Parameter	Formula	Equation Number
Friis transmission equation	$\frac{P_r}{P_t} = \left(\frac{\lambda}{4\pi R}\right)^2 G_{0t} G_{0r} \lvert \hat{\boldsymbol{\rho}}_t \cdot \hat{\boldsymbol{\rho}}_r \rvert^2$	(2-118), (2-119)
Radar range equation	$\frac{P_r}{P_t} = \sigma \frac{G_{0t} G_{0r}}{4\pi} \left[\frac{\lambda}{4\pi R_1 R_2}\right]^2 \lvert \hat{\boldsymbol{\rho}}_w \cdot \hat{\boldsymbol{\rho}}_r \rvert^2$	(2-125), (2-126)
Radar cross section (RCS)	$\sigma = \lim_{R\to\infty}\left[4\pi R^2 \frac{W_s}{W_i}\right] = \lim_{R\to\infty}\left[4\pi R^2 \frac{\lvert \mathbf{E}^s \rvert^2}{\lvert \mathbf{E}^i \rvert^2}\right] = \lim_{R\to\infty}\left[4\pi R^2 \frac{\lvert \mathbf{H}^s \rvert^2}{\lvert \mathbf{H}^i \rvert^2}\right]$	(2-120a)
Brightness temperature $T_B(\theta, \phi)$	$T_B(\theta, \phi) = \varepsilon(\theta, \phi) T_m = (1 - \lvert \Gamma \rvert^2) T_m$	(2-144)
Antenna temperature T_A	$T_A = \frac{\int_0^{2\pi}\int_0^{\pi} T_B(\theta, \phi) G(\theta, \phi) \sin\theta \, d\theta \, d\phi}{\int_{0\pi}^{2\pi}\int_0^{\pi} G(\theta, \phi) \sin\theta \, d\theta \, d\phi}$	(2-145)

REFERENCES

1. A. Z. Elsherbeni and C. D. Taylor Jr., "Antenna Pattern Plotter," Copyright © 1995, Electrical Engineering Department, The University of Mississippi, University, MS.
2. W. R. Scott Jr., "A General Program for Plotting Three-dimensional Antenna Patterns," *IEEE Antennas and Propagation Society Newsletter*, pp. 6–11, December 1989.
3. A. Z. Elsherbeni and C. D. Taylor Jr., "Interactive Antenna Pattern Visualization," *Software Book in Electromagnetics*, Vol. II, Chapter 8, CAEME Center for Multimedia Education, University of Utah, pp. 367–410, 1995.
4. J. S. Hollis, T. J. Lyon, and L. Clayton Jr. (eds.), *Microwave Antenna Measurements*, Scientific-Atlanta, Inc., July 1970.
5. J. D. Kraus, *Antennas*, McGraw-Hill, New York, 1988.
6. J. D. Kraus, *Radio Astronomy*, McGraw-Hill Book Co., 1966.
7. A. Z. Elsherbeni and P. H. Ginn. "Interactive Analysis of Antenna Arrays," *Software Book in Electromagnetics*, Vol. II, Chapter 6, CAEME Center for Multimedia Education, University of Utah, pp. 337–366, 1995.
8. J. Romeu and R. Pujol, "Array," *Software Book in Electromagnetics*, Vol. II, Chapter 12, CAEME Center for Multimedia Education, University of Utah, pp. 467–481, 1995.
9. R. S. Elliott, "Beamwidth and Directivity of Large Scanning Arrays," Last of Two Parts, *The Microwave Journal*, pp. 74–82, January 1964.
10. C.-T. Tai and C. S. Pereira, "An Approximate Formula for Calculating the Directivity of an Antenna," *IEEE Trans. Antennas Propagat.*, Vol. AP-24, No. 2, pp. 235–236, March 1976.

11. N. A. McDonald, "Approximate Relationship Between Directivity and Beamwidth for Broadside Collinear Arrays," *IEEE Trans. Antennas Propagat.*, Vol. AP-26, No. 2, pp. 340–341, March 1978.
12. D. M. Pozar, "Directivity of Omnidirectional Antennas," *IEEE Antennas Propagat. Mag.*, Vol. 35, No. 5, pp. 50–51, October 1993.
13. C. A. Balanis, *Advanced Engineering Electromagnetics*, John Wiley and Sons, New York, 1989.
14. H. Poincaré, *Theorie Mathematique de la Limiere*, Georges Carre, Paris, France, 1892.
15. G. A. Deschamps, "Part II—Geometrical Representation of the Polarization of a Plane Electromagnetic Wave," *Proc. IRE*, Vol. 39, pp. 540–544, May 1951.
16. E. F. Bolinder, "Geometrical Analysis of Partially Polarized Electromagnetic Waves," *IEEE Trans. Antennas Propagat.*, Vol. AP-15, No. 1, pp. 37–40, January 1967.
17. G. A. Deschamps and P. E. Mast, "Poincaré Sphere Representation of Partially Polarized Fields," *IEEE Trans. Antennas Propagat.*, Vol. AP-21, No. 4, pp. 474–478, July 1973.
18. G. Sinclair, "The Transmission and Reflection of Elliptically Polarized Waves," *Proc. IRE*, Vol. 38, pp. 148–151, February 1950.
19. C. A. Balanis, "Antenna Theory: A Review," *Proc. IEEE*, Vol. 80, No. 1, pp. 7–23, January 1992.
20. R. E. Collin, *Antennas and Radiowave Propagation*, McGraw-Hill Book Co., New York, 1985.
21. M. I. Skolnik, *Radar Systems*, Chapter 2, McGraw-Hill Book Co., New York, 1962.
22. J. A. Adam, "How to Design an "Invisible' Aircraft," *IEEE Spectrum*, pp. 26–31, April 1988.
23. G. T. Ruck, D. E. Barrick, W. D. Stuart, and C. K. Krichbaum, *Radar Cross Section Handbook*, Vols. 1, 2, Plenum Press, New York, 1970.
24. M. I. Skolnik (Ed.), *Radar Handbook*, Chapter 27, Section 6, McGraw-Hill Book Co., New York, pp. 27-19–27-40, 1970.
25. J. W. Crispin, Jr. and K. M. Siegel, *Methods of Radar Cross Section Analysis*, Academic Press, Inc., New York, 1968.
26. J. J. Bowman, T. B. A. Senior, and P. L. Uslenghi (Eds.), *Electromagnetic and Acoustic Scattering by Simple Shapes*, Amsterdam, The Netherland: North-Holland, 1969.
27. E. F. Knott, M. T. Turley, and J. F. Shaeffer, *Radar Cross Section*, Artech House, Inc., Norwood, MA, 1985.
28. A. K. Bhattacharya and D. L. Sengupta, *Radar Cross Section Analysis and Control*, Artech House, Inc., Norwood, MA, 1991.
29. A. F. Maffett, *Topics for a Statistical Description of Radar Cross Section*, John Wiley and Sons, New York, 1989.
30. Special issue, *Proc. IEEE*, Vol. 53, No. 8, August 1965.
31. Special issue, *Proc. IEEE*, Vol. 77, No. 5, May 1989.
32. Special issue, *IEEE Trans. Antennas Propagat.*, Vol. 37, No. 5, May 1989.
33. W. R. Stone (ed.), *Radar Cross Sections of Complex Objects*, IEEE Press, New York, 1989.
34. A. F. Stevenson, "Relations Between the Transmitting and Receiving Properties of Antennas," *Q. Appl. Math.*, pp. 369–384, January 1948.
35. R. F. Harrington, "Theory of Loaded Scatterers," *Proc. IEE* (British), Vol. 111, pp. 617–623, April 1964.
36. R. E. Collin, "The Receiving Antenna," in *Antenna Theory, Part I*, (R. E. Collin and F. J. Zucker, Eds.), McGraw-Hill Book Co., 1969.

37. R. B. Green, "The Effect of Antenna Installations on the Echo Area of an Object," Report No. 1109-3, ElectroScience Laboratory, Ohio State University, Columbus, OH, September 1961.
38. R. B. Green "Scattering from Conjugate-Matched Antennas," *IEEE Trans. Antennas Propagat.*, Vol. AP-14, No. 1, pp. 17–21, January 1966.
39. R. J. Garbacz, "The Determination of Antenna Parameters by Scattering Cross-Section Measurements, III. Antenna Scattering Cross Section," Report No. 1223-10, Antenna Laboratory, Ohio State University, November 1962.
40. R. C. Hansen, "Relationships Between Antennas as Scatterers and as Radiators," *Proc. IEEE*, Vol. 77, No. 5, pp. 659–662, May 1989.
41. S. H. Dike and D. D. King, "Absorption Gain and Backscattering Cross Section of the Cylindrical Antenna," *Proc. IRE*, Vol. 40, 1952.
42. J. Sevick, "Experimental and Theoretical Results on the Backscattering Cross Section of Coupled Antennas," Tech. Report No. 150, Cruft Laboratory, Harvard University, May 1952.
43. D. L. Moffatt, "Determination of Antenna Scattering Properties From Model Measurements," Report No. 1223-12, Antenna Laboratory, Ohio State University, January 1964.
44. J. T. Aberle, Analysis of Probe-Fed Circular Microstrip Antennas, PhD Dissertation, University of Mass., Amherst, MA, 1989.
45. J. T. Aberle, D. M. Pozar, and C. R. Birtcher, "Evaluation of Input Impedance and Radar Cross Section of Probe-Fed Microstrip Patch Elements Using an Accurate Feed Model," *IEEE Trans. Antennas Propagat.*, Vol. 39, No. 12, pp. 1691–1696, December 1991.

PROBLEMS

2.1. An antenna has a beam solid angle that is equivalent to a *trapezoidal* patch (*patch with 4 sides, 2 of which are parallel to each other*) on the surface of a sphere of radius r. The angular space of the patch on the surface of the sphere extends between $\pi/6 \leq \theta \leq \pi/3 (30^\circ \leq \theta \leq 60^\circ)$ in latitude and $\pi/4 \leq \phi \leq \pi/3 (45^\circ \leq \phi \leq 60^\circ)$ in longitude. Find the following:

(a) Equivalent *beam solid angle* [which is equal to number of *square radians/steradians* **or** $(degrees)^2$] of the patch [*in square radians/steradians* ***and*** *in* $(degrees)^2$].
- Exact.
- Approximate using $\Omega_A = \Delta\Theta \cdot \Delta\Phi = (\theta_2 - \theta_1) \cdot (\phi_2 - \phi_1)$. Compare with the exact.

(b) Corresponding antenna *maximum directivities* of part *a* (*dimensionless* ***and*** *in dB*).

2.2. Derive (2-7) given the definitions of (2-5) and (2-6)

2.3. A hypothetical isotropic antenna is radiating in free-space. At a distance of 100 m from the antenna, the total electric field (E_θ) is measured to be 5 V/m. Find the

(a) power density (W_{rad})

(b) power radiated (P_{rad})

2.4. Find the half-power beamwidth (HPBW) and first-null beamwidth (FNBW), *in radians and degrees*, for the following normalized radiation intensities:

$$\left.\begin{array}{ll}\text{(a) } U(\theta)=\cos\theta & \text{(b) } U(\theta)=\cos^2\theta \\ \text{(c) } U(\theta)=\cos(2\theta) & \text{(d) } U(\theta)=\cos^2(2\theta) \\ \text{(e) } U(\theta)=\cos(3\theta) & \text{(f) } U(\theta)=\cos^2(3\theta)\end{array}\right\} (0\le\theta\le 90^\circ, 0\le\phi\le 360^\circ)$$

2.5. Find the half-power beamwidth (HPBW) and first-null beamwidth (FNBW), *in radians and degrees*, for the following normalized radiation intensities:

$$\left.\begin{array}{l}\text{(a) } U(\theta)=\cos\theta\cos(2\theta) \\ \text{(b) } U(\theta)=\cos^2\theta\cos^2(2\theta) \\ \text{(c) } U(\theta)=\cos(\theta)\cos(3\theta) \\ \text{(d) } U(\theta)=\cos^2(\theta)\cos^2(3\theta) \\ \text{(e) } U(\theta)=\cos(2\theta)\cos(3\theta) \\ \text{(f) } U(\theta)=\cos^2(2\theta)\cos^2(3\theta)\end{array}\right\} (0\le\theta\le 90^\circ, 0\le\phi\le 360^\circ)$$

2.6. The maximum radiation intensity of a 90% efficiency antenna is 200 mW/unit solid angle. Find the directivity and gain (dimensionless and in dB) when the

(a) input power is 125.66 mW

(b) radiated power is 125.66 mW

2.7. The power radiated by a lossless antenna is 10 watts. The directional characteristics of the antenna are represented by the radiation intensity of

$$\left.\begin{array}{ll}\text{(a) } U=B_o\cos^2\theta \\ \text{(b) } U=B_o\cos^3\theta\end{array}\right\} \begin{array}{l}\text{(watts/unit solid angle)} \\ (0\le\theta\le\pi/2, 0\le\phi\le 2\pi)\end{array}$$

For each, find the

(a) maximum power density (in watts/square meter) at a distance of 1,000 m (assume far-field distance). Specify the angle where this occurs.

(b) exact and approximate beam solid angle Ω_A.

(c) directivity, exact and approximate, of the antenna (dimensionless and in dB).

(d) gain, exact and approximate, of the antenna (dimensionless and in dB).

2.8. You are an antenna engineer and you are asked to design a high directivity/gain antenna for a space-borne communication system operating at 10 GHz. The specifications of the antenna are such that its pattern consists basically of *one major lobe* and, for simplicity, *no minor lobes* (*if there are any minor lobes they are of such very low intensity and you can assume they are negligible/zero*). Also it is desired that the pattern is symmetrical in the azimuthal plane. In order to meet the desired objectives, the main lobe of the pattern should have a *half-power beamwidth* of *10 degrees*. In order to expedite the design, it is assumed that the major lobe of the normalized radiation intensity of the antenna is approximated by

$$U(\theta,\phi)=\cos^n(\theta)$$

and it exists only in the upper hemisphere $(0\le\theta\le\pi/2, 0\le\phi\le 2\pi)$. Determine the:

(a) Value of n (*not necessarily an integer*) to meet the specifications of the major lobe. *Keep 5 significant figures in your calculations*.

(b) *Exact* maximum directivity of the antenna (*dimensionless* and *in dB*).

EX2042
Page 128 of 1072

(c) *Approximate* maximum directivity of the antenna *based on Kraus'* formula (*dimensionless* and *in dB*).

(d) *Approximate* maximum directivity of the antenna based on *Tai & Pereira's* formula (*dimensionless* and *in dB*).

2.9. In target-search ground-mapping radars it is desirable to have echo power received from a target, of constant cross section, to be independent of its range. For one such application, the desirable radiation intensity of the antenna is given by

$$U(\theta,\phi)=\left\{\begin{array}{cc}1 & 0^\circ\le\theta<20^\circ\\ 0.342\csc(\theta) & 20^\circ\le\theta<60^\circ\\ 0 & 60^\circ\le\theta\le180^\circ\end{array}\right\}\ 0^\circ\le\phi\le360^\circ$$

Find the directivity (in dB) using the exact formula.

2.10. A beam antenna has half-power beamwidths of 30° and 35° in perpendicular planes intersecting at the maximum of the mainbeam. Find its approximate maximum effective aperture (in λ^2) using (a) Kraus' and (b) Tai and Pereira's formulas. The minor lobes are very small and can be neglected.

2.11. The normalized radiation intensity of a given antenna is given by

(a) $U=\sin\theta\sin\phi$ (b) $U=\sin\theta\sin^2\phi$

(c) $U=\sin\theta\sin^3\phi$ (d) $U=\sin^2\theta\sin\phi$

(e) $U=\sin^2\theta\sin^2\phi$ (f) $U=\sin^2\theta\sin^3\phi$

The intensity exists only in the $0\le\theta\le\pi, 0\le\phi\le\pi$ region, and it is zero elsewhere. Find the

(a) exact directivity (dimensionless and in dB).

(b) azimuthal and elevation plane half-power beamwidths (in degrees).

2.12. Find the directivity (dimensionless and in dB) for the antenna of Problem 2.11 using

(a) Kraus' approximate formula (2-26)

(b) Tai and Pereira's approximate formula (2-30a)

2.13. For Problem 2.5, determine the approximate directivity (in dB) using

(a) Kraus' formula

(b) Tai and Pereira's formula.

2.14. The normalized radiation intensity of an antenna is rotationally symmetric in ϕ, and it is represented by

$$U=\left\{\begin{array}{ll}1 & 0^\circ\le\theta<30^\circ\\ 0.5 & 30^\circ\le\theta<60^\circ\\ 0.1 & 60^\circ\le\theta<90^\circ\\ 0 & 90^\circ\le\theta\le180^\circ\end{array}\right.$$

(a) What is the directivity (above isotropic) of the antenna (in dB)?

(b) What is the directivity (above an infinitesimal dipole) of the antenna (in dB)?

2.15. The radiation intensity of an antenna is given by

$$U(\theta, \phi) = \cos^4 \theta \sin^2 \phi$$

for $0 \leq \theta \leq \pi/2$ and $0 \leq \phi \leq 2\pi$ (i.e., in the upper half-space). It is zero in the lower half-space.
Find the

(a) exact directivity (dimensionless and in dB)

(b) elevation plane half-power beamwidth (in degrees)

2.16. The normalized radiation intensity of an antenna is symmetric, and it can be approximated by

$$U(\theta) = \begin{cases} 1 & 0^\circ \leq \theta < 30^\circ \\ \dfrac{\cos(\theta)}{0.866} & 30^\circ \leq \theta < 90^\circ \\ 0 & 90^\circ \leq \theta \leq 180^\circ \end{cases}$$

and it is independent of ϕ. Find the

(a) exact directivity by integrating the function

(b) approximate directivity using Kraus' formula

2.17. The maximum gain of a horn antenna is $+20$ dB, while the gain of its first sidelobe is -15 dB. What is the difference in gain between the maximum and first sidelobe:

(a) in dB

(b) as a ratio of the field intensities.

2.18. The normalized radiation intensity of an antenna is approximated by

$$U = \sin \theta$$

where $0 \leq \theta \leq \pi$, and $0 \leq \phi \leq 2\pi$. Determine the directivity using the

(a) exact formula

(b) formulas of (2-33a) by McDonald and (2-33b) by Pozar

(c) computer program ***Directivity*** of this chapter.

2.19. Repeat Problem 2.18 for a $\lambda/2$ dipole whose normalized intensity is approximated by

$$U \simeq \sin^3 \theta$$

Compare the value with that of (4-91) or 1.643 (2.156 dB).

2.20. The radiation intensity of a circular loop of radius a and of constant current is given by

$$U = J_1^2(ka \sin \theta), \quad 0 \leq \theta \leq \pi \quad \text{and} \quad 0 \leq \phi \leq 2\pi$$

where $J_1(x)$ is the Bessel function of order 1. For a loop with radii of $a = \lambda/10$ and $\lambda/20$, determine the directivity using the:

EX2042
Page 130 of 1072

(a) formulas (2-33a) by McDonald and (2-33b) by Pozar.

(b) computer program ***Directivity*** of this chapter.

Compare the answers with that of a very small loop represented by 1.5 or 1.76 dB.

2.21. Find the directivity (dimensionless and in dB) for the antenna of Problem 2.11 using numerical techniques with 10° uniform divisions and with the field evaluated at the

(a) midpoint

(b) trailing edge of each division.

2.22. Compute the directivity values of Problem 2.11 using the ***Directivity*** computer program of this chapter.

2.23. The far-zone electric-field intensity (array factor) of an end-fire two-element array antenna, placed along the z-axis and radiating into free-space, is given by

$$E = \cos\left[\frac{\pi}{4}(\cos\theta - 1)\right]\frac{e^{-jkr}}{r}, \qquad 0 \le \theta \le \pi$$

Find the directivity using

(a) Kraus' approximate formula

(b) the ***Directivity*** computer program of this chapter.

2.24. Repeat Problem 2.23 when

$$E = \cos\left[\frac{\pi}{4}(\cos\theta + 1)\right]\frac{e^{-jkr}}{r}, \qquad 0 \le \theta \le \pi$$

2.25. The radiation intensity is represented by

$$U = \begin{cases} U_0 \sin(\pi \sin\theta), & 0 \le \theta \le \pi/2 \text{ and } 0 \le \phi \le 2\pi \\ 0 & \text{elsewhere} \end{cases}$$

Find the directivity

(a) exactly

(b) using the computer program ***Directivity*** of this chapter.

2.26. The radiation intensity of an aperture antenna, mounted on an infinite ground plane with z perpendicular to the aperture, is rotationally symmetric (not a function of ϕ), and it is given by

$$U = \left[\frac{\sin(\pi \sin\theta)}{\pi \sin\theta}\right]^2$$

Find the approximate directivity (dimensionless and in dB) using

(a) numerical integration. Use the ***Directivity*** computer program of this chapter.

(b) Kraus' formula

(c) Tai and Pereira's formula.

EX2042
Page 131 of 1072

2.27. The normalized far-zone field pattern of an antenna is given by

$$E = \begin{cases} (\sin\theta\cos^2\phi)^{1/2} & 0 \le \theta \le \pi \text{ and } 0 \le \phi \le \pi/2, 3\pi/2 \le \phi \le 2\pi \\ 0 & \text{elsewhere} \end{cases}$$

Find the directivity using

(a) the exact expression

(b) Kraus' approximate formula

(c) Tai and Pereira's approximate formula

(d) the computer program ***Directivity*** of this chapter

2.28. The normalized field pattern of the main beam of a conical horn antenna, mounted on an infinite ground plane with z perpendicular to the aperture, is given by

$$\frac{J_1(ka\sin\theta)}{\sin\theta}$$

where a is its radius at the aperture. Assuming that $a = \lambda$, find the

(a) half-power beamwidth

(b) directivity using Kraus' approximate formula

2.29. A base station cellular communication systems *lossless* antenna has a *maximum gain* of 16 dB (above isotropic) at 1,900 MHz. Assuming the *input power* to the antenna is 8 watts, what is the *maximum* radiated power density (in watts/cm^2) at a distance of 100 meters? This will determine the safe level for human exposure to electromagnetic radiation.

2.30. A uniform plane wave, of a form similar to (2-55), is traveling in the positive z-direction. Find the polarization (linear, circular, or elliptical), sense of rotation (CW or CCW), axial ratio (AR), and tilt angle τ (in degrees) when

(a) $E_x = E_y, \Delta\phi = \phi_y - \phi_x = 0$

(b) $E_x \neq E_y, \Delta\phi = \phi_y - \phi_x = 0$

(c) $E_x = E_y, \Delta\phi = \phi_y - \phi_x = \pi/2$

(d) $E_x = E_y, \Delta\phi = \phi_y - \phi_x = -\pi/2$

(e) $E_x = E_y, \Delta\phi = \phi_y - \phi_x = \pi/4$

(f) $E_x = E_y, \Delta\phi = \phi_y - \phi_x = -\pi/4$

(g) $E_x = 0.5E_y, \Delta\phi = \phi_y - \phi_x = \pi/2$

(h) $E_x = 0.5E_y, \Delta\phi = \phi_y - \phi_x = -\pi/2$

In all cases, justify the answer.

2.31. Derive (2-66), (2-67), and (2-68).

2.32. Write a general expression for the polarization loss factor (PLF) of two linearly polarized antennas if

(a) both lie in the same plane

(b) both do not lie in the same plane

2.33. A linearly polarized wave traveling in the positive z-direction is incident upon a circularly polarized antenna. Find the polarization loss factor PLF (dimensionless and in dB) when the antenna is (based upon its transmission mode operation)

(a) right-handed (CW)
(b) left-handed (CCW)

2.34. A 300 MHz uniform plane wave, traveling along the *x-axis in the negative x direction*, whose electric field is given by

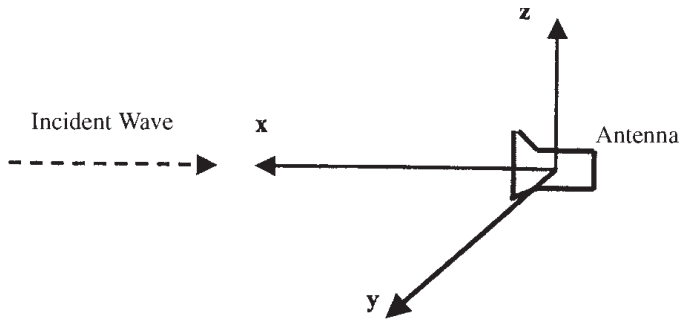
$$\mathbf{E}_w = E_o(j\hat{a}_y + 3\hat{a}_z)e^{+jkx}$$

where E_o is a real constant, impinges upon a dipole antenna that is placed at the origin and whose electric field radiated toward the *x-axis in the positive x direction* is given by

$$\mathbf{E}_a = E_a(\hat{a}_y + 2\hat{a}_z)e^{-jkx}$$

where E_a is a real constant. Determine the following:

(a) Polarization of the incident wave (*including axial ratio and sense of rotation, if any*). You must justify (state why?).
(b) Polarization of the antenna (*including axial ratio and sense of rotation, if any*). You must justify (state why?).
(c) Polarization loss factor (*dimensionless* and *in dB*).



2.35. The electric field of a uniform plane wave traveling along the *negative z* direction is given by

$$\mathbf{E}_w^i = (\hat{a}_x + j\hat{a}_y)E_o e^{+jkz}$$

and is incident upon a receiving antenna placed at the origin and *whose radiated electric field, toward the incident wave*, is given by

$$\mathbf{E}_a = (\hat{a}_x + \mathbf{2}\hat{a}_y)E_1 \frac{e^{-jkr}}{r}$$

Determine the following:

(a) Polarization of the *incident wave*, and why?
(b) Sense of rotation of the *incident wave*.
(c) Polarization *of the antenna*, and why?
(d) Sense of rotation of the *antenna polarization*.
(e) Losses (*dimensionless* and *in dB*) due to polarization mismatch between the incident wave and the antenna.

EX2042
Page 133 of 1072

2.36. A ground-based helical antenna is placed at the origin of a coordinate system and it is used as a receiving antenna. The normalized far-zone electric-field pattern of the helical antenna in the transmitting mode is represented in the direction θ_o, ϕ_o by

$$\mathbf{E}_a = E_o(j\hat{a}_\theta + 2\hat{a}_\phi) f_o(\theta_o, \phi_o) \frac{e^{-jkr}}{r}$$

The far-zone electric field transmitted by an antenna on a flying aircraft towards θ_o, ϕ_o, which is received by the ground-based helical antenna, is represented by

$$\mathbf{E}_w = E_1(2\hat{a}_\theta + j\hat{a}_\phi) f_1(\theta_o, \phi_o) \frac{e^{+jkr}}{r}$$

Determine the following:

(a) Polarization (*linear, circular, or elliptical*) of the helical antenna in the transmitting mode. *State also the sense of rotation, if any*.

(b) Polarization (*linear, circular, or elliptical*) of the incoming wave that impinges upon the helical antenna. *State also the sense of rotation, if any*.

(c) Polarization loss (*dimensionless and in dB*) due to match/mismatch of the polarizations of the antenna and incoming wave.

2.37. A circularly polarized wave, traveling in the positive z-direction, is incident upon a circularly polarized antenna. Find the polarization loss factor PLF (dimensionless and in dB) for right-hand (CW) and left-hand (CCW) wave and antenna.

2.38. The electric field radiated by a rectangular aperture, mounted on an infinite ground plane with z perpendicular to the aperture, is given by

$$\mathbf{E} = [\hat{\mathbf{a}}_\theta \cos\phi - \hat{\mathbf{a}}_\phi \sin\phi \cos\theta] f(r, \theta, \phi)$$

where $f(r, \theta, \phi)$ is a scalar function which describes the field variation of the antenna. Assuming that the receiving antenna is linearly polarized along the x-axis, find the polarization loss factor (PLF).

2.39. A circularly polarized wave, traveling in the $+z$-direction, is received by an elliptically polarized antenna whose reception characteristics near the main lobe are given approximately by

$$\mathbf{E}_a \simeq [2\hat{\mathbf{a}}_x + j\hat{\mathbf{a}}_y] f(r, \theta, \phi)$$

Find the polarization loss factor PLF (dimensionless and in dB) when the incident wave is

(a) right-hand (CW)

(b) left-hand (CCW)

circularly polarized. Repeat the problem when

$$\mathbf{E}_a \simeq [2\hat{\mathbf{a}}_x - j\hat{\mathbf{a}}_y] f(r, \theta, \phi)$$

In each case, what is the polarization of the antenna? How does it match with that of the wave?

2.40. A linearly polarized wave traveling in the negative z-direction has a tilt angle (τ) of 45°. It is incident upon an antenna whose polarization characteristics are given by

$$\hat{\boldsymbol{\rho}}_a = \frac{4\hat{\mathbf{a}}_x + j\hat{\mathbf{a}}_y}{\sqrt{17}}$$

Find the polarization loss factor PLF (dimensionless and db).

2.41. An elliptically polarized wave traveling in the negative z-direction is received by a circularly polarized antenna whose main lobe is along the $\theta = 0$ direction. The unit vector describing the polarization of the incident wave is given by

$$\hat{\boldsymbol{\rho}}_w = \frac{2\hat{\mathbf{a}}_x + j\hat{\mathbf{a}}_y}{\sqrt{5}}$$

Find the polarization loss factor PLF (dimensionless and in dB) when the wave that would be transmitted by the antenna is

(a) right-hand CP

(b) left-hand CP

2.42. A CW circularly polarized uniform plane wave is traveling in the $+z$ direction. Find the polarization loss factor PLF (dimensionless and in dB) assuming the receiving antenna (in its transmitting mode) is

(a) CW circularly polarized

(b) CCW circularly polarized

2.43. A linearly polarized uniform plane wave traveling in the $+z$ direction, with a power density of 10 milliwatts per square meter, is incident upon a CW circularly polarized antenna whose gain is 10 dB at 10 GHz. Find the

(a) maximum effective area of the antenna (in square meters)

(b) power (in watts) that will be delivered to a load attached directly to the terminals of the antenna.

2.44. A linearly polarized plane wave traveling along the negative z-axis is incident upon an elliptically polarized antenna (either CW or CCW). The axial ratio of the antenna polarization ellipse is 2:1 and its major axis coincides with the principal x-axis. Find the polarization loss factor (PLF) assuming the incident wave is linearly polarized in the

(a) x-direction

(b) y-direction

2.45. A wave traveling normally outward from the page (toward the reader) is the resultant of two elliptically polarized waves, one with components of **E** given by:

$$\mathscr{E}'_y = 3\cos\omega t$$

$$\mathscr{E}'_x = 7\cos\left(\omega t + \frac{\pi}{2}\right)$$

and the other with components given by:

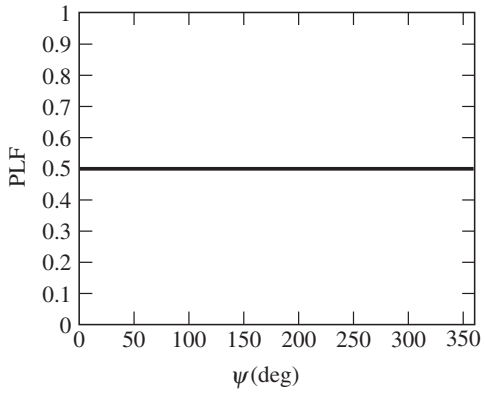
$$\mathscr{E}''_y = 2\cos\omega t$$
$$\mathscr{E}''_x = 3\cos\left(\omega t - \frac{\pi}{2}\right)$$

(a) What is the axial ratio of the resultant wave?

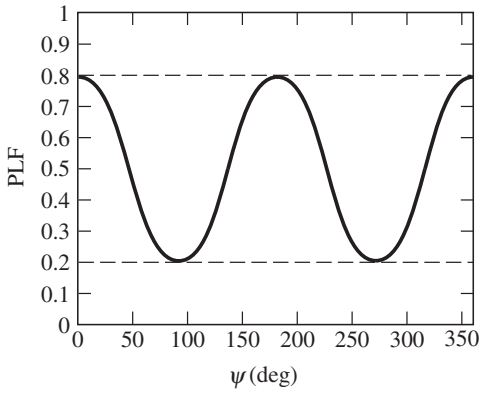
(b) Does the resultant vector **E** rotate clockwise or counterclockwise?

2.46. A linearly polarized antenna lying in the x-y plane is used to determine the polarization axial ratio of incoming plane waves traveling in the negative z-direction. The polarization of the antenna is described by the unit vector

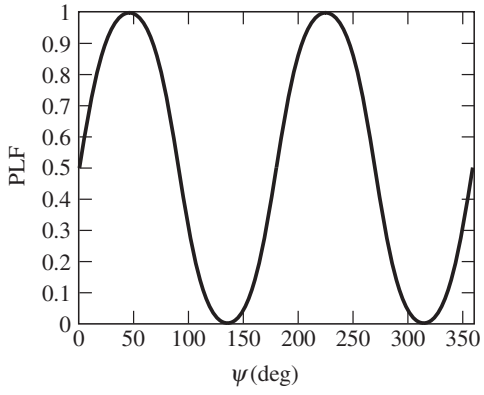
$$\hat{\boldsymbol{\rho}}_a = \hat{\mathbf{a}}_x \cos\psi + \hat{\mathbf{a}}_y \sin\psi$$



(a) PLF versus ψ



(b) PLF versus ψ



(c) PLF versus ψ

where ψ is an angle describing the orientation in the x-y plane of the receiving antenna. Above are the polarization loss factor (PLF) versus receiving antenna orientation curves obtained for three different incident plane waves. For each curve determine the axial ratio of the incident plane wave.

2.47. A $\lambda/2$ dipole, with a total loss resistance of 1 ohm, is connected to a generator whose internal impedance is $50 + j25$ ohms. Assuming that the peak voltage

EX2042
Page 136 of 1072

of the generator is 2 V and the impedance of the dipole, excluding the loss resistance, is $73 + j42.5$ ohms, find the power

(a) supplied by the source (real)

(b) radiated by the antenna

(c) dissipated by the antenna

2.48. The antenna and generator of Problem 2.47 are connected via a 50-ohm $\lambda/2$-long lossless transmission line. Find the power

(a) supplied by the source (real)

(b) radiated by the antenna

(c) dissipated by the antenna

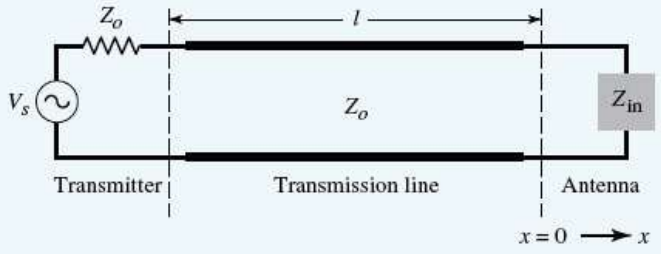
2.49. An antenna with a radiation resistance of 48 ohms, a loss resistance of 2 ohms, and a reactance of 50 ohms is connected to a generator with open-circuit voltage of 10 V and internal impedance of 50 ohms via a $\lambda/4$-long transmission line with characteristic impedance of 100 ohms.

(a) Draw the equivalent circuit

(b) Determine the power supplied by the generator

(c) Determine the power radiated by the antenna

2.50. A transmitter, with an internal impedance Z_0 (real), is connected to an antenna through a lossless transmission line of length l and characteristic impedance Z_0. Find a *simple* expression for the ratio between the antenna gain and its realized gain.



$$V(x) = A\,[e^{-jkx} + \Gamma(0)e^{+jkx}]$$

$$I(x) = \frac{A}{Z_0}\,[e^{-jkx} - \Gamma(0)e^{+jkx}]$$

V_s = strength of voltage source
$Z_{in} = R_{in} + jX_{in}$ = input impedance of the antenna
$Z_0 = R_0$ = characteristic impedance of the line
P_{accepted} = power accepted by the antenna $\{P_{\text{accepted}} = \text{Re}[V(0)I^*(0)]\}$
$P_{\text{available}}$ = power delivered to a matched load [i.e., $Z_{in} = Z_0^* = Z_0$]

2.51. The input reactance of an infinitesimal linear dipole of length $\lambda/60$ and radius $a = \lambda/200$ is given by

$$X_{in} \simeq -120\frac{[\ln(\ell/2a) - 1]}{\tan(k\ell/2)}$$

Assuming the wire of the dipole is copper with a conductivity of 5.7×10^7 S/m, determine at $f = 1$ GHz the

(a) loss resistance

(b) radiation resistance

EX2042
Page 137 of 1072

(c) radiation efficiency

(d) VSWR when the antenna is connected to a 50-ohm line

2.52. A dipole antenna consists of a circular wire of length l. Assuming the current distribution on the wire is cosinusoidal, i.e.,

$$I_z(z) = I_0 \cos\left(\frac{\pi}{l} z'\right) \quad -l/2 \le z' \le l/2$$

where I_0 is a constant, derive an expression for the loss resistance R_L, which is one-half of (2-90b).

2.53. The E-field pattern of an antenna, independent of ϕ, varies as follows:

$$E = \begin{cases} 1 & 0^\circ \le \theta \le 45^\circ \\ 0 & 45^\circ < \theta \le 90^\circ \\ \frac{1}{2} & 90^\circ < \theta \le 180^\circ \end{cases}$$

(a) What is the directivity of this antenna?

(b) What is the radiation resistance of the antenna at 200 m from it if the field is equal to 10 V/m (rms) for $\theta = 0^\circ$ at that distance and the terminal current is 5 A (rms)?

2.54. The far-zone field radiated by a rectangular aperture mounted on a ground plane, with dimensions a and b and uniform aperture distribution, is given by (see Table 12.1)

$$E \approx \hat{a}_\theta E_\theta + \hat{a}_\phi E_\phi$$

$$\left.\begin{aligned} E_\theta &= C \sin\phi \frac{\sin X}{X} \frac{\sin Y}{Y} \\ E_\phi &= C \cos\theta \cos\phi \frac{\sin X}{X} \frac{\sin Y}{Y} \end{aligned}\right\} \begin{aligned} X &= \frac{ka}{2} \sin\theta \cos\phi; \quad 0 \le \theta \le 90^\circ \\ Y &= \frac{kb}{2} \sin\theta \sin\phi; \quad 0 \le \phi \le 180^\circ \end{aligned}$$

where C is a constant and $0 \le \theta \le 90^\circ$ and $0 \le \phi \le 180^\circ$. For an aperture with $a = 3\lambda, b = 2\lambda$, determine the

(a) maximum partial directivities D_θ, D_ϕ (*dimensionless* and *in dB*) and

(b) total maximum directivity D_o (*dimensionless* and *in dB*). Compare with that computed using the equation in Table 12.1.

Use the computer program ***Directivity*** of this chapter.

2.55. Repeat Problem 2.54 when the aperture distribution is that of the dominant TE_{10} mode of a rectangular waveguide, or from Table 12.1

$$E \approx \hat{a}_\theta E_\theta + \hat{a}_\phi E_\phi$$

$$\left.\begin{aligned} E_\theta &= -\frac{\pi}{2} C \sin\phi \frac{\cos X}{(X)^2 - \left(\frac{\pi}{2}\right)^2} \frac{\sin Y}{Y} \\ E_\phi &= -\frac{\pi}{2} C \cos\theta \cos\phi \frac{\cos X}{(X)^2 - \left(\frac{\pi}{2}\right)^2} \frac{\sin Y}{Y} \end{aligned}\right\} \begin{aligned} X &= \frac{ka}{2} \sin\theta \cos\phi \\ Y &= \frac{kb}{2} \sin\theta \sin\phi \end{aligned}$$

EX2042
Page 138 of 1072

2.56. Repeat Problem 2.55 when the aperture dimensions are those of an X-band rectangular waveguide with $a = 2.286$ cm (0.9 in.), $b = 1.016$ cm (0.4 in.) and frequency of operation is 10 GHz.

2.57. Repeat Problem 2.54 for a circular aperture with a uniform distribution and whose far-zone fields are, from Table 12.2

$$\left.\begin{aligned} E &\approx \hat{a}_\theta E_\theta + \hat{a}_\phi E_\phi \\ E_\theta &= jC_1 \sin\phi \frac{J_1(Z)}{Z} \\ E_\phi &= jC_1 \cos\theta \cos\phi \frac{J_1(Z)}{Z} \end{aligned}\right\} \begin{aligned} Z &= ka \sin\theta; \qquad 0 \le \theta \le 90^\circ \\ &\qquad\qquad\quad 0 \le \phi \le 180^\circ \end{aligned}$$

where C_1 is a constant and $J_1(Z)$ is the Bessel function of the first kind. Assume $a = 1.5\lambda$.

2.58. Repeat Problem 2.57 when the aperture distribution is that of the dominant TE_{11} mode of a circular waveguide, or from Table 12.2

$$\left.\begin{aligned} E &\approx \hat{a}_\theta E_\theta + \hat{a}_\phi E_\phi \\ E_\theta &= C_2 \sin\phi \frac{J_1(Z)}{Z} \\ E_\phi &= C_2 \cos\theta \cos\phi \frac{J_z'(Z)}{(1) - \left(\dfrac{Z}{\chi_{11}'}\right)^2} \end{aligned}\right\} \begin{aligned} Z &= ka \sin\theta; \qquad 0 \le \theta \le 90^\circ \\ J_z'(Z) &= J_o(Z) \qquad 0 \le \phi \le 180^\circ \\ &\quad - J_1(Z)/Z; \end{aligned}$$

where C_2 is a constant, $J_1'(Z)$ is the derivative of $J_1(Z)$, $\chi_{11}' = 1.841$ is the first zero of $J_1'(Z)$, and $J_o(Z)$ is the Bessel function of the first kind of order zero.

2.59. Repeat 2.58 when the radius of the aperture is $a = 1.143$ cm (0.45 in.) and the frequency of operation is 10 GHz.

2.60. A 1-m long dipole antenna is driven by a 150 MHz source having a source resistance of 50 ohms and a voltage of 100 V. If the ohmic resistance of the antennas is given by $R_L = 0.625$ ohms, find the:

(a) Current going into the antenna (I_{ant})
(b) Power dissipated by the antenna
(c) Power radiated by the antenna
(d) Radiation efficiency of the antenna

2.61. The field radiated by an infinitesimal dipole of very small length ($\ell \le \lambda/50$), and of uniform current distribution I_o, is given by (4-26a) or

$$\mathbf{E} = \hat{a}_\theta E_\theta \approx \hat{a}_\theta j\eta \frac{kI_o\ell}{4\pi r} e^{-jkr} \sin\theta$$

Determine the

(a) vector effective length
(b) maximum value of the vector effective length. Specify the angle.

(c) ratio of the maximum effective length to the physical length ℓ.

2.62. The field radiated by a half-wavelength dipole ($\ell = \lambda/2$), with a sinusoidal current distribution, is given by (4-84) or

$$\mathbf{E} = \hat{a}_\theta E_\theta \approx \hat{a}_\theta j\eta \frac{I_o}{2\pi r} e^{-jkr} \left[\frac{\cos\left(\frac{\pi}{2}\cos\theta\right)}{\sin\theta} \right]$$

where I_o is the maximum current. Determine the

(a) vector effective length

(b) maximum value of the vector effective length. Specify the angle.

(c) ratio of the maximum effective length to the physical length ℓ.

2.63. A uniform plane wave, of 10^{-3}watts/cm^2 power density, is incident upon an infinitesimal dipole of length $\ell = \lambda/50$ and uniform current distribution, as shown in Figure 2.29(a). For a frequency of 10 GHz, determine the maximum open-circuited voltage at the terminals of the antenna. See Problem 2.61.

2.64. Repeat Problem 2.63 for a small dipole with triangular current distribution and length $\ell = \lambda/10$. See Example 2.14.

2.65. Repeat Problem 2.63 for a half-wavelength dipole ($\ell = \lambda/2$) with sinusoidal current distribution. See Problem 2.62.

2.66. Show that the effective length of a linear antenna can be written as

$$l_e = \sqrt{\frac{A_e |Z_t|^2}{\eta R_T}}$$

which for a lossless antenna and maximum power transfer reduces to

$$l_e = 2\sqrt{\frac{A_{em} R_r}{\eta}}$$

A_e and A_{em} represent, respectively, the effective and maximum effective apertures of the antenna while η is the intrinsic impedance of the medium.

2.67. An antenna has a maximum effective aperture of 2.147 m^2 at its operating frequency of 100 MHz. It has no conduction or dielectric losses. The input impedance of the antenna itself is 75 ohms, and it is connected to a 50-ohm transmission line. Find the directivity of the antenna system ("system" meaning includes any effects of connection to the transmission line). Assume no polarization losses.

2.68. A small circular parabolic reflector, often referred to as dish, is now being advertised as a TV antenna for direct broadcast. Assuming the diameter of the antenna is 1 meter, the frequency of operation is 3 GHz, and its aperture efficiency is 68%, determine the following:

(a) Physical area of the reflector (*in* m^2).

EX2042
Page 140 of 1072

(b) Maximum effective area of the antenna (*in* m^2).

(c) Maximum directivity (*dimensionless* and *in dB*).

(d) Maximum power (*in watts*) that can be delivered to the TV if the power density of the wave incident upon the antenna is *10* $\mu watts/m^2$. Assume *no losses* between the incident wave and the receiver (TV).

2.69. An incoming wave, with a uniform power density equal to 10^{-3} W/m^2 is incident normally upon a lossless horn antenna whose directivity is 20 dB. At a frequency of 10 GHz, determine the very maximum possible power that can be expected to be delivered to a receiver or a load connected to the horn antenna. There are no losses between the antenna and the receiver or load.

2.70. A linearly polarized aperture antenna, with a uniform field distribution over its area, is used as a receiving antenna. The antenna physical area over its aperture is 10 cm^2, and it is operating at 10 GHz. The antenna is illuminated with a circularly polarized plane wave whose incident power density is 10 mwatts/cm^2. Assuming the antenna element itself is lossless, determine its

(a) gain (*dimensionless* and *in dB*).

(b) maximum power (*in watts*) that can be delivered to a load connected to the antenna. Assume no other losses between the antenna and the load.

2.71. The *far-zone power density* radiated by a helical antenna can be approximated by

$$\mathbf{W}_{rad} = \mathbf{W}_{ave} \approx \hat{a}_r C_o \frac{1}{r^2} \cos^4 \theta$$

The radiated power density is symmetrical with respect to ϕ, and *it exists only in the upper hemisphere* $(0 \leq \theta \leq \pi/2, 0 \leq \phi \leq 2\pi)$; C_o is a constant. Determine the following:

(a) Power radiated by the antenna (*in watts*).

(b) Maximum directivity of the antenna (*dimensionless* and *in dB*)

(c) Direction (*in degrees*) along which the maximum directivity occurs.

(d) Maximum effective area (*in* m^2) at 1 GHz.

(e) Maximum power (*in watts*) received by the antenna, assuming no losses, at 1 GHz when the antenna is used as a receiver and the incident power density is *10 mwatts/*m^2.

2.72. For an *X*-band (8.2–12.4 GHz) rectangular horn, with aperture dimensions of 5.5 cm and 7.4 cm, find its maximum effective aperture (*in* cm^2) when its gain (over isotropic) is

(a) 14.8 dB at 8.2 GHz

(b) 16.5 dB at 10.3 GHz

(c) 18.0 dB at 12.4 GHz

2.73. For Problem 2.54 compute the

(a) maximum effective area (in λ^2) using the computer program ***Directivity*** of this chapter. Compare with that computed using the equation in Table 12.1.

EX2042
Page 141 of 1072

(b) aperture efficiencies of part (a). Are they smaller or larger than unity and why?

2.74. Repeat Problem 2.73 for Problem 2.55.

2.75. Repeat Problem 2.73 for Problem 2.56.

2.76. Repeat Problem 2.73 for Problem 2.57. Compare with those in Table 12.2.

2.77. Repeat Problem 2.73 for Problem 2.58. Compare with those in Table 12.2.

2.78. Repeat Problem 2.73 for Problem 2.59. Compare with those in Table 12.2.

2.79. A 30-dB, right-circularly polarized antenna in a radio link radiates 5 W of power at 2 GHz. The receiving antenna has an impedance mismatch at its terminals, which leads to a VSWR of 2. The receiving antenna is about 95% efficient and has a field pattern near the beam maximum given by $\mathbf{E}_r = (2\hat{\mathbf{a}}_x + j\hat{\mathbf{a}}_y)F_r(\theta, \phi)$. The distance between the two antennas is 4,000 km, and the receiving antenna is required to deliver 10^{-14} W to the receiver. Determine the maximum effective aperture of the receiving antenna.

2.80. The radiation intensity of an antenna can be approximated by

$$U(\theta, \phi) = \begin{cases} \cos^4(\theta) & 0^\circ \le \theta < 90^\circ \\ 0 & 90^\circ \le \theta \le 180^\circ \end{cases} \qquad \text{with } 0^\circ \le \phi \le 360^\circ$$

Determine the maximum effective aperture (*in* m^2) of the antenna if its frequency of operation is $f = 10$ GHz.

2.81. A communication satellite is in stationary (synchronous) orbit about the earth (assume altitude of 22,300 statute miles). Its transmitter generates 8.0 W. Assume the transmitting antenna is isotropic. Its signal is received by the 210-ft diameter tracking paraboloidal antenna on the earth at the NASA tracking station at Goldstone, California. Also assume no resistive losses in either antenna, perfect polarization match, and perfect impedance match at both antennas. At a frequency of 2 GHz, determine the:

(a) power density (*in watts/*m^2) incident on the receiving antenna.

(b) power received by the ground-based antenna whose gain is 60 dB.

2.82. A lossless ($e_{cd} = 1$) antenna is operating at 100 MHz and its maximum effective aperture is 0.7162 m^2 at this frequency. The input impedance of this antenna is 75 ohms, and it is attached to a 50-ohm transmission line. Find the directivity (dimensionless) of this antenna if it is polarization-matched.

2.83. A resonant, lossless ($e_{cd} = 1.0$) half-wavelength dipole antenna, having a directivity of 2.156 dB, has an input impedance of 73 ohms and is connected to a lossless, 50 ohms transmission line. A wave, having the same polarization as the antenna, is incident upon the antenna with a power density of 5 W/m^2 at a frequency of 10 MHz. Find the received power available at the end of the transmission line.

2.84. Two *X*-band (8.2–12.4 GHz) rectangular horns, with aperture dimensions of 5.5 cm and 7.4 cm and each with a gain of 16.3 dB (over isotropic) at 10 GHz,

are used as transmitting and receiving antennas. Assuming that the input power is 200 mW, the VSWR of each is 1.1, the conduction-dielectric efficiency is 100%, and the antennas are polarization-matched, find the maximum received power when the horns are separated in air by
(a) 5 m (b) 50 m (c) 500 m

2.85. Transmitting and receiving antennas operating at 1 GHz with gains (over isotropic) of 20 and 15 dB, respectively, are separated by a distance of 1 km. Find the maximum power delivered to the load when the input power is 150 W. Assume that the

(a) antennas are polarization-matched

(b) transmitting antenna is circularly polarized (either right- or left-hand) and the receiving antenna is linearly polarized.

2.86. Two lossless, polarization-matched antennas are aligned for maximum radiation between them, and are separated by a distance of 50λ. The antennas are matched to their transmission lines and have directivities of 20 dB. Assuming that the power at the input terminals of the transmitting antenna is 10 W, find the power at the terminals of the receiving antenna.

2.87. Repeat Problem 2.86 for two antennas with 30 dB directivities and separated by 100λ. The power at the input terminals is 20 W.

2.88. Transmitting and receiving antennas operating at 1 GHz with gains of 20 and 15 dB, respectively, are separated by a distance of 1 km. Find the power delivered to the load when the input power is 150 W. Assume the PLF $= 1$.

2.89. A series of microwave repeater links operating at 10 GHz are used to relay television signals into a valley that is surrounded by steep mountain ranges. Each repeater consists of a receiver, transmitter, antennas, and associated equipment. The transmitting and receiving antennas are identical horns, each having gain over isotropic of 15 dB. The repeaters are separated in distance by 10 km. For acceptable signal-to-noise ratio, the power received at each repeater must be greater than 10 nW. Loss due to polarization mismatch is not expected to exceed 3 dB. Assume matched loads and free-space propagation conditions. Determine the minimum transmitter power that should be used.

2.90. A one-way communication system, operating at 100 MHz, uses two identical $\lambda/2$ vertical, resonant, and lossless dipole antennas as transmitting and receiving elements separated by 10 km. In order for the signal to be detected by the receiver, the power level at the receiver terminals must be at least 1 μW. Each antenna is connected to the transmitter and receiver by a lossless 50-Ω transmission line. Assuming the antennas are polarization-matched and are aligned so that the maximum intensity of one is directed toward the maximum radiation intensity of the other, determine the minimum power that must be generated by the transmitter so that the signal will be detected by the receiver. Account for the proper losses from the transmitter to the receiver.

2.91. In a long-range microwave communication system operating at 9 GHz, the transmitting and receiving antennas are identical, and they are separated by

10,000 m. To meet the signal-to-noise ratio of the receiver, the received power must be at least 10 μW. Assuming the two antennas are aligned for maximum reception to each other, including being polarization-matched, what should the gains (in dB) of the transmitting and receiving antennas be when the input power to the transmitting antenna is 10 W?

2.92. A mobile wireless communication system operating at 2 GHz utilizes two antennas, one at the base station and the other at the mobile unit, which are separated by *16 kilometers*. The transmitting antenna, at the base station, is circularly-polarized while the receiving antenna, at the mobile station, is linearly polarized. The *maximum gain of the transmitting antenna is 20 dB* while the gain of the receiving antennas is unknown. The input power to the transmitting antenna is *100 watts* and the power received at the receiver, which is connected to the receiving antenna, is *5 nanowatts*. Assuming that the two antennas are aligned so that the maximum of one is directed toward the maximum of the other, *and also assuming no reflection/mismatch losses at the transmitter or the receiver*, what is the maximum gain of the receiving antenna (*dimensions* and *in dB*)?

2.93. A rectangular *X*-band horn, with aperture dimensions of 5.5 cm and 7.4 cm and a gain of 16.3 dB (over isotropic) at 10 GHz, is used to transmit and receive energy scattered from a perfectly conducting sphere of radius $a = 5\lambda$. Find the maximum scattered power delivered to the load when the distance between the horn and the sphere is
(a) 200λ (b) 500λ
Assume that the input power is 200 mW, and the radar cross section is equal to the geometrical cross section.

2.94. A radar antenna, used for both transmitting and receiving, has a gain of 150 (dimensionless) at its operating frequency of 5 GHz. It transmits 100 kW, and is aligned for maximum directional radiation and reception to a target 1 km away having a radar cross section of 3 m^2. The received signal matches the polarization of the transmitted signal. Find the received power.

2.95. In an experiment to determine the radar cross section of a Tomahawk cruise missile, a 1,000 W, 300 MHz signal was transmitted toward the target, and the received power was measured to be 0.1425 mW. The same antenna, whose gain was 75 (*dimensionless*), was used for both transmitting and receiving. The polarizations of both signals were identical (PLF = 1), and the distance between the antenna and missile was 500 m. What is the radar cross section of the cruise missile?

2.96. Repeat Problem 2.95 for a radar system with 1,000 W, 100 MHz transmitted signal, 0.01 W received signal, an antenna with a gain of 75 (*dimensionless*), and separation between the antenna and target of 700 m.

2.97. The maximum radar cross section of a resonant linear $\lambda/2$ dipole is approximately $0.86\lambda^2$. For a monostatic system (i.e., transmitter and receiver at the same location), find the received power (in W) if the transmitted power is 100 W, the distance of the dipole from the transmitting and receiving antennas is 100 m, the gain of the transmitting and receiving antennas is 15 dB each,

and the frequency of operation is 3 GHz. Assume a polarization loss factor of −1 dB.

2.98. The effective antenna temperature of an antenna looking toward zenith is approximately 5 K. Assuming that the temperature of the transmission line (waveguide) is 72 °F, find the effective temperature at the receiver terminals when the attenuation of the transmission line is 4 dB/100 ft and its length is
(a) 2 ft (b) 100 ft
Compare it to a receiver noise temperature of about 54 K.

2.99. Derive (2-146). Begin with an expression that assumes that the physical temperature and the attenuation of the transmission line are not constant.

CHAPTER 3

Radiation Integrals and Auxiliary Potential Functions

3.1 INTRODUCTION

In the analysis of radiation problems, the usual procedure is to specify the sources and then require the fields radiated by the sources. This is in contrast to the synthesis problem where the radiated fields are specified, and we are required to determine the sources.

It is a very common practice in the analysis procedure to introduce auxiliary functions, known as *vector potentials*, which will aid in the solution of the problems. The most common vector potential functions are the **A** (magnetic vector potential) and **F** (electric vector potential). Another pair is the Hertz potentials $\mathbf{\Pi}_e$ and $\mathbf{\Pi}_h$. *Although the electric and magnetic field intensities* (**E** *and* **H**) *represent physically measurable quantities, among most engineers the potentials are strictly mathematical tools*. The introduction of the potentials often simplifies the solution even though it may require determination of additional functions. While it is possible to determine the **E** and **H** fields directly from the source-current densities **J** and **M**, as shown in Figure 3.1, it is usually much simpler to find the auxiliary potential functions first and then determine the **E** and **H**. This two-step procedure is also shown in Figure 3.1.

The one-step procedure, through path 1, relates the **E** and **H** fields to **J** and **M** by integral relations. The two-step procedure, through path 2, relates the **A** and **F** (or $\mathbf{\Pi}_e$ and $\mathbf{\Pi}_h$) potentials to **J** and **M** by integral relations. The **E** and **H** are then determined simply by differentiating **A** and **F** (or $\mathbf{\Pi}_e$ and $\mathbf{\Pi}_h$). Although the two-step procedure requires both integration and differentiation, where path 1 requires only integration, the integrands in the two-step procedure are much simpler.

The most difficult operation in the two-step procedure is the integration to determine **A** and **F** (or $\mathbf{\Pi}_e$ and $\mathbf{\Pi}_h$). Once the vector potentials are known, then **E** and **H** can always be determined because any well-behaved function, no matter how complex, can always be differentiated.

The integration required to determine the potential functions is restricted over the bounds of the sources **J** and **M**. This will result in the **A** and **F** (or $\mathbf{\Pi}_e$ and $\mathbf{\Pi}_h$) to be functions of the observation point coordinates; the differentiation to determine **E** and **H** must be done in terms of the observation point coordinates. The integration

Antenna Theory: Analysis Design, Third Edition, by Constantine A. Balanis
ISBN 0-471-66782-X Copyright © 2005 John Wiley & Sons, Inc.

EX2042
Page 146 of 1072

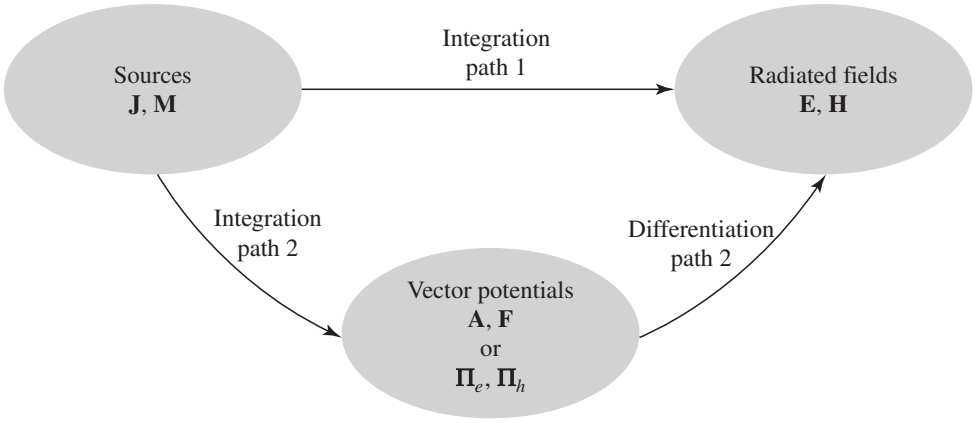


Figure 3.1 Block diagram for computing fields radiated by electric and magnetic sources.

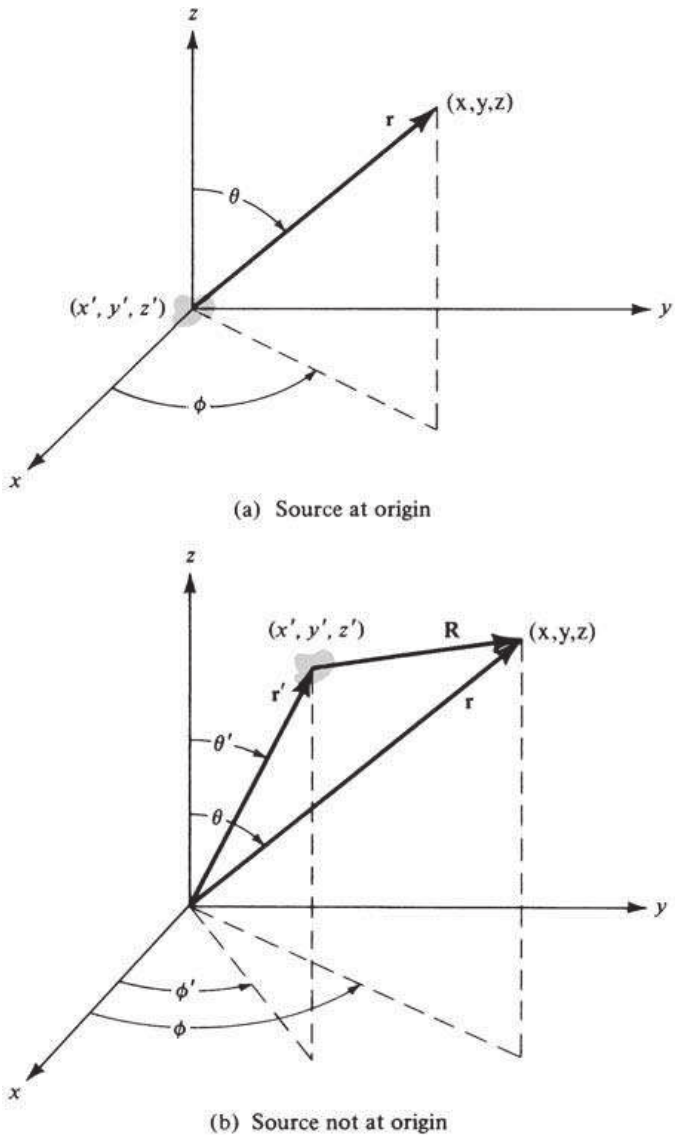


Figure 3.2 Coordinate systems for computing fields radiated by sources.

in the one-step procedure also requires that its limits be determined by the bounds of the sources.

The vector Hertz potential $\mathbf{\Pi}_e$ is analogous to $\mathbf{A}$ and $\mathbf{\Pi}_h$ is analogous to $\mathbf{F}$. The functional relation between them is a proportionality constant which is a function of the frequency and the constitutive parameters of the medium. In the solution of a problem, only one set, $\mathbf{A}$ and $\mathbf{F}$ or $\mathbf{\Pi}_e$ and $\mathbf{\Pi}_h$, is required. The author prefers the use of $\mathbf{A}$ and $\mathbf{F}$, which will be used throughout the book. The derivation of the functional relations between $\mathbf{A}$ and $\mathbf{\Pi}_e$, and $\mathbf{F}$ and $\mathbf{\Pi}_h$ are assigned at the end of the chapter as problems. (Problems 3.1 and 3.2).

3.2 THE VECTOR POTENTIAL A FOR AN ELECTRIC CURRENT SOURCE J

The vector potential $\mathbf{A}$ is useful in solving for the EM field generated by a given harmonic electric current $\mathbf{J}$. The magnetic flux $\mathbf{B}$ is always solenoidal; that is, $\nabla \cdot \mathbf{B} = 0$. Therefore, it can be represented as the curl of another vector because it obeys the vector identity

$$\nabla \cdot \nabla \times \mathbf{A} = 0 \tag{3-1}$$

where $\mathbf{A}$ is an arbitrary vector. Thus we define

$$\mathbf{B}_A = \mu \mathbf{H}_A = \nabla \times \mathbf{A} \tag{3-2}$$

or

$$\boxed{\mathbf{H}_A = \frac{1}{\mu} \nabla \times \mathbf{A}} \tag{3-2a}$$

where subscript A indicates the field due to the $\mathbf{A}$ potential. Substituting (3-2a) into Maxwell's curl equation

$$\nabla \times \mathbf{E}_A = -j\omega\mu \mathbf{H}_A \tag{3-3}$$

reduces it to

$$\nabla \times \mathbf{E}_A = -j\omega\mu \mathbf{H}_A = -j\omega \nabla \times \mathbf{A} \tag{3-4}$$

which can also be written as

$$\nabla \times [\mathbf{E}_A + j\omega \mathbf{A}] = 0 \tag{3-5}$$

From the vector identity

$$\nabla \times (-\nabla \phi_e) = 0 \tag{3-6}$$

and (3-5), it follows that

$$\mathbf{E}_A + j\omega \mathbf{A} = -\nabla \phi_e \tag{3-7}$$

or

$$\boxed{\mathbf{E}_A = -\nabla \phi_e - j\omega \mathbf{A}} \tag{3-7a}$$

EX2042
Page 148 of 1072

The scalar function ϕ_e represents an arbitrary electric scalar potential which is a function of position.

Taking the curl of both sides of (3-2) and using the vector identity

$$\nabla \times \nabla \times \mathbf{A} = \nabla(\nabla \cdot \mathbf{A}) - \nabla^2 \mathbf{A} \tag{3-8}$$

reduces it to

$$\nabla \times (\mu \mathbf{H}_A) = \nabla(\nabla \cdot \mathbf{A}) - \nabla^2 \mathbf{A} \tag{3-8a}$$

For a homogeneous medium, (3-8a) reduces to

$$\mu \nabla \times \mathbf{H}_A = \nabla(\nabla \cdot \mathbf{A}) - \nabla^2 \mathbf{A} \tag{3-9}$$

Equating Maxwell's equation

$$\boxed{\nabla \times \mathbf{H}_A = \mathbf{J} + j\omega\epsilon \mathbf{E}_A} \tag{3-10}$$

to (3-9) leads to

$$\mu \mathbf{J} + j\omega\mu\epsilon \mathbf{E}_A = \nabla(\nabla \cdot \mathbf{A}) - \nabla^2 \mathbf{A} \tag{3-11}$$

Substituting (3-7a) into (3-11) reduces it to

$$\begin{aligned} \nabla^2 \mathbf{A} + k^2 \mathbf{A} &= -\mu \mathbf{J} + \nabla(\nabla \cdot \mathbf{A}) + \nabla(j\omega\mu\epsilon\phi_e) \\ &= -\mu \mathbf{J} + \nabla(\nabla \cdot \mathbf{A} + j\omega\mu\epsilon\phi_e) \end{aligned} \tag{3-12}$$

where $k^2 = \omega^2 \mu\epsilon$.

In (3-2), the curl of $\mathbf{A}$ was defined. Now we are at liberty to define the divergence of $\mathbf{A}$, which is independent of its curl. In order to simplify (3-12), let

$$\boxed{\nabla \cdot \mathbf{A} = -j\omega\epsilon\mu\phi_e \Rightarrow \phi_e = -\frac{1}{j\omega\mu\epsilon} \nabla \cdot \mathbf{A}} \tag{3-13}$$

which is known as the *Lorentz condition*. Substituting (3-13) into (3-12) leads to

$$\boxed{\nabla^2 \mathbf{A} + k^2 \mathbf{A} = -\mu \mathbf{J}} \tag{3-14}$$

In addition, (3-7a) reduces to

$$\boxed{\mathbf{E}_A = -\nabla\phi_e - j\omega\mathbf{A} = -j\omega\mathbf{A} - j\frac{1}{\omega\mu\epsilon} \nabla(\nabla \cdot \mathbf{A})} \tag{3-15}$$

Once $\mathbf{A}$ is known, $\mathbf{H}_A$ can be found from (3-2a) and $\mathbf{E}_A$ from (3-15). $\mathbf{E}_A$ can just as easily be found from Maxwell's equation (3-10) with $\mathbf{J} = 0$. It will be shown later how to find $\mathbf{A}$ in terms of the current density $\mathbf{J}$. It will be a solution to the inhomogeneous Helmholtz equation of (3-14).

3.3 THE VECTOR POTENTIAL F FOR A MAGNETIC CURRENT SOURCE M

Although magnetic currents appear to be physically unrealizable, equivalent magnetic currents arise when we use the volume or the surface equivalence theorems. The fields generated by a harmonic magnetic current in a homogeneous region, with $\mathbf{J} = 0$ but $\mathbf{M} \neq 0$, must satisfy $\nabla \cdot \mathbf{D} = 0$. Therefore, $\mathbf{E}_F$ can be expressed as the curl of the vector potential $\mathbf{F}$ by

$$\boxed{\mathbf{E}_F = -\frac{1}{\epsilon}\nabla \times \mathbf{F}} \tag{3-16}$$

Substituting (3-16) into Maxwell's curl equation

$$\nabla \times \mathbf{H}_F = j\omega\epsilon\mathbf{E}_F \tag{3-17}$$

reduces it to

$$\nabla \times (\mathbf{H}_F + j\omega\mathbf{F}) = 0 \tag{3-18}$$

From the vector identity of (3-6), it follows that

$$\boxed{\mathbf{H}_F = -\nabla\phi_m - j\omega\mathbf{F}} \tag{3-19}$$

where ϕ_m represents an arbitrary magnetic scalar potential which is a function of position. Taking the curl of (3-16)

$$\nabla \times \mathbf{E}_F = -\frac{1}{\epsilon}\nabla \times \nabla \times \mathbf{F} = -\frac{1}{\epsilon}[\nabla\nabla \cdot \mathbf{F} - \nabla^2\mathbf{F}] \tag{3-20}$$

and equating it to Maxwell's equation

$$\boxed{\nabla \times \mathbf{E}_F = -\mathbf{M} - j\omega\mu\mathbf{H}_F} \tag{3-21}$$

leads to

$$\nabla^2\mathbf{F} + j\omega\mu\epsilon\mathbf{H}_F = \nabla\nabla \cdot \mathbf{F} - \epsilon\mathbf{M} \tag{3-22}$$

Substituting (3-19) into (3-22) reduces it to

$$\nabla^2\mathbf{F} + k^2\mathbf{F} = -\epsilon\mathbf{M} + \nabla(\nabla \cdot \mathbf{F}) + \nabla(j\omega\mu\epsilon\phi_m) \tag{3-23}$$

By letting

$$\boxed{\nabla \cdot \mathbf{F} = -j\omega\mu\epsilon\phi_m \Rightarrow \phi_m = -\frac{1}{j\omega\mu\epsilon}\nabla \cdot \mathbf{F}} \tag{3-24}$$

reduces (3-23) to

$$\boxed{\nabla^2\mathbf{F} + k^2\mathbf{F} = -\epsilon\mathbf{M}} \tag{3-25}$$

and (3-19) to

$$\boxed{\mathbf{H}_F = -j\omega\mathbf{F} - \frac{j}{\omega\mu\epsilon}\nabla(\nabla\cdot\mathbf{F})} \tag{3-26}$$

Once $\mathbf{F}$ is known, $\mathbf{E}_F$ can be found from (3-16) and $\mathbf{H}_F$ from (3-26) or (3-21) with $\mathbf{M} = 0$. It will be shown later how to find $\mathbf{F}$ once $\mathbf{M}$ is known. It will be a solution to the inhomogeneous Helmholtz equation of (3-25).

3.4 ELECTRIC AND MAGNETIC FIELDS FOR ELECTRIC (J) AND MAGNETIC (M) CURRENT SOURCES

In the previous two sections we have developed equations that can be used to find the electric and magnetic fields generated by an electric current source $\mathbf{J}$ and a magnetic current source $\mathbf{M}$. The procedure requires that the auxiliary potential functions $\mathbf{A}$ and $\mathbf{F}$ generated, respectively, by $\mathbf{J}$ and $\mathbf{M}$ are found first. In turn, the corresponding electric and magnetic fields are then determined ($\mathbf{E}_A$, $\mathbf{H}_A$ due to $\mathbf{A}$ and $\mathbf{E}_F$, $\mathbf{H}_F$ due to $\mathbf{F}$). The total fields are then obtained by the superposition of the individual fields due to $\mathbf{A}$ and $\mathbf{F}$ ($\mathbf{J}$ and $\mathbf{M}$).

In summary form, the procedure that can be used to find the fields is as follows:

Summary

1. Specify $\mathbf{J}$ and $\mathbf{M}$ (electric and magnetic current density sources).
2. a. Find $\mathbf{A}$ (due to $\mathbf{J}$) using

$$\boxed{\mathbf{A} = \frac{\mu}{4\pi}\iiint_V \mathbf{J}\frac{e^{-jkR}}{R}\,dv'} \tag{3-27}$$

which is a solution of the inhomogeneous vector wave equation of (3-14).

b. Find $\mathbf{F}$ (due to $\mathbf{M}$) using

$$\boxed{\mathbf{F} = \frac{\epsilon}{4\pi}\iiint_V \mathbf{M}\frac{e^{-jkR}}{R}\,dv'} \tag{3-28}$$

which is a solution of the inhomogeneous vector wave equation of (3-25). In (3-27) and (3-28), $k^2 = \omega^2\mu\epsilon$ and R is the distance from any point in the source to the observation point. In a latter section, we will demonstrate that (3-27) is a solution to (3-14) as (3-28) is to (3-25).

3. a. Find $\mathbf{H}_A$ using (3-2a) and $\mathbf{E}_A$ using (3-15). $\mathbf{E}_A$ can also be found using Maxwell's equation of (3-10) with $\mathbf{J} = 0$.
   b. Find $\mathbf{E}_F$ using (3-16) and $\mathbf{H}_F$ using (3-26). $\mathbf{H}_F$ can also be found using Maxwell's equation of (3-21) with $\mathbf{M} = 0$.
4. The total fields are then determined by

$$\boxed{\mathbf{E} = \mathbf{E}_A + \mathbf{E}_F = -j\omega\mathbf{A} - j\frac{1}{\omega\mu\epsilon}\nabla(\nabla \cdot \mathbf{A}) - \frac{1}{\epsilon}\nabla \times \mathbf{F}} \tag{3-29}$$

or

$$\boxed{\mathbf{E} = \mathbf{E}_A + \mathbf{E}_F = \frac{1}{j\omega\epsilon}\nabla \times \mathbf{H}_A - \frac{1}{\epsilon}\nabla \times \mathbf{F}} \tag{3-29a}$$

and

$$\boxed{\mathbf{H} = \mathbf{H}_A + \mathbf{H}_F = \frac{1}{\mu}\nabla \times \mathbf{A} - j\omega\mathbf{F} - j\frac{1}{\omega\mu\epsilon}\nabla(\nabla \cdot \mathbf{F})} \tag{3-30}$$

or

$$\boxed{\mathbf{H} = \mathbf{H}_A + \mathbf{H}_F = \frac{1}{\mu}\nabla \times \mathbf{A} - \frac{1}{j\omega\mu}\nabla \times \mathbf{E}_F} \tag{3-30a}$$

Whether (3-15) or (3-10) is used to find $\mathbf{E}_A$ and (3-26) or (3-21) to find $\mathbf{H}_F$ depends largely upon the problem. In many instances one may be more complex than the other or vice versa. In computing fields in the far-zone, it will be easier to use (3-15) for $\mathbf{E}_A$ and (3-26) for $\mathbf{H}_F$ because, as it will be shown, the second term in each expression becomes negligible in that region.

3.5 SOLUTION OF THE INHOMOGENEOUS VECTOR POTENTIAL WAVE EQUATION

In the previous section we indicated that the solution of the inhomogeneous vector wave equation of (3-14) is (3-27).

To derive it, let us assume that a source with current density J_z, which in the limit is an infinitesimal source, is placed at the origin of a *x, y, z* coordinate system, as shown in Figure 3.2(a). Since the current density is directed along the z-axis (J_z), only an A_z component will exist. Thus we can write (3-14) as

$$\nabla^2 A_z + k^2 A_z = -\mu J_z \tag{3-31}$$

At points removed from the source ($J_z = 0$), the wave equation reduces to

$$\nabla^2 A_z + k^2 A_z = 0 \tag{3-32}$$

Since in the limit the source is a point, it requires that A_z is not a function of direction (θ and ϕ); in a spherical coordinate system, $A_z = A_z(r)$ where r is the radial distance. Thus (3-32) can be written as

$$\nabla^2 A_z(r) + k^2 A_z(r) = \frac{1}{r^2}\frac{\partial}{\partial r}\left[r^2 \frac{\partial A_z(r)}{\partial r}\right] + k^2 A_z(r) = 0 \tag{3-33}$$

which when expanded reduces to

$$\frac{d^2 A_z(r)}{dr^2} + \frac{2}{r}\frac{dA_z(r)}{dr} + k^2 A_z(r) = 0 \tag{3-34}$$

The partial derivative has been replaced by the ordinary derivative since A_z is only a function of the radial coordinate.

The differential equation of (3-34) has two independent solutions

$$A_{z1} = C_1 \frac{e^{-jkr}}{r} \tag{3-35}$$

$$A_{z2} = C_2 \frac{e^{+jkr}}{r} \tag{3-36}$$

Equation (3-35) represents an outwardly (in the radial direction) traveling wave and (3-36) describes an inwardly traveling wave (assuming an $e^{j\omega t}$ time variation). For this problem, the source is placed at the origin with the radiated fields traveling in the outward radial direction. Therefore, we choose the solution of (3-35), or

$$A_z = A_{z1} = C_1 \frac{e^{-jkr}}{r} \tag{3-37}$$

In the static case ($\omega = 0, k = 0$), (3-37) simplifies to

$$A_z = \frac{C_1}{r} \tag{3-38}$$

which is a solution to the wave equation of (3-32), (3-33), or (3-34) when $k = 0$. Thus at points removed from the source, the time-varying and the static solutions of (3-37) and (3-38) differ only by the e^{-jkr} factor; or the time-varying solution of (3-37) can be obtained by multiplying the static solution of (3-38) by e^{-jkr}.

In the presence of the source ($J_z \neq 0$) and $k = 0$, the wave equation of (3-31) reduces to

$$\nabla^2 A_z = -\mu J_z \tag{3-39}$$

This equation is recognized to be Poisson's equation whose solution is widely documented. The most familiar equation with Poisson's form is that relating the scalar electric potential ϕ to the electric charge density ρ. This is given by

$$\nabla^2 \phi = -\frac{\rho}{\epsilon} \tag{3-40}$$

whose solution is

$$\phi = \frac{1}{4\pi\epsilon} \iiint_V \frac{\rho}{r}\, dv' \tag{3-41}$$

where r is the distance from any point on the charge density to the observation point. Since (3-39) is similar in form to (3-40), its solution is similar to (3-41), or

$$A_z = \frac{\mu}{4\pi} \iiint_V \frac{J_z}{r}\, dv' \tag{3-42}$$

Equation (3-42) represents the solution to (3-31) when $k = 0$ (static case). Using the comparative analogy between (3-37) and (3-38), the time-varying solution of (3-31) can be obtained by multiplying the static solution of (3-42) by e^{-jkr}. Thus

$$\boxed{A_z = \frac{\mu}{4\pi} \iiint_V J_z \frac{e^{-jkr}}{r}\, dv'} \tag{3-43}$$

which is a solution to (3-31).

If the current densities were in the x- and y-directions (J_x and J_y), the wave equation for each would reduce to

$$\nabla^2 A_x + k^2 A_x = -\mu J_x \tag{3-44}$$

$$\nabla^2 A_y + k^2 A_y = -\mu J_y \tag{3-45}$$

with corresponding solutions similar in form to (3-43), or

$$\boxed{A_x = \frac{\mu}{4\pi} \iiint_V J_x \frac{e^{-jkr}}{r}\, dv'} \tag{3-46}$$

$$\boxed{A_y = \frac{\mu}{4\pi} \iiint_V J_y \frac{e^{-jkr}}{r}\, dv'} \tag{3-47}$$

The solutions of (3-43), (3-46), and (3-47) allow us to write the solution to the vector wave equation of (3-14) as

$$\boxed{\mathbf{A} = \frac{\mu}{4\pi} \iiint_V \mathbf{J} \frac{e^{-jkr}}{r}\, dv'} \tag{3-48}$$

If the source is removed from the origin and placed at a position represented by the primed coordinates (x', y', z'), as shown in Figure 3.2(b), (3-48) can be written as

$$\mathbf{A}(x, y, z) = \frac{\mu}{4\pi} \iiint_V \mathbf{J}(x', y', z') \frac{e^{-jkR}}{R} dv' \tag{3-49}$$

where the primed coordinates represent the source, the unprimed the observation point, and R the distance from any point on the source to the observation point. In a similar fashion we can show that the solution of (3-25) is given by

$$\mathbf{F}(x, y, z) = \frac{\epsilon}{4\pi} \iiint_V \mathbf{M}(x', y', z') \frac{e^{-jkR}}{R} dv' \tag{3-50}$$

If $\mathbf{J}$ and $\mathbf{M}$ represent linear densities (m^{-1}), (3-49) and (3-50) reduce to surface integrals, or

$$\mathbf{A} = \frac{\mu}{4\pi} \iint_S \mathbf{J}_s(x', y', z') \frac{e^{-jkR}}{R} ds' \tag{3-51}$$

$$\mathbf{F} = \frac{\epsilon}{4\pi} \iint_S \mathbf{M}_s(x', y', z') \frac{e^{-jkR}}{R} ds' \tag{3-52}$$

For electric and magnetic currents $\mathbf{I}_e$ and $\mathbf{I}_m$, (3-51) and (3-52) reduce to line integrals of the form

$$\mathbf{A} = \frac{\mu}{4\pi} \int_C \mathbf{I}_e(x', y', z') \frac{e^{-jkR}}{R} dl' \tag{3-53}$$

$$\mathbf{F} = \frac{\epsilon}{4\pi} \int_C \mathbf{I}_m(x', y', z') \frac{e^{-jkR}}{R} dl' \tag{3-54}$$

3.6 FAR-FIELD RADIATION

The fields radiated by antennas of finite dimensions are spherical waves. For these radiators, a general solution to the vector wave equation of (3-14) in spherical components, each as a function of r, θ, ϕ, takes the general form of

$$\mathbf{A} = \hat{\mathbf{a}}_r A_r(r, \theta, \phi) + \hat{\mathbf{a}}_\theta A_\theta(r, \theta, \phi) + \hat{\mathbf{a}}_\phi A_\phi(r, \theta, \phi) \tag{3-55}$$

The amplitude variations of r in each component of (3-55) are of the form $1/r^n, n = 1, 2, \ldots$ [1], [2]. Neglecting higher order terms of $1/r^n (1/r^n = 0, n = 2, 3, \ldots)$ reduces (3-55) to

$$\mathbf{A} \simeq [\hat{\mathbf{a}}_r A'_r(\theta, \phi) + \hat{\mathbf{a}}_\theta A'_\theta \theta, \phi) + \hat{\mathbf{a}}_\phi A'_\phi(\theta, \phi)] \frac{e^{-jkr}}{r}, \quad r \to \infty \tag{3-56}$$

The r variations are separable from those of θ and ϕ. This will be demonstrated in the chapters that follow by many examples.

Substituting (3-56) into (3-15) reduces it to

$$\mathbf{E} = \frac{1}{r}\{-j\omega e^{-jkr}[\hat{\mathbf{a}}_r(0) + \hat{\mathbf{a}}_\theta A'_\theta(\theta, \phi) + \hat{\mathbf{a}}_\phi A'_\phi(\theta, \phi)]\} + \frac{1}{r^2}\{\cdots\} + \cdots \tag{3-57}$$

The radial **E**-field component has no $1/r$ terms, because its contributions from the first and second terms of (3-15) cancel each other.

Similarly, by using (3-56), we can write (3-2a) as

$$\mathbf{H} = \frac{1}{r}\left\{ j\frac{\omega}{\eta} e^{-jkr}[\hat{\mathbf{a}}_r(0) + \hat{\mathbf{a}}_\theta A'_\phi(\theta, \phi) - \hat{\mathbf{a}}_\phi A'_\theta(\theta, \phi)] \right\} + \frac{1}{r^2}\{\cdots\} + \cdots \tag{3-57a}$$

where $\eta = \sqrt{\mu/\epsilon}$ is the intrinsic impedance of the medium.

Neglecting higher order terms of $1/r^n$, the radiated **E**- and **H**-fields have only θ and ϕ components. They can be expressed as

Far-Field Region

$$\left.\begin{aligned} E_r &\simeq 0 \\ E_\theta &\simeq -j\omega A_\theta \\ E_\phi &\simeq -j\omega A_\phi \end{aligned}\right\} \Rightarrow \boxed{\mathbf{E}_A \simeq -j\omega\mathbf{A}} \quad \text{(for the } \theta \text{ and } \phi \text{ components only since } E_r \simeq 0) \tag{3-58a}$$

$$\left.\begin{aligned} H_r &\simeq 0 \\ H_\theta &\simeq +j\frac{\omega}{\eta}A_\phi = -\frac{E_\phi}{\eta} \\ H_\phi &\simeq -j\frac{\omega}{\eta}A_\theta = +\frac{E_\theta}{\eta} \end{aligned}\right\} \Rightarrow \boxed{\mathbf{H}_A \simeq \frac{\hat{\mathbf{a}}_r}{\eta} \times \mathbf{E}_A = -j\frac{\omega}{\eta}\hat{\mathbf{a}}_r \times \mathbf{A}} \quad \text{(for the } \theta \text{ and } \phi \text{ components only since } H_r \simeq 0) \tag{3-58b}$$

Radial field components exist only for higher order terms of $1/r^n$.

In a similar manner, the far-zone fields due to a magnetic source **M** (potential **F**) can be written as

Far-Field Region

$$\left.\begin{aligned} H_r &\simeq 0 \\ H_\theta &\simeq -j\omega F_\theta \\ H_\phi &\simeq -j\omega F_\phi \end{aligned}\right\} \Rightarrow \boxed{\mathbf{H}_F \simeq -j\omega\mathbf{F}} \quad \text{(for the } \theta \text{ and } \phi \text{ components only since } H_r \simeq 0) \tag{3-59a}$$

$$\left.\begin{aligned} E_r &\simeq 0 \\ E_\theta &\simeq -j\omega\eta F_\phi = \eta H_\phi \\ E_\phi &\simeq +j\omega\eta F_\theta = -\eta H_\theta \end{aligned}\right\} \Rightarrow \boxed{\mathbf{E}_F = -\eta\hat{\mathbf{a}}_r \times \mathbf{H}_F = j\omega\eta\hat{\mathbf{a}}_r \times \mathbf{F}} \quad \text{(for the } \theta \text{ and } \phi \text{ components only since } E_r \simeq 0) \tag{3-59b}$$

Simply stated, *the corresponding far-zone* **E**- *and* **H**-*field components are orthogonal to each other and form TEM* $(to\ r)$ *mode fields*. This is a very useful relation, and it will be adopted in the chapters that follow for the solution of the far-zone radiated fields. The far-zone (far-field) region for a radiator is defined in Figures 2.7 and 2.8. Its smallest radial distance is $2D^2/\lambda$ where D is the largest dimension of the radiator.

3.7 DUALITY THEOREM

When two equations that describe the behavior of two different variables are of the same mathematical form, their solutions will also be identical. The variables in the two equations that occupy identical positions are known as *dual* quantities and a solution of one can be formed by a systematic interchange of symbols to the other. This concept is known as the *duality theorem*.

Comparing Equations (3-2a), (3-3), (3-10), (3-14), and (3-15) to (3-16), (3-17), (3-21), (3-25), and (3-26), respectively, it is evident that they are to each other dual equations and their variables dual quantities. Thus knowing the solutions to one set (i.e., $\mathbf{J} \neq 0, \mathbf{M} = 0$), the solution to the other set ($\mathbf{J} = 0, \mathbf{M} \neq 0$) can be formed by a proper interchange of quantities. The dual equations and their dual quantities are listed, respectively in Tables 3.1 and 3.2 for electric and magnetic sources. Duality only serves as a guide to form mathematical solutions. It can be used in an abstract manner to explain the motion of magnetic charges giving rise to magnetic currents, when compared to their dual quantities of moving electric charges creating electric currents. It must, however, be emphasized that this is purely mathematical in nature since it is known, as of today, that there are no magnetic charges or currents in nature.

3.8 RECIPROCITY AND REACTION THEOREMS

We are all well familiar with the reciprocity theorem, as applied to circuits, which states that "in any network composed of linear, bilateral, lumped elements, if one places a constant **current** *(voltage)* generator between two **nodes** *(in any branch)* and

TABLE 3.1 Dual Equations for Electric (J) and Magnetic (M) Current Sources

Electric Sources ($\mathbf{J} \neq 0$, $\mathbf{M} = 0$)	**Magnetic Sources** ($\mathbf{J} = 0$, $\mathbf{M} \neq 0$)
$\nabla \times \mathbf{E}_A = -j\omega\mu\mathbf{H}_A$	$\nabla \times \mathbf{H}_F = j\omega\epsilon\mathbf{E}_F$
$\nabla \times \mathbf{H}_A = \mathbf{J} + j\omega\epsilon\mathbf{E}_A$	$-\nabla \times \mathbf{E}_F = \mathbf{M} + j\omega\mu\mathbf{H}_F$
$\nabla^2\mathbf{A} + k^2\mathbf{A} = -\mu\mathbf{J}$	$\nabla^2\mathbf{F} + k^2\mathbf{F} = -\epsilon\mathbf{M}$
$\mathbf{A} = \dfrac{\mu}{4\pi}\iiint_V \mathbf{J}\dfrac{e^{-jkR}}{R}dv'$	$\mathbf{F} = \dfrac{\epsilon}{4\pi}\iiint_V \mathbf{M}\dfrac{e^{-jkR}}{R}dv'$
$\mathbf{H}_A = \dfrac{1}{\mu}\nabla \times \mathbf{A}$	$\mathbf{E}_F = -\dfrac{1}{\epsilon}\nabla \times \mathbf{F}$
$\mathbf{E}_A = -j\omega\mathbf{A} - j\dfrac{1}{\omega\mu\epsilon}\nabla(\nabla \cdot \mathbf{A})$	$\mathbf{H}_F = -j\omega\mathbf{F} - j\dfrac{1}{\omega\mu\epsilon}\nabla(\nabla \cdot \mathbf{F})$

TABLE 3.2 Dual Quantities for Electric (J) and Magnetic (M) Current Sources

Electric Sources ($\mathbf{J} \neq 0, \mathbf{M} = 0$)	Magnetic Sources ($\mathbf{J} = 0, \mathbf{M} \neq 0$)
$\mathbf{E}_A$	$\mathbf{H}_F$
$\mathbf{H}_A$	$-\mathbf{E}_F$
$\mathbf{J}$	$\mathbf{M}$
$\mathbf{A}$	$\mathbf{F}$
ϵ	μ
μ	ϵ
k	k
η	$1/\eta$
$1/\eta$	η

places a **voltage** *(current)* meter between any other two **nodes** *(in any other branch)*, makes observation of the meter reading, then interchanges the locations of the source and the meter, the meter reading will be unchanged" [3]. We want now to discuss the reciprocity theorem as it applies to electromagnetic theory. This is done best by the use of Maxwell's equations.

Let us assume that within a linear and isotropic medium, but not necessarily homogeneous, there exist two sets of sources $\mathbf{J}_1, \mathbf{M}_1$, and $\mathbf{J}_2, \mathbf{M}_2$ which are allowed to radiate simultaneously or individually inside the same medium at the same frequency and produce fields $\mathbf{E}_1, \mathbf{H}_1$ and $\mathbf{E}_2, \mathbf{H}_2$, respectively. It can be shown [1], [2] that the sources and fields satisfy

$$-\nabla \cdot (\mathbf{E}_1 \times \mathbf{H}_2 - \mathbf{E}_2 \times \mathbf{H}_1) = \mathbf{E}_1 \cdot \mathbf{J}_2 + \mathbf{H}_2 \cdot \mathbf{M}_1 - \mathbf{E}_2 \cdot \mathbf{J}_1 - \mathbf{H}_1 \cdot \mathbf{M}_2 \tag{3-60}$$

which is called the *Lorentz Reciprocity Theorem* in differential form.

Taking a volume integral of both sides of (3-60) and using the divergence theorem on the left side, we can write it as

$$-\oiint_S (\mathbf{E}_1 \times \mathbf{H}_2 - \mathbf{E}_2 \times \mathbf{H}_1) \cdot d\mathbf{s}'$$

$$= \iiint_V (\mathbf{E}_1 \cdot \mathbf{J}_2 + \mathbf{H}_2 \cdot \mathbf{M}_1 - \mathbf{E}_2 \cdot \mathbf{J}_1 - \mathbf{H}_1 \cdot \mathbf{M}_2)\, dv' \tag{3-61}$$

which is designated as the *Lorentz Reciprocity Theorem* in integral form.

For a source-free ($\mathbf{J}_1 = \mathbf{J}_2 = \mathbf{M}_1 = \mathbf{M}_2 = 0$) region, (3-60) and (3-61) reduce, respectively, to

$$\boxed{\nabla \cdot (\mathbf{E}_1 \times \mathbf{H}_2 - \mathbf{E}_2 \times \mathbf{H}_1) = 0} \tag{3-62}$$

and

$$\boxed{\oiint_S (\mathbf{E}_1 \times \mathbf{H}_2 - \mathbf{E}_2 \times \mathbf{H}_1) \cdot d\mathbf{s}' = 0} \tag{3-63}$$

Equations (3-62) and (3-63) are special cases of the Lorentz Reciprocity Theorem and must be satisfied in source-free regions.

As an example of where (3-62) and (3-63) may be applied and what they would represent, consider a section of a waveguide where two different modes exist with fields $\mathbf{E}_1, \mathbf{H}_1$ and $\mathbf{E}_2, \mathbf{H}_2$. For the expressions of the fields for the two modes to be valid, they must satisfy (3-62) and/or (3-63).

Another useful form of (3-61) is to consider that the fields $(\mathbf{E}_1, \mathbf{H}_1, \mathbf{E}_2, \mathbf{H}_2)$ and the sources $(\mathbf{J}_1, \mathbf{M}_1, \mathbf{J}_2, \mathbf{M}_2)$ are within a medium that is enclosed by a sphere of infinite radius. Assume that the sources are positioned within a finite region and that the fields are observed in the far field (ideally at infinity). Then the left side of (3-61) is equal to zero, or

$$\oiint_S (\mathbf{E}_1 \times \mathbf{H}_2 - \mathbf{E}_2 \times \mathbf{H}_1) \cdot d\mathbf{s}' = 0 \tag{3-64}$$

which reduces (3-61) to

$$\iiint_V (\mathbf{E}_1 \cdot \mathbf{J}_2 + \mathbf{H}_2 \cdot \mathbf{M}_1 - \mathbf{E}_2 \cdot \mathbf{J}_1 - \mathbf{H}_1 \cdot \mathbf{M}_2)\, dv' = 0 \tag{3-65}$$

Equation (3-65) can also be written as

$$\boxed{\iiint_V (\mathbf{E}_1 \cdot \mathbf{J}_2 - \mathbf{H}_1 \cdot \mathbf{M}_2)\, dv' = \iiint_V (\mathbf{E}_2 \cdot \mathbf{J}_1 - \mathbf{H}_2 \cdot \mathbf{M}_1)\, dv'} \tag{3-66}$$

The reciprocity theorem, as expressed by (3-66), is the most useful form.

A close observation of (3-61) reveals that it does not, in general, represent relations of power because no conjugates appear. The same is true for the special cases represented by (3-63) and (3-66). Each of the integrals in (3-66) can be interpreted as a coupling between a set of fields and a set of sources, which produce another set of fields. This coupling has been defined as *Reaction* [4] and each of the integrals in (3-66) are denoted by

$$\langle 1, 2 \rangle = \iiint_V (\mathbf{E}_1 \cdot \mathbf{J}_2 - \mathbf{H}_1 \cdot \mathbf{M}_2)\, dv \tag{3-67}$$

$$\langle 2, 1 \rangle = \iiint_V (\mathbf{E}_2 \cdot \mathbf{J}_1 - \mathbf{H}_2 \cdot \mathbf{M}_1)\, dv \tag{3-68}$$

The relation $\langle 1, 2 \rangle$ of (3-67) relates the reaction (coupling) of fields $(\mathbf{E}_1, \mathbf{H}_1)$, which are produced by sources $\mathbf{J}_1, \mathbf{M}_1$ to sources $(\mathbf{J}_2, \mathbf{M}_2)$, which produce fields $\mathbf{E}_2, \mathbf{H}_2$; $\langle 2, 1 \rangle$ relates the reaction (coupling) of fields $(\mathbf{E}_2, \mathbf{H}_2)$ to sources $(\mathbf{J}_1, \mathbf{M}_1)$. For reciprocity to hold, it requires that the reaction (coupling) of one set of sources with the corresponding fields of another set of sources must be equal to the reaction (coupling) of the second

set of sources with the corresponding fields of the first set of sources, and vice versa. In equation form, it is written as

$$\langle 1, 2\rangle = \langle 2, 1\rangle \tag{3-69}$$

3.8.1 Reciprocity for Two Antennas

There are many applications of the reciprocity theorem. To demonstrate its potential, an antenna example will be considered. Two antennas, whose input impedances are Z_1 and Z_2, are separated by a linear and isotropic (but not necessarily homogeneous) medium, as shown in Figure 3.3. One antenna (#1) is used as a transmitter and the other (#2) as a receiver. The equivalent network of each antenna is given in Figure 3.4. The internal impedance of the generator Z_g is assumed to be the conjugate of the impedance of antenna #1 ($Z_g = Z_1^* = R_1 - jX_1$) while the load impedance Z_L is equal to the conjugate of the impedance of antenna #2 ($Z_L = Z_2^* = R_2 - jX_2$). These assumptions are made only for convenience.

The power delivered by the generator to antenna #1 is given by (2-83) or

$$P_1 = \frac{1}{2}\text{Re}[V_1 I_1^*] = \frac{1}{2}\text{Re}\left[\left(\frac{V_g Z_1}{Z_1 + Z_g}\right)\frac{V_g^*}{(Z_1 + Z_g)^*}\right] = \frac{|V_g|^2}{8R_1} \tag{3-70}$$

If the transfer admittance of the combined network consisting of the generator impedance, antennas, and load impedance is Y_{21}, the current through the load is $V_g Y_{21}$ and the power delivered to the load is

$$P_2 = \tfrac{1}{2}\text{Re}[Z_2(V_g Y_{21})(V_g Y_{21})^*] = \tfrac{1}{2}R_2|V_g|^2|Y_{21}|^2 \tag{3-71}$$

The ratio of (3-71) to (3-70) is

$$\frac{P_2}{P_1} = 4R_1 R_2|Y_{21}|^2 \tag{3-72}$$

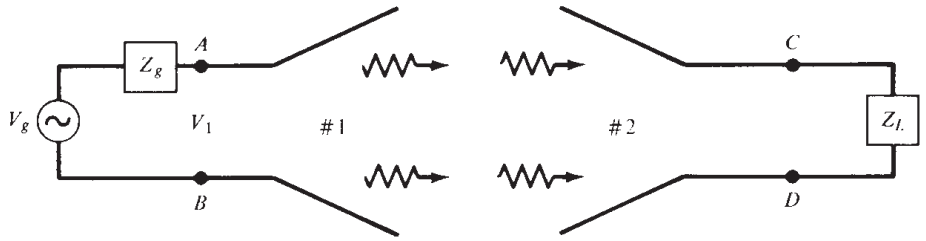


Figure 3.3 Transmitting and receiving antenna systems.

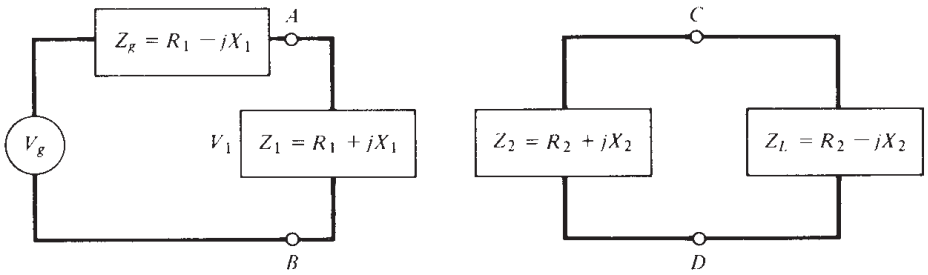


Figure 3.4 Two-antenna system with conjugate loads.

In a similar manner, we can show that when antenna #2 is transmitting and #1 is receiving, the power ratio of P_1/P_2 is given by

$$\frac{P_1}{P_2} = 4R_2R_1|Y_{12}|^2 \tag{3-73}$$

Under conditions of reciprocity ($Y_{12} = Y_{21}$), the power delivered in either direction is the same.

3.8.2 Reciprocity for Antenna Radiation Patterns

The radiation pattern is a very important antenna characteristic. Although it is usually most convenient and practical to measure the pattern in the receiving mode, it is identical, because of reciprocity, to that of the transmitting mode.

Reciprocity for antenna patterns is general provided the materials used for the antennas and feeds, and the media of wave propagation are linear. Nonlinear devices, such as diodes, can make the antenna system nonreciprocal. The antennas can be of any shape or size, and they do not have to be matched to their corresponding feed lines or loads provided there is a distinct single propagating mode at each port. The only other restriction for reciprocity to hold is for the antennas in the transmit and receive modes to be polarization matched, including the sense of rotation. This is necessary so that the antennas can transmit and receive the same field components, and thus total power. If the antenna that is used as a probe to measure the fields radiated by the antenna under test is not of the same polarization, then in some situations the transmit and receive patterns can still be the same. For example, if the transmit antenna is circularly polarized and the probe antenna is linearly polarized, then if the linearly polarized probe antenna is used twice and it is oriented one time to measure the θ-component and the other the ϕ-component, then the sum of the two components can represent the pattern of the circularly polarized antenna in either the transmit or receive modes. During this procedure, the power level and sensitivities must be held constant.

To detail the procedure and foundation of pattern measurements and reciprocity, let us refer to Figures 3.5(a) and (b). The antenna under test is #1 while the probe antenna (#2) is oriented to transmit or receive maximum radiation. The voltages and currents V_1, I_1 at terminals 1–1 of antenna #1 and V_2, I_2 at terminals 2–2 of antenna #2 are related by

$$\begin{aligned} V_1 &= Z_{11}I_1 + Z_{12}I_2 \\ V_2 &= Z_{21}I_1 + Z_{22}I_2 \end{aligned} \tag{3-74}$$

where

$$\begin{aligned} Z_{11} &= \text{self-impedance of antenna \#1} \\ Z_{22} &= \text{self-impedance of antenna \#2} \\ Z_{12}, Z_{21} &= \text{mutual impedances between antennas \#1 and \#2} \end{aligned}$$

If a current I_1 is applied at the terminals 1–1 and voltage V_2 (designated as V_{2oc}) is measured at the *open* ($I_2 = 0$) terminals of antenna #2, then an equal voltage V_{1oc}

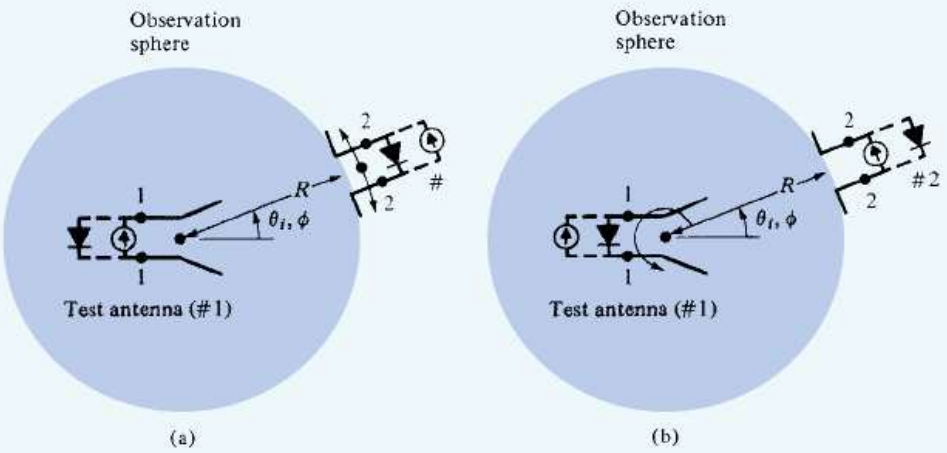


Figure 3.5 Antenna arrangement for pattern measurements and reciprocity theorem.

will be measured at the *open* ($I_1 = 0$) terminals of antenna #1 provided the current I_2 of antenna #2 is equal to I_1. In equation form, we can write

$$Z_{21} = \left.\frac{V_{2oc}}{I_1}\right|_{I_2=0} \tag{3-75a}$$

$$Z_{12} = \left.\frac{V_{1oc}}{I_2}\right|_{I_1=0} \tag{3-75b}$$

If the medium between the two antennas is linear, passive, isotropic, and the waves monochromatic, then because of reciprocity

$$Z_{21} = \left.\frac{V_{2oc}}{I_1}\right|_{I_2=0} = \left.\frac{V_{1oc}}{I_2}\right|_{I_1=0} = Z_{12} \tag{3-76}$$

If in addition $I_1 = I_2$, then

$$V_{2oc} = V_{1oc} \tag{3-77}$$

The above are valid for any position and any configuration of operation between the two antennas.

Reciprocity will now be reviewed for two modes of operation. In one mode, antenna #1 is held stationary while #2 is allowed to move on the surface of a constant radius sphere, as shown in Figure 3.5(a). In the other mode, antenna #2 is maintained stationary while #1 pivots about a point, as shown in Figure 3.5(b).

In the mode of Figure 3.5(a), antenna #1 can be used either as a transmitter or receiver. In the transmitting mode, while antenna #2 is moving on the constant radius sphere surface, the open terminal voltage V_{2oc} is measured. In the receiving mode, the open terminal voltage V_{1oc} is recorded. The three-dimensional plots of V_{2oc} and V_{1oc}, as a function of θ and ϕ, have been defined in Section 2.2 as *field patterns*. Since the three-dimensional graph of V_{2oc} is identical to that of V_{1oc} (due to reciprocity), the *transmitting* (V_{2oc}) *and receiving* (V_{1oc}) field patterns are also equal. The same conclusion can be arrived at if antenna #2 is allowed to remain stationary while #1 rotates, as shown in Figure 3.5(b).

The conditions of reciprocity hold whether antenna #1 is used as a transmitter and #2 as a receiver *or* antenna #2 as a transmitter and #1 as a receiver. In practice, the

most convenient mode of operation is that of Figure 3.5(b) with the test antenna used as a receiver. Antenna #2 is usually placed in the far-field of the test antenna (#1), and vice versa, in order that its radiated fields are plane waves in the vicinity of #1.

The receiving mode of operation of Figure 3.5(b) for the test antenna is most widely used to measure antenna patterns because the transmitting equipment is, in most cases, bulky and heavy while the receiver is small and lightweight. In some cases, the receiver is nothing more than a simple diode detector. The transmitting equipment usually consists of sources and amplifiers. To make precise measurements, especially at microwave frequencies, it is necessary to have frequency and power stabilities. Therefore, the equipment must be placed on stable and vibration-free platforms. This can best be accomplished by allowing the transmitting equipment to be held stationary and the receiving equipment to rotate.

An excellent manuscript on test procedures for antenna measurements of amplitude, phase, impedance, polarization, gain, directivity, efficiency, and others has been published by IEEE [5]. A condensed summary of it is found in [6], and a review is presented in Chapter 17 of this text.

REFERENCES

1. R. F. Harrington, *Time-Harmonic Electromagnetic Fields*, McGraw-Hill, New York, 1961.
2. C. A. Balanis, *Advanced Engineering Electromagnetics*, John Wiley & Sons, New York, 1989.
3. P. E. Mayes, personal communication.
4. V. H. Rumsey, "The Reaction Concept in Electromagnetic Theory," *Physical Review*, Series 2, Vol. 94, No. 6, June 15, 1954, pp. 1483–1491.
5. *IEEE Standard Test Procedures for Antennas*, IEEE Std 149–1979, IEEE, Inc., New York, 1979.
6. W. H. Kummer and E. S. Gillespie, "Antenna Measurements–1978," *Proc. IEEE*, Vol. 66, No. 4, April 1978, pp. 483–507.

PROBLEMS

3.1. If $\mathbf{H}_e = j\omega\epsilon\nabla \times \mathbf{\Pi}_e$, where $\mathbf{\Pi}_e$ is the electric Hertzian potential, show that

(a) $\nabla^2\mathbf{\Pi}_e + k^2\mathbf{\Pi}_e = j\dfrac{1}{\omega\epsilon}\mathbf{J}$ (b) $\mathbf{E}_e = k^2\mathbf{\Pi}_e + \nabla(\nabla \cdot \mathbf{\Pi}_e)$

(c) $\mathbf{\Pi}_e = -j\dfrac{1}{\omega\mu\epsilon}\mathbf{A}$

3.2. If $\mathbf{E}_h = -j\omega\mu\nabla \times \mathbf{\Pi}_h$, where $\mathbf{\Pi}_h$ is the magnetic Hertzian potential, show that

(a) $\nabla^2\mathbf{\Pi}_h + k^2\mathbf{\Pi}_h = j\dfrac{1}{\omega\mu}\mathbf{M}$ (b) $\mathbf{H}_h = k^2\mathbf{\Pi}_h + \nabla(\nabla \cdot \mathbf{\Pi}_h)$

(c) $\mathbf{\Pi}_h = -j\dfrac{1}{\omega\mu\epsilon}\mathbf{F}$

3.3. Verify that (3-35) and (3-36) are solutions to (3-34).

3.4. Show that (3-42) is a solution to (3-39) and (3-43) is a solution to (3-31).

3.5. Verify (3-57) and (3-57a).

3.6. Derive (3-60) and (3-61).

CHAPTER 4

Linear Wire Antennas

4.1 INTRODUCTION

Wire antennas, linear or curved, are some of the oldest, simplest, cheapest, and in many cases the most versatile for many applications. It should not then come as a surprise to the reader that we begin our analysis of antennas by considering some of the oldest, simplest, and most basic configurations. Initially we will try to minimize the complexity of the antenna structure and geometry to keep the mathematical details to a minimum.

4.2 INFINITESIMAL DIPOLE

An infinitesimal linear wire ($l \ll \lambda$) is positioned symmetrically at the origin of the coordinate system and oriented along the z axis, as shown in Figure 4.1(a). Although infinitesimal dipoles are not very practical, they are used to represent capacitor-plate (also referred to as *top-hat-loaded*) antennas. In addition, they are utilized as building blocks of more complex geometries. The end plates are used to provide capacitive loading in order to maintain the current on the dipole nearly uniform. Since the end plates are assumed to be small, their radiation is usually negligible. The wire, in addition to being very small ($l \ll \lambda$), is very thin ($a \ll \lambda$). The spatial variation of the current is assumed to be constant and given by

$$\mathbf{I}(z') = \hat{\mathbf{a}}_z I_0 \tag{4-1}$$

where $I_0 =$ constant.

4.2.1 Radiated Fields

To find the fields radiated by the current element, the two-step procedure of Figure 3.1 is used. It will be required to determine first **A** and **F** and then find the **E** and **H**. The functional relation between **A** and the source **J** is given by (3-49), (3-51), or (3-53). Similar relations are available for **F** and **M**, as given by (3-50), (3-52), and (3-54).

Antenna Theory: Analysis Design, Third Edition, by Constantine A. Balanis
ISBN 0-471-66782-X Copyright © 2005 John Wiley & Sons, Inc.

EX2042
Page 164 of 1072

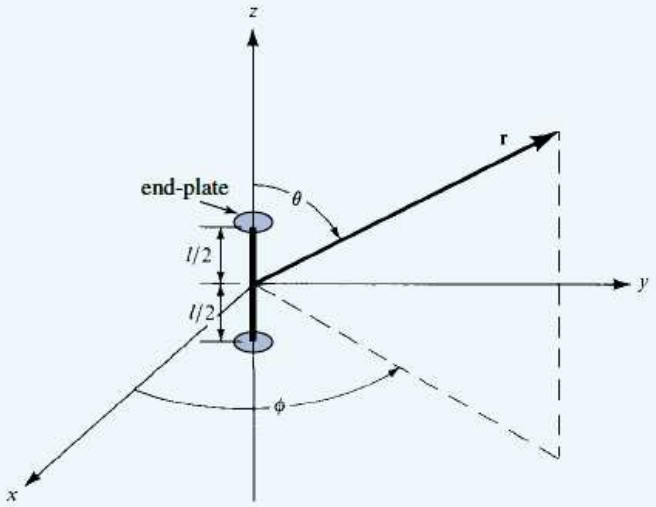
Since the source only carries an electric current $\mathbf{I}_e$, $\mathbf{I}_m$ and the potential function $\mathbf{F}$ are zero. To find $\mathbf{A}$ we write

$$\mathbf{A}(x, y, z) = \frac{\mu}{4\pi} \int_C \mathbf{I}_e(x', y', z') \frac{e^{-jkR}}{R} dl' \tag{4-2}$$

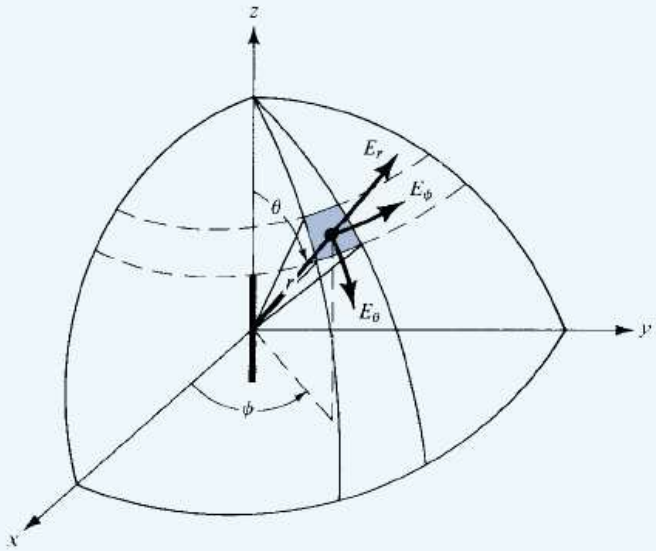
where (x, y, z) represent the observation point coordinates, (x', y', z') represent the coordinates of the source, R is the distance from any point on the source to the observation point, and path C is along the length of the source. For the problem of Figure 4.1

$$\mathbf{I}_e(x', y', z') = \hat{\mathbf{a}}_z I_0 \tag{4-3a}$$

$$x' = y' = z' = 0 \text{ (infinitesimal dipole)} \tag{4-3b}$$



(a) Infinitesimal dipole



(b) Electric field orientation

Figure 4.1 Geometrical arrangement of an infinitesimal dipole and its associated electric-field components on a spherical surface.

EX2042
Page 165 of 1072

$$R = \sqrt{(x-x')^2 + (y-y')^2 + (z-z')^2} = \sqrt{x^2+y^2+z^2}$$
$$= r = \text{constant} \tag{4-3c}$$
$$dl' = dz' \tag{4-3d}$$

so we can write (4-2) as

$$\boxed{\mathbf{A}(x,y,z) = \hat{\mathbf{a}}_z \frac{\mu I_0}{4\pi r} e^{-jkr} \int_{-l/2}^{+l/2} dz' = \hat{\mathbf{a}}_z \frac{\mu I_0 l}{4\pi r} e^{-jkr}} \tag{4-4}$$

The next step of the procedure is to find $\mathbf{H}_A$ using (3-2a) and then $\mathbf{E}_A$ using (3-15) or (3-10) with $\mathbf{J} = 0$. To do this, it is often much simpler to transform (4-4) from rectangular to spherical components and then use (3-2a) and (3-15) or (3-10) in spherical coordinates to find $\mathbf{H}$ and $\mathbf{E}$.

The transformation between rectangular and spherical components is given, in matrix form, by (VII-12a) (see Appendix VII)

$$\begin{bmatrix} A_r \\ A_\theta \\ A_\phi \end{bmatrix} = \begin{bmatrix} \sin\theta\cos\phi & \sin\theta\sin\phi & \cos\theta \\ \cos\theta\cos\phi & \cos\theta\sin\phi & -\sin\theta \\ -\sin\phi & \cos\phi & 0 \end{bmatrix} \begin{bmatrix} A_x \\ A_y \\ A_z \end{bmatrix} \tag{4-5}$$

For this problem, $A_x = A_y = 0$, so (4-5) using (4-4) reduces to

$$A_r = A_z \cos\theta = \frac{\mu I_0 l e^{-jkr}}{4\pi r} \cos\theta \tag{4-6a}$$
$$A_\theta = -A_z \sin\theta = -\frac{\mu I_0 l e^{-jkr}}{4\pi r} \sin\theta \tag{4-6b}$$
$$A_\phi = 0 \tag{4-6c}$$

Using the symmetry of the problem (no ϕ variations), (3-2a) can be expanded in spherical coordinates and written in simplified form as

$$\mathbf{H} = \hat{\mathbf{a}}_\phi \frac{1}{\mu r} \left[\frac{\partial}{\partial r}(r A_\theta) - \frac{\partial A_r}{\partial \theta} \right] \tag{4-7}$$

Substituting (4-6a)–(4-6c) into (4-7) reduces it to

$$\boxed{\begin{aligned} H_r &= H_\theta = 0 \qquad (4\text{-}8a) \\ H_\phi &= j \frac{k I_0 l \sin\theta}{4\pi r} \left[1 + \frac{1}{jkr} \right] e^{-jkr} \qquad (4\text{-}8b) \end{aligned}}$$

The electric field $\mathbf{E}$ can now be found using (3-15) or (3-10) with $\mathbf{J} = 0$. That is,

$$\mathbf{E} = \mathbf{E}_A = -j\omega\mathbf{A} - j\frac{1}{\omega\mu\epsilon}\nabla(\nabla \cdot \mathbf{A}) = \frac{1}{j\omega\epsilon}\nabla \times \mathbf{H} \tag{4-9}$$

EX2042
Page 166 of 1072

Substituting (4-6a)–(4-6c) or (4-8a)–(4-8b) into (4-9) reduces it to

$$E_r = \eta \frac{I_0 l \cos\theta}{2\pi r^2}\left[1 + \frac{1}{jkr}\right] e^{-jkr} \tag{4-10a}$$

$$E_\theta = j\eta \frac{kI_0 l \sin\theta}{4\pi r}\left[1 + \frac{1}{jkr} - \frac{1}{(kr)^2}\right] e^{-jkr} \tag{4-10b}$$

$$E_\phi = 0 \tag{4-10c}$$

The **E**- and **H**-field components are valid everywhere, except on the source itself, and they are sketched in Figure 4.1(b) on the surface of a sphere of radius r. It is a straightforward exercise to verify Equations (4-10a)–(4-10c), and this is left as an exercise to the reader (Prob. 4.13).

4.2.2 Power Density and Radiation Resistance

The input impedance of an antenna, which consists of real and imaginary parts, was discussed in Section 2.13. For a lossless antenna, the real part of the input impedance was designated as radiation resistance. It is through the mechanism of the radiation resistance that power is transferred from the guided wave to the free-space wave. To find the input resistance for a lossless antenna, the Poynting vector is formed in terms of the **E**- and **H**-fields radiated by the antenna. By integrating the Poynting vector over a closed surface (usually a sphere of constant radius), the total power radiated by the source is found. The real part of it is related to the input resistance.

For the infinitesimal dipole, the complex Poynting vector can be written using (4-8a)–(4-8b) and (4-10a)–(4-10c) as

$$\begin{aligned}\mathbf{W} &= \tfrac{1}{2}(\mathbf{E} \times \mathbf{H}^*) = \tfrac{1}{2}(\hat{\mathbf{a}}_r E_r + \hat{\mathbf{a}}_\theta E_\theta) \times (\hat{\mathbf{a}}_\phi H_\phi^*) \\ &= \tfrac{1}{2}(\hat{\mathbf{a}}_r E_\theta H_\phi^* - \hat{\mathbf{a}}_\theta E_r H_\phi^*)\end{aligned} \tag{4-11}$$

whose radial W_r and transverse W_θ components are given, respectively, by

$$W_r = \frac{\eta}{8}\left|\frac{I_0 l}{\lambda}\right|^2 \frac{\sin^2\theta}{r^2}\left[1 - j\frac{1}{(kr)^3}\right] \tag{4-12a}$$

$$W_\theta = j\eta \frac{k|I_0 l|^2 \cos\theta \sin\theta}{16\pi^2 r^3}\left[1 + \frac{1}{(kr)^2}\right] \tag{4-12b}$$

The complex power moving in the radial direction is obtained by integrating (4-11)–(4-12b) over a closed sphere of radius r. Thus it can be written as

$$P = \oiint_S \mathbf{W} \cdot d\mathbf{s} = \int_0^{2\pi}\int_0^{\pi} (\hat{\mathbf{a}}_r W_r + \hat{\mathbf{a}}_\theta W_\theta) \cdot \hat{\mathbf{a}}_r r^2 \sin\theta \, d\theta \, d\phi \tag{4-13}$$

which reduces to

$$P = \int_0^{2\pi}\int_0^{\pi} W_r r^2 \sin\theta \, d\theta \, d\phi = \eta\frac{\pi}{3}\left|\frac{I_0 l}{\lambda}\right|^2\left[1 - j\frac{1}{(kr)^3}\right] \tag{4-14}$$

EX2042
Page 167 of 1072

The transverse component W_θ of the power density does not contribute to the integral. Thus (4-14) does not represent the total complex power radiated by the antenna. Since W_θ, as given by (4-12b), is purely imaginary, it will not contribute to any real radiated power. However, it does contribute to the imaginary (reactive) power which along with the second term of (4-14) can be used to determine the total reactive power of the antenna. *The reactive power density, which is most dominant for small values of kr, has both radial and transverse components. It merely changes between outward and inward directions to form a standing wave at a rate of twice per cycle. It also moves in the transverse direction as suggested by (4-12b).*

Equation (4-13), which gives the real and imaginary power that is moving outwardly, can also be written as

$$P = \frac{1}{2}\iint_S \mathbf{E} \times \mathbf{H}^* \cdot d\mathbf{s} = \eta\left(\frac{\pi}{3}\right)\left|\frac{I_0 l}{\lambda}\right|^2\left[1 - j\frac{1}{(kr)^3}\right]$$

$$= P_{\text{rad}} + j2\omega(\tilde{W}_m - \tilde{W}_e) \tag{4-15}$$

where

P = power (in radial direction)
P_{rad} = time-average power radiated
$\tilde{W}_m$ = time-average magnetic energy density (in radial direction)
$\tilde{W}_e$ = time-average electric energy density (in radial direction)
$2\omega(\tilde{W}_m - \tilde{W}_e)$ = time-average imaginary (reactive) power (in radial direction)

From (4-14)

$$P_{\text{rad}} = \eta\left(\frac{\pi}{3}\right)\left|\frac{I_0 l}{\lambda}\right|^2 \tag{4-16}$$

and

$$2\omega(\tilde{W}_m - \tilde{W}_e) = -\eta\left(\frac{\pi}{3}\right)\left|\frac{I_0 l}{\lambda}\right|^2 \frac{1}{(kr)^3} \tag{4-17}$$

It is clear from (4-17) that the radial electric energy must be larger than the radial magnetic energy. For large values of kr ($kr \gg 1$ or $r \gg \lambda$), the reactive power diminishes and vanishes when $kr = \infty$.

Since the antenna radiates its real power through the radiation resistance, for the infinitesimal dipole it is found by equating (4-16) to

$$\boxed{P_{\text{rad}} = \eta\left(\frac{\pi}{3}\right)\left|\frac{I_0 l}{\lambda}\right|^2 = \frac{1}{2}|I_0|^2 R_r} \tag{4-18}$$

where R_r is the radiation resistance. Equation (4-18) reduces to

$$\boxed{R_r = \eta\left(\frac{2\pi}{3}\right)\left(\frac{l}{\lambda}\right)^2 = 80\pi^2\left(\frac{l}{\lambda}\right)^2} \tag{4-19}$$

for a free-space medium ($\eta \simeq 120\pi$). It should be pointed out that the radiation resistance of (4-19) represents the total radiation resistance since (4-12b) does not contribute to it.

For a wire antenna to be classified as an infinitesimal dipole, its overall length must be very small (usually $l \leq \lambda/50$).

Example 4.1

Find the radiation resistance of an infinitesimal dipole whose overall length is $l = \lambda/50$.

Solution: Using (4-19)

$$R_r = 80\pi^2 \left(\frac{l}{\lambda}\right)^2 = 80\pi^2 \left(\frac{1}{50}\right)^2 = 0.316 \text{ ohms}$$

Since the radiation resistance of an infinitesimal dipole is about 0.3 ohms, it will present a very large mismatch when connected to practical transmission lines, many of which have characteristic impedances of 50 or 75 ohms. The reflection efficiency (e_r) and hence the overall efficiency (e_0) will be very small.

The reactance of an infinitesimal dipole is capacitive. This can be illustrated by considering the dipole as a flared open-circuited transmission line, as discussed in Section 1.4. Since the input impedance of an open-circuited transmission line a distance $l/2$ from its open end is given by $Z_{in} = -jZ_c \cot(\beta l/2)$, where Z_c is its characteristic impedance, it will always be negative (capacitive) for $l \ll \lambda$.

4.2.3 Radian Distance and Radian Sphere

The **E**- and **H**-fields for the infinitesimal dipole, as represented by (4-8a)–(4-8b) and (4-10a)–(4-10c), are valid everywhere (except on the source itself). An inspection of these equations reveals the following:

(a) At a distance $r = \lambda/2\pi$ (or $kr = 1$), which is referred to as the *radian distance*, the magnitude of the first and second terms within the brackets of (4-8b) and (4-10a) is the same. Also at the radian distance the magnitude of all three terms within the brackets of (4-10b) is identical; the only term that contributes to the total field is the second, because the first and third terms cancel each other. This is illustrated in Figure 4.2.

(b) At distances less than the radian distance $r < \lambda/2\pi$ ($kr < 1$), the magnitude of the second term within the brackets of (4-8b) and (4-10a) is greater than the first term and begins to dominate as $r \ll \lambda/2\pi$. For (4-10b) and $r < \lambda/2\pi$, the magnitude of the third term within the brackets is greater than the magnitude of the first and second terms while the magnitude of the second term is greater than that of the first one; each of these terms begins to dominate as $r \ll \lambda/2\pi$. This is illustrated in Figure 4.2. The region $r < \lambda/2\pi$ ($kr < 1$) is referred to as the *near-field* region, and the energy in that region is basically imaginary (stored).

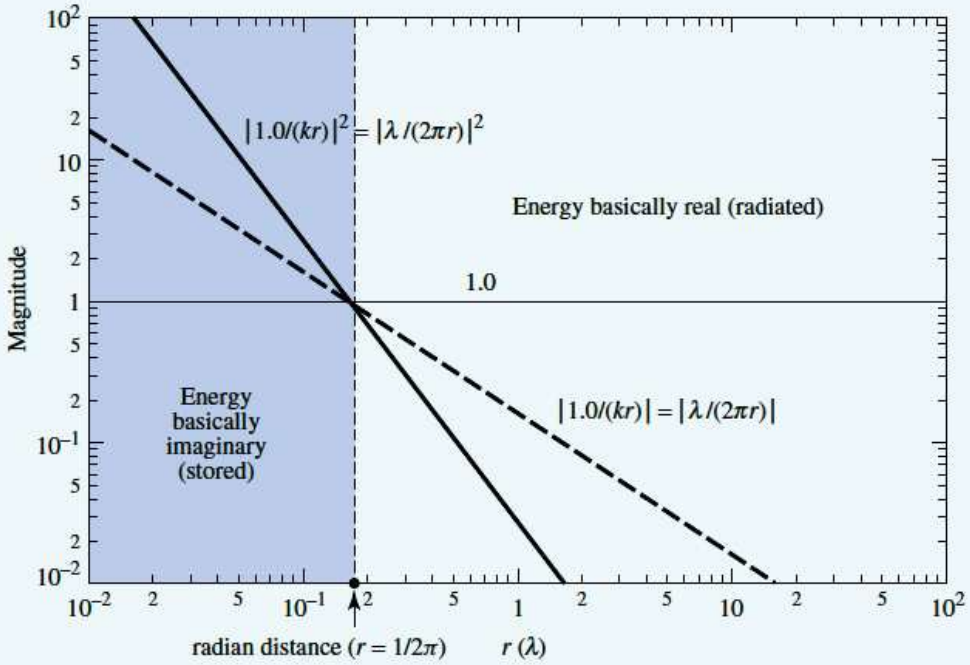


Figure 4.2 Magnitude variation, as a function of the radial distance, of the field terms radiated by an infinitesimal dipole.

(c) At distances greater than the radian distance $r > \lambda/2\pi$ $(kr > 1)$, the first term within the brackets of (4-8b) and (4-10a) is greater than the magnitude of the second term and begins to dominate as $r \gg \lambda/2\pi$ $(kr \gg 1)$. For (4-10b) and $r > \lambda/2\pi$, the first term within the brackets is greater than the magnitude of the second and third terms while the magnitude of the second term is greater than that of the third; each of these terms begins to dominate as $r \gg \lambda/2\pi$. This is illustrated in Figure 4.2. The region $r > \lambda/2\pi$ $(kr > 1)$ is referred to as the *intermediate-field* region while that for $r \gg \lambda/2\pi$ $(kr \gg 1)$ is referred to as the *far-field* region, and the energy in that region is basically real (radiated).

(d) The sphere with radius equal to the radian distance $(r = \lambda/2\pi)$ is referred as the *radian sphere*, and it defines the region within which the reactive power density is greater than the radiated power density [1]–[3]. For an antenna, the radian sphere represents the volume occupied mainly by the stored energy of the antenna's electric and magnetic fields. Outside the radian sphere the radiated power density is greater than the reactive power density and begins to dominate as $r \gg \lambda/2\pi$. *Therefore the radian sphere can be used as a reference, and it defines the transition between stored energy pulsating primarily in the $\pm\theta$ direction [represented by (4-12b)] and energy radiating in the radial (r) direction [represented by the first term of (4-12a); the second term represents stored energy pulsating inwardly and outwardly in the radial (r) direction].* Similar behavior, where the power density near the antenna is primarily reactive and far away is primarily real, is exhibited by all antennas, although not exactly at the radian distance.

4.2.4 Near-Field ($kr \ll 1$) Region

An inspection of (4-8a)–(4-8b) and (4-10a)–(4-10c) reveals that for $kr \ll \lambda$ or $r \ll \lambda/2\pi$ they can be reduced in much simpler form and can be approximated by

$$\left.\begin{aligned} E_r &\simeq -j\eta \frac{I_0 l e^{-jkr}}{2\pi kr^3}\cos\theta && \text{(4-20a)}\\ E_\theta &\simeq -j\eta \frac{I_0 l e^{-jkr}}{4\pi kr^3}\sin\theta && \text{(4-20b)}\\ E_\phi &= H_r = H_\theta = 0 && \text{(4-20c)}\\ H_\phi &\simeq \frac{I_0 l e^{-jkr}}{4\pi r^2}\sin\theta && \text{(4-20d)} \end{aligned}\right\} \quad kr \ll 1$$

The **E**-field components, E_r and E_θ, are in time-phase but they are in time-phase quadrature with the **H**-field component H_ϕ; therefore there is no time-average power flow associated with them. This is demonstrated by forming the time-average power density as

$$\mathbf{W}_{\text{av}} = \tfrac{1}{2}\text{Re}[\mathbf{E} \times \mathbf{H}^*] = \tfrac{1}{2}\text{Re}[\hat{\mathbf{a}}_r E_\theta H^*{}_\phi - \hat{\mathbf{a}}_\theta E_r H^*{}_\phi] \tag{4-21}$$

which by using (4-20a)–(4-20d) reduces to

$$\mathbf{W}_{\text{av}} = \frac{1}{2}\text{Re}\left[-\hat{\mathbf{a}}_r j\frac{\eta}{k}\left|\frac{I_0 l}{4\pi}\right|^2 \frac{\sin^2\theta}{r^5} + \hat{\mathbf{a}}_\theta j\frac{\eta}{k}\frac{|I_0 l|^2}{8\pi^2}\frac{\sin\theta\cos\theta}{r^5}\right] = 0 \tag{4-22}$$

The condition of $kr \ll 1$ can be satisfied at moderate distances away from the antenna provided that the frequency of operation is very low. Equations (4-20a) and (4-20b) are similar to those of a static electric dipole and (4-20d) to that of a static current element. Thus we usually refer to (4-20a)–(4-20d) as the *quasistationary fields*.

4.2.5 Intermediate-Field ($kr > 1$) Region

As the values of kr begin to increase and become greater than unity, the terms that were dominant for $kr \ll 1$ become smaller and eventually vanish. For moderate values of kr the **E**-field components lose their in-phase condition and approach time-phase quadrature. Since their magnitude is not the same, in general, they form a rotating vector whose extremity traces an ellipse. This is analogous to the polarization problem except that the vector rotates in a plane parallel to the direction of propagation and is usually referred to as the *cross field*. At these intermediate values of kr, the E_θ and H_ϕ components approach time-phase, which is an indication of the formation of time-average power flow in the outward (radial) direction (radiation phenomenon).

As the values of kr become moderate ($kr > 1$), the field expressions can be approximated again but in a different form. In contrast to the region where $kr \ll 1$, the first term within the brackets in (4-8b) and (4-10a) becomes more dominant and the second term can be neglected. The same is true for (4-10b) where the second and third terms

become less dominant than the first. Thus we can write for $kr > 1$

$$\left.\begin{aligned} E_r &\simeq \eta \frac{I_0 l e^{-jkr}}{2\pi r^2} \cos\theta && \text{(4-23a)} \\ E_\theta &\simeq j\eta \frac{k I_0 l e^{-jkr}}{4\pi r} \sin\theta && \text{(4-23b)} \\ E_\phi &= H_r = H_\theta = 0 && \text{(4-23c)} \\ H_\phi &\simeq j \frac{k I_0 l e^{-jkr}}{4\pi r} \sin\theta && \text{(4-23d)} \end{aligned}\right\} \quad kr > 1$$

The total electric field is given by

$$\mathbf{E} = \hat{\mathbf{a}}_r E_r + \hat{\mathbf{a}}_\theta E_\theta \tag{4-24}$$

whose magnitude can be written as

$$|\mathbf{E}| = \sqrt{|E_r|^2 + |E_\theta|^2} \tag{4-25}$$

4.2.6 Far-Field ($kr \gg 1$) Region

Since (4-23a)–(4-23d) are valid only for values of $kr > 1$ ($r > \lambda$), then E_r will be smaller than E_θ because E_r is inversely proportional to r^2 where E_θ is inversely proportional to r. In a region where $kr \gg 1$, (4-23a)–(4-23d) can be simplified and approximated by

$$\left.\begin{aligned} E_\theta &\simeq j\eta \frac{k I_0 l e^{-jkr}}{4\pi r} \sin\theta && \text{(4-26a)} \\ E_r &\simeq E_\phi = H_r = H_\theta = 0 && \text{(4-26b)} \\ H_\phi &\simeq j \frac{k I_0 l e^{-jkr}}{4\pi r} \sin\theta && \text{(4-26c)} \end{aligned}\right\} \quad kr \gg 1$$

The ratio of E_θ to H_ϕ is equal to

$$Z_w = \frac{E_\theta}{H_\phi} \simeq \eta \tag{4-27}$$

where

Z_w = wave impedance

η = intrinsic impedance ($377 \simeq 120\pi$ ohms for free-space)

The **E**- and **H**-field components are perpendicular to each other, transverse to the radial direction of propagation, and the r variations are separable from those of θ and ϕ. The shape of the pattern is not a function of the radial distance r, and the fields form a *T*ransverse *E*lectro*M*agnetic (TEM) wave whose wave impedance is equal to the intrinsic impedance of the medium. As it will become even more evident in

later chapters, *this relationship is applicable in the far-field region of all antennas of finite dimensions*. Equations (4-26a)–(4-26c) can also be derived using the procedure outlined and relationships developed in Section 3.6. This is left as an exercise to the reader (Prob. 4.15).

Example 4.2

For an infinitesimal dipole determine and interpret the vector effective length [see Section 2.15, Figure 2.29(a)]. At what incidence angle does the open-circuit maximum voltage occurs at the output terminals of the dipole if the electric-field intensity of the incident wave is 10 mV/m? The length of the dipole is 10 cm.

Solution: Using (4-26a) and the effective length as defined by (2-92), we can write that

$$E_\theta = j\eta \frac{kI_0 l e^{-jkr}}{4\pi r}\sin\theta = -\hat{\mathbf{a}}_\theta j\eta \frac{kI_0 e^{-jkr}}{4\pi r}\cdot(-\hat{\mathbf{a}}_\theta l\sin\theta)$$
$$= -\hat{\mathbf{a}}_\theta j\eta \frac{kI_0 e^{-jkr}}{4\pi r}\cdot \boldsymbol{\ell}_e$$

Therefore, the effective length is

$$\boldsymbol{\ell}_e = -\hat{\mathbf{a}}_\theta l\sin\theta$$

whose maximum value occurs when $\theta = 90^\circ$, and it is equal to l. Therefore, to achieve maximum output the wave must be incident upon the dipole at a normal incidence angle ($\theta = 90^\circ$).

The open-circuit maximum voltage is equal to

$$V_{oc}|_{\max} = |\mathbf{E}^i\cdot\boldsymbol{\ell}_e|_{\max} = |\hat{\mathbf{a}}_\theta 10\times 10^{-3}\cdot(-\hat{\mathbf{a}}_\theta l\sin\theta)|_{\max}$$
$$= 10\times 10^{-3} l = 10^{-3}\ \text{volts}$$

4.2.7 Directivity

The real power P_{rad} radiated by the dipole was found in Section 4.2.2, as given by (4-16). The same expression can be obtained by first forming the average power density, using (4-26a)–(4-26c). That is,

$$\mathbf{W}_{\text{av}} = \frac{1}{2}\text{Re}(\mathbf{E}\times\mathbf{H}^*) = \hat{\mathbf{a}}_r\frac{1}{2\eta}|E_\theta|^2 = \hat{\mathbf{a}}_r\frac{\eta}{2}\left|\frac{kI_0 l}{4\pi}\right|^2\frac{\sin^2\theta}{r^2} \tag{4-28}$$

Integrating (4-28) over a closed sphere of radius r reduces it to (4-16). This is left as an exercise to the reader (Prob. 4.14).

Associated with the average power density of (4-28) is a radiation intensity U which is given by

$$U = r^2\ W_{\text{av}} = \frac{\eta}{2}\left(\frac{kI_0 l}{4\pi}\right)^2\sin^2\theta = \frac{r^2}{2\eta}|E_\theta(r,\theta,\phi)|^2 \tag{4-29}$$

and it conforms with (2-12a). The normalized pattern of (4-29) is shown in Figure 4.3. The maximum value occurs at $\theta = \pi/2$ and it is equal to

$$U_{\max} = \frac{\eta}{2}\left(\frac{kI_0 l}{4\pi}\right)^2 \tag{4-30}$$

EX2042
Page 173 of 1072

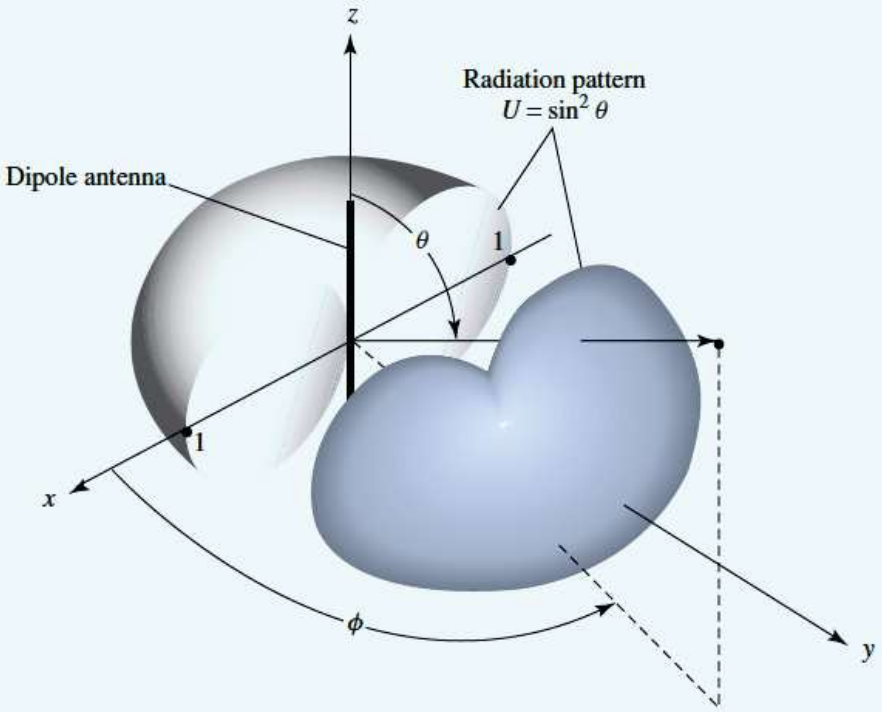


Figure 4.3 Three-dimensional radiation pattern of infinitesimal dipole.

Using (4-16) and (4-30), the directivity reduces to

$$D_0 = 4\pi \frac{U_{\max}}{P_{\text{rad}}} = \frac{3}{2} \tag{4-31}$$

and the maximum effective aperture to

$$A_{em} = \left(\frac{\lambda^2}{4\pi}\right) D_0 = \frac{3\lambda^2}{8\pi} \tag{4-32}$$

The radiation resistance of the dipole can be obtained by the definition of (4-18). Since the radiated power obtained by integrating (4-28) over a closed sphere is the same as that of (4-16), the radiation resistance using it will also be the same as obtained previously and given by (4-19).

Integrating the complex Poynting vector over a closed sphere, as was done in (4-13), results in the power (real and imaginary) directed in the radial direction. Any transverse components of power density, as given by (4-12b), will not be captured by the integration even though they are part of the overall power. *Because of this limitation, this method cannot be used to derive the input reactance of the antenna.*

The procedure that can be used to derive the far-zone electric and magnetic fields radiated by an antenna, along with some of the most important parameters/figures of merit that are used to describe the performance of an antenna, are summarized in Table 4.1.

TABLE 4.1 Summary of Procedure to Determine the Far-Field Radiation Characteristics of an Antenna

1. Specify electric and/or magnetic current densities **J, M** [physical or equivalent (see Chapter 3, Figure 3.1)]
2. Determine vector potential components $A_\theta,\ A_\phi$ and/or $F_\theta,\ F_\phi$ using (3-46)–(3-54) in far field
3. Find far-zone **E** and **H** radiated fields ($E_\theta,\ E_\phi;\ H_\theta,\ H_\phi$) using (3-58a)–(3-58b)
4. Form either

   a. $$\mathbf{W}_{\text{rad}}(r,\theta,\phi) = \mathbf{W}_{\text{av}}(r,\theta,\phi) = \frac{1}{2}\text{Re}[\mathbf{E}\times\mathbf{H}^*]$$
   $$\simeq \frac{1}{2}\text{Re}\ [(\hat{a}_\theta E_\theta + \hat{a}_\phi E_\phi)\times(\hat{a}_\theta H_\theta^* + \hat{a}_\phi H_\phi^*)]$$
   $$\mathbf{W}_{\text{rad}}(r,\theta,\phi) = \hat{a}_r\frac{1}{2}\left[\frac{|E_\theta|^2+|E_\phi|^2}{\eta}\right] = \hat{a}_r\frac{1}{r^2}|f(\theta,\phi)|^2$$

   or

   b. $U(\theta,\phi) = r^2\ W_{\text{rad}}(r,\theta,\phi) = |f(\theta,\phi)|^2$
5. Determine either

   a. $$P_{\text{rad}} = \int_0^{2\pi}\int_0^{\pi} W_{\text{rad}}(r,\theta,\phi)r^2\sin\theta\,d\theta\,d\phi$$

   or

   b. $$P_{\text{rad}} = \int_0^{2\pi}\int_0^{\pi} U(\theta,\phi)\sin\theta\,d\theta\,d\phi$$
6. Find directivity using
   $$D(\theta,\phi) = \frac{U(\theta,\phi)}{U_0} = \frac{4\pi U(\theta,\phi)}{P_{\text{rad}}}$$
   $$D_0 = D_{\max} = D(\theta,\phi)|_{\max} = \frac{U(\theta,\phi)|_{\max}}{U_0} = \frac{4\pi U(\theta,\phi)|_{\max}}{P_{\text{rad}}}$$
7. Form *normalized* power amplitude pattern:
   $$P_n(\theta,\phi) = \frac{U(\theta,\phi)}{U_{\max}}$$
8. Determine radiation and input resistance:
   $$R_r = \frac{2P_{\text{rad}}}{|I_0|^2};\qquad R_{in} = \frac{R_r}{\sin^2\left(\frac{kl}{2}\right)}$$
9. Determine maximum effective area
   $$A_{em} = \frac{\lambda^2}{4\pi}D_0$$

4.3 SMALL DIPOLE

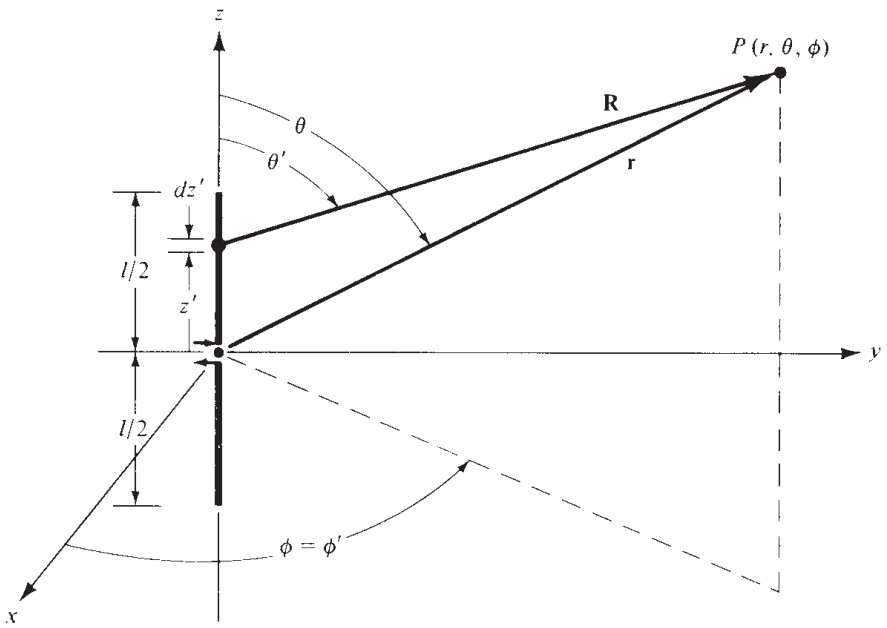
The creation of the current distribution on a thin wire was discussed in Section 1.4, and it was illustrated with some examples in Figure 1.16. The radiation properties of an infinitesimal dipole, which is usually taken to have a length $l \le \lambda/50$, were discussed

EX2042
Page 175 of 1072

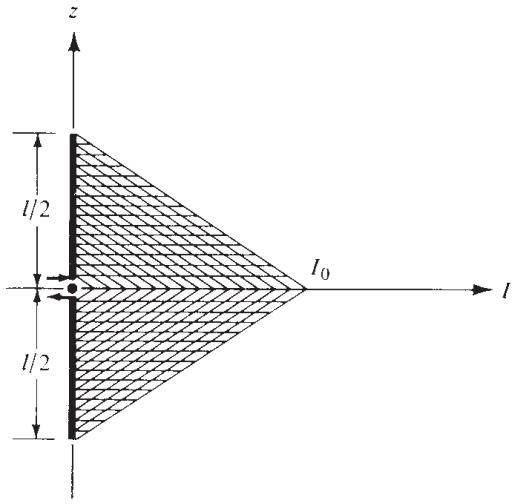
in the previous section. Its current distribution was assumed to be constant. Although a constant current distribution is not realizable (other than top-hat-loaded elements), it is a mathematical quantity that is used to represent actual current distributions of antennas that have been incremented into many small lengths.

A better approximation of the current distribution of wire antennas, whose lengths are usually $\lambda/50 < l \leq \lambda/10$, is the triangular variation of Figure 1.16(a). The sinusoidal variations of Figures 1.16(b)–(c) are more accurate representations of the current distribution of any length wire antenna.

The most convenient geometrical arrangement for the analysis of a dipole is usually to have it positioned symmetrically about the origin with its length directed along the z-axis, as shown in Figure 4.4(a). This is not necessary, but it is usually the most convenient. The current distribution of a small dipole ($\lambda/50 < l \leq \lambda/10$) is shown in



(a) Dipole and geometry



(b) Current distribution

Figure 4.4 Geometrical arrangement of dipole and current distribution.

Figure 4.4(b), and it is given by

$$\mathbf{I}_e(x', y', z') = \begin{cases} \hat{\mathbf{a}}_z I_0 \left(1 - \dfrac{2}{l} z'\right), & 0 \le z' \le l/2 \\ \hat{\mathbf{a}}_z I_0 \left(1 + \dfrac{2}{l} z'\right), & -l/2 \le z' \le 0 \end{cases} \tag{4-33}$$

where $I_0 =$ constant.

Following the procedure established in the previous section, the vector potential of (4-2) can be written using (4-33) as

$$\begin{aligned} \mathbf{A}(x, y, z) = \frac{\mu}{4\pi} \Bigg[& \hat{\mathbf{a}}_z \int_{-l/2}^{0} I_0 \left(1 + \frac{2}{l} z'\right) \frac{e^{-jkR}}{R} \, dz' \\ & + \hat{\mathbf{a}}_z \int_{0}^{l/2} I_0 \left(1 - \frac{2}{l} z'\right) \frac{e^{-jkR}}{R} \, dz' \Bigg] \end{aligned} \tag{4-34}$$

Because the overall length of the dipole is very small (usually $l \le \lambda/10$), the values of R for different values of z' along the length of the wire ($-l/2 \le z' \le l/2$) are not much different from r. Thus R can be approximated by $R \simeq r$ throughout the integration path. The maximum phase error in (4-34) by allowing $R = r$ for $\lambda/50 < l \le \lambda/10$, will be $kl/2 = \pi/10$ rad $= 18^\circ$ for $l = \lambda/10$. Smaller values will occur for the other lengths. As it will be shown in the next section, this amount of phase error is usually considered negligible and has very little effect on the overall radiation characteristics. Performing the integration, (4-34) reduces to

$$\mathbf{A} = \hat{\mathbf{a}}_z A_z = \hat{\mathbf{a}}_z \frac{1}{2} \left[\frac{\mu I_0 l e^{-jkr}}{4\pi r} \right] \tag{4-35}$$

which is one-half of that obtained in the previous section for the infinitesimal dipole and given by (4-4).

The potential function given by (4-35) becomes a more accurate approximation as $kr \to \infty$. This is also the region of most practical interest, and it has been designated as the *far-field* region. Since the potential function for the triangular distribution is one-half of the corresponding one for the constant (uniform) current distribution, the corresponding fields of the former are one-half of the latter. Thus we can write the **E**- and **H**-fields radiated by a small dipole as

$$\left.\begin{aligned} E_\theta &\simeq j\eta \frac{k I_0 l e^{-jkr}}{8\pi r} \sin\theta && \text{(4-36a)} \\ E_r &\simeq E_\phi = H_r = H_\theta = 0 && \text{(4-36b)} \\ H_\phi &\simeq j \frac{k I_0 l e^{-jkr}}{8\pi r} \sin\theta && \text{(4-36c)} \end{aligned}\right\} \quad kr \gg 1$$

with the wave impedance equal, as before, to (4-27).

Since the directivity of an antenna is controlled by the relative shape of the field or power pattern, the directivity, and maximum effective area of this antenna are the

EX2042
Page 177 of 1072

same as the ones with the constant current distribution given by (4-31) and (4-32), respectively.

The radiation resistance of the antenna is strongly dependent upon the current distribution. Using the procedure established for the infinitesimal dipole, it can be shown that for the small dipole its radiated power is one-fourth ($\frac{1}{4}$) of (4-18). Thus the radiation resistance reduces to

$$R_r = \frac{2P_{\text{rad}}}{|I_0|^2} = 20\pi^2 \left(\frac{l}{\lambda}\right)^2 \tag{4-37}$$

which is also one-fourth ($\frac{1}{4}$) of that obtained for the infinitesimal dipole as given by (4-19). Their relative patterns (shapes) are the same and are shown in Figure 4.3.

4.4 REGION SEPARATION

Before we attempt to solve for the fields radiated by a finite dipole of any length, it would be very desirable to discuss the separation of the space surrounding an antenna into three regions; namely, the *reactive near-field, radiating near-field* (*Fresnel*) and the *far-field* (*Fraunhofer*) which were introduced briefly in Section 2.2.4. This is necessary because for a dipole antenna of any length and any current distribution, it will become increasingly difficult to solve for the fields everywhere. Approximations can be made, especially for the far-field (Fraunhofer) region, which is usually the one of most practical interest, to simplify the formulation to yield closed form solutions. The same approximations used to simplify the formulation of the fields radiated by a finite dipole are also used to formulate the fields radiated by most practical antennas. So it will be very important to introduce them properly and understand their implications upon the solution.

The difficulties in obtaining closed form solutions that are valid everywhere for any practical antenna stem from the inability to perform the integration of

$$\mathbf{A}(x, y, z) = \frac{\mu}{4\pi} \int_C \mathbf{I}_e(x', y', z') \frac{e^{-jkR}}{R}\, dl' \tag{4-38}$$

where

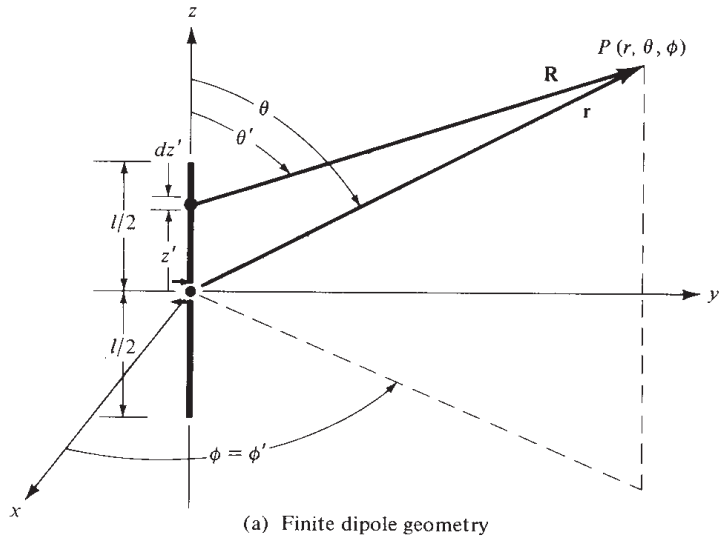
$$R = \sqrt{(x - x')^2 + (y - y')^2 + (z - z')^2} \tag{4-38a}$$

For a finite dipole with sinusoidal current distribution, the integral of (4-38) can be reduced to a closed form that is valid everywhere! This will be shown in Chapter 8. The length R is defined as the distance from any point on the source to the observation point. The integral of (4-38) was used to solve for the fields of infinitesimal and small dipoles in Sections 4.1 and 4.2. However in the first case (infinitesimal dipole) $R = r$ and in the second case (small dipole) R was approximated by $r (R \simeq r)$ because the length of the dipole was restricted to be $l \leq \lambda/10$. The major simplification of (4-38) will be in the approximation of R.

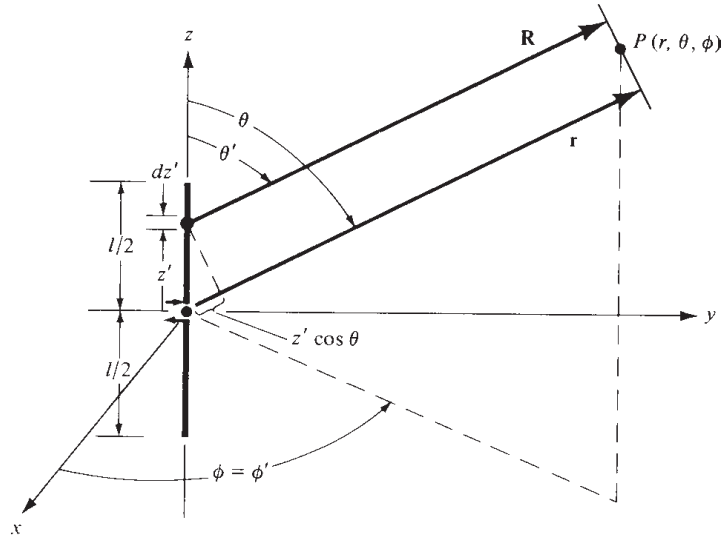
A very thin dipole of finite length l is symmetrically positioned about the origin with its length directed along the z-axis, as shown in Figure 4.5(a). Because the wire is assumed to be very thin ($x' = y' = 0$), we can write (4-38) as

$$R = \sqrt{(x - x')^2 + (y - y')^2 + (z - z')^2} = \sqrt{x^2 + y^2 + (z - z')^2} \tag{4-39}$$

EX2042
Page 178 of 1072



(a) Finite dipole geometry



(b) Geometrical arrangement for far–field approximations

Figure 4.5 Finite dipole geometry and far-field approximations.

which when expanded can be written as

$$R = \sqrt{(x^2 + y^2 + z^2) + (-2zz' + z'^2)} = \sqrt{r^2 + (-2rz'\cos\theta + z'^2)} \tag{4-40}$$

where

$$r^2 = x^2 + y^2 + z^2 \tag{4-40a}$$

$$z = r\cos\theta \tag{4-40b}$$

Using the binomial expansion, we can write (4-40) in a series as

$$R = r - z'\cos\theta + \frac{1}{r}\left(\frac{z'^2}{2}\sin^2\theta\right) + \frac{1}{r^2}\left(\frac{z'^3}{2}\cos\theta\sin^2\theta\right) + \cdots \tag{4-41}$$

whose higher order terms become less significant provided $r \gg z'$.

EX2042
Page 179 of 1072

4.4.1 Far-Field (Fraunhofer) Region

The most convenient simplification of (4-41), other than $R \simeq r$, will be to approximate it by its first two terms, or

$$R \simeq r - z' \cos\theta \tag{4-42}$$

The most significant neglected term of (4-41) is the third whose maximum value is

$$\frac{1}{r}\left(\frac{z'^2}{2}\sin^2\theta\right)_{\max} = \frac{z'^2}{2r} \qquad \text{when } \theta = \pi/2 \tag{4-43}$$

When (4-43) attains its maximum value, the fourth term of (4-41) vanishes because $\theta = \pi/2$. It can be shown that the higher order terms not shown in (4-41) also vanish. Therefore approximating (4-41) by (4-42) introduces a *maximum* error given by (4-43).

It has been shown by many investigators through numerous examples that for most practical antennas, *with overall lengths greater than a wavelength* ($l > \lambda$), a maximum total phase error of $\pi/8$ rad (22.5°) is not very detrimental in the analytical formulations. Using that as a criterion we can write, using (4-43), that the maximum phase error should always be

$$\frac{k(z')^2}{2r} \le \frac{\pi}{8} \tag{4-44}$$

which for $-l/2 \le z' \le l/2$ reduces to

$$r \ge 2\left(\frac{l^2}{\lambda}\right) \tag{4-45}$$

Equation (4-45) simply states that to maintain the maximum phase error of an antenna equal to or less than $\pi/8$ rad (22.5°), the observation distance r must equal or be greater than $2l^2/\lambda$ where l is the largest* dimension of the antenna structure. The usual simplification for the far-field region is to approximate the R in the exponential (e^{-jkR}) of (4-38) by (4-42) and the R in the denominator of (4-38) by $R \simeq r$. These simplifications are designated as the far-field approximations and are usually denoted in the literature as

Far-field Approximations

$$\begin{aligned} R &\simeq r - z'\cos\theta \qquad \text{for phase terms} \\ R &\simeq r \qquad\qquad\qquad\quad \text{for amplitude terms} \end{aligned} \tag{4-46}$$

provided r satisfies (4-45).

It may be advisable to illustrate the approximation (4-46) geometrically. For $R \simeq r - z'\cos\theta$, where θ is the angle measured from the z-axis, the radial vectors $\mathbf{R}$ and $\mathbf{r}$ must be parallel to each other, as shown in Figure 4.5(b). For any other antenna whose maximum dimension is D, the approximation of (4-46) is valid provided the observations are made at a distance

$$r \ge 2\frac{D^2}{\lambda} \tag{4-47}$$

For an aperture antenna the maximum dimension is taken to be its diagonal.

*Provided the overall length (l) of the antenna is large compared to the wavelength [see IEEE Standard Definitions of Terms for Antennas, IEEE Std (145-1983)].

For most practical antennas, whose overall length is large compared to the wavelength, these are adequate approximations which have been shown by many investigators through numerous examples to give valid results in pattern predictions. Some discrepancies are evident in regions of low intensity (usually below -25 dB). This is illustrated in Figure 2.9 where the patterns of a paraboloidal antenna for $R = \infty$ and $R = 2D^2/\lambda$ differ at levels below -25 dB. Allowing R to have a value of $R = 4D^2/\lambda$ gives better results.

It would seem that the approximation of R in (4-46) for the amplitude is more severe than that for the phase. However a close observation reveals this is not the case. Since the observations are made at a distance where r is very large, any small error in the approximation of the denominator (amplitude) will not make much difference in the answer. However, because of the periodic nature of the phase (repeats every 2π rad), it can be a major fraction of a period. The best way to illustrate it will be to consider an example.

Example 4.3

For an antenna with an overall length $l = 5\lambda$, the observations are made at $r = 60\lambda$. Find the errors in phase and amplitude using (4-46).

Solution: For $\theta = 90^\circ$, $z' = 2.5\lambda$, and $r = 60\lambda$, (4-40) reduces to

$$R_1 = \lambda\sqrt{(60)^2 + (2.5)^2} = 60.052\lambda$$

and (4-46) to

$$R_2 = r = 60\lambda$$

Therefore the phase difference is

$$\Delta\phi = k\Delta R = \frac{2\pi}{\lambda}(R_1 - R_2) = 2\pi(0.052) = 0.327 \text{ rad} = 18.74^\circ$$

which is an appreciable fraction ($\simeq \frac{1}{20}$) of a full period (360°).

The difference of the inverse values of R is

$$\frac{1}{R_2} - \frac{1}{R_1} = \frac{1}{\lambda}\left(\frac{1}{60} - \frac{1}{60.052}\right) = \frac{1.44 \times 10^{-5}}{\lambda}$$

which should always be a very small value in amplitude.

4.4.2 Radiating Near-Field (Fresnel) Region

If the observation point is chosen to be smaller than $r = 2l^2/\lambda$, the maximum phase error by the approximation of (4-46) is greater than $\pi/8$ rad (22.5°) which may be undesirable in many applications. If it is necessary to choose observation distances smaller than (4-45), another term (the third) in the series solution of (4-41) must be retained to maintain a maximum phase error of $\pi/8$ rad (22.5°). Doing this, the infinite series of (4-41) can be approximated by

$$R \simeq r - z'\cos\theta + \frac{1}{r}\left(\frac{z'^2}{2}\sin^2\theta\right) \tag{4-48}$$

EX2042
Page 181 of 1072

The most significant term that we are neglecting from the infinite series of (4-41) is the fourth. To find the maximum phase error introduced by the omission of the next most significant term, the angle θ at which this occurs must be found. To do this, the neglected term is differentiated with respect to θ and the result is set equal to zero. Thus

$$\frac{\partial}{\partial\theta}\left[\frac{1}{r^2}\left(\frac{z'^3}{2}\cos\theta\sin^2\theta\right)\right] = \frac{z'^3}{2r^2}\sin\theta[-\sin^2\theta + 2\cos^2\theta] = 0 \tag{4-49}$$

The angle $\theta = 0$ is not chosen as a solution because for that value the fourth term is equal to zero. In other words, $\theta = 0$ gives the minimum error. The maximum error occurs when the second term of (4-49) vanishes; that is when

$$[-\sin^2\theta + 2\cos^2\theta]_{\theta=\theta_1} = 0 \tag{4-50}$$

or

$$\theta_1 = \tan^{-1}(\pm\sqrt{2}) \tag{4-50a}$$

If the maximum phase error is allowed to be equal or less than $\pi/8$ rad, the distance r at which this occurs can be found from

$$\frac{kz'^3}{2r^2}\cos\theta\sin^2\theta\Big|_{\substack{z'=l/2\\ \theta=\tan^{-1}\sqrt{2}}} = \frac{\pi}{\lambda}\frac{l^3}{8r^2}\left(\frac{1}{\sqrt{3}}\right)\left(\frac{2}{3}\right) = \frac{\pi}{12\sqrt{3}}\left(\frac{l^3}{\lambda r^2}\right) \le \frac{\pi}{8} \tag{4-51}$$

which reduces to

$$r^2 \ge \frac{2}{3\sqrt{3}}\left(\frac{l^3}{\lambda}\right) = 0.385\left(\frac{l^3}{\lambda}\right) \tag{4-52}$$

or

$$r \ge 0.62\sqrt{l^3/\lambda} \tag{4-52a}$$

A value of r greater than that of (4-52a) will lead to an error less than $\pi/8$ rad (22.5°). Thus the region where the first three terms of (4-41) are significant, and the omission of the fourth introduces a maximum phase error of $\pi/8$ rad (22.5°), is defined by

$$2l^2/\lambda > r \ge 0.62\sqrt{l^3/\lambda} \tag{4-53}$$

where l is the length of the antenna. This region is designated as *radiating near-field* because the radiating power density is greater than the reactive power density and the field pattern (its shape) is a function of the radial distance r. This region is also called the *Fresnel region* because the field expressions in this region reduce to Fresnel integrals.

The discussion has centered around the finite length antenna of length l with the observation considered to be a point source. If the antenna is not a line source, l in (4-53) must represent the largest dimension of the antenna (which for an aperture is the diagonal). *Also if the transmitting antenna has maximum length l_t and the receiving antenna has maximum length l_r, then the sum of l_t and l_r must be used in place of l in (4-53).*

EX2042
Page 182 of 1072

The boundaries for separating the far-field (Fraunhofer), the radiating near-field (Fresnel), and the reactive near-field regions are not very rigid. Other criteria have also been established [4] but the ones introduced here are the most "popular." Also the fields, as the boundaries from one region to the other are crossed, do not change abruptly but undergo a very gradual transition.

4.4.3 Reactive Near-Field Region

If the distance of observation is smaller than the inner boundary of the Fresnel region, this region is usually designated as *reactive near-field* with inner and outer boundaries defined by

$$0.62\sqrt{l^3/\lambda} > r > 0 \tag{4-54}$$

where l is the length of the antenna. In this region the reactive power density predominates, as was demonstrated in Section 4.1 for the infinitesimal dipole.

In summary, the space surrounding an antenna is divided into three regions whose boundaries are determined by

$$\text{reactive near-field } [0.62\sqrt{D^3/\lambda} > r > 0] \tag{4-55a}$$

$$\text{radiating near-field (Fresnel) } [2D^2/\lambda > r \geq 0.62\sqrt{D^3/\lambda}] \tag{4-55b}$$

$$\text{far-field (Fraunhofer) } [\infty \geq r \geq 2D^2/\lambda] \tag{4-55c}$$

where D is the largest dimension of the antenna ($D = l$ for a wire antenna).

4.5 FINITE LENGTH DIPOLE

The techniques that were developed previously can also be used to analyze the radiation characteristics of a linear dipole of any length. To reduce the mathematical complexities, it will be assumed in this chapter that the dipole has a negligible diameter (ideally zero). This is a good approximation provided the diameter is considerably smaller than the operating wavelength. Finite radii dipoles will be analyzed in Chapters 8 and 9.

4.5.1 Current Distribution

For a very thin dipole (ideally zero diameter), the current distribution can be written, to a good approximation, as

$$\mathbf{I}_e(x' = 0, y' = 0, z') = \begin{cases} \hat{\mathbf{a}}_z I_0 \sin\left[k\left(\dfrac{l}{2} - z'\right)\right], & 0 \leq z' \leq l/2 \\ \hat{\mathbf{a}}_z I_0 \sin\left[k\left(\dfrac{l}{2} + z'\right)\right], & -l/2 \leq z' \leq 0 \end{cases} \tag{4-56}$$

This distribution assumes that the antenna is *center-fed and the current vanishes at the end points* ($z' = \pm l/2$). Experimentally it has been verified that the current in a center-fed wire antenna has sinusoidal form with nulls at the end points. For $l = \lambda/2$

and $\lambda/2 < l < \lambda$ the current distribution of (4-56) is shown plotted in Figures 1.16(b) and 1.12(c), respectively. The geometry of the antenna is that shown in Figure 4.5.

4.5.2 Radiated Fields: Element Factor, Space Factor, and Pattern Multiplication

For the current distribution of (4-56) it will be shown in Chapter 8 that closed form expressions for the **E**- and **H**-fields can be obtained which are valid in all regions (any observation point except on the source itself). In general, however, this is not the case. Usually we are limited to the far-field region, because of the mathematical complications provided in the integration of the vector potential **A** of (4-2). Since closed form solutions, which are valid everywhere, cannot be obtained for many antennas, the observations will be restricted to the far-field region. This will be done first in order to illustrate the procedure. In some cases, even in that region it may become impossible to obtain closed form solutions.

The finite dipole antenna of Figure 4.5 is subdivided into a number of infinitesimal dipoles of length $\Delta z'$. As the number of subdivisions is increased, each infinitesimal dipole approaches a length dz'. For an infinitesimal dipole of length dz' positioned along the z-axis at z', the electric and magnetic field components in the far field are given, using (4-26a)–(4-26c), as

$$dE_\theta \simeq j\eta \frac{kI_e(x', y', z')e^{-jkR}}{4\pi R} \sin\theta \, dz' \tag{4-57a}$$

$$dE_r \simeq dE_\phi = dH_r = dH_\theta = 0 \tag{4-57b}$$

$$dH_\phi \simeq j \frac{kI_e(x', y', z')e^{-jkR}}{4\pi R} \sin\theta \, dz' \tag{4-57c}$$

where R is given by (4-39) or (4-40).

Using the far-field approximations given by (4-46), (4-57a) can be written as

$$dE_\theta \simeq j\eta \frac{kI_e(x', y', z')e^{-jkr}}{4\pi r} \sin\theta e^{+jkz'\cos\theta} \, dz' \tag{4-58}$$

Summing the contributions from all the infinitesimal elements, the summation reduces, in the limit, to an integration. Thus

$$\boxed{E_\theta = \int_{-l/2}^{+l/2} dE_\theta = j\eta \frac{ke^{-jkr}}{4\pi r} \sin\theta \left[\int_{-l/2}^{+l/2} I_e(x', y', z')e^{jkz'\cos\theta} \, dz' \right]} \tag{4-58a}$$

The factor outside the brackets is designated as the *element factor* and that within the brackets as the *space factor*. For this antenna, the element factor is equal to the field of a unit length infinitesimal dipole located at a reference point (the origin). In general, the element factor depends on the type of current and its direction of flow while the space factor is a function of the current distribution along the source.

The total field of the antenna is equal to the product of the element and space factors. This is referred to as *pattern multiplication* for continuously distributed sources (see also Chapter 7), and it can be written as

$$\boxed{\text{total field} = (\text{element factor}) \times (\text{space factor})} \tag{4-59}$$

The pattern multiplication for continuous sources is analogous to the pattern multiplication of (6-5) for discrete-element antennas (arrays).

For the current distribution of (4-56), (4-58a) can be written as

$$E_\theta \simeq j\eta \frac{kI_0 e^{-jkr}}{4\pi r} \sin\theta \left\{ \int_{-l/2}^{0} \sin\left[k\left(\frac{l}{2} + z'\right)\right] e^{+jkz'\cos\theta}\, dz' + \int_{0}^{+l/2} \sin\left[k\left(\frac{l}{2} - z'\right)\right] e^{+jkz'\cos\theta}\, dz' \right\} \tag{4-60}$$

Each one of the integrals in (4-60) can be integrated using

$$\int e^{\alpha x} \sin(\beta x + \gamma)\, dx = \frac{e^{\alpha x}}{\alpha^2 + \beta^2} [\alpha \sin(\beta x + \gamma) - \beta \cos(\beta x + \gamma)] \tag{4-61}$$

where

$$\alpha = \pm jk\cos\theta \tag{4-61a}$$

$$\beta = \pm k \tag{4-61b}$$

$$\gamma = kl/2 \tag{4-61c}$$

After some mathematical manipulations, (4-60) takes the form of

$$\boxed{E_\theta \simeq j\eta \frac{I_0 e^{-jkr}}{2\pi r} \left[\frac{\cos\left(\frac{kl}{2}\cos\theta\right) - \cos\left(\frac{kl}{2}\right)}{\sin\theta} \right]} \tag{4-62a}$$

In a similar manner, or by using the established relationship between the E_θ and H_ϕ in the far field as given by (3-58b) or (4-27), the total H_ϕ component can be written as

$$\boxed{H_\phi \simeq \frac{E_\theta}{\eta} \simeq j \frac{I_0 e^{-jkr}}{2\pi r} \left[\frac{\cos\left(\frac{kl}{2}\cos\theta\right) - \cos\left(\frac{kl}{2}\right)}{\sin\theta} \right]} \tag{4-62b}$$

4.5.3 Power Density, Radiation Intensity, and Radiation Resistance

For the dipole, the average Poynting vector can be written as

$$\mathbf{W}_{\text{av}} = \frac{1}{2}\text{Re}[\mathbf{E} \times \mathbf{H}^*] = \frac{1}{2}\text{Re}[\hat{\mathbf{a}}_\theta E_\theta \times \hat{\mathbf{a}}_\phi H_\phi^*] = \frac{1}{2}\text{Re}\left[\hat{\mathbf{a}}_\theta E_\theta \times \hat{\mathbf{a}}_\phi \frac{E_\theta^*}{\eta}\right]$$

$$\mathbf{W}_{\text{av}} = \hat{\mathbf{a}}_r W_{\text{av}} = \hat{\mathbf{a}}_r \frac{1}{2\eta}|E_\theta|^2 = \hat{\mathbf{a}}_r \eta \frac{|I_0|^2}{8\pi^2 r^2}\left[\frac{\cos\left(\frac{kl}{2}\cos\theta\right) - \cos\left(\frac{kl}{2}\right)}{\sin\theta}\right]^2 \quad (4\text{-}63)$$

and the radiation intensity as

$$U = r^2 \, W_{\text{av}} = \eta \frac{|I_0|^2}{8\pi^2}\left[\frac{\cos\left(\frac{kl}{2}\cos\theta\right) - \cos\left(\frac{kl}{2}\right)}{\sin\theta}\right]^2 \quad (4\text{-}64)$$

The normalized (to 0 dB) elevation power patterns, as given by (4-64) for $l = \lambda/4, \lambda/2, 3\lambda/4$, and λ are shown plotted in Figure 4.6. The current distribution of each is given by (4-56). The power patterns for an infinitesimal dipole $l \ll \lambda$ ($U \sim \sin^2\theta$) is also included for comparison. As the length of the antenna increases, the beam becomes narrower. Because of that, the directivity should also increase with length. It is found that the 3-dB beamwidth of each is equal to

$l \ll \lambda$	3-dB beamwidth $= 90^\circ$
$l = \lambda/4$	3-dB beamwidth $= 87^\circ$
$l = \lambda/2$	3-dB beamwidth $= 78^\circ$
$l = 3\lambda/4$	3-dB beamwidth $= 64^\circ$
$l = \lambda$	3-dB beamwidth $= 47.8^\circ$

(4-65)

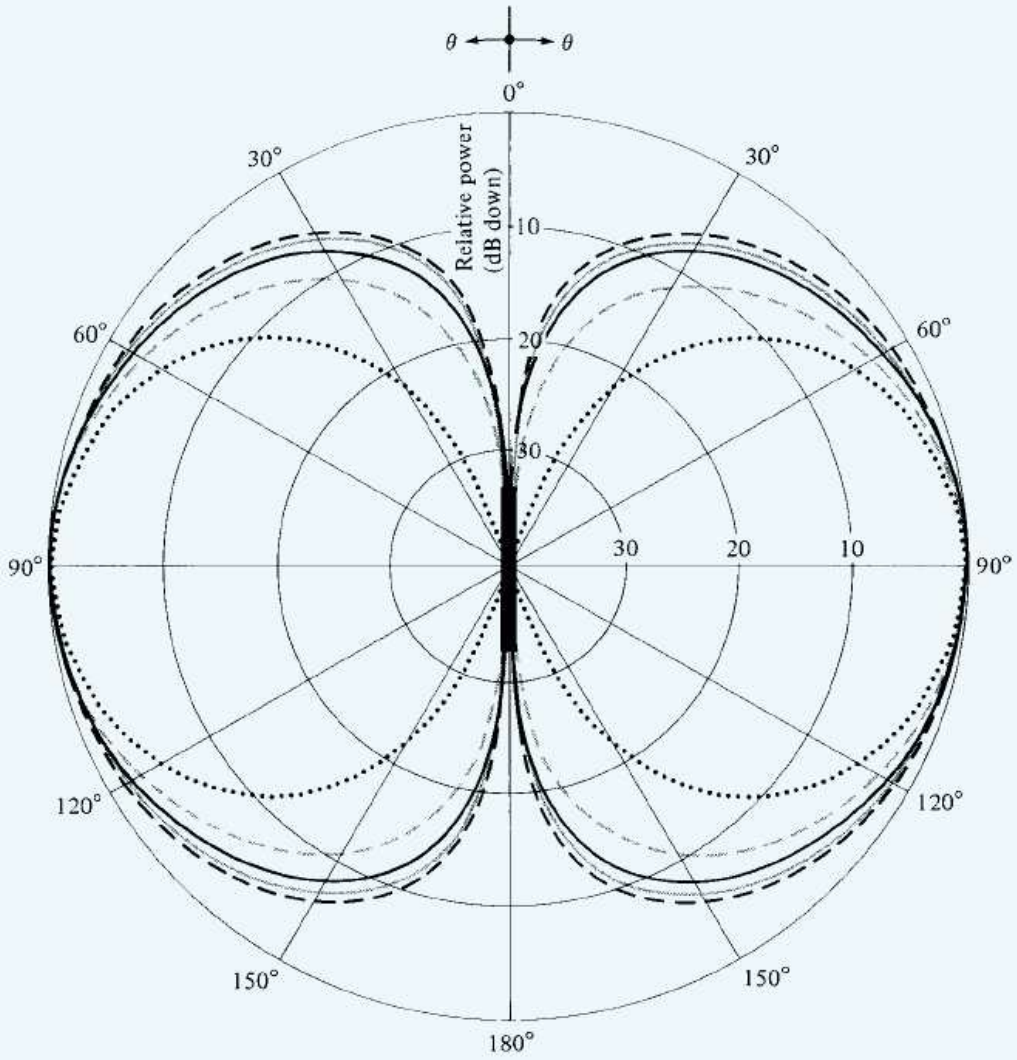
As the length of the dipole increases beyond one wavelength ($l > \lambda$), the number of lobes begin to increase. The normalized power pattern for a dipole with $l = 1.25\lambda$ is shown in Figure 4.7. In Figure 4.7(a) the three-dimensional pattern is illustrated using the software from [5], while in Figure 4.7(b) the two-dimensional (elevation pattern) is depicted. For the three-dimensional illustration, a 90° angular section of the pattern has been omitted to illustrate the elevation plane directional pattern variations. The current distribution for the dipoles with $l = \lambda/4, \lambda/2, \lambda, 3\lambda/2$, and 2λ, as given by (4-56), is shown in Figure 4.8.

To find the total power radiated, the average Poynting vector of (4-63) is integrated over a sphere of radius r. Thus

$$P_{\text{rad}} = \oiint_S \mathbf{W}_{\text{av}} \cdot d\mathbf{s} = \int_0^{2\pi}\int_0^{\pi} \hat{\mathbf{a}}_r W_{\text{av}} \cdot \hat{\mathbf{a}}_r r^2 \sin\theta \, d\theta \, d\phi$$

$$= \int_0^{2\pi}\int_0^{\pi} W_{\text{av}} r^2 \sin\theta \, d\theta \, d\phi \quad (4\text{-}66)$$

EX2042
Page 186 of 1072



– – – – – $l = \lambda/50$	$l = \lambda/50$	3-dB beamwidth = 90°
····· $l = \lambda/4$	$l = \lambda/4$	3-dB beamwidth = 87°
——— $l = \lambda/2$	$l = \lambda/2$	3-dB beamwidth = 78°
– · – · – · $l = 3\lambda/4$	$l = 3\lambda/4$	3-dB beamwidth = 64°
····· $l = \lambda$	$l = \lambda$	3-dB beamwidth = 47.8°

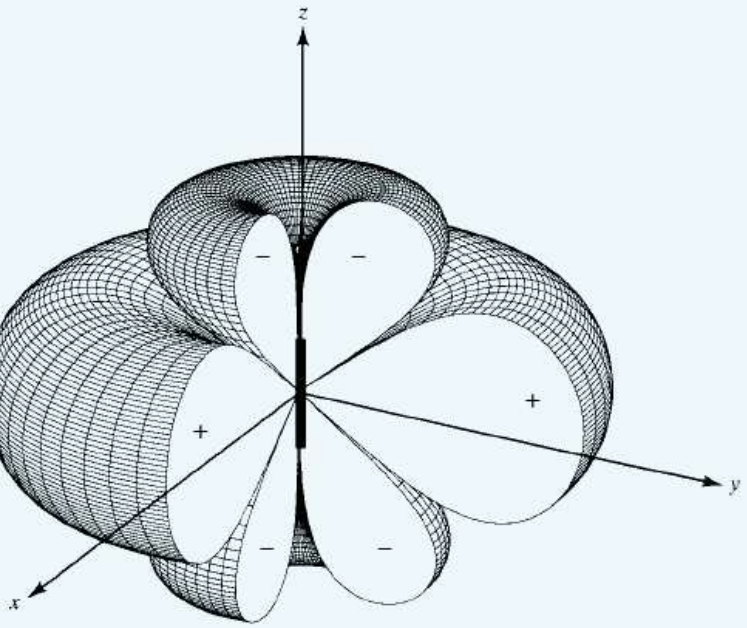
Figure 4.6 Elevation plane amplitude patterns for a thin dipole with sinusoidal current distribution ($l = \lambda/50, \lambda/4, \lambda/2, 3\lambda/4, \lambda$).

Using (4-63), we can write (4-66) as

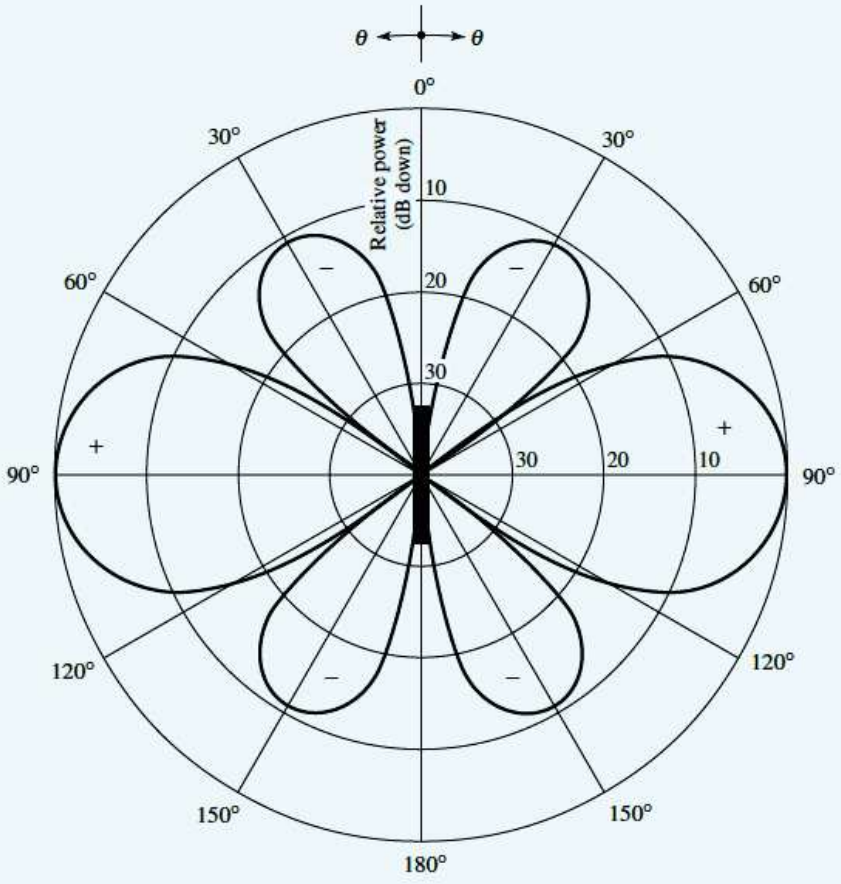
$$P_{\text{rad}} = \int_0^{2\pi} \int_0^{\pi} W_{\text{av}} r^2 \sin\theta \, d\theta \, d\phi$$

$$= \eta \frac{|I_0|^2}{4\pi} \int_0^{\pi} \frac{\left[\cos\left(\frac{kl}{2}\cos\theta\right) - \cos\left(\frac{kl}{2}\right)\right]^2}{\sin\theta} d\theta \tag{4-67}$$

EX2042
Page 187 of 1072



(a) Three-dimensional



(b) Two-dimensional

Figure 4.7 Three- and two-dimensional amplitude patterns for a thin dipole of $l = 1.25\lambda$ and sinusoidal current distribution.

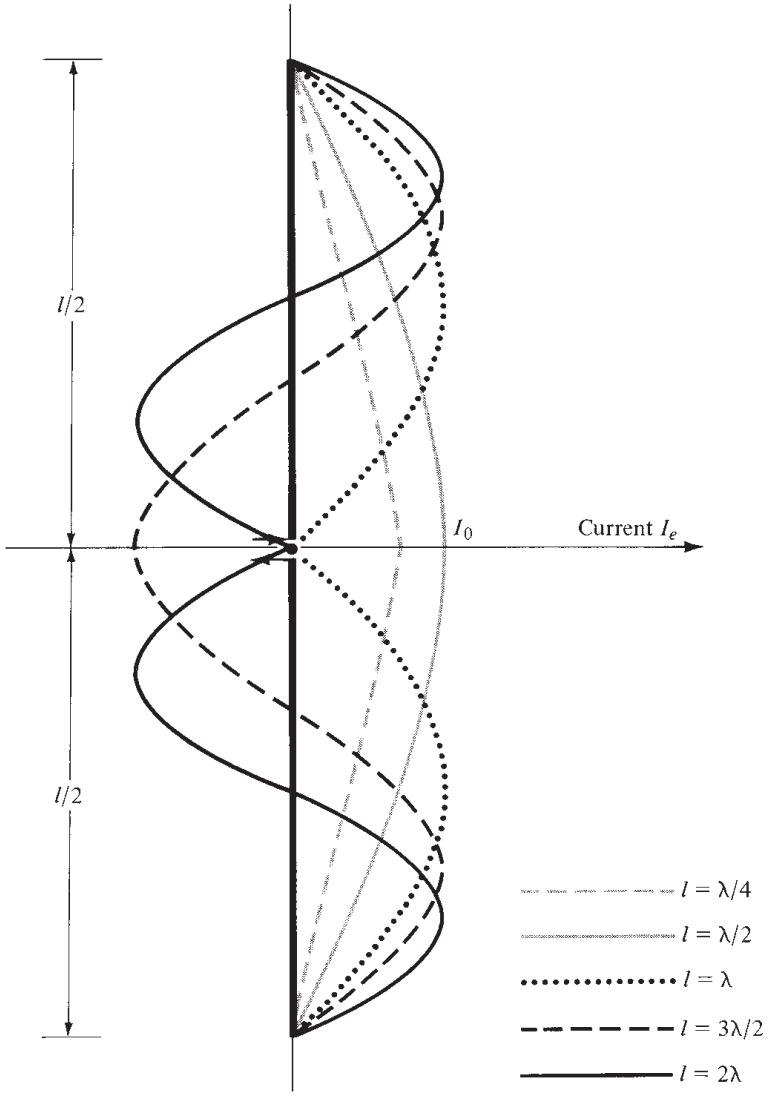


Figure 4.8 Current distributions along the length of a linear wire antenna.

After some extensive mathematical manipulations, it can be shown that (4-67) reduces to

$$P_{\text{rad}} = \eta \frac{|I_0|^2}{4\pi}\{C + \ln(kl) - C_i(kl) + \tfrac{1}{2}\sin(kl)[S_i(2kl) - 2S_i(kl)] + \tfrac{1}{2}\cos(kl)[C + \ln(kl/2) + C_i(2kl) - 2C_i(kl)]\} \tag{4-68}$$

where $C = 0.5772$ (Euler's constant) and $C_i(x)$ and $S_i(x)$ are the cosine and sine integrals (see Appendix III) given by

$$C_i(x) = -\int_x^\infty \frac{\cos y}{y}\,dy = \int_\infty^x \frac{\cos y}{y}\,dy \tag{4-68a}$$

$$S_i(x) = \int_0^x \frac{\sin y}{y}\,dy \tag{4-68b}$$

EX2042
Page 189 of 1072

The derivation of (4-68) from (4-67) is assigned as a problem at the end of the chapter (Prob. 4.21). $C_i(x)$ is related to $C_{in}(x)$ by

$$\begin{aligned} C_{in}(x) &= \ln(\gamma x) - C_i(x) = \ln(\gamma) + \ln(x) - C_i(x) \\ &= 0.5772 + \ln(x) - C_i(x) \end{aligned} \tag{4-69}$$

where

$$C_{in}(x) = \int_0^x \left(\frac{1-\cos y}{y}\right) dy \tag{4-69a}$$

$C_i(x)$, $S_i(x)$ and $C_{in}(x)$ are tabulated in Appendix III.

The radiation resistance can be obtained using (4-18) and (4-68) and can be written as

$$\begin{aligned} R_r = \frac{2P_{\text{rad}}}{|I_0|^2} = \frac{\eta}{2\pi}\{&C + \ln(kl) - C_i(kl) \\ &+ \tfrac{1}{2}\sin(kl) \times [S_i(2kl) - 2S_i(kl)] \\ &+ \tfrac{1}{2}\cos(kl) \times [C + \ln(kl/2) + C_i(2kl) - 2C_i(kl)]\} \end{aligned} \tag{4-70}$$

Shown in Figure 4.9 is a plot of R_r as a function of l (in wavelengths) when the antenna is radiating into free-space ($\eta \simeq 120\pi$).

The imaginary part of the impedance cannot be derived using the same method as the real part because, as was explained in Section 4.2.2, the integration over a closed sphere in (4-13) does not capture the imaginary power contributed by the transverse component W_θ of the power density. Therefore, the EMF method is used in Chapter 8 as

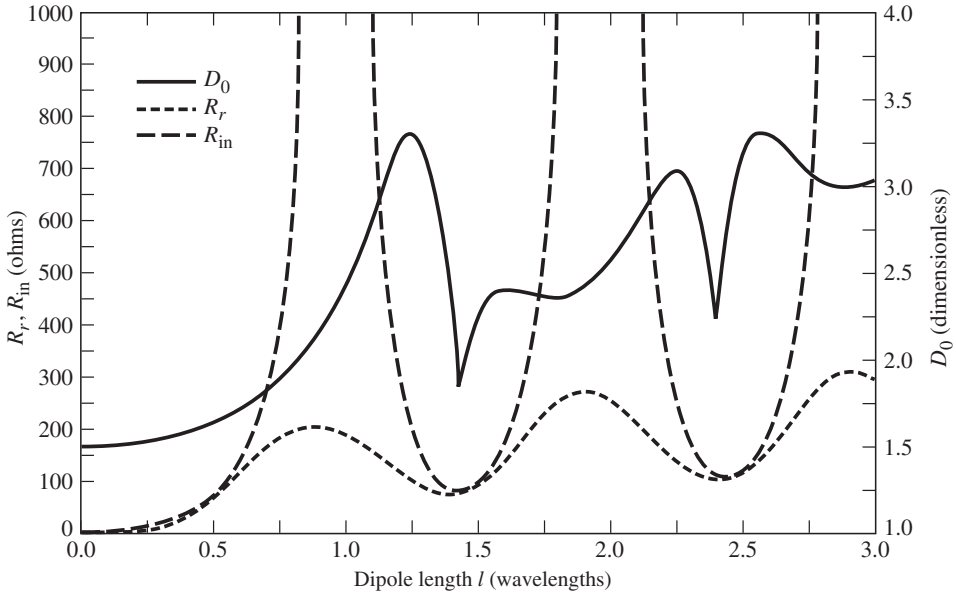


Figure 4.9 Radiation resistance, input resistance and directivity of a thin dipole with sinusoidal current distribution.

an alternative approach. Using the EMF method, the imaginary part of the impedance, relative to the current maximum, is given by (8-60b) or

$$X_m = \frac{\eta}{4\pi}\left\{2S_i(kl) + \cos(kl)[2S_i(kl) - S_i(2kl)] - \sin(kl)\left[2C_i(kl) - C_i(2kl) - C_i\left(\frac{2ka^2}{l}\right)\right]\right\} \tag{4-70a}$$

An approximate form of (4-60b) for small dipoles is given by (8-62).

4.5.4 Directivity

As was illustrated in Figure 4.6, the radiation pattern of a dipole becomes more directional as its length increases. When the overall length is greater than one wavelength, the number of lobes increases and the antenna loses its directional properties. The parameter that is used as a "figure of merit" for the directional properties of the antenna is the directivity which was defined in Section 2.6.

The directivity was defined mathematically by (2-22), or

$$D_0 = 4\pi \frac{F(\theta,\phi)|_{\max}}{\int_0^{2\pi}\int_0^{\pi} F(\theta,\phi)\sin\theta\, d\theta\, d\phi} \tag{4-71}$$

where $F(\theta,\phi)$ is related to the radiation intensity U by (2-19), or

$$U = B_0 F(\theta,\phi) \tag{4-72}$$

From (4-64), the dipole antenna of length l has

$$F(\theta,\phi) = F(\theta) = \left[\frac{\cos\left(\frac{kl}{2}\cos\theta\right) - \cos\left(\frac{kl}{2}\right)}{\sin\theta}\right]^2 \tag{4-73}$$

and

$$B_0 = \eta\frac{|I_0|^2}{8\pi^2} \tag{4-73a}$$

Because the pattern is not a function of ϕ, (4-71) reduces to

$$D_0 = \frac{2F(\theta)|_{\max}}{\int_0^{\pi} F(\theta)\sin\theta\, d\theta} \tag{4-74}$$

Equation (4-74) can be written, using (4-67), (4-68), and (4-73), as

$$D_0 = \frac{2F(\theta)|_{\max}}{Q} \tag{4-75}$$

EX2042
Page 191 of 1072

where

$$Q = \{C + \ln(kl) - C_i(kl) + \tfrac{1}{2}\sin(kl)[S_i(2kl) - 2S_i(kl)] + \tfrac{1}{2}\cos(kl)[C + \ln(kl/2) + C_i(2kl) - 2C_i(kl)]\} \tag{4-75a}$$

The maximum value of $F(\theta)$ varies and depends upon the length of the dipole.

Values of the directivity, as given by (4-75) and (4-75a), have been obtained for $0 < l \leq 3\lambda$ and are shown plotted in Figure 4.9. The corresponding values of the maximum effective aperture are related to the directivity by

$$A_{em} = \frac{\lambda^2}{4\pi} D_0 \tag{4-76}$$

4.5.5 Input Resistance

In Section 2.13 the input impedance was defined as "the ratio of the voltage to current at a pair of terminals or the ratio of the appropriate components of the electric to magnetic fields at a point." The real part of the input impedance was defined as the input resistance which for a lossless antenna reduces to the radiation resistance, a result of the radiation of real power.

In Section 4.2.2, the radiation resistance of an infinitesimal dipole was derived using the definition of (4-18). The radiation resistance of a dipole of length l with sinusoidal current distribution, of the form given by (4-56), is expressed by (4-70). By this definition, the radiation resistance is referred to the maximum current which for some lengths ($l = \lambda/4, 3\lambda/4, \lambda$, etc.) does not occur at the input terminals of the antenna (see Figure 4.8). To refer the radiation resistance to the input terminals of the antenna, the antenna itself is first assumed to be lossless ($R_L = 0$). Then the power at the input terminals is equated to the power at the current maximum.

Referring to Figure 4.10, we can write

$$\frac{|I_{in}|^2}{2} R_{in} = \frac{|I_0|^2}{2} R_r \tag{4-77}$$

or

$$R_{in} = \left[\frac{I_0}{I_{in}}\right]^2 R_r \tag{4-77a}$$

where

R_{in} = radiation resistance at input (feed) terminals
R_r = radiation resistance at current maximum Eq. (4-70)
I_0 = current maximum
I_{in} = current at input terminals

For a dipole of length l, the current at the input terminals (I_{in}) is related to the current maximum (I_0) referring to Figure 4.10, by

$$I_{in} = I_0 \sin\left(\frac{kl}{2}\right) \tag{4-78}$$

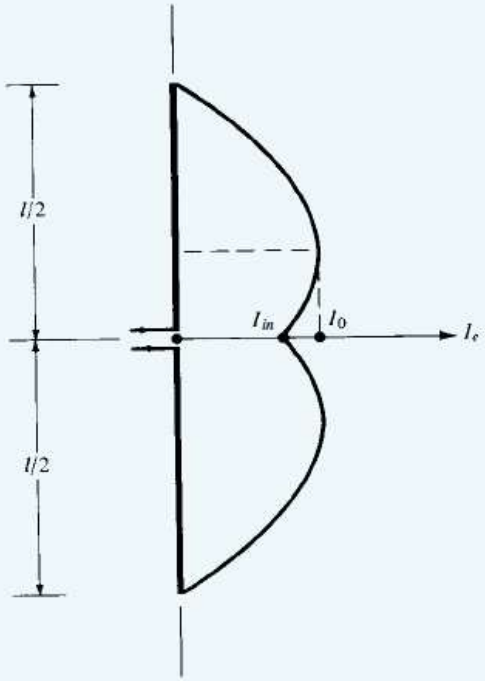


Figure 4.10 Current distribution of a linear wire antenna when current maximum does not occur at the input terminals.

Thus the input radiation resistance of (4-77a) can be written as

$$R_{in} = \frac{R_r}{\sin^2\left(\frac{kl}{2}\right)} \tag{4-79}$$

Values of R_{in} for $0 < l \leq 3\lambda$ are shown in Figure 4.9.

To compute the radiation resistance (in ohms), directivity (dimensionless and in dB), and input resistance (in ohms) for a dipole of length l, a MATLAB and FORTRAN computer program has been developed. The program is based on the definitions of each as given by (4-70), (4-71), and (4-79). The radiated power P_{rad} is computed by numerically integrating (over a closed sphere) the radiation intensity of (4-72)–(4-73a). The program, both in MATLAB and FORTRAN, is included in the computer disc made available with the book. The length of the dipole (in wavelengths) must be inserted as an input.

When the overall length of the antenna is a multiple of λ (i.e., $l = n\lambda, n = 1, 2, 3, \ldots$), it is apparent from (4-56) and from Figure 4.8 that $I_{in} = 0$. That is,

$$I_{in} = I_0 \sin\left[k\left(\frac{l}{2} \pm z'\right)\right]\Big|_{\substack{z'=0 \\ l=n\lambda, n=0,1,2,\ldots}} = 0 \tag{4-80}$$

which indicates that the input resistance at the input terminals, as given by (4-77a) or (4-79) is infinite. In practice this is not the case because the current distribution does not follow an exact sinusoidal distribution, especially at the feed point. It has, however, very high values. Two of the primary factors which contribute to the nonsinusoidal

EX2042
Page 193 of 1072

current distribution on an actual wire antenna are the nonzero radius of the wire and finite gap spacing at the terminals.

The radiation resistance and input resistance, as predicted, respectively, by (4-70) and (4-79), are based on the ideal current distribution of (4-56) and do not account for the finite radius of the wire or the gap spacing at the feed. Although the radius of the wire does not strongly influence the resistances, the gap spacing at the feed does play a significant role especially when the current at and near the feed point is small.

4.5.6 Finite Feed Gap

To analytically account for a nonzero current at the feed point for antennas with a finite gap at the terminals, Schelkunoff and Friis [6] have changed the current of (4-56) by including a quadrature term in the distribution. The additional term is inserted to take into account the effects of radiation on the antenna current distribution. In other words, once the antenna is excited by the "ideal" current distribution of (4-56), electric and magnetic fields are generated which in turn disturb the "ideal" current distribution. This reaction is included by modifying (4-56) to

$$\mathbf{I}_e(x', y', z') = \begin{cases} \hat{\mathbf{a}}_z \left\{ I_0 \sin\left[k\left(\frac{l}{2} - z'\right)\right] + jpI_0\left[\cos(kz') - \cos\left(\frac{k}{2}l\right)\right]\right\}, \\ \qquad\qquad 0 \le z' \le l/2 \\ \hat{\mathbf{a}}_z \left\{ I_0 \sin\left[k\left(\frac{l}{2} + z'\right)\right] + jpI_0\left[\cos(kz') - \cos\left(\frac{k}{2}l\right)\right]\right\}, \\ \qquad\qquad -l/2 \le z' \le 0 \end{cases} \tag{4-81}$$

where p is a coefficient that is dependent upon the overall length of the antenna and the gap spacing at the terminals. The values of p become smaller as the radius of the wire and the gap decrease.

When $l = \lambda/2$,

$$\mathbf{I}_e(x', y', z') = \hat{\mathbf{a}}_z I_0(1 + jp)\cos(kz') \quad 0 \le |z'| \le \lambda/4 \tag{4-82}$$

and for $l = \lambda$

$$\mathbf{I}_e(x', y', z') = \begin{cases} \hat{\mathbf{a}}_z I_0\{\sin(kz') + jp[1 + \cos(kz')]\} & 0 \le z' \le \lambda/2 \\ \hat{\mathbf{a}}_z I_0\{-\sin(kz') + jp[1 + \cos(kz')]\} & -\lambda/2 \le z' \le 0 \end{cases} \tag{4-83}$$

Thus for $l = \lambda/2$ the shape of the current is not changed while for $l = \lambda$ it is modified by the second term which is more dominant for small values of z'.

The variations of the current distribution and impedances, especially of wire-type antennas, as a function of the radius of the wire and feed gap spacing can be easily taken into account by using advanced computational methods and numerical techniques, especially Integral Equations and Moment Method [7]–[12], which are introduced in Chapter 8.

To illustrate the point, the current distribution of an $l = \lambda/2$ and $l = \lambda$ dipole has been computed using an integral equation formulation with a moment method numerical solution, and it is shown in Figure 8.13(b) where it is compared with the ideal distribution of (4-56) and other available data. For the moment method solution, a gap at the feed has been inserted. As expected and illustrated in Figure 8.13(b), the current

distribution for the $l = \lambda/2$ dipole based on (4-56) is not that different from that based on the moment method. This is also illustrated by (4-82). Therefore the input resistance based on these two methods will not be that different. However, for the $l = \lambda$ dipole, the current distribution based on (4-56) is quite different, especially at and near the feed point, compared to that based on the moment method, as shown in Figure 8.13(b). This is expected since the current distribution based on the ideal current distribution is zero at the feed point; for practical antennas it is very small. Therefore the gap at the feed plays an important role on the current distribution at and near the feed point. In turn, the values of the input resistance based on the two methods will be quite different, since there is a significant difference in the current between the two methods. This is discussed further in Chapter 8.

4.6 HALF-WAVELENGTH DIPOLE

One of the most commonly used antennas is the half-wavelength ($l = \lambda/2$) dipole. Because its radiation resistance is 73 ohms, which is very near the 50-ohm or 75-ohm characteristic impedances of some transmission lines, its matching to the line is simplified especially at resonance. Because of its wide acceptance in practice, we will examine in a little more detail its radiation characteristics.

The electric and magnetic field components of a half-wavelength dipole can be obtained from (4-62a) and (4-62b) by letting $l = \lambda/2$. Doing this, they reduce to

$$E_\theta \simeq j\eta \frac{I_0 e^{-jkr}}{2\pi r} \left[\frac{\cos\left(\frac{\pi}{2}\cos\theta\right)}{\sin\theta} \right] \tag{4-84}$$

$$H_\phi \simeq j \frac{I_0 e^{-jkr}}{2\pi r} \left[\frac{\cos\left(\frac{\pi}{2}\cos\theta\right)}{\sin\theta} \right] \tag{4-85}$$

In turn, the time-average power density and radiation intensity can be written, respectively, as

$$W_{\text{av}} = \eta \frac{|I_0|^2}{8\pi^2 r^2} \left[\frac{\cos\left(\frac{\pi}{2}\cos\theta\right)}{\sin\theta} \right]^2 \simeq \eta \frac{|I_0|^2}{8\pi^2 r^2} \sin^3\theta \tag{4-86}$$

and

$$U = r^2\ W_{\text{av}} = \eta \frac{|I_0|^2}{8\pi^2} \left[\frac{\cos\left(\frac{\pi}{2}\cos\theta\right)}{\sin\theta} \right]^2 \simeq \eta \frac{|I_0|^2}{8\pi^2} \sin^3\theta \tag{4-87}$$

whose two-dimensional pattern is shown plotted in Figure 4.6 while the three-dimensional pattern is depicted in Figure 4.11. For the three-dimensional pattern of Figure 4.11, a 90° angular sector has been removed to illustrate the figure-eight elevation plane pattern variations.

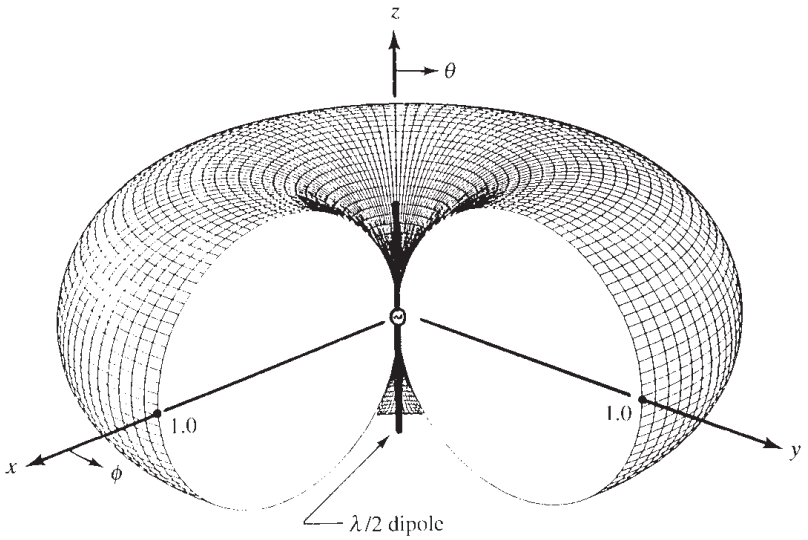


Figure 4.11 Three-dimensional pattern of a $\lambda/2$ dipole. (SOURCE: C. A. Balanis, "Antenna Theory: A Review" *Proc. IEEE*, Vol. 80, No 1. Jan. 1992. © 1992 IEEE).

The total power radiated can be obtained as a special case of (4-67), or

$$P_{\text{rad}} = \eta \frac{|I_0|^2}{4\pi} \int_0^{\pi} \frac{\cos^2\left(\frac{\pi}{2}\cos\theta\right)}{\sin\theta}\, d\theta \tag{4-88}$$

which when integrated reduces, as a special case of (4-68), to

$$P_{\text{rad}} = \eta \frac{|I_0|^2}{8\pi} \int_0^{2\pi} \left(\frac{1-\cos y}{y}\right) dy = \eta \frac{|I_0|^2}{8\pi} C_{in}(2\pi) \tag{4-89}$$

By the definition of $C_{in}(x)$, as given by (4-69), $C_{in}(2\pi)$ is equal to

$$C_{in}(2\pi) = 0.5772 + \ln(2\pi) - C_i(2\pi) = 0.5772 + 1.838 - (-0.02) \simeq 2.435 \tag{4-90}$$

where $C_i(2\pi)$ is obtained from the tables in Appendix III.

Using (4-87), (4-89), and (4-90), the maximum directivity of the half-wavelength dipole reduces to

$$\boxed{D_0 = 4\pi \frac{U_{\max}}{P_{\text{rad}}} = 4\pi \frac{U|_{\theta=\pi/2}}{P_{\text{rad}}} = \frac{4}{C_{in}(2\pi)} = \frac{4}{2.435} \simeq 1.643} \tag{4-91}$$

The corresponding maximum effective area is equal to

$$\boxed{A_{em} = \frac{\lambda^2}{4\pi} D_0 = \frac{\lambda^2}{4\pi}(1.643) \simeq 0.13\lambda^2} \tag{4-92}$$

EX2042
Page 196 of 1072

and the radiation resistance, for a free-space medium ($\eta \simeq 120\pi$), is given by

$$\boxed{R_r = \frac{2P_{\text{rad}}}{|I_0|^2} = \frac{\eta}{4\pi} C_{in}(2\pi) = 30(2.435) \simeq 73} \tag{4-93}$$

The radiation resistance of (4-93) is also the radiation resistance at the input terminals (input resistance) since the current maximum for a dipole of $l = \lambda/2$ occurs at the input terminals (see Figure 4.8). As it will be shown in Chapter 8, the imaginary part (reactance) associated with the input impedance of a dipole is a function of its length (for $l = \lambda/2$, it is equal to $j42.5$). Thus the total input impedance for $l = \lambda/2$ is equal to

$$\boxed{Z_{in} = 73 + j42.5} \tag{4-93a}$$

To reduce the imaginary part of the input impedance to zero, the antenna is matched or reduced in length until the reactance vanishes. The latter is most commonly used in practice for half-wavelength dipoles.

Depending on the radius of the wire, the length of the dipole for first resonance is about $l = 0.47\lambda$ to 0.48λ; the thinner the wire, the closer the length is to 0.48λ. Thus, for thicker wires, a larger segment of the wire has to be removed from $\lambda/2$ to achieve resonance.

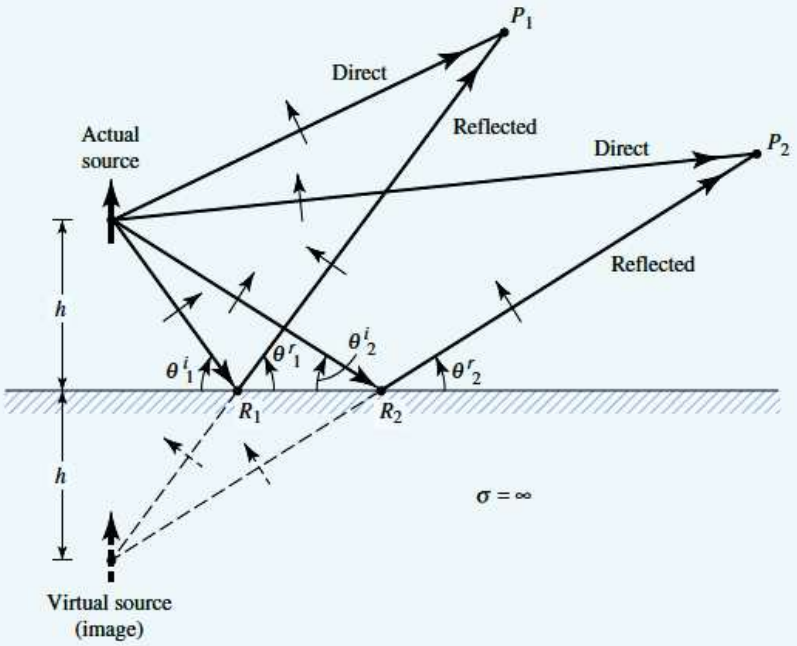
4.7 LINEAR ELEMENTS NEAR OR ON INFINITE PERFECT CONDUCTORS

Thus far we have considered the radiation characteristics of antennas radiating into an unbounded medium. The presence of an obstacle, especially when it is near the radiating element, can significantly alter the overall radiation properties of the antenna system. In practice the most common obstacle that is always present, even in the absence of anything else, is the ground. Any energy from the radiating element directed toward the ground undergoes a reflection. The amount of reflected energy and its direction are controlled by the geometry and constitutive parameters of the ground.

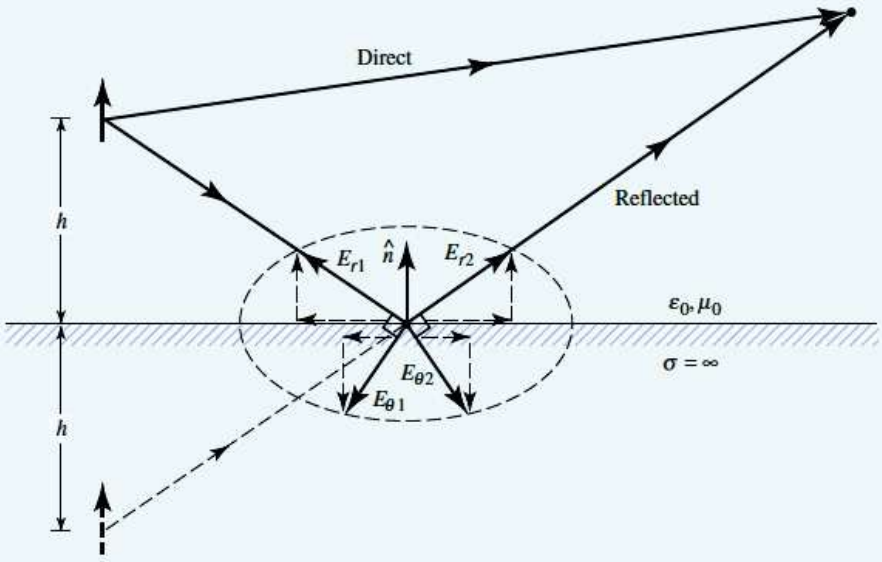
In general, the ground is a lossy medium ($\sigma \neq 0$) whose effective conductivity increases with frequency. Therefore it should be expected to act as a very good conductor above a certain frequency, depending primarily upon its composition and moisture content. To simplify the analysis, it will first be assumed that the ground is a perfect electric conductor, flat, and infinite in extent. The effects of finite conductivity and earth curvature will be incorporated later. The same procedure can also be used to investigate the characteristics of any radiating element near any other infinite, flat, perfect electric conductor. Although infinite structures are not realistic, the developed procedures can be used to simulate very large (electrically) obstacles. The effects that finite dimensions have on the radiation properties of a radiating element can be conveniently accounted for by the use of the Geometrical Theory of Diffraction (Chapter 12, Section 12.10) and/or the Moment Method (Chapter 8, Section 8.4).

4.7.1 Image Theory

To analyze the performance of an antenna near an infinite plane conductor, virtual sources (images) will be introduced to account for the reflections. As the name implies, these are not real sources but imaginary ones, which when combined with the real



(a) Vertical electric dipole



(b) Field components at point of reflection

Figure 4.12 Vertical electric dipole above an infinite, flat, perfect electric conductor.

sources, form an equivalent system. For analysis purposes only, the equivalent system gives the same radiated field on and above the conductor as the actual system itself. Below the conductor, the equivalent system does not give the correct field. However, in this region the field is zero and there is no need for the equivalent.

To begin the discussion, let us assume that a vertical electric dipole is placed a distance h above an infinite, flat, perfect electric conductor as shown in Figure 4.12(a). The arrow indicates the polarity of the source. Energy from the actual source is radiated in all directions in a manner determined by its unbounded medium directional properties. For an observation point P_1, there is a direct wave. In addition, a wave from the actual source radiated toward point R_1 of the interface undergoes a reflection.

EX2042
Page 198 of 1072

The direction is determined by the law of reflection ($\theta_1^i = \theta_1^r$) which assures that the energy in homogeneous media travels in straight lines along the shortest paths. This wave will pass through the observation point P_1. By extending its actual path below the interface, it will seem to originate from a virtual source positioned a distance h below the boundary. For another observation point P_2 the point of reflection is R_2, but the virtual source is the same as before. The same is concluded for all other observation points above the interface.

The amount of reflection is generally determined by the respective constitutive parameters of the media below and above the interface. For a perfect electric conductor below the interface, the incident wave is completely reflected and the field below the boundary is zero. According to the boundary conditions, the tangential components of the electric field must vanish at all points along the interface. Thus for an incident electric field with vertical polarization shown by the arrows, the polarization of the reflected waves must be as indicated in the figure to satisfy the boundary conditions. To excite the polarization of the reflected waves, the virtual source must also be vertical and with a polarity in the same direction as that of the actual source (thus a reflection coefficient of $+1$).

Another orientation of the source will be to have the radiating element in a horizontal position, as shown in Figure 4.24. Following a procedure similar to that of the vertical dipole, the virtual source (image) is also placed a distance h below the interface but with a 180° polarity difference relative to the actual source (thus a reflection coefficient of -1).

In addition to electric sources, artificial equivalent "magnetic" sources and magnetic conductors have been introduced to aid in the analyses of electromagnetic boundary-value problems. Figure 4.13(a) displays the sources and their images for an electric plane conductor. The single arrow indicates an electric element and the double a magnetic one. The direction of the arrow identifies the polarity. Since many problems can be solved using duality, Figure 4.13(b) illustrates the sources and their images when the obstacle is an infinite, flat, perfect "magnetic" conductor.

4.7.2 Vertical Electric Dipole

The analysis procedure for vertical and horizontal electric and magnetic elements near infinite electric and magnetic plane conductors, using image theory, was illustrated graphically in the previous section. Based on the graphical model of Figure 4.12, the mathematical expressions for the fields of a vertical linear element near a perfect electric conductor will now be developed. For simplicity, only far-field observations will be considered.

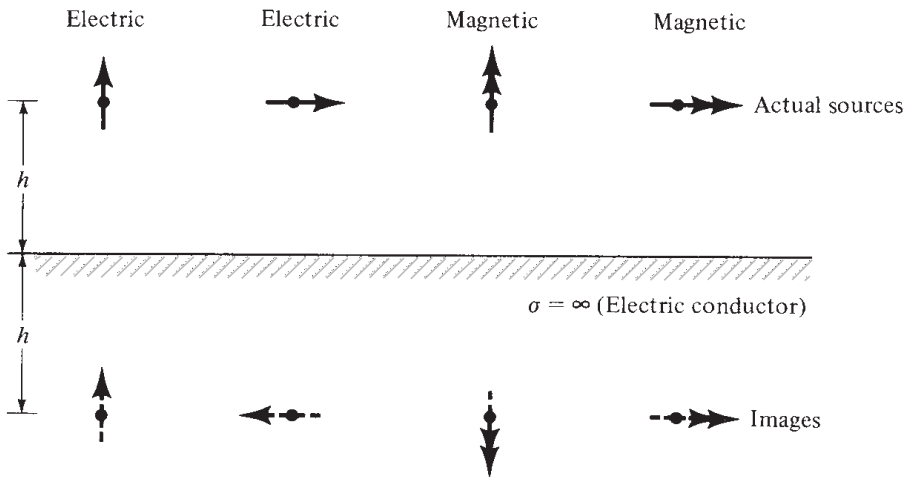
Referring to the geometry of Figure 4.14(a), the far-zone direct component of the electric field of the infinitesimal dipole of length l, constant current I_0, and observation point P is given according to (4-26a) by

$$E_\theta^d = j\eta \frac{kI_0 l e^{-jkr_1}}{4\pi r_1} \sin\theta_1 \tag{4-94}$$

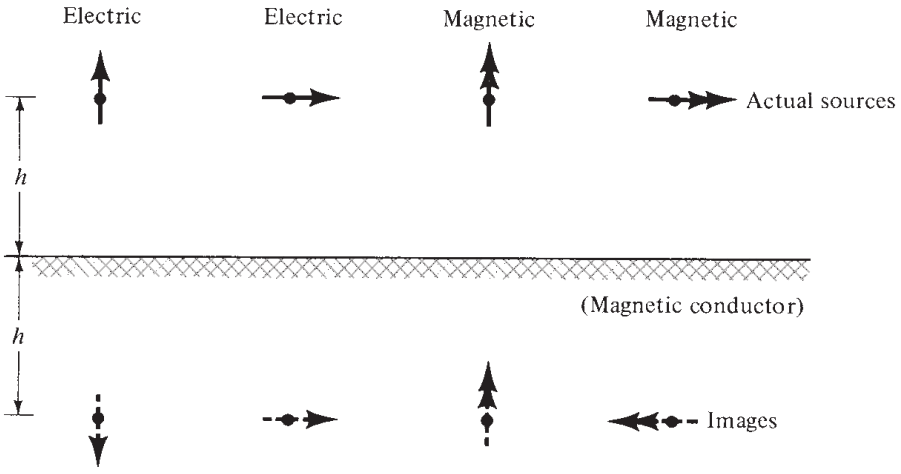
The reflected component can be accounted for by the introduction of the virtual source (image), as shown in Figure 4.14(a), and it can be written as

$$E_\theta^r = jR_v\eta \frac{kI_0 l e^{-jkr_2}}{4\pi r_2} \sin\theta_2 \tag{4-95}$$

EX2042
Page 199 of 1072



(a) Electric conductor



(b) Magnetic conductor

Figure 4.13 Electric and magnetic sources and their images near electric (PEC) and magnetic (PMC) conductors.

or

$$E_\theta^r = j\eta \frac{kI_0 l e^{-jkr_2}}{4\pi r_2} \sin\theta_2 \tag{4-95a}$$

since the reflection coefficient R_v is equal to unity.

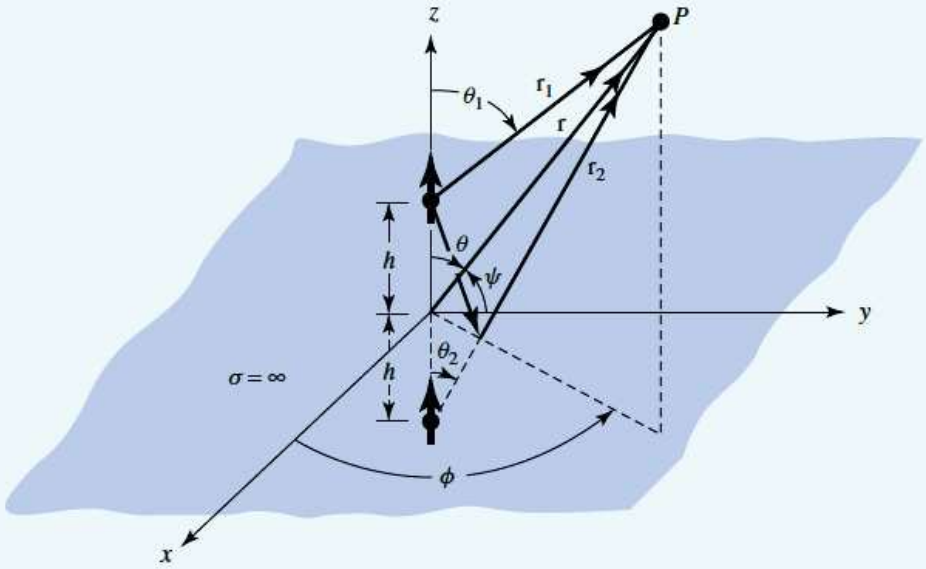
The total field above the interface ($z \geq 0$) is equal to the sum of the direct and reflected components as given by (4-94) and (4-95a). Since a field cannot exist inside a perfect electric conductor, it is equal to zero below the interface. To simplify the expression for the total electric field, it is referred to the origin of the coordinate system ($z = 0$).

In general, we can write that

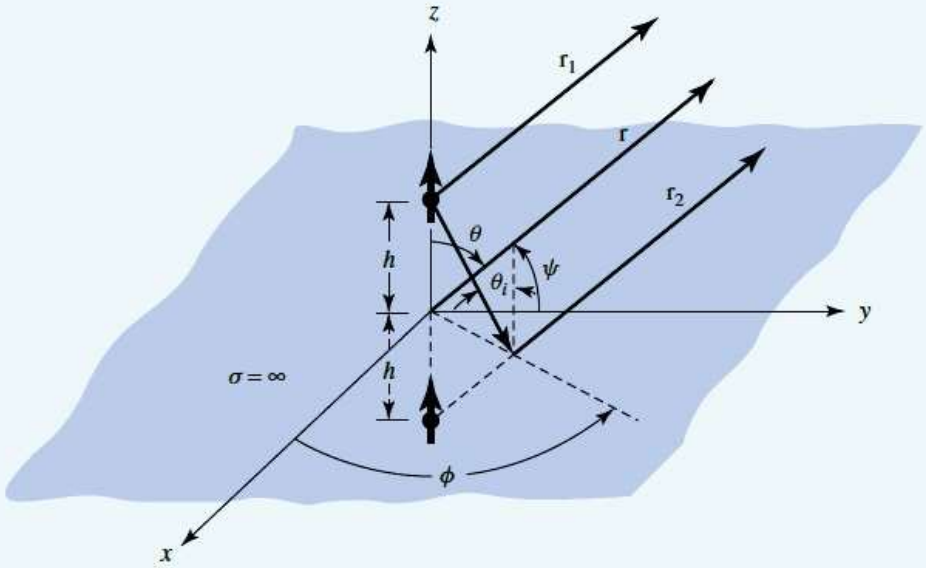
$$r_1 = [r^2 + h^2 - 2rh\cos\theta]^{1/2} \tag{4-96a}$$

$$r_2 = [r^2 + h^2 - 2rh\cos(\pi - \theta)]^{1/2} \tag{4-96b}$$

EX2042
Page 200 of 1072



(a) Vertical electric dipole above ground plane



(b) Far-field observations

Figure 4.14 Vertical electric dipole above infinite perfect electric conductor.

For far-field observations ($r \gg h$), (4-96a) and (4-96b) reduce using the binomial expansion to

$$r_1 \simeq r - h\cos\theta \tag{4-97a}$$

$$r_2 \simeq r + h\cos\theta \tag{4-97b}$$

As shown in Figure 4.14(b), geometrically (4-97a) and (4-97b) represent parallel lines. Since the amplitude variations are not as critical

$$r_1 \simeq r_2 \simeq r \quad \text{for amplitude variations} \tag{4-98}$$

EX2042
Page 201 of 1072

Using (4-97a)–(4-98), the sum of (4-94) and (4-95a) can be written as

$$\left.\begin{aligned} E_\theta &\simeq j\eta\frac{kI_0le^{-jkr}}{4\pi r}\sin\theta[2\cos(kh\cos\theta)] && z\geq 0\\ E_\theta &= 0 && z<0 \end{aligned}\right\} \tag{4-99}$$

It is evident that the total electric field is equal to the product of the field of a single source positioned symmetrically about the origin and a factor [within the brackets in (4-99)] which is a function of the antenna height (h) and the observation angle (θ). This is referred to as *pattern multiplication* and the factor is known as the *array factor* [see also (6-5)]. This will be developed and discussed in more detail and for more complex configurations in Chapter 6.

The shape and amplitude of the field is not only controlled by the field of the single element but also by the positioning of the element relative to the ground. To examine the field variations as a function of the height h, the normalized (to 0 dB) power patterns for $h = 0, \lambda/8, \lambda/4, 3\lambda/8, \lambda/2$, and λ have been plotted in Figure 4.15. Because of symmetry, only half of each pattern is shown. For $h > \lambda/4$ more minor lobes, in addition to the major ones, are formed. As h attains values greater than λ, an even greater number of minor lobes is introduced. These are shown in Figure 4.16 for $h = 2\lambda$ and 5λ. The introduction of the additional lobes in Figure 4.16 is usually called *scalloping*. In general, the total number of lobes is equal to the integer that is closest to

$$\boxed{\text{number of lobes} \simeq \frac{2h}{\lambda}+1} \tag{4-100}$$

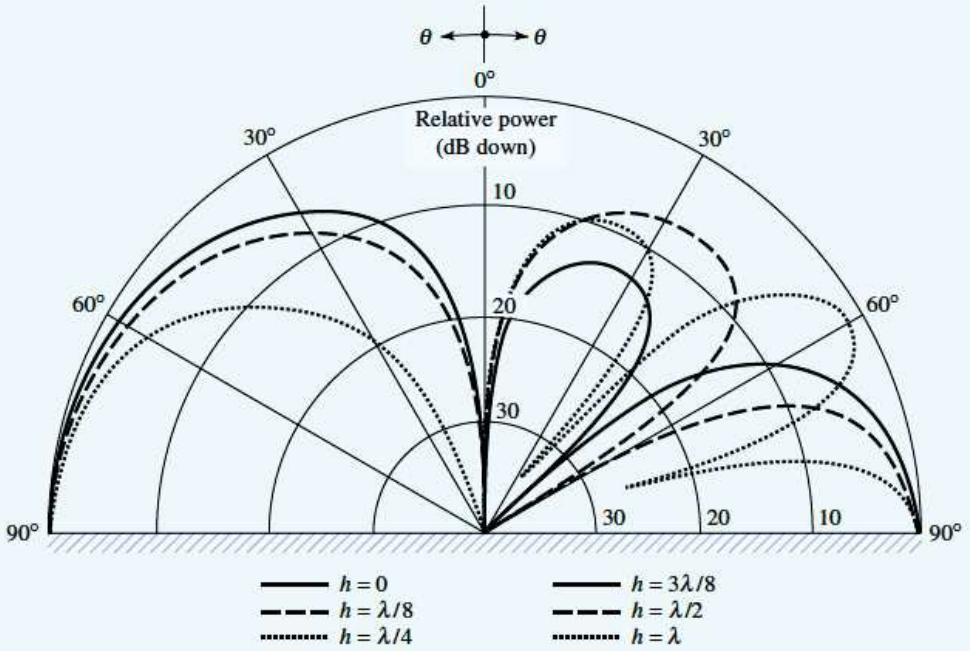


Figure 4.15 Elevation plane amplitude patterns of a vertical infinitesimal electric dipole for different heights above an infinite perfect electric conductor.

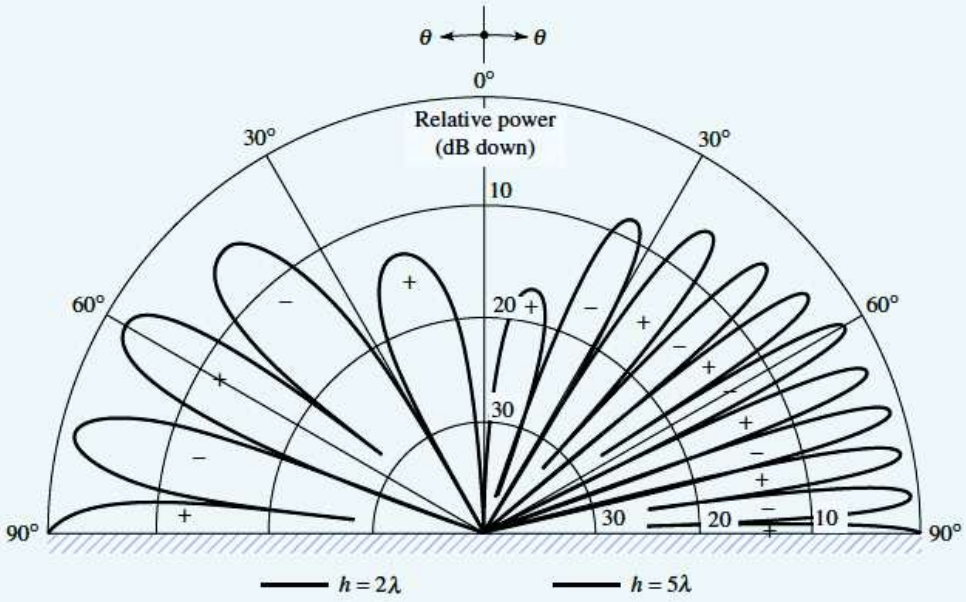


Figure 4.16 Elevation plane amplitude patterns of a vertical infinitesimal electric dipole for heights of 2λ and 5λ above an infinite perfect electric conductor.

Since the total field of the antenna system is different from that of a single element, the directivity and radiation resistance are also different. To derive expressions for them, we first find the total radiated power over the upper hemisphere of radius r using

$$P_{\text{rad}} = \oiint_S \mathbf{W}_{\text{av}} \cdot d\mathbf{s} = \frac{1}{2\eta} \int_0^{2\pi} \int_0^{\pi/2} |E_\theta|^2 r^2 \sin\theta \, d\theta \, d\phi$$

$$= \frac{\pi}{\eta} \int_0^{\pi/2} |E_\theta|^2 r^2 \sin\theta \, d\theta \tag{4-101}$$

which simplifies, with the aid of (4-99), to

$$P_{\text{rad}} = \pi\eta \left| \frac{I_0 l}{\lambda} \right|^2 \left[\frac{1}{3} - \frac{\cos(2kh)}{(2kh)^2} + \frac{\sin(2kh)}{(2kh)^3} \right] \tag{4-102}$$

As $kh \to \infty$ the radiated power, as given by (4-102), is equal to that of an isolated element. However, for $kh \to 0$, it can be shown by expanding the sine and cosine functions into series that the power is twice that of an isolated element. Using (4-99), the radiation intensity can be written as

$$U = r^2 \, W_{\text{av}} = r^2 \left(\frac{1}{2\eta} |E_\theta|^2 \right) = \frac{\eta}{2} \left| \frac{I_0 l}{\lambda} \right|^2 \sin^2\theta \cos^2(kh\cos\theta) \tag{4-103}$$

The maximum value of (4-103) occurs at $\theta = \pi/2$ and is given, excluding $kh \to \infty$, by

$$U_{\text{max}} = U|_{\theta=\pi/2} = \frac{\eta}{2} \left| \frac{I_0 l}{\lambda} \right|^2 \tag{4-103a}$$

EX2042
Page 203 of 1072

which is four times greater than that of an isolated element. With (4-102) and (4-103a), the directivity can be written as

$$D_0 = \frac{4\pi U_{\max}}{P_{\text{rad}}} = \frac{2}{\left[\frac{1}{3} - \frac{\cos(2kh)}{(2kh)^2} + \frac{\sin(2kh)}{(2kh)^3}\right]} \tag{4-104}$$

whose value for $kh = 0$ is 3. The maximum value occurs when $kh = 2.881$ ($h = 0.4585\lambda$), and it is equal to 6.566 which is greater than four times that of an isolated element (1.5). The pattern for $h = 0.4585\lambda$ is shown plotted in Figure 4.17 while the directivity, as given by (4-104), is displayed in Figure 4.18 for $0 \le h \le 5\lambda$.

Using (4-102), the radiation resistance can be written as

$$R_r = \frac{2P_{\text{rad}}}{|I_0|^2} = 2\pi\eta\left(\frac{l}{\lambda}\right)^2\left[\frac{1}{3} - \frac{\cos(2kh)}{(2kh)^2} + \frac{\sin(2kh)}{(2kh)^3}\right] \tag{4-105}$$

whose value for $kh \to \infty$ is the same and for $kh = 0$ is twice that of the isolated element as given by (4-19). When $kh = 0$, the value of R_r as given by (4-105) is only one-half the value of an $l' = 2l$ isolated element according to (4-19). The radiation resistance, as given by (4-105), is plotted in Figure 4.18 for $0 \le h \le 5\lambda$ when $l = \lambda/50$ and the element is radiating into free-space ($\eta \simeq 120\pi$). It can be compared to the value of $R_r = 0.316$ ohms for the isolated element of Example 4.1.

In practice, a wide use has been made of a quarter-wavelength monopole ($l = \lambda/4$) mounted above a ground plane, and fed by a coaxial line, as shown in Figure 4.19(a). For analysis purposes, a $\lambda/4$ image is introduced and it forms the $\lambda/2$ equivalent of Figure 4.19(b). It should be emphasized that the $\lambda/2$ equivalent of Figure 4.19(b) gives

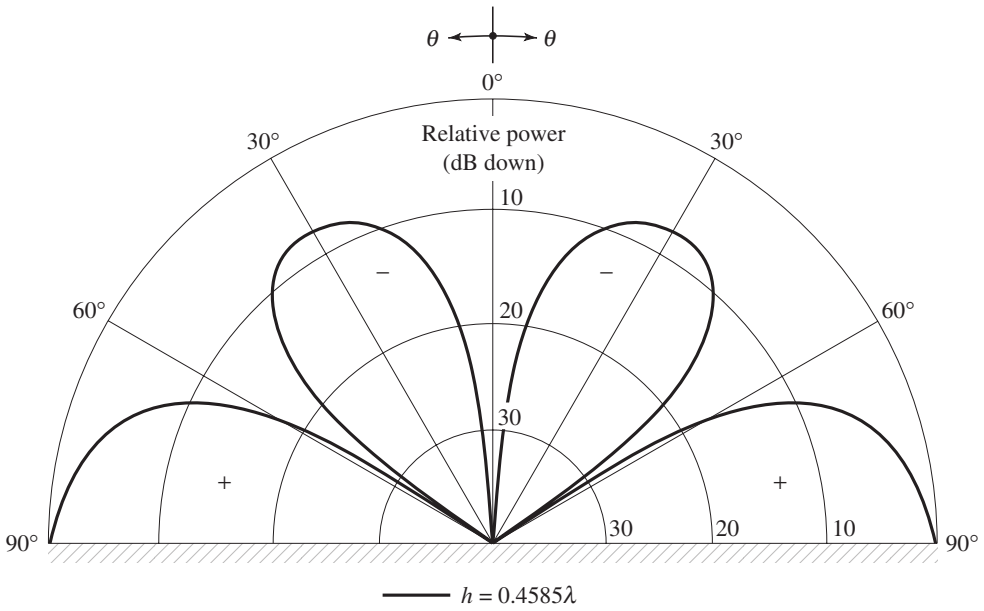


Figure 4.17 Elevation plane amplitude pattern of a vertical infinitesimal electric dipole at a height of 0.4585λ above an infinite perfect electric conductor.

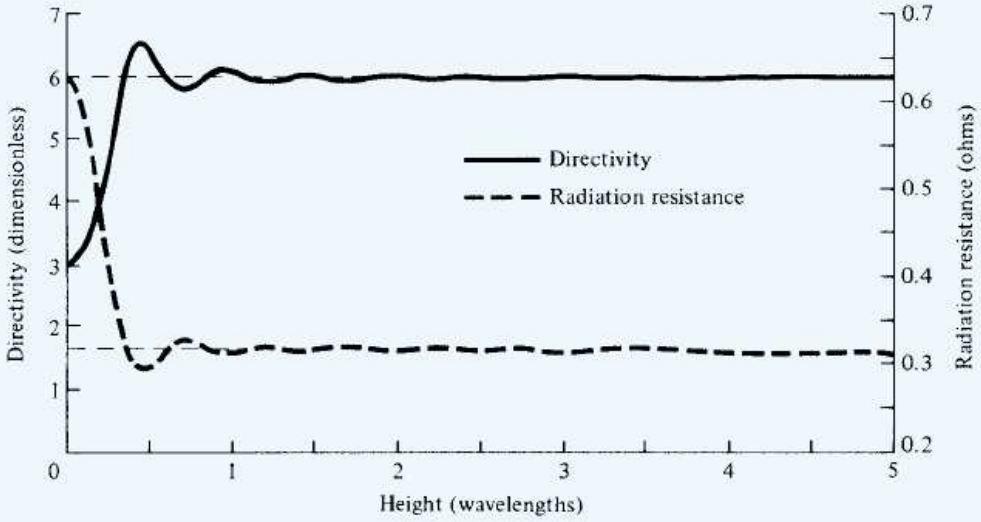
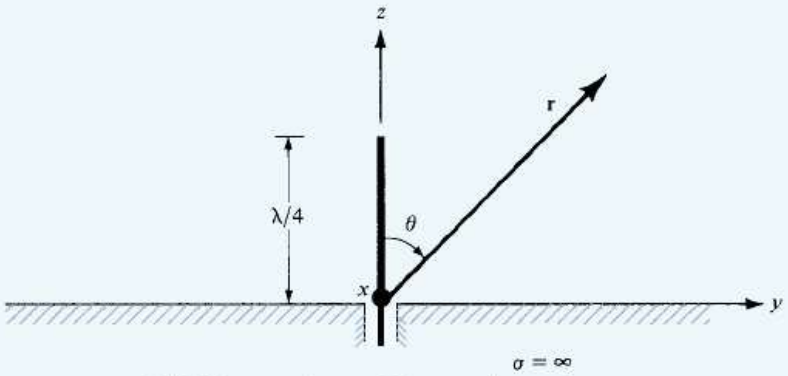
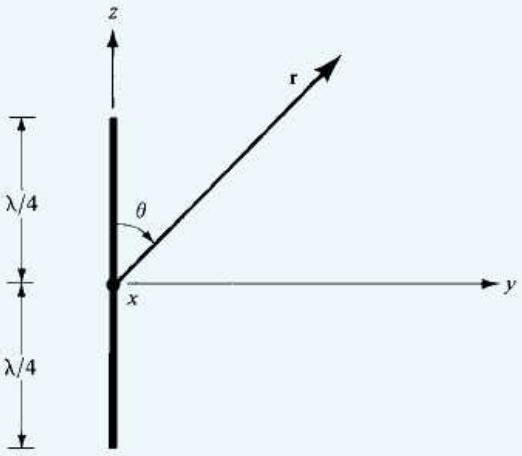


Figure 4.18 Directivity and radiation resistance of a vertical infinitesimal electric dipole as a function of its height above an infinite perfect electric conductor.



(a) λ/4 monopole on infinite electric conductor



(b) Equivalent of λ/4 monopole on infinite electric conductor

Figure 4.19 Quarter-wavelength monopole on an infinite perfect electric conductor.

the correct field values for the actual system of Figure 4.19(a) only above the interface ($z \geq 0, 0 \leq \theta \leq \pi/2$). Thus, the far-zone electric and magnetic fields for the $\lambda/4$ monopole above the ground plane are given, respectively, by (4-84) and (4-85).

From the discussions of the resistance of an infinitesimal dipole above a ground plane for $kh = 0$, it follows that the input impedance of a $\lambda/4$ monopole above a ground plane is equal to one-half that of an isolated $\lambda/2$ dipole. Thus, referred to the current maximum, the input impedance Z_{im} is given by

$$Z_{im}\ (\text{monopole}) = \tfrac{1}{2} Z_{im}\ (\text{dipole}) = \tfrac{1}{2}[73 + j42.5] = 36.5 + j21.25 \qquad (4\text{-}106)$$

where $73 + j42.5$ is the input impedance (and also the impedance referred to the current maximum) of a $\lambda/2$ dipole as given by (4-93a).

The same procedure can be followed for any other length. The input impedance $Z_{im} = R_{im} + jX_{im}$ (referred to the current maximum) of a vertical $\lambda/2$ dipole placed near a flat lossy electric conductor, as a function of height above the ground plane, is plotted in Figure 4.20, for $0 \leq h \leq \lambda$. Conductivity values considered were 10^{-2}, 10^{-1}, 1, 10 S/m, and infinity (PEC). It is apparent that the conductivity does not strongly influence the impedance values. The conductivity values used are representative of dry to wet earth. It is observed that the values of the resistance and reactance approach, as the height increases, the corresponding ones of the isolated element (73 ohms for the resistance and 42.5 ohms for the reactance).

4.7.3 Approximate Formulas for Rapid Calculations and Design

Although the input resistance of a dipole of any length can be computed using (4-70) and (4-79), while that of the corresponding monopole using (4-106), very good answers

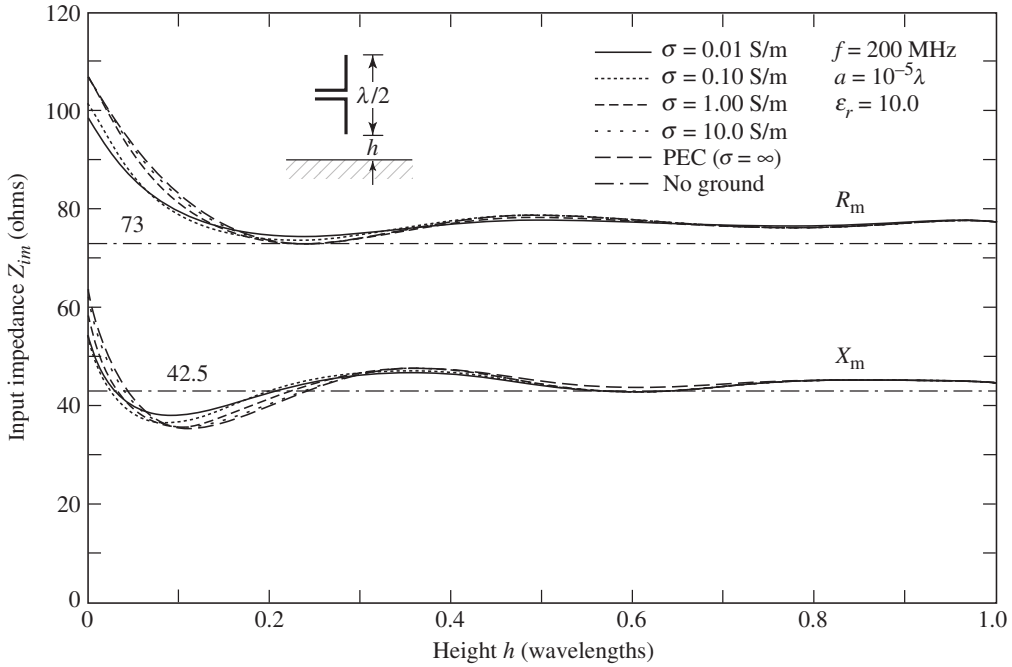


Figure 4.20 Input impedance of a vertical $\lambda/2$ dipole above a flat lossy electric conducting surface.

can be obtained using simpler but approximate expressions. Defining G as

$$G = kl/2 \text{ for dipole} \tag{4-107a}$$

$$G = kl \text{ for monopole} \tag{4-107b}$$

where l is the total length of each respective element, it has been shown that the input resistance of the dipole and monopole can be computed approximately using [13]

$$\frac{0 < G < \pi/4}{(\textit{maximum input resistance of dipole is less than 12.337 ohms})}$$

$$R_{in}\ (\text{dipole}) = 20G^2 \qquad 0 < l < \lambda/4 \tag{4-108a}$$

$$R_{in}\ (\text{monopole}) = 10G^2 \quad 0 < l < \lambda/8 \tag{4-108b}$$

$$\frac{\pi/4 \leq G < \pi/2}{(\textit{maximum input resistance of dipole is less than 76.383 ohms})}$$

$$R_{in}\ (\text{dipole}) = 24.7G^{2.5} \qquad \lambda/4 \leq l < \lambda/2 \tag{4-109a}$$

$$R_{in}\ (\text{monopole}) = 12.35G^{2.5} \quad \lambda/8 \leq l < \lambda/4 \tag{4-109b}$$

$$\frac{\pi/2 \leq G < 2}{(\textit{maximum input resistance of dipole is less than 200.53 ohms})}$$

$$R_{in}\ (\text{dipole}) = 11.14G^{4.17} \qquad \lambda/2 \leq l < 0.6366\lambda \tag{4-110a}$$

$$R_{in}\ (\text{monopole}) = 5.57G^{4.17} \quad \lambda/4 \leq l < 0.3183\lambda \tag{4-110b}$$

Besides being much simpler in form, these formulas are much more convenient in design (synthesis) problems where the input resistance is given and it is desired to determine the length of the element. These formulas can be verified by plotting the actual resistance versus length on a log–log scale and observe the slope of the line [13]. For example, the slope of the line for values of G up to about $\pi/4 \simeq 0.75$ is 2.

Example 4.4

Determine the length of the dipole whose input resistance is 50 ohms. Verify the answer.

Solution: Using (4-109a)

$$50 = 24.7G^{2.5}$$

or

$$G = 1.3259 = kl/2$$

Therefore

$$l = 0.422\lambda$$

Using (4-70) and (4-79) R_{in} for 0.422λ is 45.816 ohms, which closely agrees with the desired value of 50 ohms. To obtain 50 ohms using (4-70) and (4-79), $l = 0.4363\lambda$.

4.7.4 Antennas for Mobile Communication Systems

The dipole and monopole are two of the most widely used antennas for wireless mobile communication systems [14]–[18]. An array of dipole elements is extensively used as an antenna at the base station of a land mobile system while the monopole, because of its broadband characteristics and simple construction, is perhaps to most common antenna element for portable equipment, such as cellular telephones, cordless telephones, automobiles, trains, etc. The radiation efficiency and gain characteristics of both of these elements are strongly influenced by their electrical length which is related to the frequency of operation. In a handheld unit, such as a cellular telephone, the position of the monopole element on the unit influences the pattern while it does not strongly affect the input impedance and resonant frequency. In addition to its use in mobile communication systems, the quarter-wavelength monopole is very popular in many other applications. An alternative to the monopole for the handheld unit is the loop, which is discussed in Chapter 5. Other elements include the inverted F, planar inverted F antenna (PIFA), microstrip (patch), spiral, and others [14]–[18].

The variation of the input impedance, real and imaginary parts, of a vertical monopole antenna mounted on an experimental unit, simulating a cellular telephone, are shown in Figure 4.21(a,b) [17]. It is apparent that the first resonance, around 1,000 MHz, is of the *series type* with slowly varying values of impedance versus frequency, and of desirable magnitude, for practical implementation. For frequencies below the first resonance, the impedance is capacitive (imaginary part is negative), as is typical of linear elements of small lengths (see Figure 8.17); above the first resonance, the impedance is inductive (positive imaginary part). The second resonance, around 1,500 MHz, is of the *parallel type* (*antiresonance*) with large and rapid changes in the values of the impedance. These values and variation of impedance are usually undesirable for practical implementation. The order of the types of resonance (*series* vs. *parallel*) can be interchanged by choosing another element, such as a loop, as illustrated in Chapter 5, Section 5.8, Figure 5.20 [18]. The radiation amplitude patterns are those of a typical dipole with intensity in the lower hemisphere.

Examples of monopole type antennas used in cellular and cordless telephones, walkie-talkies, and CB radios are shown in Figure 4.22. The monopoles used in these units are either stationary or retractable/telescopic. The length of the retractable/telescopic monopole, such as the one used in the Motorola StarTAC and in others, is varied during operation to improve the radiation characteristics, such as the amplitude pattern and input impedance. During nonusage, the element is usually retracted within the body of the device to prevent it from damage. Units that do not utilize a visible monopole type of antenna, such as the one of the cellular telephones in Figure 4.22, use embedded/hidden type of antenna element. One such embedded/hidden element that is often used is a planar inverted F antenna (PIFA) [16]; there are others. Many of the stationary monopoles are often covered with a dielectric cover. Within the cover, there is typically a straight wire. *However, another design that is often used is a helix antenna* (see Chapter 10, Section 10.3.1) *with a very small circumference and overall length so that the helix operates in the normal mode, whose relative pattern is exhibited in Figure 10.14(a) and which resembles that of a straight-wire monopole. The helix is used, in lieu of a straight wire, because it can be designed to have larger input impedance, which is more attractive for matching to typical feed lines, such as a coaxial line* (see Problem 10.18).

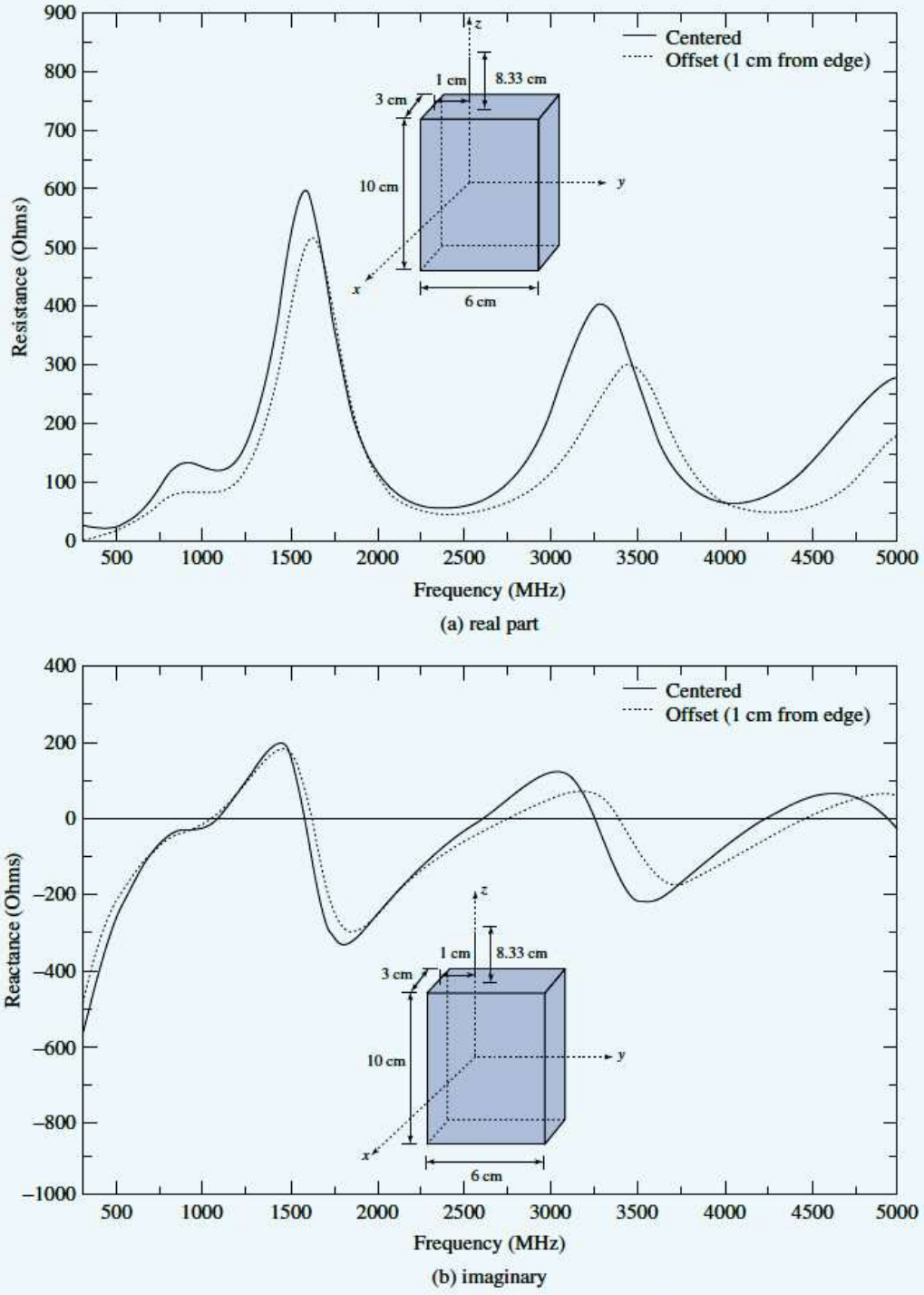


Figure 4.21 Input impedance, real and imaginary parts, of a vertical monopole mounted on an experimental cellular telephone device.

An antenna configuration that is widely used as a base-station antenna for mobile communication and is seen almost everywhere is shown in Figure 4.23. It is a triangular array configuration consisting of twelve dipoles, with four dipoles on each side of the triangle. Each four-element array, on each side of the triangle, is used to cover an angular sector of 120°, forming what is usually referred to as a sectoral array [see Section 16.3.1(B) and Figure 16.6(a)].



Figure 4.22 Examples of stationary, retractable/telescopic and embedded/hidden antennas used in commercial cellular and cordless telephones, walkie-talkies, and CB radios. (SOURCE: Reproduced with permissions from Motorola, Inc. © Motorola, Inc.; Samsung © Samsung; Midland Radio Corporation © Midland Radio Corporation).

4.7.5 Horizontal Electric Dipole

Another dipole configuration is when the linear element is placed horizontally relative to the infinite electric ground plane, as shown in Figure 4.24. The analysis procedure of this is identical to the one of the vertical dipole. Introducing an image and assuming far-field observations, as shown in Figure 4.25(a,b), the direct component can be written as

$$E_{\psi}^{d} = j\eta \frac{kI_0 l e^{-jkr_1}}{4\pi r_1} \sin\psi \tag{4-111}$$

and the reflected one by

$$E_{\psi}^{r} = jR_h \eta \frac{kI_0 l e^{-jkr_2}}{4\pi r_2} \sin\psi \tag{4-112}$$

or

$$E_{\psi}^{r} = -j\eta \frac{kI_0 l e^{-jkr_2}}{4\pi r_2} \sin\psi \tag{4-112a}$$

since the reflection coefficient is equal to $R_h = -1$.

To find the angle ψ, which is measured from the y-axis toward the observation point, we first form

$$\cos\psi = \hat{\mathbf{a}}_y \cdot \hat{\mathbf{a}}_r = \hat{\mathbf{a}}_y \cdot (\hat{\mathbf{a}}_x \sin\theta\cos\phi + \hat{\mathbf{a}}_y \sin\theta\sin\phi + \hat{\mathbf{a}}_z \cos\theta) = \sin\theta\sin\phi \tag{4-113}$$

EX2042
Page 210 of 1072



Figure 4.23 Triangular array of dipoles used as a sectoral base-station antenna for mobile communication.

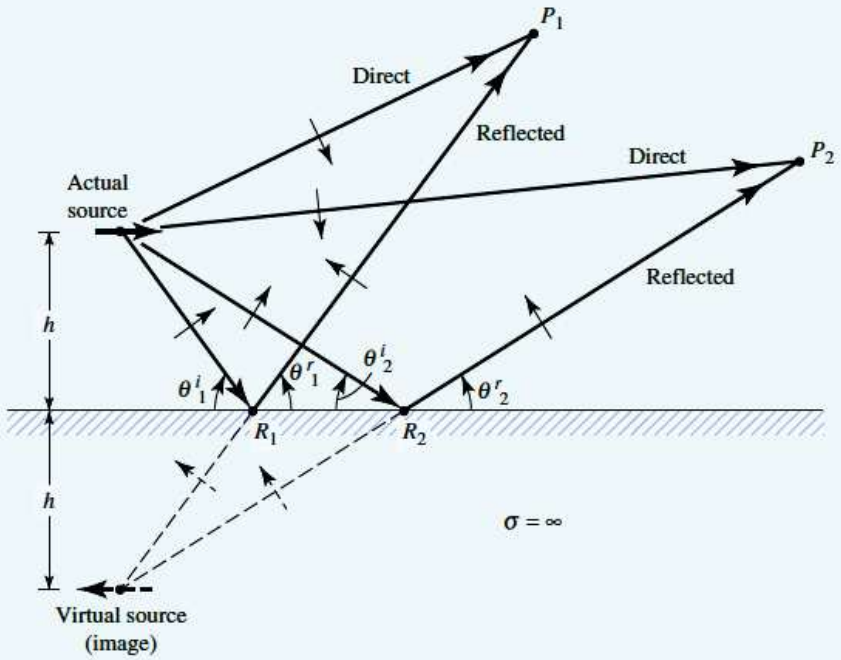
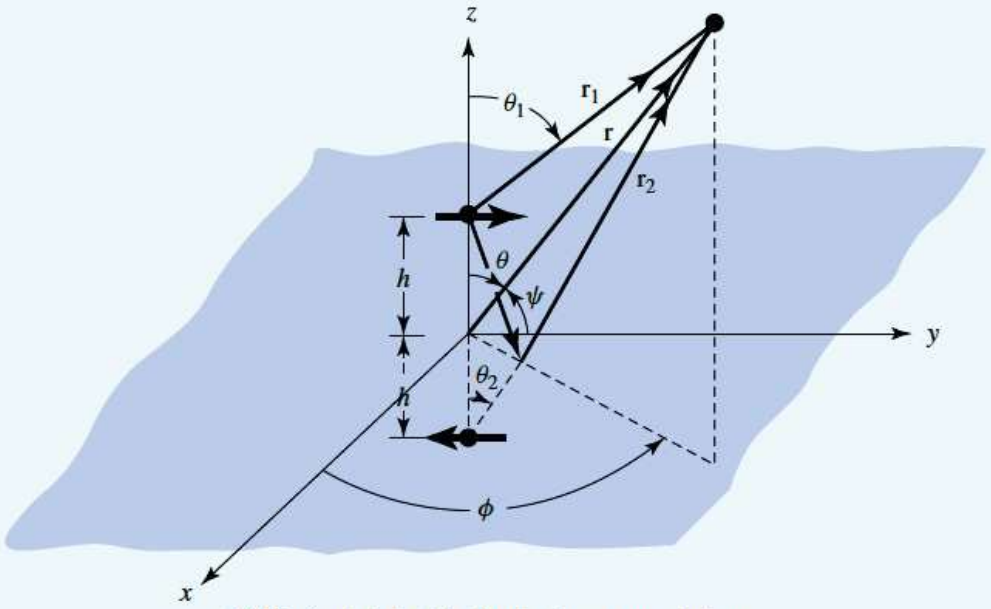
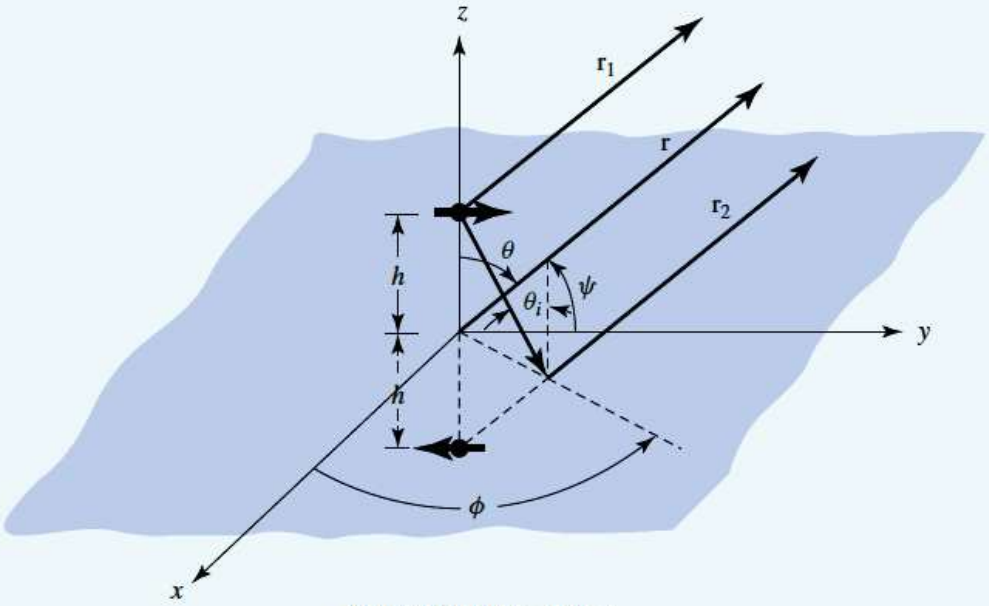


Figure 4.24 Horizontal electric dipole, and its associated image, above an infinite, flat, perfect electric conductor.

EX2042
Page 211 of 1072



(a) Horizontal electric dipole above ground plane



(b) Far-field observations

Figure 4.25 Horizontal electric dipole above an infinite perfect electric conductor.

from which we find

$$\sin\psi = \sqrt{1-\cos^2\psi} = \sqrt{1-\sin^2\theta\sin^2\phi} \tag{4-114}$$

Since for far-field observations

$$\left.\begin{aligned} r_1 &\simeq r - h\cos\theta \\ r_2 &\simeq r + h\cos\theta \end{aligned}\right\} \quad \text{for phase variations} \tag{4-115a}$$

$$r_1 \simeq r_2 \simeq r \qquad \text{for amplitude variations} \tag{4-115b}$$

EX2042
Page 212 of 1072

the total field, which is valid only above the ground plane ($z \geq h; 0 \leq \theta \leq \pi/2, 0 \leq \phi \leq 2\pi$), can be written as

$$E_\psi = E_\psi^d + E_\psi^r = j\eta \frac{kI_0 l e^{-jkr}}{4\pi r} \sqrt{1 - \sin^2\theta \sin^2\phi}\ [2j \sin(kh\cos\theta)] \qquad (4\text{-}116)$$

Equation (4-116) again consists of the product of the field of a single isolated element placed symmetrically at the origin and a factor (within the brackets) known as the *array factor*. This again is the pattern multiplication rule of (6-5) which is discussed in more detail in Chapter 6.

Example 4.5

Using the vector potential **A** and the procedure outlined in Section 3.6 of Chapter 3, derive the far-zone spherical electric and magnetic field components of a horizontal infinitesimal dipole placed at the origin of the coordinate system of Figure 4.1.

Solution: Using (4-4), but for a horizontal infinitesimal dipole of uniform current directed along the y-axis, the corresponding vector potential can be written as

$$\underline{A} = \hat{a}_y \frac{\mu I_0 \ell e^{-jkr}}{4\pi r}$$

with the corresponding spherical components, using the rectangular to spherical components transformation of (4-5), expressed as

$$A_\theta = A_y \cos\theta \sin\phi = \frac{\mu I_0 \ell e^{-jkr}}{4\pi r} \cos\theta \sin\phi$$

$$A_\phi = A_y \cos\phi = \frac{\mu I_0 \ell e^{-jkr}}{4\pi r} \cos\phi$$

Using (3-58a) and (3-58b), we can write the corresponding far-zone electric and magnetic field components as

$$E_\theta \cong -j\omega A_\theta = -j \frac{\omega\mu I_0 \ell e^{-jkr}}{4\pi r} \cos\theta \sin\phi$$

$$E_\phi \cong -j\omega A_\phi = -j \frac{\omega\mu I_0 \ell e^{-jkr}}{4\pi r} \cos\phi$$

$$H_\theta \cong -\frac{E_\phi}{\eta} = j \frac{\omega\mu I_0 \ell e^{-jkr}}{4\pi\eta r} \cos\phi$$

$$H_\phi \cong +\frac{E_\theta}{\eta} = +j \frac{\omega\mu I_0 \ell e^{-jkr}}{4\pi\eta r} \cos\theta \sin\phi$$

Although the electric-field components, and thus the magnetic field components, take a different analytical form than (4-111), the patterns are the same.

To examine the variations of the total field as a function of the element height above the ground plane, the two-dimensional elevation plane patterns (normalized to 0 dB) for $\phi = 90^\circ$ (y-z plane) when $h = 0, \lambda/8, \lambda/4, 3\lambda/8, \lambda/2$, and λ are plotted

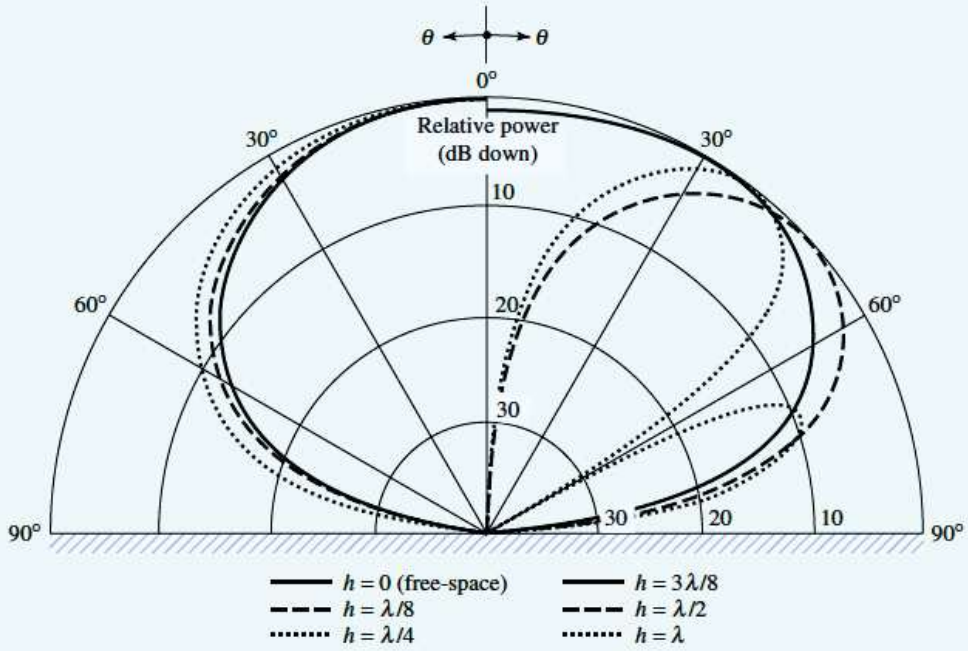


Figure 4.26 Elevation plane ($\phi = 90°$) amplitude patterns of a horizontal infinitesimal electric dipole for different heights above an infinite perfect electric conductor.

in Figure 4.26. Since this antenna system is not symmetric with respect to the z axis, the azimuthal plane (x-y plane) pattern is not isotropic.

To obtain a better visualization of the radiation intensity in all directions above the interface, the three-dimensional pattern for $h = \lambda$ is shown plotted in Figure 4.27. The radial distance on the x-y plane represents the elevation angle θ from 0° to 90°, and the z-axis represents the normalized amplitude of the radiation field intensity from 0 to 1. The azimuthal angle ϕ ($0 \leq \phi \leq 2\pi$) is measured from the x- toward the y-axis on the x-y plane.

As the height increases beyond one wavelength ($h > \lambda$), a larger number of lobes is again formed. This is illustrated in Figure 4.28 for $h = 2\lambda$ and 5λ. The scalloping effect is evident here, as in Figure 4-16 for the vertical dipole. The total number of lobes is equal to the integer that most closely is equal to

$$\boxed{\text{number of lobes} \simeq 2\left(\frac{h}{\lambda}\right)} \tag{4-117}$$

with unity being the smallest number.

Following a procedure similar to the one performed for the vertical dipole, the radiated power can be written as

$$P_{\text{rad}} = \eta\frac{\pi}{2}\left|\frac{I_0 l}{\lambda}\right|^2\left[\frac{2}{3} - \frac{\sin(2kh)}{2kh} - \frac{\cos(2kh)}{(2kh)^2} + \frac{\sin(2kh)}{(2kh)^3}\right] \tag{4-118}$$

and the radiation resistance as

$$R_r = \eta\pi\left(\frac{l}{\lambda}\right)^2\left[\frac{2}{3} - \frac{\sin(2kh)}{2kh} - \frac{\cos(2kh)}{(2kh)^2} + \frac{\sin(2kh)}{(2kh)^3}\right] \tag{4-119}$$

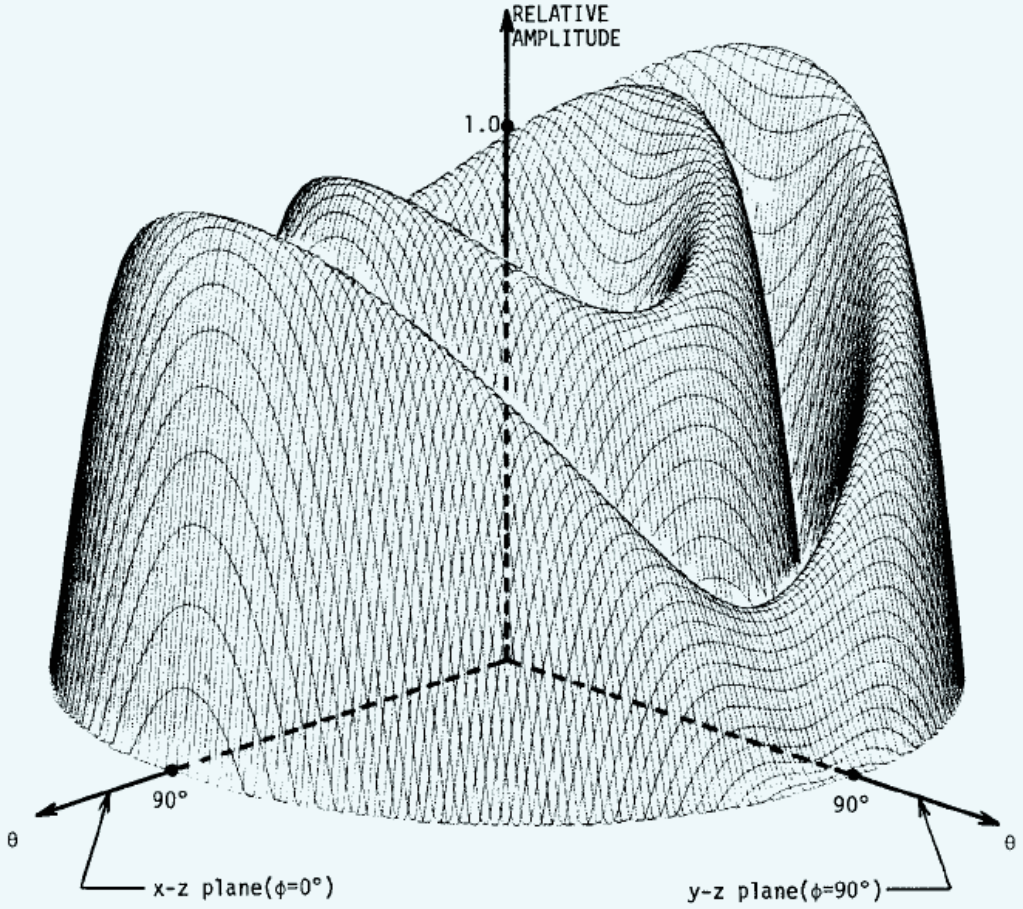


Figure 4.27 Three-dimensional amplitude pattern of an infinitesimal horizontal dipole a distance $h = \lambda$ above an infinite perfect electric conductor.

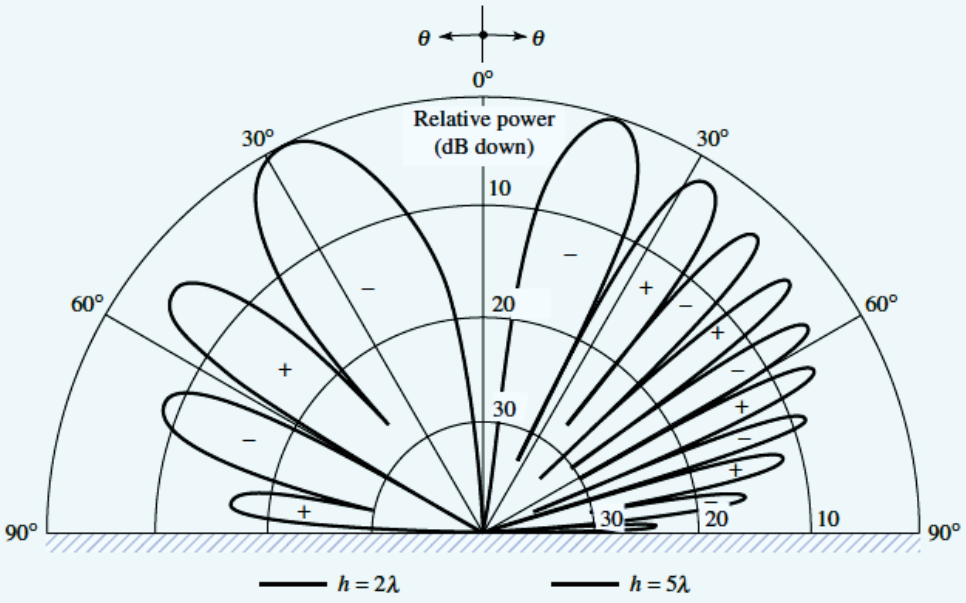


Figure 4.28 Elevation plane ($\phi = 90°$) amplitude patterns of a horizontal infinitesimal electric dipole for heights 2λ and 5λ above an infinite perfect electric conductor.

EX2042
Page 215 of 1072

By expanding the sine and cosine functions into series, it can be shown that (4-119) reduces for small values of kh to

$$R_r \overset{kh\to 0}{=} \eta\pi\left(\frac{l}{\lambda}\right)^2\left[\frac{2}{3}-\frac{2}{3}+\frac{8}{15}\left(\frac{2\pi h}{\lambda}\right)^2\right]=\eta\frac{32\pi^3}{15}\left(\frac{l}{\lambda}\right)^2\left(\frac{h}{\lambda}\right)^2 \tag{4-120}$$

For $kh \to \infty$, (4-119) reduces to that of an isolated element. The radiation resistance, as given by (4-119), is plotted in Figure 4.29 for $0 \le h \le 5\lambda$ when $l = \lambda/50$ and the antenna is radiating into free-space ($\eta \simeq 120\pi$).

The radiation intensity is given by

$$U \simeq \frac{r^2}{2\eta}|E_\psi|^2=\frac{\eta}{2}\left|\frac{I_0 l}{\lambda}\right|^2(1-\sin^2\theta\sin^2\phi)\sin^2(kh\cos\theta) \tag{4-121}$$

The maximum value of (4-121) depends on the value of kh (whether $kh \le \pi/2, h \le \lambda/4$ or $kh > \pi/2, h > \lambda/4$). It can be shown that the maximum of (4-121) is:

$$U_{\max}=\begin{cases}\dfrac{\eta}{2}\left|\dfrac{I_0 l}{\lambda}\right|^2\sin^2(kh) & kh\le\pi/2\ (h\le\lambda/4)\\ & (\theta=0^\circ)\end{cases} \tag{4-122a}$$

$$\begin{cases}\dfrac{\eta}{2}\left|\dfrac{I_0 l}{\lambda}\right|^2 & kh>\pi/2\ (h>\lambda/4)\\ & [\phi=0^\circ \text{ and } \sin(kh\cos\theta_{\max})=1\\ & \text{or } \theta_{\max}=\cos^{-1}(\pi/2kh)]\end{cases} \tag{4-122b}$$

Using (4-118) and (4-122a), (4-122b), the directivity can be written as

$$D_0=\frac{4\pi U_{\max}}{P_{\text{rad}}}=\begin{cases}\dfrac{4\sin^2(kh)}{R(kh)} & kh\le\pi/2\ (h\le\lambda/4)\\ \dfrac{4}{R(kh)} & kh>\pi/2\ (h>\lambda/4)\end{cases} \tag{4-123a, 4-123b}$$

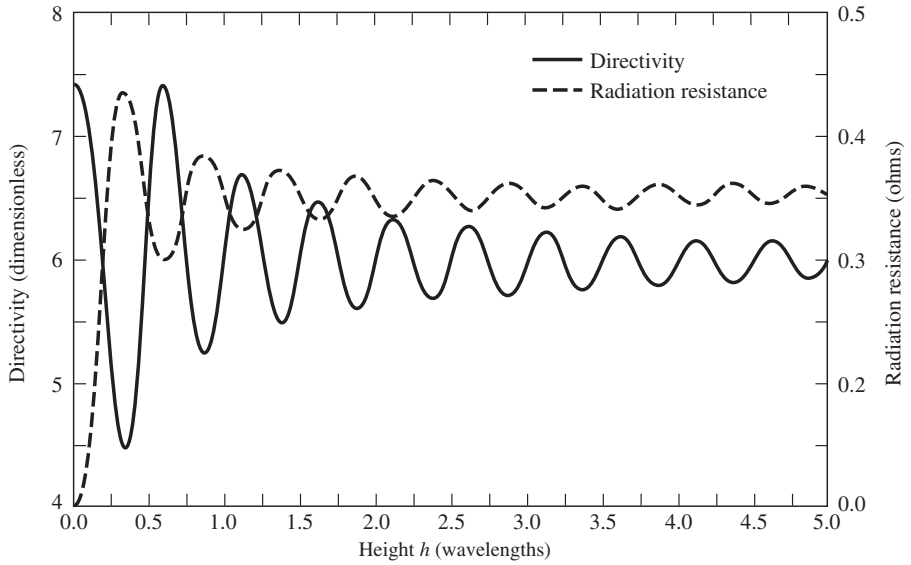


Figure 4.29 Radiation resistance and maximum directivity of a horizontal infinitesimal electric dipole as a function of its height above an infinite perfect electric conductor.

where

$$R(kh) = \left[\frac{2}{3} - \frac{\sin(2kh)}{2kh} - \frac{\cos(2kh)}{(2kh)^2} + \frac{\sin(2kh)}{(2kh)^3}\right] \tag{4-123c}$$

For small values of kh ($kh \to 0$), (4-123a) reduces to

$$D_0 \overset{kh\to 0}{=} \frac{4\sin^2(kh)}{\left[\frac{2}{3} - \frac{2}{3} + \frac{8}{15}(kh)^2\right]} = 7.5\left(\frac{\sin\ kh}{kh}\right)^2 \tag{4-124}$$

For $h = 0$ the element is shorted and it does not radiate. The directivity, as given by (4-123a)–(4-123b) is plotted for $0 \le h \le 5\lambda$ in Figure 4.29. It exhibits a maximum value of 7.5 for small values of h. Maximum values of slightly greater than 6 occur when $h \simeq (0.615 + n/2)\lambda$, $n = 1, 2, 3, \ldots$.

The input impedance $Z_{im} = R_{im} + jX_{im}$ (referred to the current maximum) of a horizontal $\lambda/2$ dipole above a flat lossy electric conductor is shown plotted in Figure 4.30 for $0 \le h \le \lambda$. Conductivities of 10^{-2}, 10^{-1}, 1, 10 S/m, and infinity (PEC) were considered. It is apparent that the conductivity does have a more pronounced effect on the impedance values, compared to those of the vertical dipole shown in Figure 4.20. The conductivity values used are representative of those of the dry to wet earth. The values of the resistance and reactance approach, as the height increases, the corresponding values of the isolated element (73 ohms for the resistance and 42.5 ohms for the reactance).

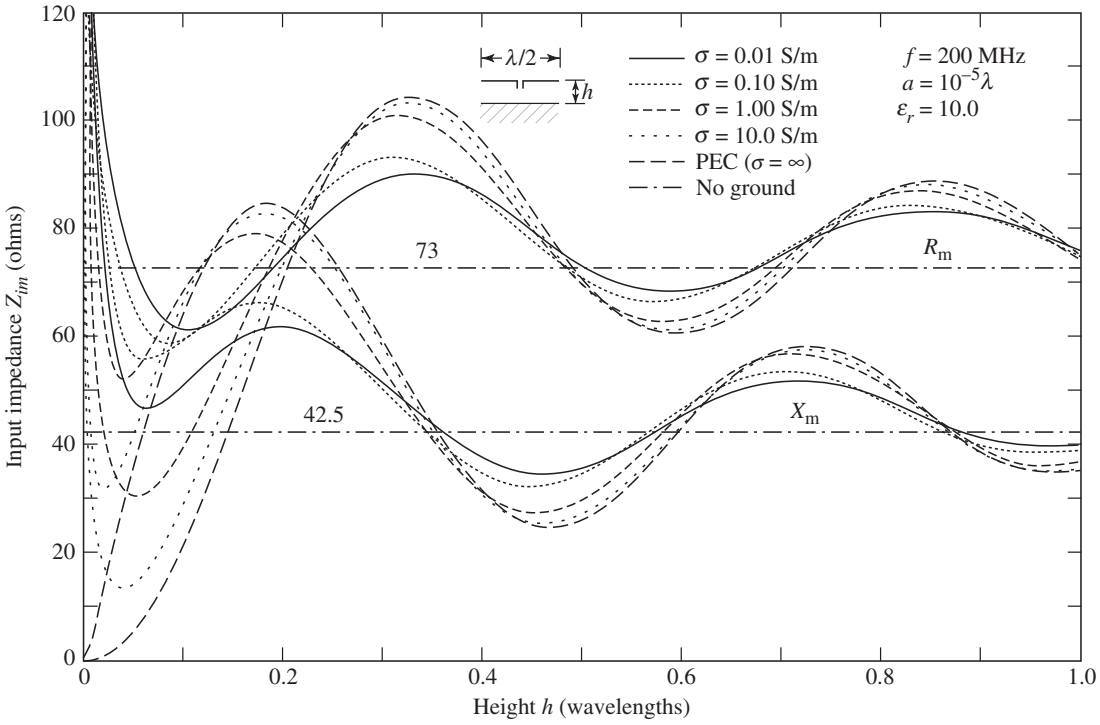


Figure 4.30 Input impedance of a horizontal $\lambda/2$ above a flat lossy electric conducting surface.

EX2042
Page 217 of 1072

4.8 GROUND EFFECTS

In the previous two sections the variations of the radiation characteristics (pattern, radiation resistance, directivity) of infinitesimal vertical and horizontal linear elements were examined when they were placed above plane perfect electric conductors. Although ideal electric conductors ($\sigma = \infty$) are not realizable, their effects can be used as guidelines for good conductors ($\sigma \gg \omega\epsilon$, where ϵ is the permittivity of the medium).

One obstacle that is not an ideal conductor, and it is always present in any antenna system, is the ground (earth). In addition, the earth is not a plane surface. To simplify the analysis, however, the earth will initially be assumed to be flat. For pattern analysis, this is a very good engineering approximation provided the radius of the earth is large compared to the wavelength and the observation angles are greater than about $57.3/(ka)^{1/3}$ degrees from grazing (a is the earth radius) [19]. Usually these angles are greater than about 3°.

In general, the characteristics of an antenna at low (LF) and medium (MF) frequencies are profoundly influenced by the lossy earth. This is particularly evident in the input resistance. When the antenna is located at a height that is small compared to the skin depth of the conducting earth, the input resistance may even be greater than its free-space values [19]. This leads to antennas with very low efficiencies. Improvements in the efficiency can be obtained by placing radial wires or metallic disks on the ground.

The analytical procedures that are introduced to examine the ground effects are based on the geometrical optics models of the previous sections. The image (virtual) source is again placed a distance h below the interface to account for the reflection. However, for each polarization nonunity reflection coefficients are introduced which, in general, will be a function of the angles of incidence and the constitutive parameters of the two media. Although plane wave reflection coefficients are used, even though spherical waves are radiated by the source, the error is small for conducting media [20]. The spherical nature of the wavefront begins to dominate the reflection phenomenon at grazing angles (i.e., as the point of reflection approaches the horizon) [21]. If the height (h) of the antenna above the interface is much less than the skin depth $\delta[\delta = \sqrt{2/(\omega\mu\sigma)}]$ of the ground, the image depth h below the interface should be increased [20] by a complex distance $\delta(1 - j)$.

The geometrical optics formulations are valid provided the sources are located inside the lossless medium. When the sources are placed within the ground, the formulations should include possible surface-wave contributions. Exact boundary-value solutions, based on Sommerfeld integral formulations, are available [19]. However they are too complex to be included in an introductory chapter.

4.8.1 Vertical Electric Dipole

The field radiated by an electric infinitesimal dipole when placed above the ground can be obtained by referring to the geometry of Figures 4.14(a) and (b). Assuming the earth is flat and the observations are made in the far field, the direct component of the field is given by (4-94) and the reflected component by (4-95) where the reflection coefficient R_v is given by

$$R_v = \frac{\eta_0 \cos\theta_i - \eta_1 \cos\theta_t}{\eta_0 \cos\theta_i + \eta_1 \cos\theta_t} = -R_{\parallel} \tag{4-125}$$

where $R_{\parallel}$ is the reflection coefficient for parallel polarization [7] and

$\eta_0 = \sqrt{\dfrac{\mu_0}{\epsilon_0}}$ = intrinsic impedance of free-space (air)

$\eta_1 = \sqrt{\dfrac{j\omega\mu_1}{\sigma_1 + j\omega\epsilon_1}}$ = intrinsic impedance of the ground

θ_i = angle of incidence (relative to the normal)

θ_t = angle of refraction (relative to the normal)

The angles θ_i and θ_t are related by Snell's law of refraction

$$\gamma_0 \sin\theta_i = \gamma_1 \sin\theta_t \tag{4-126}$$

where

$\gamma_0 = jk_0$ = propagation constant for free-space (air)

k_0 = phase constant for free-space (air)

$\gamma_1 = (\alpha_1 + jk_1)$ = propagation constant for the ground

α_1 = attenuation constant for the ground

k_1 = phase constant for the ground

Using the far-field approximations of (4-97a)–(4-98), the total electric field above the ground ($z \geq 0$) can be written as

$$E_\theta = j\eta \frac{kI_0 l e^{-jkr}}{4\pi r} \sin\theta [e^{jkh\cos\theta} + R_v e^{-jkh\cos\theta}] \quad z \geq 0 \tag{4-127}$$

where R_v is given by (4-125).

The permittivity and conductivity of the earth are strong functions of the ground's geological constituents, especially its moisture. Typical values for the relative permittivity ϵ_r (dielectric constant) are in the range of 5–100 and for the conductivity σ in the range of $10^{-4} - 1$ S/m.

A normalized (to 0 dB) pattern for an infinitesimal dipole above the ground with $h = \lambda/4$, $\epsilon_{r1} = 5$, $f = 1$ GHz, $\sigma_1 = 10^{-2}$ S/m is shown plotted in Figure 4.31 (dashed curves) where it is compared with that (solid curve) of a perfect conductor ($\sigma_1 = \infty$). In the presence of the ground, the radiation toward the vertical direction ($60^\circ > \theta > 0^\circ$) is more intense than that for the perfect electric conductor, but it vanishes for grazing angles ($\theta = 90^\circ$). The null field toward the horizon ($\theta = 90^\circ$) is formed because the reflection coefficient R_v approaches -1 as $\theta_i \to 90^\circ$. Thus the ground effects on the pattern of a vertically polarized antenna are significantly different from those of a perfect conductor.

Significant changes also occur in the impedance. Because the formulation for the impedance is much more complex [19], it will not be presented here. Graphical illustrations for the impedance change of a vertical dipole placed a height h above a homogeneous lossy half-space, as compared to those in free-space, can be found in [22].

4.8.2 Horizontal Electric Dipole

The analytical formulation of the horizontal dipole above the ground can also be obtained in a similar manner as for the vertical electric dipole. Referring to

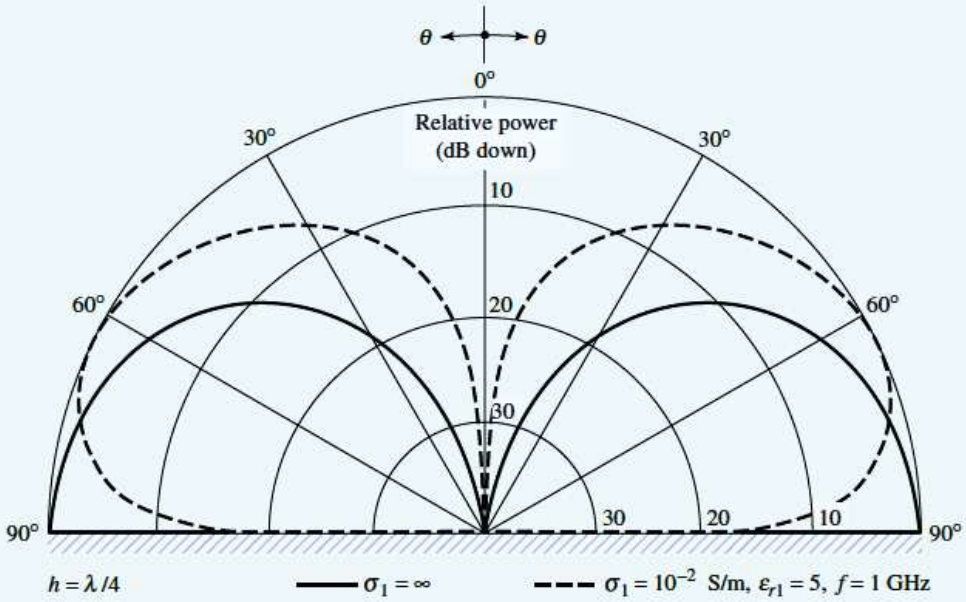


Figure 4.31 Elevation plane amplitude patterns of an infinitesimal vertical dipole above a perfect electric conductor ($\sigma_1 = \infty$) and a flat earth ($\sigma_1 = 0.01$ S/m, $\epsilon_{r1} = 5$, $f = 1$ GHz).

Figure 4.25(a) and (b), the direct component is given by (4-111) and the reflected by (4-112) where the reflection coefficient R_h is given by

$$R_h = \begin{cases} R_\perp \text{ for } \phi = 0^\circ, 180^\circ \text{ plane} \\ R_\parallel \text{ for } \phi = 90^\circ, 270^\circ \text{ plane} \end{cases} \tag{4-128}$$

where $R_\parallel$ is the reflection coefficient for parallel polarization, as given by (4-125), and $R_\perp$ is the reflection coefficient for perpendicular polarization given by [7]

$$R_\perp = \frac{\eta_1 \cos\theta_i - \eta_0 \cos\theta_t}{\eta_1 \cos\theta_i + \eta_0 \cos\theta_t} \tag{4-128a}$$

The angles θ_i and θ_t are again related by Snell's law of refraction as given by (4-126).

Using the far-field approximations of (4-115a) and (4-115b), the total field above the ground ($z \geq h$) can be written as

$$E_\psi = j\eta \frac{kI_0 e^{-jkr}}{4\pi r} \sqrt{1 - \sin^2\theta \sin^2\phi}\, [e^{jkh\cos\theta} + R_h e^{-jkh\cos\theta}], \quad z \geq h \tag{4-129}$$

where R_h is given by (4-128).

The normalized (to 0 dB) pattern in the y-z plane ($\phi = 90^\circ$) for $h = \lambda/4$ is shown plotted in Figure 4.32 (dashed curve) where it is compared with that (solid curve) of a perfect conductor ($\sigma_1 = \infty$). In the space above the interface, the relative pattern in the presence of the ground is not significantly different from that of a perfect conductor. This becomes more evident by examining R_h as given by (4-128). For a ground medium, the values of R_h for most observation angles are not much different from -1 (the value of R_h for a perfect conductor). For grazing angles ($\theta_i \to 90^\circ$), the values of R_h for the lossy ground approach -1 very rapidly. Thus the relative pattern

EX2042
Page 220 of 1072

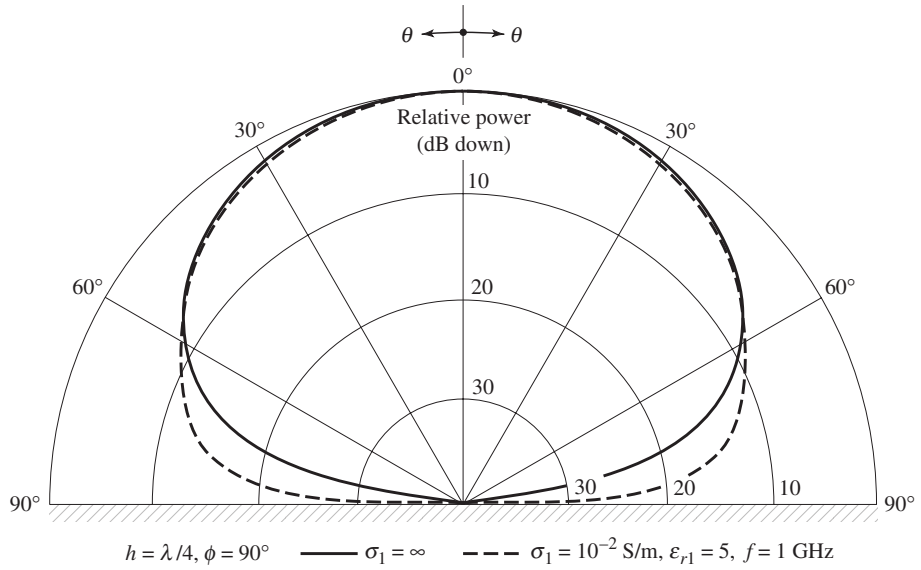


Figure 4.32 Elevation plane ($\phi = 90^\circ$) amplitude patterns of an infinitesimal horizontal dipole above a perfect electric conductor ($\sigma_1 = \infty$) and a flat earth ($\sigma_1 = 0.01$ S/m, $\epsilon_{r1} = 5$, $f = 1$ GHz).

of a horizontal dipole above a lossy surface is not significantly different from that above a perfect conductor.

4.8.3 Earth Curvature

Antenna pattern measurements on aircraft can be made using either scale models or full scale in-flight. Scale model measurements usually are made indoors using electromagnetic anechoic chambers, as described in Chapter 17. The indoor facilities provide a controlled environment, and all-weather capability, security, and minimize electromagnetic interference. However, scale model measurements may not always simulate real-life outdoor conditions, such as the reflecting surface of seawater. Therefore full-scale model measurements may be necessary. For in-flight measurements, reflecting surfaces, such as seawater, introduce reflections, which usually interfere with the direct signal. These unwanted signals are usually referred to as *multipath*. Therefore the total measured signal in an outdoor system configuration is the combination of the direct signal and that due to multipath, and usually it cannot be easily separated in its parts using measuring techniques. Since the desired signal is that due to the direct path, it is necessary to be able to subtract from the total response the contributions due to multipath. This can be accomplished by developing analytical models to predict the contributions due to multipath, which can then be subtracted from the total signal in order to be left with the desired direct path signal. In this section we will briefly describe techniques that have been used to accomplish this [23], [24].

The analytical formulations of Sections 4.8.1 and 4.8.2 for the patterns of vertical and horizontal dipoles assume that the earth is flat. This is a good approximation provided the curvature of the earth is large compared to the wavelength and the angle of observation is greater than about 3° from grazing [or more accurately greater than about $57.3/(ka)^{1/3}$ degrees, where a is the radius of the earth] from grazing [25]. The curvature of the earth has a tendency to spread out (weaken, diffuse, diverge) the

EX2042
Page 221 of 1072

reflected energy more than a corresponding flat surface. The spreading of the reflected energy from a curved surface as compared to that from a flat surface is taken into account by introducing a divergence factor D [21], [23], [24], defined as

$$D = \text{divergence factor} = \frac{\text{reflected field from curved surface}}{\text{reflected field from flat surface}} \tag{4-130}$$

The formula for D can be derived using purely geometrical considerations. It is accomplished by comparing the ray energy density in a small cone reflected from a sphere near the principal point of reflection with the energy density the rays (within the same cone) would have if they were reflected from a plane surface. Based on the geometrical optics energy conservation law for a bundle of rays within a cone, the reflected rays within the cone will subtend a circle on a perpendicular plane for reflections from a flat surface, as shown in Figure 4.33(a). However, according to the geometry of Figure 4.33(b), it will subtend an ellipse for a spherical reflecting surface. Therefore the divergence factor of (4-130) can also be defined as

$$D = \frac{E_s^r}{E_f^r} = \left[\frac{\text{area contained in circle}}{\text{area contained in ellipse}}\right]^{1/2} \tag{4-131}$$

where

E_s^r = reflected field from spherical surface
E_f^r = reflected field from flat surface

Using the geometry of Figure 4.34, the divergence factor can be written as [7] and [24]

$$D = \frac{\sqrt{\dfrac{\rho_1^r \rho_2^r}{(\rho_1^r + s)(\rho_2^r + s)}}}{\dfrac{s'}{s' + s}} \tag{4-132}$$

where ρ_1^r and ρ_2^r are the principal radii of curvature of the reflected wavefront at the point of reflection and are given, according to the geometry of Figure 4.34, by

$$\frac{1}{\rho_1^r} = \frac{1}{s'} + \frac{1}{\rho \sin\psi} + \sqrt{\frac{1}{(\rho \sin\psi)^2} - \frac{4}{a^2}} \tag{4-132a}$$

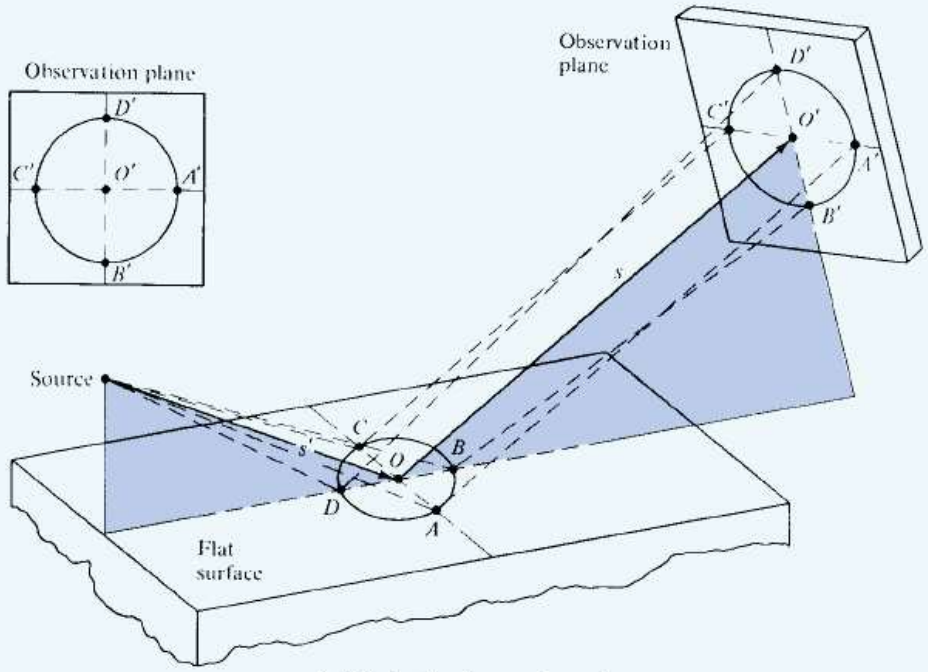
$$\frac{1}{\rho_2^r} = \frac{1}{s'} + \frac{1}{\rho \sin\psi} - \sqrt{\frac{1}{(\rho \sin\psi)^2} - \frac{4}{a^2}} \tag{4-132b}$$

$$\rho = \frac{a}{1 + \sin^2\psi} \tag{4-132c}$$

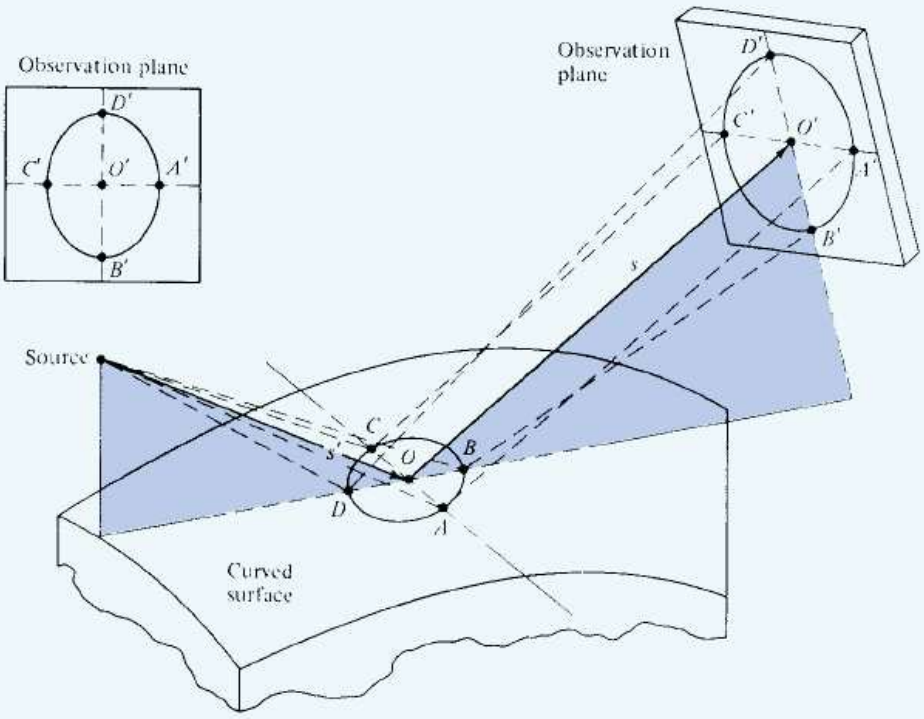
A simplified form of the divergence factor is that of [26]

$$D \cong \left[1 + \frac{2s's}{a(s' + s)\sin\psi}\right]^{-1/2} \cdot \left[1 + \frac{2s's}{a(s' + s)}\right]^{-1/2} \tag{4-133}$$

Both (4-132) and (4-133) take into account the earth curvature in two orthogonal planes.



(a) Reflection from a flat surface



(b) Reflection from a spherical surface

Figure 4.33 Reflection from flat and spherical surfaces.

Assuming that the divergence of rays in the azimuthal plane (plane vertical to the page) is negligible (two-dimensional case), the divergence factor can be written as

$$D \simeq \left[1 + 2\frac{ss'}{ad\tan\psi}\right]^{-1/2} \tag{4-134}$$

EX2042
Page 223 of 1072

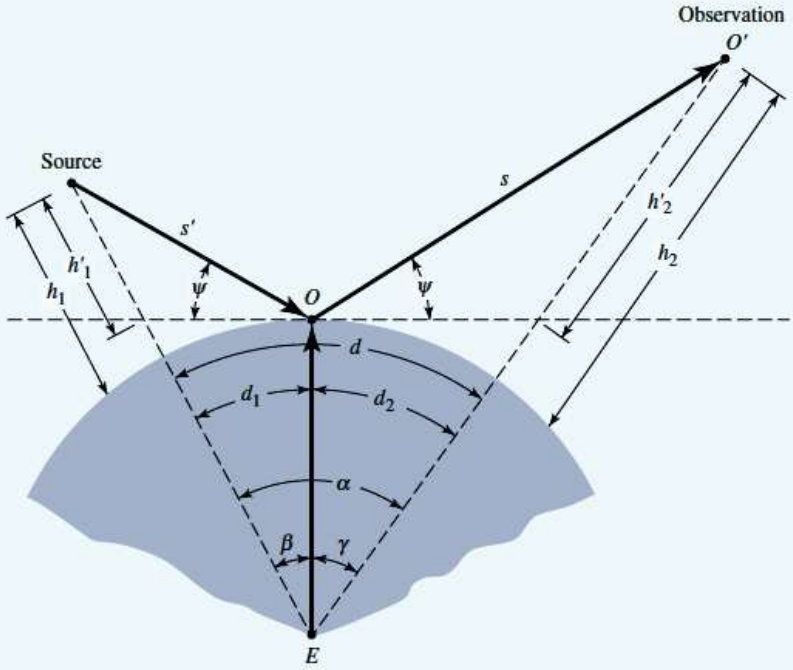


Figure 4.34 Geometry for reflections from a spherical surface.

where ψ is the grazing angle. Thus the divergence factor of (4-134) takes into account energy spreading primarily in the elevation plane. According to Figure 4.34

h_1' = height of the source above the earth (with respect to the tangent at the point of reflection)
h_2' = height of the observation point above the earth (with respect to the tangent at the point of reflection)
d = range (along the surface of the earth) between the source and the observation point
a = radius of the earth (3,959 mi). Usually a $\frac{4}{3}$ radius ($\simeq$ 5,280 mi) is used.
ψ = reflection angle (with respect to the tangent at the point of reflection).
d_1 = distance (along the surface of the earth) from the source to the reflection point
d_2 = distance (along the surface of the earth) from the observation point to the reflection point

The divergence factor can be included in the formulation of the fields radiated by a vertical or a horizontal dipole, in the presence of the earth, by modifying (4-127) and (4-129) and writing them, respectively, as

$$E_\theta = j\eta \frac{kI_0 l e^{-jkr}}{4\pi r} \sin\theta [e^{jkh\cos\theta} + DR_v e^{-jkh\cos\theta}] \tag{4-135a}$$

$$E_\psi = j\eta \frac{kI_0 l e^{-jkr}}{4\pi r} \sqrt{1 - \sin^2\theta \sin^2\phi} [e^{jkh\cos\theta} + DR_h e^{-jkh\cos\theta}] \tag{4-135b}$$

While the previous formulations are valid for smooth surfaces, they can still be used with rough surfaces, provided the surface geometry satisfies the Rayleigh criterion [21] and [26]

$$h_m < \frac{\lambda}{8\sin\psi} \tag{4-136}$$

where h_m is the maximum height of the surface roughness. Since the dividing line between a smooth and a rough surface is not that well defined, (4-136) should only be used as a guideline.

The *coherent* contributions due to scattering by a surface with Gaussian rough surface statistics can be approximately accounted for by modifying the vertical and horizontal polarization smooth surface reflection coefficients of (4-125) and (4-128) and express them as

$$R_{v,h}^{s} = R_{v,h}^{0} e^{-2(k_0 h_0 \cos\theta_i)^2} \tag{4-137}$$

where

$R_{v,h}^{s}$ = reflection coefficient of a rough surface for either vertical or horizontal polarization
$R_{v,h}^{0}$ = reflection coefficient of a smooth surface for either vertical (4-125) or horizontal (4-128) polarization
h_0^2 = mean-square roughness height

A *slightly rough surface* is defined as one whose rms height is much smaller than the wavelength, while a *very rough surface* is defined as one whose rms height is much greater than the wavelength.

Plots of the divergence factor as a function of the grazing angle ψ (or as a function of the observation point h_2') for different source heights are shown in Figure 4.35. It is observed that the divergence factor is somewhat different and smaller than unity for small grazing angles, and it approaches unity as the grazing angle becomes larger. The variations of D displayed in Figure 4.35 are typical but not unique. For different positions of the source and observation point, the variations will be somewhat different. More detailed information on the variation of the divergence factor and its effect on the overall field pattern is available [24].

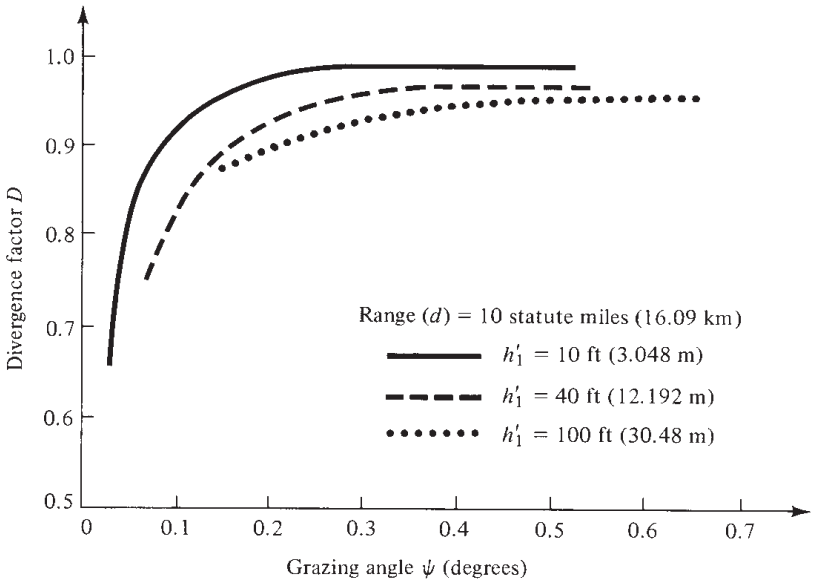


Figure 4.35 Divergence factor for a 4/3 radius earth (a_e = 5,280 mi = 8,497.3 km) as a function of grazing angle ψ.

The most difficult task usually involves the determination of the reflection point from a knowledge of the heights of the source and observation points, and the range d between them. Procedures to do this have been developed [21], [23]–[27].

However, the one presented here is more accurate and does not require either iterative or graphical solutions. To find d_1 and d_2 (given d, h_1, and h_2), the cubic equation of [21] is utilized

$$2d_1^3 - 3dd_1^2 + [d^2 - 2a(h_1 + h_2)]d_1 + 2ah_1d = 0 \tag{4-138}$$

with solution given by

$$d_1 = \frac{d}{2} + p\cos\left(\frac{\Omega + \pi}{3}\right) \tag{4-138a}$$

$$d_2 = d - d_1 \tag{4-138b}$$

$$p = \frac{2}{\sqrt{3}}\sqrt{a(h_1 + h_2) + \left(\frac{d}{2}\right)^2} \tag{4-138c}$$

$$\Omega = \cos^{-1}\left[\frac{2a(h_1 - h_2)\,d}{p^3}\right] \tag{4-138d}$$

Equation (4-138) is valid provided that $\alpha - \beta$ is small, such that $\sin(\alpha - \beta) \simeq \alpha - \beta$, $\cos(\alpha - \beta) \simeq 1 - (\alpha - \beta)^2/2$, $\sin\beta \simeq \beta$, and $\cos\beta \simeq 1 - (\beta)^2/2$. Once d_1 and d_2 are found, then successively β, γ, s', s, ψ, r_1, r_2, α_1^r, α_1^d, α_2^r, and α_2^d can be determined using the geometry of Figure 4.34.

Using the analytical model developed here, computations were made to see how well the predictions compared with measurements. For the computations it was assumed that the reflecting surface is seawater possessing a dielectric constant of 81 and a conductivity of 4.64 S/m [23], [24]. To account for atmospheric refraction, a 4/3 earth was assumed [21], [23], [28] so the atmosphere above the earth can be considered homogeneous with propagation occurring along straight lines.

For computations using the earth as the reflecting surface, all three divergence factors of (4-132)–(4-134) gave the same results. However, for nonspherical reflecting surfaces and for those with smaller radii of curvature, the divergence factor of (4-132) is slightly superior followed by (4-133) and then by (4-134). In Figure 4.36 we display and compare the predicted and measured *height gain* versus range d ($4 < d < 14$ nautical miles) for a vertical-vertical polarization system configuration at a frequency of 167.5 MHz. The *height gain* is defined as the ratio of the total field in the presence of the earth divided by the total field in the absence of the earth. A good agreement is noted between the two. The peaks and nulls are formed by constructive and destructive interferences between the direct and reflected components. If the reflecting surface were perfectly conducting, the maximum height gain would be 2 (6 dB). Because the modeled reflecting surface of Figure 4.36 was seawater with a dielectric constant of 81 and a conductivity of 4.64 S/m, the maximum height gain is less than 6 dB. The measurements were taken by aircraft and facilities of the Naval Air Warfare Center, Patuxent River, MD. Additional measurements were made but are not included here; they can be found in [29] and [30].

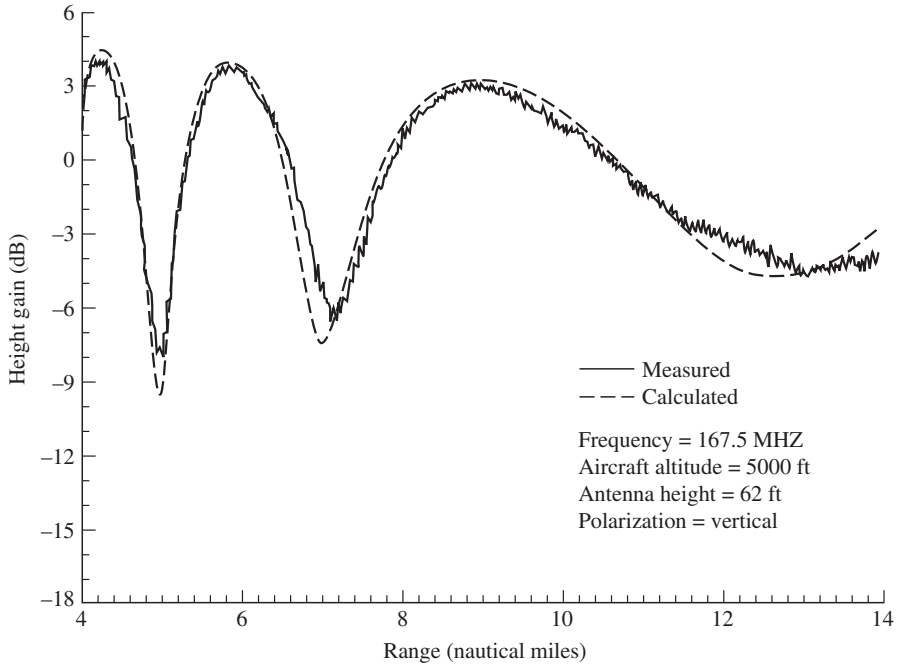


Figure 4.36 Measured and calculated height gain over the ocean ($\epsilon_r = 81, \sigma = 4.64$ S/m) for vertical polarization.

A summary of the pertinent parameters, and associated formulas and equation numbers for this chapter are listed in Table 4.2.

4.9 COMPUTER CODES

There are many computer codes that have been developed to analyze wire-type linear antennas, such as the dipole, and they are too numerous to mention here. One simple program to characterize the radiation characteristics of a dipole, designated as *Dipole* (both in FORTRAN and MATLAB), is included in the attached CD. Another much more advanced program, designated as the **Numerical Electromagnetics Code (NEC)**, is a user-oriented software developed by Lawrence Livermore National Laboratory [31]. It is a Method of Moments (MoM) code for analyzing the interaction of electromagnetic waves with arbitrary structures consisting of conducting wires and surfaces. It is probably the most widely distributed and used electromagnetics code. Included with the distribution are graphics programs for generating plots of the structure, antenna patterns, and impedance. There are also other commercial software that are based on the NEC. A compact version of the NEC is the **MININEC (Mini-Numerical Electromagnetics Code)** [31]–[33]. The MININEC is more convenient for the analysis of wire-type antennas. More information can be obtained by contacting:

G. J. Burke, L-156
Lawrence Livermore National Laboratory
P. O. Box 5504
Livermore, CA 94550

TABLE 4.2 Summary of Important Parameters and Associated Formulas and Equation Numbers for a Dipole in the Far Field

Parameter	Formula	Equation Number
	Infinitesimal Dipole $(l \leq \lambda/50)$	
Normalized power pattern	$U = (E_{\theta n})^2 = C_0 \sin^2\theta$	(4-29)
Radiation resistance R_r	$R_r = \eta\left(\frac{2\pi}{3}\right)\left(\frac{l}{\lambda}\right)^2 = 80\pi^2\left(\frac{l}{\lambda}\right)^2$	(4-19)
Input resistance R_{in}	$R_{in} = R_r = \eta\left(\frac{2\pi}{3}\right)\left(\frac{l}{\lambda}\right)^2 = 80\pi^2\left(\frac{l}{\lambda}\right)^2$	(4-19)
Wave impedance Z_w	$Z_w = \frac{E_\theta}{H_\phi} \simeq \eta = 377$ ohms	
Directivity D_0	$D_0 = \frac{3}{2} = 1.761$ dB	(4-31)
Maximum effective area A_{em}	$A_{em} = \frac{3\lambda^2}{8\pi}$	(4-32)
Vector effective length $\boldsymbol{\ell}_e$	$\boldsymbol{\ell}_e = -\hat{\mathbf{a}}_\theta l \sin\theta$ $\lvert\boldsymbol{\ell}_e\rvert_{\max} = \lambda$	(2-91), Example 4.2
Half-power beamwidth	$\text{HPBW} = 90^\circ$	(4-65)
Loss resistance R_L	$R_L = \frac{l}{P}\sqrt{\frac{\omega\mu_0}{2\sigma}} = \frac{l}{2\pi b}\sqrt{\frac{\omega\mu_0}{2\sigma}}$	(2-90b)
	Small Dipole $(\lambda/50 < \ell \leq \lambda/10)$	
Normalized power pattern	$U = (E_{\theta n})^2 = C_1 \sin^2\theta$	(4-36a)
Radiation resistance R_r	$R_r = 20\pi^2\left(\frac{l}{\lambda}\right)^2$	(4-37)
Input resistance R_{in}	$R_{in} = R_r = 20\pi^2\left(\frac{l}{\lambda}\right)^2$	(4-37)

(*continued overleaf*)

TABLE 4.2 (*continued*)

Parameter	Formula	Equation Number
Wave impedance Z_w	$Z_w = \dfrac{E_\theta}{H_\phi} \simeq \eta = 377 \text{ ohms}$	(4-36a), (4-36c)
Directivity D_0	$D_0 = \dfrac{3}{2} = 1.761 \text{ dB}$	
Maximum effective area A_{em}	$A_{em} = \dfrac{3\lambda^2}{8\pi}$	
Vector effective length $\boldsymbol{\ell}_e$	$\boldsymbol{\ell}_e = -\hat{\mathbf{a}}_\theta \dfrac{l}{2} \sin\theta$ $\lvert\boldsymbol{\ell}_e\rvert_{\max} = \dfrac{l}{2}$	(2-91), (4-36a)
Half-power beamwidth	$\text{HPBW} = 90^\circ$	(4-65)
	Half Wavelength Dipole $(l = \lambda/2)$	
Normalized power pattern	$U = (E_{\theta n})^2 = C_2 \left[\dfrac{\cos\left(\dfrac{\pi}{2}\cos\theta\right)}{\sin\theta} \right]^2 \simeq C_2 \sin^3\theta$	(4-87)
Radiation resistance R_r	$R_r = \dfrac{\eta}{4\pi} C_{in}(2\pi) \simeq 73 \text{ ohms}$	(4-93)
Input resistance R_{in}	$R_{in} = R_r = \dfrac{\eta}{4\pi} C_{in}(2\pi) \simeq 73 \text{ ohms}$	(4-79), (4-93)
Input impedance Z_{in}	$Z_{in} = 73 + j42.5$	(4-93a)
Wave impedance Z_w	$Z_w = \dfrac{E_\theta}{H_\phi} \simeq \eta = 377 \text{ ohms}$	
Directivity D_0	$D_0 = \dfrac{4}{C_{in}(2\pi)} \simeq 1.643 = 2.156 \text{ dB}$	(4-91)
Vector effective length $\boldsymbol{\ell}_e$	$\boldsymbol{\ell}_e = -\hat{\mathbf{a}}_\theta \dfrac{\lambda}{\pi} \dfrac{\cos\left(\dfrac{\pi}{2}\cos\theta\right)}{\sin\theta}$ $\lvert\boldsymbol{\ell}_e\rvert_{\max} = \dfrac{\lambda}{\pi} = 0.3183\lambda$	(2-91), (4-84)
Half-power beamwidth	$\text{HPBW} = 78^\circ$	(4-65)

TABLE 4.2 (*continued*)

Parameter	Formula	Equation Number
Loss resistance R_L	$R_L = \dfrac{l}{2P}\sqrt{\dfrac{\omega\mu_0}{2\sigma}} = \dfrac{l}{4\pi b}\sqrt{\dfrac{\omega\mu_0}{2\sigma}}$	Example (2-13)
	Quarter-Wavelength Monopole $(l = \lambda/4)$	
Normalized power pattern	$U = (E_{\theta n})^2 = C_2\left[\dfrac{\cos\left(\dfrac{\pi}{2}\cos\theta\right)}{\sin\theta}\right]^2 \simeq C_2\sin^3\theta$	(4-87)
Radiation resistance R_r	$R_r = \dfrac{\eta}{8\pi}C_{in}(2\pi) \simeq 36.5$ ohms	(4-106)
Input resistance R_{in}	$R_{in} = R_r = \dfrac{\eta}{8\pi}C_{in}(2\pi) \simeq 36.5$ ohms	(4-106)
Input impedance Z_{in}	$Z_{in} = 36.5 + j21.25$	(4-106)
Wave impedance Z_w	$Z_w = \dfrac{E_\theta}{H_\phi} \simeq \eta = 377$ ohms	
Directivity D_0	$D_0 = 3.286 = 5.167$ dB	
Vector effective length $\boldsymbol{\ell}_e$	$\boldsymbol{\ell}_e = -\hat{\mathbf{a}}_\theta\dfrac{\lambda}{\pi}\cos\left(\dfrac{\pi}{2}\cos\theta\right)$	(2-91)
	$\lvert\boldsymbol{\ell}_e\rvert_{\max} = \dfrac{\lambda}{\pi} = 0.3183\lambda$	(4-84)

4.10 MULTIMEDIA

In the CD that is part of the book, the following multimedia resources are included for the review, understanding, and visualization of the material of this chapter.

a. **Java**-based **interactive questionnaire**, with answers.
b. **Java**-based **applet** for computing and displaying the radiation characteristics of a dipole.
c. **Java**-based **visualization/animation** for displaying the radiation characteristics of a dipole of different lengths.
d. **Matlab** and **Fortran** computer program, designated ***Dipole***, for computing the radiation characteristics of a dipole. The description of the program is found in the corresponding READ ME file of the attached CD.
e. **Power Point (PPT)** viewgraphs, in multicolor.

EX2042
Page 230 of 1072

REFERENCES

1. W. A. Wheeler, "The Spherical Coil as an Inductor, Shield, or Antenna," *Proc. IRE*, Vol. 46, pp. 1595–1602, September 1958 (correction, Vol. 48, p. 328, March 1960).
2. W. A. Wheeler, "The Radiansphere Around a Small Antenna," *Proc. IRE*, Vol. 47, pp. 1325–1331, August 1959.
3. W. A. Wheeler, "Small Antennas," *IEEE Trans. Antennas Propagat.*, Vol. AP-23, No. 4, pp. 462–469, July 1975.
4. C. H. Walter, *Traveling Wave Antennas*, McGraw-Hill, 1965, pp. 32–44.
5. W. R. Scott, Jr., "A General Program for Plotting Three-Dimensional Antenna Patterns," *IEEE Antennas Propagat. Soc. Newsletter*, pp. 6–11, December 1989.
6. S. K. Schelkunoff and H. T. Friis, *Antennas: Theory and Practice*, Wiley, New York, 1952, pp. 229–244, 351–353.
7. C. A. Balanis, *Advanced Engineering Electromagnetics*, John Wiley & Sons, Inc., New York, 1989.
8. R. F. Harrington, "Matrix Methods for Field Problems," *Proc. IEEE*, Vol. 55, No. 2, pp. 136–149, February 1967.
9. R. F. Harrington, *Field Computation by Moment Methods*, Macmillan, New York, 1968.
10. R. Mittra (Ed.), *Computer Techniques for Electromagnetics*, Pergamon, New York, 1973.
11. J. Moore and P. Pizer (Eds.), *Moment Methods in Electromagnetics: Techniques and Applications*, Research Studies Press, Letchworth, UK, 1984.
12. J. J. Wang, *Generalized Moment Methods in Electromagnetics*, John Wiley & Sons, Inc., New York, 1991.
13. R. F. Schwartz, "Input Impedance of a Dipole or Monopole," *Microwave J.*, Vol. 15, No. 12, p. 22, December 1972.
14. K. Fujimoto and J. R. James, *Mobile Antenna Systems Handbook*, Artech House, Norwood, MA, 1994.
15. M. A. Jensen and Y. Rahmat-Samii, "Performance Analysis of Antennas for Hand-Held Transceivers Using FDTD," *IEEE Trans. Antennas Propagat.*, Vol. 42, No. 8, pp. 1106–1113, August 1994.
16. M. A. Jensen and Y. Rahmat-Samii, "EM Interaction of Handset Antennas and a Human in Personal Communications," *Proc. IEEE*, Vol. 83, No. 1, pp. 7–17, January 1995.
17. K. D. Katsibas, "Analysis and Design of Mobile Antennas for Handheld Units," Master's Thesis, Arizona State University, Tempe, AZ, August 1996.
18. K. D. Katsibas, C. A. Balanis, P. A. Tirkas, and C. R. Birtcher, "Folded Loop Antenna for Mobile Handheld Units," *IEEE Trans. Antennas Propagat.*, Vol. 46, No. 2, pp. 260–266, February 1998.
19. R. E. Collin and F. J. Zucker (Eds.), *Antenna Theory Part 2*, Chapters 23 and 24 (by J. R. Wait), McGraw-Hill, New York, 1969.
20. P. R. Bannister, "Image Theory Results for the Mutual Impedance of Crossing Earth Return Circuits," *IEEE Trans. Electromagn. Compat.*, Vol. 15, No. 4, pp. 158–160, 1973.
21. D. E. Kerr, *Propagation of Short Radio Waves*, MIT Radiation Laboratory Series, McGraw-Hill, New York, 1951, Vol. 13, pp. 98–109, 112–122, 396–444.
22. L. E. Vogler and J. L. Noble, "Curves of Input Impedance Change due to Ground for Dipole Antennas," U.S. National Bureau of Standards, Monograph 72, January 31, 1964.
23. H. R. Reed and C. M. Russell, *Ultra High Frequency Propagation*, Boston Technical Publishers, Inc., Lexington, Mass., 1964, Chapter 4, pp. 102–116.

24. C. A. Balanis, R. Hartenstein, and D. DeCarlo, "Multipath Interference for In-Flight Antenna Measurements," *IEEE Trans. Antennas Propagat.*, Vol. AP-32, No. 1, pp. 100–104, January 1984.
25. J. R. Wait and A. M. Conda, "Pattern of an Antenna on a Curved Lossy Surface," *IRE Trans. Antennas Propagat.*, Vol. AP-6, No. 4, pp. 348–359, October 1958.
26. P. Bechmann and A. Spizzichino, *The Scattering of Electromagnetic Waves from Rough Surfaces*, Macmillan, New York, 1963.
27. G. May, "Determining the Point of Reflection on MW Radio Links," *Microwave J.*, Vol. 20, No. 9, pp. 74, 76, September 1977.
28. D. T. Paris and F. K. Hurd, *Basic Electromagnetic Theory*, McGraw-Hill Book Co., pp. 385–386, 1969.
29. C. A. Balanis, "Multipath Interference in Airborne Antenna Measurements," Final Report, prepared for Naval Air Station, Patuxent River, MD, May 28, 1982.
30. D. DeCarlo, "Automation of In-Flight Antenna Measurements," MSEE Problem Report, Dept. of Electrical Engineering, West Virginia University, July 1980.
31. G. J. Burke and A. J. Poggio, "Numerical Electromagnetics Code (NEC)-Method of Moments," Technical Document 116, Naval Ocean Systems Center, San Diego, CA, January 1981.
32. A. J. Julian, J. M. Logan, and J. W. Rockway, "MININEC: A Mini-Numerical Electromagnetics Code," Technical Document 516, Naval Ocean Systems Center, San Diego, CA, September 6, 1982.
33. J. Rockway, J. Logan, D. Tam, and S. Li, *The MININEC SYSTEM: Microcomputer Analysis of Wire Antennas*, Artech House, Inc., Norwood, MA, 1988.

PROBLEMS

4.1. A horizontal infinitesimal electric dipole of constant current I_0 is placed symmetrically about the origin and directed along the x-axis. Derive the
(a) far-zone fields radiated by the dipole
(b) directivity of the antenna

4.2. Repeat Problem 4.1 for a horizontal infinitesimal electric dipole directed along the y-axis.

4.3. Repeat Problem 4.1 using the procedure of Example 4.5.

4.4. For Example 4.5,
(a) formulate an expression for the directivity.
(b) determine the radiated power.
(c) determine the maximum directivity by integrating the radiated power. Compare with that of Problem 4.2 or any other infinitesimal dipole.
(d) determine the maximum directivity using the computer program **Dipole**; compare with that of part (c).

4.5. For Problem 4.1 determine the polarization of the radiated far-zone electric fields (E_θ, E_ϕ) and normalized amplitude pattern in the following planes:
(a) $\phi = 0^\circ$ (b) $\phi = 90^\circ$ (c) $\theta = 90^\circ$

4.6. Repeat Problem 4.5 for the horizontal infinitesimal electric dipole of Problem 4.2, which is directed along the y-axis.

EX2042
Page 232 of 1072

4.7. For Problem 4.3, determine the polarization of the radiated far-zone fields (E_θ, E_ϕ) in the following planes:
(a) $\phi = 0^\circ$ (b) $\phi = 90^\circ$ (c) $\theta = 90^\circ$
Compare with those of Problem 4.5.

4.8. For Example 4.5, determine the polarization of the radiated far-zone fields (E_θ, E_ϕ) in the following planes:
(a) $\phi = 0^\circ$ (b) $\phi = 90^\circ$ (c) $\theta = 90^\circ$
Compare with those of Problem 4.6.

4.9. An infinitesimal magnetic dipole of constant current I_m and length l is symmetrically placed about the origin along the z-axis. Find the
(a) spherical **E**- and **H**-field components radiated by the dipole in all space
(b) directivity of the antenna

4.10. For the infinitesimal magnetic dipole of Problem 4.9, find the far-zone fields when the element is placed along the
(a) x-axis, (b) y-axis

4.11. An infinitesimal electric dipole is centered at the origin and lies on the x-y plane along a line which is at an angle of 45° with respect to the x-axis. Find the far-zone electric and magnetic fields radiated. The answer should be a function of spherical coordinates.

4.12. Repeat Problem 4.11 for an infinitesimal magnetic dipole.

4.13. Derive (4-10a)–(4-10c) using (4-8a)–(4-9).

4.14. Derive the radiated power of (4-16) by forming the average power density, using (4-26a)–(4-26c), and integrating it over a sphere of radius r.

4.15. Derive the far-zone fields of an infinitesimal electric dipole, of length l and constant current I_0, using (4-4) and the procedure outlined in Section 3.6. Compare the results with (4-26a)–(4-26c).

4.16. Derive the fifth term of (4-41).

4.17. For an antenna with a maximum linear dimension of D, find the inner and outer boundaries of the Fresnel region so that the maximum phase error does not exceed
(a) $\pi/16$ rad (b) $\pi/4$ rad (c) 18° (d) 15°

4.18. The boundaries of the far-field (Fraunhofer) and Fresnel regions were selected based on a maximum phase error of 22.5°, which occur, respectively, at directions of 90° and 54.74° from the axis along the largest dimension of the antenna. For an antenna of maximum length of 5λ, what do these maximum phase errors reduce to at an angle of 30° from the axis along the length of the antenna? Assume that the phase error in each case is totally contributed by the respective first higher order term that is being neglected in the infinite series expansion of the distance from the source to the observation point.

4.19. The current distribution on a terminated and matched long linear (traveling wave) antenna of length l, positioned along the z-axis and fed at its one end, is given by

$$\mathbf{I} = \hat{\mathbf{a}}_z I_0 e^{-jkz'}, \quad 0 \le z' \le l$$

EX2042
Page 233 of 1072

where I_0 is a constant. Derive expressions for the

(a) far-zone spherical electric and magnetic field components

(b) radiation power density

4.20. A line source of infinite length and constant current I_0 is positioned along the z-axis. Find the

(a) vector potential $\mathbf{A}$

(b) cylindrical $\mathbf{E}$- and $\mathbf{H}$-field components radiated

$$\text{Hint: } \int_{-\infty}^{+\infty} \frac{e^{-j\beta\sqrt{b^2+t^2}}}{\sqrt{b^2+t^2}}\,dt = -j\pi H_0^{(2)}(\beta b)$$

where $H_0^{(2)}(\alpha x)$ is the Hankel function of the second kind of order zero.

4.21. Show that (4-67) reduces to (4-68) and (4-88) to (4-89).

4.22. A thin linear dipole of length l is placed symmetrically about the z-axis. Find the far-zone spherical electric and magnetic components radiated by the dipole whose current distribution can be approximated by

(a) $I_z(z') = \begin{cases} I_0\left(1+\dfrac{2}{l}z'\right), & -l/2 \le z' \le 0 \\ I_0\left(1-\dfrac{2}{l}z'\right), & 0 \le z' \le l/2 \end{cases}$

(b) $I_z(z') = I_0 \cos\left(\dfrac{\pi}{l}z'\right), \quad -l/2 \le z' \le l/2$

(c) $I_z(z') = I_0 \cos^2\left(\dfrac{\pi}{l}z'\right), \quad -l/2 \le z' \le l/2$

4.23. A center-fed electric dipole of length l is attached to a balanced lossless transmission line whose characteristic impedance is 50 ohms. Assuming the dipole is resonant at the given length, find the input VSWR when
(a) $l = \lambda/4$ (b) $l = \lambda/2$ (c) $l = 3\lambda/4$ (d) $l = \lambda$

4.24. Use the equations in the book or the computer program of this chapter. Find the radiation efficiency of resonant linear electric dipoles of length
(a) $l = \lambda/50$ (b) $l = \lambda/4$ (c) $l = \lambda/2$ (d) $l = \lambda$
Assume that each dipole is made out of copper [$\sigma = 5.7 \times 10^7$ S/m], has a radius of $10^{-4}\lambda$, and is operating at $f = 10$ MHz. Use the computer program of this chapter to find the radiation resistances.

4.25. Write the far-zone electric and magnetic fields radiated by a magnetic dipole of $l = \lambda/2$ aligned with the z-axis. Assume a sinusoidal magnetic current with maximum value I_{mo}.

4.26. A resonant center-fed dipole is connected to a 50-ohm line. It is desired to maintain the input VSWR = 2.

(a) What should the largest input resistance of the dipole be to maintain the VSWR = 2?

(b) What should the length (in wavelengths) of the dipole be to meet the specification?

(c) What is the radiation resistance of the dipole?

EX2042
Page 234 of 1072

4.27. The radiation field of a particular antenna is given by:

$$\mathbf{E} = \hat{\mathbf{a}}_\theta j\omega\mu k \sin\theta \frac{I_0 A_1 e^{-jkr}}{4\pi r} + \hat{\mathbf{a}}_\phi \omega\mu \sin\theta \frac{I_0 A_2 e^{-jkr}}{2\pi r}$$

The values A_1 and A_2 depend on the antenna geometry. Obtain an expression for the radiation resistance. What is the polarization of the antenna?

4.28. For a $\lambda/2$ dipole placed symmetrical along the z-axis, determine the

(a) vector effective height

(b) maximum value (magnitude) of the vector effective height

(c) ratio (in percent) of the maximum value (magnitude) of the vector effective height to its total length

(d) maximum open-circuit output voltage when a uniform plane wave with an electric field of

$$\mathbf{E}^i|_{\theta=90^\circ} = -\hat{\mathbf{a}}_\theta 10^{-3} \text{ volts/wavelength}$$

impinges at broadside incidence on the dipole.

4.29. A base-station cellular communication system utilizes arrays of $\lambda/2$ dipoles as transmitting and receiving antennas. Assuming that each element is *lossless* and that the *input power* to each of the $\lambda/2$ dipoles is 1 watt, determine at *1,900 MHz* and a distance of *5 km* the maximum

(a) radiation intensity *Specify also the units.*

(b) radiation density (*in watts*$/m^2$)

for each $\lambda/2$ *dipole*. This determines the safe level for human exposure to EM radiation.

4.30. A $\lambda/2$ dipole situated with its center at the origin radiates a time-averaged power of 600 W at a frequency of 300 MHz. A second $\lambda/2$ dipole is placed with its center at a point $P(r, \theta, \phi)$, where $r = 200$ m, $\theta = 90^\circ$, $\phi = 40^\circ$. It is oriented so that its axis is parallel to that of the transmitting antenna. What is the available power at the terminals of the second (receiving) dipole?

4.31. A half-wave dipole is radiating into free-space. The coordinate system is defined so that the origin is at the center of the dipole and the z-axis is aligned with the dipole. Input power to the dipole is 100 W. Assuming an overall efficiency of 50%, find the power density (in W/m^2) at $r = 500$ m, $\theta = 60^\circ$, $\phi = 0^\circ$.

4.32. A small dipole of length $l = \lambda/20$ and of wire radius $a = \lambda/400$ is fed symmetrically, and it is used as a communications antenna at the lower end of the VHF band ($f = 30$ *MHz*). *The antenna is made of perfect electric conductor (PEC)*. The *input reactance* of the dipole is given by

$$X_{in} = -j120 \frac{[\ln(l/2a) - 1]}{\tan\left(\dfrac{\pi l}{\lambda}\right)}$$

EX2042
Page 235 of 1072

Determine the following:

(a) Input impedance of the antenna. *State whether it is inductive or capacitive.*

(b) Radiation efficiency (*in percent*).

(c) Capacitor (*in farads*) *or* inductor (*in henries*) that must be connected *in series* with the dipole at the feed in order to resonate the element. *Specify which element is used and its value.*

4.33. A half-wavelength ($l = \lambda/2$) dipole is connected to a transmission line with a characteristic impedance of 75 ohms. Determine the following:

(a) Reflection coefficient. Magnitude and phase (*in degrees*).

(b) VSWR.

It is now desired to resonate the dipole using, *in series*, an inductor or capacitor. At a frequency of 100 MHz, determine:

(c) What kind of an element, inductor or capacitor, is needed to resonate the dipole?

(d) What is the inductance or capacitance?

(e) The new VSWR of the resonant dipole.

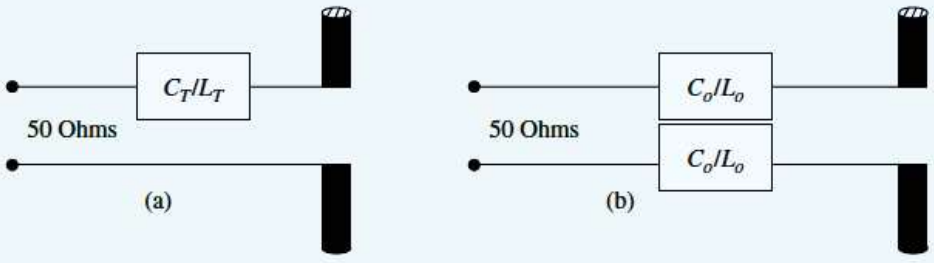
4.34. A $\lambda/2$ dipole is used as a radiating element while it is connected to a 50-ohm lossless transmission line. It is desired to resonate the element at *1.9 GHz* by placing *in series capacitor(s) or inductor(s)* (whichever are appropriate) at its input terminals. Determine the following:

(a) VSWR inside the transmission line *before the dipole is resonated [before the capacitor(s) or inductor(s) are placed in series].*

(b) Total single capacitance C_T (in farads) or inductance L_T (in henries) that must be placed *in series* with the element at its input terminals in order to resonate it. (*See diagram a*).

(c) Individual two capacitances C_o (in farads) or inductances L_o (in henries) that must be placed *in series* with the element at its input terminals in order to resonate it. We need to use two capacitors or two inductors to keep the system balanced by placing in series one with each arm of the dipole (*see diagram b*).

(d) VSWR after the element is resonated with capacitor(s) or inductor(s).



4.35. The input impedance of a $\lambda/2$ dipole, assuming the input (feed) terminals are at the center of the dipole, is equal to $73 + j42.5$. Assuming the dipole is lossless, find the

(a) input impedance (real and imaginary parts) assuming the input (feed) terminals have been shifted to a point on the dipole which is $\lambda/8$ from either end point of the dipole length

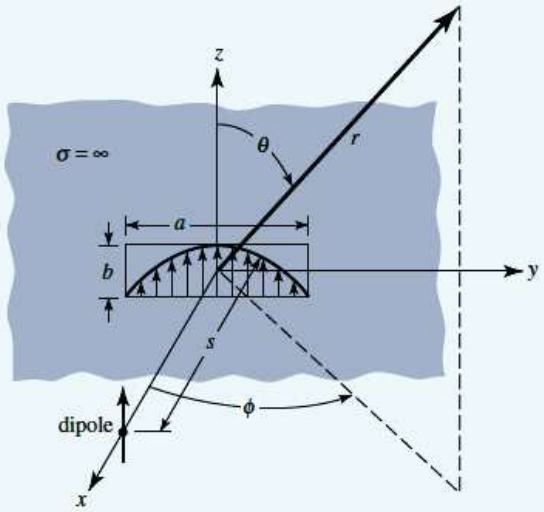
(b) capacitive or inductive reactance that must be placed across the new input terminals of part (a) so that the dipole is self-resonant

(c) VSWR at the new input terminals when the self-resonant dipole of part (b) is connected to a "twin-lead" 300-ohm line

4.36. A linear half-wavelength dipole is operating at a frequency of 1 GHz; determine the capacitance *or* inductance that must be placed *across* (in parallel) the input terminals of the dipole so that the antenna becomes resonant (make the total input impedance real). What is then the VSWR of the resonant half-wavelength dipole when it is connected to a 50-ohm line?

4.37. The field radiated by an infinitesimal electric dipole, placed along the z-axis a distance s along the x-axis, is incident upon a waveguide aperture antenna of dimensions a and b, mounted on an infinite ground plane, as shown in the figure. The normalized electric field radiated by the aperture in the E-plane (x-z plane; $\phi = 0°$) is given by

$$\mathbf{E} = -\hat{\mathbf{a}}_\theta j \frac{\omega\mu b I_0 e^{-jkr}}{4\pi r} \frac{\sin\left(\frac{kb}{2}\cos\theta\right)}{\frac{kb}{2}\cos\theta}$$



Assuming the dipole and aperture antennas are in the far field of each other, determine the polarization loss (in dB) between the two antennas.

4.38. We are given the following information about antenna A:

(a) When A is transmitting, its radiated far-field expression for the E field is given by:

$$\mathbf{E}_a(z) = E_0 \frac{e^{-jkz}}{4\pi z}\left(\frac{\hat{\mathbf{a}}_x + j\hat{\mathbf{a}}_y}{\sqrt{2}}\right) \quad V/m$$

(b) When A is receiving an incident plane wave given by:

$$\mathbf{E}_1(z) = \hat{\mathbf{a}}_y e^{jkz} \quad V/m$$

its open-circuit voltage is $V_1 = 4e^{j20°}\,V$.

EX2042
Page 237 of 1072

If we use the same antenna to receive a second incident plane given by:

$$\mathbf{E}_2(z) = 10(2\hat{\mathbf{a}}_x + \hat{\mathbf{a}}_y E^{j30^\circ})e^{jkz} \quad V/m$$

find its received open-circuit voltage V_2.

4.39. A 3-cm long dipole carries a phasor current $I_0 = 10e^{j60}$A. Assuming that $\lambda = 5$ cm, determine the E- and H-fields at 10 cm away from the dipole and at $\theta = 45^\circ$.

4.40. The radiation resistance of a thin, lossless linear electric dipole of length $l = 0.6\lambda$ is 120 ohms. What is the input resistance?

4.41. A lossless, resonant, center-fed $3\lambda/4$ linear dipole, radiating in free-space is attached to a balanced, lossless transmission line whose characteristic impedance is 300 ohms. Calculate the

(a) radiation resistance (referred to the current maximum)

(b) input impedance (referred to the input terminals)

(c) VSWR on the transmission line

For parts (a) and (b) use the computer program at the end of the chapter.

4.42. Repeat Problem 4.41 for a center-fed $5\lambda/8$ dipole.

4.43. A dipole antenna, with a triangular current distribution, is used for communication with submarines at a frequency of 150 kHz. The overall length of the dipole is 200 m, and its radius is 1 m. Assume a loss resistance of 2 ohms in series with the radiation resistance of the antenna.

(a) Evaluate the input impedance of the antenna including the loss resistance. The input reactance can be approximated by

$$X_{in} = -120\frac{[\ln(l/2a) - 1]}{\tan(\pi l/\lambda)}$$

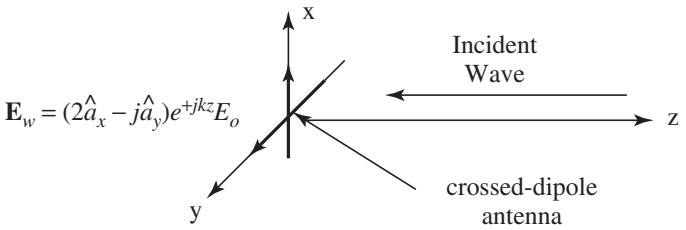
(b) Evaluate the radiation efficiency of the antenna.

(c) Evaluate the radiation power factor of the antenna.

(d) Design a conjugate-matching network to provide a perfect match between the antenna and a 50-ohm transmission line. Give the value of the series reactance X and the turns ratio n of the ideal transformer.

(e) Assuming a conjugate match, evaluate the instantaneous 2:1 VSWR bandwidth of the antenna.

4.44. A uniform plane wave traveling along the negative z-axis given by



EX2042
Page 238 of 1072

impinges upon an crossed-dipole antenna consisting of *two identical dipoles*, one directed along the x-axis and the other directed along the y-axis, *both fed with the same amplitude*. The *y-directed dipole is fed with a* 90° *phase lead* compared to the x-directed dipole.

(a) Write an expression for the polarization unit vector of the incident wave.

(b) Write an expression for the polarization unit vector of the receiving antenna *along the* $+ z$*-axis*.

(c) For the incident wave, state the following:
   1. Polarization (linear, circular, elliptical) and axial ratio.
   2. Rotation of the polarization vector (CW, CCW).

(d) For the receiving antenna, state the following:
   1. Polarization (linear, circular, elliptical) and axial ratio.
   2. Rotation of the polarization vector (CW, CCW).

(e) Determine the polarization loss factor (*dimensionless* and *in dB*) between the incident wave and the receiving antenna.

4.45. A half-wavelength ($l = \lambda/2$) dipole, positioned symmetrically about the origin along the z-axis, is used as a receiving antenna. A 300 MHz uniform plane wave, traveling along the x-axis in the negative x direction, impinges upon the $\lambda/2$ dipole. The incident plane wave has a power density of 2μ watts/m^2, and its electric field is given by

$$\mathbf{E}^{\mathbf{i}}{}_w = (3\hat{a}_z + j\hat{a}_y)E_0 e^{+\mathrm{jkx}}$$

where E_0 is a constant. Determine the following:

(a) Polarization of the incident wave (*including its axial ratio and sense of rotation*, if applicable).

(b) Polarization of the antenna toward the x-axis (*including its axial ratio and sense of direction*, if applicable).

(c) Polarization losses (*in dB*) between the antenna and the incoming wave (assume far-zone fields for the antenna).

(d) Maximum power (*in watts*) that can be delivered to a matched load connected to the $\lambda/2$ dipole (assume no other losses).

4.46. Derive (4-102) using (4-99).

4.47. Determine the smallest height that an infinitesimal vertical electric dipole of $l = \lambda/50$ must be placed above an electric ground plane so that its pattern has only one null (aside from the null toward the vertical), and it occurs at 30° from the vertical. For that height, find the directivity and radiation resistance.

4.48. A $\lambda/50$ linear dipole is placed vertically at a height $h = 2\lambda$ above an infinite electric ground plane. Determine the angles (in degrees) where all the nulls of its pattern occur.

4.49. A linear infinitesimal dipole of length l and constant current is placed vertically a distance h above an infinite electric ground plane. Find the first five smallest heights (in ascending order) so that a null is formed (for each height) in the far-field pattern at an angle of 60° from the vertical.

EX2042
Page 239 of 1072

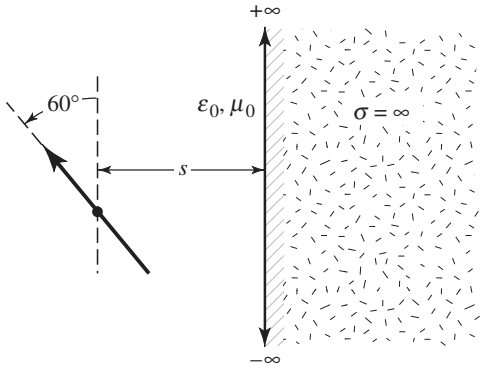
4.50. A vertical infinitesimal linear dipole is placed a distance $h = 3\lambda/2$ above an infinite perfectly conducting flat ground plane. Determine the

(a) angle (*in degrees* from the vertical) where the *array factor* of the system will achieve its *maximum* value

(b) angle (*in degrees* from the vertical) where the maximum of the *total field* will occur

(c) relative (compared to its maximum) field strength (*in dB*) of the total field at the angles where the array factor of the system achieves its maximum value (as obtained in part a).

4.51. An infinitesimal dipole of length ℓ is placed a distance s from an air-conductor interface and at an angle of $\theta = 60^\circ$ from the vertical axis, as shown in the figure. Determine the location and direction of the image source which can be used to account for reflections. Be very clear in indicating the location and direction of the image. Your answer can be in the form of a very clear sketch.



4.52. It is desired to design an antenna system, which utilizes a vertical infinitesimal dipole of length ℓ placed a height h above a flat, perfect electric conductor of infinite extent. The design specifications require that the pattern of the array factor of the source and its image has only one maximum, and that maximum is pointed at an angle of 60° from the vertical. Determine (in wavelengths) the height of the source to achieve this desired design specification.

4.53. A very short ($l \leq \lambda/50$) vertical electric dipole is mounted on a pole a height h above the ground, which is assumed to be flat, perfectly conducting, and of infinite extent. The dipole is used as a transmitting antenna in a VHF ($f =$ 50 MHz) ground-to-air communication system. In order for the communication system transmitting antenna signal not to interfere with a nearby radio station, it is necessary to place a null in the vertical dipole system pattern at an angle of 80° from the vertical. What should the shortest height (in meters) of the dipole be to achieve the desired specifications?

4.54. A half-wavelength dipole is placed vertically on an infinite electric ground plane. Assuming that the dipole is fed at its base, find the

(a) radiation impedance (referred to the current maximum)

(b) input impedance (referred to the input terminals)

(c) VSWR when the antenna is connected to a lossless 50-ohm transmission line.

EX2042
Page 240 of 1072

4.55. A vertical $\lambda/2$ *dipole* is the radiating element in a circular array used for over-the-horizon communication system operating at *1 GHz*. The circular array (*center of the dipoles*) is placed at a *height h* above the ground that is assumed to be flat, perfect electric conducting, and infinite in extent.

(a) In order for the array not to be interfered with by another communication system that is operating in the same frequency, it is desired to place *only one null* in the *elevation pattern of the array factor* of a single vertical $\lambda/2$ dipole at an angle of $\theta = 30^\circ$ from zenith (axis of the dipole). Determine the *smallest nonzero height h* (*in meters*) above the ground at which the center of the dipole must be placed to accomplish this.

(b) If the height (*at its center*) of the vertical dipole is *0.3 m* above ground, determine *all the angles* θ from zenith (*in degrees*) where *all* the

1. null(s) of the *array factor* of a single dipole in the elevation plane will be directed toward.
2. main maximum (maxima) of the *array factor* of a single dipole in the elevation plane will be directed toward.

4.56. A vertical $\lambda/2$ dipole antenna is used as a ground-to-air, over-the-horizon communication antenna at the VHF band ($f = 200$ *MHz*). The antenna is elevated at a height *h* (*measured from its center/feed point*) above ground (*assume the ground is flat, smooth, and perfect electric conductor extending to infinity*). In order to avoid interference with other simultaneously operating communication systems, it is desired to place a null in the far-field amplitude pattern of the antenna system at an angle of 60° *from the vertical*.
Determine the *three smallest physical/nontrivial heights* (*in meters at 200 MHz*) above the ground at which the antenna can be placed to meet the desired pattern specifications.

4.57. A base-station cellular communication systems lossless antenna, which is placed in a residential area of a city, has a maximum gain of *16 dB* (above isotropic) *toward the residential area* at *1,900 MHz*. Assuming the *input* power to the antenna is 8 watts, what is the

(a) maximum radiated power density (*in watts*$/cm^2$) at a distance of 100 m (*line of sight*) from the base station to the residential area? This will determine the safe level for human exposure to electromagnetic radiation.

(b) power (*in watts*) received at that point of the residential area by a cellular telephone whose antenna is a *lossless* $\lambda/4$ vertical monopole and whose maximum value of the amplitude pattern is directed toward the maximum incident power density. *Assume the* $\lambda/4$ *monopole is mounted on an infinite ground plane*.

4.58. A vertical $\lambda/4$ monopole is used as the antenna on a cellular telephone operating at 1.9 GHz. Even though the monopole is mounted on a box-type cellular telephone, for simplicity purposes, assume here that it is mounted on a perfectly electric conducting (PEC) ground plane. Assuming an incident maximum power density of 10^{-6} watts/m^2, *state or determine*, for the monopole's omnidirectional pattern, the

(a) maximum directivity (*dimensionless and in dB*). *You must state the rationale or method you are using to find the directivity*.

(b) maximum power that can be delivered to the cellular telephone receiver. *Assume no losses.*

4.59. A homeowner uses a CB antenna mounted on the top of his house. Let us assume that the operating frequency is 900 MHz and the radiated power is *1,000 watts*. In order not to be exposed to a long-term microwave radiation, there have been some standards, although controversial, developed that set the maximum safe power density that humans can be exposed to and not be subject to any harmful effects. Let us assume that the maximum safe power density of long-term human RF exposure is 10^{-3} *watts*$/cm^2$ or *10 watts*$/m^2$. Assuming no losses, determine the *shortest distance* (*in meters*) from the CB antenna you must be in order not to exceed the safe level of power density exposure. Assume that the CB antenna is radiating into free-space and it is

(a) an isotropic radiator.

(b) a $\lambda/4$ monopole mounted on an infinite PEC and radiating towards its maximum.

4.60. Derive (4-118) using (4-116).

4.61. An infinitesimal horizontal electric dipole of length $l = \lambda/50$ is placed parallel to the y-axis a height h above an infinite electric ground plane.

(a) Find the smallest height h (excluding $h = 0$) that the antenna must be elevated so that a null in the $\phi = 90^\circ$ plane will be formed at an angle of $\theta = 45^\circ$ from the vertical axis.

(b) For the height of part (a), determine the (1) radiation resistance and (2) directivity (for $\theta = 0^\circ$) of the antenna system.

4.62. A horizontal $\lambda/50$ infinitesimal dipole of constant current and length l is placed parallel to the y-axis a distance $h = 0.707\lambda$ above an infinite electric ground plane. Find *all* the nulls formed by the antenna system in the $\phi = 90^\circ$ plane.

4.63. An infinitesimal electric dipole of length $l = \lambda/50$ is placed horizontally at a height of $h = 2\lambda$ above a flat, smooth, perfect electric conducting plane which extends to infinity. It is desired to measure its far-field radiation characteristics (e.g. amplitude pattern, phase pattern, polarization pattern, etc.). The system is operating at 300 MHz. What should the minimum radius (*in meters*) of the circle be where the measurements should be carried out? The radius should be measured from the origin of the coordinate system, which is taken at the interface between the actual source and image.

4.64. An infinitesimal magnetic dipole is placed vertically a distance h above an infinite, perfectly conducting electric ground plane. Derive the far-zone fields radiated by the element above the ground plane.

4.65. Repeat Problem 4.64 for an electric dipole above an infinite, perfectly conducting magnetic ground plane.

4.66. Repeat Problem 4.64 for a magnetic dipole above an infinite, perfectly conducting magnetic ground plane.

4.67. An infinitesimal vertical electric dipole is placed at height h above an infinite PMC (perfect magnetic conductor) ground plane.

EX2042
Page 242 of 1072

(a) Find the smallest height h (excluding $h = 0$) to which the antenna must be elevated so that a null is formed at an angle $\theta = 60^\circ$ from the vertical axis

(b) For the value of h found in part (a), determine

1. the directive gain of the antenna in the $\theta = 45^\circ$ direction
2. the radiation resistance of the antenna normalized to the intrinsic impedance of the medium above the ground plane

Assume that the length of the antenna is $l = \lambda/100$.

4.68. A vertical $\lambda/2$ dipole, operating at 1 GHz, is placed a distance of 5 m (with respect to the tangent at the point of reflections) above the earth. Find the total field at a point 20 km from the source ($d = 20 \times 10^3$ m), at a height of 1,000 m (with respect to the tangent) above the ground. Use a 4/3 radius earth and assume that the electrical parameters of the earth are $\epsilon_r = 5, \sigma = 10^{-2}$ S/m.

4.69. Two astronauts equipped with handheld radios land on different parts of a large asteroid. The radios are identical and transmit 5 W average power at 300 MHz. Assume the asteroid is a smooth sphere with physical radius of 1,000 km, has no atmosphere, and consists of a lossless dielectric material with relative permittivity $\epsilon_r = 9$. Assume that the radios' antennas can be modeled as vertical infinitesimal electric dipoles. Determine the signal power (in microwatts) received by each radio from the other, if the astronauts are separated by a range (distance along the asteroid's surface) of 2 km, and hold their radios vertically at heights of 1.5 m above the asteroid's surface.

Additional Information Required to Answer this Question: Prior to landing on the asteroid the astronauts calibrated their radios. Separating themselves in outer space by 10 km, the astronauts found the received signal power at each radio from the other was 10 microwatts, when both antennas were oriented in the same direction.

4.70. A satellite S transmits an electromagnetic wave, at 10 GHz, via its transmitting antenna. The characteristics of the satellite-based transmitter are:

(a) The power radiated from the satellite antenna is 10 W.

(b) The distance between the satellite antenna and a point A on the earth's surface is 3.7×10^7 m, and

(c) The satellite transmitting antenna directivity in the direction SA is 50 dB Ignoring ground effects,

1. Determine the magnitude of the E-field at A.
2. If the receiver at point A is a $\lambda/2$ dipole, what would be the voltage reading at the terminals of the antenna?

4.71. Derive (4-133) based on geometrical optics as presented in section 13.2 of [7].

CHAPTER 5

Loop Antennas

5.1 INTRODUCTION

Another simple, inexpensive, and very versatile antenna type is the loop antenna. Loop antennas take many different forms such as a rectangle, square, triangle, ellipse, circle, and many other configurations. Because of the simplicity in analysis and construction, the circular loop is the most popular and has received the widest attention. It will be shown that a small loop (circular or square) is equivalent to an infinitesimal magnetic dipole whose axis is perpendicular to the plane of the loop. That is, the fields radiated by an electrically small circular or square loop are of the same mathematical form as those radiated by an infinitesimal magnetic dipole.

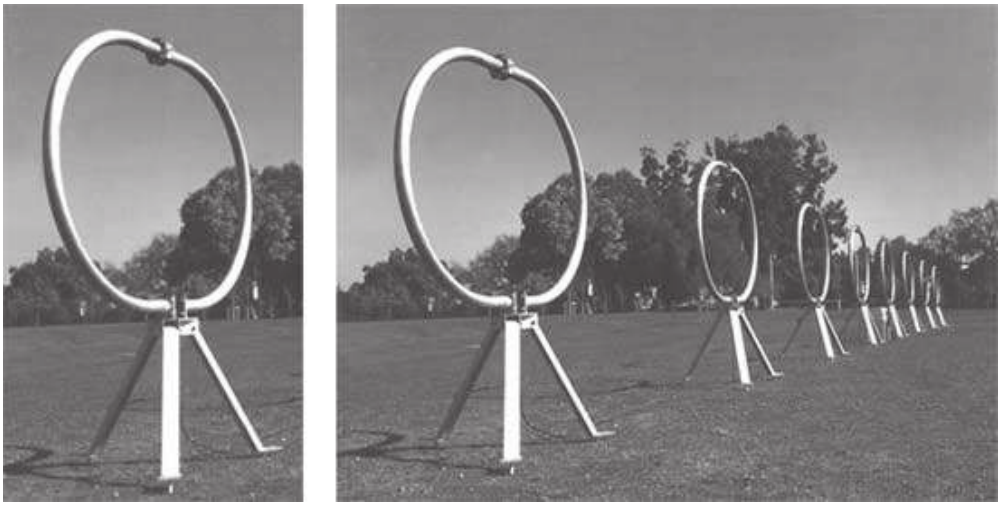
Loop antennas are usually classified into two categories, electrically small and electrically large. Electrically small antennas are those whose overall length (circumference) is usually less than about one-tenth of a wavelength ($C < \lambda/10$). However, electrically large loops are those whose circumference is about a free-space wavelength ($C \sim \lambda$). Most of the applications of loop antennas are in the HF (3–30 MHz), VHF (30–300 MHz), and UHF (300–3,000 MHz) bands. When used as field probes, they find applications even in the microwave frequency range.

Loop antennas with electrically small circumferences or perimeters have small radiation resistances that are usually smaller than their loss resistances. Thus they are very poor radiators, and they are seldom employed for transmission in radio communication. When they are used in any such application, it is usually in the receiving mode, such as in portable radios and pagers, where antenna efficiency is not as important as the signal-to-noise ratio. They are also used as probes for field measurements and as directional antennas for radiowave navigation. The field pattern of electrically small antennas of any shape (circular, elliptical, rectangular, square, etc.) is similar to that of an infinitesimal dipole with a null perpendicular to the plane of the loop and with its maximum along the plane of the loop. As the overall length of the loop increases and its circumference approaches one free-space wavelength, the maximum of the pattern shifts from the plane of the loop to the axis of the loop which is perpendicular to its plane.

The radiation resistance of the loop can be increased, and made comparable to the characteristic impedance of practical transmission lines, by increasing (electrically) its perimeter and/or the number of turns. Another way to increase the radiation resistance

Antenna Theory: Analysis Design, Third Edition, by Constantine A. Balanis
ISBN 0-471-66782-X Copyright © 2005 John Wiley & Sons, Inc.

EX2042
Page 244 of 1072



(a) single element (b) array of eight elements

Figure 5.1 Commercial loop antenna as a single vertical element and in the form of an eight-element linear array. (Courtesy: TCI, A Dielectric Company).

of the loop is to insert, within its circumference or perimeter, a ferrite core of very high permeability which will raise the magnetic field intensity and hence the radiation resistance. This forms the so-called ferrite loop.

Electrically large loops are used primarily in directional arrays, such as in helical antennas (see Section 10.3.1), Yagi-Uda arrays (see Section 10.3.3), quad arrays (see Section 10.3.4), and so on. For these and other similar applications, the maximum radiation is directed toward the axis of the loop forming an end-fire antenna. To achieve such directional pattern characteristics, the circumference (perimeter) of the loop should be about one free-space wavelength. The proper phasing between turns enhances the overall directional properties.

Loop antennas can be used as single elements, as shown in Figure 5.1(a), whose plane of its area is perpendicular to the ground. The relative orientation of the loop can be in other directions, including its plane being parallel relative to the ground. Thus, its mounting orientation will determine its radiation characteristics relative to the ground. Loops are also used in arrays of various forms. The particular array configuration will determine its overall pattern and radiation characteristics. One form of arraying is shown in Figure 5.1(b), where eight loops of Figure 5.1(a) are placed to form a linear array of eight vertical elements.

5.2 SMALL CIRCULAR LOOP

The most convenient geometrical arrangement for the field analysis of a loop antenna is to position the antenna symmetrically on the x-y plane, at $z = 0$, as shown in Figure 5.2(a). The wire is assumed to be very thin and the current spatial distribution is given by

$$I_\phi = I_0 \tag{5-1}$$

where I_0 is a constant. Although this type of current distribution is accurate only for a loop antenna with a very small circumference, a more complex distribution makes the mathematical formulation quite cumbersome.

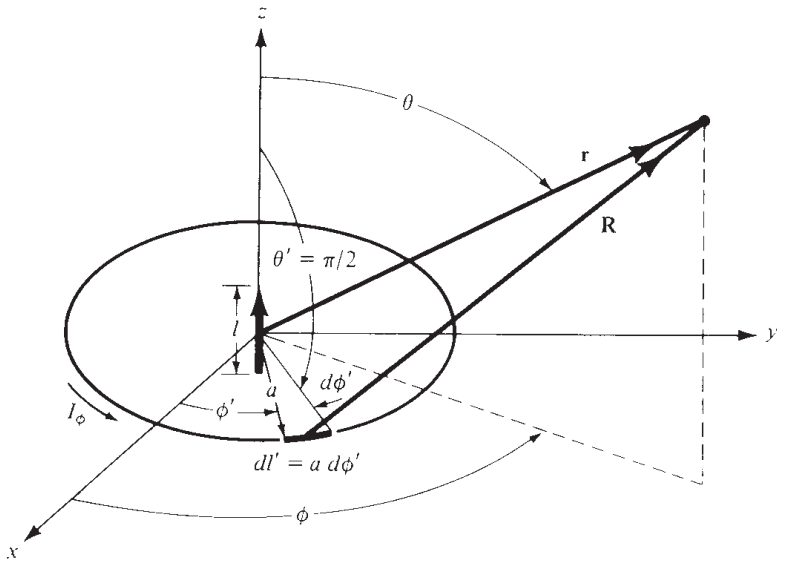
5.2.1 Radiated Fields

To find the fields radiated by the loop, the same procedure is followed as for the linear dipole. The potential function **A** given by (3-53) as

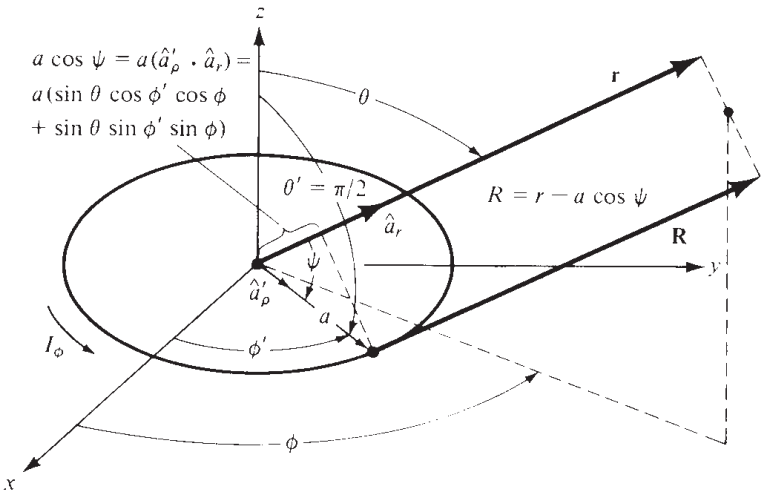
$$\mathbf{A}(x, y, z) = \frac{\mu}{4\pi} \int_C \mathbf{I}_e(x', y', z') \frac{e^{-jkR}}{R} dl' \tag{5-2}$$

is first evaluated. Referring to Figure 5.2(a), R is the distance from any point on the loop to the observation point and dl' is an infinitesimal section of the loop antenna. In general, the current spatial distribution $\mathbf{I}_e(x', y', z')$ can be written as

$$\mathbf{I}_e(x', y', z') = \hat{\mathbf{a}}_x I_x(x', y', z') + \hat{\mathbf{a}}_y I_y(x', y', z') + \hat{\mathbf{a}}_z I_z(x', y', z') \tag{5-3}$$



(a) Geometry for circular loop



(b) Geometry for far-field observations

Figure 5.2 Geometrical arrangement for loop antenna analysis.

whose form is more convenient for linear geometries. For the circular-loop antenna of Figure 5.2(a), whose current is directed along a circular path, it would be more convenient to write the rectangular current components of (5-3) in terms of the cylindrical components using the transformation (see Appendix VII)

$$\begin{bmatrix} I_x \\ I_y \\ I_z \end{bmatrix} = \begin{bmatrix} \cos\phi' & -\sin\phi' & 0 \\ \sin\phi' & \cos\phi' & 0 \\ 0 & 0 & 1 \end{bmatrix} \begin{bmatrix} I_\rho \\ I_\phi \\ I_z \end{bmatrix} \tag{5-4}$$

which when expanded can be written as

$$\left.\begin{aligned} I_x &= I_\rho \cos\phi' - I_\phi \sin\phi' \\ I_y &= I_\rho \sin\phi' + I_\phi \cos\phi' \\ I_z &= I_z \end{aligned}\right\} \tag{5-5}$$

Since the radiated fields are usually determined in spherical components, the rectangular unit vectors of (5-3) are transformed to spherical unit vectors using the transformation matrix given by (4-5). That is,

$$\left.\begin{aligned} \hat{\mathbf{a}}_x &= \hat{\mathbf{a}}_r \sin\theta\cos\phi + \hat{\mathbf{a}}_\theta \cos\theta\cos\phi - \hat{\mathbf{a}}_\phi \sin\phi \\ \hat{\mathbf{a}}_y &= \hat{\mathbf{a}}_r \sin\theta\sin\phi + \hat{\mathbf{a}}_\theta \cos\theta\sin\phi + \hat{\mathbf{a}}_\phi \cos\phi \\ \hat{\mathbf{a}}_z &= \hat{\mathbf{a}}_r \cos\theta - \hat{\mathbf{a}}_\theta \sin\theta \end{aligned}\right\} \tag{5-6}$$

Substituting (5-5) and (5-6) in (5-3) reduces it to

$$\begin{aligned} \mathbf{I}_e = {} & \hat{\mathbf{a}}_r [I_\rho \sin\theta\cos(\phi - \phi') + I_\phi \sin\theta \sin(\phi - \phi') + I_z \cos\theta] \\ & + \hat{\mathbf{a}}_\theta [I_\rho \cos\theta\cos(\phi - \phi') + I_\phi \cos\theta \sin(\phi - \phi') - I_z \sin\theta] \\ & + \hat{\mathbf{a}}_\phi [-I_\rho \sin(\phi - \phi') + I_\phi \cos(\phi - \phi')] \end{aligned} \tag{5-7}$$

It should be emphasized that the source coordinates are designated as primed (ρ', ϕ', z') and the observation coordinates as unprimed (r, θ, ϕ). For the circular loop, the current is flowing in the ϕ direction (I_ϕ) so that (5-7) reduces to

$$\mathbf{I}_e = \hat{\mathbf{a}}_r I_\phi \sin\theta \sin(\phi - \phi') + \hat{\mathbf{a}}_\theta I_\phi \cos\theta \sin(\phi - \phi') + \hat{\mathbf{a}}_\phi I_\phi \cos(\phi - \phi') \tag{5-8}$$

The distance R, from any point on the loop to the observation point, can be written as

$$R = \sqrt{(x - x')^2 + (y - y')^2 + (z - z')^2} \tag{5-9}$$

Since

$$\begin{aligned} x &= r\sin\theta\cos\phi \\ y &= r\sin\theta\sin\phi \\ z &= r\cos\theta \\ x^2 + y^2 + z^2 &= r^2 \\ x' &= a\cos\phi' \end{aligned} \tag{5-10}$$

EX2042
Page 247 of 1072

$$y' = a\sin\phi'$$
$$z' = 0$$
$$x'^2 + y'^2 + z'^2 = a^2$$

(5-9) reduces to

$$R = \sqrt{r^2 + a^2 - 2ar\sin\theta\cos(\phi - \phi')} \tag{5-11}$$

By referring to Figure 5.2(a), the differential element length is given by

$$dl' = a\,d\phi' \tag{5-12}$$

Using (5-8), (5-11), and (5-12), the ϕ-component of (5-2) can be written as

$$A_\phi = \frac{a\mu}{4\pi}\int_0^{2\pi} I_\phi\cos(\phi - \phi')\frac{e^{-jk\sqrt{r^2+a^2-2ar\sin\theta\cos(\phi-\phi')}}}{\sqrt{r^2 + a^2 - 2ar\sin\theta\cos(\phi - \phi')}}\,d\phi' \tag{5-13}$$

Since the spatial current I_ϕ as given by (5-1) is constant, the field radiated by the loop will not be a function of the observation angle ϕ. Thus any observation angle ϕ can be chosen; for simplicity $\phi = 0$. Therefore (5-13) reduces to

$$A_\phi = \frac{a\mu I_0}{4\pi}\int_0^{2\pi}\cos\phi'\frac{e^{-jk\sqrt{r^2+a^2-2ar\sin\theta\cos\phi'}}}{\sqrt{r^2 + a^2 - 2ar\sin\theta\cos\phi'}}\,d\phi' \tag{5-14}$$

The integration of (5-14), for very thin circular loop of any radius, can be carried out and is represented by a complex infinite series whose real part contains complete elliptic integrals of the first and second kind while the imaginary part consists of elementary functions [1]. This treatment is only valid provided the observation distance is greater than the radius of the loop ($r > a$). Another very detailed and systematic treatment is that of [2], [3] which is valid for any observation distance ($r < a, r > a$) except when the observation point is on the loop itself ($r = a, \theta = \pi/2$). The development in [2], [3] has been applied to circular loops whose current distribution is uniform, cosinusoidal, and Fourier cosine series. Asymptotic expansions have been presented in [2], [3] to find simplified and approximate forms for far-field observations.

Both treatments, [1]–[3], are too complex to be presented here. The reader is referred to the literature. In this chapter a method will be presented that approximates the integration of (5-14). For small loops, the function

$$f = \frac{e^{-jk\sqrt{r^2+a^2-2ar\sin\theta\cos\phi'}}}{\sqrt{r^2 + a^2 - 2ar\sin\theta\cos\phi'}} \tag{5-15}$$

which is part of the integrand of (5-14), can be expanded in a Maclaurin series in a using

$$f = f(0) + f'(0)a + \frac{1}{2!}f''(0)a^2 + \cdots + \frac{1}{(n-1)!}f^{(n-1)}(0)a^{n-1} + \cdots \tag{5-15a}$$

EX2042
Page 248 of 1072

where $f'(0) = \partial f/\partial a|_{a=0}$, $f''(0) = \partial^2 f/\partial a^2|_{a=0}$, and so forth. Taking into account only the first two terms of (5-15a), or

$$f(0) = \frac{e^{-jkr}}{r} \tag{5-15b}$$

$$f'(0) = \left(\frac{jk}{r} + \frac{1}{r^2}\right) e^{-jkr} \sin\theta \cos\phi' \tag{5-15c}$$

$$f \simeq \left[\frac{1}{r} + a\left(\frac{jk}{r} + \frac{1}{r^2}\right) \sin\theta \cos\phi'\right] e^{-jkr} \tag{5-15d}$$

reduces (5-14) to

$$A_\phi \simeq \frac{a\mu I_0}{4\pi} \int_0^{2\pi} \cos\phi' \left[\frac{1}{r} + a\left(\frac{jk}{r} + \frac{1}{r^2}\right) \sin\theta \cos\phi'\right] e^{-jkr}\, d\phi'$$

$$A_\phi \simeq \frac{a^2\mu I_0}{4} e^{-jkr} \left(\frac{jk}{r} + \frac{1}{r^2}\right) \sin\theta \tag{5-16}$$

In a similar manner, the r- and θ-components of (5-2) can be written as

$$A_r \simeq \frac{a\mu I_0}{4\pi} \sin\theta \int_0^{2\pi} \sin\phi' \left[\frac{1}{r} + a\left(\frac{jk}{r} + \frac{1}{r^2}\right) \sin\theta \cos\phi'\right] e^{-jkr}\, d\phi' \tag{5-16a}$$

$$A_\theta \simeq -\frac{a\mu I_0}{4\pi} \cos\theta \int_0^{2\pi} \sin\phi' \left[\frac{1}{r} + a\left(\frac{jk}{r} + \frac{1}{r^2}\right) \sin\theta \cos\phi'\right] e^{-jkr}\, d\phi' \tag{5-16b}$$

which when integrated reduce to zero. Thus

$$\mathbf{A} \simeq \hat{\mathbf{a}}_\phi A_\phi = \hat{\mathbf{a}}_\phi \frac{a^2\mu I_0}{4} e^{-jkr} \left[\frac{jk}{r} + \frac{1}{r^2}\right] \sin\theta$$

$$= \hat{\mathbf{a}}_\phi j \frac{k\mu a^2 I_0 \sin\theta}{4r} \left[1 + \frac{1}{jkr}\right] e^{-jkr} \tag{5-17}$$

Substituting (5-17) into (3-2a) reduces the magnetic field components to

$$H_r = j \frac{ka^2 I_0 \cos\theta}{2r^2} \left[1 + \frac{1}{jkr}\right] e^{-jkr} \tag{5-18a}$$

$$H_\theta = -\frac{(ka)^2 I_0 \sin\theta}{4r} \left[1 + \frac{1}{jkr} - \frac{1}{(kr)^2}\right] e^{-jkr} \tag{5-18b}$$

$$H_\phi = 0 \tag{5-18c}$$

EX2042
Page 249 of 1072

Using (3-15) or (3-10) with $\mathbf{J} = 0$, the corresponding electric-field components can be written as

$$\boxed{\begin{aligned} E_r &= E_\theta = 0 \qquad (5\text{-}19a)\\ E_\phi &= \eta \frac{(ka)^2 I_0 \sin\theta}{4r}\left[1 + \frac{1}{jkr}\right] e^{-jkr} \qquad (5\text{-}19b)\end{aligned}}$$

5.2.2 Small Loop and Infinitesimal Magnetic Dipole

A comparison of (5-18a)–(5-19b) with those of the infinitesimal magnetic dipole indicates that they have similar forms. In fact, the electric and magnetic field components of an infinitesimal magnetic dipole of length l and constant "magnetic" spatial current I_m are given by

$$E_r = E_\theta = H_\phi = 0 \qquad (5\text{-}20a)$$

$$E_\phi = -j \frac{k I_m l \sin\theta}{4\pi r}\left[1 + \frac{1}{jkr}\right] e^{-jkr} \qquad (5\text{-}20b)$$

$$H_r = \frac{I_m l \cos\theta}{2\pi\eta r^2}\left[1 + \frac{1}{jkr}\right] e^{-jkr} \qquad (5\text{-}20c)$$

$$H_\theta = j \frac{k I_m l \sin\theta}{4\pi\eta r}\left[1 + \frac{1}{jkr} - \frac{1}{(kr)^2}\right] e^{-jkr} \qquad (5\text{-}20d)$$

These can be obtained, using duality, from the fields of an infinitesimal electric dipole, (4-8a)–(4-10c). When (5-20a)–(5-20d) are compared with (5-18a)–(5-19b), they indicate that *a magnetic dipole of magnetic moment $I_m l$ is equivalent to a small electric loop of radius a and constant electric current I_0 provided that*

$$\boxed{I_m l = jS\omega\mu I_0} \qquad (5\text{-}21)$$

where $S = \pi a^2$ (area of the loop). Thus, for analysis purposes, the small electric loop can be replaced by a small linear magnetic dipole of constant current. The geometrical equivalence is illustrated in Figure 5.2(a) where the magnetic dipole is directed along the z-axis which is also perpendicular to the plane of the loop.

5.2.3 Power Density and Radiation Resistance

The fields radiated by a small loop, as given by (5-18a)–(5-19b), are valid everywhere except at the origin. As was discussed in Section 4.1 for the infinitesimal dipole, the power in the region very close to the antenna (near field, $kr \ll 1$) is predominantly reactive and in the far field ($kr \gg 1$) is predominantly real. To illustrate this for the loop, the complex power density

$$\begin{aligned}\mathbf{W} &= \tfrac{1}{2}(\mathbf{E} \times \mathbf{H}^*) = \tfrac{1}{2}[(\hat{\mathbf{a}}_\phi E_\phi) \times (\hat{\mathbf{a}}_r H_r^* + \hat{\mathbf{a}}_\theta H_\theta^*)]\\ &= \tfrac{1}{2}(-\hat{\mathbf{a}}_r E_\phi H_\theta^* + \hat{\mathbf{a}}_\theta E_\phi H_r^*) \qquad (5\text{-}22)\end{aligned}$$

is first formed. When (5-22) is integrated over a closed sphere, only its radial component given by

$$W_r = \eta \frac{(ka)^4}{32} |I_0|^2 \frac{\sin^2\ \theta}{r^2} \left[1 + j \frac{1}{(kr)^3}\right] \tag{5-22a}$$

contributes to the complex power P_r. Thus

$$P_r = \oiint_S \mathbf{W} \cdot d\mathbf{s} = \eta \frac{(ka)^4}{32} |I_0|^2 \int_0^{2\pi} \int_0^{\pi} \left[1 + j \frac{1}{(kr)^3}\right] \sin^3\ \theta\, d\theta\, d\phi \tag{5-23}$$

which reduces to

$$P_r = \eta \left(\frac{\pi}{12}\right) (ka)^4 |I_0|^2 \left[1 + j \frac{1}{(kr)^3}\right] \tag{5-23a}$$

and whose real part is equal to

$$P_{\text{rad}} = \eta \left(\frac{\pi}{12}\right) (ka)^4 |I_0|^2 \tag{5-23b}$$

For small values of $kr (kr \ll 1)$, the second term within the brackets of (5-23a) is dominant which makes the power mainly reactive. In the far field ($kr \gg 1$), the second term within the brackets diminishes, which makes the power real. *A comparison between (5-23a) with (4-14) indicates a difference in sign between the terms within the brackets. Whereas for the infinitesimal dipole the radial power density in the near field is capacitive, for the small loop it is inductive. This is illustrated in Figure 4.21 for the dipole and in Figures 5.13 and 5.20 for the loop.*

The radiation resistance of the loop is found by equating (5-23b) to $|I_0|^2 R_r/2$. Doing this, the radiation resistance can be written as

$$\boxed{R_r = \eta \left(\frac{\pi}{6}\right) (k^2a^2)^2 = \eta \frac{2\pi}{3} \left(\frac{kS}{\lambda}\right)^2 = 20\pi^2 \left(\frac{C}{\lambda}\right)^4 \simeq 31{,}171 \left(\frac{S^2}{\lambda^4}\right)} \tag{5-24}$$

where $S = \pi a^2$ is the area and $C = 2\pi a$ is the circumference of the loop. The last form of (5-24) holds for loops of other configurations, such as rectangular, elliptical, etc. (See Problem 5.30).

The radiation resistance as given by (5-24) is only for a single-turn loop. If the loop antenna has N turns wound so that the magnetic field passes through all the loops, the radiation resistance is equal to that of single turn multiplied by N^2. That is,

$$\boxed{R_r = \eta \left(\frac{2\pi}{3}\right) \left(\frac{kS}{\lambda}\right)^2 N^2 = 20\pi^2 \left(\frac{C}{\lambda}\right)^4 N^2 \simeq 31{,}171\, N^2 \left(\frac{S^2}{\lambda^4}\right)} \tag{5-24a}$$

Even though the radiation resistance of a single-turn loop may be small, the overall value can be increased by including many turns. This is a very desirable and practical mechanism that is not available for the infinitesimal dipole.

EX2042
Page 251 of 1072

Example 5.1

Find the radiation resistance of a single-turn and an eight-turn small circular loop. The radius of the loop is $\lambda/25$ and the medium is free-space.

Solution:

$$S = \pi a^2 = \pi \left(\frac{\lambda}{25}\right)^2 = \frac{\pi\lambda^2}{625}$$

$$R_r \text{ (single turn)} = 120\pi \left(\frac{2\pi}{3}\right)\left(\frac{2\pi^2}{625}\right)^2 = 0.788 \text{ ohms}$$

$$R_r \text{ (8 turns)} = 0.788(8)^2 = 50.43 \text{ ohms}$$

The radiation and loss resistances of an antenna determine the radiation efficiency, as defined by (2-90). The loss resistance of a single-turn small loop is, in general, much larger than its radiation resistance; thus the corresponding radiation efficiencies are very low and depend on the loss resistance. To increase the radiation efficiency, multiturn loops are often employed. However, because the current distribution in a multiturn loop is quite complex, great confidence has not yet been placed in analytical methods for determining the radiation efficiency. Therefore greater reliance has been placed on experimental procedures. Two experimental techniques that can be used to measure the radiation efficiency of a small multiturn loop are those that are usually referred to as the *Wheeler method* and the *Q method* [4].

Usually it is assumed that the loss resistance of a small loop is the same as that of a straight wire whose length is equal to the circumference of the loop, and it is computed using (2-90b). Although this assumption is adequate for single-turn loops, it is not valid for multiturn loops. In a multiturn loop, the current is not uniformly distributed around the wire but depends on the skin and proximity effects [5]. In fact, for close spacings between turns, the contribution to the loss resistance due to the proximity effect can be larger than that due to the skin effect.

The total ohmic resistance for an N-turn circular-loop antenna with loop radius a, wire radius b, and loop separation $2c$, shown in Figure 5.3(a) is given by [6]

$$R_{\text{ohmic}} = \frac{Na}{b} R_s \left(\frac{R_p}{R_0} + 1\right) \tag{5-25}$$

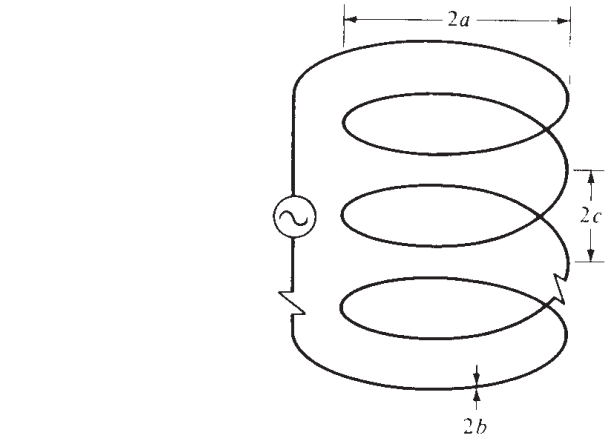
where

$$R_s = \sqrt{\frac{\omega\mu_0}{2\sigma}} = \text{surface impedance of conductor}$$

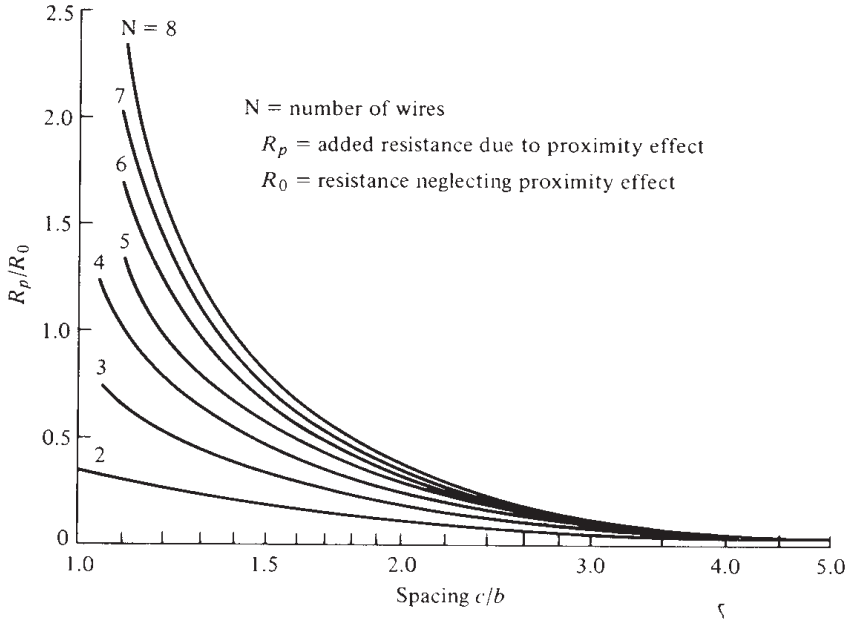
$$R_p = \text{ohmic resistance per unit length due to proximity effect}$$

$$R_0 = \frac{NR_s}{2\pi b} = \text{ohmic skin effect resistance per unit length (ohms/m)}$$

The ratio of R_p/R_0 has been computed [6] as a function of the spacing c/b for loops with $2 \leq N \leq 8$ and it is shown plotted in Figure 5.3(b). It is evident that for close spacing the ohmic resistance is twice as large as that in the absence of the proximity effect ($R_p/R_0 = 0$).



(a) N-turn circular loop



(b) Ohmic resistance due to proximity (after G. N. Smith)

Figure 5.3 N-turn circular loop and ohmic resistance due to proximity effect. (SOURCE: G. S. Smith, "Radiation Efficiency of Electrically Small Multiturn Loop Antennas," *IEEE Trans. Antennas Propagat.*, Vol. AP-20, No. 5, September, pp. 656–657. 1972 © 1972 IEEE).

Example 5.2

Find the radiation efficiency of a single-turn and an eight-turn small circular loop at $f =$ 100 MHz. The radius of the loop is $\lambda/25$, the radius of the wire is $10^{-4}\lambda$, and the turns are spaced $4 \times 10^{-4}\lambda$ apart. Assume the wire is copper with a conductivity of 5.7×10^7(S/m) and the antenna is radiating into free-space.

Solution: From Example 5.1

$$R_r \text{ (single turn)} = 0.788 \text{ ohms}$$

$$R_r \text{ (8 turns)} = 50.43 \text{ ohms}$$

The loss resistance for a single turn is given, according to (2-90b), by

$$R_L = R_{hf} = \frac{a}{b}\sqrt{\frac{\omega\mu_0}{2\sigma}} = \frac{1}{25(10^{-4})}\sqrt{\frac{\pi(10^8)(4\pi \times 10^{-7})}{5.7 \times 10^7}}$$
$$= 1.053 \text{ ohms}$$

and the radiation efficiency, according to (2-90), by

$$e_{cd} = \frac{0.788}{0.788 + 1.053} = 0.428 = 42.8\%$$

From Figure 5.3(b)

$$\frac{R_p}{R_0} = 0.38$$

and from (5-25)

$$R_L = R_{\text{ohmic}} = \frac{8}{25(10^{-4})}\sqrt{\frac{\pi(10^8)(4\pi \times 10^{-7})}{5.7 \times 10^7}}(1.38) = 11.62$$

Thus

$$e_{cd} = \frac{50.43}{50.43 + 11.62} = 0.813 = 81.3\%$$

5.2.4 Near-Field ($kr \ll 1$) Region

The expressions for the fields, as given by (5-18a)–(5-19b), can be simplified if the observations are made in the near field ($kr \ll 1$). As for the infinitesimal dipole, the predominant term in each expression for the field in the near-zone region is the last one within the parentheses of (5-18a)–(5-19b). Thus for $kr \ll 1$

$$\left.\begin{aligned} H_r &\simeq \frac{a^2 I_0 e^{-jkr}}{2r^3}\cos\theta && \text{(5-26a)}\\ H_\theta &\simeq \frac{a^2 I_0 e^{-jkr}}{4r^3}\sin\theta && \text{(5-26b)}\\ H_\phi &= E_r = E_\theta = 0 && \text{(5-26c)}\\ E_\phi &\simeq -j\frac{a^2 k I_0 e^{-jkr}}{4r^2}\sin\theta && \text{(5-26d)} \end{aligned}\right\} \quad kr \ll 1$$

The two **H**-field components are in time-phase. However, they are in time quadrature with those of the electric field. This indicates that the average power (real power) is zero, as is for the infinitesimal electric dipole. The condition of $kr \ll 1$ can be satisfied at moderate distances away from the antenna provided the frequency of operation is very low. The fields of (5-26a)–(5-26d) are usually referred to as *quasi-stationary*.

5.2.5 Far-Field ($kr \gg 1$) Region

The other space of interest where the fields can be approximated is the far-field ($kr \gg 1$) region. In contrast to the near field, the dominant term in (5-18a)–(5-19b) for $kr \gg 1$ is the first one within the parentheses. Since for $kr > 1$ the H_r component will be inversely proportional to r^2 whereas H_θ will be inversely proportional to r. For large values of $kr (kr \gg 1)$, the H_r component will be small compared to H_θ. Thus it can be assumed that it is approximately equal to zero. Therefore for $kr \gg 1$,

$$\left.\begin{aligned} H_\theta &\simeq -\frac{k^2 a^2 I_0 e^{-jkr}}{4r}\sin\theta = -\frac{\pi S I_0 e^{-jkr}}{\lambda^2 r}\sin\theta \\ E_\phi &\simeq \eta\frac{k^2 a^2 I_0 e^{-jkr}}{4r}\sin\theta = \eta\frac{\pi S I_0 e^{-jkr}}{\lambda^2 r}\sin\theta \end{aligned}\right\} \quad kr \gg 1 \tag{5-27a}$$

$$E_\phi \simeq \eta\frac{k^2 a^2 I_0 e^{-jkr}}{4r}\sin\theta = \eta\frac{\pi S I_0 e^{-jkr}}{\lambda^2 r}\sin\theta \tag{5-27b}$$

$$H_r \simeq H_\phi = E_r = E_\theta = 0 \tag{5-27c}$$

where $S = \pi a^2$ is the geometrical area of the loop.

Forming the ratio of $-E_\phi/H_\theta$, the wave impedance can be written as

$$Z_w = -\frac{E_\phi}{H_\theta} \simeq \eta \tag{5-28}$$

where

Z_w = wave impedance
η = intrinsic impedance

As for the infinitesimal dipole, the **E**- and **H**-field components of the loop in the far-field ($kr \gg 1$) region are perpendicular to each other and transverse to the direction of propagation. They form a *T*ransverse *E*lectro *M*agnetic (TEM) field whose wave impedance is equal to the intrinsic impedance of the medium. Equations (5-27a)– (5-27c) can also be derived using the procedure outlined and relationships developed in Section 3.6. This is left as an exercise to the reader (Problem 5.9).

5.2.6 Radiation Intensity and Directivity

The real power P_{rad} radiated by the loop was found in Section 5.2.3 and is given by (5-23b). The same expression can be obtained by forming the average power density, using (5-27a)–(5-27c), and integrating it over a closed sphere of radius r. This is left as an exercise to the reader (Problem 5.8). Associated with the radiated power P_{rad} is an average power density $\mathbf{W}_{\text{av}}$. It has only a radial component W_r which is related to the radiation intensity U by

$$U = r^2 W_r = \frac{\eta}{2}\left(\frac{k^2 a^2}{4}\right)^2 |I_0|^2 \sin^2\theta = \frac{r^2}{2\eta}|E_\phi(r,\theta,\phi)|^2 \tag{5-29}$$

and it conforms to (2-12a). The normalized pattern of the loop, as given by (5-29), is identical to that of the infinitesimal dipole shown in Figure 4.3. The maximum value

EX2042
Page 255 of 1072

occurs at $\theta = \pi/2$, and it is given by

$$U_{\max} = U|_{\theta=\pi/2} = \frac{\eta}{2}\left(\frac{k^2a^2}{4}\right)^2 |I_0|^2 \tag{5-30}$$

Using (5-30) and (5-23b), the directivity of the loop can be written as

$$\boxed{D_0 = 4\pi\frac{U_{\max}}{P_{\text{rad}}} = \frac{3}{2}} \tag{5-31}$$

and its maximum effective area as

$$\boxed{A_{em} = \left(\frac{\lambda^2}{4\pi}\right)D_0 = \frac{3\lambda^2}{8\pi}} \tag{5-32}$$

It is observed that the directivity, and as a result the maximum effective area, of a small loop is the same as that of an infinitesimal electric dipole. This should be expected since their patterns are identical.

The far-field expressions for a small loop, as given by (5-27a)–(5-27c), will be obtained by another procedure in the next section. In that section a loop of any radius but of constant current will be analyzed. The small loop far-field expressions will then be obtained as a special case of that problem.

Example 5.3

The radius of a small loop of constant current is $\lambda/25$. Find the physical area of the loop and compare it with its maximum effective aperture.

Solution:

$$S\ (\text{physical}) = \pi a^2 = \pi\left(\frac{\lambda}{25}\right)^2 = \frac{\pi\lambda^2}{625} = 5.03\times10^{-3}\lambda^2$$

$$A_{em} = \frac{3\lambda^2}{8\pi} = 0.119\lambda^2$$

$$\frac{A_{em}}{S} = \frac{0.119\lambda^2}{5.03\times10^{-3}\lambda^2} = 23.66$$

Electrically the loop is about 24 times larger than its physical size, which should not be surprising. To be effective, a small loop must be larger electrically than its physical size.

5.2.7 Equivalent Circuit

A small loop is primarily inductive, and it can be represented by a lumped element equivalent circuit similar to those of Figure 2.28.

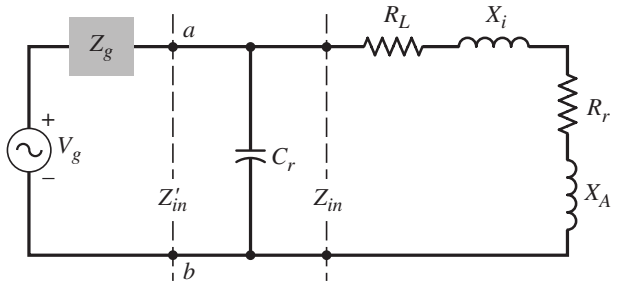


Figure 5.4 Equivalent circuit of loop antenna in transmitting mode.

A. Transmitting Mode

The equivalent circuit for its input impedance when the loop is used as a transmitting antenna is that shown in Figure 5.4. This is similar to the equivalent circuit of Figure 2.28(b). Therefore its input impedance Z_{in} is represented by

$$Z_{in} = R_{in} + jX_{in} = (R_r + R_L) + j(X_A + X_i) \tag{5-33}$$

where

R_r = radiation resistance as given by (5-24)
R_L = loss resistance of loop conductor
X_A = external inductive reactance of loop antenna = ωL_A
X_i = internal high-frequency reactance of loop conductor = ωL_i

In Figure 5.4 the capacitor C_r is used in parallel to (5-33) to resonate the antenna; it can also be used to represent distributed stray capacitances. In order to determine the capacitance of C_r at resonance, it is easier to represent (5-33) by its equivalent admittance Y_{in} of

$$Y_{in} = G_{in} + jB_{in} = \frac{1}{Z_{in}} = \frac{1}{R_{in} + jX_{in}} \tag{5-34}$$

where

$$G_{in} = \frac{R_{in}}{R_{in}^2 + X_{in}^2} \tag{5-34a}$$

$$B_{in} = -\frac{X_{in}}{R_{in}^2 + X_{in}^2} \tag{5-34b}$$

At resonance, the susceptance B_r of the capacitor C_r must be chosen to eliminate the imaginary part B_{in} of (5-34) given by (5-34b). This is accomplished by choosing C_r according to

$$C_r = \frac{B_r}{2\pi f} = -\frac{B_{in}}{2\pi f} = \frac{1}{2\pi f}\frac{X_{in}}{R_{in}^2 + X_{in}^2} \tag{5-35}$$

Under resonance the input impedance Z'_{in} is then equal to

$$Z'_{in} = R'_{in} = \frac{1}{G_{in}} = \frac{R_{in}^2 + X_{in}^2}{R_{in}} = R_{in} + \frac{X_{in}^2}{R_{in}} \tag{5-36}$$

EX2042
Page 257 of 1072

The loss resistance R_L of the loop conductor can be computed using techniques illustrated in Example 5.2. The inductive reactance X_A of the loop is computed using the inductance L_A [7] of:

Circular loop of radius a and wire radius b:

$$L_A = \mu_0 a \left[\ln\left(\frac{8a}{b}\right) - 2 \right] \tag{5-37a}$$

Square loop with sides a and wire radius b:

$$L_A = 2\mu_0 \frac{a}{\pi} \left[\ln\left(\frac{a}{b}\right) - 0.774 \right] \tag{5-37b}$$

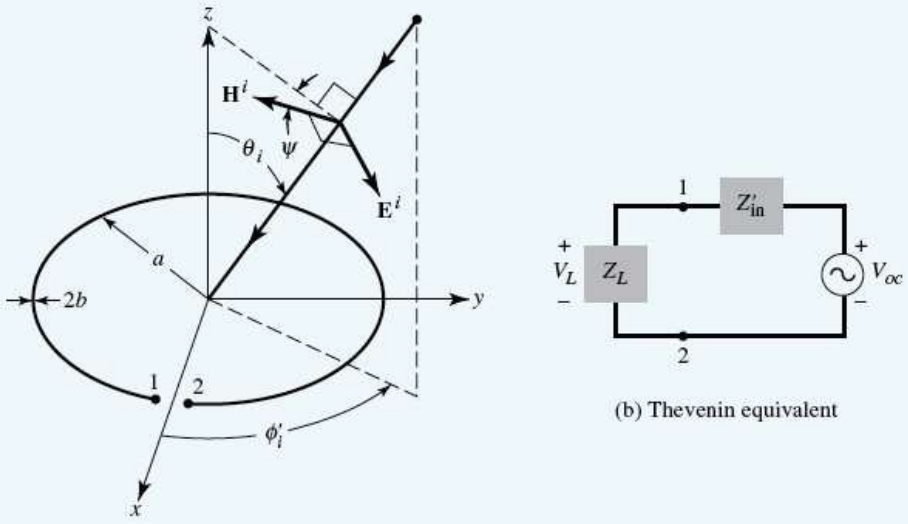
The internal reactance of the loop conductor X_i can be found using the internal inductance L_i of the loop which for a single turn can be approximated by

$$L_i = \frac{l}{\omega P}\sqrt{\frac{\omega\mu_0}{2\sigma}} = \frac{a}{\omega b}\sqrt{\frac{\omega\mu_0}{2\sigma}} \tag{5-38}$$

where l is the length and P is the perimeter (circumference) of the wire of the loop.

B. Receiving Mode

The loop antenna is often used as a receiving antenna or as a probe to measure magnetic flux density. Therefore when a plane wave impinges upon it, as shown in Figure 5.5(a), an open-circuit voltage develops across its terminals. This open-circuit voltage is related according to (2-93) to its vector effective length and incident electric field. This open-circuit voltage is proportional to the incident magnetic flux density B_z^i, which is normal



(b) Thevenin equivalent

(a) Plane wave incident on a receiving loop (G.S. Smith, "Loop Antennas," Copyright © 1984, McGraw-Hill, Inc. Permission by McGraw-Hill, Inc.)

Figure 5.5 Loop antenna and its equivalent in receiving mode.

to the plane of the loop. Assuming the incident field is uniform over the plane of the loop, the open-circuit voltage for a single-turn loop can be written as [8]

$$V_{oc} = j\omega\pi a^2 B_z^i \tag{5-39}$$

Defining in Figure 5.5(a) the plane of incidence as the plane formed by the z axis and radical vector, then the open-circuit voltage of (5-39) can be related to the magnitude of the incident magnetic and electric fields by

$$V_{oc} = j\omega\pi a^2 \mu_0 H^i \cos\psi_i \sin\theta_i = jk_0\pi a^2 E^i \cos\psi_i \sin\theta_i \tag{5-39a}$$

where ψ_i is the angle between the direction of the magnetic field of the incident plane wave and the plane of incidence, as shown in Figure 5.5(a).

Since the open-circuit voltage is also related to the vector effective length by (2-93), then the effective length for a single-turn loop can be written as

$$\boldsymbol{\ell}_e = \hat{\mathbf{a}}_\phi l_e = \hat{\mathbf{a}}_\phi jk_0\pi a^2 \cos\psi_i \sin\theta_i = \hat{\mathbf{a}}_\phi jk_0 S \cos\psi_i \sin\theta_i \tag{5-40}$$

where S is the area of the loop. The factor $\cos\psi_i \sin\theta_i$ is introduced because the open-circuit voltage is proportional to the magnetic flux density component B_z^i which is normal to the plane of the loop.

When a load impedance Z_L is connected to the output terminals of the loop as shown in Figure 5.5(b), the voltage V_L across the load impedance Z_L is related to the input impedance Z'_{in} of Figure 5.5(b) and the open-circuit voltage of (5-39a) by

$$V_L = V_{oc} \frac{Z_L}{Z'_{in} + Z_L} \tag{5-41}$$

5.3 CIRCULAR LOOP OF CONSTANT CURRENT

Let us now reconsider the loop antenna of Figure 5.2(a) but with a radius that may not necessarily be small. The current in the loop will again be assumed to be constant, as given by (5-1). For this current distribution, the vector potential is given by (5-14). The integration in (5-14) is quite complex, as is indicated right after (5-14). However, if the observation are restricted in the far-field ($r \gg a$) region, the small radius approximation is not needed to simplify the integration of (5-14).

Although the uniform current distribution along the perimeter of the loop is only valid provided the circumference is less than about 0.1λ (radius less than about 0.016λ), the procedure developed here for a constant current can be followed to find the far-zone fields of any size loop with not necessarily uniform current.

5.3.1 Radiated Fields

To find the fields in the far-field region, the distance R can be approximated by

$$R = \sqrt{r^2 + a^2 - 2ar\sin\theta\cos\phi'} \simeq \sqrt{r^2 - 2ar\sin\theta\cos\phi'} \quad \text{for} \quad r \gg a \tag{5-42}$$

which can be reduced, using the binomial expansion, to

$$\left.\begin{aligned} R &\simeq r\sqrt{1-\frac{2a}{r}\sin\theta\cos\phi'} = r - a\sin\theta\cos\phi' = r - a\cos\psi_0 \\ &\qquad\qquad\qquad\qquad\qquad\qquad\qquad\qquad \text{for phase terms} \\ R &\simeq r \qquad\qquad\qquad\qquad\qquad\qquad\qquad\qquad \text{for amplitude terms} \end{aligned}\right\} \tag{5-43}$$

since

$$\begin{aligned} \cos\psi_0 = \hat{\mathbf{a}}'_\rho \cdot \hat{\mathbf{a}}_r|_{\phi=0} &= (\hat{\mathbf{a}}_x\cos\phi' + \hat{\mathbf{a}}_y\sin\phi') \\ &\quad\cdot(\hat{\mathbf{a}}_x\sin\theta\cos\phi + \hat{\mathbf{a}}_y\sin\theta\sin\phi + \hat{\mathbf{a}}_z\cos\theta)|_{\phi=0} \\ &= \sin\theta\cos\phi' \end{aligned} \tag{5-43a}$$

The geometrical relation between R and r, for any observation angle ϕ in the far-field region, is shown in Figure 5.2(b). For observations at $\phi = 0$, it simplifies to that given by (5-43) and shown in Figure 5.6. Thus (5-14) can be simplified to

$$A_\phi \simeq \frac{a\mu I_0 e^{-jkr}}{4\pi r}\int_0^{2\pi}\cos\phi' e^{+jka\sin\theta\cos\phi'}\,d\phi' \tag{5-44}$$

and it can be separated into two terms as

$$A_\phi \simeq \frac{a\mu I_0 e^{-jkr}}{4\pi r}\left[\int_0^{\pi}\cos\phi' e^{+jka\sin\theta\cos\phi'}\,d\phi' + \int_\pi^{2\pi}\cos\phi' e^{+jka\sin\theta\cos\phi'}\,d\phi'\right] \tag{5-45}$$

The second term within the brackets can be rewritten by making a change of variable of the form

$$\phi' = \phi'' + \pi \tag{5-46}$$

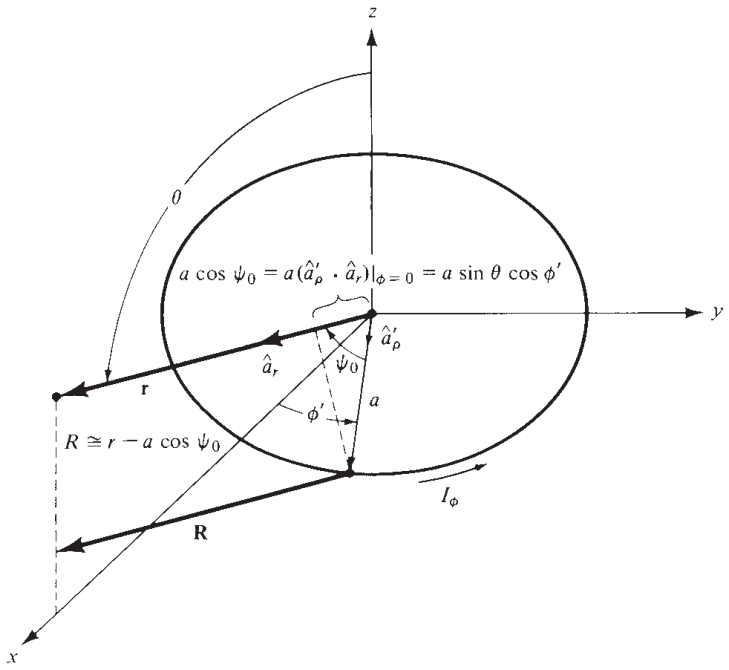


Figure 5.6 Geometry for far-field analysis of a loop antenna.

EX2042
Page 260 of 1072

Thus (5-45) can also be written as

$$A_\phi \simeq \frac{a\mu I_0 e^{-jkr}}{4\pi r}\left[\int_0^\pi \cos\phi' e^{+jka\sin\theta\cos\phi'}\,d\phi' - \int_0^\pi \cos\phi'' e^{-jka\sin\theta\cos\phi''}\,d\phi''\right] \tag{5-47}$$

Each of the integrals in (5-47) can be integrated by the formula (see Appendix V)

$$\pi j^n J_n(z) = \int_0^\pi \cos(n\phi) e^{+jz\cos\phi}\,d\phi \tag{5-48}$$

where $J_n(z)$ is the Bessel function of the first kind of order n. Using (5-48) reduces (5-47) to

$$A_\phi \simeq \frac{a\mu I_0 e^{-jkr}}{4\pi r}[\pi j J_1(ka\sin\theta) - \pi j J_1(-ka\sin\theta)] \tag{5-49}$$

The Bessel function of the first kind and order n is defined (see Appendix V) by the infinite series

$$J_n(z) = \sum_{m=0}^{\infty} \frac{(-1)^m (z/2)^{n+2m}}{m!(m+n)!} \tag{5-50}$$

By a simple substitution into (5-50), it can be shown that

$$J_n(-z) = (-1)^n J_n(z) \tag{5-51}$$

which for $n = 1$ is equal to

$$J_1(-z) = -J_1(z) \tag{5-52}$$

Using (5-52) we can write (5-49) as

$$A_\phi \simeq j\frac{a\mu I_0 e^{-jkr}}{2r} J_1(ka\sin\theta) \tag{5-53}$$

The next step is to find the **E-** and **H-**fields associated with the vector potential of (5-53). Since (5-53) is only valid for far-field observations, the procedure outlined in Section 3.6 can be used. The vector potential **A**, as given by (5-53), is of the form suggested by (3-56). That is, the r variations are separable from those of θ and ϕ. Therefore according to (3-58a)–(3-58b) and (5-53)

$$E_r \simeq E_\theta = 0 \tag{5-54a}$$

$$E_\phi \simeq \frac{ak\eta I_0 e^{-jkr}}{2r} J_1(ka\sin\theta) \tag{5-54b}$$

$$H_r \simeq H_\phi = 0 \tag{5-54c}$$

$$H_\theta \simeq -\frac{E_\phi}{\eta} = -\frac{akI_0 e^{-jkr}}{2r} J_1(ka\sin\theta) \tag{5-54d}$$

EX2042
Page 261 of 1072

5.3.2 Power Density, Radiation Intensity, Radiation Resistance, and Directivity

The next objective for this problem will be to find the power density, radiation intensity, radiation resistance, and directivity. To do this, the time-average power density is formed. That is,

$$\mathbf{W}_{\text{av}} = \frac{1}{2}\text{Re}[\mathbf{E} \times \mathbf{H}^*] = \frac{1}{2}\text{Re}[\hat{\mathbf{a}}_\phi E_\phi \times \hat{\mathbf{a}}_\theta H_\theta^*] = \hat{\mathbf{a}}_r \frac{1}{2\eta}|E_\phi|^2 \tag{5-55}$$

which can be written using (5-54b) as

$$\mathbf{W}_{\text{av}} = \hat{\mathbf{a}}_r W_r = \hat{\mathbf{a}}_r \frac{(a\omega\mu)^2|I_0|^2}{8\eta r^2} J_1{}^2(ka\sin\theta) \tag{5-56}$$

with the radiation intensity given by

$$U = r^2 W_r = \frac{(a\omega\mu)^2|I_0|^2}{8\eta} J_1{}^2(ka\sin\theta) \tag{5-57}$$

The radiation patterns for $a = \lambda/10, \lambda/5$, and $\lambda/2$ are shown in Figure 5.7. These patterns indicate that the field radiated by the loop along its axis ($\theta = 0^\circ$) is zero. Also the shape of these patterns is similar to that of a linear dipole with $l \leq \lambda$ (a figure-eight shape). As the radius a increases beyond 0.5λ, the field intensity along the plane of the loop ($\theta = 90^\circ$) diminishes and eventually it forms a null when $a \simeq 0.61\lambda$. This is left as an exercise to the reader for verification (Prob. 5.18). Beyond $a = 0.61\lambda$, the radiation along the plane of the loop begins to intensify and the pattern attains a multilobe form.

Three-dimensional patterns for loop circumferences of $C = 0.1\lambda$ and 5λ, assuming uniform current distribution, are shown in Figure 5.8. It is apparent that for the 0.1λ circumference the pattern is basically that of figure eight ($\sin\theta$), while for the 5λ loop it exhibits multiple lobes. The multiple lobes in a large loop begin to form when the circumference exceeds about 3.83λ (radius exceeds about 0.61λ); see Problem 5.18.

The patterns represented by (5-57) (some of them are illustrated in Figure 5.7) assume that the current distribution, no matter what the loop size, is constant. This is not a valid assumption if the loop circumference $C(C = 2\pi a)$ exceeds about 0.1λ (i.e., $a > 0.016\lambda$) [9]. For radii much greater than about 0.016λ, the current variation along the circumference of the loop begins to attain a distribution that is best represented by a Fourier series [8]. Although a most common assumption is that the current distribution is nearly cosinusoidal, it is not satisfactory particularly near the driving point of the antenna.

A uniform and nonuniform in-phase current distribution can be attained on a loop antenna even if the radius is large. To accomplish this, the loop is subdivided into sections, with each section/arc of the loop fed with a different feed line; all feed lines are typically fed from a common feed source. Such an arrangement, although more complex, can approximate either uniform or nonuniform in-phase current distribution.

It has been shown [10] that when the circumference of the loop is about one wavelength ($C \simeq \lambda$), its maximum radiation based on a nonuniform current distribution is along its axis ($\theta = 0^\circ, 180^\circ$) which is perpendicular to the plane of the loop. This

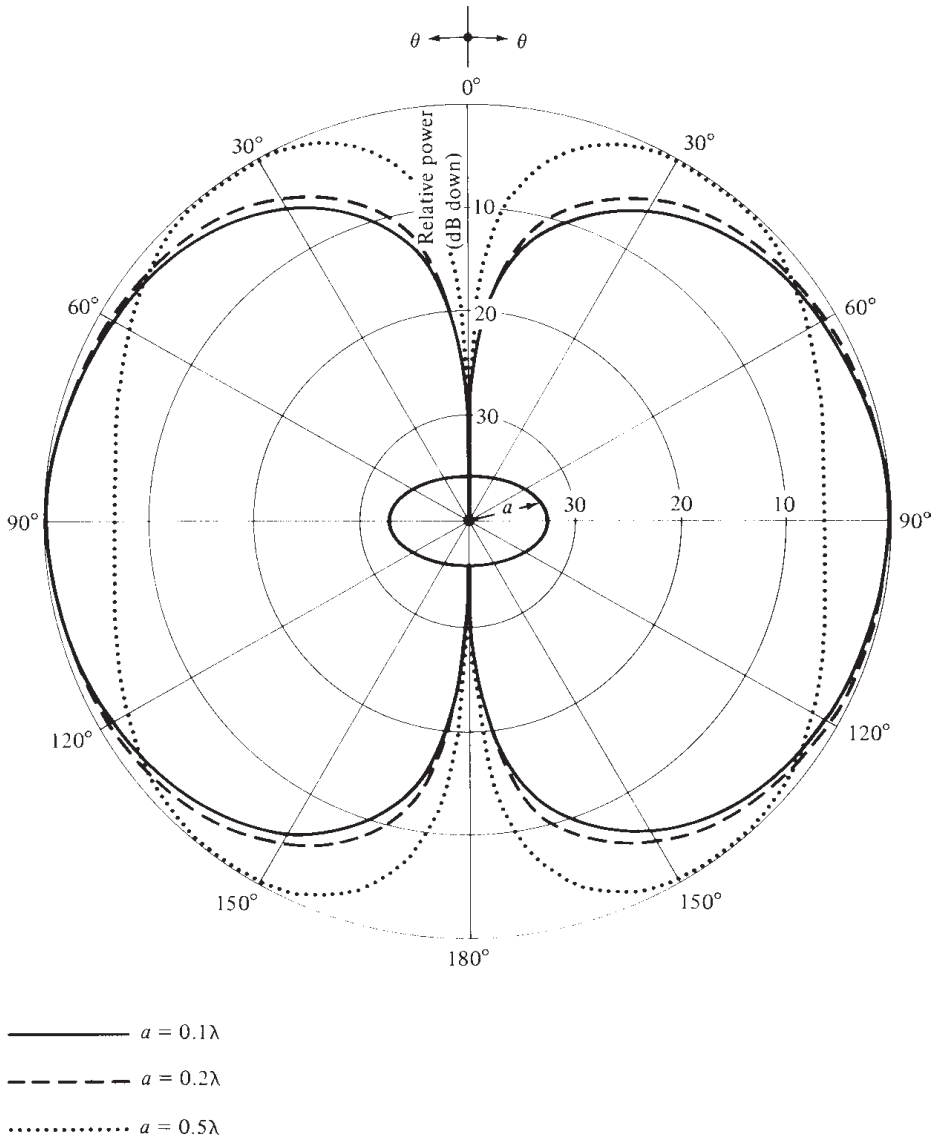


Figure 5.7 Elevation plane amplitude patterns for a circular loop of constant current ($a = 0.1\lambda, 0.2\lambda$, and 0.5λ).

feature of the loop antenna has been utilized to design Yagi-Uda arrays whose basic elements (feed, directors, and reflectors) are circular loops [11]–[14]. Because of its many applications, the one-wavelength circumference circular-loop antenna is considered as fundamental as a half-wavelength dipole.

The radiated power can be written using (5-56) as

$$P_{\text{rad}} = \iint_S \mathbf{W}_{\text{av}} \cdot d\mathbf{s} = \frac{\pi(a\omega\mu)^2|I_0|^2}{4\eta} \int_0^\pi J_1{}^2(ka\sin\theta)\sin\theta\, d\theta \tag{5-58}$$

The integral in (5-58) can be rewritten [15] as

$$\int_0^\pi J_1{}^2(ka\sin\theta)\sin\theta\, d\theta = \frac{1}{ka}\int_0^{2ka} J_2(x)\, dx \tag{5-59}$$

EX2042
Page 263 of 1072

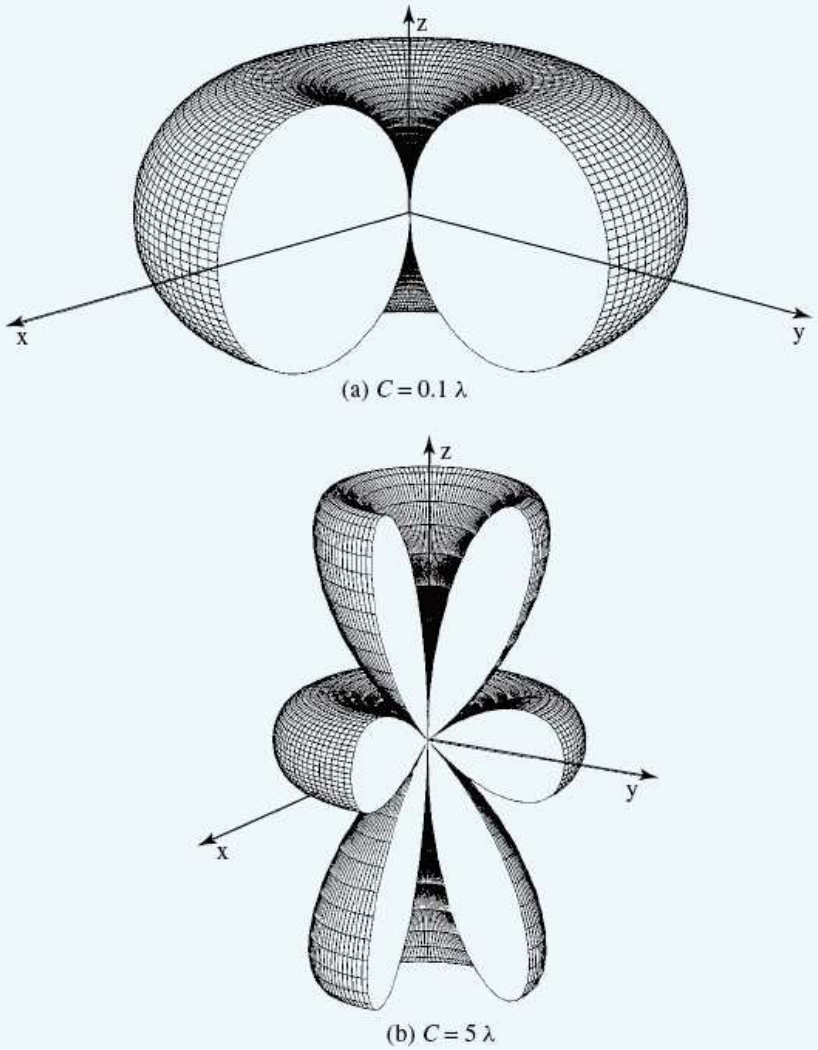


Figure 5.8 Three-dimensional amplitude patterns of a circular loop with constant current distribution.

The evaluation of the integral of (5-59) has been the subject of recent papers [16]–[20]. In these references, *along with some additional corrections*, the integral of (5-59)

$$Q_{11}^{(1)}(ka) = \frac{1}{2}\int_0^{\pi} J_1^2(ka\sin\theta)\sin\theta\, d\theta = \frac{1}{2ka}\int_0^{2ka} J_2(x)\, dx \tag{5-59a}$$

can be represented by a series of Bessel functions

$$Q_{11}^{(1)}(ka) = \frac{1}{ka}\sum_{m=0}^{\infty} J_{2m+3}(2ka) \tag{5-59b}$$

where $J_m(x)$ is the Bessel function of the first kind, mth order. This is a highly convergent series (typically no more than $2ka$ terms are necessary), and its numerical evaluation is very efficient. Approximations to (5-59) can be made depending upon the values of the upper limit (large or small radii of the loop).

EX2042
Page 264 of 1072

A. Large Loop Approximation ($a \geq \lambda/2$)

To evaluate (5-59), the first approximation will be to assume that the radius of the loop is large ($a \geq \lambda/2$). For that case, the integral in (5-59) can be approximated by

$$\int_0^{\pi} J_1{}^2(ka\sin\theta)\sin\theta\, d\theta = \frac{1}{ka}\int_0^{2ka} J_2(x)\, dx \simeq \frac{1}{ka} \tag{5-60}$$

and (5-58) by

$$P_{\text{rad}} \simeq \frac{\pi(a\omega\mu)^2|I_0|^2}{4\eta(ka)} \tag{5-61}$$

The maximum radiation intensity occurs when $ka\sin\theta = 1.84$ so that

$$U|_{\max} = \frac{(a\omega\mu)^2|I_0|^2}{8\eta} J_1{}^2(ka\sin\theta)|_{ka\sin\theta=1.84} = \frac{(a\omega\mu)^2|I_0|^2}{8\eta}(0.582)^2 \tag{5-62}$$

Thus

$$R_r = \frac{2P_{\text{rad}}}{|I_0|^2} = \frac{2\pi(a\omega\mu)^2}{4\eta(ka)} = \eta\left(\frac{\pi}{2}\right)ka = 60\pi^2(ka) = 60\pi^2\left(\frac{C}{\lambda}\right) \tag{5-63a}$$

$$D_0 = 4\pi\frac{U_{\max}}{P_{\text{rad}}} = 4\pi\frac{ka(0.582)^2}{2\pi} = 2ka(0.582)^2 = 0.677\left(\frac{C}{\lambda}\right) \tag{5-63b}$$

$$A_{em} = \frac{\lambda^2}{4\pi}D_0 = \frac{\lambda^2}{4\pi}\left[0.677\left(\frac{C}{\lambda}\right)\right] = 5.39\times 10^{-2}\lambda C \tag{5-63c}$$

where C(circumference) $= 2\pi a$ and $\eta \simeq 120\pi$.

B. Intermediate Loop Approximation ($\lambda/6\pi \leq a < \lambda/2$)

If the radius of the loop is $\lambda/(6\pi) = 0.053\lambda \leq a < \lambda/2$, the integral of (5-59) for $Q_{11}^1(ka)$ is approximated by (5-59a) and (5-59b), and the radiation resistance and directivity can be expressed, respectively, as

$$R_r = \frac{2P_{rad}}{|I_0|^2} = \eta\pi(ka)^2 Q_{11}^{(1)}(ka) \tag{5-64a}$$

$$D_0 = \frac{4\pi U_{\max}}{P_{rad}} = \frac{F_m(ka)}{Q_{11}^{(1)}(ka)} \tag{5-64b}$$

where

$$F_m(ka) = J_1^2(ka\sin\theta)|_{\max} = \begin{cases} J_1^2(1.840) = (0.582)^2 = 0.339 & \text{(5-64c)} \\ \quad ka > 1.840\ (a > 0.293\lambda) & \\ J_1^2(ka) & \\ \quad ka < 1.840\ (a < 0.293\lambda) & \text{(5-64d)} \end{cases}$$

C. Small Loop Approximation ($a < \lambda/6\pi$)

If the radius of the loop is small ($a < \lambda/6\pi$), the expressions for the fields as given by (5-54a)–(5-54d) can be simplified. To do this, the Bessel function $J_1(ka\sin\theta)$ is expanded, by the definition of (5-50), in an infinite series of the form (see Appendix V)

$$J_1(ka\sin\theta) = \tfrac{1}{2}(ka\sin\theta) - \tfrac{1}{16}(ka\sin\theta)^3 + \cdots \tag{5-65}$$

For small values of $ka (ka < \frac{1}{3})$, (5-65) can be approximated by its first term, or

$$J_1(ka \sin\theta) \simeq \frac{ka \sin\theta}{2} \tag{5-65a}$$

Thus (5-54a)–(5-54d) can be written as

$$\left.\begin{aligned} E_r &\simeq E_\theta = 0 && \text{(5-66a)}\\ E_\phi &\simeq \frac{a^2\omega\mu k I_0 e^{-jkr}}{4r}\sin\theta = \eta\frac{a^2k^2 I_0 e^{-jkr}}{4r}\sin\theta && \text{(5-66b)}\\ H_r &\simeq H_\phi = 0 && \text{(5-66c)}\\ H_\theta &\simeq -\frac{a^2\omega\mu k I_0 e^{-jkr}}{4\eta r}\sin\theta = -\frac{a^2k^2 I_0 e^{-jkr}}{4r}\sin\theta && \text{(5-66d)} \end{aligned}\right\} \quad a < \lambda/6\pi$$

which are identical to those of (5-27a)–(5-27c). Thus the expressions for the radiation resistance, radiation intensity, directivity, and maximum effective aperture are those given by (5-24), (5-29), (5-31), and (5-32).

To demonstrate the variation of the radiation resistance as a function of the radius a of the loop, it is plotted in Figure 5.9 for $\lambda/100 \le a \le \lambda/30$, based on the approximation of (5-65a). It is evident that the values are extremely low (less than 1 ohm), and they are usually smaller than the loss resistances of the wires. These radiation resistances also lead to large mismatch losses when connected to practical transmission

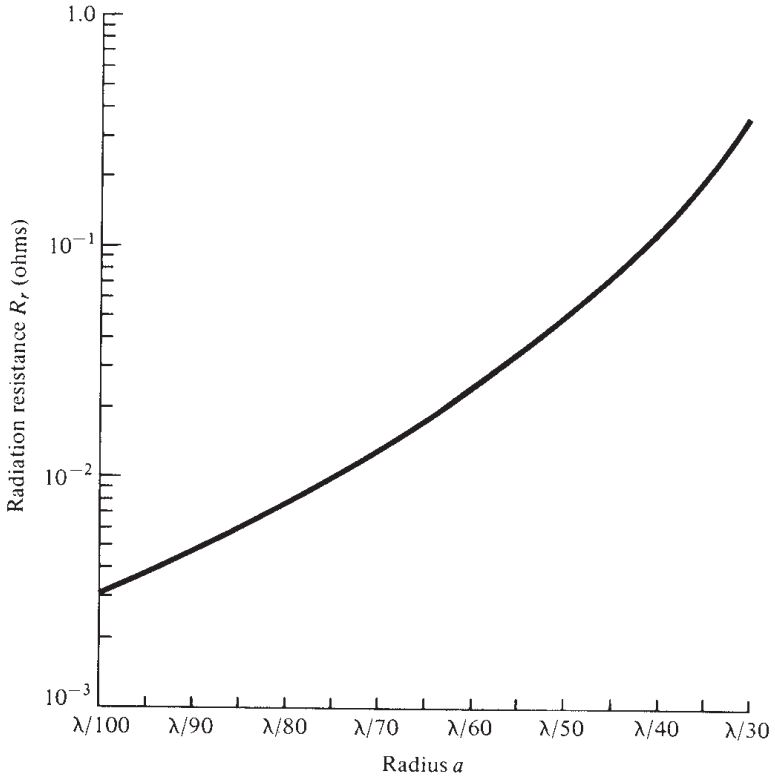


Figure 5.9 Radiation resistance for a constant current circular-loop antenna based on the approximation of (5-65a).

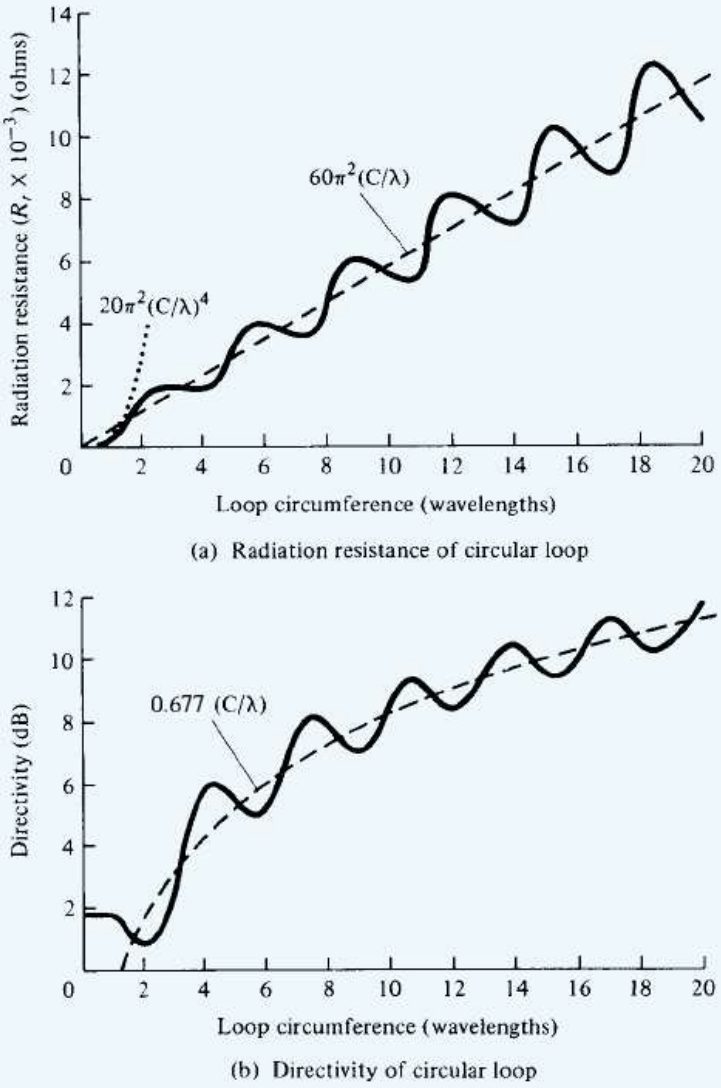


Figure 5.10 Radiation resistance and directivity for circular loop of constant current. (SOURCE: E. A. Wolff, *Antenna Analysis*, Wiley, New York, 1966).

lines of 50 or 75 ohms. To increase the radiation resistance, it would require multiple turns as suggested by (5-24a). This, however, also increases the loss resistance which contributes to the inefficiency of the antenna. A plot of the radiation resistance for $0 < ka = C/\lambda < 20$, based on the evaluation of (5-59) by numerical techniques, is shown in Figure 5.10. The dashed line represents the values based on the large loop approximation of (5-60) and the dotted ($\cdots\cdots$) represents the values based on the small loop approximation of (5-65a).

In addition to the real part of the input impedance, there is also an imaginary component which would increase the mismatch losses even if the real part is equal to the characteristic impedance of the lossless transmission line. However, the imaginary component can always, in principle at least, be eliminated by connecting a reactive element (capacitive or inductive) across the terminals of the loop to make the antenna a resonant circuit.

To facilitate the computations for the directivity and radiation resistance of a circular loop with a constant current distribution, a MATLAB and FORTRAN computer

program has been developed. The program utilizes (5-62) and (5-58) to compute the directivity [(5-58) is integrated numerically]. The program requires as an input the radius of the loop (in wavelengths). A Bessel function subroutine is contained within the FORTRAN program. A listing of the program is included in the CD attached with the book.

5.4 CIRCULAR LOOP WITH NONUNIFORM CURRENT

The analysis in the previous sections was based on a uniform current, which would be a valid approximation when the radius of the loop is small electrically (usually $a < 0.016\lambda$). As the dimensions of the loop increase, the current variations along the circumference of the loop must be taken into account. As stated previously, a very common assumption for the current distribution is a cosinusoidal variation [21], [22]. This, however, is not a satisfactory approximation particularly near the driving point of the antenna [9]. A better distribution would be to represent the current by a Fourier series [23]

$$I(\phi') = I_0 + 2\sum_{n=1}^{M} I_n \cos(n\phi') \tag{5-67}$$

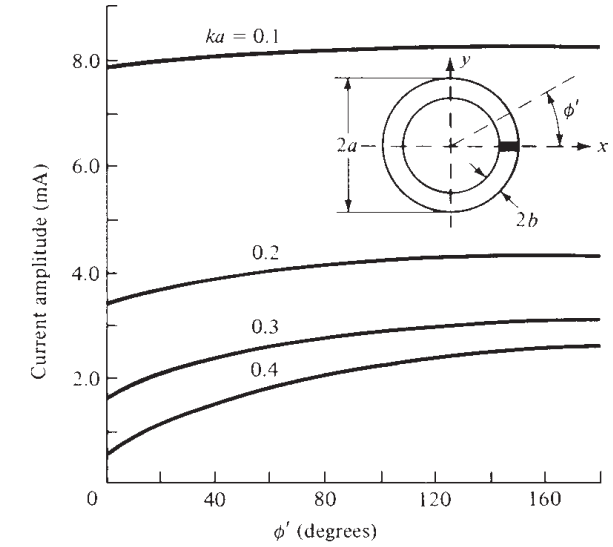
where ϕ' is measured from the feed point of the loop along the circumference, as shown at the inset of Figure 5.11.

A complete analysis of the fields radiated by a loop with nonuniform current distribution is somewhat complex, laborious, and quite lengthy [2], [3]. Instead of attempting to include the analytical formulations, which are cumbersome but well documented in the cited references, a number of graphical illustrations of numerical and experimental data is presented. These curves can be used in facilitating designs.

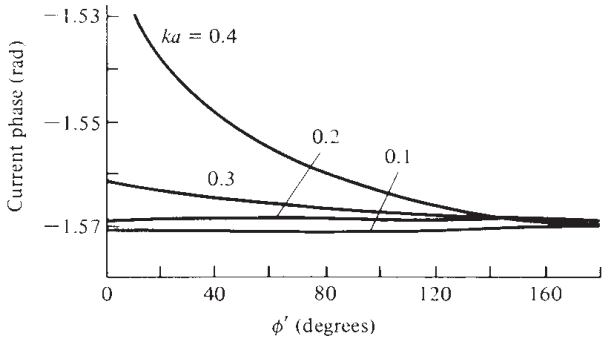
To illustrate that the current distribution of a wire loop antenna is not uniform unless its radius is very small, the magnitude and phase of it have been plotted in Figure 5.11 as a function of ϕ' (in degrees). The loop circumference C is $ka = C/\lambda = 0.1$, 0.2, 0.3, and 0.4 and the wire size was chosen so that $\Omega = 2\ln(2\pi a/b) = 10$. It is apparent that for $ka = 0.1$ the current is nearly uniform. For $ka = 0.2$ the variations are slightly greater and become even larger as ka increases. On the basis of these results, loops much larger than $ka = 0.1$ (radius much greater than 0.016λ) cannot be considered small.

As was indicated earlier, the maximum of the pattern for a loop antenna shifts from the plane of the loop ($\theta = 90^\circ$) to its axis ($\theta = 0^\circ, 180^\circ$) as the circumference of the loop approaches one wavelength, assuming that simultaneously the current changes from uniform to nonuniform. Based on the nonuniform current distribution of (5-67), the directivity of the loop along $\theta = 0^\circ$ has been computed, and it is plotted in Figure 5.12 versus the circumference of the loop in wavelengths [8]. The maximum directivity is about 4.5 dB, and it occurs when the circumference is about 1.4λ. For a one-wavelength circumference, which is usually the optimum design for a helical antenna, the directivity is about 3.4 dB. It is also apparent that the directivity is basically independent of the radius of the wire, as long as the circumference is equal or less than about 1.3 wavelengths; there are differences in directivity as a function of the wire radius for greater circumferences.

Computed impedances, based on the Fourier series representation of the current, are shown plotted in Figure 5.13. The input resistance and reactance are plotted as



(a) Magnitude



(b) Phase

Figure 5.11 Current magnitude and phase distributions on small circular loop antennas. (SOURCE: J. E. Storer, "Impedance of Thin-Wire Loop Antennas," *AIEE Trans.*, Vol. 75, November 1956. © 1956 IEEE).

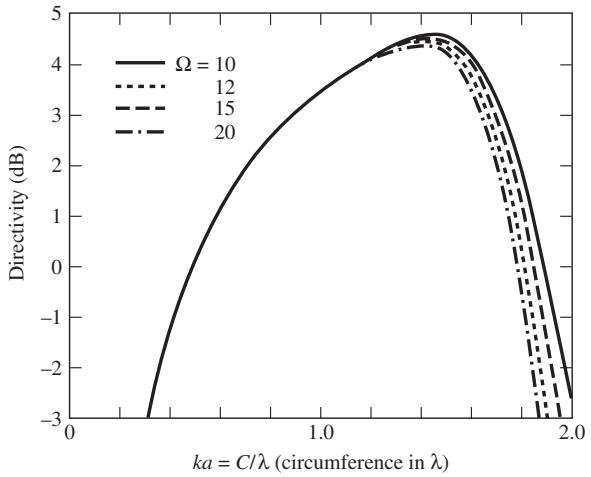
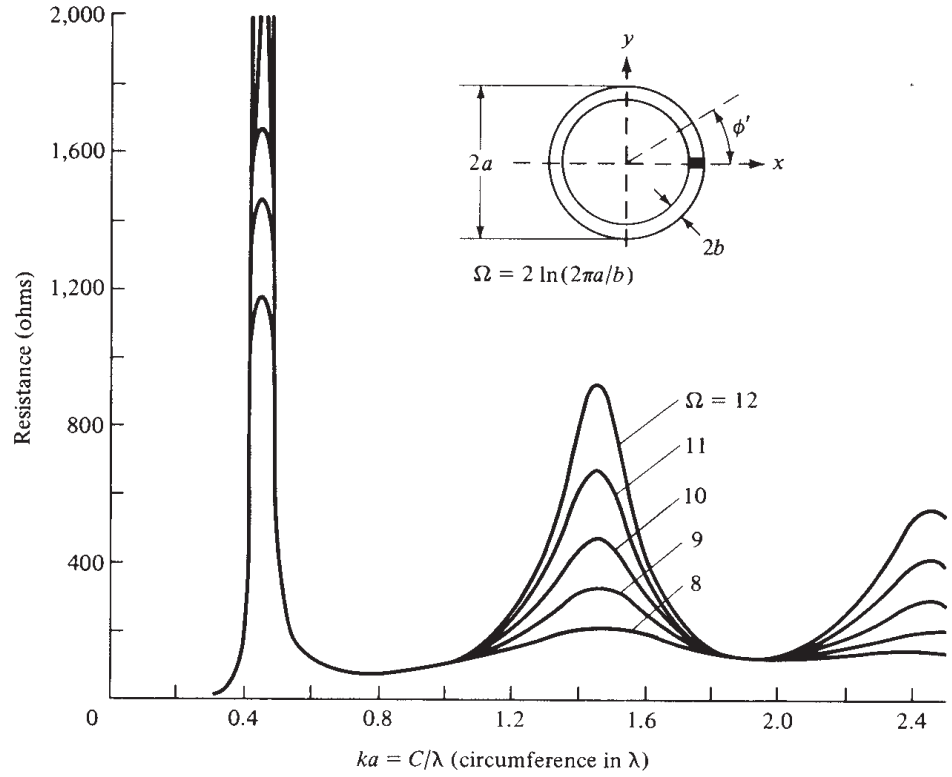
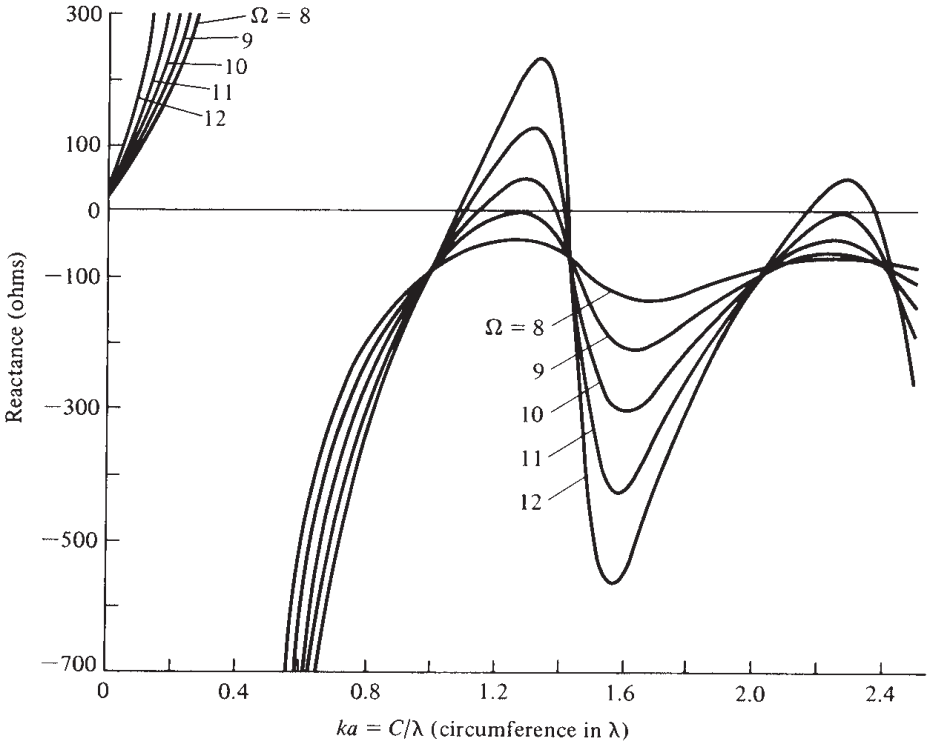


Figure 5.12 Directivity of circular-loop antenna for $\theta = 0, \pi$ versus electrical size (circumference/wavelength). (SOURCE: G. S. Smith, "Loop Antennas," Chapter 5 of *Antenna Engineering Handbook*, 1984, © 1984 McGraw-Hill, Inc. Permission by McGraw-Hill, Inc).

EX2042
Page 269 of 1072



(a) Resistance



(b) Reactance

Figure 5.13 Input impedance of circular-loop antennas. (SOURCE: J. E. Storer, "Impedance of Thin-Wire Loop Antennas," *AIEE Trans.*, Vol. 75, November 1956. © 1956 IEEE).

a function of the circumference C (in wavelengths) for $0 \leq ka = C/\lambda \leq 2.5$. The diameter of the wire was chosen so that $\Omega = 2\ln(2\pi a/b) = 8$, 9, 10, 11, and 12. It is apparent that the first antiresonance occurs when the circumference of the loop is about $\lambda/2$, and it is extremely sharp. It is also noted that as the loop wire increases in thickness, there is a rapid disappearance of the resonances. As a matter of fact, for $\Omega < 9$ there is only one antiresonance point. These curves (for $C > \lambda$) are similar, both qualitatively and quantitatively, to those of a linear dipole. The major difference is that the loop is more capacitive (by about 130 ohms) than a dipole. This shift in reactance allows the dipole to have several resonances and antiresonances while moderately thick loops ($\Omega < 9$) have only one antiresonance. *Also small loops are primarily inductive while small dipoles are primarily capacitive*. The resistance curves for the loop and the dipole are very similar.

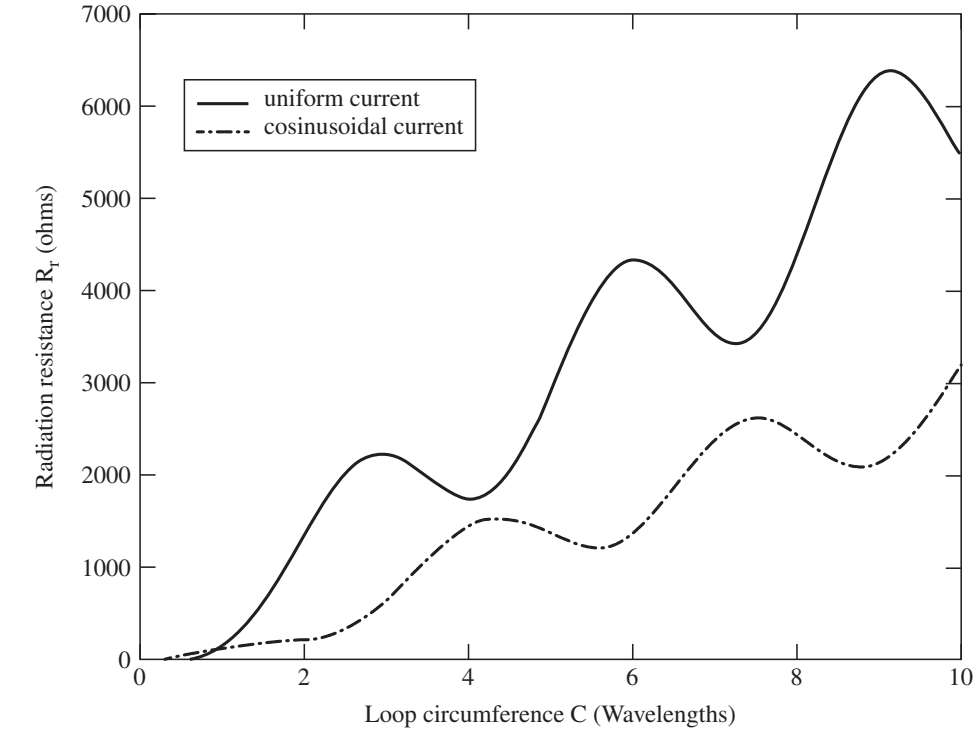
To verify the analytical formulations and the numerical computations, loop antennas were built and measurements of impedance were made [9]. The measurements were conducted using a half-loop over an image plane, and it was driven by a two-wire line. An excellent agreement between theory and experiment was indicated everywhere except near resonances where computed conductance curves were slightly higher than those measured. This is expected since ohmic losses were not taken into account in the analytical formulation. It was also noted that the measured susceptance curve was slightly displaced vertically by a constant value. This can be attributed to the "end effect" of the experimental feeding line and the "slice generator" used in the analytical modeling of the feed. For a dipole, the correction to the analytical model is usually a negative capacitance in shunt with the antenna [24]. A similar correction for the loop would result in a better agreement between the computed and measured susceptances. Computations for a half-loop above a ground plane were also performed by J. E. Jones [25] using the Moment Method.

The radiation resistance and directivity of a loop antenna with a cosinusoidal current distribution $I_\phi(\phi) = I_0 \cos\phi$ was derived in [2] and evaluated in [16] by integrating in far-zone fields and expressing the integral in terms of five $Q_{mn}^{(1)}(ka)$ integrals of similar form as (5-59a) and (5-59b). Doing this, the values are plotted, respectively, in Figures 5.14(a,b) where they are compared with those based on a uniform current distribution.

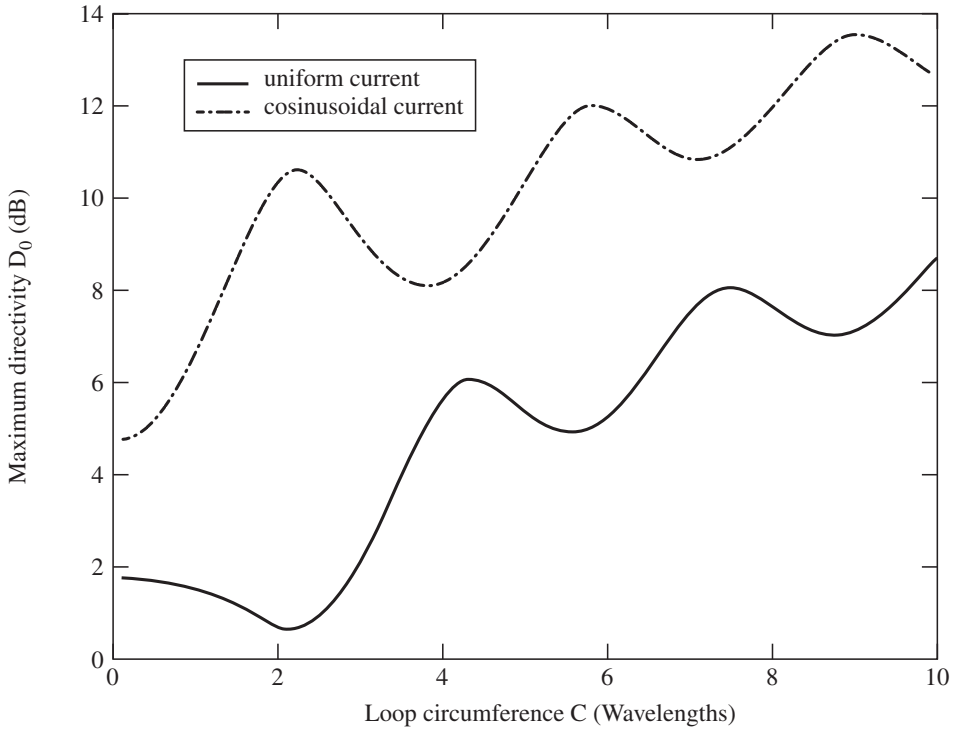
5.4.1 Arrays

In addition to being used as single elements and in arrays, as shown in Figure 5.1(a,b), there are some other classic arrays of loop configurations. Two of the most popular arrays of loop antennas are the helical antenna and the Yagi-Uda array. The loop is also widely used to form a solenoid which in conjunction with a ferrite cylindrical rod within its circumference is used as a receiving antenna and as a tuning element, especially in transistor radios. This is discussed in Section 5.7.

The helical antenna, which is discussed in more detail in Section 10.3.1, is a wire antenna, which is wound in the form of a helix, as shown in Figure 10.13. It is shown that it can be modeled approximately by a series of loops and vertical dipoles, as shown in Figure 10.15. The helical antenna possesses in general elliptical polarization, but it can be designed to achieve nearly circular polarization. There are two primary modes of operation for a helix, the normal mode and the axial mode. The helix operates in its normal mode when its overall length is small compared to the wavelength, and it has a pattern with a null along its axis and the maximum along



(a) Radiation resistance R_r



(b) Maximum directivity D_o

Figure 5.14 Radiation resistance (R_r) and maximum directivity (D_0) of a circular loop with constant current distribution. (SOURCE: S. V. Savov, "An Efficient Solution of a Class of Integrals Arising in Antenna Theory," *IEEE Antennas and Propagation Magazine*, Vol. 44, October 2002, pp. 98–101. © 2002 IEEE).

EX2042
Page 272 of 1072

the plane of the loop. This pattern (figure-eight type in the elevation plane) is similar to that of a dipole or a small loop. *A helical antenna operating in the normal mode is sometimes used as a monopole antenna for mobile cell and cordless telephones, and it is usually covered with a plastic cover. This helix monopole is used because its input impedance is larger than that of a regular monopole and more attractive for matching to typical transmission lines used as feed lines, such as a coaxial line* (see Problem 10.18).

The helix operates in the axial mode when the circumference of the loop is between $3/4\lambda < C < 4/3\lambda$ with an optimum design when the circumference is nearly one wavelength. When the circumference of the loop approaches one wavelength, the maximum of the pattern is along its axis. In addition, the phasing among the turns is such that overall the helix forms an end-fire antenna with attractive impedance and polarization characteristics (see Example 10.1). In general, the helix is a popular communication antenna in the VHF and UHF bands.

The Yagi-Uda antenna is primarily an array of linear dipoles with one element serving as the feed while the others act as parasitic. However this arrangement has been extended to include arrays of loop antennas, as shown in Figure 10.30. As for the helical antenna, in order for this array to perform as an end-fire array, the circumference of each of the elements is near one wavelength. More details can be found in Section 10.3.4 and especially in [11]–[14]. A special case is the quad antenna which is very popular amongst ham radio operators. It consists of two square loops, one serving as the excitation while the other is acting as a reflector; there are no directors. The overall perimeter of each loop is one wavelength.

5.4.2 Design Procedure

The design of small loops is based on the equations for the radiation resistance (5-24), (5-24a), directivity (5-31), maximum effective aperture (5-32), resonance capacitance (5-35), resonance input impedance (5-36) and inductance (5-37a), (5-37b). In order to resonate the element, the capacitor C_r of Figure 5.4 is chosen based on (5-35) so as to cancel out the imaginary part of the input impedance Z_{in}.

For large loops with a nonuniform current distribution, the design is accomplished using the curves of Figure 5.12 for the axial directivity and those of Figure 5.13 for the impedance. To resonate the loop, usually a capacitor in parallel or an inductor in series is added, depending on the radius of the loop and that of the wire.

Example 5.4

Design a resonant loop antenna to operate at 100 MHz so that the pattern maximum is along the axis of the loop. Determine the radius of the loop and that of the wire (in meters), the axial directivity (in dB), and the parallel lumped element (capacitor in parallel or inductor in series) that must be used in order to resonate the antenna.

Solution: In order for the pattern maximum to be along the axis of the loop, the circumference of the loop must be large compared to the wavelength. Therefore the current distribution will be nonuniform. To accomplish this, Figure 5.13 should be used. There is not only one unique design which meets the specifications, but there are many designs that can accomplish the goal.

One design is to select a circumference where the loop is self resonant, and there is no need for a resonant capacitor. For example, referring to Figure 5.13(b) and choosing an $\Omega = 12$, the circumference of the loop is nearly 1.125λ. Since the free-space wavelength at 100 MHz is 3 meters, then the circumference is

$$\text{circumference} \simeq 1.125(3) = 3.375 \text{ meters}$$

while the radius of the loop is

$$\text{radius} = a = \frac{3.375}{2\pi} = 0.5371 \text{ meters}$$

The radius of the wire is obtained using

$$\Omega = 12 = 2 \ln\left(\frac{2\pi a}{b}\right)$$

or

$$\frac{a}{b} = 64.2077$$

Therefore the radius of the wire is

$$b = \frac{a}{64.2077} = \frac{0.5371}{64.2077} = 0.8365 \text{ cm} = 8.365 \times 10^{-3} \text{meters}$$

Using Figure 5.12, the axial directivity for this design is approximately 3.6 dB. Using Figure 5.13(a), the input impedance is approximately

$$Z_{in} = Z'_{in} \simeq 840 \text{ ohms}$$

Since the antenna chosen is self resonant, there is no need for a lumped element to resonate the radiator.

Another design will be to use another circumference where the loop is not self resonant. This will necessitate the use of a capacitor C_r to resonate the antenna. This is left as an end of the chapter exercise.

5.5 GROUND AND EARTH CURVATURE EFFECTS FOR CIRCULAR LOOPS

The presence of a lossy medium can drastically alter the performance of a circular loop. The parameters mostly affected are the pattern, directivity, input impedance, and antenna efficiency. The amount of energy dissipated as heat by the lossy medium directly affects the antenna efficiency. As for the linear elements, geometrical optics techniques can be used to analyze the radiation characteristics of loops in the presence of conducting surfaces. The reflections are taken into account by introducing appropriate image (virtual) sources. Divergence factors are introduced to take into account the effects of the ground curvature. Because the techniques are identical to the formulations of Section 4.8, they will not be repeated here. The reader is directed to that section for the details. It should be pointed out, however, that a horizontal loop has horizontal polarization in contrast to the vertical polarization of a vertical electric dipole. Exact boundary-value solutions, based on Sommerfeld integral formulations, are available [25]. However they are too complex to be included in an introductory chapter.

By placing the loop above a reflector, the pattern is made unidirectional and the directivity is increased. To simplify the problem, initially the variations of the axial directivity ($\theta = 0^\circ$) of a circular loop with a circumference of one wavelength ($ka = 1$) when placed horizontally a height h above an infinite in extent perfect electric conductor are examined as a function of the height above the ground plane. These were obtained using image theory and the array factor of two loops, and they are shown for $10 < \Omega < 20$ in Figure 5.15[8], [26]. Since only one curve is shown for $10 < \Omega < 20$, it is evident that the directivity variations as a function of the height are not strongly dependent on the radius of the wire of the loop. It is also apparent that for $0.05\lambda < h < 0.2\lambda$ and $0.65\lambda < h < 0.75\lambda$ the directivity is about 9 dB. For the same size loop, the corresponding variations of the impedance as a function of the height are shown in Figure 5.16[8], [26]. While the directivity variations are not strongly influenced by the radius of the wire, the variations of the impedance do show a dependence on the radius of the wire of the loop for $10 < \Omega < 20$.

A qualitative criterion that can be used to judge the antenna performance is the ratio of the radiation resistance in free-space to that in the presence of the homogeneous lossy medium [27]. This is a straightforward but very tedious approach. A much simpler method [28] is to find directly the self-impedance changes (real and imaginary) that result from the presence of the conducting medium.

Since a small horizontal circular loop is equivalent to a small vertical magnetic dipole (see Section 5.2.2), computations [29] were carried out for a vertical magnetic dipole placed a height h above a homogeneous lossy half-space. The changes in the self-impedance, normalized with respect to the free-space radiation resistance R_0 given by (5-24), are found in [29]. Significant changes, compared to those of a perfect conductor, are introduced by the presence of the ground.

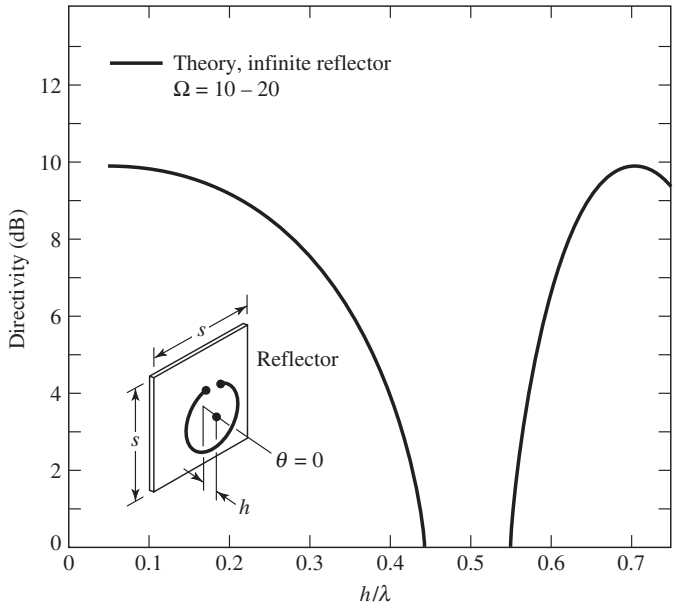


Figure 5.15 Directivity of circular-loop antenna, $C = ka = 1$, for $\theta = 0$ versus distance from reflector h/λ. Theoretical curve is for infinite planar reflector. (SOURCE: G. S. Smith, "Loop Antennas," Chapter 5 of *Antenna Engineering Handbook*, 1984, © 1984 McGraw-Hill, Inc. Permission by McGraw-Hill, Inc).

EX2042
Page 275 of 1072

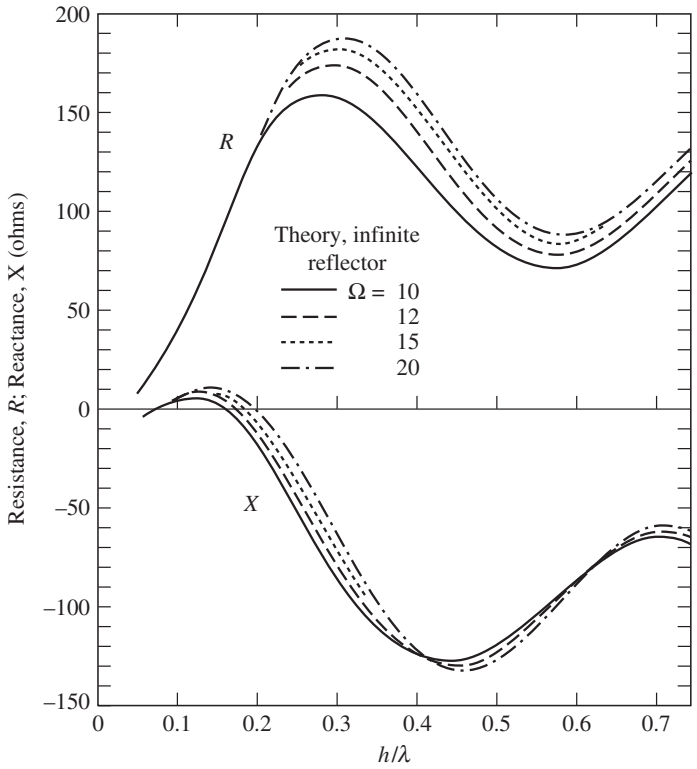


Figure 5.16 Input impedance of circular-loop antenna $C = ka = 1$ versus distance from reflector h/λ. Theoretical curves are for infinite planar reflector; measured points are for square reflector. (SOURCE: G. S. Smith, "Loop Antennas," Chapter 5 of *Antenna Engineering Handbook*, 1984, © 1984, McGraw-Hill, Inc. Permission by McGraw-Hill, Inc).

The effects that a stratified lossy half-space have on the characteristics of a horizontal small circular loop have also been investigated and documented [30]. It was found that when a resonant loop is close to the interface, the changes in the input admittance as a function of the antenna height and the electrical properties of the lossy medium were very pronounced. This suggests that a resonant loop can be used effectively to sense and to determine the electrical properties of an unknown geological structure.

5.6 POLYGONAL LOOP ANTENNAS

The most attractive polygonal loop antennas are the square, rectangular, triangular, and rhombic. These antennas can be used for practical applications such as for aircraft, missiles, and communications systems. However, because of their more complex structure, theoretical analyses seem to be unsuccessful [31]. Thus the application of these antennas has received much less attention. However design curves, computed using the Moment Method, do exist [32] and can be used to design polygonal loop antennas for practical applications. Usually the circular loop has been used in the UHF range because of its higher directivity while triangular and square loops have been applied in the HF and UHF bands because of advantages in their mechanical construction. Broadband impedance characteristics can be obtained from the different polygonal loops.

EX2042
Page 276 of 1072

5.6.1 Square Loop

Next to the circular loop, the square loop is the simplest loop configuration. The far-field pattern for a small loop, in each of its principal planes, can be obtained by assuming that each of its sides is a small linear dipole of constant current I_0 and length a. Referring to Figure 5.17, the field in the y-z plane is given according to (4-26a) by

$$E_\phi = E_{\phi 1} + E_{\phi 2} = -j\eta \frac{kI_0 a}{4\pi}\left[\frac{e^{-jkr_1}}{r_1} - \frac{e^{-jkr_2}}{r_2}\right] \tag{5-68}$$

since the pattern of each element is omnidirectional in that plane. Using the far-field approximations of

$$\left.\begin{aligned} r_1 &\simeq r - \frac{a}{2}\sin\theta \\ r_2 &\simeq r + \frac{a}{2}\sin\theta \end{aligned}\right\} \quad \text{for phase variations} \tag{5-68a}$$

$$r_1 \simeq r_2 \simeq r \qquad \text{for amplitude variations} \tag{5-68b}$$

(5-68) can be written as

$$E_\phi = \eta \frac{kI_0 a e^{-jkr}}{2\pi r}\sin\left(\frac{ka}{2}\sin\theta\right) \tag{5-69}$$

For small values of $a(a < \lambda/50)$, (5-69) reduces to

$$\boxed{E_\phi = \eta \frac{(ka)^2 I_0 e^{-jkr}}{4\pi r}\sin\theta = \eta \frac{\pi S I_0 e^{-jkr}}{\lambda^2 r}\sin\theta} \tag{5-70}$$

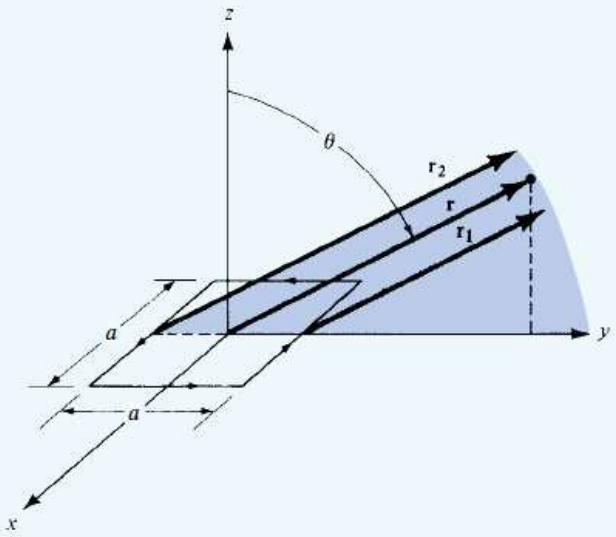


Figure 5.17 Square loop geometry for far-field observations on the y-z plane.

where $S = a^2$ is the geometrical area of the loop. The corresponding magnetic field is given by

$$H_\theta = -\frac{E_\phi}{\eta} = -\frac{\pi S I_0 e^{-jkr}}{\lambda^2 r} \sin\theta \tag{5-71}$$

Equations (5-70) and (5-71) are identical to (5-27b) and (5-27a), respectively, for the small circular loop. Thus the far-zone principal-plane fields of a small square loop are identical to those of a small circular loop. The fields in the other planes are more difficult to obtain, and they will not be attempted here. However design curves are included which can be used for practical design applications.

5.6.2 Triangular, Rectangular, and Rhombic Loops

Shown in Figure 5.18 are the polygonal loops for which design data will be presented. They consist of top- and base-driven triangular loops, a rectangular loop, and a rhombic loop. The top-driven triangular loop has its feed at the top corner of the isosceles triangle while the base-driven configuration has its terminals at the base. The rectangular loop has its feed at the center of one of its sides while the rhombic configuration has its terminals at one of its corners.

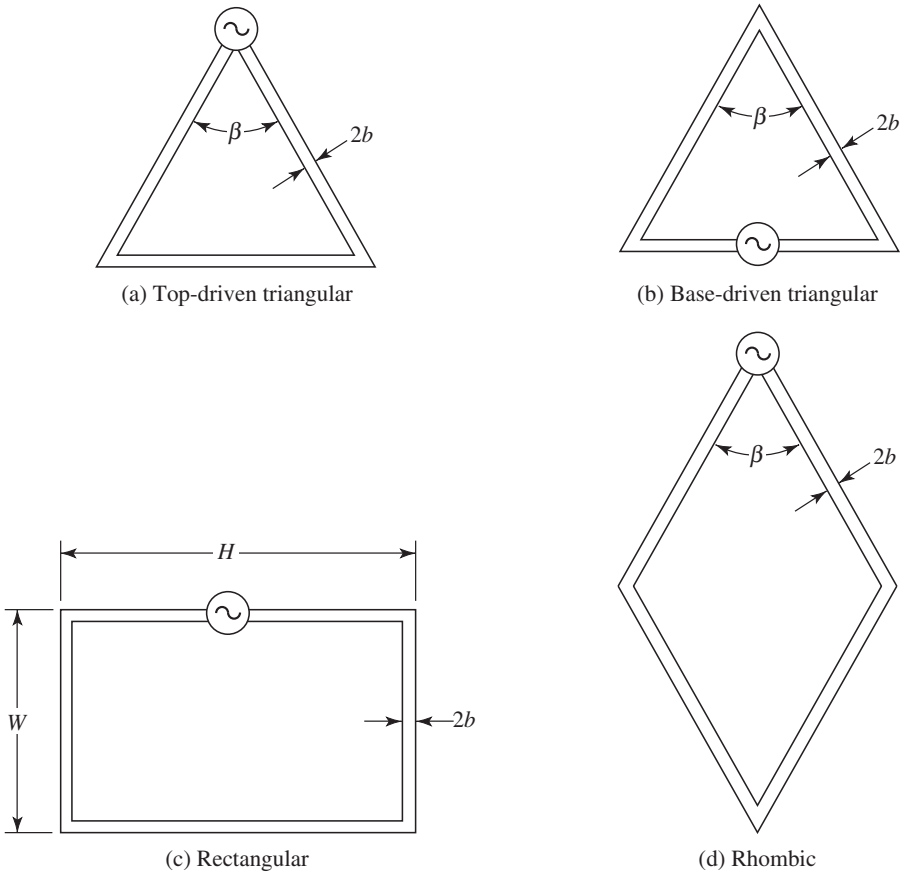


Figure 5.18 Typical configurations of polygonal loop antennas. (SOURCE: T. Tsukiji and S. Tou, "On Polygonal Loop Antennas," *IEEE Trans. Antennas Propagat.*, Vol. AP-28, No. 4, July 1980. © 1980 IEEE).

The parameter β defines the angle of the top corner of the isosceles triangle for the triangular and rhombic loops while $\gamma = W/H$ is used to identify the relative side dimensions of the rectangular loop. The perimeter of each loop is given by P; for the rectangular loop, $P = 2(H + W)$. For all configurations, the radius of the wire is b.

Included in [32] are the input impedance ($Z = R + jX$) variations, as a function of P (in wavelengths), of the four configurations shown in Figure 5.18. The interval between adjacent points on each curve is $\Delta P/\lambda = 0.2$. Depending on the parameters β or γ, the input resistance of polygonal loops near the resonance frequency changes drastically. The reactance goes to zero when a loop approaches a short-circuited $\lambda/2$ long transmission line. In design then, the shape of the loop can be chosen so that the input impedance is equal to the characteristic impedance of the transmission line. Although the curves in [32] are for specific wire radii, the impedance variations of the polygonal antennas as a function of the wire diameter are similar to those of the dipole.

Because the radius of the impedance locus for the $\beta = 60^\circ$ of the top-driven triangular loop [Figure 5.18(a)] is smaller than for the other values of β, the $\beta = 60^\circ$ has the broadest impedance bandwidth compared with other triangular shapes or with the same shape but different feed points. Similar broadband impedance characteristics are indicated in [32] for a rectangular loop with $\gamma = 0.5$ (the side with the feed point is twice as large as the other).

It can then be concluded that if the proper shape and feed point are chosen, a polygonal loop can have broadband impedance characteristics. The most attractive are the top-driven triangular loop with $\beta = 60^\circ$ and the rectangular loop with $\gamma = 0.5$. A 50–70 ohm coaxial cable can be matched with a triangular loop with $\beta = 40^\circ$. Rectangular loops with greater directivities, but with less ideal impedance characteristics, are those with larger values of γ.

The frequency characteristics of a polygonal loop can be estimated by inspecting its current distribution. When the current standing wave pattern has, at its antiresonant frequency, a null at a sharp corner of the loop, the loop has a very low current standing wave and, hence, broadband impedance characteristics.

Radiation patterns for the $\beta = 60^\circ$ top- and base-driven triangular loops and the $\gamma = 4$ rectangular loop, for various values of P (in wavelengths), were also computed [32]. It was noted that for low frequencies near the resonance, the patterns of the top- and base-driven triangular loops were not too different. However, for higher frequencies the base-driven triangular loop had a greater gain than its corresponding top-driven configuration. In general, rectangular loops with larger γ's have greater gains.

5.7 FERRITE LOOP

Because the loss resistance is comparable to the radiation resistance, electrically small loops are very poor radiators and are seldom used in the transmitting mode. However, they are often used for receiving signals, such as in radios and pagers, where the signal-to-noise ratio is much more important than the efficiency.

5.7.1 Radiation Resistance

The radiation resistance, and in turn the antenna efficiency, can be raised by increasing the circumference of the loop. Another way to increase the radiation resistance, without increasing the electrical dimensions of the antenna, would be to insert within

its circumference a ferrite core that has a tendency to increase the magnetic flux, the magnetic field, the open-circuit voltage, and in turn the radiation resistance of the loop [33], [34]. This is the so-called *ferrite loop* and the ferrite material can be a rod of very few inches in length. The radiation resistance of the ferrite loop is given by

$$\frac{R_f}{R_r} = \left(\frac{\mu_{ce}}{\mu_0}\right)^2 = \mu_{cer}^2 \tag{5-72}$$

where

R_f = radiation resistance of ferrite loop
R_r = radiation resistance of air core loop
μ_{ce} = effective permeability of ferrite core
μ_0 = permeability of free-space
μ_{cer} = relative effective permeability of ferrite core

Using (5-24), the radiation resistance of (5-72) for a single-turn small ferrite loop can be written as

$$\boxed{R_f = 20\pi^2 \left(\frac{C}{\lambda}\right)^4 \left(\frac{\mu_{ce}}{\mu_0}\right)^2 = 20\pi^2 \left(\frac{C}{\lambda}\right)^4 \mu_{cer}^2} \tag{5-73}$$

and for an N-turn loop, using (5-24a), as

$$\boxed{R_f = 20\pi^2 \left(\frac{C}{\lambda}\right)^4 \left(\frac{\mu_{ce}}{\mu_0}\right)^2 N^2 = 20\pi^2 \left(\frac{C}{\lambda}\right)^4 \mu_{cer}^2 N^2} \tag{5-74}$$

The relative effective permeability of the ferrite core μ_{cer} is related to the relative intrinsic permeability of the unbounded ferrite material $\mu_{fr}(\mu_{fr} = \mu_f/\mu_0)$ by

$$\mu_{cer} = \frac{\mu_{ce}}{\mu_0} = \frac{\mu_{fr}}{1 + D(\mu_{fr} - 1)} \tag{5-75}$$

where D is the demagnetization factor which has been found experimentally for different core geometries, as shown in Figure 5.19. For most ferrite material, the relative intrinsic permeability μ_{fr} is very large ($\mu_{fr} \gg 1$) so that the relative effective permeability of the ferrite core μ_{cer} is approximately inversely proportional to the demagnetization factor, or $\mu_{cer} \sim 1/D = D^{-1}$. In general, the demagnetization factor is a function of the geometry of the ferrite core. For example, the demagnetization factor for a sphere is $D = \frac{1}{3}$ while that for an ellipsoid of length $2l$ and radius a, such that $l \gg a$, is

$$D = \left(\frac{a}{l}\right)^2 \left[\ln\left(\frac{2l}{a}\right) - 1\right], \qquad l \gg a \tag{5-75a}$$

5.7.2 Ferrite-Loaded Receiving Loop

Because of their smallness, ferrite loop antennas of few turns wound around a small ferrite rod are used as antennas especially in pocket transistor radios. The antenna is

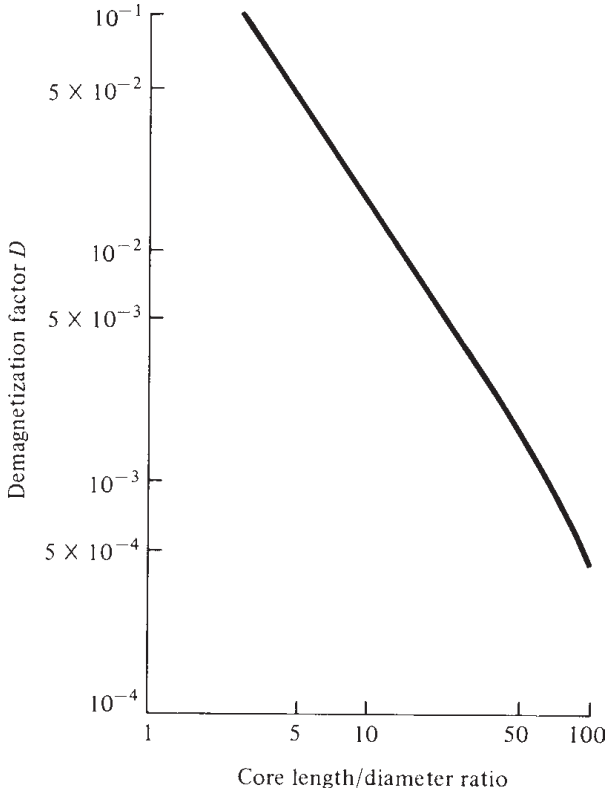


Figure 5.19 Demagnetization factor as a function of core length/diameter ratio. (SOURCE: E. A. Wolff, *Antenna Analysis*, Wiley, New York, 1966).

usually connected in parallel with the RF amplifier tuning capacitance and, in addition to acting as an antenna, it furnishes the necessary inductance to form a tuned circuit. Because the inductance is obtained with only few turns, the loss resistance is kept small. Thus the Q is usually very high, and it results in high selectivity and greater induced voltage.

The equivalent circuit for a ferrite-loaded loop antenna is similar to that of Figure 5.4 except that a loss resistance R_M, in addition to R_L, is needed to account for the power losses in the ferrite core. Expressions for the loss resistance R_M and inductance L_A for the ferrite-loaded loop of N turns can be found in [7] and depend on some empirical factors which are determined from an average of experimental results. The inductance L_i is the same as that of the unloaded loop.

5.8 MOBILE COMMUNICATION SYSTEMS APPLICATIONS

As was indicated in Section 4.7.4 of Chapter 4, the monopole is one of the most widely used elements for handheld units of mobile communication systems. An alternative to the monopole is the loop, [35]–[40], which has been often used in pagers but has found very few applications in handheld transceivers. This is probably due to loop's high resistance and inductive reactance which are more difficult to match to standard feed lines. The fact that loop antennas are more immune to noise makes them more

attractive for an interfering and fading environment, like that of mobile communication systems. In addition, loop antennas become more viable candidates for wireless communication systems which utilize devices operating at higher frequency bands, particularly in designs where balanced amplifiers must interface with the antenna. Relative to top side of the handheld unit, such as the telephone, the loop can be placed either horizontally [36] or vertically [38]–[40]. Either configuration presents attractive radiation characteristics for land-based mobile systems.

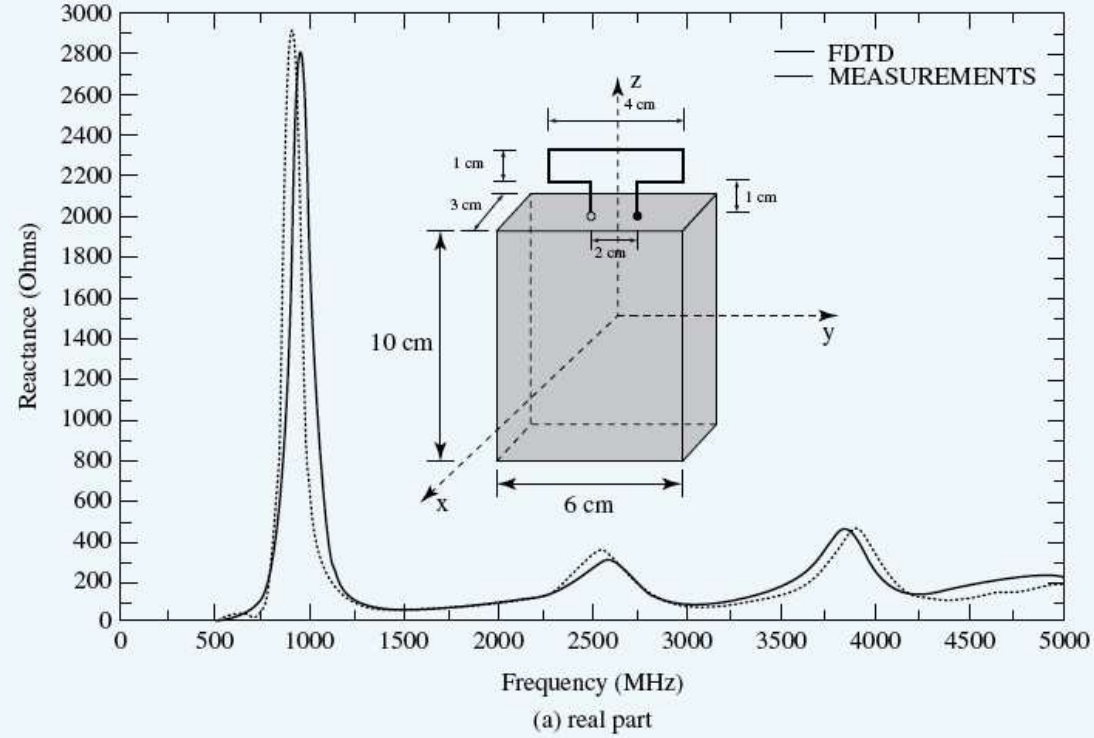
The radiation characteristics, normalized pattern and input impedance, of a monopole and vertical loop mounted on an experimental mobile handheld device were examined in [38]–[40]. The loop was in the form of a folded configuration mounted vertically on the handheld conducting device with its one end either grounded or ungrounded to the device. The predicted and measured input impedance of the folded loop, when its terminating end was grounded to the box, are displayed in Figure 5.20(a,b). It is evident that the first resonance, around 900 MHz, of the folded loop is of the *parallel type* (*antiresonance*) with a very high, and rapidly changing versus frequency, resistance, and reactance. These values and variations of impedance are usually undesirable for practical implementation. For frequencies below the first resonance, the impedance is inductive (imaginary part is positive), as is typical of small loop antennas (see Figure 5.13); above the first resonance, the impedance is capacitive (negative imaginary part). The second resonance, around 2,100 MHz, is of the *series type* with slowly varying values of impedance, and of desirable magnitude, for practical implementation. The resonance forms (*parallel* vs. *series*) can be interchanged if the terminating end of the folded loop is ungrounded with the element then operating as an L monopole [38]–[40] and exhibiting the same resonance behavior as that of a monopole mounted on the device (see Chapter 4, Section 4.7.4, Figure 4.21). Even though the radiating element is a loop whose plane is vertical to the box, the amplitude pattern, in both cases (loop and L), is similar and nearly omnidirectional as that of the monopole of Figure 4.21 because the PEC box is also part of the radiating system.

A summary of the pertinent parameters and associated formulas and equation numbers for this chapter are listed in Table 5.1.

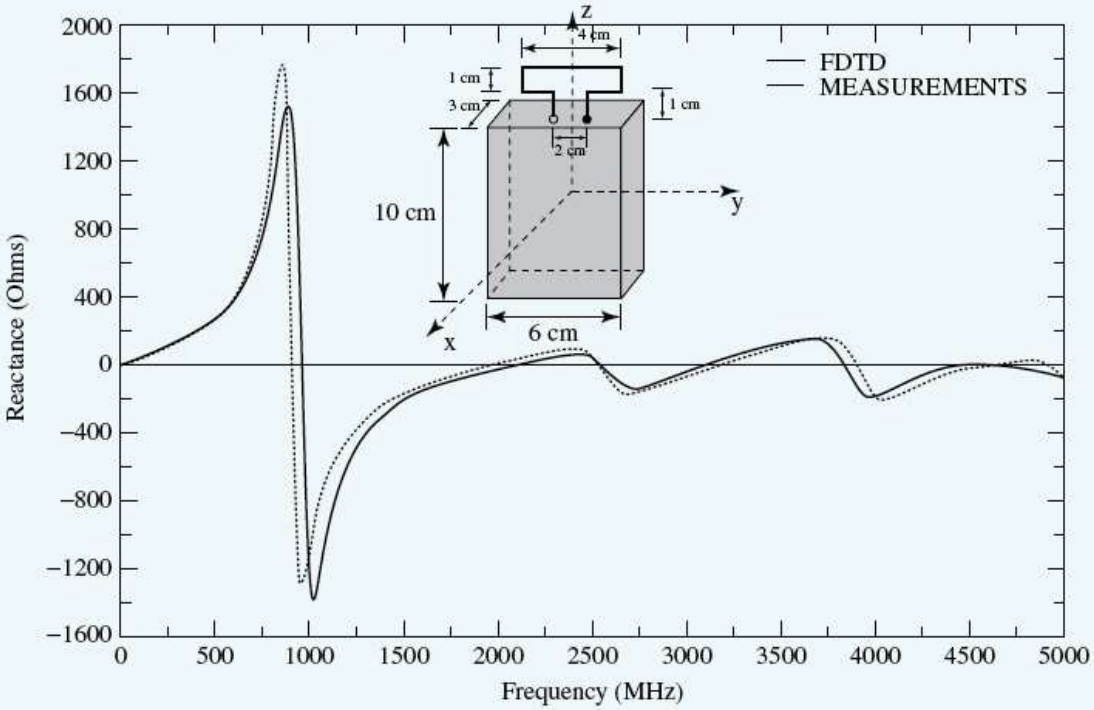
5.9 MULTIMEDIA

In the CD that is part of the book, the following multimedia resources are included for the review, understanding, and visualization of the material of this chapter:

a. **Java**-based **interactive questionnaire**, with answers.
b. **Java**-based **applet** for computing and displaying the radiation characteristics of a loop.
c. **Java**-based animation of loop amplitude pattern.
d. **Matlab** and **Fortran** computer program, designated ***Loop***, for computing the radiation characteristics of a loop. A description of the program is found in the READ ME file of the corresponding program in the attached CD.
e. **Power Point (PPT)** viewgraphs, in multicolor.



(a) real part



(b) imaginary part

Figure 5.20 Input impedance, real and imaginary parts of a wire folded loop mounted vertically on a conducting mobile hand-held unit (SOURCE: K. D. Katsibas, et. al., "Folded Loop Antenna for Mobile Hand-Held Units," *IEEE Transactions Antennas Propagat.*, Vol. 46, No. 2, February 1998, pp. 260–266. © 1998 IEEE).

TABLE 5.1 Summary of Important Parameters, and Associated Formulas and Equation Numbers for Loop in Far Field

Parameter	Formula	Equation Number
	Small Circular Loop $(a < \lambda/6\pi, C < \lambda/3)$ **(Uniform Current)**	
Normalized power pattern	$U = \lvert E_{\phi n}\rvert^2 = C_0 \sin^2\theta$	(5-27b)
Wave impedance Z_w	$Z_w = -\dfrac{E_\phi}{H_\theta} \simeq \eta = 377 \ \text{Ohms}$	(5-28)
Directivity D_0	$D_0 = \dfrac{3}{2} = 1.761 \ \text{dB}$	(5-31)
Maximum effective area A_{em}	$A_{em} = \dfrac{3\lambda^2}{8\pi}$	(5-32)
Radiation resistance R_r (one turn)	$R_r = 20\pi^2 \left(\dfrac{C}{\lambda}\right)^4$	(5-24)
Radiation resistance R_r (N turns)	$R_r = 20\pi^2 \left(\dfrac{C}{\lambda}\right)^4 N^2$	(5-24a)
Input resistance R_{in}	$R_{in} = R_r = 20\pi^2 \left(\dfrac{C}{\lambda}\right)^4$	(5-24)
Loss resistance R_L (one turn)	$R_L = \dfrac{l}{P}\sqrt{\dfrac{\omega\mu_0}{2\sigma}} = \dfrac{C}{2\pi b}\sqrt{\dfrac{\omega\mu_0}{2\sigma}}$	(2-90b)
Loss resistance R_L (N turns)	$R_L = \dfrac{Na}{b} R_s \left(\dfrac{R_p}{R_0} + 1\right)$	(5-25)
Loop external inductance L_A	$L_A = \mu_0 a \left[\ln\left(\dfrac{8a}{b}\right) - 2\right]$	(5-37a)
Loop internal inductance L_i	$L_i = \dfrac{a}{\omega b}\sqrt{\dfrac{\omega\mu_0}{2\sigma}}$	(5-38)
Vector effective length $\boldsymbol{\ell}_e$	$\boldsymbol{\ell}_e = \hat{\mathbf{a}}_\phi \, jk_0\pi a^2 \cos\psi_i \sin\theta_i$	(5-40)
Half-power beamwidth	$\text{HPBW} = 90^\circ$	(4-65)

(*continued overleaf*)

TABLE 5.1 (*continued*)

Parameter	Formula	Equation Number
	Large Circular Loop $(a \geq \lambda/2, C \geq 3.14\lambda)$ **(Uniform Current)**	
Normalized power pattern	$U = \lvert E_{\phi n}\rvert^2 = C_1 J_1^2(ka \sin\theta)$	(5-57)
Wave impedance Z_w	$Z_w = -\dfrac{E_\phi}{H_\theta} \simeq \eta = 377 \ \text{Ohms}$	(5-28)
Directivity D_0 $(a > \lambda/2)$	$D_0 = 0.677\left(\dfrac{C}{\lambda}\right)$	(5-63b)
Maximum effective area A_{em} $(a > \lambda/2)$	$A_{em} = \dfrac{\lambda^2}{4\pi}\left[0.677\left(\dfrac{C}{\lambda}\right)\right]$	(5-63c)
Radiation resistance $(a > \lambda/2)$, (one turn)	$R_r = 60\pi^2\left(\dfrac{C}{\lambda}\right)$	(5-63a)
Input resistance $(a > \lambda/2)$, (one turn)	$R_{in} = R_r = 60\pi^2\left(\dfrac{C}{\lambda}\right)$	(5-63a)
Loss resistance R_L (one turn)	$R_L = \dfrac{l}{P}\sqrt{\dfrac{\omega\mu_0}{2\sigma}} = \dfrac{C}{2\pi b}\sqrt{\dfrac{\omega\mu_0}{2\sigma}}$	(2-90b)
Loss resistance R_L (N turns)	$R_L = \dfrac{Na}{b}R_s\left(\dfrac{R_p}{R_0} + 1\right)$	(5-25)
External inductance L_A	$L_A = \mu_0 a\left[\ln\left(\dfrac{8a}{b}\right) - 2\right]$	(5-37a)
Internal inductance L_i	$L_i = \dfrac{a}{\omega b}\sqrt{\dfrac{\omega\mu_0}{2\sigma}}$	(5-38)
Vector effective length $\boldsymbol{\ell}_e$	$\boldsymbol{\ell}_e = \hat{\mathbf{a}}_\phi jk_0\pi a^2 \cos\psi_i \sin\theta_i$	(5-40)
	Small Square Loop **(Figure 5.17)** **(Uniform Current, *a* on Each Side**	
Normalized power pattern (principal plane)	$U = \lvert E_{\phi n}\rvert^2 = C_2 \sin^2\theta$	(5-70)

TABLE 5.1 (*continued*)

Parameter	Formula	Equation Number
Wave impedance Z_w	$Z_w = -\dfrac{E_\phi}{H_\theta} \simeq \eta = 377 \ \text{Ohms}$	(5-28)
Radiation resistance R_r	$R_r = 20\left(\dfrac{2\pi a}{\lambda}\right)^4 = 20\left(\dfrac{C}{\lambda}\right)^4$	
Input resistance R_{in}	$R_{in} = R_r = 20\left(\dfrac{4a}{\lambda}\right)^4 = 20\left(\dfrac{P}{\lambda}\right)^4$	
Loss resistance R_L	$R_L = \dfrac{4a}{P}\sqrt{\dfrac{\omega\mu_0}{2\sigma}} = \dfrac{4a}{2\pi b}\sqrt{\dfrac{\omega\mu_0}{2\sigma}}$	(2-90b)
External inductance L_A	$L_A = 2\mu_0\dfrac{a}{\pi}\left[\ln\left(\dfrac{a}{b}\right) - 0.774\right]$	(5-37b)
Internal inductance L_i	$L_i = \dfrac{4a}{\omega P}\sqrt{\dfrac{\omega\mu_0}{2\sigma}} = \dfrac{4a}{2\pi b\omega}\sqrt{\dfrac{\omega\mu_0}{2\sigma}}$	(5-38)
	Ferrite Circular Loop $(a < \lambda/6\pi, C < \lambda/3)$ **(uniform current)**	
Radiation resistance R_f (one turn)	$R_f = 20\pi^2\left(\dfrac{C}{\lambda}\right)^4 \mu_{cer}^2$	(5-73)
	$\mu_{cer} = \dfrac{\mu_{fr}}{1 + D(\mu_{fr} - 1)}$	(5-75)
Radiation resistance R_f (N turns)	$R_f = 20\pi^2\left(\dfrac{C}{\lambda}\right)^4 \mu_{cer}^2 N^2$	(5-74)
Demagnetizing factor D	Ellipsoid: $D = \left(\dfrac{a}{l}\right)^2\left[\ln\left(\dfrac{2l}{a}\right) - 1\right]$ $l \gg a$ Sphere: $D = \dfrac{1}{3}$	(5-75a)

REFERENCES

1. P. L. Overfelt, "Near Fields of the Constant Current Thin Circular Loop Antenna of Arbitrary Radius," *IEEE Trans. Antennas Propagat.*, Vol. 44, No. 2, February 1996, pp. 166–171.
2. D. H. Werner, "An Exact Integration Procedure for Vector Potentials of Thin Circular Loop Antennas," *IEEE Trans. Antennas Propagat.*, Vol. 44, No. 2, February 1996, pp. 157–165.
3. D. H. Werner, "Lommel Expansions in Electromagnetics," Chapter in *Frontiers in Electromagnetics*, (D. H. Werner and R. Mittra, eds.), IEEE Press/John Wiley, New York, 2000.

4. E. H. Newman, P. Bohley, and C. H. Walter, "Two Methods for Measurement of Antenna Efficiency," *IEEE Trans. Antennas Propagat.*, Vol. AP-23, No. 4, July 1975, pp. 457–461.
5. G. S. Smith, "Radiation Efficiency of Electrically Small Multiturn Loop Antennas," *IEEE Trans. Antennas Propagat.*, Vol. AP-20, No. 5, September 1972, pp. 656–657.
6. G. S. Smith, "The Proximity Effect in Systems of Parallel Conductors," *J. Appl. Phys.*, Vol. 43, No. 5, May 1972, pp. 2196–2203.
7. J. D. Kraus, *Electromagnetics*, 4th ed., McGraw-Hill Book Co., New York, 1992.
8. G. S. Smith, "Loop Antennas," Chapter 5 in *Antenna Engineering Handbook*, 2nd ed., McGraw-Hill Book Co., New York, 1984.
9. J. E. Storer, "Impedance of Thin-Wire Loop Antennas," *AIEE Trans., (Part I. Communication and Electronics)*, Vol. 75, Nov. 1956, pp. 606–619.
10. S. Adachi and Y. Mushiake, "Studies of Large Circular Loop Antenna," *Sci. Rep. Research Institute of Tohoku University (RITU), B*, Vol. 9, No. 2, 1957, pp. 79–103.
11. S. Ito, N. Inagaki, and T. Sekiguchi, "An Investigation of the Array of Circular-Loop Antennas," *IEEE Trans. Antennas Propagat.*, Vol. AP-19, No. 4, July 1971, pp. 469–476.
12. A. Shoamanesh and L. Shafai, "Properties of Coaxial Yagi Loop Arrays," *IEEE Trans. Antennas Propagat.*, Vol. AP-26, No. 4, July 1978, pp. 547–550.
13. A. Shoamanesh and L. Shafai, "Design Data for Coaxial Yagi Array of Circular Loops," *IEEE Trans. Antennas Propagat.*, Vol. AP-27, September 1979, pp. 711–713.
14. D. DeMaw (ed.), *The Radio Amateur's Handbook*, American Radio Relay League, 56th ed., 1979, pp. 20–18.
15. G. N. Watson, *A Treatise on the Theory of Bessel Functions*, Cambridge University Press, London, 1922.
16. S. V. Savov, "An Efficient Solution of a Class of Integrals Arising in Antenna Theory," *IEEE Antennas Propagat. Mag.*, Vol. 44, No. 5, October 2002, pp. 98–101.
17. J. D. Mahony, "Circular Microstrip-Patch Directivity Revisited: An Easily Computable Exact Expression," *IEEE Antennas Propagat. Mag.*, Vol. 45, No. 1, February 2003, pp. 120–122.
18. J. D. Mahony, "A Comment on Q-Type Integrals and Their Use in Expressions for Radiated Power," *IEEE Antennas Propagat. Mag.*, Vol. 45, No. 3, June 2003, pp. 127–138.
19. S. V. Savov, "A Comment on the Radiation Resistance," *IEEE Antennas Propagat. Mag.*, Vol. 45, No. 3, June 2003, p. 129.
20. I. Gradshteyn and I. Ryzhik, *Tables of Integrals, Series and Products*, Academic Press, New York, 1965.
21. J. E. Lindsay, Jr., "A Circular Loop Antenna with Non-Uniform Current Distribution," *IRE Trans. Antennas Propagat.*, Vol. AP-8, No. 4, July 1960, pp. 438–441.
22. E. A. Wolff, *Antenna Analysis*, Wiley, New York, 1966.
23. H. C. Pocklington, "Electrical Oscillations in Wire," Cambridge Philosophical Society Proceedings, London, England, Vol. 9, 1897, p. 324.
24. R. King, "Theory of Antennas Driven from Two-Wire Line," *J. Appl. Phys.*, Vol. 20, 1949, p. 832.
25. D. G. Fink (ed.), *Electronics Engineers' Handbook*, Section 18, "Antennas" (by W. F. Croswell), McGraw-Hill, New York, pp. 18–22.
26. K. Iizuka, R. W. P. King, and C. W. Harrison, Jr., "Self- and Mutual Admittances of Two Identical Circular Loop Antennas in a Conducting Medium and in Air," *IEEE Trans. Antennas Propagat.*, Vol. AP-14, No. 4, July 1966, pp. 440–450.
27. R. E. Collin and F. J. Zucher (eds.), *Antenna Theory Part 2*, Chapter 23 (by J. R. Wait), McGraw-Hill, New York, 1969.

28. J. R. Wait, "Possible Influence of the Ionosphere on the Impedance of a Ground-Based Antenna," *J. Res. Natl. Bur. Std.* (U.S.), Vol. 66D, September–October 1962, pp. 563–569.
29. L. E. Vogler and J. L. Noble, "Curves of Input Impedance Change Due to Ground for Dipole Antennas," U.S. National Bureau of Standards, Monograph 72, January 31, 1964.
30. D. C. Chang, "Characteristics of a Horizontal Circular Loop Antenna over a Multilayered, Dissipative Half-Space," *IEEE Trans. Antennas Propagat.*, Vol. AP-21, No. 6, November 1973, pp. 871–874.
31. R. W. P. King, "Theory of the Center-Driven Square Loop Antenna," *IRE Trans. Antennas Propagat.*, Vol. AP-4, No. 4, July 1956, p. 393.
32. T. Tsukiji and S. Tou, "On Polygonal Loop Antennas," *IEEE Trans. Antennas Propagat.*, Vol. AP-28, No. 4, July 1980, pp. 571–575.
33. M. A. Islam, "A Theoretical Treatment of Low-Frequency Loop Antennas with Permeable Cores," *IEEE Trans. Antennas Propagat.*, Vol. AP-11, No. 2, March 1963, pp. 162–169.
34. V. H. Rumsey and W. L. Weeks, "Electrically Small Ferrite Loaded Loop Antennas," *IRE Convention Rec.*, Vol. 4, Part 1, 1956, pp. 165–170.
35. K. Fujimoto and J. R. James, *Mobile Antenna Systems Handbook*, Artech House, Norwood, MA, 1994.
36. M. A. Jensen and Y. Rahmat-Samii, "Performance Analysis of Antennas for Hand-Held Transceivers Using FDTD," *IEEE Trans. Antennas Propagat.*, Vol. 42, No. 8, August 1994, pp. 1106–1113.
37. M. A. Jensen and Y. Rahmat-Samii, "EM Interaction of Handset Antennas and a Human in Personal Communications," *Proc. IEEE*, Vol. 83, No. 1, January 1995, pp. 7–17.
38. K. D. Katsibas, C. A. Balanis, P. A. Tirkas, and C. R. Birtcher, "Folded Loop Antenna for Mobile Communication Systems," 1996 IEEE Antennas and Propagation Society International Symposium, Baltimore, MD, July 21–26, 1996, pp. 1582–1585.
39. C. A. Balanis, K. D. Katsibas, P. A. Tirkas, and C. R. Birtcher, "Loop Antenna for Mobile and Personal Communication Systems," IEEE International Vehicular Technology Conference (IEEE VTC '97), Phoenix, AZ, May 5–7, 1997.
40. K. D. Katsibas, C. A. Balanis, P. A. Tirkas, and C. R. Birtcher, "Folded Loop Antenna for Mobile Handheld Units," *IEEE Trans. Antennas Propagat.*, Vol. 46, No. 2, February 1998, pp. 260–266.

PROBLEMS

5.1. Derive

(a) (5-18a)–(5-18c) using (5-17) and (3-2a)

(b) (5-19a)–(5-19b) using (5-18a)–(5-18c)

5.2. Write the fields of an infinitesimal linear magnetic dipole of constant current I_m, length l, and positioned along the z-axis. Use the fields of an infinitesimal electric dipole, (4-8a)–(4-10c), and apply the principle of duality. Compare with (5-20a)–(5-20d).

5.3. A circular loop, *of loop radius* $\lambda/30$ *and wire radius* $\lambda/1000$, is used as a transmitting/receiving antenna in a back-pack radio communication system at *10 MHz*. The wire of the loop is made of copper with a conductivity of 5.7×10^7 S/m. Assuming the antenna is *radiating in free space*, determine the

(a) radiation resistance of the loop;

(b) loss resistance of the loop (*assume that its value is the same as if the wire were straight*);

(c) input resistance;

(d) input impedance;

(e) radiation efficiency.

5.4. A small circular loop with a uniform current distribution, and with its classical omnidirectional pattern, is used as a receiving antenna. Determine the maximum directivity (*dimensionless* and *in dB*) using:

(a) Exact method.

(b) An approximate method appropriate for this pattern. Specify the method used.

(c) Another approximate method appropriate for this pattern. Specify the method used.

Hint: *For the approximate methods, the word omnidirectional is a clue*.

5.5. A *N-turn* resonant circular loop *with a uniform current distribution* and with a *circumference of* $\lambda/4$, is fed by a lossless balanced twin-lead transmission line with a characteristic impedance of 300 ohms. *Neglecting proximity effects*, determine the

(a) *closest integer number* of turns so that the input impedance is nearly 300 ohms;

(b) input impedance of the antenna;

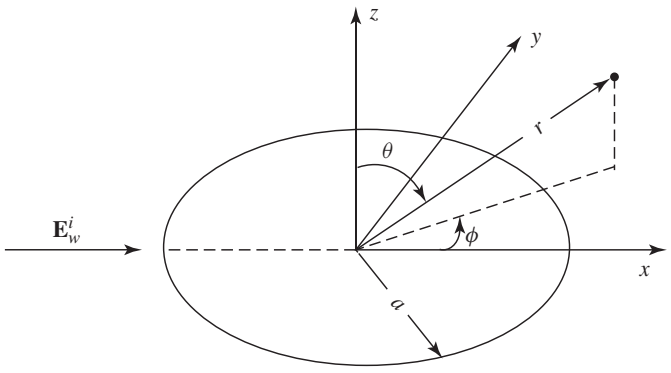
(c) reflection coefficient;

(d) VSWR inside the transmission line.

5.6. A small circular loop with circumference $C < \lambda/20$ is used as a receiving antenna. A uniform plane wave traveling along the x-axis and toward the positive (+) x direction (as shown in the figure), whose electric field is given by

$$\mathbf{E}_w^i = (\hat{\mathbf{a}}_y + \mathbf{2}\hat{\mathbf{a}}_z)e^{-jkx}$$

is incident upon the antenna. Determine the



(a) polarization of the incident wave. Justify your answer.

(b) axial ratio of the polarization ellipse of the incident wave.

(c) polarization of the loop antenna toward the x-axis.

(d) polarization loss factor (*dimensionless* and *in dB*).

(e) maximum power at *1 GHz* that can be delivered to a load connected to the antenna, if the power density of the above incident wave is *5 mwatts/cm*^{2}. Assume no other losses.

Hint: $\hat{\mathbf{a}}_\phi = -\hat{\mathbf{a}}_x \sin\phi + \hat{\mathbf{a}}_y \cos\phi$

5.7. Find the radiation efficiency of a single-turn and a four-turn circular loop each of radius $\lambda/(10\pi)$ and operating at 10 MHz. The radius of the wire is $10^{-3}\lambda$ and the turns are spaced $3 \times 10^{-3}\lambda$ apart. Assume the wire is copper with a conductivity of 5.7×10^7 S/m, and the antenna is radiating into free-space.

5.8. Find the power radiated by a small loop by forming the average power density, using (5-27a)–(5-27c), and integrating over a sphere of radius r. Compare the answer with (5-23b).

5.9. For a small loop of constant current, derive its far-zone fields using (5-17) and the procedure outlined and relationships developed in Section 3.6. Compare the answers with (5-27a)–(5-27c).

5.10. A single-turn resonant circular loop with a $\lambda/8\pi$ radius is made of copper wire with a wire radius of $10^{-4}\lambda/2\pi$ and conductivity of 5.7×10^7 S/m. For a frequency of 100 MHz, determine, *assuming uniform current*, the

(a) radiation efficiency (assume the wire is straight);

(b) *maximum gain* of the antenna (*dimensionless* and *in dB*).

5.11. Design a lossless resonant circular loop operating at 10 MHz so that its single-turn radiation resistance is 0.73 ohms. The resonant loop is to be connected to a matched load through a balanced "twin-lead" 300-ohm transmission line.

(a) Determine the radius of the loop (in meters and wavelengths).

(b) To minimize the matching reflections between the resonant loop and the 300-ohm transmission line, determine the closest number of integer turns the loop must have.

(c) For the loop of part b, determine the maximum power that can be expected to be delivered to a receiver matched load if the incident wave is polarization matched to the lossless resonant loop. The power density of the incident wave is 10^{-6}watts/m^2.

5.12. A resonant six-turn loop of *closely spaced turns* is operating at 50 MHz. The radius of the loop is $\lambda/30$, and the loop is connected to a 50-ohm transmission line. The radius of the wire is $\lambda/300$, its conductivity is $\sigma = 5.7 \times 10^7$ S/m, and the spacing between the turns is $\lambda/100$. Determine the

(a) directivity of the antenna (in dB)

(b) radiation efficiency taking into account the proximity effects of the turns

(c) reflection efficiency

(d) gain of the antenna (in dB)

5.13. Find the radiation efficiency (in percent) of an eight-turn circular-loop antenna operating at 30 MHz. The radius of each turn is $a = 15$ cm, the radius of the wire is $b = 1$ mm, and the spacing between turns is $2c = 3.6$ mm. Assume

EX2042
Page 290 of 1072

the wire is copper ($\sigma = 5.7 \times 10^7$ S/m), and the antenna is radiating into free-space. Account for the *proximity effect*.

5.14. A very small circular loop of radius $a (a < \lambda/6\pi)$ and constant current I_0 is symmetrically placed about the origin at $x = 0$ and with the plane of its area parallel to the y-z plane. Find the

(a) spherical **E**- and **H**-field components radiated by the loop in the far zone

(b) directivity of the antenna

5.15. Repeat Problem 5.14 when the plane of the loop is parallel to the x-z plane at $y = 0$.

5.16. Using the computer program of this chapter, compute the radiation resistance and the directivity of a circular loop of constant current with a radius of

(a) $a = \lambda/50$ (b) $a = \lambda/10$ (c) $a = \lambda/4$ (d) $a = \lambda/2$

5.17. A constant current circular loop of radius $a = 5\lambda/4$ is placed on the x-y plane. Find the *two* smallest angles (excluding $\theta = 0^\circ$) where a null is formed in the far-field pattern.

5.18. Design a circular loop of constant current such that its field intensity vanishes only at $\theta = 0^\circ (\theta = 180^\circ)$ and 90°. Find its

(a) radius

(b) radiation resistance

(c) directivity

5.19. Design a constant current circular loop so that its first minimum, aside from $\theta = 0^\circ$, in its far-field pattern is at 30° from a normal to the plane of the loop. Find the

(a) smallest radius of the antenna (in wavelengths)

(b) relative (to the maximum) radiation intensity (in dB) in the plane of the loop

5.20. Design a constant current circular loop so that its pattern has a null in the plane of the loop, and two nulls above and two nulls below the plane of the loop. Find the

(a) radius of the loop

(b) angles where the nulls occur

5.21. A constant current circular loop is placed on the x-y plane. Find the far-field position, relative to that of the loop, that a linearly polarized probe antenna must have so that the polarization loss factor (PLF) is maximized.

5.22. A very small $(a \ll \lambda)$ circular loop of constant current is placed a distance h above an infinite electric ground plane. Assuming z is perpendicular to the ground plane, find the total far-zone field radiated by the loop when its plane is parallel to the

(a) x-z plane

(b) y-z plane

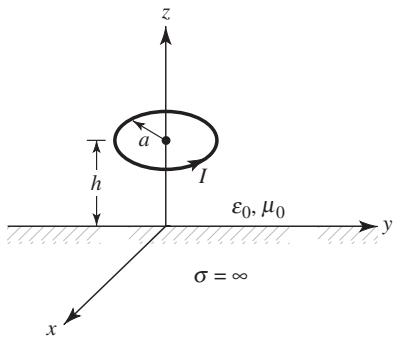
5.23. A very small loop antenna $(a \ll \lambda/30)$ of constant current is placed a height h above a flat, perfectly conducting ground plane of infinite extent. The area plane of the loop is parallel to the interface (x-y plane). For far-field observations

EX2042
Page 291 of 1072

(a) find the total electric field radiated by the loop in the presence of the ground plane

(b) all the angles (in degrees) from the vertical to the interface where the total field will vanish when the height is λ

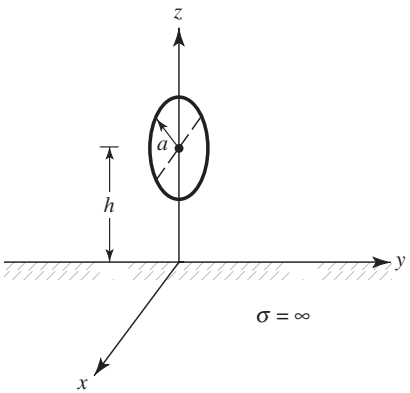
(c) the smallest nonzero height (in λ) such that the total far-zone field exhibits a null at an angle of 60° from the vertical



5.24. A small circular loop, with its area parallel to the *x-z* plane, is placed a height h above an infinite flat perfectly electric conducting ground plane. Determine

(a) the array factor for the equivalent problem which allows you to find the total field on and above the ground plane

(b) angle(s) θ (in degrees) where the array factor will vanish when the loop is placed at a height $\lambda/2$ above the ground plane



5.25. A small circular loop with its area parallel to the x-z plane is placed at a height h above an infinite perfectly conducting ground plane, as shown in the figure for Problem 5.24. Determine the

(a) array factor for the equivalent problem which will allow you to find the total field *on and above* the ground plane.

(b) two *smallest* heights h (*in* λ) *greater than* $h = 0$ (i.e., $h > 0$) that will form a maximum on the magnitude of the array factor toward $\theta = 0^\circ$.

5.26. For the loop of Problem 5.22(a), find the smallest height h so that a null is formed in the *y-z* plane at an angle of 45° above the ground plane.

5.27. A small single-turn circular loop of radius $a = 0.05\lambda$ is operating at 300 MHz. Assuming the radius of the wire is $10^{-4}\lambda$, determine the

EX2042
Page 292 of 1072

(a) loss resistance

(b) radiation resistance

(c) loop inductance

Show that the loop inductive reactance is much greater than the loss resistance and radiation resistance indicating that a small loop acts primarily as an inductor.

5.28. Determine the radiation resistance of a single-turn small loop, assuming the geometrical shape of the loop is

(a) rectangular with dimensions a and b $(a, b \ll \lambda)$

(b) elliptical with major axis a and minor axis b $(a, b, \ll \lambda)$

5.29. A one-turn small circular loop is used as a radiating element for a VHF ($f =$ 100 MHz) communications system. The loop is constructed out of a perfect electric conducting wire. The circumference of the loop is $C = \lambda/20$ while the radius of the wire is $\lambda/400$. Determine, using $\sigma = 5.7 \times 10^7$ S/m, the

(a) input resistance of the wire for a single turn.

(b) input reactance of the loop. *Is it inductive or capacitive? Be specific*.

(c) inductance (*in henries*) or capacitance (*in farads*) that can be placed *in series* with the loop at the feed to resonate the antenna at $f = 100$ MHz; choose the element that will accomplish the desired objective.

5.30. Show that for the rectangular loop the radiation resistance is represented by

$$R_r = 31{,}171\left(\frac{a^2b^2}{\lambda^4}\right)$$

while for the elliptical loop is represented by

$$R_r = 31{,}171\left(\frac{\pi^2a^2b^2}{16\lambda^4}\right)$$

5.31 Assuming the direction of the magnetic field of the incident plane wave coincides with the plane of incidence, derive the effective length of a small circular loop of radius a based on the definition of (2-92). Show that its effective length is

$$\boldsymbol{\ell}_e = \hat{\mathbf{a}}_\phi jkS\sin(\theta)$$

where $S = \pi a^2$.

5.32. A circular loop of nonconstant current distribution, with circumference of 1.4λ, is attached to a 300-ohm line. Assuming the radius of the wire is $1.555 \times 10^{-2}\lambda$, find the

(a) input impedance of the loop

(b) VSWR of the system

(c) inductance or capacitance that must be placed across the feed points so that the loop becomes resonant at $f = 100$ MHz.

5.33. A very popular antenna for amateur radio operators is a square loop antenna (referred to as *quad antenna*) whose circumference is one wavelength. Assuming the radiation characteristics of the square loop are well represented by those of a circular loop:

(a) What is the input impedance (real and imaginary parts) of the antenna?

(b) What element (inductor or capacitor), and of what value, must be placed in series with the loop at the feed point to resonate the radiating element at a frequency of 1 GHz?

(c) What is the input VSWR, having the inductor or capacitor in place, if the loop is connected to a 78-ohm coaxial cable?

5.34. Design circular loops of wire radius b, which resonate at the first resonance. Find

(a) four values of a/b where the first resonance occurs (a is the radius of the loop)

(b) the circumference of the loops and the corresponding radii of the wires for the antennas of part (a).

5.35. Using the asymptotic form of (5-59b) for small argument, show that the radiation resistance of (5-64a) for a small loop of uniform current is given by

$$R_r = 20\pi^2(ka)^4 = 20\pi^2\left(\frac{C}{\lambda}\right)^4$$

5.36. Consider a circular loop of wire of radius a on the x-y plane and centered about the origin. Assume the current on the loop is given by

$$I_\phi(\phi') = I_0\cos(\phi')$$

(a) Show that the far-zone electric field of the loop is given by

$$E_\theta = \frac{j\eta ka}{2} I_0 \frac{e^{-jkr}}{r} \frac{J_1(ka\sin\theta)}{ka\sin\theta}\cos\theta\sin\phi$$

$$E_\phi = \frac{j\eta ka}{2} I_0 \frac{e^{-jkr}}{r} J_1{}'(ka\sin\theta)\cos\phi$$

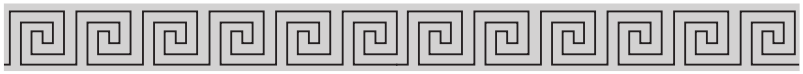
where

$$J_1{}'(x) = \frac{dJ_1(x)}{dx}$$

(b) Evaluate the radiation intensity $U(\theta, \phi)$ in the direction $\theta = 0$ and $\phi = \frac{\pi}{2}$ as a function of ka.

EX2042
Page 294 of 1072

CHAPTER 6



Arrays: Linear, Planar, and Circular

6.1 INTRODUCTION

In the previous chapter, the radiation characteristics of single-element antennas were discussed and analyzed. Usually the radiation pattern of a single element is relatively wide, and each element provides low values of directivity (gain). In many applications it is necessary to design antennas with very directive characteristics (very high gains) to meet the demands of long distance communication. This can only be accomplished by increasing the electrical size of the antenna.

Enlarging the dimensions of single elements often leads to more directive characteristics. Another way to enlarge the dimensions of the antenna, without necessarily increasing the size of the individual elements, is to form an assembly of radiating elements in an electrical and geometrical configuration. This new antenna, formed by multielements, is referred to as an *array*. In most cases, the elements of an array are identical. This is not necessary, but it is often convenient, simpler, and more practical. The individual elements of an array may be of any form (wires, apertures, etc.).

The total field of the array is determined by the vector addition of the fields radiated by the individual elements. This assumes that the current in each element is the same as that of the isolated element (neglecting coupling). This is usually not the case and depends on the separation between the elements. To provide very directive patterns, it is necessary that the fields from the elements of the array interfere constructively (add) in the desired directions and interfere destructively (cancel each other) in the remaining space. Ideally this can be accomplished, but practically it is only approached. In an array of identical elements, there are at least five controls that can be used to shape the overall pattern of the antenna. These are:

1. the geometrical configuration of the overall array (linear, circular, rectangular, spherical, etc.)
2. the relative displacement between the elements
3. the excitation amplitude of the individual elements
4. the excitation phase of the individual elements
5. the relative pattern of the individual elements

Antenna Theory: Analysis Design, Third Edition, by Constantine A. Balanis
ISBN 0-471-66782-X Copyright © 2005 John Wiley & Sons, Inc.

EX2042
Page 295 of 1072

The influence that each one of the above has on the overall radiation characteristics will be the subject of this chapter. In many cases the techniques will be illustrated with examples.

There are a plethora of antenna arrays used for personal, commercial, and military applications utilizing different elements including dipoles, loops, apertures, microstrips, horns, reflectors, and so on. Arrays of dipoles are shown in Figures 4.21, 10.19, and 11.12. The one in Figure 4.21 is an array that is widely used as a base-station antenna for mobile communication. It is a triangular array consisting of twelve dipoles, with four dipoles on each side of the triangle. Each four-element array, on each side of the triangle, is basically used to cover an angular sector of 120° forming what is usually referred to as a *sectoral array*. The one in Figure 10.19 is a classic array of dipoles, referred to as the *Yagi-Uda* array, and it is primarily used for TV and amateur radio applications. The array of Figure 11.12 is also an array of dipoles, which is referred to as the *log-periodic* antenna, which is primarily used for TV reception and has wider bandwidth than the Yagi-Uda array but slightly smaller directivity. An array of loops is shown in Figure 5.1 and one utilizing microstrips as elements is displayed in Figure 14.35. An advanced array design of slots, used in the AWACS, is shown in Figure 6.27.

The simplest and one of the most practical arrays is formed by placing the elements along a line. To simplify the presentation and give a better physical interpretation of the techniques, a two-element array will first be considered. The analysis of an N-element array will then follow. Two-dimensional analysis will be the subject at first. In latter sections, three-dimensional techniques will be introduced.

6.2 TWO-ELEMENT ARRAY

Let us assume that the antenna under investigation is an array of two infinitesimal horizontal dipoles positioned along the z-axis, as shown in Figure 6.1(a). The total field radiated by the two elements, *assuming no coupling between the elements*, is equal to the sum of the two and in the y-z plane it is given by

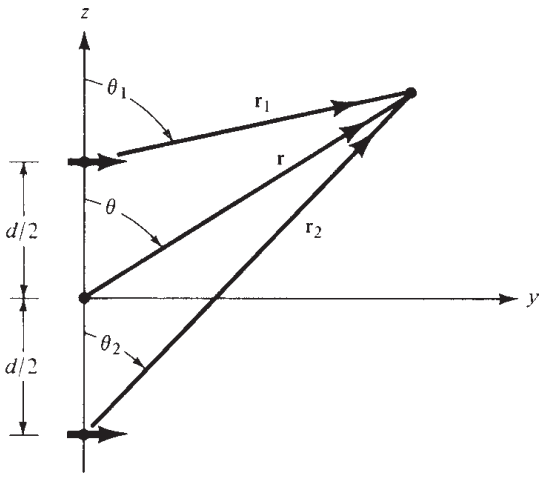
$$\mathbf{E}_t = \mathbf{E}_1 + \mathbf{E}_2 = \hat{\mathbf{a}}_\theta \, j\eta \frac{kI_0 l}{4\pi} \left\{ \frac{e^{-j[kr_1 - (\beta/2)]}}{r_1} \cos\theta_1 + \frac{e^{-j[kr_2 + (\beta/2)]}}{r_2} \cos\theta_2 \right\} \tag{6-1}$$

where β is the difference in phase excitation between the elements. The magnitude excitation of the radiators is identical. Assuming far-field observations and referring to Figure 6.1(b),

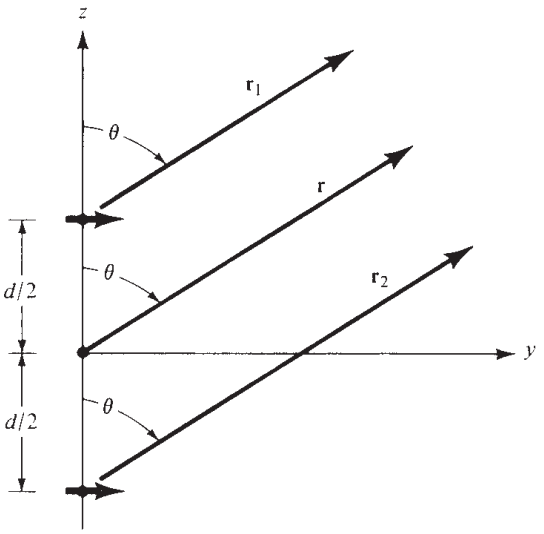
$$\theta_1 \simeq \theta_2 \simeq \theta \tag{6-2a}$$

$$\left.\begin{aligned} r_1 &\simeq r - \frac{d}{2}\cos\theta \\ r_2 &\simeq r + \frac{d}{2}\cos\theta \end{aligned}\right\} \quad \text{for phase variations} \tag{6-2b}$$

$$r_1 \simeq r_2 \simeq r \qquad \text{for amplitude variations} \tag{6-2c}$$



(a) Two infinitesimal dipoles



(b) Far-field observations

Figure 6.1 Geometry of a two-element array positioned along the z-axis.

Equation 6-1 reduces to

$$\mathbf{E}_t = \hat{\mathbf{a}}_\theta j\eta \frac{kI_0 l e^{-jkr}}{4\pi r} \cos\theta [e^{+j(kd\cos\theta+\beta)/2} + e^{-j(kd\cos\theta+\beta)/2}]$$

$$\mathbf{E}_t = \hat{\mathbf{a}}_\theta j\eta \frac{kI_0 l e^{-jkr}}{4\pi r} \cos\theta \left\{2\cos\left[\frac{1}{2}(kd\cos\theta+\beta)\right]\right\} \tag{6-3}$$

It is apparent from (6-3) that the total field of the array is equal to the field of a single element positioned at the origin multiplied by a factor which is widely referred to as the *array factor*. Thus for the two-element array of constant amplitude, the array factor is given by

$$\text{AF} = 2\cos[\tfrac{1}{2}(kd\cos\theta+\beta)] \tag{6-4}$$

which in normalized form can be written as

$$(\text{AF})_n = \cos[\tfrac{1}{2}(kd\cos\theta + \beta)] \tag{6-4a}$$

The array factor is a function of the geometry of the array and the excitation phase. By varying the separation d and/or the phase β between the elements, the characteristics of the array factor and of the total field of the array can be controlled.

It has been illustrated that the far-zone field of a uniform two-element array of identical elements is equal to the *product of the field of a single element, at a selected reference point (usually the origin), and the array factor of that array*. That is,

$$\boxed{\mathbf{E}(\text{total}) = [\mathbf{E}(\text{single element at reference point})] \times [\text{array factor}]} \tag{6-5}$$

This is referred to as *pattern multiplication* for arrays of identical elements, and it is analogous to the pattern multiplication of (4-59) for continuous sources. Although it has been illustrated only for an array of two elements, each of identical magnitude, it is also valid for arrays with any number of identical elements which do not necessarily have identical magnitudes, phases, and/or spacings between them. This will be demonstrated in this chapter by a number of different arrays.

Each array has its own array factor. The array factor, in general, is a function of the number of elements, their geometrical arrangement, their relative magnitudes, their relative phases, and their spacings. The array factor will be of simpler form if the elements have identical amplitudes, phases, and spacings. Since the array factor does not depend on the directional characteristics of the radiating elements themselves, it can be formulated by replacing the actual elements with isotropic (point) sources. Once the array factor has been derived using the point-source array, the total field of the actual array is obtained by the use of (6-5). Each point-source is assumed to have the amplitude, phase, and location of the corresponding element it is replacing.

In order to synthesize the total pattern of an array, the designer is not only required to select the proper radiating elements but the geometry (positioning) and excitation of the individual elements. To illustrate the principles, let us consider some examples.

Example 6.1

Given the array of Figures 6.1(a) and (b), find the nulls of the total field when $d = \lambda/4$ and

a. $\beta = 0$
b. $\beta = +\dfrac{\pi}{2}$
c. $\beta = -\dfrac{\pi}{2}$

Solution:

a. $\beta = 0$

The normalized field is given by

$$E_{tn} = \cos\theta \cos\left(\frac{\pi}{4}\cos\theta\right)$$

The nulls are obtained by setting the total field equal to zero, or

$$E_{tn} = \cos\theta \cos\left(\frac{\pi}{4}\cos\theta\right)|_{\theta=\theta_n} = 0$$

Thus

$$\cos\theta_n = 0 \Rightarrow \theta_n = 90^\circ$$

and

$$\cos\left(\frac{\pi}{4}\cos\theta_n\right) = 0 \Rightarrow \frac{\pi}{4}\cos\theta_n = \frac{\pi}{2}, -\frac{\pi}{2} \Rightarrow \theta_n = \text{does not exist}$$

The only null occurs at $\theta = 90^\circ$ and is due to the pattern of the individual elements. The array factor does not contribute any additional nulls because there is not enough separation between the elements to introduce a phase difference of 180° between the elements, for any observation angle.

b. $\beta = +\dfrac{\pi}{2}$

The normalized field is given by

$$E_{tn} = \cos\theta \cos\left[\frac{\pi}{4}(\cos\theta + 1)\right]$$

The nulls are found from

$$E_{tn} = \cos\theta \cos\left[\frac{\pi}{4}(\cos\theta + 1)\right]|_{\theta=\theta_n} = 0$$

Thus

$$\cos\theta_n = 0 \Rightarrow \theta_n = 90^\circ$$

and

$$\cos\left[\frac{\pi}{4}(\cos\theta + 1)\right]|_{\theta=\theta_n} = 0 \Rightarrow \frac{\pi}{4}(\cos\theta_n + 1) = \frac{\pi}{2} \Rightarrow \theta_n = 0^\circ$$

and

$$\Rightarrow \frac{\pi}{4}(\cos\theta_n + 1) = -\frac{\pi}{2} \Rightarrow \theta_n = \text{does not exist}$$

The nulls of the array occur at $\theta = 90^\circ$ and 0°. The null at 0° is introduced by the arrangement of the elements (array factor). This can also be shown by physical reasoning, as shown in Figure 6.2(a). The element in the negative z-axis has an initial phase lag of 90° relative to the other element. As the wave from that element travels toward the positive z-axis ($\theta = 0^\circ$ direction), it undergoes an additional 90° phase retardation when it arrives at the other element on the positive z-axis. Thus there is a total of 180° phase difference between the waves of the two elements when travel is toward the positive z-axis ($\theta = 0^\circ$). The waves

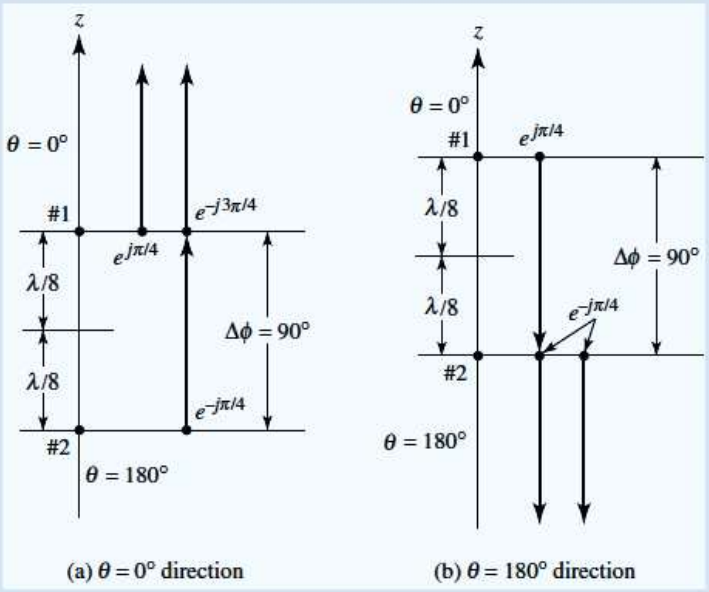


Figure 6.2 Phase accumulation for two-element array for null formation toward $\theta = 0°$ and 180°.

of the two elements are in phase when they travel in the negative z-axis ($\theta = 180°$), as shown in Figure 6.2(b).

c. $\beta = -\dfrac{\pi}{2}$

The normalized field is given by

$$E_{tn} = \cos\theta \cos\left[\frac{\pi}{4}(\cos\theta - 1)\right]$$

and the nulls by

$$E_{tn} = \cos\theta \cos\left[\frac{\pi}{4}(\cos\theta - 1)\right]|_{\theta=\theta_n} = 0$$

Thus

$$\cos\theta_n = 0 \Rightarrow \theta_n = 90°$$

and

$$\cos\left[\frac{\pi}{4}(\cos\theta_n - 1)\right] = 0 \Rightarrow \frac{\pi}{4}(\cos\theta_n - 1) = \frac{\pi}{2} \Rightarrow \theta_n = \text{does not exist}$$

and

$$\Rightarrow \frac{\pi}{4}(\cos\theta_n - 1) = -\frac{\pi}{2} \Rightarrow \theta_n = 180°$$

The nulls occur at 90° and 180°. The element at the positive z-axis has a phase lag of 90° relative to the other, and the phase difference is 180° when travel is restricted toward the negative z-axis. There is no phase difference when the waves travel toward the positive z-axis. A diagram similar to that of Figure 6.2 can be used to illustrate this case.

To better illustrate the pattern multiplication rule, the normalized patterns of the single element, the array factor, and the total array for each of the above array examples are shown in Figures 6.3, 6.4(a), and 6.4(b). In each figure, the total pattern of the array is obtained by multiplying the pattern of the single element by that of the array factor. *In each case, the pattern is normalized to its own maximum.* Since the array factor for the example of Figure 6.3 is nearly isotropic (within 3 dB), the element pattern and the total pattern are almost identical in shape. The largest magnitude difference between the two is about 3 dB, and for each case it occurs toward the direction along which the phases of the two elements are in phase quadrature (90° out of phase). For Figure 6.3 this occurs along $\theta = 0^\circ$ while for Figures 6.4(a,b) this occurs along $\theta = 90^\circ$. Because the array factor for Figure 6.4(a) is of cardioid form, its corresponding element and total patterns are considerably different. In the total pattern, the null at $\theta = 90^\circ$ is due to the element pattern while that toward $\theta = 0^\circ$ is due to the array factor. Similar results are displayed in Figure 6.4(b).

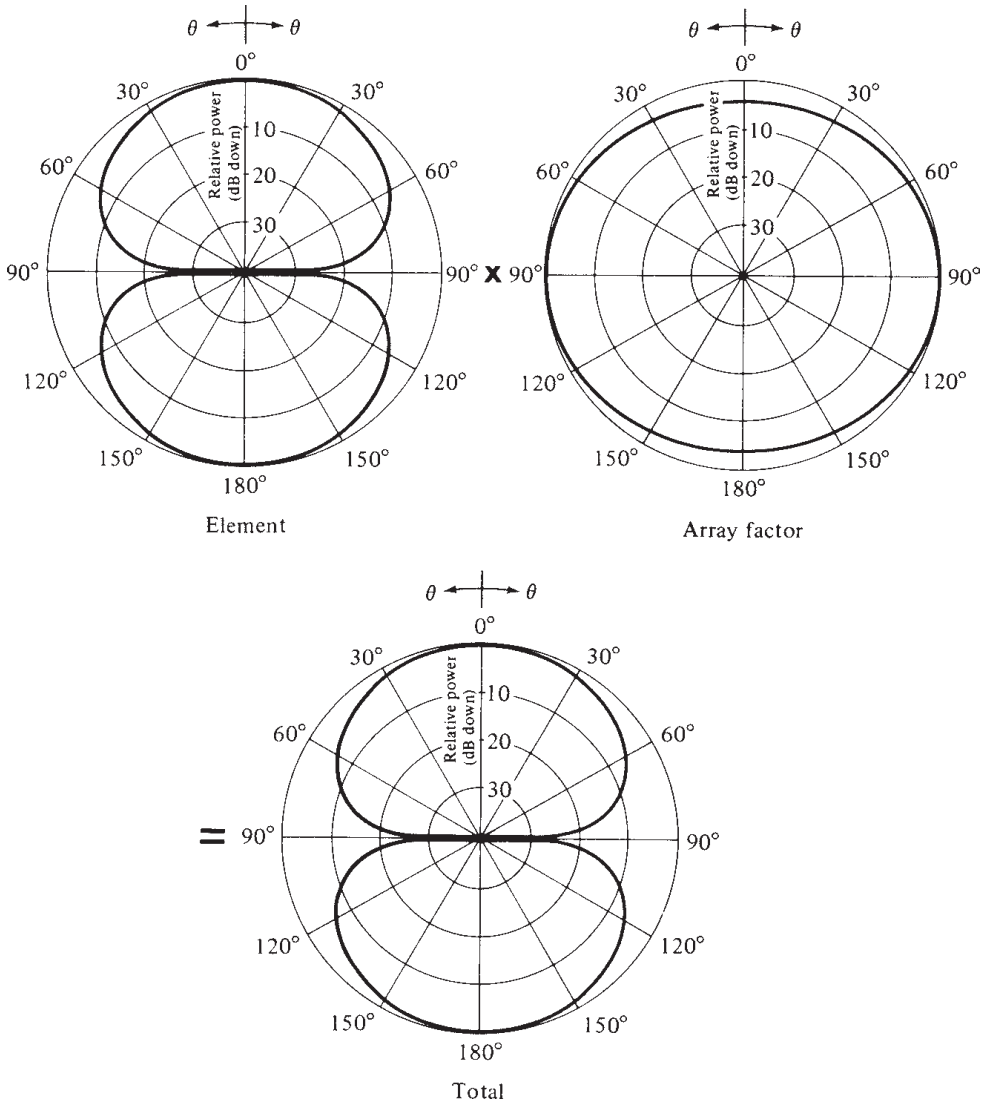


Figure 6.3 Element, array factor, and total field patterns of a two-element array of infinitesimal horizontal dipoles with identical phase excitation ($\beta = 0^\circ, d = \lambda/4$).

Example 6.2

Consider an array of two identical infinitesimal dipoles oriented as shown in Figures 6.1(a) and (b). For a separation d and phase excitation difference β between the elements, find the angles of observation where the nulls of the array occur. The magnitude excitation of the elements is the same.

Solution: The normalized total field of the array is given by (6-3) as

$$E_{tn} = \cos\theta \cos[\tfrac{1}{2}(kd\cos\theta + \beta)]$$

To find the nulls, the field is set equal to zero, or

$$E_{tn} = \cos\theta \cos[\tfrac{1}{2}(kd\cos\theta + \beta)]|_{\theta=\theta_n} = 0$$

Thus

$$\cos\theta_n = 0 \Rightarrow \theta_n = 90^\circ$$

and

$$\cos\left[\frac{1}{2}(kd\cos\theta_n + \beta)\right] = 0 \Rightarrow \frac{1}{2}(kd\cos\theta_n + \beta) = \pm\left(\frac{2n+1}{2}\right)\pi$$

$$\Rightarrow \theta_n = \cos^{-1}\left(\frac{\lambda}{2\pi d}[-\beta \pm (2n+1)\pi]\right),$$

$$n = 0, 1, 2, \ldots$$

The null at $\theta = 90^\circ$ is attributed to the pattern of the individual elements of the array while the remaining ones are due to the formation of the array. For no phase difference between the elements ($\beta = 0$), the separation d must be equal or greater than half a wavelength ($d \geq \lambda/2$) in order for at least one null, due to the array, to occur.

6.3 *N*-ELEMENT LINEAR ARRAY: UNIFORM AMPLITUDE AND SPACING

Now that the arraying of elements has been introduced and it was illustrated by the two-element array, let us generalize the method to include N elements. Referring to the geometry of Figure 6.5(a), let us assume that all the elements have identical amplitudes but each succeeding element has a β progressive phase lead current excitation relative to the preceding one (β represents the phase by which the current in each element leads the current of the preceding element). *An array of identical elements all of identical magnitude and each with a progressive phase is referred to as a uniform array*. The array factor can be obtained by considering the elements to be point sources. If the actual elements are not isotropic sources, the total field can be formed by multiplying the array factor of the isotropic sources by the field of a single element. This is the pattern multiplication rule of (6-5), and it applies only for arrays of identical elements.

The array factor is given by

$$\text{AF} = 1 + e^{+j(kd\cos\theta+\beta)} + e^{+j2(kd\cos\theta+\beta)} + \cdots + e^{j(N-1)(kd\cos\theta+\beta)}$$

$$\text{AF} = \sum_{n=1}^{N} e^{j(n-1)(kd\cos\theta+\beta)} \tag{6-6}$$

which can be written as

$$\boxed{\text{AF} = \sum_{n=1}^{N} e^{j(n-1)\psi}} \tag{6-7}$$

$$\text{where} \quad \psi = kd\cos\theta + \beta \tag{6-7a}$$

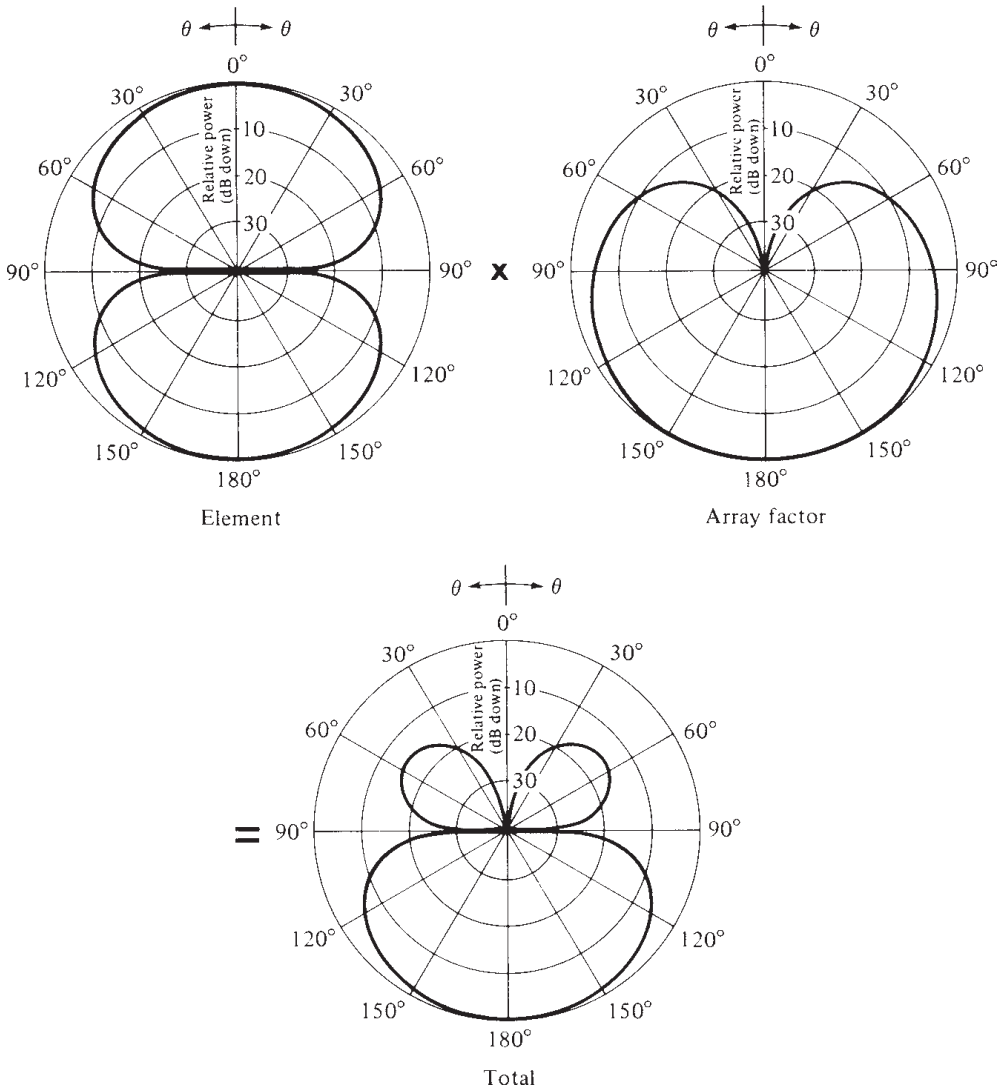


Figure 6.4 Pattern multiplication of element, array factor, and total array patterns of a two-element array of infinitesimal horizontal dipoles with (a) $\beta = +90°$, $d = \lambda/4$.

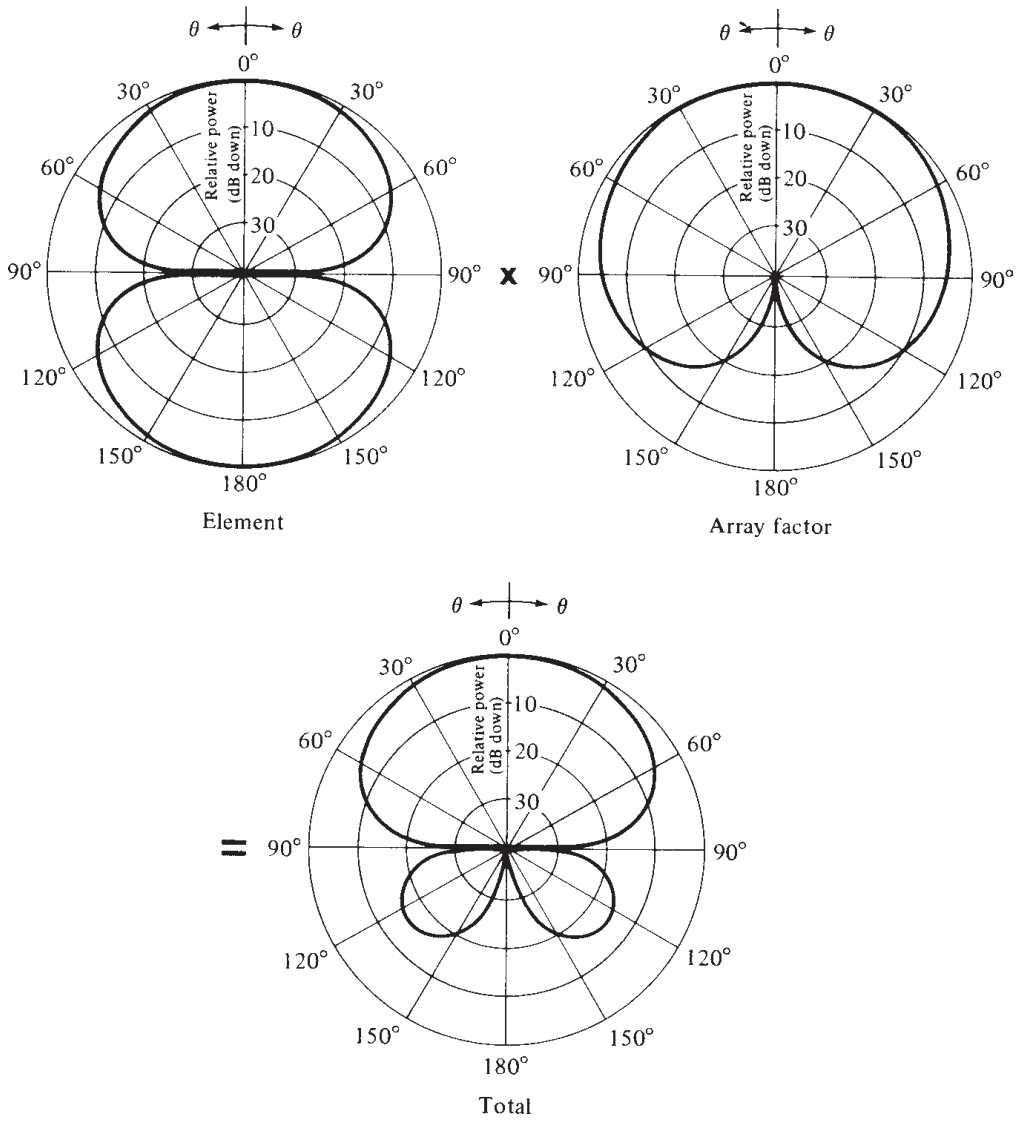


Figure 6.4 (b) $\beta = -90^\circ$, $d = \lambda/4$ (*continued*).

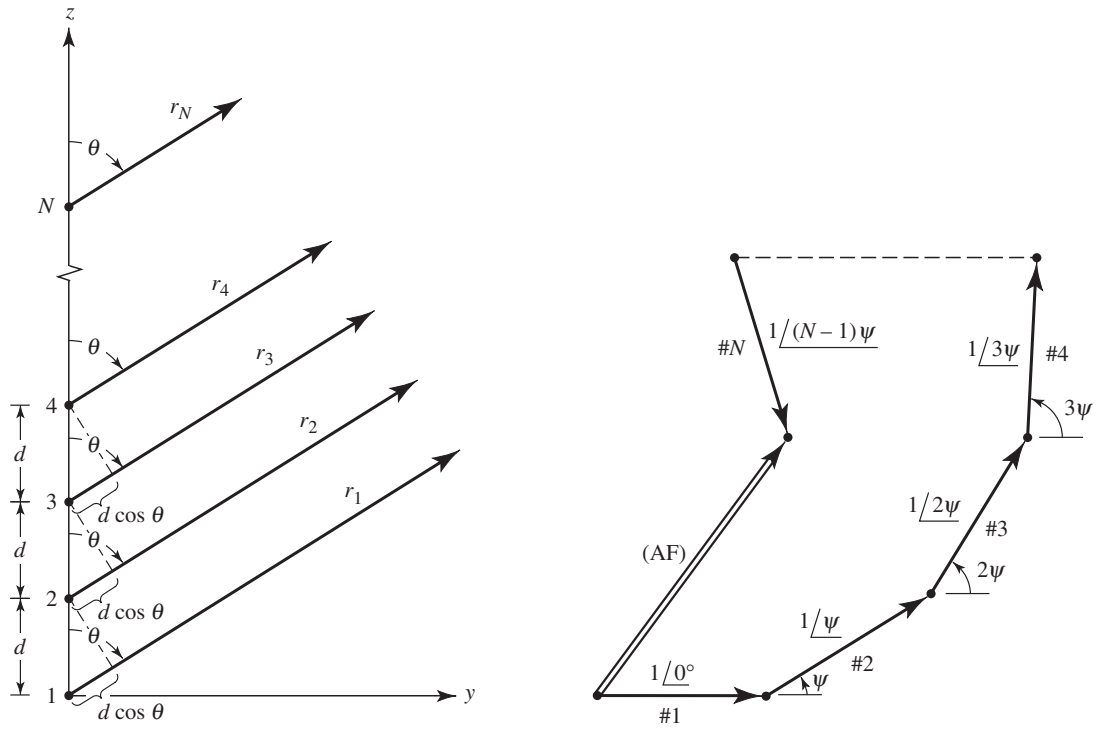
Since the total array factor for the uniform array is a summation of exponentials, it can be represented by the vector sum of N phasors each of unit amplitude and progressive phase ψ relative to the previous one. Graphically this is illustrated by the phasor diagram in Figure 6.5(b). It is apparent from the phasor diagram that the amplitude and phase of the AF can be controlled in uniform arrays by properly selecting the relative phase ψ between the elements; in nonuniform arrays, the amplitude as well as the phase can be used to control the formation and distribution of the total array factor.

The array factor of (6-7) can also be expressed in an alternate, compact and closed form whose functions and their distributions are more recognizable. This is accomplished as follows.

Multiplying both sides of (6-7) by $e^{j\psi}$, it can be written as

$$(\text{AF})e^{j\psi} = e^{j\psi} + e^{j2\psi} + e^{j3\psi} + \cdots + e^{j(N-1)\psi} + e^{jN\psi} \tag{6-8}$$

EX2042
Page 304 of 1072



(a) Geometry (b) Phasor diagram

Figure 6.5 Far-field geometry and phasor diagram of N-element array of isotropic sources positioned along the z-axis.

Subtracting (6-7) from (6-8) reduces to

$$\text{AF}(e^{j\psi} - 1) = (-1 + e^{jN\psi}) \tag{6-9}$$

which can also be written as

$$\begin{aligned} \text{AF} &= \left[\frac{e^{jN\psi} - 1}{e^{j\psi} - 1}\right] = e^{j[(N-1)/2]\psi}\left[\frac{e^{j(N/2)\psi} - e^{-j(N/2)\psi}}{e^{j(1/2)\psi} - e^{-j(1/2)\psi}}\right] \\ &= e^{j[(N-1)/2]\psi}\left[\frac{\sin\left(\frac{N}{2}\psi\right)}{\sin\left(\frac{1}{2}\psi\right)}\right] \end{aligned} \tag{6-10}$$

If the reference point is the physical center of the array, the array factor of (6-10) reduces to

$$\text{AF} = \left[\frac{\sin\left(\frac{N}{2}\psi\right)}{\sin\left(\frac{1}{2}\psi\right)}\right] \tag{6-10a}$$

For small values of ψ, the above expression can be approximated by

$$\text{AF} \simeq \left[\frac{\sin\left(\frac{N}{2}\psi\right)}{\frac{\psi}{2}} \right] \tag{6-10b}$$

The maximum value of (6-10a) or (6-10b) is equal to N. To normalize the array factors so that the maximum value of each is equal to unity, (6-10a) and (6-10b) are written in normalized form as (see Appendix II)

$$\boxed{(\text{AF})_n = \frac{1}{N}\left[\frac{\sin\left(\frac{N}{2}\psi\right)}{\sin\left(\frac{1}{2}\psi\right)} \right]} \tag{6-10c}$$

and (see Appendix I)

$$\boxed{(\text{AF})_n \simeq \left[\frac{\sin\left(\frac{N}{2}\psi\right)}{\frac{N}{2}\psi} \right]} \tag{6-10d}$$

To find the nulls of the array, (6-10c) or (6-10d) is set equal to zero. That is,

$$\sin\left(\frac{N}{2}\psi\right) = 0 \Rightarrow \frac{N}{2}\psi|_{\theta=\theta_n} = \pm n\pi \Rightarrow \theta_n = \cos^{-1}\left[\frac{\lambda}{2\pi d}\left(-\beta \pm \frac{2n}{N}\pi\right)\right] \tag{6-11}$$

$$n = 1, 2, 3, \ldots$$

$$n \neq N, 2N, 3N, \ldots \text{ with (6-10c)}$$

For $n = N, 2N, 3N, \ldots$, (6-10c) attains its maximum values because it reduces to a sin(0)/0 form. The values of n determine the order of the nulls (first, second, etc.). For a zero to exist, the argument of the arccosine cannot exceed unity. Thus the number of nulls that can exist will be a function of the element separation d and the phase excitation difference β.

The maximum values of (6-10c) occur when

$$\frac{\psi}{2} = \frac{1}{2}(kd\cos\theta + \beta)|_{\theta=\theta_m} = \pm m\pi \Rightarrow \theta_m = \cos^{-1}\left[\frac{\lambda}{2\pi d}(-\beta \pm 2m\pi)\right] \tag{6-12}$$

$$m = 0, 1, 2, \ldots$$

The array factor of (6-10d) has only one maximum and occurs when $m = 0$ in (6-12). That is,

$$\theta_m = \cos^{-1}\left(\frac{\lambda\beta}{2\pi d}\right) \tag{6-13}$$

which is the observation angle that makes $\psi = 0$.

The 3-dB point for the array factor of (6-10d) occurs when (see Appendix I)

$$\frac{N}{2}\psi = \frac{N}{2}(kd\cos\theta + \beta)|_{\theta=\theta_h} = \pm 1.391$$

$$\Rightarrow \theta_h = \cos^{-1}\left[\frac{\lambda}{2\pi d}\left(-\beta \pm \frac{2.782}{N}\right)\right] \tag{6-14}$$

which can also be written as

$$\theta_h = \frac{\pi}{2} - \sin^{-1}\left[\frac{\lambda}{2\pi d}\left(-\beta \pm \frac{2.782}{N}\right)\right] \tag{6-14a}$$

For large values of $d (d \gg \lambda)$, it reduces to

$$\theta_h \simeq \left[\frac{\pi}{2} - \frac{\lambda}{2\pi d}\left(-\beta \pm \frac{2.782}{N}\right)\right] \tag{6-14b}$$

The half-power beamwidth Θ_h can be found once the angles of the first maximum (θ_m) and the half-power point (θ_h) are determined. For a symmetrical pattern

$$\Theta_h = 2|\theta_m - \theta_h| \tag{6-14c}$$

For the array factor of (6-10d), there are secondary maxima (maxima of minor lobes) which occur *approximately* when the numerator of (6-10d) attains its maximum value. That is,

$$\sin\left(\frac{N}{2}\psi\right) = \sin\left[\frac{N}{2}(kd\cos\theta + \beta)\right]|_{\theta=\theta_s} \simeq \pm 1 \Rightarrow \frac{N}{2}(kd\cos\theta + \beta)|_{\theta=\theta_s}$$

$$\simeq \pm\left(\frac{2s+1}{2}\right)\pi \Rightarrow \theta_s \simeq \cos^{-1}\left\{\frac{\lambda}{2\pi d}\left[-\beta \pm \left(\frac{2s+1}{N}\right)\pi\right]\right\},$$

$$s = 1, 2, 3, \ldots \tag{6-15}$$

which can also be written as

$$\theta_s \simeq \frac{\pi}{2} - \sin^{-1}\left\{\frac{\lambda}{2\pi d}\left[-\beta \pm \left(\frac{2s+1}{N}\right)\pi\right]\right\}, \quad s = 1, 2, 3, \ldots \tag{6-15a}$$

For large values of $d (d \gg \lambda)$, it reduces to

$$\theta_s \simeq \frac{\pi}{2} - \frac{\lambda}{2\pi d}\left[-\beta \pm \left(\frac{2s+1}{N}\right)\pi\right], \quad s = 1, 2, 3, \ldots \tag{6-15b}$$

The maximum of the first minor lobe of (6-10c) occurs *approximately* when (see Appendix I)

$$\frac{N}{2}\psi = \frac{N}{2}(kd\cos\theta + \beta)|_{\theta=\theta_s} \simeq \pm\left(\frac{3\pi}{2}\right) \tag{6-16}$$

or when

$$\theta_s = \cos^{-1}\left\{\frac{\lambda}{2\pi d}\left[-\beta \pm \frac{3\pi}{N}\right]\right\} \tag{6-16a}$$

At that point, the magnitude of (6-10d) reduces to

$$(\mathrm{AF})_n \simeq \left[\frac{\sin\left(\frac{N}{2}\psi\right)}{\frac{N}{2}\psi}\right]_{\substack{\theta=\theta_s \\ s=1}} = \frac{2}{3\pi} = 0.212 \tag{6-17}$$

which in dB is equal to

$$(\mathrm{AF})_n = 20\log_{10}\left(\frac{2}{3\pi}\right) = -13.46 \text{ dB} \tag{6-17a}$$

Thus the maximum of the first minor lobe of the array factor of (6-10d) is 13.46 dB down from the maximum at the major lobe. More accurate expressions for the angle, beamwidth, and magnitude of first minor lobe of the array factor of (6-10d) can be obtained. These will be discussed in Chapter 12.

6.3.1 Broadside Array

In many applications it is desirable to have the maximum radiation of an array directed normal to the axis of the array [broadside; $\theta_0 = 90^\circ$ of Figure 6.5(a)]. To optimize the design, the maxima of the single element and of the array factor should both be directed toward $\theta_0 = 90^\circ$. The requirements of the single elements can be accomplished by the judicious choice of the radiators, and those of the array factor by the proper separation and excitation of the individual radiators. In this section, the requirements that allow the array factor to "radiate" efficiently broadside will be developed.

Referring to (6-10c) or (6-10d), the first maximum of the array factor occurs when

$$\psi = kd\cos\theta + \beta = 0 \tag{6-18}$$

Since it is desired to have the first maximum directed toward $\theta_0 = 90^\circ$, then

$$\boxed{\psi = kd\cos\theta + \beta|_{\theta=90^\circ} = \beta = 0} \tag{6-18a}$$

Thus to have the maximum of the array factor of a uniform linear array directed broadside to the axis of the array, it is necessary that all the elements have the same phase excitation (in addition to the same amplitude excitation). The separation between the elements can be of any value. To ensure that there are no principal maxima in other directions, which are referred to as *grating lobes*, the separation between the elements

should not be equal to multiples of a wavelength ($d \neq n\lambda$, $n = 1, 2, 3 \ldots$) when $\beta = 0$. If $d = n\lambda$, $n = 1, 2, 3, \ldots$ and $\beta = 0$, then

$$\psi = kd\cos\theta + \beta\big|_{\substack{d=n\lambda \\ \beta=0 \\ n=1,2,3,\ldots}} = 2\pi n\cos\theta\big|_{\theta=0^\circ,180^\circ} = \pm 2n\pi \tag{6-19}$$

This value of ψ when substituted in (6-10c) makes the array factor attain its maximum value. Thus for a uniform array with $\beta = 0$ and $d = n\lambda$, in addition to having the maxima of the array factor directed broadside ($\theta_0 = 90^\circ$) to the axis of the array, there are additional maxima directed along the axis ($\theta_0 = 0^\circ, 180^\circ$) of the array (end-fire radiation).

One of the objectives in many designs is to avoid multiple maxima, in addition to the main maximum, which are referred to as *grating lobes*. Often it may be required to select the largest spacing between the elements but with no grating lobes. *To avoid any grating lobe, the largest spacing between the elements should be less than one wavelength* ($d_{\max} < \lambda$).

To illustrate the method, the three-dimensional array factor of a 10-element ($N = 10$) uniform array with $\beta = 0$ and $d = \lambda/4$ is shown plotted in Figure 6.6(a). A 90° angular sector has been removed for better view of the pattern distribution in the elevation plane. The only maximum occurs at broadside ($\theta_0 = 90^\circ$). To form a comparison, the three-dimensional pattern of the same array but with $d = \lambda$ is also plotted in Figure 6.6(b). For this pattern, in addition to the maximum at $\theta_0 = 90^\circ$, there are additional maxima directed toward $\theta_0 = 0^\circ, 180^\circ$. The corresponding two-dimensional patterns of Figures 6.6(a,b) are shown in Figure 6.7.

If the spacing between the elements is chosen between $\lambda < d < 2\lambda$, then the maximum of Figure 6.6 toward $\theta_0 = 0^\circ$ shifts toward the angular region $0^\circ < \theta_0 < 90^\circ$ while the maximum toward $\theta_0 = 180^\circ$ shifts toward $90^\circ < \theta_0 < 180^\circ$. When $d = 2\lambda$, there are maxima toward $0^\circ, 60^\circ, 90^\circ, 120^\circ$ and 180°.

In Tables 6.1 and 6.2 the expressions for the nulls, maxima, half-power points, minor lobe maxima, and beamwidths for broadside arrays have been listed. They are derived from (6-10c)–(6-16a).

6.3.2 Ordinary End-Fire Array

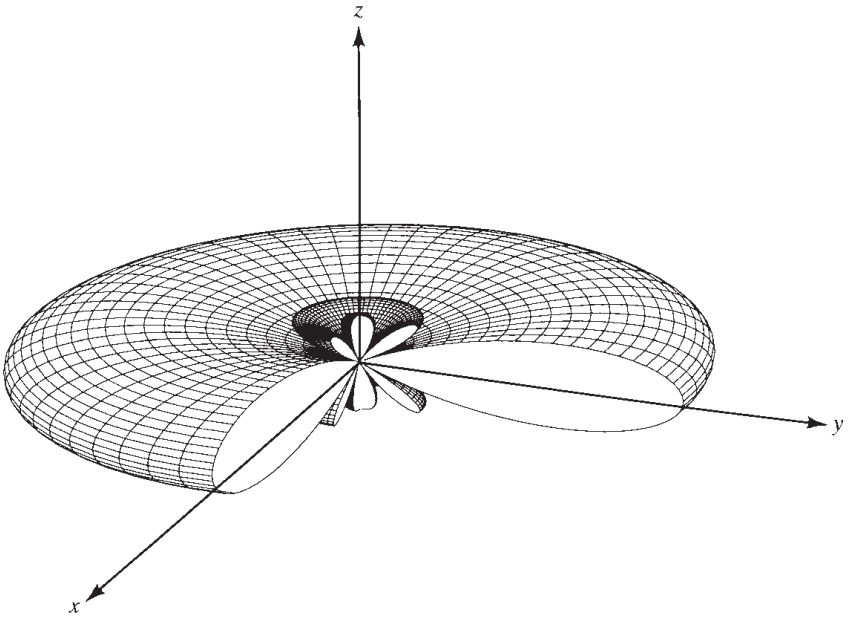
Instead of having the maximum radiation broadside to the axis of the array, it may be desirable to direct it along the axis of the array (end-fire). As a matter of fact, it may be necessary that it radiates toward only one direction (either $\theta_0 = 0^\circ$ or 180° of Figure 6.5).

To direct the first maximum toward $\theta_0 = 0^\circ$,

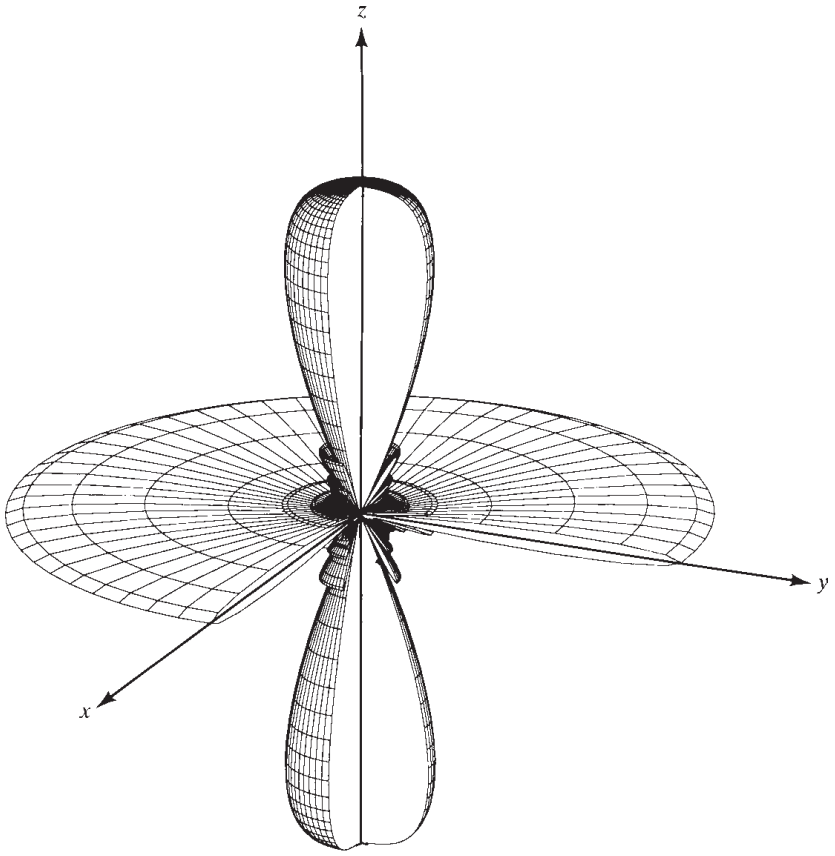
$$\boxed{\psi = kd\cos\theta + \beta|_{\theta=0^\circ} = kd + \beta = 0 \Rightarrow \beta = -kd} \tag{6-20a}$$

If the first maximum is desired toward $\theta_0 = 180^\circ$, then

$$\boxed{\psi = kd\cos\theta + \beta|_{\theta=180^\circ} = -kd + \beta = 0 \Rightarrow \beta = kd} \tag{6-20b}$$



(a) Broadside ($\beta = 0$, $d = \lambda/4$)



(b) Broadside/end-fire ($\beta = 0$, $d = \lambda$)

Figure 6.6 Three-dimensional amplitude patterns for broadside, and broadside/end-fire arrays ($N = 10$).

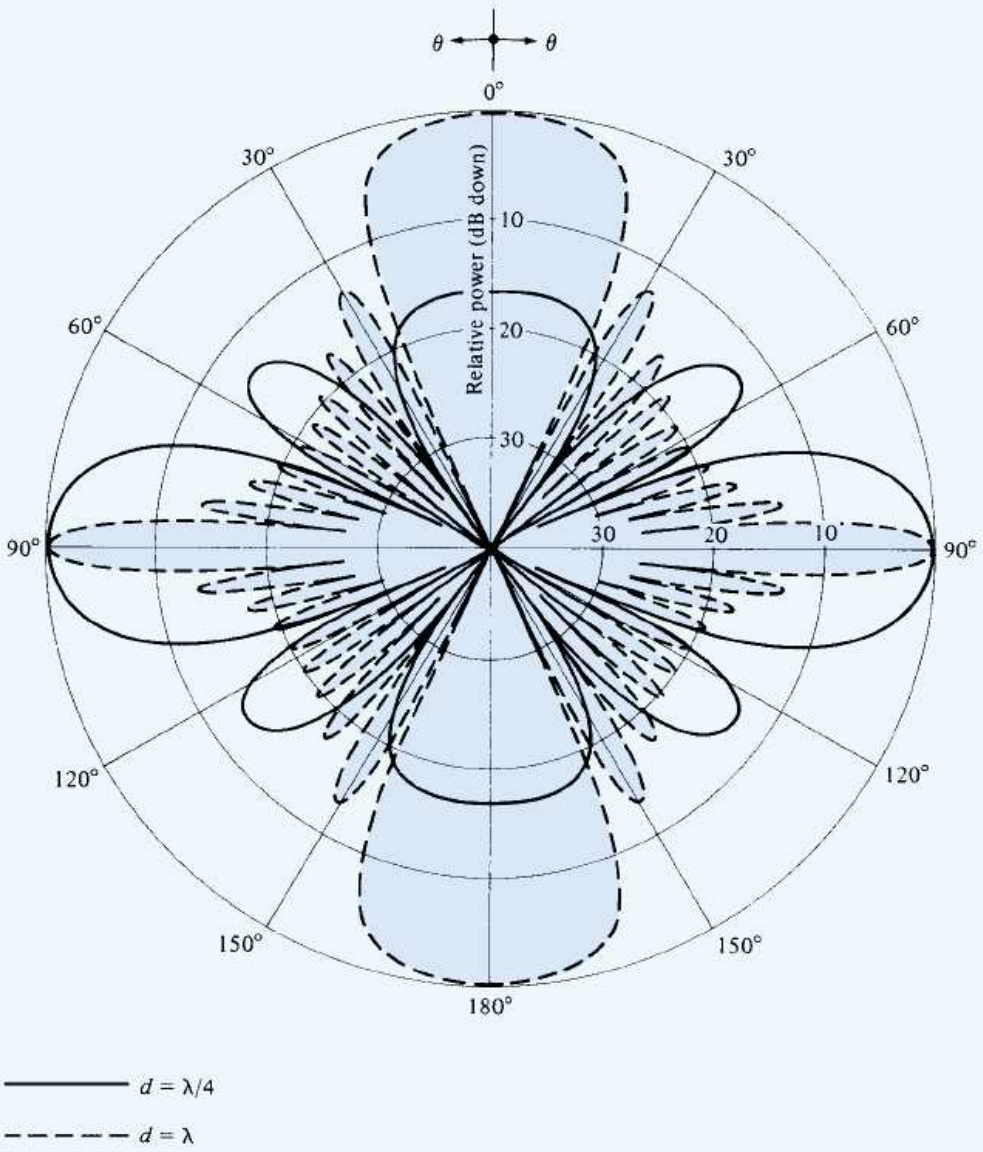


Figure 6.7 Array factor patterns of a 10-element uniform amplitude broadside array ($N = 10, \beta = 0$).

Thus end-fire radiation is accomplished when $\beta = -kd$ (for $\theta_0 = 0°$) or $\beta = kd$ (for $\theta_0 = 180°$).

If the element separation is $d = \lambda/2$, end-fire radiation exists simultaneously in both directions ($\theta_0 = 0°$ and $\theta_0 = 180°$). If the element spacing is a multiple of a wavelength ($d = n\lambda$, $n = 1, 2, 3, \ldots$), then in addition to having end-fire radiation in both directions, there also exist maxima in the broadside directions. Thus for $d = n\lambda, n = 1, 2, 3, \ldots$ there exist four maxima; two in the broadside directions and two along the axis of the array. *To have only one end-fire maximum and to avoid any grating lobes, the maximum spacing between the elements should be less than* $d_{\max} < \lambda/2$.

The three-dimensional radiation patterns of a 10-element ($N = 10$) array with $d = \lambda/4$, $\beta = +kd$ are plotted in Figure 6.8. When $\beta = -kd$, the maximum is directed along $\theta_0 = 0°$ and the three-dimensional pattern is shown in Figure 6.8(a). However, when $\beta = +kd$, the maximum is oriented toward $\theta_0 = 180°$, and the three-dimensional

TABLE 6.1 Nulls, Maxima, Half-Power Points, and Minor Lobe Maxima for Uniform Amplitude Broadside Arrays

NULLS	$\theta_n = \cos^{-1}\left(\pm\frac{n}{N}\frac{\lambda}{d}\right)$ $n = 1, 2, 3, \ldots$ $n \neq N, 2N, 3N, \ldots$
MAXIMA	$\theta_m = \cos^{-1}\left(\pm\frac{m\lambda}{d}\right)$ $m = 0, 1, 2, \ldots$
HALF-POWER POINTS	$\theta_h \simeq \cos^{-1}\left(\pm\frac{1.391\lambda}{\pi N d}\right)$ $\pi d/\lambda \ll 1$
MINOR LOBE MAXIMA	$\theta_s \simeq \cos^{-1}\left[\pm\frac{\lambda}{2d}\left(\frac{2s+1}{N}\right)\right]$ $s = 1, 2, 3, \ldots$ $\pi d/\lambda \ll 1$

TABLE 6.2 Beamwidths for Uniform Amplitude Broadside Arrays

FIRST-NULL BEAMWIDTH (FNBW)	$\Theta_n = 2\left[\frac{\pi}{2} - \cos^{-1}\left(\frac{\lambda}{Nd}\right)\right]$
HALF-POWER BEAMWIDTH (HPBW)	$\Theta_h \simeq 2\left[\frac{\pi}{2} - \cos^{-1}\left(\frac{1.391\lambda}{\pi N d}\right)\right]$ $\pi d/\lambda \ll 1$
FIRST SIDE LOBE BEAMWIDTH (FSLBW)	$\Theta_s \simeq 2\left[\frac{\pi}{2} - \cos^{-1}\left(\frac{3\lambda}{2dN}\right)\right]$ $\pi d/\lambda \ll 1$

pattern is shown in Figure 6.8(b). The two-dimensional patterns of Figures 6.8(a,b) are shown in Figure 6.9. To form a comparison, the array factor of the same array ($N = 10$) but with $d = \lambda$ and $\beta = -kd$ has been calculated. Its pattern is identical to that of a broadside array with $N = 10$, $d = \lambda$, and it is shown plotted in Figure 6.7. It is seen that there are four maxima; two broadside and two along the axis of the array.

The expressions for the nulls, maxima, half-power points, minor lobe maxima, and beamwidths, as applied to ordinary end-fire arrays, are listed in Tables 6.3 and 6.4.

6.3.3 Phased (Scanning) Array

In the previous two sections it was shown how to direct the major radiation from an array, by controlling the phase excitation between the elements, in directions normal

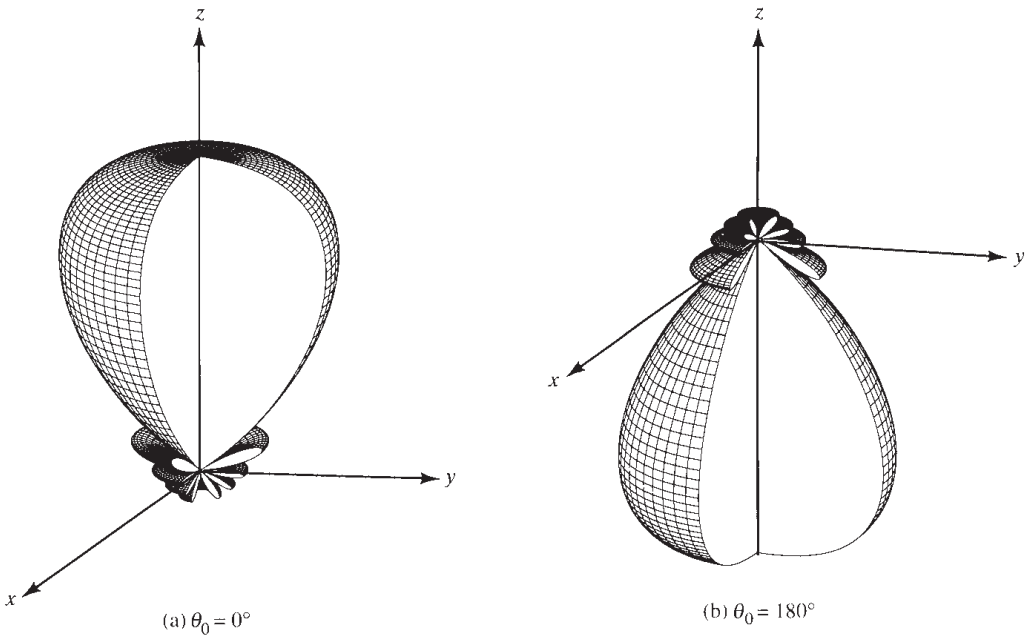


Figure 6.8 Three-dimensional amplitude patterns for end-fire arrays toward $\theta_0 = 0^\circ$ and 180° ($N = 10$, $d = \lambda/4$).

(broadside) and along the axis (end fire) of the array. It is then logical to assume that the maximum radiation can be oriented in any direction to form a scanning array. The procedure is similar to that of the previous two sections.

Let us assume that the maximum radiation of the array is required to be oriented at an angle $\theta_0(0^\circ \le \theta_0 \le 180^\circ)$. To accomplish this, the phase excitation β between the elements must be adjusted so that

$$\boxed{\psi = kd\cos\theta + \beta|_{\theta=\theta_0} = kd\cos\theta_0 + \beta = 0 \Rightarrow \beta = -kd\cos\theta_0} \tag{6-21}$$

Thus by controlling the progressive phase difference between the elements, the maximum radiation can be squinted in any desired direction to form a scanning array. This is the basic principle of electronic scanning phased array operation. Since in phased array technology the scanning must be continuous, the system should be capable of continuously varying the progressive phase between the elements. In practice, this is accomplished electronically by the use of ferrite or diode phase shifters. For ferrite phase shifters, the phase shift is controlled by the magnetic field within the ferrite, which in turn is controlled by the amount of current flowing through the wires wrapped around the phase shifter.

For diode phase shifter using balanced, hybrid-coupled varactors, the actual phase shift is controlled either by varying the analog bias dc voltage (typically 0–30 volts) or by a digital command through a digital-to-analog (D/A) converter [1]–[3].

Shown in Figure 6.10 is an *incremental switched-line* PIN-diode phase shifter [2]–[3]. This design is simple, straightforward, lightweight, and high speed. The lines of lengths l_1 and l_2 are switched on and off by controlling the bias of the PIN diodes, using two single-pole double-throw switches, as illustrated in Figure 6.10. The

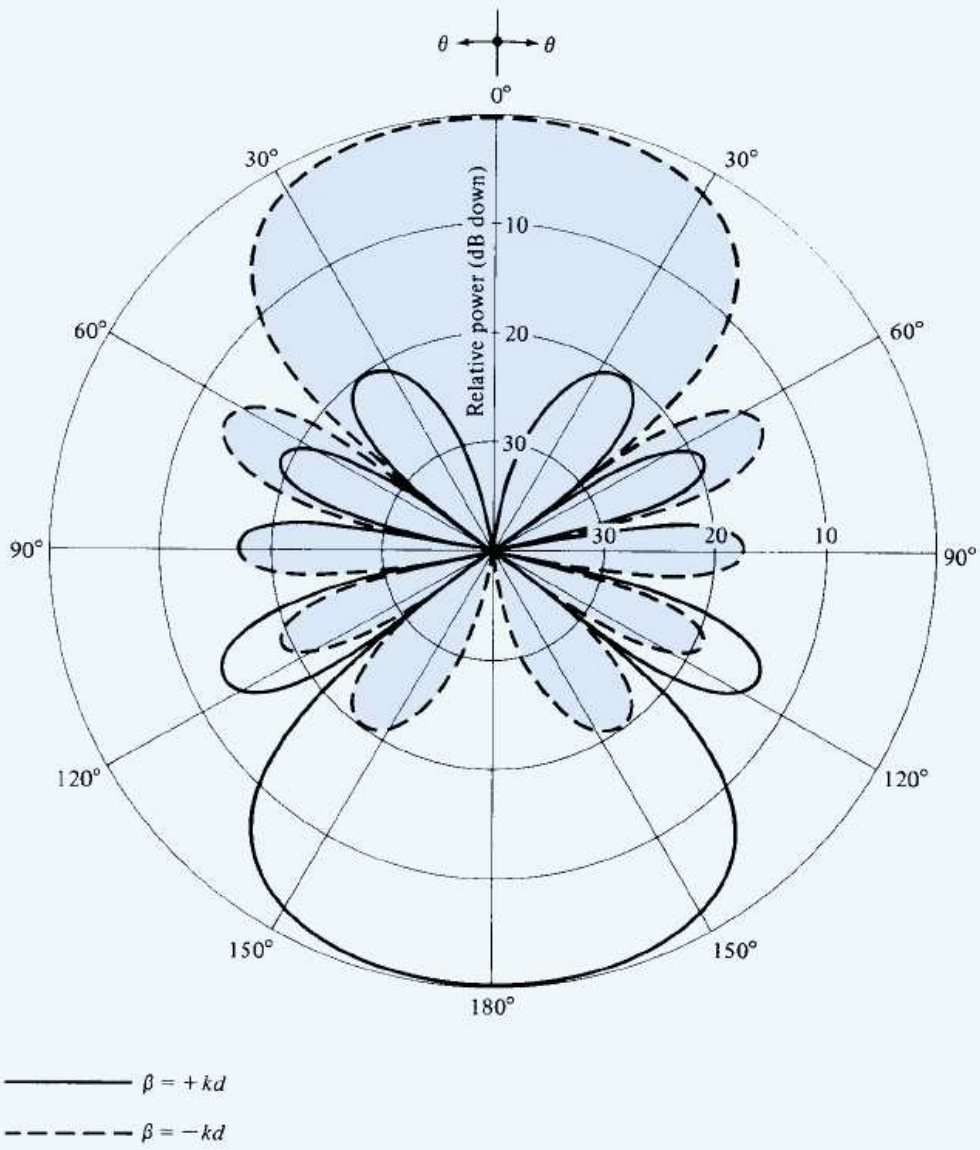


Figure 6.9 Array factor patterns of a 10-element uniform amplitude end-fire array ($N = 10, d = \lambda/4$).

differential phase shift, provided by switching on and off the two paths, is given by

$$\Delta\phi = k(l_2 - l_1) \tag{6-21a}$$

By properly choosing l_1 and l_2, and the operating frequency, the differential phase shift (in degrees) provided by each incremental line phase shifter can be as small as desired, and it determines the resolution of the phase shifter. The design of an entire phase shifter typically utilizes several such incremental phase shifters to cover the entire range ($0 - 180^\circ$) of phase. However, the *switched-line* phase shifter, as well as many other ones, are usually designed for binary phase shifts of $\Delta\phi = 180^\circ, 90^\circ, 45^\circ, 22.5^\circ$, etc. [3]. There are other designs of PIN-diode phase shifters, including those that utilize open-circuited stubs and reactive elements [2]. The basic designs of a phase shifter utilizing PIN diodes are typically classified into three categories: *switched line, loaded*

EX2042
Page 314 of 1072

TABLE 6.3 Nulls, Maxima, Half-Power Points, and Minor Lobe Maxima for Uniform Amplitude Ordinary End-Fire Arrays

NULLS	$\theta_n = \cos^{-1}\left(1 - \frac{n\lambda}{Nd}\right)$ $n = 1, 2, 3, \ldots$ $n \neq N, 2N, 3N, \ldots$
MAXIMA	$\theta_m = \cos^{-1}\left(1 - \frac{m\lambda}{d}\right)$ $m = 0, 1, 2, \ldots$
HALF-POWER POINTS	$\theta_h \simeq \cos^{-1}\left(1 - \frac{1.391\lambda}{\pi dN}\right)$ $\pi d/\lambda \ll 1$
MINOR LOBE MAXIMA	$\theta_s \simeq \cos^{-1}\left[1 - \frac{(2s+1)\lambda}{2Nd}\right]$ $s = 1, 2, 3, \ldots$ $\pi d/\lambda \ll 1$

TABLE 6.4 Beamwidths for Uniform Amplitude Ordinary End-Fire Arrays

FIRST-NULL BEAMWIDTH (FNBW)	$\Theta_n = 2\cos^{-1}\left(1 - \frac{\lambda}{Nd}\right)$
HALF-POWER BEAMWIDTH (HPBW)	$\Theta_h \simeq 2\cos^{-1}\left(1 - \frac{1.391\lambda}{\pi dN}\right)$ $\pi d/\lambda \ll 1$
FIRST SIDE LOBE BEAMWIDTH (FSLBW)	$\Theta_s \simeq 2\cos^{-1}\left(1 - \frac{3\lambda}{2Nd}\right)$ $\pi d/\lambda \ll 1$

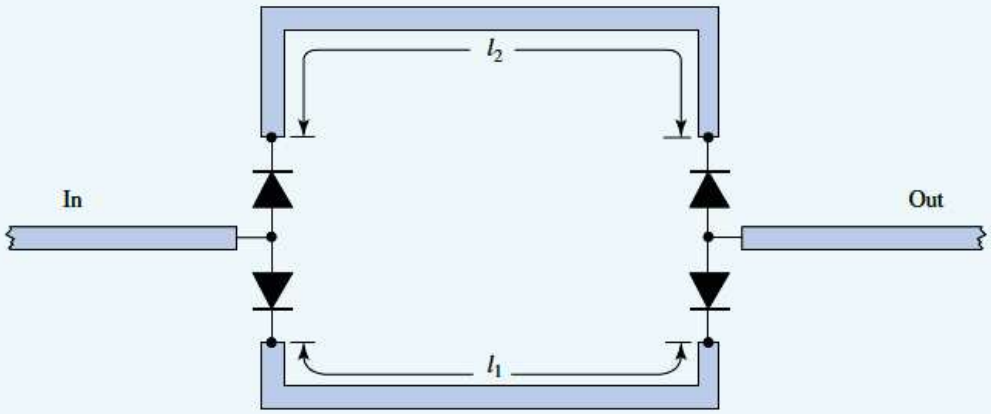


Figure 6.10 Incremental switched-line phase shifter using PIN diodes. (SOURCE: D.M. Pozar, *Microwave Engineering*, John Wiley & Sons, Inc. 2004).

line, and *reflection type* [3]. The *loaded-line* phase shifter can be used for phase shifts generally 45° or smaller. Phase shifters that utilize PIN diodes are not ideal switches since the PIN diodes usually possess finite series resistance and reactance that can contribute significant insertion loss if several of them are used. These phase shifters can also be used as time-delay devices.

To demonstrate the principle of scanning, the three-dimensional radiation pattern of a 10-element array, with a separation of $\lambda/4$ between the elements and with the maximum squinted in the $\theta_0 = 60^\circ$ direction, is plotted in Figure 6.11(a). The corresponding two-dimensional pattern is shown in Figure 6.11(b).

The half-power beamwidth of the scanning array is obtained using (6-14) with $\beta = -kd\cos\theta_0$. Using the minus sign in the argument of the inverse cosine function in (6-14) to represent one angle of the half-power beamwidth and the plus sign to represent the other angle, then the total beamwidth is the difference between these two angles and can be written as

$$\begin{aligned}\Theta_h &= \cos^{-1}\left[\frac{\lambda}{2\pi d}\left(kd\cos\theta_0 - \frac{2.782}{N}\right)\right] - \cos^{-1}\left[\frac{\lambda}{2\pi d}\left(kd\cos\theta_0 + \frac{2.782}{N}\right)\right] \\ &= \cos^{-1}\left(\cos\theta_0 - \frac{2.782}{Nkd}\right) - \cos^{-1}\left(\cos\theta_0 + \frac{2.782}{Nkd}\right)\end{aligned} \tag{6-22}$$

Since $N = (L + d)/d$, (6-22) reduces to [4]

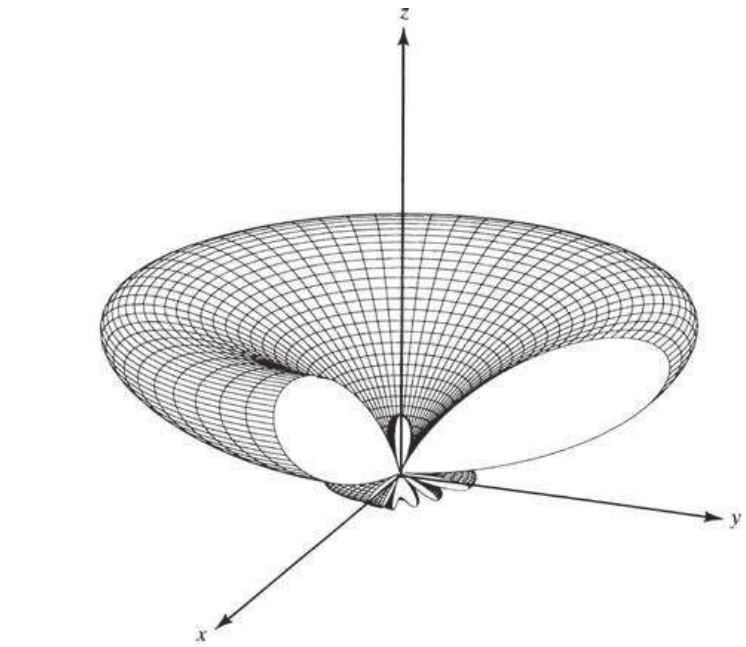
$$\boxed{\begin{aligned}\Theta_h &= \cos^{-1}\left[\cos\theta_0 - 0.443\frac{\lambda}{(L+d)}\right] \\ &\quad - \cos^{-1}\left[\cos\theta_0 + 0.443\frac{\lambda}{(L+d)}\right]\end{aligned}} \tag{6-22a}$$

where L is the length of the array. Equation (6-22a) can also be used to compute the half-power beamwidth of a broadside array. However, it is not valid for an end-fire array. A plot of the half-power beamwidth (in degrees) as a function of the array length is shown in Figure 6.12. These curves are valid for broadside, ordinary end-fire, and scanning uniform arrays (constant magnitude but with progressive phase shift). In a later section it will be shown that the curves of Figure 6.12 can be used, in conjunction with a beam broadening factor [4], to compute the directivity of nonuniform amplitude arrays.

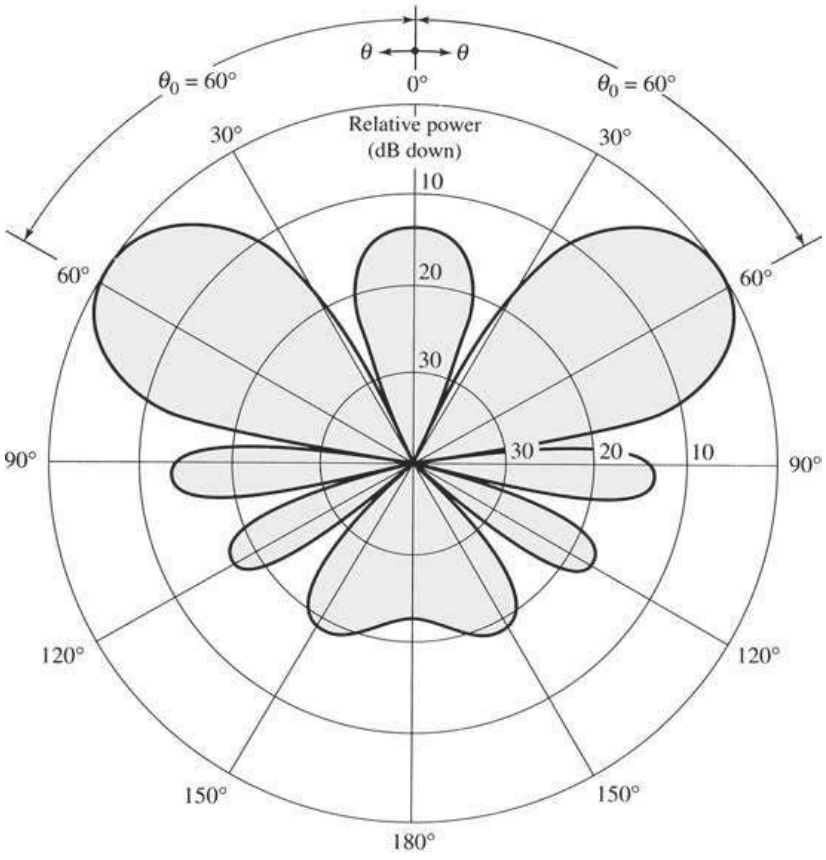
6.3.4 Hansen-Woodyard End-Fire Array

The conditions for an ordinary end-fire array were discussed in Section 6.3.2. It was concluded that the maximum radiation can be directed along the axis of the uniform array by allowing the progressive phase shift β between elements to be equal to (6-20a) for $\theta_0 = 0^\circ$ and (6-20b) for $\theta_0 = 180^\circ$.

To enhance the directivity of an end-fire array without destroying any of the other characteristics, Hansen and Woodyard [5] in 1938 proposed that the required phase



(a) Three-dimensional



(b) Two-dimensional

Figure 6.11 Three- and two-dimensional array factor patterns of a 10-element uniform amplitude scanning array ($N = 10$, $\beta = -kd\cos\theta_0$, $\theta_0 = 60^\circ$, $d = \lambda/4$).

EX2042
Page 317 of 1072

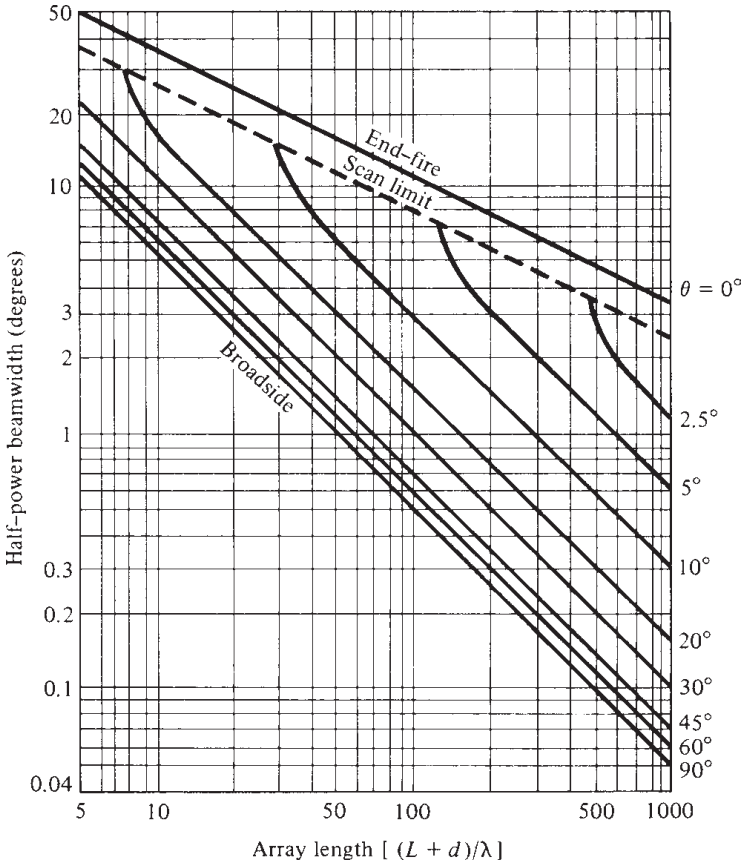


Figure 6.12 Half-power beamwidth for broadside, ordinary end-fire, and scanning uniform linear arrays. (SOURCE: R. S. Elliott, "Beamwidth and Directivity of Large Scanning Arrays," First of Two Parts, *The Microwave Journal*, December 1963).

shift between *closely spaced elements of a very long array*[†] should be

$$\boxed{\beta = -\left(kd + \frac{2.92}{N}\right) \simeq -\left(kd + \frac{\pi}{N}\right) \Rightarrow \text{for maximum in } \theta_0 = 0^\circ} \tag{6-23a}$$

$$\boxed{\beta = +\left(kd + \frac{2.92}{N}\right) \simeq +\left(kd + \frac{\pi}{N}\right) \Rightarrow \text{for maximum in } \theta_0 = 180^\circ} \tag{6-23b}$$

These requirements are known today as the *Hansen-Woodyard conditions for end-fire radiation*. They lead to a *larger* directivity than the conditions given by (6-20a) and (6-20b). It should be pointed out, however, that *these conditions do not necessarily yield the maximum possible directivity*. In fact, the maximum may not even occur at $\theta_0 = 0^\circ$ or 180°, its value found using (6-10c) or (6-10d) may not be unity, and the side lobe level may not be -13.46 dB. Both of them, maxima and side lobe levels, depend on the number of array elements, as will be illustrated.

[†]In principle, the Hansen-Woodyard condition was derived for an infinitely long antenna with continuous distribution. It thus gives good results for very long, finite length discrete arrays with closely spaced elements.

To realize the increase in directivity as a result of the Hansen-Woodyard conditions, it is necessary that, in addition to the conditions of (6-23a) and (6-23b), $|\psi|$ assumes values of

For maximum radiation along $\theta_0 = 0^\circ$

$$|\psi| = |kd\cos\theta + \beta|_{\theta=0^\circ} = \frac{\pi}{N} \quad \text{and} \quad |\psi| = |kd\cos\theta + \beta|_{\theta=180^\circ} \simeq \pi \tag{6-24a}$$

For maximum radiation along $\theta_0 = 180^\circ$

$$|\psi| = |kd\cos\theta + \beta|_{\theta=180^\circ} = \frac{\pi}{N} \quad \text{and} \quad |\psi| = |kd\cos\theta + \beta|_{\theta=0^\circ} \simeq \pi \tag{6-24b}$$

The condition of $|\psi| = \pi/N$ in (6-24a) or (6-24b) is realized by the use of (6-23a) or (6-23b), respectively. Care must be exercised in meeting the requirement of $|\psi| \simeq \pi$ for each array. For an array of N elements, the condition of $|\psi| \simeq \pi$ is satisfied by using (6-23a) for $\theta = 0^\circ$, (6-23b) for $\theta = 180^\circ$, and choosing for each a spacing of

$$d = \left(\frac{N-1}{N}\right)\frac{\lambda}{4} \tag{6-25}$$

If the number of elements is large, (6-25) can be approximated by

$$d \simeq \frac{\lambda}{4} \tag{6-25a}$$

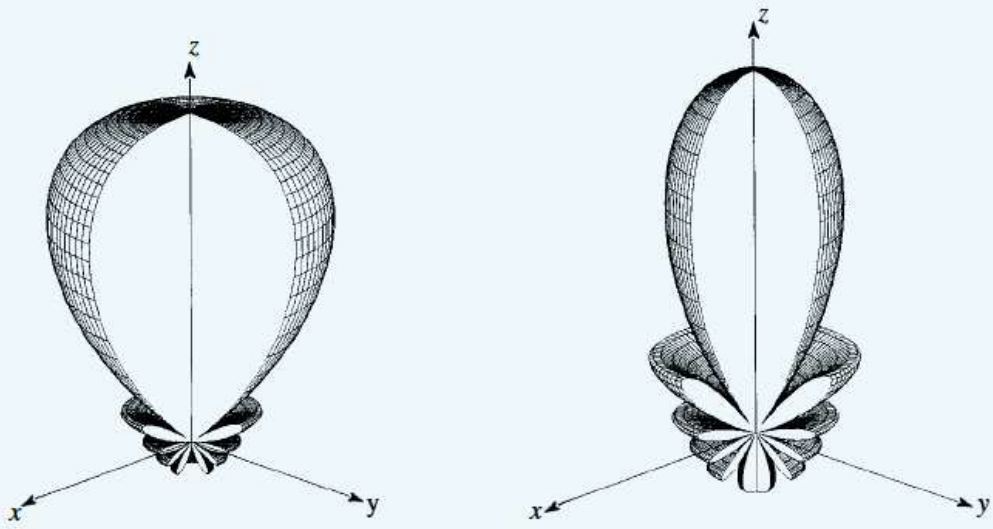
Thus for a large uniform array, the Hansen-Woodyard condition can only yield an improved directivity provided the spacing between the elements is approximately $\lambda/4$.

This is also illustrated in Figure 6.13 where the 3-D field patterns of the *ordinary* and the *Hansen-Woodyard* end-fire designs, for $N = 10$ and $d = \lambda/4$, are placed next to each other. It is apparent that the major lobe of the ordinary end-fire is wider (HPBW = 74°) than that of the Hansen-Woodyard (HPBW = 37°); thus, higher directivity for the Hansen-Woodyard. However, the side lobe of the ordinary end-fire is lower (about −13.5 dB) compared to that of the Hansen-Woodyard, which is about −8.9 dB. *The lower side lobe by the ordinary end-fire is not sufficient to offset the benefit from the narrower beamwidth of the Hansen-Woodyard that leads to the higher directivity*. A comparison between the ordinary and Hansen-Woodyard end-fire array patterns is also illustrated in Figure 10.16 for the design of a helical antenna.

To make the comparisons more meaningful, the directivities for each of the patterns of Figures 6.13 have been calculated, using numerical integration, and it is found that they are equal to 11 and 19, respectively. Thus the Hansen-Woodyard conditions realize a 73% increase in directivity for this case.

As will be shown in Section 6.4 and listed in Table 6.8, the directivity of a Hansen-Woodyard end-fire array is always approximately 1.805 times (or 2.56 dB) greater than the directivity of an ordinary end-fire array. The increase in directivity of the pattern in Figure 6.13 for the Hansen-Woodyard design is at the expense of an increase of about 4 dB in side lobe level. Therefore in the design of an array, there is a trade-off between directivity (or half-power beamwidth) and side lobe level.

To show that (6-23a) and (6-23b) do *not* lead to improved directivities over those of (6-20a) and (6-20b) if (6-24a) and (6-24b) are not satisfied, the pattern for the same



(a) Ordinary (b) Hansen-Woodyard

Figure 6.13 Three-dimensional patterns for ordinary and Hansen-Woodyard end-fire designs ($N = 10, d = \lambda/4$).

array ($N = 10$) with $d = \lambda/4(\beta = -3\pi/5)$ and $d = \lambda/2(\beta = -11\pi/10)$ are plotted in Figure 6.14. Even though the $d = \lambda/2$ pattern exhibits a very narrow lobe in the $\theta_0 = 0°$ direction, its back lobes are larger than its main lobe. The $d = \lambda/2$ pattern fails to realize a larger directivity because the necessary $|\psi|_{\theta=180°} \simeq \pi$ condition of (6-24a) is not satisfied. That is,

$$|\psi| = |(kd\cos\theta + \beta)|_{\substack{\theta=180° \\ \beta=-(kd+\pi/N)}} = |-(2kd + \pi/N)|_{\substack{d=\lambda/2 \\ N=10}} = 2.1\pi \tag{6-26}$$

which is not equal to π as required by (6-24a). Similar results occur for spacings other than those specified by (6-25) or (6-25a).

To better understand and appreciate the Hansen-Woodyard conditions, a succinct derivation of (6-23a) will be outlined. The procedure is identical to that reported by Hansen and Woodyard in their classic paper [5].

The array factor of an N-element array is given by (6-10c) as

$$(\text{AF})_n = \frac{1}{N}\left\{\frac{\sin\left[\frac{N}{2}(kd\cos\theta + \beta)\right]}{\sin\left[\frac{1}{2}(kd\cos\theta + \beta)\right]}\right\} \tag{6-27}$$

and approximated, for small values of $\psi(\psi = kd\cos\theta + \beta)$, by (6-10d) or

$$(\text{AF})_n \simeq \frac{\sin\left[\frac{N}{2}(kd\cos\theta + \beta)\right]}{\left[\frac{N}{2}(kd\cos\theta + \beta)\right]} \tag{6-27a}$$

EX2042
Page 320 of 1072

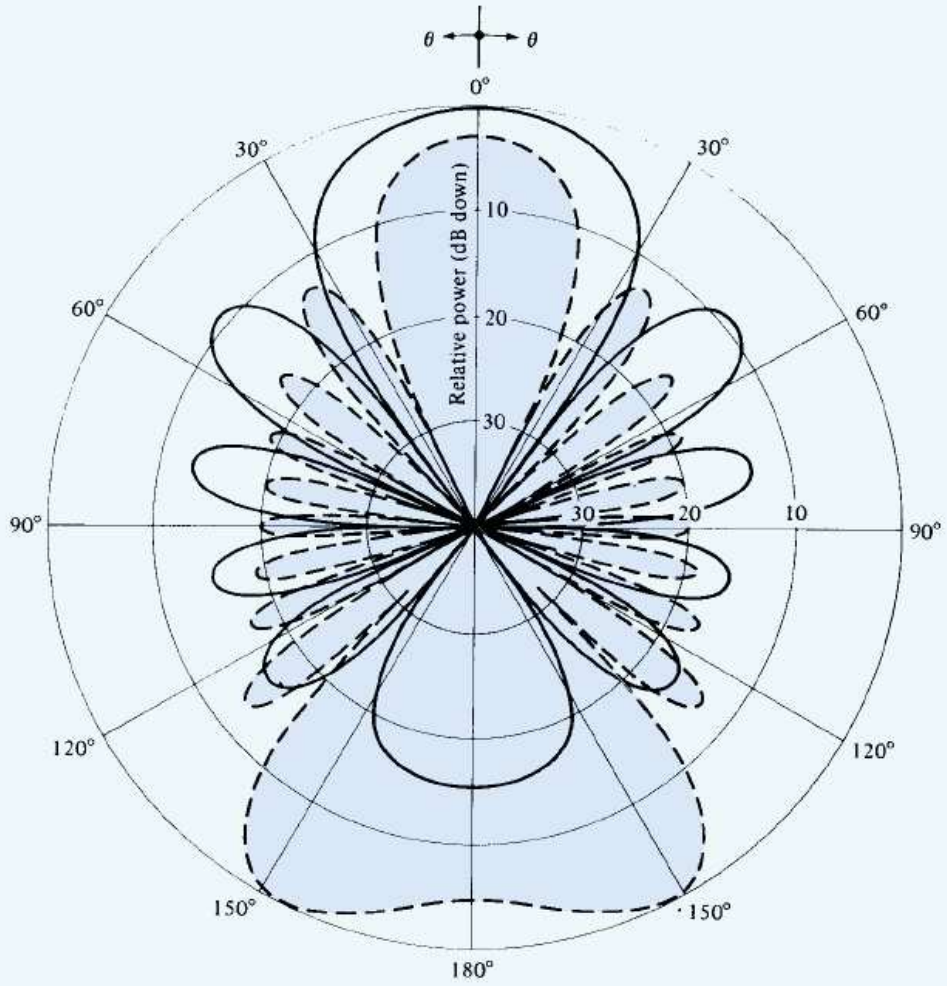


Figure 6.14 Array factor patterns of a 10-element uniform amplitude Hansen-Woodyard end-fire array [$N = 10$, $\beta = -(kd + \pi/N)$].

If the progressive phase shift between the elements is equal to

$$\beta = -pd \tag{6-28}$$

where p is a constant, (6-27a) can be written as

$$(\mathrm{AF})_n = \left\{ \frac{\sin[q(k\cos\theta - p)]}{q(k\cos\theta - p)} \right\} = \left[\frac{\sin(Z)}{Z} \right] \tag{6-29}$$

where

$$q = \frac{Nd}{2} \tag{6-29a}$$

$$Z = q(k\cos\theta - p) \tag{6-29b}$$

EX2042
Page 321 of 1072

The radiation intensity can be written as

$$U(\theta) = [(\mathrm{AF})_n]^2 = \left[\frac{\sin(Z)}{Z}\right]^2 \tag{6-30}$$

whose value at $\theta = 0^\circ$ is equal to

$$U(\theta)|_{\theta=0^\circ} = \left\{\frac{\sin[q(k\cos\theta - p)]}{q(k\cos\theta - p)}\right\}^2\Bigg|_{\theta=0^\circ} = \left\{\frac{\sin[q(k-p)]}{q(k-p)}\right\}^2 \tag{6-30a}$$

Dividing (6-30) by (6-30a), so that the value of the array factor is equal to unity at $\theta = 0^\circ$, leads to

$$U(\theta)_n = \left\{\frac{q(k-p)}{\sin[q(k-p)]}\frac{\sin[q(k\cos\theta - p)]}{[q(k\cos\theta - p)]}\right\}^2 = \left[\frac{\upsilon}{\sin(\upsilon)}\frac{\sin(Z)}{Z}\right]^2 \tag{6-31}$$

where

$$\upsilon = q(k-p) \tag{6-31a}$$

$$Z = q(k\cos\theta - p) \tag{6-31b}$$

The directivity of the array factor can be evaluated using

$$D_0 = \frac{4\pi U_{\max}}{P_{\mathrm{rad}}} = \frac{U_{\max}}{U_0} \tag{6-32}$$

where U_0 is the average radiation intensity and it is given by

$$\begin{aligned} U_0 &= \frac{P_{\mathrm{rad}}}{4\pi} = \frac{1}{4\pi}\int_0^{2\pi}\int_0^{\pi} U(\theta)\sin\theta\, d\theta\, d\phi \\ &= \frac{1}{2}\left[\frac{\upsilon}{\sin(\upsilon)}\right]^2 \int_0^{\pi}\left[\frac{\sin(Z)}{Z}\right]^2 \sin\theta\, d\theta \end{aligned} \tag{6-33}$$

By using (6-31a) and (6-31b), (6-33) can be written as

$$U_0 = \frac{1}{2}\left[\frac{q(k-p)}{\sin[q(k-p)]}\right]^2 \int_0^{\pi}\left[\frac{\sin[q(k\cos\theta - p)]}{q(k\cos\theta - p)}\right]^2 \sin\theta\, d\theta \tag{6-33a}$$

To maximize the directivity, as given by (6-32), (6-33a) must be minimized. Performing the integration, (6-33a) reduces to

$$U_0 = \frac{1}{2kq}\left[\frac{\upsilon}{\sin(\upsilon)}\right]^2 \left[\frac{\pi}{2} + \frac{[\cos(2\upsilon) - 1]}{2\upsilon} + S_i(2\upsilon)\right] = \frac{1}{2kq}g(\upsilon) \tag{6-34}$$

where

$$\upsilon = q(k - p) \tag{6-34a}$$

$$S_i(z) = \int_0^z \frac{\sin t}{t}\, dt \tag{6-34b}$$

$$g(\upsilon) = \left[\frac{\upsilon}{\sin(\upsilon)}\right]^2 \left[\frac{\pi}{2} + \frac{[\cos(2\upsilon) - 1]}{2\upsilon} + S_i(2\upsilon)\right] \tag{6-34c}$$

The function $g(\upsilon)$ is plotted in Figure 6.15 and its minimum value occurs when

$$\upsilon = q(k - p) = \frac{Nd}{2}(k - p) = -1.46 \tag{6-35}$$

Thus

$$\beta = -pd = -\left(kd + \frac{2.92}{N}\right) \tag{6-36}$$

which is the condition for end-fire radiation with improved directivity (Hansen-Woodyard condition) along $\theta_0 = 0^\circ$, as given by (6-23a). Similar procedures can be followed to establish (6-23b).

Ordinarily, (6-36) is approximated by

$$\beta = -\left(kd + \frac{2.92}{N}\right) \simeq -\left(kd + \frac{\pi}{N}\right) \tag{6-37}$$

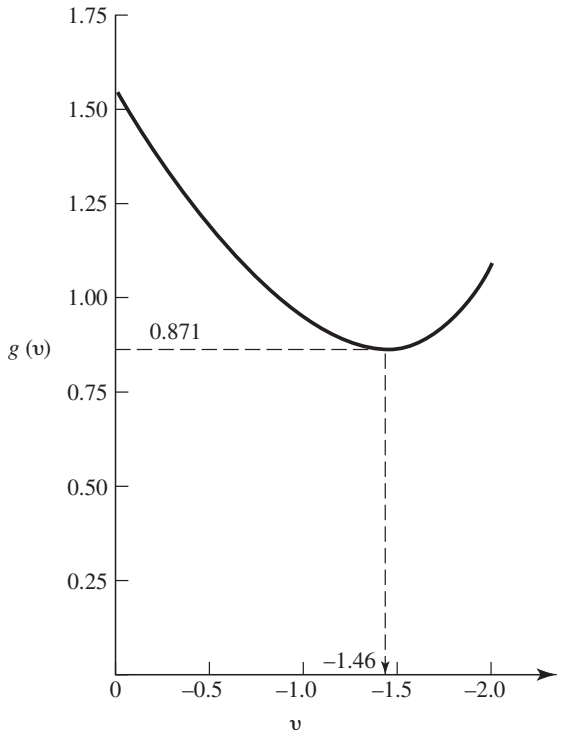


Figure 6.15 Variation of $g(\upsilon)$ (see Eq. 6-34c) as a function of υ.

with not too much relaxation in the condition since the curve of Figure 6.15 is broad around the minimum point $\upsilon = -1.46$. Its value at $\upsilon = -1.57$ is almost the same as the minimum at $\upsilon = -1.46$.

The expressions for the nulls, maxima, half-power points, minor lobe maxima, and beamwidths are listed in Tables 6.5 and 6.6.

For the broadside, end-fire and scanning linear designs, there is a maximum spacing $d_{\max}$ that should not be exceeded to maintain in the amplitude pattern either one or

TABLE 6.5 Nulls, Maxima, Half-Power Points, and Minor Lobe Maxima for Uniform Amplitude Hansen-Woodyard End-Fire Arrays

NULLS	$\theta_n = \cos^{-1}\left[1 + (1-2n)\dfrac{\lambda}{2dN}\right]$ $n = 1, 2, 3, \ldots$ $n \neq N, 2N, 3N, \ldots$
MAXIMA	$\theta_m = \cos^{-1}\left\{1 + [1-(2m+1)]\dfrac{\lambda}{2Nd}\right\}$ $m = 1, 2, 3, \ldots$ $\pi d/\lambda \ll 1$
HALF-POWER POINTS	$\theta_h = \cos^{-1}\left(1 - 0.1398\dfrac{\lambda}{Nd}\right)$ $\pi d/\lambda \ll 1$ N large
MINOR LOBE MAXIMA	$\theta_s = \cos^{-1}\left(1 - \dfrac{s\lambda}{Nd}\right)$ $s = 1, 2, 3, \ldots$ $\pi d/\lambda \ll 1$

TABLE 6.6 Beamwidths for Uniform Amplitude Hansen-Woodyard End-Fire Arrays

FIRST-NULL BEAMWIDTH (FNBW)	$\Theta_n = 2\cos^{-1}\left(1 - \dfrac{\lambda}{2dN}\right)$
HALF-POWER BEAMWIDTH (HPBW)	$\Theta_h = 2\cos^{-1}\left(1 - 0.1398\dfrac{\lambda}{Nd}\right)$ $\pi d/\lambda \ll 1$ N large
FIRST SIDE LOBE BEAMWIDTH (FSLBW)	$\Theta_s = 2\cos^{-1}\left(1 - \dfrac{\lambda}{Nd}\right)$ $\pi d/\lambda \ll 1$

EX2042
Page 324 of 1072

TABLE 6.7 Maximum Element Spacing d_{max} to Maintain Either One or Two Amplitude Maxima of a Linear Array

Array	Distribution	Type	Direction of Maximum	Element Spacing
Linear	Uniform	Broadside	$\theta_0 = 90^\circ$ *only* $\theta_0 = 0^\circ, 90^\circ, 180^\circ$ *simultaneously*	$d_{max} < \lambda$ $d = \lambda$
Linear	Uniform	Ordinary end-fire	$\theta_0 = 0^\circ$ *only* $\theta_0 = 180^\circ$ *only* $\theta_0 = 0^\circ, 90^\circ, 180^\circ$ *simultaneously*	$d_{max} < \lambda/2$ $d_{max} < \lambda/2$ $d = \lambda$
Linear	Uniform	Hansen-Woodyard end-fire	$\theta_0 = 0^\circ$ *only* $\theta_0 = 180^\circ$ *only*	$d \simeq \lambda/4$ $d \simeq \lambda/4$
Linear	Uniform	Scanning	$\theta_0 = \theta_{max}$ $0 < \theta_0 < 180^\circ$	$d_{max} < \lambda$
Linear	Nonuniform	Binomial	$\theta_0 = 90^\circ$ *only* $\theta_0 = 0^\circ, 90^\circ, 180^\circ$ *simultaneously*	$d_{max} < \lambda$ $d = \lambda$
Linear	Nonuniform	Dolph-Tschebyscheff	$\theta_0 = 90^\circ$ *only* $\theta_0 = 0^\circ, 90^\circ, 180^\circ$ *simultaneously*	$d_{max} \leq \frac{\lambda}{\pi} \cos^{-1}\left(-\frac{1}{z_o}\right)$ $d = \lambda$
Planar	Uniform	Planar	$\theta_0 = 0^\circ$ *only* $\theta_0 = 0^\circ, 90^\circ$ and 180°; $\phi_0 = 0^\circ, 90^\circ, 180^\circ, 270^\circ$ *simultaneously*	$d_{max} < \lambda$ $d = \lambda$

two maxima. *Table 6.7 lists the maximum element spacing d_{max} for the various linear and planar arrays, uniform and nonuniform, in order to maintain either one or two amplitude maxima.*

6.4 *N*-ELEMENT LINEAR ARRAY: DIRECTIVITY

The criteria that must be met to achieve broadside and end-fire radiation by a uniform linear array of N elements were discussed in the previous section. It would be instructive to investigate the directivity of each of the arrays, since it represents a figure of merit on the operation of the system.

6.4.1 Broadside Array

As a result of the criteria for broadside radiation given by (6-18a), the array factor for this form of the array reduces to

$$(\mathrm{AF})_n = \frac{1}{N}\left[\frac{\sin\left(\frac{N}{2}kd\cos\theta\right)}{\sin\left(\frac{1}{2}kd\cos\theta\right)}\right] \tag{6-38}$$

which for a small spacing between the elements ($d \ll \lambda$) can be approximated by

$$(\mathrm{AF})_n \simeq \left[\frac{\sin\left(\frac{N}{2}kd\cos\theta\right)}{\left(\frac{N}{2}kd\cos\theta\right)}\right] \tag{6-38a}$$

The radiation intensity can be written as

$$U(\theta) = [(\mathrm{AF})_n]^2 = \left[\frac{\sin\left(\frac{N}{2}kd\cos\theta\right)}{\frac{N}{2}kd\cos\theta}\right]^2 = \left[\frac{\sin(Z)}{Z}\right]^2 \tag{6-39}$$

$$Z = \frac{N}{2}kd\cos\theta \tag{6-39a}$$

The directivity can be obtained using (6-32) where $U_{\max}$ of (6-39) is equal to unity ($U_{\max} = 1$) and it occurs at $\theta = 90^\circ$. The average value U_0 of the intensity reduces to

$$\begin{aligned} U_0 &= \frac{1}{4\pi}P_{\mathrm{rad}} = \frac{1}{2}\int_0^\pi \left[\frac{\sin(Z)}{Z}\right]^2 \sin\theta\, d\theta \\ &= \frac{1}{2}\int_0^\pi \left[\frac{\sin\left(\frac{N}{2}kd\cos\theta\right)}{\frac{N}{2}kd\cos\theta}\right]^2 \sin\theta\, d\theta \end{aligned} \tag{6-40}$$

By making a change of variable, that is,

$$Z = \frac{N}{2}kd\cos\theta \tag{6-40a}$$

$$dZ = -\frac{N}{2}kd\sin\theta\, d\theta \tag{6-40b}$$

(6-40) can be written as

$$U_0 = -\frac{1}{Nkd}\int_{+Nkd/2}^{-Nkd/2}\left[\frac{\sin Z}{Z}\right]^2 dZ = \frac{1}{Nkd}\int_{-Nkd/2}^{+Nkd/2}\left[\frac{\sin Z}{Z}\right]^2 dZ \tag{6-41}$$

For a large array ($Nkd/2 \rightarrow$ large), (6-41) can be approximated by extending the limits to infinity. That is,

$$U_0 = \frac{1}{Nkd}\int_{-Nkd/2}^{+Nkd/2}\left[\frac{\sin Z}{Z}\right]^2 dZ \simeq \frac{1}{Nkd}\int_{-\infty}^{+\infty}\left[\frac{\sin Z}{Z}\right]^2 dZ \tag{6-41a}$$

Since

$$\int_{-\infty}^{+\infty}\left[\frac{\sin(Z)}{Z}\right]^2 dZ = \pi \tag{6-41b}$$

(6-41a) reduces to

$$U_0 \simeq \frac{\pi}{Nkd} \tag{6-41c}$$

The directivity of (6-32) can now be written as

$$D_0 = \frac{U_{\max}}{U_0} \simeq \frac{Nkd}{\pi} = 2N\left(\frac{d}{\lambda}\right) \tag{6-42}$$

Using

$$L = (N-1)d \tag{6-43}$$

where L is the overall length of the array, (6-42) can be expressed as

$$D_0 \simeq 2N\left(\frac{d}{\lambda}\right) \simeq 2\left(1+\frac{L}{d}\right)\left(\frac{d}{\lambda}\right) \tag{6-44}$$

which for a large array ($L \gg d$) reduces to

$$D_0 \simeq 2N\left(\frac{d}{\lambda}\right) = 2\left(1+\frac{L}{d}\right)\left(\frac{d}{\lambda}\right) \overset{L \gg d}{\simeq} 2\left(\frac{L}{\lambda}\right) \tag{6-44a}$$

Example 6.3

Given a linear, broadside, uniform array of 10 isotropic elements ($N = 10$) with a separation of $\lambda/4(d = \lambda/4)$ between the elements, find the directivity of the array.

Solution: Using (6-44a)

$$D_0 \simeq 2N\left(\frac{d}{\lambda}\right) = 5 \text{ (dimensionless)} = 10\log_{10}(5) = 6.99 \text{ dB}$$

6.4.2 Ordinary End-Fire Array

For an end-fire array, with the maximum radiation in the $\theta_0 = 0^\circ$ direction, the array factor is given by

$$(\text{AF})_n = \left[\frac{\sin\left[\frac{N}{2}kd(\cos\theta - 1)\right]}{N\sin\left[\frac{1}{2}kd(\cos\theta - 1)\right]}\right] \tag{6-45}$$

which, for a small spacing between the elements ($d \ll \lambda$), can be approximated by

$$(\mathrm{AF})_n \simeq \left[\frac{\sin\left[\frac{N}{2}kd(\cos\theta - 1)\right]}{\left[\frac{N}{2}kd(\cos\theta - 1)\right]} \right] \tag{6-45a}$$

The corresponding radiation intensity can be written as

$$U(\theta) = [(\mathrm{AF})_n]^2 = \left[\frac{\sin\left[\frac{N}{2}kd(\cos\theta - 1)\right]}{\frac{N}{2}kd(\cos\theta - 1)} \right]^2 = \left[\frac{\sin(Z)}{Z}\right]^2 \tag{6-46}$$

$$Z = \frac{N}{2}kd(\cos\theta - 1) \tag{6-46a}$$

whose maximum value is unity ($U_{\max} = 1$) and it occurs at $\theta = 0^\circ$. The average value of the radiation intensity is given by

$$\begin{aligned} U_0 &= \frac{1}{4\pi}\int_0^{2\pi}\int_0^{\pi} \left[\frac{\sin\left[\frac{N}{2}kd(\cos\theta - 1)\right]}{\frac{N}{2}kd(\cos\theta - 1)} \right]^2 \sin\theta\, d\theta\, d\phi \\ &= \frac{1}{2}\int_0^{\pi} \left[\frac{\sin\left[\frac{N}{2}kd(\cos\theta - 1)\right]}{\frac{N}{2}kd(\cos\theta - 1)} \right]^2 \sin\theta\, d\theta \end{aligned} \tag{6-47}$$

By letting

$$Z = \frac{N}{2}kd(\cos\theta - 1) \tag{6-47a}$$

$$dZ = -\frac{N}{2}kd\sin\theta\, d\theta \tag{6-47b}$$

(6-47) can be written as

$$U_0 = -\frac{1}{Nkd}\int_0^{-Nkd}\left[\frac{\sin(Z)}{Z}\right]^2 dZ = \frac{1}{Nkd}\int_0^{Nkd}\left[\frac{\sin(Z)}{Z}\right]^2 dZ \tag{6-48}$$

For a large array ($Nkd \rightarrow$ large), (6-48) can be approximated by extending the limits to infinity. That is,

$$U_0 = \frac{1}{Nkd}\int_0^{Nkd}\left[\frac{\sin(Z)}{Z}\right]^2 dZ \simeq \frac{1}{Nkd}\int_0^{\infty}\left[\frac{\sin(Z)}{Z}\right]^2 dZ \tag{6-48a}$$

Using (6-41b) reduces (6-48a) to

$$U_0 \simeq \frac{\pi}{2Nkd} \tag{6-48b}$$

and the directivity to

$$D_0 = \frac{U_{\max}}{U_0} \simeq \frac{2Nkd}{\pi} = 4N\left(\frac{d}{\lambda}\right) \tag{6-49}$$

Another form of (6-49), using (6-43), is

$$D_0 \simeq 4N\left(\frac{d}{\lambda}\right) = 4\left(1 + \frac{L}{d}\right)\left(\frac{d}{\lambda}\right) \tag{6-49a}$$

which for a large array ($L \gg d$) reduces to

$$D_0 \simeq 4N\left(\frac{d}{\lambda}\right) = 4\left(1 + \frac{L}{d}\right)\left(\frac{d}{\lambda}\right) \overset{L \gg d}{\simeq} 4\left(\frac{L}{\lambda}\right) \tag{6-49b}$$

It should be noted that the directivity of the end-fire array, as given by (6-49)–(6-49b), is twice that for the broadside array as given by (6-42)–(6-44a).

Example 6.4

Given a linear, end-fire, uniform array of 10 elements ($N = 10$) with a separation of $\lambda/4$($d = \lambda/4$) between the elements, find the directivity of the array factor. This array is identical to the broadside array of Example 6.3.

Solution: Using (6-49)

$$D_0 \simeq 4N\left(\frac{d}{\lambda}\right) = 10 \text{ (dimensionless)} = 10\log_{10}(10) = 10 \text{ dB}$$

This value for the directivity ($D_0 = 10$) is approximate, based on the validity of (6-48a). However, it compares very favorably with the value of $D_0 = 10.05$ obtained by numerically integrating (6-45) using the DIRECTIVITY computer program of Chapter 2.

6.4.3 Hansen-Woodyard End-Fire Array

For an end-fire array with improved directivity (Hansen-Woodyard designs) and maximum radiation in the $\theta_0 = 0°$ direction, the radiation intensity (for small spacing between the elements, $d \ll \lambda$) is given by (6-31)–(6-31b). The maximum radiation intensity is unity ($U_{\max} = 1$), and the average radiation intensity is given by (6-34) where q and υ are defined, respectively, by (6-29a) and (6-34a). Using (6-29a), (6-34a), (6-35), and (6-37), the radiation intensity of (6-34) reduces to

$$U_0 = \frac{1}{Nkd}\left(\frac{\pi}{2}\right)^2\left[\frac{\pi}{2} + \frac{2}{\pi} - 1.8515\right] = \frac{0.871}{Nkd} \tag{6-50}$$

which can also be written as

$$U_0 = \frac{0.871}{Nkd} = \frac{1.742}{2Nkd} = 0.554\left(\frac{\pi}{2Nkd}\right) \tag{6-50a}$$

The average value of the radiation intensity, as given by (6-50a), is 0.554 times that for the ordinary end-fire array of (6-48b). Thus the directivity can be expressed, using (6-50a), as

$$D_0 = \frac{U_{\max}}{U_0} = \frac{1}{0.554}\left[\frac{2Nkd}{\pi}\right] = 1.805\left[4N\left(\frac{d}{\lambda}\right)\right] \tag{6-51}$$

which is 1.805 times that of the ordinary end-fire array as given by (6-49). Using (6-43), (6-51) can also be written as

$$D_0 = 1.805\left[4N\left(\frac{d}{\lambda}\right)\right] = 1.805\left[4\left(1+\frac{L}{d}\right)\frac{d}{\lambda}\right] \tag{6-51a}$$

which for a large array ($L \gg d$) reduces to

$$\begin{aligned} D_0 &= 1.805\left[4N\left(\frac{d}{\lambda}\right)\right] = 1.805\left[4\left(1+\frac{L}{d}\right)\left(\frac{d}{\lambda}\right)\right] \\ &\simeq 1.805\left[4\left(\frac{L}{\lambda}\right)\right] \end{aligned} \tag{6-51b}$$

Example 6.5

Given a linear, end-fire (with improved directivity) Hansen-Woodyard, uniform array of 10 elements ($N = 10$) with a separation of $\lambda/4(d = \lambda/4)$ between the elements, find the directivity of the array factor. This array is identical to that of Examples 6.3 (broadside) and 6.4 (ordinary end-fire), and it is used for comparison.

Solution: Using (6-51b)

$$D_0 = 1.805\left[4N\left(\frac{d}{\lambda}\right)\right] = 18.05 \text{ (dimensionless)} = 10\log_{10}(18.05) = 12.56 \text{ dB}$$

The value of this directivity ($D_0 = 18.05$) is 1.805 times greater than that of Example 6.4 (ordinary end-fire) and 3.61 times greater than that found in Example 6.3 (broadside).

Table 6.8 lists the directivities for broadside, ordinary end fire, and Hansen-Woodyard arrays.

6.5 DESIGN PROCEDURE

In the design of any antenna system, the most important design parameters are usually the number of elements, spacing between the elements, excitation (amplitude and phase), half-power beamwidth, directivity, and side lobe level. In a design procedure some of these parameters are specified and the others are then determined.

TABLE 6.8 Directivities for Broadside and End-Fire Arrays

Array	Directivity
BROADSIDE	$D_0 = 2N\left(\frac{d}{\lambda}\right) = 2\left(1+\frac{L}{d}\right)\frac{d}{\lambda} \simeq 2\left(\frac{L}{\lambda}\right)$ $N\pi d/\lambda \to \infty,\ L \gg d$
END-FIRE (ORDINARY)	$D_0 = 4N\left(\frac{d}{\lambda}\right) = 4\left(1+\frac{L}{d}\right)\frac{d}{\lambda} \simeq 4\left(\frac{L}{\lambda}\right)$ Only one maximum ($\theta_0 = 0^\circ$ or 180°) $2N\pi d/\lambda \to \infty,\ L \gg d$
	$D_0 = 2N\left(\frac{d}{\lambda}\right) = 2\left(1+\frac{L}{d}\right)\frac{d}{\lambda} \simeq 2\left(\frac{L}{\lambda}\right)$ Two maxima ($\theta_0 = 0^\circ$ and 180°)
END-FIRE (HANSEN-WOODYARD)	$D_0 = 1.805\left[4N\left(\frac{d}{\lambda}\right)\right] = 1.805\left[4\left(1+\frac{L}{d}\right)\frac{d}{\lambda}\right] = 1.805\left[4\left(\frac{L}{\lambda}\right)\right]$ $2N\pi d/\lambda \to \infty,\ L \gg d$

The parameters that are specified and those that are determined vary among designs. For a uniform array, other than for the Hansen-Woodyard end-fire, the side lobe is always approximately -13.5 dB. For the Hansen-Woodyard end-fire array the side lobe level is somewhat compromised above the -13.5 dB in order to gain about 1.805 (or 2.56 dB) in directivity. The order in which the other parameters are specified and determined varies among designs. For each of the uniform linear arrays that have been discussed, equations and some graphs have been presented which can be used to determine the half-power beamwidth and directivity, once the number of elements and spacing (or the total length of the array) are specified. In fact, some of the equations have been boxed or listed in tables. This may be considered more of an analysis procedure. The other approach is to specify the half-power beamwidth or directivity and to determine most of the other parameters. This can be viewed more as a design approach, and can be accomplished to a large extent with equations or graphs that have been presented. More exact values can be obtained, if necessary, using iterative or numerical methods.

Example 6.6

Design a uniform linear scanning array whose maximum of the array factor is 30° from the axis of the array ($\theta_0 = 30^\circ$). The desired half-power beamwidth is 2° while the spacing between the elements is $\lambda/4$. Determine the excitation of the elements (amplitude and phase), length of the array (in wavelengths), number of elements, and directivity (in dB).

Solution: Since the desired design is a uniform linear scanning array, the amplitude excitation is uniform. However, the progressive phase between the elements is, using (6-21)

$$\beta = -kd\cos\theta_0 = -\frac{2\pi}{\lambda}\left(\frac{\lambda}{4}\right)\cos(30^\circ) = -1.36 \text{ radians} = -77.94^\circ$$

The length of the array is obtained using an iterative procedure of (6-22) or its graphical solution of Figure 6.12. Using the graph of Figure 6.12 for a scan angle of 30° and 2° half-power beamwidth, the approximate length plus one spacing ($L + d$) of the array is 50λ. For the 50λ length plus one spacing dimension from Figure 6.12 and 30° scan angle, (6-22) leads to a half-power beamwidth of 2.03°, which is very close to the desired value of 2°. Therefore, the length of the array for a spacing of $\lambda/4$ is 49.75λ.

Since the length of the array is 49.75λ and the spacing between the elements is $\lambda/4$, the total number of elements is

$$N = \frac{L}{d} + 1 = \left(\frac{L+d}{d}\right) = \frac{50}{1/4} = 200$$

The directivity of the array is obtained using the radiation intensity and the computer program DIRECTIVITY of Chapter 2, and it is equal to 100.72 or 20.03 dB.

6.6 *N*-ELEMENT LINEAR ARRAY: THREE-DIMENSIONAL CHARACTERISTICS

Up to now, the two-dimensional array factor of an N-element linear array has been investigated. Although in practice only two-dimensional patterns can be measured, a collection of them can be used to reconstruct the three-dimensional characteristics of an array. It would then be instructive to examine the three-dimensional patterns of an array of elements. Emphasis will be placed on the array factor.

6.6.1 *N*-Elements Along *Z*-Axis

A linear array of N isotropic elements are positioned along the z-axis and are separated by a distance d, as shown in Figure 6.5(a). The amplitude excitation of each element is a_n and there exists a progressive phase excitation β between the elements. For far-field observations, the array factor can be written according to (6-6) as

$$\text{AF} = \sum_{n=1}^{N} a_n e^{j(n-1)(kd\cos\gamma+\beta)} = \sum_{n=1}^{N} a_n e^{j(n-1)\psi} \tag{6-52}$$

$$\psi = kd\cos\gamma + \beta \tag{6-52a}$$

where the a_n's are the amplitude excitation coefficients and γ is the angle between the axis of the array (z-axis) and the radial vector from the origin to the observation point.

In general, the angle γ can be obtained from the dot product of a unit vector along the axis of the array with a unit vector directed toward the observation point. For the geometry of Figure 6.5(a)

$$\cos\gamma = \hat{\mathbf{a}}_z \cdot \hat{\mathbf{a}}_r = \hat{\mathbf{a}}_z \cdot (\hat{\mathbf{a}}_x \sin\theta\cos\phi + \hat{\mathbf{a}}_y \sin\theta\sin\phi + \hat{\mathbf{a}}_z \cos\theta) = \cos\theta \Rightarrow \gamma = \theta \tag{6-53}$$

Thus (6-52) along with (6-53) is identical to (6-6), because the system of Figure 6.5(a) possesses a symmetry around the z-axis (no ϕ variations). This is not the case when the elements are placed along any of the other axes, as will be shown next.

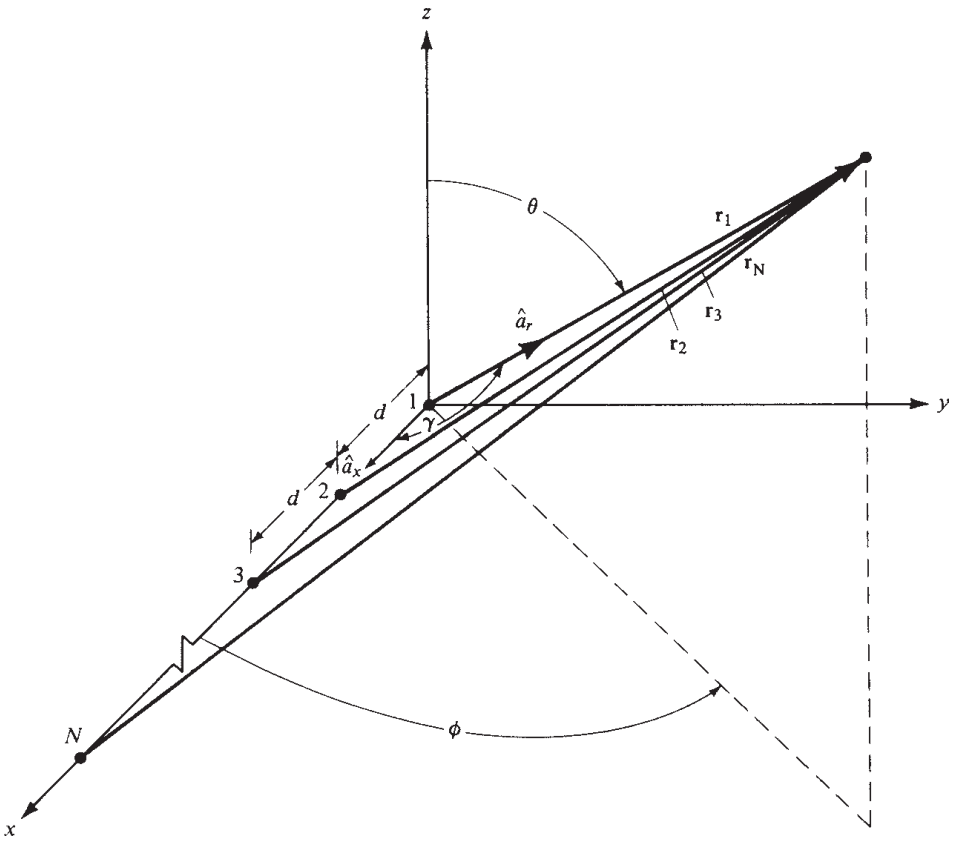


Figure 6.16 Linear array of N isotropic elements positioned along the x-axis.

6.6.2 *N*-Elements Along *X*- or *Y*-Axis

To demonstrate the simplicity that a judicious coordinate system and geometry can provide in the solution of a problem, let us consider an array of N isotropic elements along the x-axis, as shown in Figure 6.16. The far-zone array factor for this array is identical in form to that of Figure 6.5(a) except for the phase factor ψ. For this geometry

$$\cos\gamma = \hat{\mathbf{a}}_x \cdot \hat{\mathbf{a}}_r = \hat{\mathbf{a}}_x \cdot (\hat{\mathbf{a}}_x \sin\theta\cos\phi + \hat{\mathbf{a}}_y \sin\theta\sin\phi + \hat{\mathbf{a}}_z \cos\theta) = \sin\theta\cos\phi \quad (6\text{-}54)$$

$$\cos\gamma = \sin\theta\cos\phi \Rightarrow \gamma = \cos^{-1}(\sin\theta\cos\phi) \quad (6\text{-}54a)$$

The array factor of this array is also given by (6-52) but with γ defined by (6-54a). For this system, the array factor is a function of both angles (θ and ϕ).

In a similar manner, the array factor for N isotropic elements placed along the y-axis is that of (6-52) but with γ defined by

$$\cos\gamma = \hat{\mathbf{a}}_y \cdot \hat{\mathbf{a}}_r = \sin\theta\sin\phi \Rightarrow \gamma = \cos^{-1}(\sin\theta\sin\phi) \quad (6\text{-}55)$$

Physically placing the elements along the z-, x-, or y-axis does not change the characteristics of the array. Numerically they yield identical patterns even though their mathematical forms are different.

Example 6.7

Two half-wavelength dipole ($l = \lambda/2$) are positioned along the x-axis and are separated by a distance d, as shown in Figure 6.17. The lengths of the dipoles are parallel to the z-axis. Find the total field of the array. Assume uniform amplitude excitation and a progressive phase difference of β.

Solution: The field pattern of a single element placed at the origin is given by (4-84) as

$$E_\theta = j\eta \frac{I_0 e^{-jkr}}{2\pi r} \left[\frac{\cos\left(\frac{\pi}{2}\cos\theta\right)}{\sin\theta} \right]$$

Using (6-52), (6-54a), and (6-10c), the array factor can be written as

$$(\mathrm{AF})_n = \frac{\sin(kd\sin\theta\cos\phi + \beta)}{2\sin\left[\frac{1}{2}(kd\sin\theta\cos\phi + \beta)\right]}$$

The total field of the array is then given, using the pattern multiplication rule of (6-5), by

$$E_{\theta t} = E_\theta \cdot (\mathrm{AF})_n = j\eta \frac{I_0 e^{-jkr}}{2\pi r} \frac{\cos\left(\frac{\pi}{2}\cos\theta\right)}{\sin\theta} \left[\frac{\sin(kd\sin\theta\cos\phi + \beta)}{2\sin\left[\frac{1}{2}(kd\sin\theta\cos\phi + \beta)\right]} \right]$$

To illustrate the techniques, the three-dimensional patterns of the two-element array of Example 6.7 have been sketched in Figures 6.17(a) and (b). For both, the element separation is $\lambda/2(d = \lambda/2)$. For the pattern of Figure 6.17(a), the phase excitation between the elements is identical ($\beta = 0$). In addition to the nulls in the $\theta = 0^\circ$ direction, provided by the individual elements of the array, there are additional nulls along the x-axis ($\theta = \pi/2, \phi = 0$ and $\phi = \pi$) provided by the formation of the array. The 180° phase difference required to form the nulls along the x-axis is a result of the separation of the elements [$kd = (2\pi/\lambda)(\lambda/2) = \pi$].

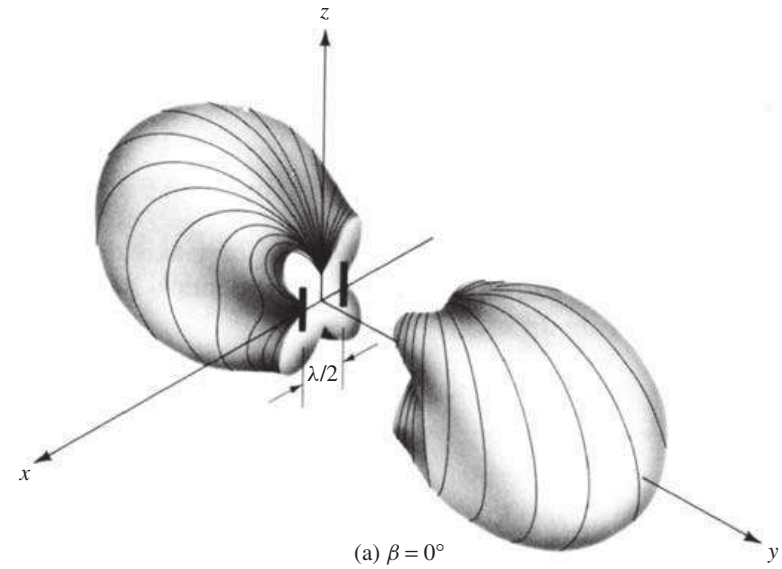
To form a comparison, the three-dimensional pattern of the same array but with a 180° phase excitation ($\beta = 180^\circ$) between the elements is sketched in Figure 6.17(b). The overall pattern of this array is quite different from that shown in Figure 6.17(a). In addition to the nulls along the z-axis ($\theta = 0^\circ$) provided by the individual elements, there are nulls along the y-axis formed by the 180° excitation phase difference.

6.7 RECTANGULAR-TO-POLAR GRAPHICAL SOLUTION

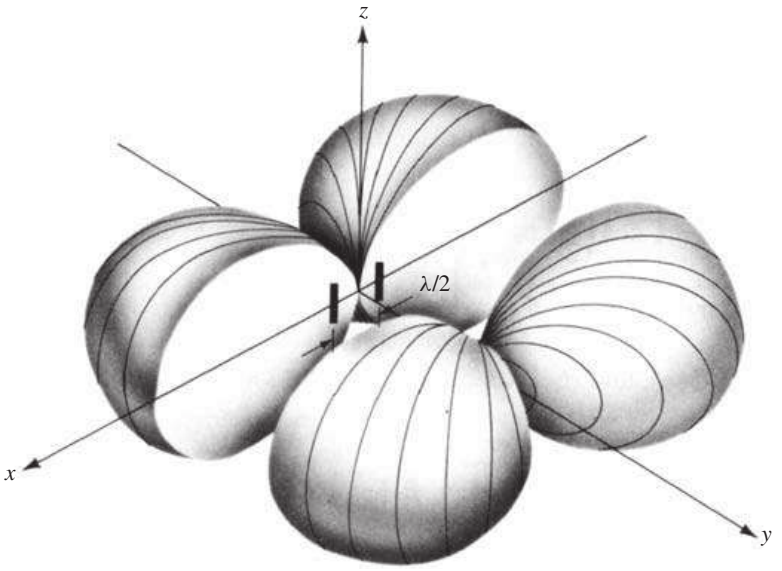
In antenna theory, many solutions are of the form

$$f(\zeta) = f(C\cos\gamma + \delta) \tag{6-56}$$

EX2042
Page 334 of 1072



(a) $\beta = 0°$



(b) $\beta = \pm 180°$

Figure 6.17 Three-dimensional patterns for two $\lambda/2$ dipoles spaced $\lambda/2$. (SOURCE: P. Lorrain and D. R. Corson, *Electromagnetic Fields and Waves*, 2nd ed., W. H. Freeman and Co., Copyright © 1970).

where C and δ are constants and γ is a variable. For example, the approximate array factor of an N-element, uniform amplitude linear array [Equation (6-10d)] is that of a $\sin(\zeta)/\zeta$ form with

$$\zeta = C\cos\gamma + \delta = \frac{N}{2}\psi = \frac{N}{2}(kd\cos\theta + \beta) \tag{6-57}$$

where

$$C = \frac{N}{2}kd \tag{6-57a}$$

$$\delta = \frac{N}{2}\beta \tag{6-57b}$$

Usually the $f(\zeta)$ function can be sketched as a function of ζ in rectilinear coordinates. Since ζ in (6-57) has no physical analog, in many instances it is desired that a graphical representation of $|f(\zeta)|$ be obtained as a function of the physically observable angle θ. This can be constructed graphically from the rectilinear graph, and it forms a polar plot.

The procedure that must be followed in the construction of the polar graph is as follows:

1. Plot, using rectilinear coordinates, the function $|f(\zeta)|$.
2. a. Draw a circle with radius C and with its center on the abscissa at $\zeta = \delta$.
   b. Draw vertical lines to the abscissa so that they will intersect the circle.
   c. From the center of the circle, draw radial lines through the points on the circle intersected by the vertical lines.
   d. Along the radial lines, mark off corresponding magnitudes from the linear plot.
   e. Connect all points to form a continuous graph.

To better illustrate the procedure, the polar graph of the function

$$f(\zeta) = \frac{\sin\left(\frac{N}{2}\psi\right)}{N\sin\left(\frac{\psi}{2}\right)}, \quad \zeta = \frac{5\pi}{2}\cos\theta - \frac{5\pi}{4} \tag{6-58}$$

has been constructed in Figure 6.18. The function $f(\zeta)$ of (6-58) represents the array factor of a 10-element ($N = 10$) uniform linear array with a spacing of $\lambda/4(d = \lambda/4)$ and progressive phase shift of $-\pi/4(\beta = -\pi/4)$ between the elements. The constructed graph can be compared with its exact form shown in Figure 6.11.

From the construction of Figure 6.18, it is evident that the angle at which the maximum is directed is controlled by the radius of the circle C and the variable δ. For the array factor of Figure 6.18, the radius C is a function of the number of elements (N) and the spacing between the elements (d). In turn, δ is a function of the number of elements (N) and the progressive phase shift between the elements (β). Making $\delta = 0$ directs the maximum toward $\theta = 90^\circ$ (broadside array). The part of the linear graph that is used to construct the polar plot is determined by the radius of the circle and the relative position of its center along the abscissa. The usable part of the linear graph is referred to as the *visible* region and the remaining part as the *invisible* region. Only the *visible* region of the linear graph is related to the physically observable angle θ (hence its name).

6.8 *N*-ELEMENT LINEAR ARRAY: UNIFORM SPACING, NONUNIFORM AMPLITUDE

The theory to analyze linear arrays with uniform spacing, uniform amplitude, and a progressive phase between the elements was introduced in the previous sections of this chapter. A number of numerical and graphical solutions were used to illustrate

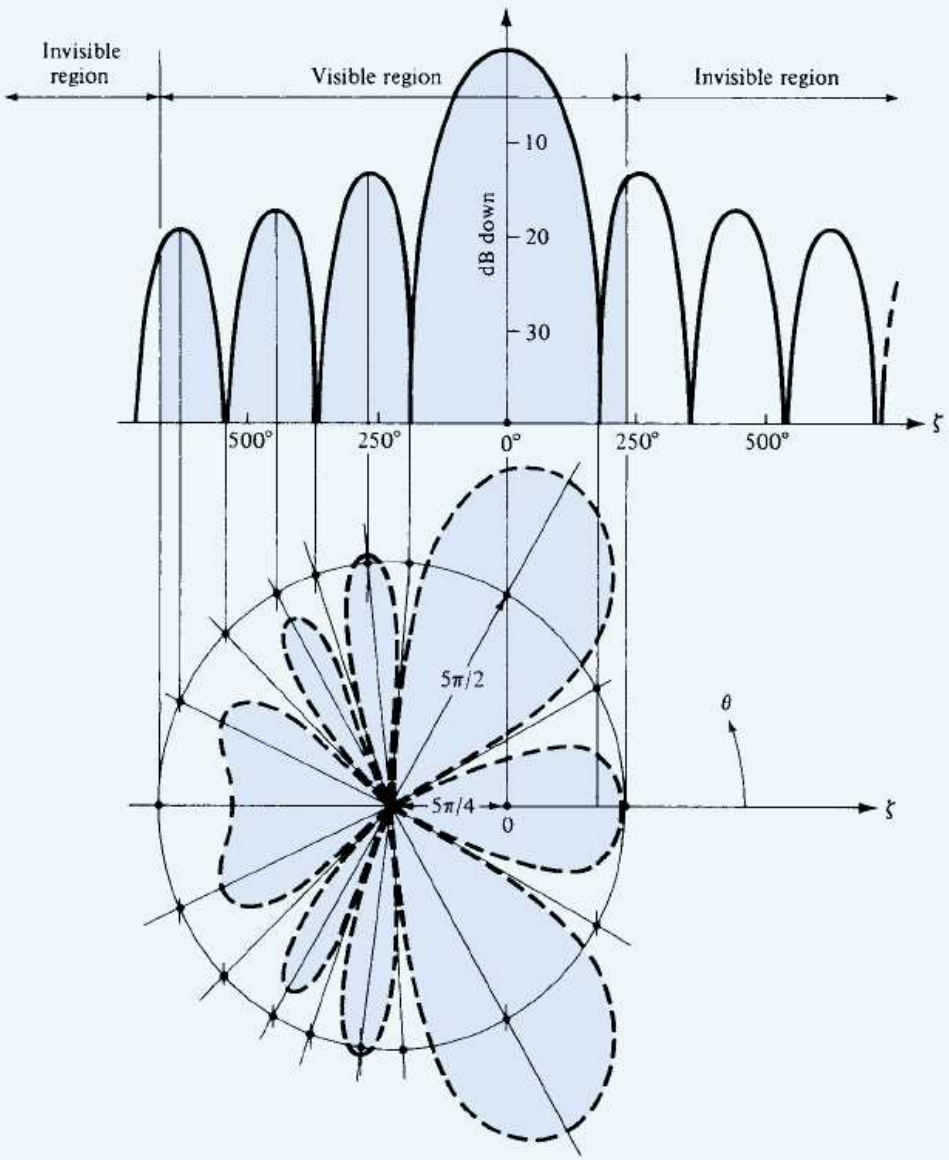


Figure 6.18 Rectangular-to-polar plot graphical solution.

some of the principles. In this section, broadside arrays with uniform spacing but nonuniform amplitude distribution will be considered. Most of the discussion will be directed toward binomial [6] and Dolph-Tschebyscheff [7] broadside arrays (also spelled Tchebyscheff or Chebyshev).

Of the three distributions (uniform, binomial, and Tschebyscheff), a uniform amplitude array yields the smallest half-power beamwidth. It is followed, in order, by the Dolph-Tschebyscheff and binomial arrays. In contrast, binomial arrays usually possess the smallest side lobes followed, in order, by the Dolph-Tschebyscheff and uniform arrays. As a matter of fact, binomial arrays with element spacing equal or less than $\lambda/2$ have no side lobes. It is apparent that the designer must compromise between side lobe level and beamwidth.

A criterion that can be used to judge the relative beamwidth and side lobe level of one design to another is the amplitude distribution (tapering) along the source. *It*

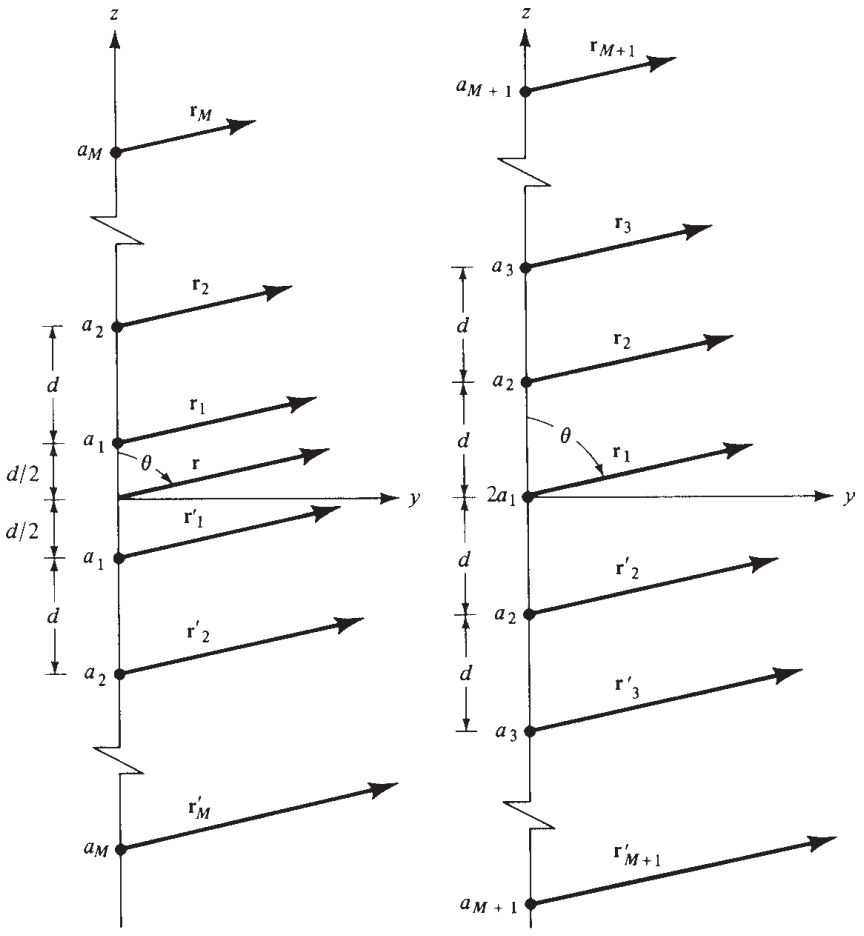
has been shown analytically that for a given side lobe level the Dolph-Tschebyscheff array produces the smallest beamwidth between the first nulls. Conversely, for a given beamwidth between the first nulls, the Dolph-Tschebyscheff design leads to the smallest possible side lobe level.

Uniform arrays usually possess the largest directivity. However, superdirective (or super gain as most people refer to them) antennas possess directivities higher than those of a uniform array [8]. Although a certain amount of superdirectivity is practically possible, superdirective arrays usually require very large currents with opposite phases between adjacent elements. Thus the net total current and efficiency of each array are very small compared to the corresponding values of an individual element.

Before introducing design methods for specific nonuniform amplitude distributions, let us first derive the array factor.

6.8.1 Array Factor

An array of an even number of isotropic elements $2M$ (where M is an integer) is positioned symmetrically along the z-axis, as shown in Figure 6.19(a). The separation between the elements is d, and M elements are placed on each side of the origin.



(a) Even number of elements (b) Odd number of elements

Figure 6.19 Nonuniform amplitude arrays of even and odd number of elements.

EX2042
Page 338 of 1072

Assuming that the amplitude excitation is symmetrical about the origin, the array factor for a nonuniform amplitude broadside array can be written as

$$\begin{aligned}(\text{AF})_{2M} = a_1 e^{+j(1/2)kd\cos\theta} &+ a_2 e^{+j(3/2)kd\cos\theta} + \cdots \\ &+ a_M e^{+j[(2M-1)/2]kd\cos\theta} \\ &+ a_1 e^{-j(1/2)kd\cos\theta} + a_2 e^{-j(3/2)kd\cos\theta} + \cdots \\ &+ a_M e^{-j[(2M-1)/2]kd\cos\theta}\end{aligned}$$

$$(\text{AF})_{2M} = 2\sum_{n=1}^{M} a_n \cos\left[\frac{(2n-1)}{2} kd\cos\theta\right] \tag{6-59}$$

which in normalized form reduces to

$$(\text{AF})_{2M} = \sum_{n=1}^{M} a_n \cos\left[\frac{(2n-1)}{2} kd\cos\theta\right] \tag{6-59a}$$

where a_n's are the excitation coefficients of the array elements.

If the total number of isotropic elements of the array is odd $2M + 1$ (where M is an integer), as shown in Figure 6.19(b), the array factor can be written as

$$\begin{aligned}(\text{AF})_{2M+1} = 2a_1 &+ a_2 e^{+jkd\cos\theta} + a_3 e^{j2kd\cos\theta} + \cdots + a_{M+1} e^{jMkd\cos\theta} \\ &+ a_2 e^{-jkd\cos\theta} + a_3 e^{-j2kd\cos\theta} + \cdots + a_{M+1} e^{-jMkd\cos\theta}\end{aligned}$$

$$(\text{AF})_{2M+1} = 2\sum_{n=1}^{M+1} a_n \cos[(n-1)kd\cos\theta] \tag{6-60}$$

which in normalized form reduces to

$$(\text{AF})_{2M+1} = \sum_{n=1}^{M+1} a_n \cos[(n-1)kd\cos\theta] \tag{6-60a}$$

The amplitude excitation of the center element is $2a_1$.

Equations (6-59a) and (6-60a) can be written in normalized form as

$$(\text{AF})_{2M}(\text{even}) = \sum_{n=1}^{M} a_n \cos[(2n-1)u] \tag{6-61a}$$

$$(\text{AF})_{2M+1}(\text{odd}) = \sum_{n=1}^{M+1} a_n \cos[2(n-1)u] \tag{6-61b}$$

where

$$u = \frac{\pi d}{\lambda}\cos\theta \tag{6-61c}$$

The next step will be to determine the values of the excitation coefficients (a_n's).

6.8.2 Binomial Array

The array factor for the binomial array is represented by (6-61a)–(6-61c) where the a_n's are the excitation coefficients which will now be derived.

A. Excitation Coefficients

To determine the excitation coefficients of a binomial array, J. S. Stone [6] suggested that the function $(1+x)^{m-1}$ be written in a series, using the binomial expansion, as

$$(1+x)^{m-1} = 1 + (m-1)x + \frac{(m-1)(m-2)}{2!}x^2 + \frac{(m-1)(m-2)(m-3)}{3!}x^3 + \dots \tag{6-62}$$

The positive coefficients of the series expansion for different values of m are

$m=1$									1										
$m=2$								1		1									
$m=3$							1		2		1								
$m=4$						1		3		3		1							
$m=5$					1		4		6		4		1						
$m=6$				1		5		10		10		5		1					
$m=7$			1		6		15		20		15		6		1				
$m=8$		1		7		21		35		35		21		7		1			
$m=9$	1		8		28		56		70		56		28		8		1		
$m=10$	1	9		36		84		126		126		84		36		9		1	

(6-63)

The above represents Pascal's triangle. If the values of m are used to represent the number of elements of the array, then the coefficients of the expansion represent the relative amplitudes of the elements. Since the coefficients are determined from a binomial series expansion, the array is known as a *binomial array*.

Referring to (6-61a), (6-61b), and (6-63), the amplitude coefficients for the following arrays are:

1. Two elements $(2M = 2)$

$$a_1 = 1$$

2. Three elements $(2M + 1 = 3)$

$$2a_1 = 2 \Rightarrow a_1 = 1$$
$$a_2 = 1$$

3. Four elements $(2M = 4)$

$$a_1 = 3$$
$$a_2 = 1$$

4. Five elements $(2M + 1 = 5)$

$$2a_1 = 6 \Rightarrow a_1 = 3$$
$$a_2 = 4$$
$$a_3 = 1$$

The coefficients for other arrays can be determined in a similar manner.

B. Design Procedure

One of the objectives of any method is its use in a design. For the binomial method, as for any other nonuniform array method, one of the requirements is the amplitude excitation coefficients for a given number of elements. This can be accomplished using either (6-62) or the Pascal triangle of (6-63) or extensions of it. Other figures of merit are the directivity, half-power beamwidth and side lobe level. It already has been stated that *binomial arrays do not exhibit any minor lobes provided the spacing between the elements is equal or less than one-half of a wavelength.* Unfortunately, closed-form expressions for the directivity and half-power beamwidth for binomial arrays of any spacing between the elements are not available. However, because the design using a $\lambda/2$ spacing leads to a pattern with no minor lobes, approximate closed-form expressions for the half-power beamwidth and maximum directivity for the $d = \lambda/2$ spacing only have been derived [9] in terms of the numbers of elements or the length of the array, and they are given, respectively, by

$$\text{HPBW}(d = \lambda/2) \simeq \frac{1.06}{\sqrt{N-1}} = \frac{1.06}{\sqrt{2L/\lambda}} = \frac{0.75}{\sqrt{L/\lambda}} \tag{6-64}$$

$$D_0 = \frac{2}{\displaystyle\int_0^{\pi} \left[\cos\left(\frac{\pi}{2}\cos\theta\right)\right]^{2(N-1)} \sin\theta \, d\theta} \tag{6-65}$$

$$D_0 = \frac{(2N-2)(2N-4)\cdots 2}{(2N-3)(2N-5)\cdots 1} \tag{6-65a}$$

$$D_0 \simeq 1.77\sqrt{N} = 1.77\sqrt{1 + 2L/\lambda} \tag{6-65b}$$

These expressions can be used effectively to design binomial arrays with a desired half-power beamwidth or directivity. The value of the directivity as obtained using (6-65) to (6-65b) can be compared with the value using the array factor and the computer program DIRECTIVITY of Chapter 2.

To illustrate the method, the patterns of a 10-element binomial array $(2M = 10)$ with spacings between the elements of $\lambda/4$, $\lambda/2$, $3\lambda/4$, and λ, respectively, have been plotted in Figure 6.20. The patterns are plotted using (6-61a) and (6-61c) with the coefficients of $a_1 = 126, a_2 = 84, a_3 = 36, a_4 = 9$, and $a_5 = 1$. It is observed that there are no minor lobes for the arrays with spacings of $\lambda/4$ and $\lambda/2$ between the elements. While binomial arrays have very low level minor lobes, they exhibit larger beamwidths (compared to uniform and Dolph-Tschebyscheff designs). A major practical disadvantage of binomial arrays is the wide variations between the amplitudes of the different

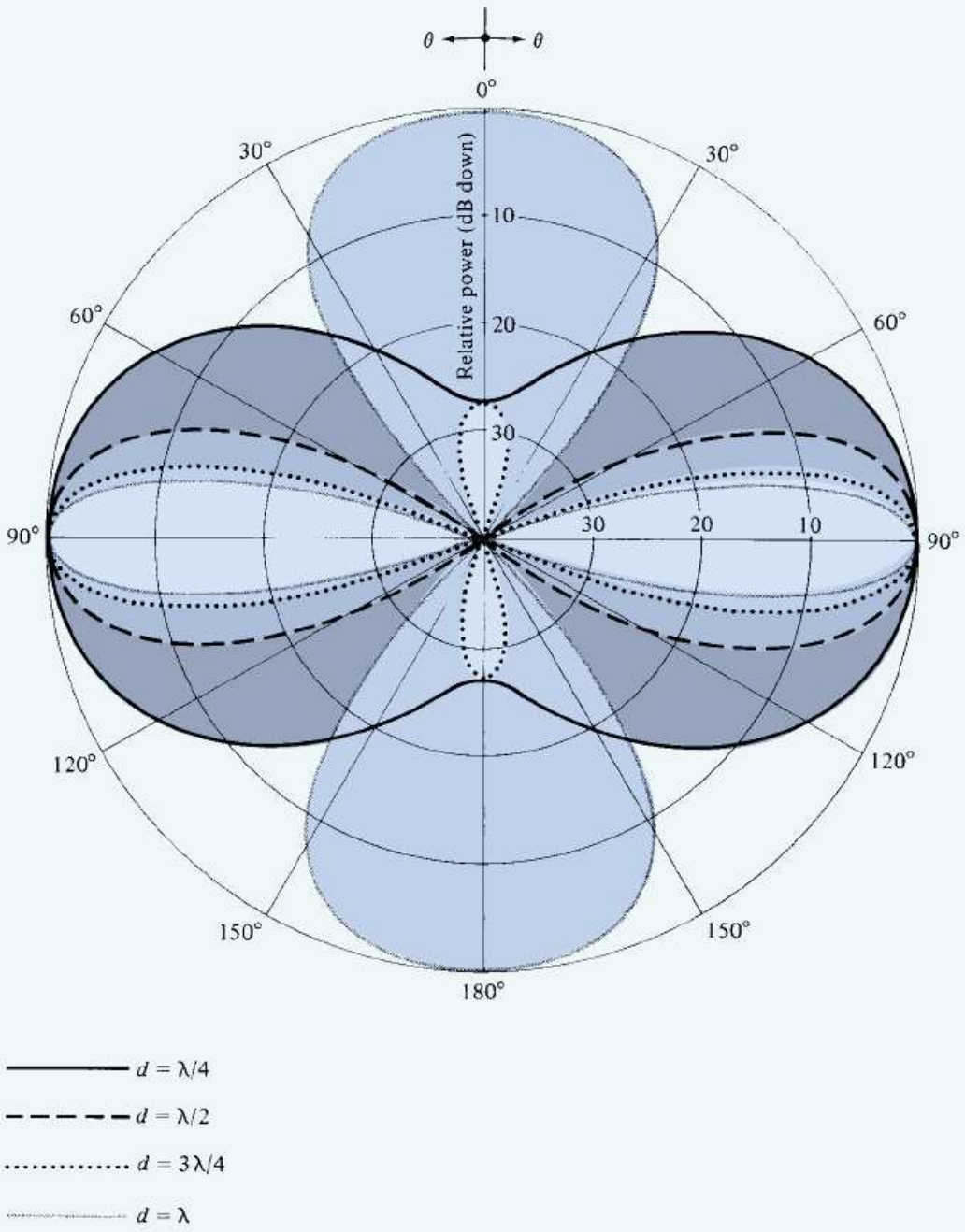


Figure 6.20 Array factor power patterns for a 10-element broadside binomial array with $N = 10$ and $d = \lambda/4, \lambda/2, 3\lambda/4$, and λ.

elements of an array, especially for an array with a large number of elements. This leads to very low efficiencies for the feed network, and it makes the method not very desirable in practice. For example, the relative amplitude coefficient of the end elements of a 10-element array is 1 while that of the center element is 126. Practically, it would be difficult to obtain and maintain such large amplitude variations among the elements. They would also lead to very inefficient antenna systems. Because the magnitude distribution is monotonically decreasing from the center toward the edges

EX2042
Page 342 of 1072

and the magnitude of the extreme elements is negligible compared to those toward the center, a very low side lobe level is expected.

Table 6.7 lists the maximum element spacing $d_{\max}$ for the various linear and planar arrays, including binomial arrays, in order to maintain either one or two amplitude maxima.

Example 6.8

For a 10-element binomial array with a spacing of $\lambda/2$ between the elements, whose amplitude pattern is displayed in Figure 6.20, determine the half-power beamwidth (in degrees) and the maximum directivity (in dB). Compare the answers with other available data.

Solution: Using (6-64), the half-power beamwidth is equal to

$$\text{HPBW} \simeq \frac{1.06}{\sqrt{10-1}} = \frac{1.06}{3} = 0.353 \text{ radians} = 20.23^\circ$$

The value obtained using the array factor, whose pattern is shown in Figure 6.20, is 20.5° which compares well with the approximate value.

Using (6-65a), the value of the directivity is equal for $N = 10$

$$D_0 = 5.392 = 7.32 \text{ dB}$$

while the value obtained using (6-65b) is

$$D_0 = 1.77\sqrt{10} = 5.597 = 7.48 \text{ dB}$$

The value obtained using the array factor and the computer program DIRECTIVITY is $D_0 = 5.392 = 7.32$ dB. These values compare favorably with each other.

6.8.3 Dolph-Tschebyscheff Array

Another array, with many practical applications, is the *Dolph-Tschebyscheff array*. The method was originally introduced by Dolph [7] and investigated afterward by others [10]–[13]. It is primarily a compromise between uniform and binomial arrays. Its excitation coefficients are related to Tschebyscheff polynomials. A Dolph-Tschebyscheff array with no side lobes (or side lobes of $-\infty$ dB) reduces to the binomial design. The excitation coefficients for this case, as obtained by both methods, would be identical.

A. Array Factor

Referring to (6-61a) and (6-61b), the array factor of an array of even or odd number of elements with symmetric amplitude excitation is nothing more than a summation of M or $M + 1$ cosine terms. The largest harmonic of the cosine terms is one less than the total number of elements of the array. Each cosine term, whose argument is an integer times a fundamental frequency, can be rewritten as a series of cosine functions

with the fundamental frequency as the argument. That is,

$$
\begin{aligned}
m = 0 \quad & \cos(mu) = 1 \\
m = 1 \quad & \cos(mu) = \cos u \\
m = 2 \quad & \cos(mu) = \cos(2u) = 2\cos^2 u - 1 \\
m = 3 \quad & \cos(mu) = \cos(3u) = 4\cos^3 u - 3\cos u \\
m = 4 \quad & \cos(mu) = \cos(4u) = 8\cos^4 u - 8\cos^2 u + 1 \\
m = 5 \quad & \cos(mu) = \cos(5u) = 16\cos^5 u - 20\cos^3 u + 5\cos u \\
m = 6 \quad & \cos(mu) = \cos(6u) = 32\cos^6 u - 48\cos^4 u + 18\cos^2 u - 1 \\
m = 7 \quad & \cos(mu) = \cos(7u) = 64\cos^7 u - 112\cos^5 u + 56\cos^3 u - 7\cos u \\
m = 8 \quad & \cos(mu) = \cos(8u) = 128\cos^8 u - 256\cos^6 u + 160\cos^4 u \\
& \qquad\qquad - 32\cos^2 u + 1 \\
m = 9 \quad & \cos(mu) = \cos(9u) = 256\cos^9 u - 576\cos^7 u + 432\cos^5 u \\
& \qquad\qquad - 120\cos^3 u + 9\cos u
\end{aligned}
\tag{6-66}
$$

The above are obtained by the use of Euler's formula

$$[e^{ju}]^m = (\cos u + j\sin u)^m = e^{jmu} = \cos(mu) + j\sin(mu) \tag{6-67}$$

and the trigonometric identity $\sin^2 u = 1 - \cos^2 u$.

If we let

$$z = \cos u \tag{6-68}$$

(6-66) can be written as

$$
\begin{aligned}
m = 0 \quad & \cos(mu) = 1 = T_0(z) \\
m = 1 \quad & \cos(mu) = z = T_1(z) \\
m = 2 \quad & \cos(mu) = 2z^2 - 1 = T_2(z) \\
m = 3 \quad & \cos(mu) = 4z^3 - 3z = T_3(z) \\
m = 4 \quad & \cos(mu) = 8z^4 - 8z^2 + 1 = T_4(z) \\
m = 5 \quad & \cos(mu) = 16z^5 - 20z^3 + 5z = T_5(z) \\
m = 6 \quad & \cos(mu) = 32z^6 - 48z^4 + 18z^2 - 1 = T_6(z) \\
m = 7 \quad & \cos(mu) = 64z^7 - 112z^5 + 56z^3 - 7z = T_7(z) \\
m = 8 \quad & \cos(mu) = 128z^8 - 256z^6 + 160z^4 - 32z^2 + 1 = T_8(z) \\
m = 9 \quad & \cos(mu) = 256z^9 - 576z^7 + 432z^5 - 120z^3 + 9z = T_9(z)
\end{aligned}
\tag{6-69}
$$

and each is related to a Tschebyscheff (Chebyshev) polynomial $T_m(z)$. These relations between the cosine functions and the Tschebyscheff polynomials are valid only in the $-1 \le z \le +1$ range. Because $|\cos(mu)| \le 1$, each Tschebyscheff polynomial is $|T_m(z)| \le 1$ for $-1 \le z \le +1$. For $|z| > 1$, the Tschebyscheff polynomials are related to the hyperbolic cosine functions.

The recursion formula for Tschebyscheff polynomials is

$$\boxed{T_m(z) = 2zT_{m-1}(z) - T_{m-2}(z)} \tag{6-70}$$

It can be used to find one Tschebyscheff polynomial if the polynomials of the previous two orders are known. Each polynomial can also be computed using

$$T_m(z) = \cos[m \cos^{-1}(z)] \qquad -1 \le z \le +1 \tag{6-71a}$$

$$T_m(z) = \cosh[m \cosh^{-1}(z)]^{\dagger} \qquad z < -1, z > +1 \tag{6-71b}$$

In Figure 6.21 the first six Tschebyscheff polynomials have been plotted. The following properties of the polynomials are of interest:

1. All polynomials, of any order, pass through the point (1, 1).
2. Within the range $-1 \le z \le 1$, the polynomials have values within -1 to $+1$.
3. All roots occur within $-1 \le z \le 1$, and all maxima and minima have values of $+1$ and -1, respectively.

Since the array factor of an even or odd number of elements is a summation of cosine terms whose form is the same as the Tschebyscheff polynomials, the unknown coefficients of the array factor can be determined by equating the series representing the cosine terms of the array factor to the appropriate Tschebyscheff polynomial. *The order of the polynomial should be one less than the total number of elements of the array.*

The design procedure will be outlined first, and it will be illustrated with an example. In outlining the procedure, it will be assumed that the number of elements, spacing between the elements, and ratio of major-to-minor lobe intensity (R_0) are known. The requirements will be to determine the excitation coefficients and the array factor of a Dolph-Tschebyscheff array.

B. Array Design

Statement. Design a broadside Dolph-Tschebyscheff array of $2M$ or $2M + 1$ elements with spacing d between the elements. The side lobes are R_0 dB below the maximum of the major lobe. Find the excitation coefficients and form the array factor.

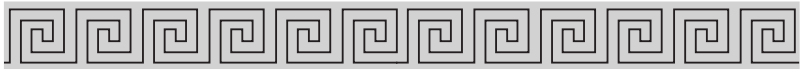
Procedure

a. Select the appropriate array factor as given by (6-61a) or (6-61b).
b. Expand the array factor. Replace each cos(*mu*) function ($m = 0, 1, 2, 3, \ldots$) by its appropriate series expansion found in (6-66).
c. Determine the point $z = z_0$ such that $T_m(z_0) = R_0$ (voltage ratio). *The order m of the Tschebyscheff polynomial is always one less than the total number of elements*. The design procedure requires that the Tschebyscheff polynomial in the $-1 \le z \le z_1$, where z_1 is the null nearest to $z = +1$, be used to represent the minor lobes of the array. The major lobe of the pattern is formed from the remaining part of the polynomial up to point $z_0 (z_1 < z \le z_0)$.
d. Substitute

$$\cos(u) = \frac{z}{z_0} \tag{6-72}$$

$^{\dagger} x = \cosh^{-1}(y) = \ln[y \pm (y^2 - 1)^{1/2}]$

CHAPTER 7



Antenna Synthesis and Continuous Sources

7.1 INTRODUCTION

Thus far in the book we have concentrated primarily on the analysis and design of antennas. In the analysis problem an antenna model is chosen, and it is analyzed for its radiation characteristics (pattern, directivity, impedance, beamwidth, efficiency, polarization, and bandwidth). This is usually accomplished by initially specifying the current distribution of the antenna, and then analyzing it using standard procedures. If the antenna current is not known, it can usually be determined from integral equation formulations. Numerical techniques, such as the Moment Method of Chapter 8, can be used to numerically solve the integral equations.

In practice, it is often necessary to design an antenna system that will yield desired radiation characteristics. For example, a very common request is to design an antenna whose far-field pattern possesses nulls in certain directions. Other common requests are for the pattern to exhibit a desired distribution, narrow beamwidth and low sidelobes, decaying minor lobes, and so forth. The task, in general, is to find not only the antenna configuration but also its geometrical dimensions and excitation distribution. The designed system should yield, either exactly or approximately, an acceptable radiation pattern, and it should satisfy other system constraints. This method of design is usually referred to as *synthesis*. Although synthesis, in its broadest definition, usually refers to antenna pattern synthesis, it is often used interchangeably with design. Since design methods have been outlined and illustrated previously, as in Chapter 6, in this chapter we want to introduce and illustrate antenna pattern synthesis methods.

Antenna pattern synthesis usually requires that first an approximate analytical model is chosen to represent, either exactly or approximately, the desired pattern. The second step is to match the analytical model to a physical antenna model. Generally speaking, antenna pattern synthesis can be classified into three categories. One group requires that the antenna patterns possess nulls in desired directions. The method introduced by Schelkunoff [1] can be used to accomplish this; it will be discussed in Section 7.3. Another category requires that the patterns exhibit a desired distribution in the entire visible region. This is referred to as *beam shaping*, and it can be accomplished using the Fourier transform [2] and the Woodward-Lawson [3], [4] methods. They will be

Antenna Theory: Analysis Design, Third Edition, by Constantine A. Balanis
ISBN 0-471-66782-X Copyright © 2005 John Wiley & Sons, Inc.

EX2042
Page 346 of 1072

discussed and illustrated in Sections 7.4 and 7.5, respectively. A third group includes techniques that produce patterns with narrow beams and low sidelobes. Some methods that accomplish this have already been discussed; namely the binomial method (Section 6.8.2) and the Dolph-Tschebyscheff method (also spelled Tchebyscheff or Chebyshev) of Section 6.8.3. Other techniques that belong to this family are the Taylor line-source (Tschebyscheff-error) [5] and the Taylor line-source (one parameter) [6]. They will be outlined and illustrated in Sections 7.6 and 7.7, respectively.

The synthesis methods will be utilized to design line-sources and linear arrays whose space factors [as defined by (4-58a)] and array factors [as defined by (6-52)] will yield desired far-field radiation patterns. The total pattern is formed by multiplying the space factor (or array factor) by the element factor (or element pattern) as dictated by (4-59) [or (6-5)]. For very narrow beam patterns, the total pattern is nearly the same as the space factor or array factor. This is demonstrated by the dipole antenna ($l \ll \lambda$) of Figure 4.3 whose element factor, as given by (4-58a), is $\sin\theta$; for values of θ near $90^\circ(\theta \simeq 90^\circ)$, $\sin\theta \simeq 1$.

The synthesis techniques will be followed with a brief discussion of some very popular line-source distributions (triangular, cosine, cosine-squared) and continuous aperture distributions (rectangular and circular).

7.2 CONTINUOUS SOURCES

Very long (in terms of a wavelength) arrays of discrete elements usually are more difficult to implement, more costly, and have narrower bandwidths. For such applications, antennas with continuous distributions would be convenient to use. A very long wire and a large reflector represent, respectively, antennas with continuous line and aperture distributions. Continuous distribution antennas usually have larger sidelobes, are more difficult to scan, and in general, they are not as versatile as arrays of discrete elements. The characteristics of continuously distributed sources can be approximated by discrete-element arrays, and vice-versa, and their development follows and parallels that of discrete-element arrays.

7.2.1 Line-Source

Continuous line-source distributions are functions of only one coordinate, and they can be used to approximate linear arrays of discrete elements and vice-versa.

The array factor of a discrete-element array, placed along the z-axis, is given by (6-52) and (6-52a). As the number of elements increases in a fixed-length array, the source approaches a continuous distribution. In the limit, the array factor summation reduces to an integral. For a continuous distribution, the factor that corresponds to the array factor is known as the *space factor*. For a line-source distribution of length l placed symmetrically along the z-axis as shown in Figure 7.1(a), the space factor (SF) is given by

$$\boxed{\mathrm{SF}(\theta) = \int_{-l/2}^{+l/2} I_n(z') e^{j[kz'\cos\theta + \phi_n(z')]}\, dz'} \tag{7-1}$$

where $I_n(z')$ and $\phi_n(z')$ represent, respectively, the amplitude and phase distributions along the source. For a uniform phase distribution $\phi_n(z') = 0$.

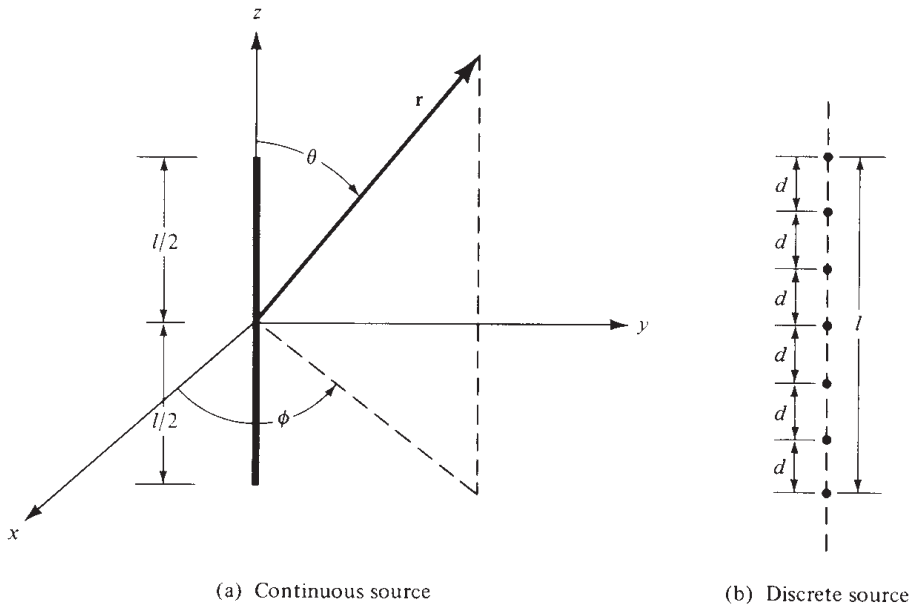


Figure 7.1 Continuous and discrete linear sources.

Equation (7-1) is a finite one-dimensional Fourier transform relating the far-field pattern of the source to its excitation distribution. Two-dimensional Fourier transforms are used to represent the space factors for two-dimensional source distributions. These relations are results of the angular spectrum concept for plane waves, introduced first by Booker and Clemmow [2], and it relates the angular spectrum of a wave to the excitation distribution of the source.

For a continuous source distribution, the total field is given by the product of the *element* and *space* factors as defined in (4-59). This is analogous to the pattern multiplication of (6-5) for arrays. *The type of current and its direction of flow on a source determine the element factor*. For a finite length linear dipole, for example, the total field of (4-58a) is obtained by summing the contributions of small infinitesimal elements which are used to represent the entire dipole. In the limit, as the infinitesimal lengths become very small, the summation reduces to an integration. In (4-58a), the factor outside the brackets is the element factor and the one within the brackets is the space factor and corresponds to (7-1).

7.2.2 Discretization of Continuous Sources

The radiation characteristics of continuous sources can be approximated by discrete-element arrays, and vice-versa. This is illustrated in Figure 7.1(b) whereby discrete elements, with a spacing d between them, are placed along the length of the continuous source. Smaller spacings between the elements yield better approximations, and they can even capture the fine details of the continuous distribution radiation characteristics. For example, the continuous line-source distribution $I_n(z')$ of (7-1) can be approximated by a discrete-element array whose element excitation coefficients, at the specified element positions within $-l/2 \leq z' \leq l/2$, are determined by the sampling of $I_n(z')e^{j\phi_n(z')}$. The radiation pattern of the digitized discrete-element array will approximate the pattern of the continuous source.

EX2042
Page 348 of 1072

The technique can be used for the discretization of any continuous distribution. The accuracy increases as the element spacing decreases; in the limit, the two patterns will be identical. For large element spacing, the patterns of the two antennas will not match well. To avoid this, another method known as *root-matching* can be used [7]. Instead of sampling the continuous current distribution to determine the element excitation coefficients, the root-matching method requires that the nulls of the continuous distribution pattern also appear in the initial pattern of the discrete-element array. If the synthesized pattern using this method still does not yield (within an acceptable accuracy) the desired pattern, a perturbation technique [7] can then be applied to the distribution of the discrete-element array to improve its accuracy.

7.3 SCHELKUNOFF POLYNOMIAL METHOD

A method that is conducive to the synthesis of arrays whose patterns possess nulls in desired directions is that introduced by Schelkunoff [1]. To complete the design, this method requires information on the number of nulls and their locations. The number of elements and their excitation coefficients are then derived. The analytical formulation of the technique follows.

Referring to Figure 6.5(a), the array factor for an N-element, equally spaced, nonuniform amplitude, and progressive phase excitation is given by (6-52) as

$$\text{AF} = \sum_{n=1}^{N} a_n e^{j(n-1)(kd\cos\theta+\beta)} = \sum_{n=1}^{N} a_n e^{j(n-1)\psi} \tag{7-2}$$

where a_n accounts for the nonuniform amplitude excitation of each element. The spacing between the elements is d and β is the progressive phase shift.

Letting

$$z = x + jy = e^{j\psi} = e^{j(kd\cos\theta+\beta)} \tag{7-3}$$

we can rewrite (7-2) as

$$\text{AF} = \sum_{n=1}^{N} a_n z^{n-1} = a_1 + a_2 z + a_3 z^2 + \cdots + a_N z^{N-1} \tag{7-4}$$

which is a polynomial of degree $(N-1)$. From the mathematics of complex variables and algebra, any polynomial of degree $(N-1)$ has $(N-1)$ roots and can be expressed as a product of $(N-1)$ linear terms. Thus we can write (7-4) as

$$\boxed{\text{AF} = a_n(z-z_1)(z-z_2)(z-z_3)\cdots(z-z_{N-1})} \tag{7-5}$$

where $z_1, z_2, z_3, \ldots, z_{N-1}$ are the roots, which may be complex, of the polynomial. The magnitude of (7-5) can be expressed as

$$\boxed{|\text{AF}| = |a_n||z-z_1||z-z_2||z-z_3|\cdots|z-z_{N-1}|} \tag{7-6}$$

Some very interesting observations can be drawn from (7-6) which can be used judiciously for the analysis and synthesis of arrays. Before tackling that phase of the problem, let us first return and examine the properties of (7-3).

The complex variable z of (7-3) can be written in another form as

$$z = |z|e^{j\psi} = |z| \angle\psi = 1 \angle\psi \tag{7-7}$$

$$\psi = kd\cos\theta + \beta = \frac{2\pi}{\lambda} d\cos\theta + \beta \tag{7-7a}$$

It is clear that for any value of d, θ, or β the magnitude of z lies always on a *unit* circle; however its phase depends upon d, θ, and β. For $\beta = 0$, we have plotted in Figures 7-2(a)–(d) the value of z, magnitude and phase, as θ takes values of 0 to π rad. It is observed that for $d = \lambda/8$ the values of z, for all the physically observable

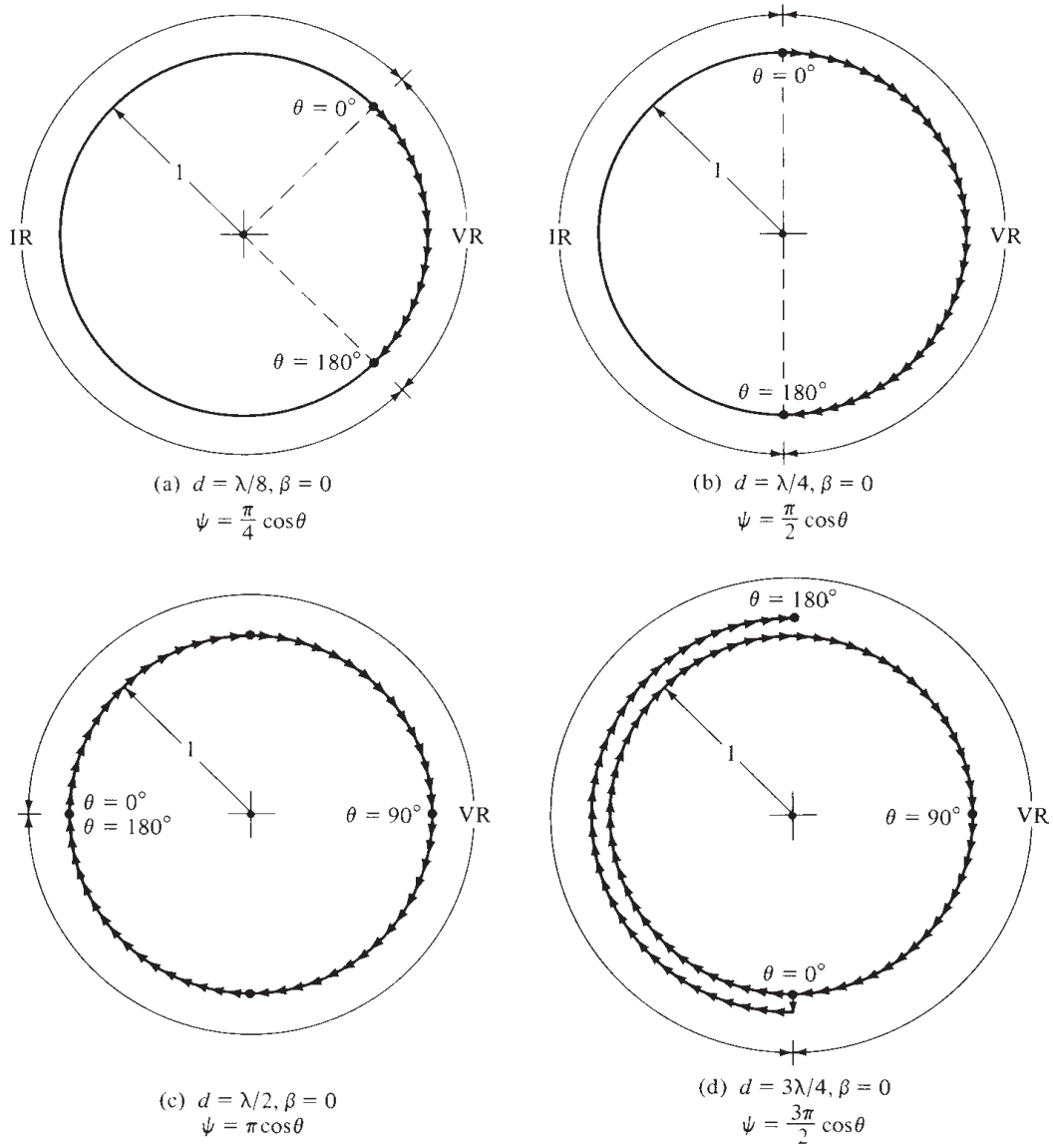


Figure 7.2 *V*isible *R*egion (VR) and *I*nvisible *R*egion (IR) boundaries for complex variable z when $\beta = 0$.

angles of θ, only exist over the part of the circle shown in Figure 7.2(a). Any values of z outside that arc are not realizable by any physical observation angle θ for the spacing $d = \lambda/8$. We refer to the realizable part of the circle as the *visible region* and the remaining as the *invisible region*. In Figure 7.2(a) we also observe the path of the z values as θ changes from 0° to 180°.

In Figures 7.2(b)–(d) we have plotted the values of z when the spacing between the elements is $\lambda/4$, $\lambda/2$, and $3\lambda/4$. It is obvious that the visible region can be extended by increasing the spacing between the elements. It requires a spacing of at least $\lambda/2$ to encompass, at least once, the entire circle. Any spacing greater than $\lambda/2$ leads to multiple values for z. In Figure 7.2(d) we have double values for z for half of the circle when $d = 3\lambda/4$.

To demonstrate the versatility of the arrays, in Figures 7.3(a)–(d) we have plotted the values of z for the same spacings as in Figure 7.2(a)–(d) but with a $\beta = \pi/4$. A

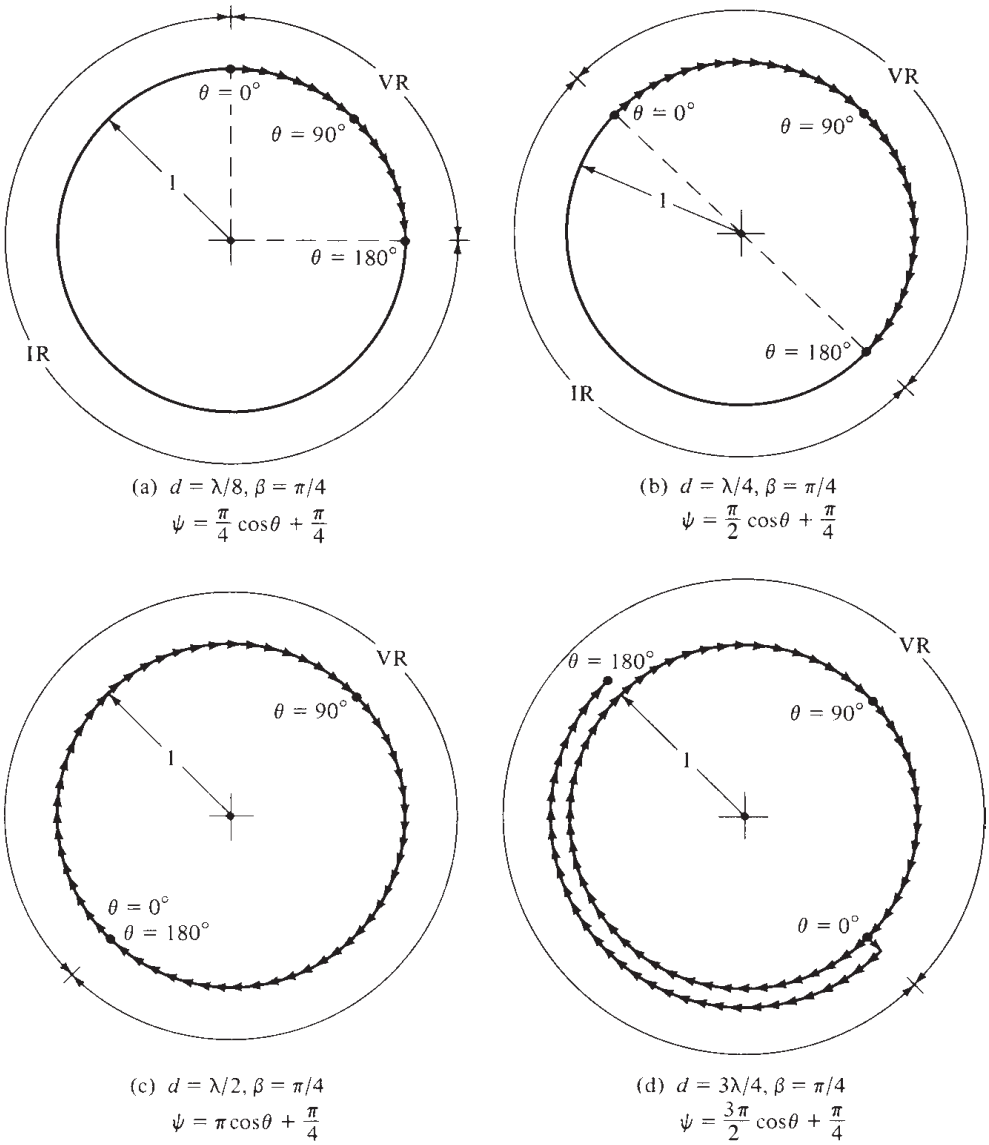


Figure 7.3 *V*isible *R*egion (VR) and *I*nvisible *R*egion (IR) boundaries for complex variable z when $\beta = \pi/4$.

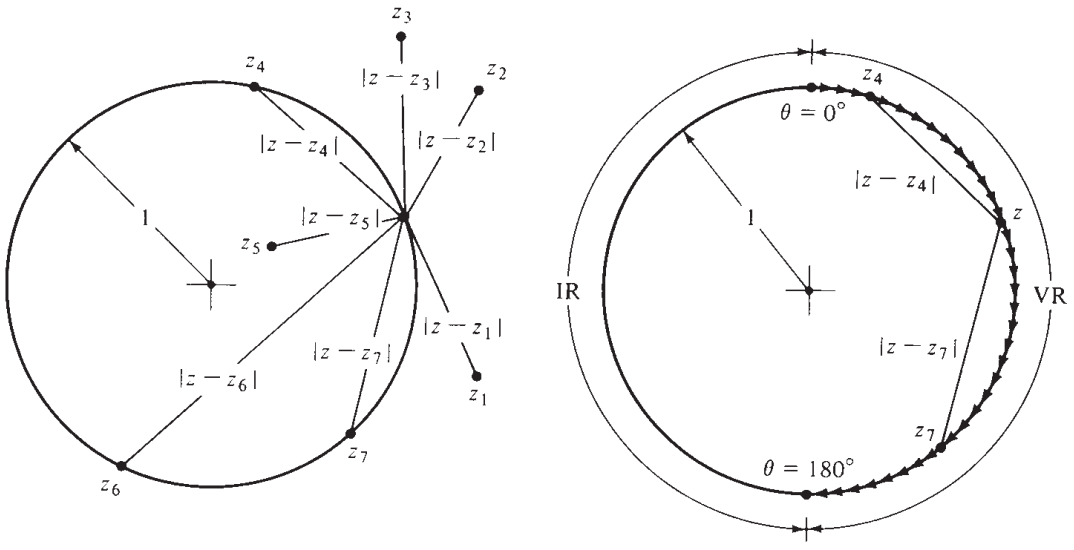
EX2042
Page 351 of 1072

comparison between the corresponding figures indicates that the overall visible region for each spacing has not changed but its relative position on the unit circle has rotated counterclockwise by an amount equal to β.

We can conclude then that the overall extent of the visible region can be controlled by the spacing between the elements and its relative position on the unit circle by the progressive phase excitation of the elements. These two can be used effectively in the design of the array factors.

Now let us return to (7-6). The magnitude of the array factor, its form as shown in (7-6), has a geometrical interpretation. For a given value of z in the visible region of the unit circle, corresponding to a value of θ as determined by (7-3), |AF| is proportional to the product of the distances between z and $z_1, z_2, z_3, \ldots, z_{N-1}$, the roots of AF. In addition, apart from a constant, the phase of AF is equal to the sum of the phases between z and each of the zeros (roots). This is best demonstrated geometrically in Figure 7.4(a). If all the roots $z_1, z_2, z_3, \ldots, z_{N-1}$ are located in the visible region of the unit circle, then each one corresponds to a null in the pattern of |AF| because as θ changes z changes and eventually passes through each of the z_n's. When it does, the length between z and that z_n is zero and (7-6) vanishes. When all the zeros (roots) are not in the visible region of the unit circle, but some lie outside it and/or any other point not on the unit circle, then only those zeros on the visible region will contribute to the nulls of the pattern. This is shown geometrically in Figure 7.4(b). If no zeros exist in the visible region of the unit circle, then that particular array factor has no nulls for any value of θ. However, if a given zero lies on the unit circle but not in its visible region, that zero can be included in the pattern by changing the phase excitation β so that the visible region is rotated until it encompasses that root. Doing this, and not changing d, may exclude some other zero(s).

To demonstrate all the principles, we will consider an example along with some computations.



(a) Roots of array factor

(b) Roots of array factor on unit circle and within visible region

Figure 7.4 Array factor roots within and outside unit circle, and visible and invisible regions.

Example 7.1

Design a linear array with a spacing between the elements of $d = \lambda/4$ such that it has zeros at $\theta = 0°, 90°$, and $180°$. Determine the number of elements, their excitation, and plot the derived pattern. Use Schelkunoff's method.

Solution: For a spacing of $\lambda/4$ between the elements and a phase shift $\beta = 0°$, the visible region is shown in Figure 7.2(b). If the desired zeros of the array factor must occur at $\theta = 0°, 90°$, and $180°$, then these correspond to $z = j, 1, -j$ on the unit circle. Thus a normalized form of the array factor is given by

$$\text{AF} = (z - z_1)(z - z_2)(z - z_3) = (z - j)(z - 1)(z + j)$$

$$\text{AF} = z^3 - z^2 + z - 1$$

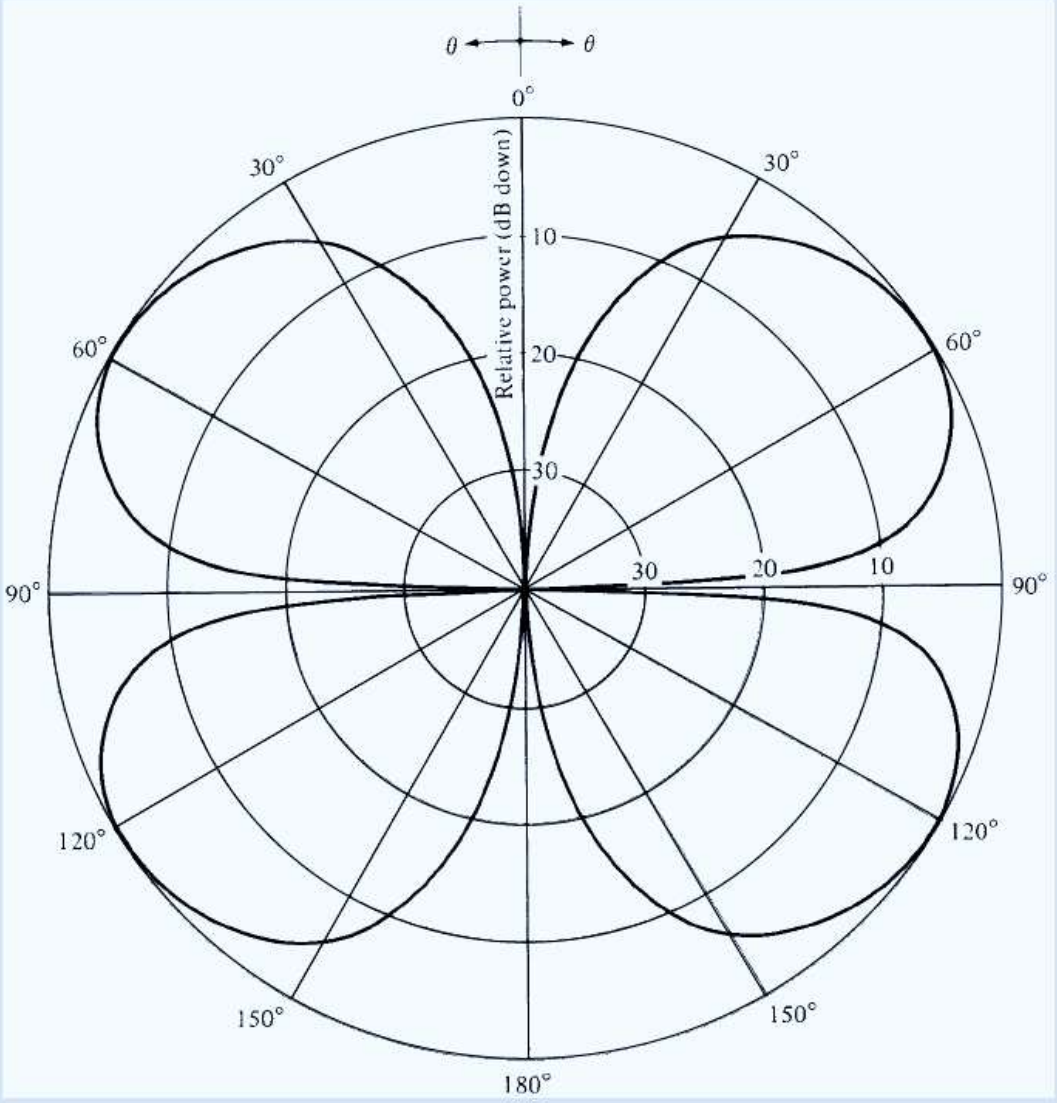


Figure 7.5 Amplitude radiation pattern of a four-element array of isotropic sources with a spacing of $\lambda/4$ between them, zero degrees progressive phase shift, and zeros at $\theta = 0°, 90°$, and $180°$.

Referring to (7-4), the above array factor and the desired radiation characteristics can be realized when there are four elements and their excitation coefficients are equal to

$$a_1 = -1$$

$$a_2 = +1$$

$$a_3 = -1$$

$$a_4 = +1$$

To illustrate the method, we plotted in Figure 7.5 the pattern of that array; it clearly meets the desired specifications. Because of the symmetry of the array, the pattern of the left hemisphere is identical to that of the right.

7.4 FOURIER TRANSFORM METHOD

This method can be used to determine, given a complete description of the desired pattern, the excitation distribution of a continuous or a discrete source antenna system. The derived excitation will yield, either exactly or approximately, the desired antenna pattern. The pattern synthesis using this method is referred to as *beam shaping*.

7.4.1 Line-Source

For a continuous line-source distribution of length l, as shown in Figure 7.1, the normalized space factor of (7-1) can be written as

$$\mathrm{SF}(\theta) = \int_{-l/2}^{l/2} I(z') e^{j(k\cos\theta - k_z)z'}\, dz' = \int_{-l/2}^{l/2} I(z') e^{j\xi z'}\, dz' \tag{7-8}$$

$$\xi = k\cos\theta - k_z \Rightarrow \theta = \cos^{-1}\left(\frac{\xi + k_z}{k}\right) \tag{7-8a}$$

where k_z is the excitation phase constant of the source. For a normalized uniform current distribution of the form $I(z') = I_0/l$, (7-8) reduces to

$$\mathrm{SF}(\theta) = I_0 \frac{\sin\left[\dfrac{kl}{2}\left(\cos\theta - \dfrac{k_z}{k}\right)\right]}{\dfrac{kl}{2}\left(\cos\theta - \dfrac{k_z}{k}\right)} \tag{7-9}$$

The observation angle θ of (7-9) will have real values (visible region) provided that $-(k + k_z) \le \xi \le (k - k_z)$ as obtained from (7-8a).

Since the current distribution of (7-8) extends only over $-l/2 \le z' \le l/2$ (and it is zero outside it), the limits can be extended to infinity and (7-8) can be written as

$$\boxed{\mathrm{SF}(\theta) = \mathrm{SF}(\xi) = \int_{-\infty}^{+\infty} I(z') e^{j\xi z'}\, dz'} \tag{7-10a}$$

The form of (7-10a) is a Fourier transform, and it relates the excitation distribution $I(z')$ of a continuous source to its far-field space factor $\mathrm{SF}(\theta)$. The transform pair of (7-10a) is given by

$$\boxed{I(z') = \frac{1}{2\pi}\int_{-\infty}^{+\infty} \mathrm{SF}(\xi)e^{-jz'\xi}\,d\xi = \frac{1}{2\pi}\int_{-\infty}^{+\infty} \mathrm{SF}(\theta)e^{-jz'\xi}\,d\xi} \tag{7-10b}$$

Whether (7-10a) represents the direct transform and (7-10b) the inverse transform, or vice-versa, does not matter here. The most important thing is that the excitation distribution and the far-field space factor are related by Fourier transforms.

Equation (7-10b) indicates that if $\mathrm{SF}(\theta)$ represents the desired pattern, the excitation distribution $I(z')$ that will yield the exact desired pattern must in general exist for all values of $z'(-\infty \le z' \le \infty)$. Since physically only sources of finite dimensions are realizable, the excitation distribution of (7-10b) is usually truncated at $z' = \pm l/2$ (beyond $z' = \pm l/2$ it is set to zero). Thus the approximate source distribution is given by

$$I_a(z') \simeq \begin{cases} I(z') = \dfrac{1}{2\pi}\displaystyle\int_{-\infty}^{+\infty} \mathrm{SF}(\xi)e^{-jz'\xi}\,d\xi & -l/2 \le z' \le l/2 \\ 0 & \text{elsewhere} \end{cases} \tag{7-11}$$

and it yields an approximate pattern $\mathrm{SF}(\theta)_a$. The approximate pattern is used to represent, within certain error, the desired pattern $\mathrm{SF}(\theta)_d$. Thus

$$\boxed{\mathrm{SF}(\theta)_d \simeq \mathrm{SF}(\theta)_a = \int_{-l/2}^{l/2} I_a(z')e^{j\xi z'}\,dz'} \tag{7-12}$$

It can be shown that, over all values of ξ, the synthesized approximate pattern $\mathrm{SF}(\theta)_a$ yields the least-mean-square error or deviation from the desired pattern $\mathrm{SF}(\theta)_d$. However that criterion is not satisfied when the values of ξ are restricted only in the visible region [8], [9].

To illustrate the principles of this design method, an example is taken.

Example 7.2

Determine the current distribution and the approximate radiation pattern of a line-source placed along the z-axis whose desired radiation pattern is symmetrical about $\theta = \pi/2$, and it is given by

$$\mathrm{SF}(\theta) = \begin{cases} 1 & \pi/4 \le \theta \le 3\pi/4 \\ 0 & \text{elsewhere} \end{cases}$$

This is referred to as a sectoral pattern, and it is widely used in radar search and communication applications.

Solution: Since the pattern is symmetrical, $k_z = 0$. The values of ξ, as determined by (7-8a), are given by $k/\sqrt{2} \geq \xi \geq -k/\sqrt{2}$. In turn, the current distribution is given by (7-10b) or

$$I(z') = \frac{1}{2\pi}\int_{-\infty}^{+\infty} \mathrm{SF}(\xi)e^{-jz'\xi}\,d\xi$$

$$= \frac{1}{2\pi}\int_{-k/\sqrt{2}}^{k/\sqrt{2}} e^{-jz'\xi}\,d\xi = \frac{k}{\pi\sqrt{2}}\left[\frac{\sin\left(\frac{kz'}{\sqrt{2}}\right)}{\frac{kz'}{\sqrt{2}}}\right]$$

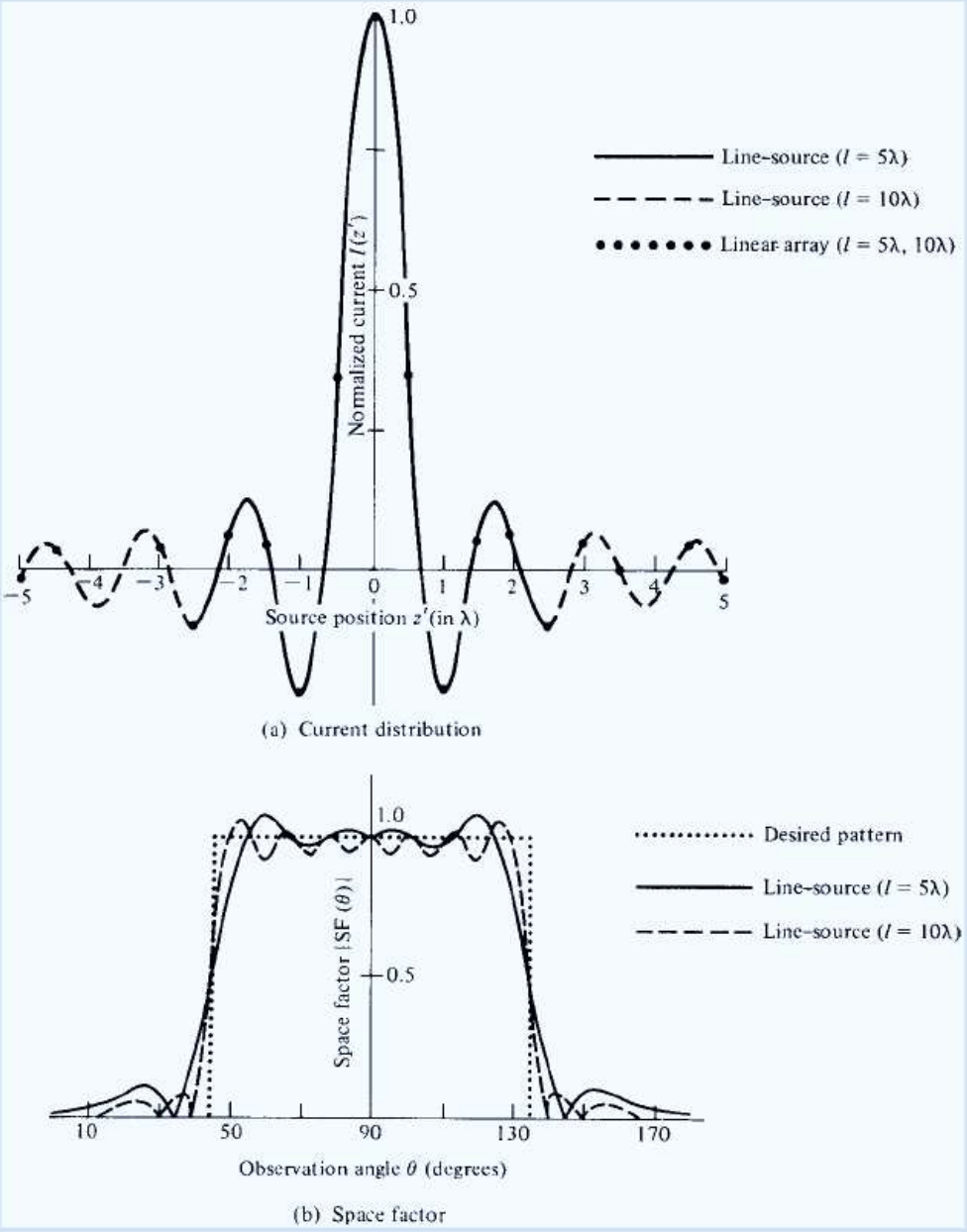


Figure 7.6 Normalized current distribution, desired pattern, and synthesized patterns using the Fourier transform method.

and it exists over all values of $z'(-\infty \le z' \le \infty)$. Over the extent of the line-source, the current distribution is approximated by

$$I_a(z') \simeq I(z'), \qquad -l/2 \le z' \le l/2$$

If the derived current distribution $I(z')$ is used in conjunction with (7-10a) and it is assumed to exist over all values of z', the exact and desired sectoral pattern will result. If however it is truncated at $z' = \pm l/2$ (and assumed to be zero outside), then the desired pattern is approximated by (7-12) or

$$\begin{aligned} \mathrm{SF}(\theta)_d \simeq \mathrm{SF}(\theta)_a &= \int_{-l/2}^{l/2} I_a(z') e^{j\xi z'}\, dz' \\ &= \frac{1}{\pi}\left\{ S_i\left[\frac{l}{\lambda}\pi\left(\cos\theta + \frac{1}{\sqrt{2}}\right)\right] - S_i\left[\frac{l}{\lambda}\pi\left(\cos\theta - \frac{1}{\sqrt{2}}\right)\right]\right\} \end{aligned}$$

where $S_i(x)$ is the sine integral of (4-68b).

The approximate current distribution (normalized so that its maximum is unity) is plotted in Figure 7.6(a) for $l = 5\lambda$ and $l = 10\lambda$. The corresponding approximate normalized patterns are shown in Figure 7.6(b) where they are compared with the desired pattern. A very good reconstruction is indicated. The longer line-source ($l = 10\lambda$) provides a better realization. The sidelobes are about 0.102 (-19.83 dB) for $l = 5\lambda$ and 0.081 (-21.83 dB) for $l = 10\lambda$ (relative to the pattern at $\theta = 90^\circ$).

7.4.2 Linear Array

The array factor of an N-element linear array of equally spaced elements and nonuniform excitation is given by (7-2). If the reference point is taken at the physical center of the array, the array factor can also be written as

Odd Number of Elements $(N = 2M + 1)$

$$\boxed{\mathrm{AF}(\theta) = \mathrm{AF}(\psi) = \sum_{m=-M}^{M} a_m e^{jm\psi}} \tag{7-13a}$$

Even Number of Elements $(\mathrm{N} = 2\mathrm{M})$

$$\boxed{\mathrm{AF}(\theta) = \mathrm{AF}(\psi) = \sum_{m=-M}^{-1} a_m e^{j[(2m+1)/2]\psi} + \sum_{m=1}^{M} a_m e^{j[(2m-1)/2]\psi}} \tag{7-13b}$$

where

$$\boxed{\psi = kd\cos\theta + \beta} \tag{7-13c}$$

For an odd number of elements ($N = 2M + 1$), the elements are placed at

$$z'_m = md, \quad m = 0, \pm 1, \pm 2, \ldots, \pm M \tag{7-13d}$$

and for an even number ($N = 2M$) at

$$z'_m = \begin{cases} \dfrac{2m-1}{2}\, d, & 1 \le m \le M \\ \dfrac{2m+1}{2}\, d, & -M \le m \le -1 \end{cases} \tag{7-13e}$$

An odd number of elements must be utilized to synthesize a desired pattern whose average value, over all angles, is not equal to zero. The $m = 0$ term of (7-13a) is analogous to the d.c. term in a Fourier series expansion of functions whose average value is not zero.

In general, the array factor of an antenna is a periodic function of ψ, and it must repeat for every 2π radians. In order for the array factor to satisfy the periodicity requirements for real values of θ (visible region), then $2kd = 2\pi$ or $d = \lambda/2$. The periodicity and visible region requirement of $d = \lambda/2$ can be relaxed; in fact, it can be made $d < \lambda/2$. However, the array factor $\mathrm{AF}(\psi)$ must be made pseudoperiodic by using fill-in functions, as is customarily done in Fourier series analysis. Such a construction leads to nonunique solutions, because each new fill-in function will result in a different solution. In addition, spacings smaller than $\lambda/2$ lead to superdirective arrays that are undesirable and impractical. If $d > \lambda/2$, the derived patterns exhibit undesired grating lobes; in addition, they must be restricted to satisfy the periodicity requirements.

If $\mathrm{AF}(\psi)$ represents the desired array factor, the excitation coefficients of the array can be obtained by the Fourier formula of

Odd Number of Elements ($N = 2M + 1$)

$$a_m = \frac{1}{T}\int_{-T/2}^{T/2} \mathrm{AF}(\psi) e^{-jm\psi}\, d\psi = \frac{1}{2\pi}\int_{-\pi}^{\pi} \mathrm{AF}(\psi) e^{-jm\psi}\, d\psi \qquad -M \le m \le M \tag{7-14a}$$

Even Number of Elements ($N = 2M$)

$$a_m = \begin{cases} \dfrac{1}{T}\displaystyle\int_{-T/2}^{T/2} \mathrm{AF}(\psi) e^{-j[(2m+1)/2]\psi}\, d\psi \\ \quad = \dfrac{1}{2\pi}\displaystyle\int_{-\pi}^{\pi} \mathrm{AF}(\psi) e^{-j[(2m+1)/2]\psi}\, d\psi \qquad -M \le m \le -1 \end{cases} \tag{7-14b}$$

$$a_m = \begin{cases} \dfrac{1}{T}\displaystyle\int_{-T/2}^{T/2} \mathrm{AF}(\psi) e^{-j[(2m-1)/2]\psi}\, d\psi \\ \quad = \dfrac{1}{2\pi}\displaystyle\int_{-\pi}^{\pi} \mathrm{AF}(\psi) e^{-j[(2m-1)/2]\psi}\, d\psi \qquad 1 \le m \le M \end{cases} \tag{7-14c}$$

Simplifications in the forms of (7-13a)–(7-13b) and (7-14a)–(7-14c) can be obtained when the excitations are symmetrical about the physical center of the array.

Example 7.3

Determine the excitation coefficients and the resultant pattern for a broadside discrete-element array whose array factor closely approximates the desired symmetrical sectoral pattern of Example 7.2. Use 11 elements with a spacing of $d = \lambda/2$ between them. Repeat the design for 21 elements.

Solution: Since the array is broadside, the progressive phase shift between the elements as required by (6-18a) is zero ($\beta = 0$). Since the pattern is nonzero only for $\pi/4 \le \theta \le 3\pi/4$, the corresponding values of ψ are obtained from (7-13c) or $\pi/\sqrt{2} \ge \psi \ge -\pi/\sqrt{2}$. The excitation coefficients are obtained from (7-14a) or

$$a_m = \frac{1}{2\pi}\int_{-\pi/\sqrt{2}}^{\pi/\sqrt{2}} e^{-jm\psi}\, d\psi = \frac{1}{\sqrt{2}}\left[\frac{\sin\left(\frac{m\pi}{\sqrt{2}}\right)}{\frac{m\pi}{\sqrt{2}}}\right]$$

and they are symmetrical about the physical center of the array $[a_m(-z'_m) = a_m(z'_m)]$. The corresponding array factor is given by (7-13a).

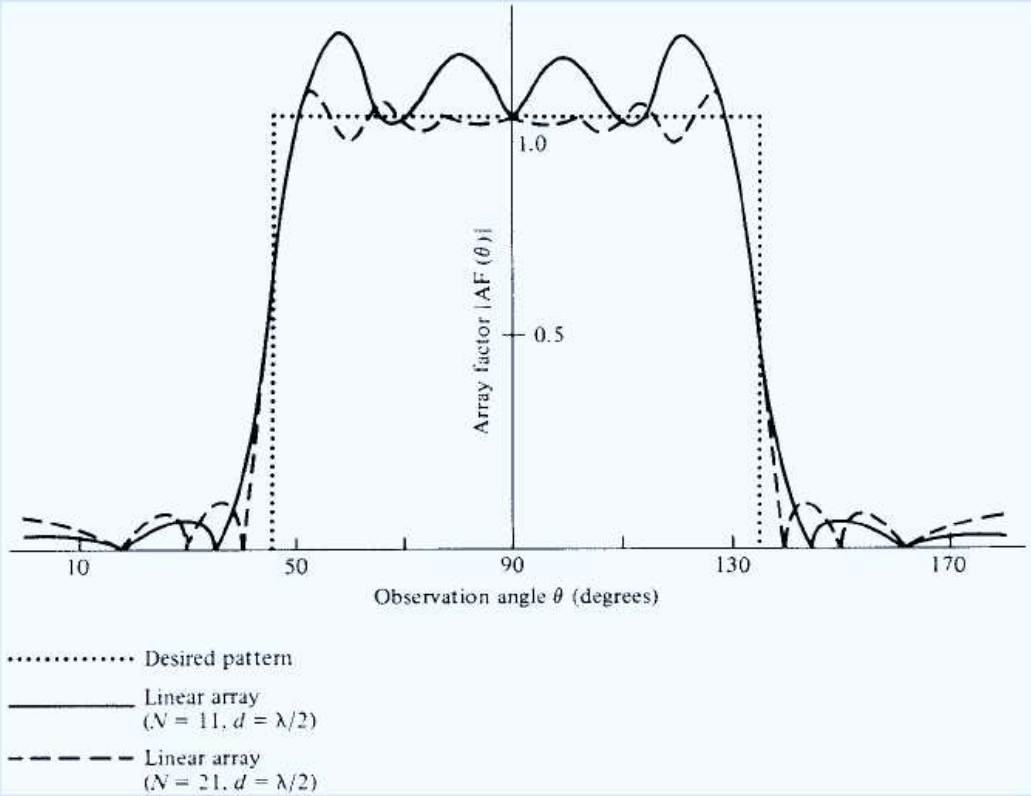


Figure 7.7 Desired array factor and synthesized normalized patterns for linear array of 11 and 21 elements using the Fourier transform method.

The normalized excitation coefficients are

$$
\begin{aligned}
a_0 &= 1.0000 & a_{\pm 4} &= 0.0578 & a_{\pm 8} &= -0.0496 \\
a_{\pm 1} &= 0.3582 & a_{\pm 5} &= -0.0895 & a_{\pm 9} &= 0.0455 \\
a_{\pm 2} &= -0.2170 & a_{\pm 6} &= 0.0518 & a_{\pm 10} &= -0.0100 \\
a_{\pm 3} &= 0.0558 & a_{\pm 7} &= 0.0101 &
\end{aligned}
$$

They are displayed graphically by a dot (•) in Figure 7.6(a) where they are compared with the continuous current distribution of Example 7.2. It is apparent that at the element positions, the line-source and linear array excitation values are identical. This is expected since the two antennas are of the same length (for $N = 11, d = \lambda/2 \Rightarrow l = 5\lambda$ and for $N = 21, d = \lambda/2 \Rightarrow l = 10\lambda$).

The corresponding normalized array factors are displayed in Figure 7.7. As it should be expected, the larger array ($N = 21, d = \lambda/2$) provides a better reconstruction of the desired pattern. The sidelobe levels, relative to the value of the pattern at $\theta = 90^\circ$, are 0.061 (-24.29 dB) for $N = 11$ and 0.108 (-19.33 dB) for $N = 21$.

Discrete-element linear arrays only approximate continuous line-sources. Therefore, their patterns shown in Figure 7.7 do not approximate as well the desired pattern as the corresponding patterns of the line-source distributions shown in Figure 7.6(b).

Whenever the desired pattern contains discontinuities or its values in a given region change very rapidly, the reconstruction pattern will exhibit oscillatory overshoots which are referred to as *Gibbs' phenomena*. Since the desired sectoral patterns of Examples 7.2 and 7.3 are discontinuous at $\theta = \pi/4$ and $3\pi/4$, the reconstructed patterns displayed in Figures 7.6(b) and 7.7 exhibit these oscillatory overshoots.

7.5 WOODWARD-LAWSON METHOD

A very popular antenna pattern synthesis method used for beam shaping was introduced by Woodward and Lawson [3], [4], [10]. The synthesis is accomplished by sampling the desired pattern at various discrete locations. Associated with each pattern sample is a harmonic current of uniform amplitude distribution and uniform progressive phase, whose corresponding field is referred to as a *composing function*. For a line-source, each composing function is of an $b_m \sin(\psi_m)/\psi_m$ form whereas for a linear array it takes an $b_m \sin(N\phi_m)/N \sin(\phi_m)$ form. The excitation coefficient b_m of each harmonic current is such that its field strength is equal to the amplitude of the desired pattern at its corresponding sampled point. The total excitation of the source is comprised of a finite summation of space harmonics. The corresponding synthesized pattern is represented by a finite summation of composing functions with each term representing the field of a current harmonic with uniform amplitude distribution and uniform progressive phase.

The formation of the overall pattern using the Woodward-Lawson method is accomplished as follows. The first composing function produces a pattern whose main beam placement is determined by the value of its uniform progressive phase while its innermost sidelobe level is about -13.5 dB; the level of the remaining sidelobes

monotonically decreases. The second composing function has also a similar pattern except that its uniform progressive phase is adjusted so that its main lobe maximum coincides with the innermost null of the first composing function. This results in the filling-in of the innermost null of the pattern of the first composing function; the amount of filling-in is controlled by the amplitude excitation of the second composing function. Similarly, the uniform progressive phase of the third composing function is adjusted so that the maximum of its main lobe occurs at the second innermost null of the first composing function; it also results in filling-in of the second innermost null of the first composing function. This process continues with the remaining finite number of composing functions.

The Woodward-Lawson method is simple, elegant, and provides insight into the process of pattern synthesis. However, because the pattern of each composing function perturbs the entire pattern to be synthesized, it lacks local control over the sidelobe level in the unshaped region of the entire pattern. In 1988 and 1989 a spirited and welcomed dialogue developed concerning the Woodward-Lawson method [11]–[14]. The dialogue centered whether the Woodward-Lawson method should be taught and even appear in textbooks, and whether it should be replaced by an alternate method [15] which overcomes some of the shortcomings of the Woodward-Lawson method. The alternate method of [15] is more of a numerical and iterative extension of Schelkunoff's polynomial method which may be of greater practical value because it provides superior beamshape and pattern control. One of the distinctions of the two methods is that the Woodward-Lawson method deals with the synthesis of *field patterns* while that of [15] deals with the synthesis of *power patterns*.

The analytical formulation of this method is similar to the Shannon sampling theorem used in communications which states that "if a function $g(t)$ is band-limited, with its highest frequency being f_h, the function $g(t)$ can be reconstructed using samples taken at a frequency f_s. To faithfully reproduce the original function $g(t)$, the sampling frequency f_s should be at least twice the highest frequency f_h ($f_s \geq 2f_h$) or the function should be sampled at points separated by no more than $\Delta t \leq 1/f_s \geq 1/(2f_h) = T_h/2$ where T_h is the period of the highest frequency f_h." In a similar manner, the radiation pattern of an antenna can be synthesized by sampling functions whose samples are separated by λ/l rad, where l is the length of the source [9], [10].

7.5.1 Line-Source

Let the current distribution of a continuous source be represented, within $-l/2 \leq z' \leq l/2$, by a finite summation of normalized sources each of constant amplitude and linear phase of the form

$$i_m(z') = \frac{b_m}{l} e^{-jkz' \cos\theta_m} \qquad -l/2 \leq z' \leq l/2 \tag{7-15}$$

As it will be shown later, θ_m represents the angles where the desired pattern is sampled. The total current $I(z')$ is given by a finite summation of $2M$ (even samples) or $2M + 1$ (odd samples) current sources each of the form of (7-15). Thus

$$I(z') = \frac{1}{l} \sum_{m=-M}^{M} b_m e^{-jkz' \cos\theta_m} \tag{7-16}$$

where

$$m = \pm 1, \pm 2, \ldots, \pm M \text{ (for } 2M \text{ even number of samples)} \tag{7-16a}$$

$$m = 0, \pm 1, \pm 2, \ldots, \pm M \text{ (for } 2M + 1 \text{ odd number of samples)} \tag{7-16b}$$

For simplicity use odd number of samples.

Associated with each current source of (7-15) is a corresponding field pattern of the form given by (7-9) or

$$s_m(\theta) = b_m \left\{ \frac{\sin\left[\frac{kl}{2}(\cos\theta - \cos\theta_m)\right]}{\frac{kl}{2}(\cos\theta - \cos\theta_m)} \right\} \tag{7-17}$$

whose maximum occurs when $\theta = \theta_m$. The total pattern is obtained by summing $2M$ (even samples) or $2M + 1$ (odd samples) terms each of the form given by (7-17). Thus

$$\mathrm{SF}(\theta) = \sum_{m=-M}^{M} b_m \left\{ \frac{\sin\left[\frac{kl}{2}(\cos\theta - \cos\theta_m)\right]}{\frac{kl}{2}(\cos\theta - \cos\theta_m)} \right\} \tag{7-18}$$

The maximum of each individual term in (7-18) occurs when $\theta = \theta_m$, and it is equal to $\mathrm{SF}(\theta = \theta_m)$. In addition, when one term in (7-18) attains its maximum value at its sample at $\theta = \theta_m$, all other terms of (7-18) which are associated with the other samples are zero at $\theta = \theta_m$. In other words, all sampling terms (composing functions) of (7-18) are zero at all sampling points other than at their own. Thus at each sampling point the total field is equal to that of the sample. This is one of the most appealing properties of this method. If the desired space factor is sampled at $\theta = \theta_m$, the excitation coefficients b_m can be made equal to its value at the sample points θ_m. Thus

$$b_m = \mathrm{SF}(\theta = \theta_m)_d \tag{7-19}$$

The reconstructed pattern is then given by (7-18), and it approximates closely the desired pattern.

In order for the synthesized pattern to satisfy the periodicity requirements of 2π for real values of θ (visible region) and to faithfully reconstruct the desired pattern, each sample should be separated by

$$kz'\Delta|_{|z'|=l} = 2\pi \Rightarrow \Delta = \frac{\lambda}{l} \tag{7-19a}$$

The location of each sample is given by

$$\cos\theta_m = m\Delta = m\left(\frac{\lambda}{l}\right), m = 0, \pm1, \pm2, .. \quad \text{for } odd \text{ samples} \tag{7-19b}$$

$$\cos\theta_m = \begin{cases} \dfrac{(2m-1)}{2}\Delta = \dfrac{(2m-1)}{2}\left(\dfrac{\lambda}{l}\right), \\ \qquad m = +1, +2, .. \quad \text{for } even \text{ samples} \\ \dfrac{(2m+1)}{2}\Delta = \dfrac{(2m+1)}{2}\left(\dfrac{\lambda}{l}\right), \\ \qquad m = -1, -2, .. \quad \text{for } even \text{ samples} \end{cases} \tag{7-19c}$$

Therefore, M should be the closest integer to $M = l/\lambda$.

As long as the location of each sample is determined by (7-19b or 7-19c), the pattern value at the sample points is determined solely by that of one sample and it is not correlated to the field of the other samples.

Example 7.4

Repeat the design of Example 7.2 for $l = 5\lambda$ using odd samples and the Woodward-Lawson line-source synthesis method.

Solution: Since $l = 5\lambda$, $M = 5$ and the sampling separation is 0.2. The total number of sampling points is 11. The angles where the sampling is performed are given, according to (7-19b), by

$$\theta_m = \cos^{-1}\left(m\frac{\lambda}{l}\right) = \cos^{-1}(0.2m), \quad m = 0, \pm1, \ldots, \pm5$$

The angles and the excitation coefficients at the sample points are listed below.

m	θ_m	$b_m = \mathrm{SF}(\theta_m)_d$	m	θ_m	$b_m = \mathrm{SF}(\theta_m)_d$
0	90°	1			
1	78.46°	1	−1	101.54°	1
2	66.42°	1	−2	113.58°	1
3	53.13°	1	−3	126.87°	1
4	36.87°	0	−4	143.13°	0
5	0°	0	−5	180°	0

The computed pattern is shown in Figure 7.8(a) where it is compared with the desired pattern. A good reconstruction is indicated. The sidelobe level, relative to the value of the pattern at $\theta = 90°$, is 0.160 (−15.92 dB).

To demonstrate the synthesis of the pattern using the sampling concept, we have plotted in Figure 7.8(b) all seven nonzero composing functions $s_m(\theta)$ used for the reconstruction of the $l = 5\lambda$ line-source pattern of Figure 7.8(a). Each nonzero $s_m(\theta)$ composing function

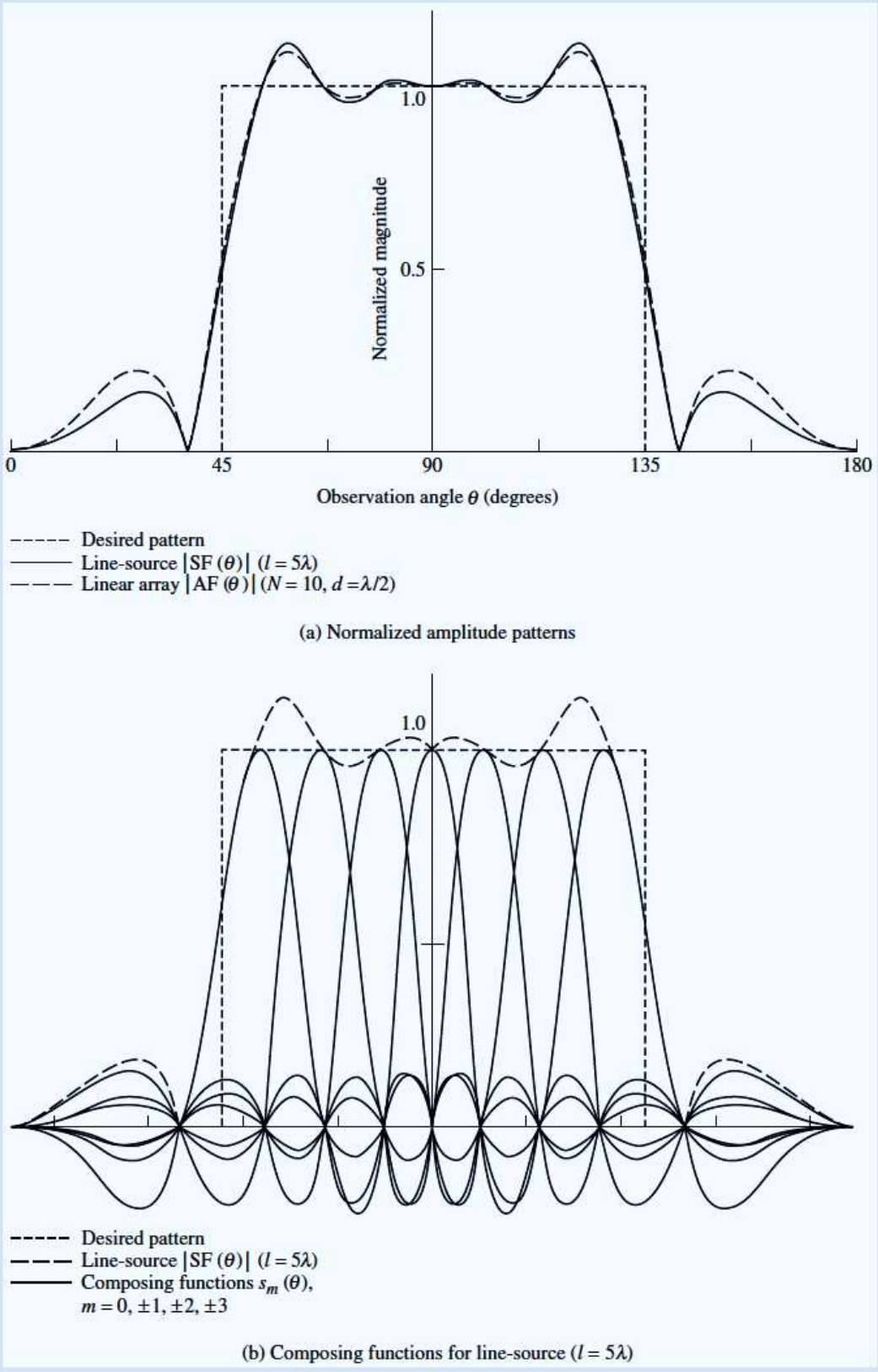


Figure 7.8 Desired and synthesized patterns, and composing functions for Woodward-Lawson designs.

was computed using (7-17) for $m = 0, \pm1, \pm2, \pm3$. It is evident that at each sampling point all the composing functions are zero, except the one that represents that sample. Thus the value of the desired pattern at each sampling point is determined solely by the maximum value of a single composing function. The angles where the composing functions attain their maximum values are listed in the previous table.

7.5.2 Linear Array

The Woodward-Lawson method can also be implemented to synthesize discrete linear arrays. The technique is similar to the Woodward-Lawson method for line-sources except that the pattern of each sample, as given by (7-17), is replaced by the array factor of a uniform array as given by (6-10c). The pattern of each sample can be written as

$$f_m(\theta) = b_m \frac{\sin\left[\frac{N}{2}kd(\cos\theta - \cos\theta_m)\right]}{N\sin\left[\frac{1}{2}kd(\cos\theta - \cos\theta_m)\right]} \tag{7-20}$$

$l = Nd$ assumes the array is equal to the length of the line-source (*for this design only, the length l of the line includes a distance d/2 beyond each end element*). The total array factor can be written as a superposition of $2M + 1$ sampling terms (as was done for the line-source) each of the form of (7-20). Thus

$$\boxed{\mathrm{AF}(\theta) = \sum_{m=-M}^{M} b_m \frac{\sin\left[\frac{N}{2}kd(\cos\theta - \cos\theta_m)\right]}{N\sin\left[\frac{1}{2}kd(\cos\theta - \cos\theta_m)\right]}} \tag{7-21}$$

As for the line-sources, the excitation coefficients of the array elements at the sample points are equal to the value of the desired array factor at the sample points. That is,

$$\boxed{b_m = \mathrm{AF}(\theta = \theta_m)_d} \tag{7-22}$$

The sample points are taken at

$$\cos\theta_m = m\Delta = m\left(\frac{\lambda}{l}\right), m = 0, \pm1, \pm2, .. \quad \text{for } odd \text{ samples} \tag{7-23a}$$

$$\cos\theta_m = \begin{cases} \dfrac{(2m-1)}{2}\Delta = \dfrac{(2m-1)}{2}\left(\dfrac{\lambda}{Nd}\right), \\ \qquad m = +1, +2, .. \quad \text{for } even \text{ samples} \\ \dfrac{(2m+1)}{2}\Delta = \dfrac{(2m+1)}{2}\left(\dfrac{\lambda}{Nd}\right), \\ \qquad m = -1, -2, .. \quad \text{for } even \text{ samples} \end{cases} \tag{7-23b}$$

The normalized excitation coefficient of each array element, required to give the desired pattern, is given by

$$a_n(z') = \frac{1}{N} \sum_{m=-M}^{M} b_m e^{-jkz_n' \cos\theta_m} \tag{7-24}$$

where z_n' indicates the position of the nth element (element in question) symmetrically placed about the geometrical center of the array.

Example 7.5

Repeat the design of Example 7.4 for a linear array of 10 elements using the Woodward-Lawson method with odd samples and an element spacing of $d = \lambda/2$.

Solution: According to (7-19), (7-19b), (7-22) and (7-23a), the excitation coefficients of the array at the sampling points are the same as those of the line-source. Using the values of b_m as listed in Example 7.4, the computed array factor pattern using (7-21) is shown in Figure 7.8(a). A good synthesis of the desired pattern is displayed. The sidelobe level, relative to the pattern value at $\theta = 90^\circ$, is 0.221 (-13.1 dB). The agreement between the line-source and the linear array Woodward-Lawson designs are also good.

The normalized pattern of the symmetrical discrete array can also be generated using the array factor of (6-61a) or (6-61b), where the normalized excitation coefficients a_n's of the array elements are obtained using (7-24). For this example, the excitation coefficients of the 10-element array, along with their symmetrical position, are listed below. To achieve the normalized amplitude pattern of unity at $\theta = 90^\circ$ in Figure 7.8(a), the array factor of (6-61a) must be multiplied by $1/\Sigma a_n = 1/0.4482 = 2.2312$.

Element Number n	Element Position z'_n	Excitation Coefficient a_n
± 1	$\pm 0.25\lambda$	0.6080
± 2	$\pm 0.75\lambda$	-0.1295
± 3	$\pm 1.25\lambda$	0.0000
± 4	$\pm 1.75\lambda$	0.0660
± 5	$\pm 2.25\lambda$	-0.0963

In general, the Fourier transform synthesis method yields reconstructed patterns whose mean-square error (or deviation) from the desired pattern is a minimum. However, the Woodward-Lawson synthesis method reconstructs patterns whose values at the sampled points are identical to the ones of the desired pattern; it does not have any control of the pattern between the sample points, and it does not yield a pattern with least-mean-square deviation.

Ruze [9] points out that the least-mean-square error design is not necessarily the best. The particular application will dictate the preference between the two. However, the Fourier transform method is best suited for reconstruction of desired patterns which are analytically simple and which allow the integrations to be performed in closed form. Today, with the advancements in high-speed computers, this is not a major restriction since the integration

can be performed (with high efficiency) numerically. In contrast, the Woodward-Lawson method is more flexible, and it can be used to synthesize any desired pattern. In fact, it can even be used to reconstruct patterns which, because of their complicated nature, cannot be expressed analytically. Measured patterns, either of analog or digital form, can also be synthesized using the Woodward-Lawson method.

7.6 TAYLOR LINE-SOURCE (TSCHEBYSCHEFF-ERROR)

In Chapter 6 we discussed the classic Dolph-Tschebyscheff array design which yields, for a given sidelobe level, the smallest possible first-null beamwidth (or the smallest possible sidelobe level for a given first-null beamwidth). Another classic design that is closely related to it, but is more applicable for continuous distributions, is that by Taylor [5] (this method is different from that by Taylor [6] which will be discussed in the next section).

The Taylor design [5] yields a pattern that is an optimum compromise between beamwidth and sidelobe level. In an ideal design, the minor lobes are maintained at an equal and specific level. Since the minor lobes are of equal ripple and extend to infinity, this implies an infinite power. More realistically, however, the technique as introduced by Taylor leads to a pattern whose first few minor lobes (closest to the main lobe) are maintained at an equal and specified level; the remaining lobes decay monotonically. Practically, even the level of the closest minor lobes exhibits a slight monotonic decay. This decay is a function of the space u over which these minor lobes are required to be maintained at an equal level. As this space increases, the rate of decay of the closest minor lobes decreases. For a very large space of u (over which the closest minor lobes are required to have an equal ripple), the rate of decay is negligible. It should be pointed out, however, that the other method by Taylor [6] (of Section 7.7) yields minor lobes, all of which decay monotonically.

The details of the analytical formulation are somewhat complex (for the average reader) and lengthy, and they will not be included here. The interested reader is referred to the literature [5], [16]. Instead, a succinct outline of the salient points of the method and of the design procedure will be included. The design is for far-field patterns, and it is based on the formulation of (7-1).

Ideally the normalized space factor that yields a pattern with equal-ripple minor lobes is given by

$$\mathrm{SF}(\theta) = \frac{\cosh[\sqrt{(\pi A)^2 - u^2}]}{\cosh(\pi A)} \tag{7-25}$$

$$u = \pi \frac{l}{\lambda} \cos\theta \tag{7-25a}$$

whose maximum value occurs when $u = 0$. The constant A is related to the maximum desired sidelobe level R_0 by

$$\cosh(\pi A) = R_0 \text{ (voltage ratio)} \tag{7-26}$$

EX2042
Page 367 of 1072

The space factor of (7-25) can be derived from the Dolph-Tschebyscheff array formulation of Section 6.8.3, if the number of elements of the array are allowed to become infinite.

Since (7-25) is ideal and cannot be realized physically, Taylor [5] suggested that it be approximated (within a certain error) by a space factor comprised of a product of factors whose roots are the zeros of the pattern. Because of its approximation to the ideal Tschebyscheff design, it is also referred to as *Tschebyscheff-error*. The Taylor space factor is given by

$$\mathrm{SF}(u, A, \overline{n}) = \frac{\sin(u)}{u} \frac{\prod_{n=1}^{\overline{n}-1} \left[1 - \left(\frac{u}{u_n} \right)^2 \right]}{\prod_{n=1}^{\overline{n}-1} \left[1 - \left(\frac{u}{n\pi} \right)^2 \right]} \tag{7-27}$$

$$u = \pi v = \pi \frac{l}{\lambda} \cos\theta \tag{7-27a}$$

$$u_n = \pi v_n = \pi \frac{l}{\lambda} \cos\theta_n \tag{7-27b}$$

where θ_n represents the locations of the nulls. The parameter $\overline{n}$ is a constant chosen by the designer so that the minor lobes for $|v| = |u/\pi| \leq \overline{n}$ are maintained at a nearly constant voltage level of $1/R_0$ while for $|v| = |u/\pi| > \overline{n}$ the envelope, through the maxima of the remaining minor lobes, decays at a rate of $1/v = \pi/u$. In addition, the nulls of the pattern for $|v| \geq \overline{n}$ occur at integer values of v.

In general, there are $\overline{n} - 1$ inner nulls for $|v| < \overline{n}$ and an infinite number of outer nulls for $|v| \geq \overline{n}$. To provide a smooth transition between the inner and the outer nulls (at the expense of slight beam broadening), Taylor introduced a parameter σ. It is usually referred to as the *scaling factor*, and it spaces the inner nulls so that they blend smoothly with the outer ones. In addition, it is the factor by which the beamwidth of the Taylor design is greater than that of the Dolph-Tschebyscheff, and it is given by

$$\sigma = \frac{\overline{n}}{\sqrt{A^2 + \left(\overline{n} - \frac{1}{2}\right)^2}} \tag{7-28}$$

The location of the nulls are obtained using

$$u_n = \pi v_n = \pi \frac{l}{\lambda} \cos\theta_n = \begin{cases} \pm\pi\sigma\sqrt{A^2 + \left(n - \frac{1}{2}\right)^2} & 1 \leq n < \overline{n} \\ \pm n\pi & \overline{n} \leq n \leq \infty \end{cases} \tag{7-29}$$

The normalized line-source distribution, which yields the desired pattern, is given by

$$I(z') = \frac{\lambda}{l} \left[1 + 2 \sum_{p=1}^{\overline{n}-1} \mathrm{SF}(p, A, \overline{n}) \cos\left(2\pi p \frac{z'}{l} \right) \right] \tag{7-30}$$

The coefficients $\mathrm{SF}(p, A, \overline{n})$ represent samples of the Taylor pattern, and they can be obtained from (7-27) with $u = \pi p$. They can also be found using

$$\mathrm{SF}(p, A, \overline{n}) = \begin{cases} \dfrac{[(\overline{n}-1)!]^2}{(\overline{n}-1+p)!(\overline{n}-1-p)!} \displaystyle\prod_{m=1}^{\overline{n}-1} \left[1 - \left(\frac{\pi p}{u_m}\right)^2\right] & |p| < \overline{n} \\ 0 & |p| \geq \overline{n} \end{cases} \tag{7-30a}$$

with $\mathrm{SF}(-p, A, \overline{n}) = \mathrm{SF}(p, A, \overline{n})$.

The half-power beamwidth is given approximately by [8]

$$\boxed{\Theta_0 \simeq 2\sin^{-1}\left\{\frac{\lambda\sigma}{\pi l}\left[(\cosh^{-1}R_0)^2 - \left(\cosh^{-1}\frac{R_0}{\sqrt{2}}\right)^2\right]^{1/2}\right\}} \tag{7-31}$$

7.6.1 Design Procedure

To initiate a Taylor design, you must

1. specify the normalized maximum tolerable sidelobe level $1/R_0$ of the pattern.
2. choose a positive integer value for $\overline{n}$ such that for $|v| = |(l/\lambda)\cos\theta| \leq \overline{n}$ the normalized level of the minor lobes is nearly constant at $1/R_0$. For $|v| > \overline{n}$, the minor lobes decrease monotonically. In addition, for $|v| < \overline{n}$ there exist $(\overline{n}-1)$ nulls. The position of all the nulls is found using (7-29). Small values of $\overline{n}$ yield source distributions which are maximum at the center and monotonically decrease toward the edges. In contrast, large values of $\overline{n}$ result in sources which are peaked simultaneously at the center and at the edges, and they yield sharper main beams. Therefore, very small and very large values of $\overline{n}$ should be avoided. Typically, the value of $\overline{n}$ should be at least 3 and at least 6 for designs with sidelobes of -25 and -40 dB, respectively.

To complete the design, you do the following:

1. Determine A using (7-26), σ using (7-28), and the nulls using (7-29).
2. Compute the space factor using (7-27), the source distribution using (7-30) and (7-30a), and the half-power beamwidth using (7-31).

Example 7.6

Design a -20 dB Taylor, Tschebyscheff-error, distribution line-source with $\overline{n} = 5$. Plot the pattern and the current distribution for $l = 7\lambda(-7 \leq v = u/\pi \leq 7)$.

Solution: For a -20 dB sidelobe level

$$R_0 \text{ (voltage ratio)} = 10$$

Using (7-26)

$$A = \frac{1}{\pi}\cosh^{-1}(10) = 0.95277$$

and by (7-28)

$$\sigma = \frac{5}{\sqrt{(0.95277)^2 + (5 - 0.5)^2}} = 1.0871$$

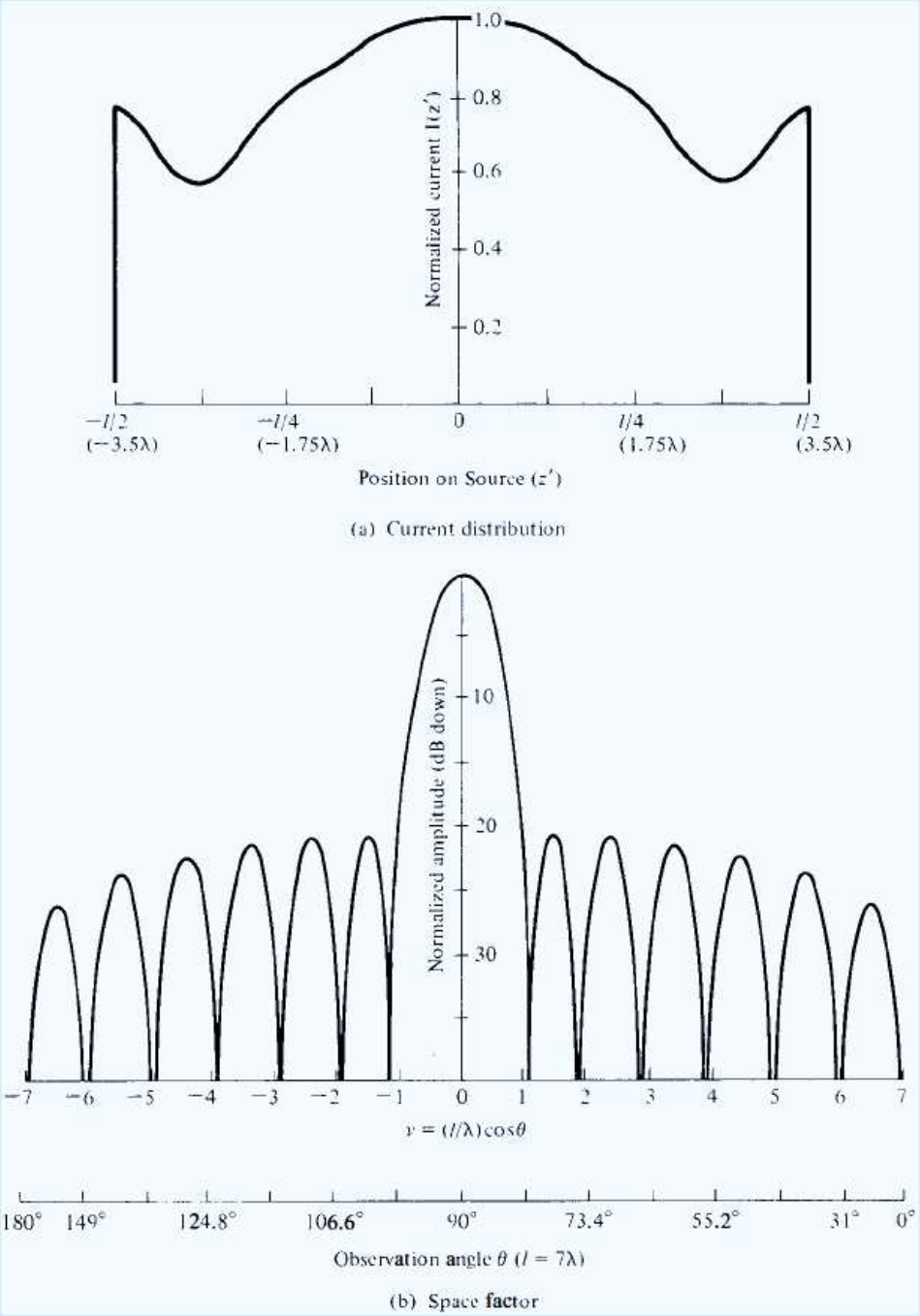


Figure 7.9 Normalized current distribution and far-field space factor pattern for a −20 dB sidelobe and $\bar{n} = 5$ Taylor (Tschebyscheff-error) line-source of $l = 7\lambda$.

The nulls are given by (7-29) or

$$v_n = u_n/\pi = \pm 1.17, \pm 1.932, \pm 2.91, \pm 3.943, \pm 5.00, \pm 6.00, \pm 7.00, \ldots$$

The corresponding null angles for $l = 7\lambda$ are

$$\theta_n = 80.38^\circ(99.62^\circ), 73.98^\circ(106.02^\circ), 65.45^\circ(114.55^\circ),$$
$$55.71^\circ(124.29^\circ), 44.41^\circ(135.59^\circ), \text{ and } 31.00^\circ(149.00^\circ)$$

The half-power beamwidth for $l = 7\lambda$ is found using (7-31), or

$$\Theta_0 \simeq 7.95^\circ$$

The source distribution, as computed using (7-30) and (7-30a), is displayed in Figure 7.9(a). The corresponding radiation pattern for $-7 \leq v = u/\pi \leq 7$ ($0^\circ \leq \theta \leq 180^\circ$ for $l = 7\lambda$) is shown in Figure 7.9(b).

All the computed parameters compare well with results reported in [5] and [16].

7.7 TAYLOR LINE-SOURCE (ONE-PARAMETER)

The Dolph-Tschebyscheff array design of Section 6.8.3 yields minor lobes of equal intensity while the Taylor (Tschebyscheff-error) produces a pattern whose inner minor lobes are maintained at a constant level and the remaining ones decrease monotonically. For some applications, such as radar and low-noise systems, it is desirable to sacrifice some beamwidth and low inner minor lobes to have all the minor lobes decay as the angle increases on either side of the main beam. In radar applications this is preferable because interfering or spurious signals would be reduced further when they try to enter through the decaying minor lobes. Thus any significant contributions from interfering signals would be through the pattern in the vicinity of the major lobe. Since in practice it is easier to maintain pattern symmetry around the main lobe, it is also possible to recognize that such signals are false targets. In low-noise applications, it is also desirable to have minor lobes that decay away from the main beam in order to diminish the radiation accepted through them from the relatively "hot" ground.

A continuous line-source distribution that yields decaying minor lobes and, in addition, controls the amplitude of the sidelobe is that introduced by Taylor [6] in an unpublished classic memorandum. It is referred to as the *Taylor (one-parameter)* design and its source distribution is given by

$$I_n(z') = \begin{cases} J_0\left[j\pi B\sqrt{1-\left(\dfrac{2z'}{l}\right)^2}\right] & -l/2 \leq z' \leq +l/2 \\ 0 & \text{elsewhere} \end{cases} \tag{7-32}$$

where J_0 is the Bessel function of the first kind of order zero, l is the total length of the continuous source [see Figure 7.1(a)], and B is a constant to be determined from the specified sidelobe level.

The space factor associated with (7-32) can be obtained by using (7-1). After some intricate mathematical manipulations, utilizing Gegenbauer's finite integral and Gegenbauer polynomials [17], the space factor for a Taylor amplitude distribution line-source with uniform phase $[\phi_n(z') = \phi_0 = 0]$ can be written as

$$\boxed{\mathrm{SF}(\theta) = \begin{cases} l\dfrac{\sinh[\sqrt{(\pi B)^2 - u^2}]}{\sqrt{(\pi B)^2 - u^2}}, & u^2 < (\pi B)^2 \\ l\dfrac{\sin[\sqrt{u^2 - (\pi B)^2}]}{\sqrt{u^2 - (\pi B)^2}}, & u^2 > (\pi B)^2 \end{cases}} \tag{7-33}$$

where

$$\boxed{u = \pi \frac{l}{\lambda} \cos\theta} \tag{7-33a}$$

B = constant determined from sidelobe level
l = line-source dimension

The derivation of (7-33) is assigned as an exercise to the reader (Problem 7.28). When $(\pi B)^2 > u^2$, (7-33) represents the region near the main lobe. The minor lobes are represented by $(\pi B)^2 < u^2$ in (7-33). Either form of (7-33) can be obtained from the other by knowing that (see Appendix VI)

$$\begin{aligned} \sin(jx) &= j\sinh(x) \\ \sinh(jx) &= j\sin(x) \end{aligned} \tag{7-34}$$

When $u = 0$ ($\theta = \pi/2$ and maximum radiation), the normalized pattern height is equal to

$$(\mathrm{SF})_{\max} = \frac{\sinh(\pi B)}{\pi B} = H_0 \tag{7-35}$$

For $u^2 \gg (\pi B)^2$, the normalized form of (7-33) reduces to

$$\mathrm{SF}(\theta) = \frac{\sin[\sqrt{u^2 - (\pi B)^2}]}{\sqrt{u^2 - (\pi B)^2}} \simeq \frac{\sin(u)}{u} \quad u \gg \pi B \tag{7-36}$$

and it is identical to the pattern of a uniform distribution. The maximum height H_1 of the sidelobe of (7-36) is $H_1 = 0.217233$ (or 13.2 dB down from the maximum), and it occurs when (see Appendix I)

$$[u^2 - (\pi B)^2]^{1/2} \simeq u = 4.494 \tag{7-37}$$

Using (7-35), the maximum voltage height of the sidelobe (relative to the maximum H_0 of the major lobe) is equal to

$$\frac{H_1}{H_0} = \frac{1}{R_0} = \frac{0.217233}{\sinh(\pi B)/(\pi B)} \tag{7-38}$$

or

$$\boxed{R_0 = \frac{1}{0.217233}\frac{\sinh(\pi B)}{\pi B} = 4.603\frac{\sinh(\pi B)}{\pi B}} \tag{7-38a}$$

Equation (7-38a) can be used to find the constant B when the intensity ratio R_0 of the major-to-the-sidelobe is specified. Values of B for typical sidelobe levels are

Sidelobe Level (dB)	−10	−15	−20	−25	−30	−35	−40
B	$j0.4597$	0.3558	0.7386	1.0229	1.2761	1.5136	1.7415

The disadvantage of designing an array with decaying minor lobes as compared to a design with equal minor lobe level (Dolph-Tschebyscheff), is that it yields about 12 to 15% greater half-power beamwidth. However such a loss in beamwidth is a small penalty to pay when the extreme minor lobes decrease as $1/u$.

To illustrate the principles, let us consider an example.

Example 7.7

Given a continuous line-source, whose total length is 4λ, design a Taylor, one-parameter, distribution array whose sidelobe is 30 dB down from the maximum of the major lobe.

a. Find the constant B.
b. Plot the pattern (in dB) of the continuous line-source distribution.
c. For a spacing of $\lambda/4$ between the elements, find the number of discrete isotropic elements needed to approximate the continuous source. Assume that the two extreme elements are placed at the edges of the continuous line source.
d. Find the normalized coefficients of the discrete array of part (c).
e. Write the array factor of the discrete array of parts (c) and (d).
f. Plot the array factor (in dB) of the discrete array of part (e).
g. For a corresponding Dolph-Tschebyscheff array, find the normalized coefficients of the discrete elements.
h. Compare the patterns of the Taylor continuous line-source distribution and discretized array, and the corresponding Dolph-Tschebyscheff discrete-element array.

Solution: For a −30 dB maximum sidelobe, the voltage ratio of the major-to-the-sidelobe level is equal to

$$30 = 20 \log_{10} (R_0) \Rightarrow R_0 = 31.62$$

a. The constant B is obtained using (7-38a) or

$$R_0 = 31.62 = 4.603 \frac{\sinh(\pi B)}{\pi B} \Rightarrow B = 1.2761$$

b. The normalized space factor pattern is obtained using (7-33), and it is shown plotted in Figure 7.10.

c. For $d = \lambda/4$ and with elements at the extremes, the number of elements is 17.

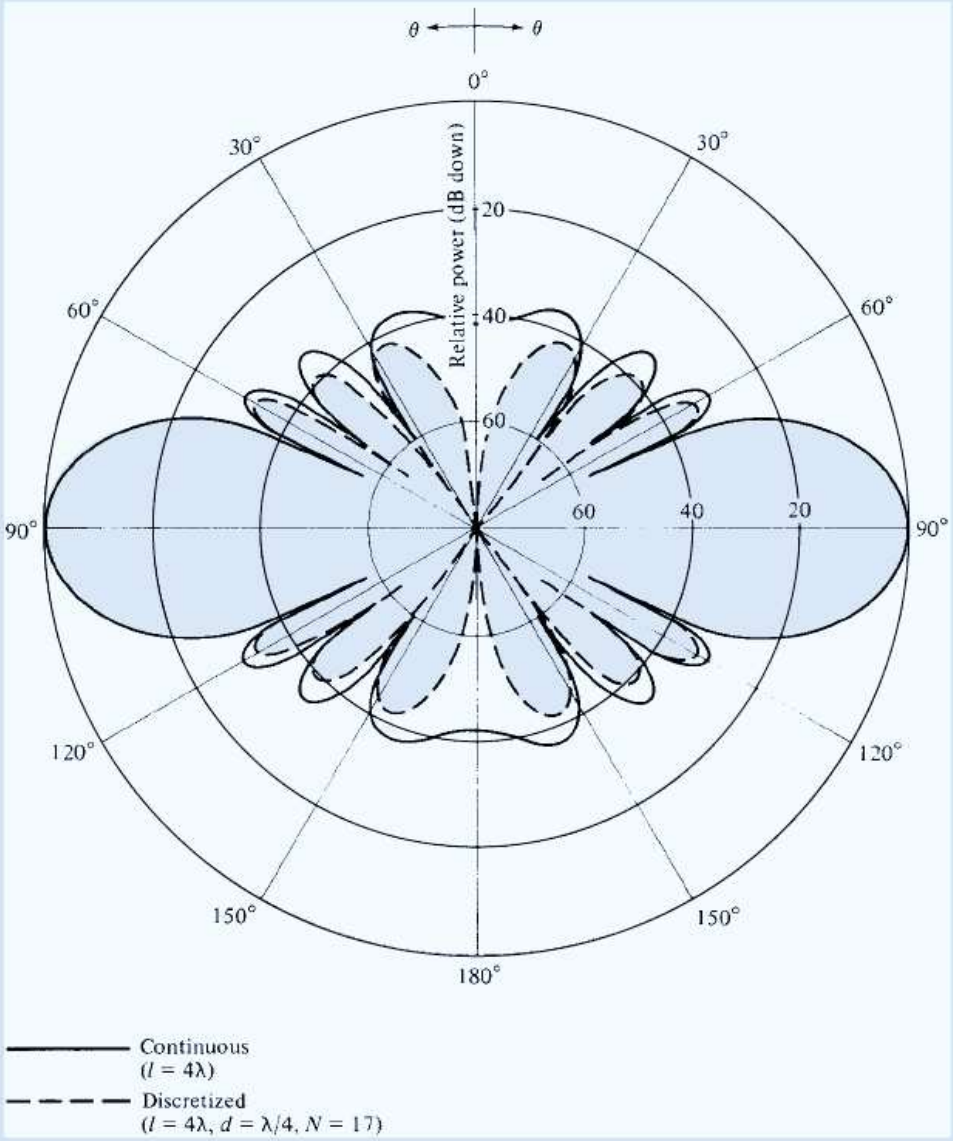


Figure 7.10 Far-field amplitude patterns of continuous and discretized Taylor (one-parameter) distributions.

d. The coefficients are obtained using (7-32). Since we have an odd number of elements, their positioning and excitation coefficients are those shown in Figure 6.19(b). Thus the total excitation coefficient of the center element is

$$2a_1 = I_n(z')|_{z'=0} = J_0(j4.009) = 11.400 \Rightarrow a_1 = 5.70$$

The coefficients of the elements on either side of the center element are identical (because of symmetry), and they are obtained from

$$a_2 = I(z')|_{z'=\pm\lambda/4} = J_0(j3.977) = 11.106$$

The coefficients of the other elements are obtained in a similar manner, and they are given by

$$a_3 = 10.192$$
$$a_4 = 8.889$$
$$a_5 = 7.195$$
$$a_6 = 5.426$$
$$a_7 = 3.694$$
$$a_8 = 2.202$$
$$a_9 = 1.000$$

e. The array factor is given by (6-61b) and (6-61c), or

$$(\text{AF})_{17} = \sum_{n=1}^{9} a_n \cos[2(n-1)u]$$

$$u = \pi \frac{d}{\lambda} \cos\theta = \frac{\pi}{4} \cos\theta$$

where the coefficients (a_n's) are those found in part (d).

f. The normalized pattern (in dB) of the discretized distribution (discrete-element array) is shown in Figure 7.10.

g. The normalized coefficients of a 17-element Dolph-Tschebyscheff array, with −30 dB sidelobes, are obtained using the method outlined in the Design Section of Section 6.8.3 and are given by

Unnormalized	Normalized
$a_1 = 2.858$	$a_{1n} = 1.680$
$a_2 = 5.597$	$a_{2n} = 3.290$
$a_3 = 5.249$	$a_{3n} = 3.086$
$a_4 = 4.706$	$a_{4n} = 2.767$
$a_5 = 4.022$	$a_{5n} = 2.364$
$a_6 = 3.258$	$a_{6n} = 1.915$
$a_7 = 2.481$	$a_{7n} = 1.459$
$a_8 = 1.750$	$a_{8n} = 1.029$
$a_9 = 1.701$	$a_{9n} = 1.000$

As with the discretized Taylor distribution array, the coefficients are symmetrical, and the form of the array factor is that given in part (e).

h. The normalized pattern (in dB) is plotted in Figure 7.11 where it is compared with that of the discretized Taylor distribution. From the patterns in Figures 7.10 and 7.11, it can be concluded that

1. the main lobe of the continuous line-source Taylor design is well approximated by the discretized distribution with a $\lambda/4$ spacing between the elements. Even the minor lobes are well represented, and a better approximation can be obtained with more elements and smaller spacing between them.
2. the Taylor distribution array pattern has a wider main lobe than the corresponding Dolph-Tschebyscheff, but it displays decreasing minor lobes away from the main beam.

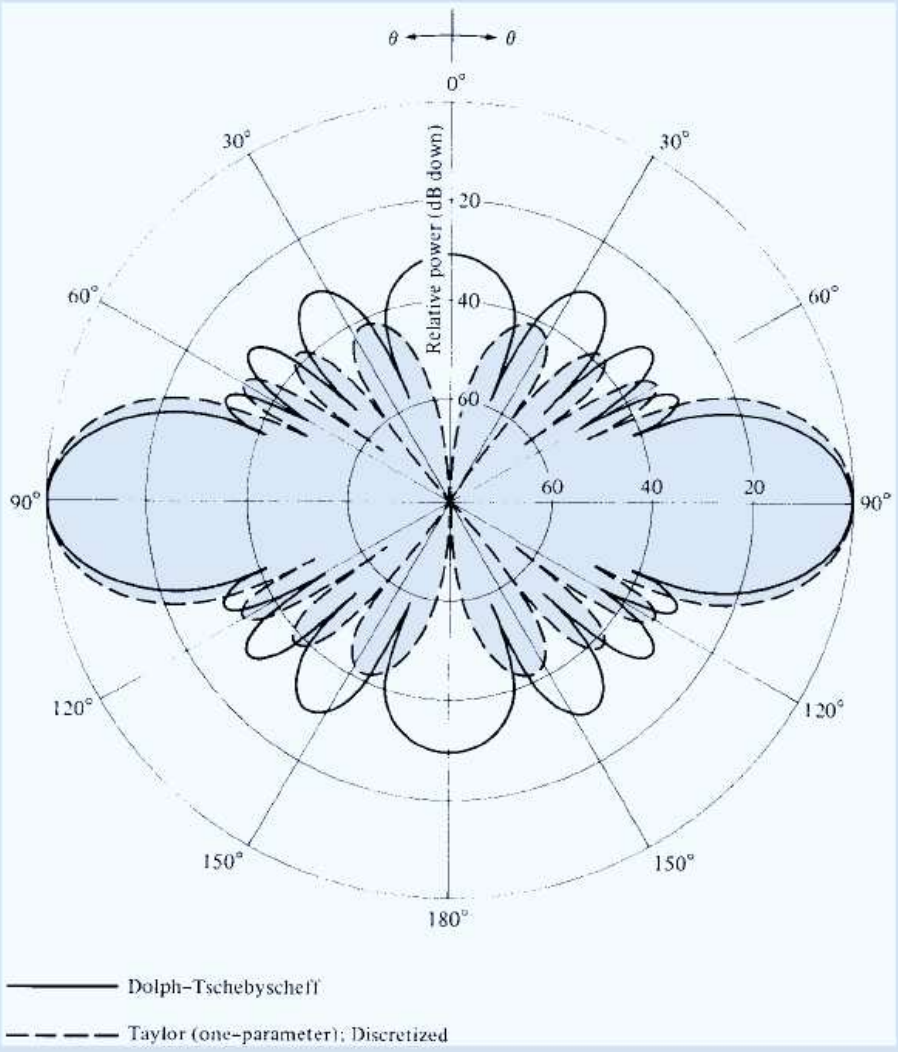
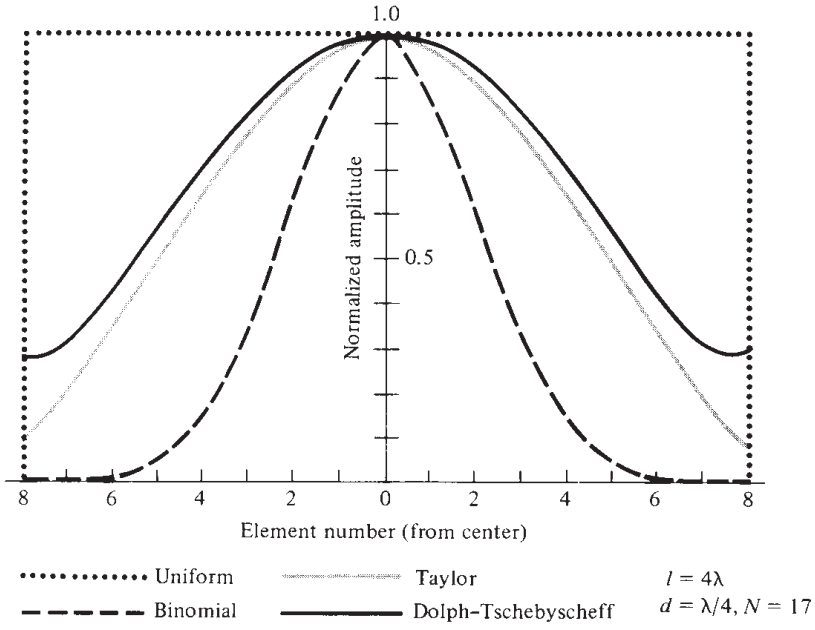


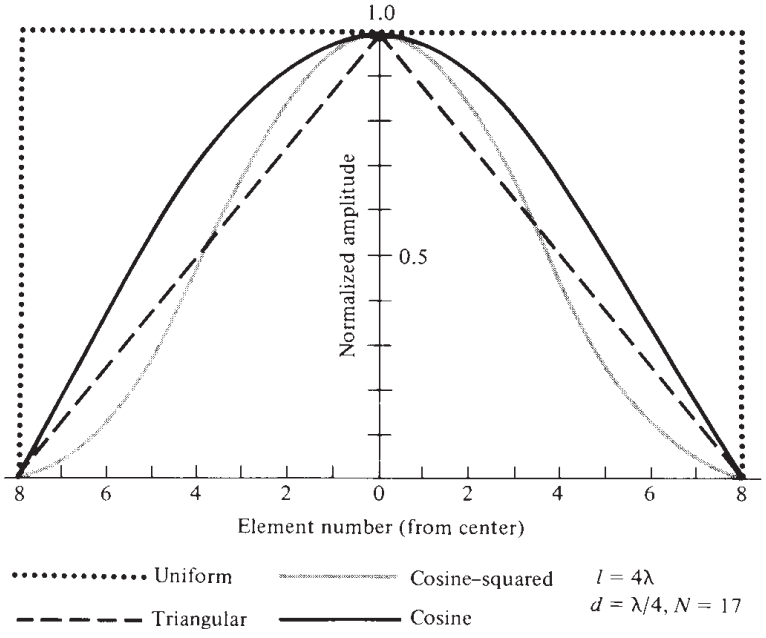
Figure 7.11 Far-field amplitude patterns of Taylor (discretized) and Dolph-Tschebyscheff distributions ($l = 4\lambda, d = \lambda/4, N = 17$).

A larger spacing between the elements does not approximate the continuous distribution as accurately. The design of Taylor and Dolph-Tschebyscheff arrays for $l = 4\lambda$ and $d = \lambda/2 (N = 9)$ is assigned as a problem at the end of the chapter (Problem 7.29).

To qualitatively assess the performance between uniform, binomial, Dolph-Tschebyscheff, and Taylor (one-parameter) array designs, the amplitude distribution of each has been plotted in Figure 7.12(a). It is assumed that $l = 4\lambda$, $d = \lambda/4$, $N = 17$,



(a) Amplitude distribution of uniform, binomial, Taylor, and Dolph–Tschebyscheff discrete-element arrays



(b) Amplitude distribution of uniform, triangular, cosine, and cosine squared discrete-element arrays

Figure 7.12 Amplitude distribution of nonuniform amplitude linear arrays.

EX2042
Page 377 of 1072

and the maximum sidelobe is 30 dB down. The coefficients are normalized with respect to the amplitude of the corresponding element at the center of that array.

The binomial design possesses the smoothest amplitude distribution (between 1 and 0) from the center to the edges (the amplitude toward the edges is vanishingly small). Because of this characteristic, the binomial array displays the smallest sidelobes followed, in order, by the Taylor, Tschebyscheff, and the uniform arrays. In contrast, the uniform array possesses the smallest half-power beamwidth followed, in order, by the Tschebyscheff, Taylor, and binomial arrays. *As a rule of thumb, the array with the smoothest amplitude distribution (from the center to the edges) has the smallest sidelobes and the larger half-power beamwidths*. The best design is a trade-off between sidelobe level and beamwidth.

A MATLAB computer program entitled ***Synthesis*** has been developed, and it performs synthesis using the Schelkunoff, Fourier transform, Woodward-Lawson, Taylor (Tschebyscheff-error) and Taylor (one-parameter) methods. The program is included in the CD attached to the book. The description of the program is provided in the corresponding READ ME file.

7.8 TRIANGULAR, COSINE, AND COSINE-SQUARED AMPLITUDE DISTRIBUTIONS

Some other very common and simple line-source amplitude distributions are those of the triangular, cosine, cosine-squared, cosine on-a-pedestal, cosine-squared on-a-pedestal, Gaussian, inverse taper, and edge. Instead of including many details, the pattern, half-power beamwidth, first-null beamwidth, magnitude of sidelobes, and directivity for uniform, triangular, cosine, and cosine-squared amplitude distributions (with constant phase) are summarized in Table 7.1 [18], [19].

The normalized coefficients for a uniform, triangular, cosine, and cosine-squared arrays of $l = 4\lambda, d = \lambda/4, N = 17$ are shown plotted in Figure 7.12(b). The array with the smallest sidelobes and the larger half-power beamwidth is the cosine-squared, because it possesses the smoothest distribution. It is followed, in order, by the triangular, cosine, and uniform distributions. This is verified by examining the characteristics in Table 7.1.

Cosine on-a-pedestal distribution is obtained by the superposition of the uniform and the cosine distributions. Thus it can be represented by

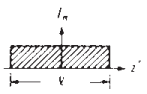
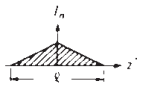
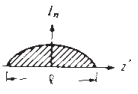
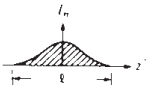
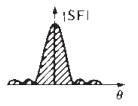
$$I_n(z') = \begin{cases} I_0 + I_2 \cos\left(\dfrac{\pi}{l} z'\right), & -l/2 \le z' \le l/2 \\ 0 & \text{elsewhere} \end{cases} \tag{7-39}$$

where I_0 and I_2 are constants. The space factor pattern of such a distribution is obtained by the addition of the patterns of the uniform and the cosine distributions found in Table 7.1. That is,

$$\text{SF}(\theta) = I_0 l \frac{\sin(u)}{u} + I_2 \frac{\pi l}{2} \frac{\cos u}{(\pi/2)^2 - u^2} \tag{7-40}$$

A similar procedure is used to represent and analyze a cosine-squared on-a-pedestal distribution.

TABLE 7.1 Radiation Characteristics for Line-Sources and Linear Arrays with Uniform, Triangular, Cosine, and Cosine-Squared Distributions

Distribution	Uniform	Triangular	Cosine	Cosine-Squared
Distribution I_n (analytical)	I_0	$I_1\left(1-\frac{2}{l}\lvert z'\rvert\right)$	$I_2\cos\left(\frac{\pi}{l}z'\right)$	$I_3\cos^2\left(\frac{\pi}{l}z'\right)$
Distribution (graphical)				
Space factor (SF) $u=\left(\frac{\pi l}{\lambda}\right)\cos\theta$	$I_0 l\frac{\sin(u)}{u}$	$I_1\frac{l}{2}\left[\frac{\sin\left(\frac{u}{2}\right)}{\frac{u}{2}}\right]^2$	$I_2 l\frac{\pi}{2}\frac{\cos(u)}{(\pi/2)^2-u^2}$	$I_3\frac{l}{2}\frac{\sin(u)}{u}\left[\frac{\pi^2}{\pi^2-u^2}\right]$
Space factor |SF|				
Half-power beamwidth (degrees) $l \gg \lambda$	$\frac{50.6}{(l/\lambda)}$	$\frac{73.4}{(l/\lambda)}$	$\frac{68.8}{(l/\lambda)}$	$\frac{83.2}{(l/\lambda)}$
First-null beamwidth (degrees) $l \gg \lambda$	$\frac{114.6}{(l/\lambda)}$	$\frac{229.2}{(l/\lambda)}$	$\frac{171.9}{(l/\lambda)}$	$\frac{229.2}{(l/\lambda)}$
First sidelobe max. (to main max.) (dB)	-13.2	-26.4	-23.2	-31.5
Directivity factor (l large)	$2\left(\frac{l}{\lambda}\right)$	$0.75\left[2\left(\frac{l}{\lambda}\right)\right]$	$0.810\left[2\left(\frac{l}{\lambda}\right)\right]$	$0.667\left[2\left(\frac{l}{\lambda}\right)\right]$

7.9 LINE-SOURCE PHASE DISTRIBUTIONS

The amplitude distributions of the previous section were assumed to have uniform phase variations throughout the physical extent of the source. Practical radiators (such as reflectors, lenses, horns, etc.) have nonuniform phase fronts caused by one or more of the following:

1. displacement of the reflector feed from the focus
2. distortion of the reflector or lens surface

3. feeds whose wave fronts are not ideally cylindrical or spherical (as they are usually presumed to be)
4. physical geometry of the radiator

These are usually referred to *phase errors*, and they are more evident in radiators with tilted beams.

To simplify the analytical formulations, most of the phase fronts are represented with linear, quadratic, or cubic distributions. Each of the phase distributions can be associated with each of the amplitude distributions. In (7-1), the phase distribution of the source is represented by $\phi_n(z')$. For linear, quadratic, and cubic phase variations, $\phi_n(z')$ takes the form of

$$linear: \qquad \phi_1(z') = \beta_1 \frac{2}{l} z', \qquad -l/2 \le z' \le l/2 \tag{7-41a}$$

$$quadratic: \quad \phi_2(z') = \beta_2 \left(\frac{2}{l}\right)^2 z'^2, \quad -l/2 \le z' \le l/2 \tag{7-41b}$$

$$cubic: \qquad \phi_3(z') = \beta_3 \left(\frac{2}{l}\right)^3 z'^3, \quad -l/2 \le z' \le l/2 \tag{7-41c}$$

and it is shown plotted in Figure 7.13. The quadratic distribution is used to represent the phase variations at the aperture of a horn and of defocused (along the symmetry axis) reflector and lens antennas.

The space factor patterns corresponding to the phase distributions of (7-41a)–(7-41c) can be obtained by using (7-1). Because the analytical formulations become lengthy and complex, especially for the quadratic and cubic distributions, they will not be included here. Instead, a general guideline of their effects will be summarized [18], [19].

Linear phase distributions have a tendency to tilt the main beam of an antenna by an angle θ_0 and to form an asymmetrical pattern. The pattern of this distribution can be obtained by replacing the u (for uniform phase) in Table 7.1 by $(u - \theta_0)$. In general, the half-power beamwidth of the tilted pattern is increased by $1/\cos\theta_0$ while the directivity is decreased by $\cos\theta_0$. This becomes more apparent by realizing that the projected length of the line-source toward the maximum is reduced by $\cos\theta_0$. Thus the effective length of the source is reduced.

Quadratic phase errors lead primarily to a reduction of directivity, and an increase in sidelobe level on either side of the main lobe. The symmetry of the original pattern is maintained. In addition, for moderate phase variations, ideal nulls in the patterns disappear. Thus the minor lobes blend into each other and into the main beam, and they represent shoulders of the main beam instead of appearing as separate lobes. Analytical formulations for quadratic phase distributions are introduced in Chapter 13 on horn antennas.

Cubic phase distributions introduce not only a tilt in the beam but also decrease the directivity. The newly formed patterns are asymmetrical. The minor lobes on one side are increased in magnitude and those on the other side are reduced in intensity.

7.10 CONTINUOUS APERTURE SOURCES

Space factors for aperture (two-dimensional) sources can be introduced in a similar manner as in Section 7.2.1 for line-sources.

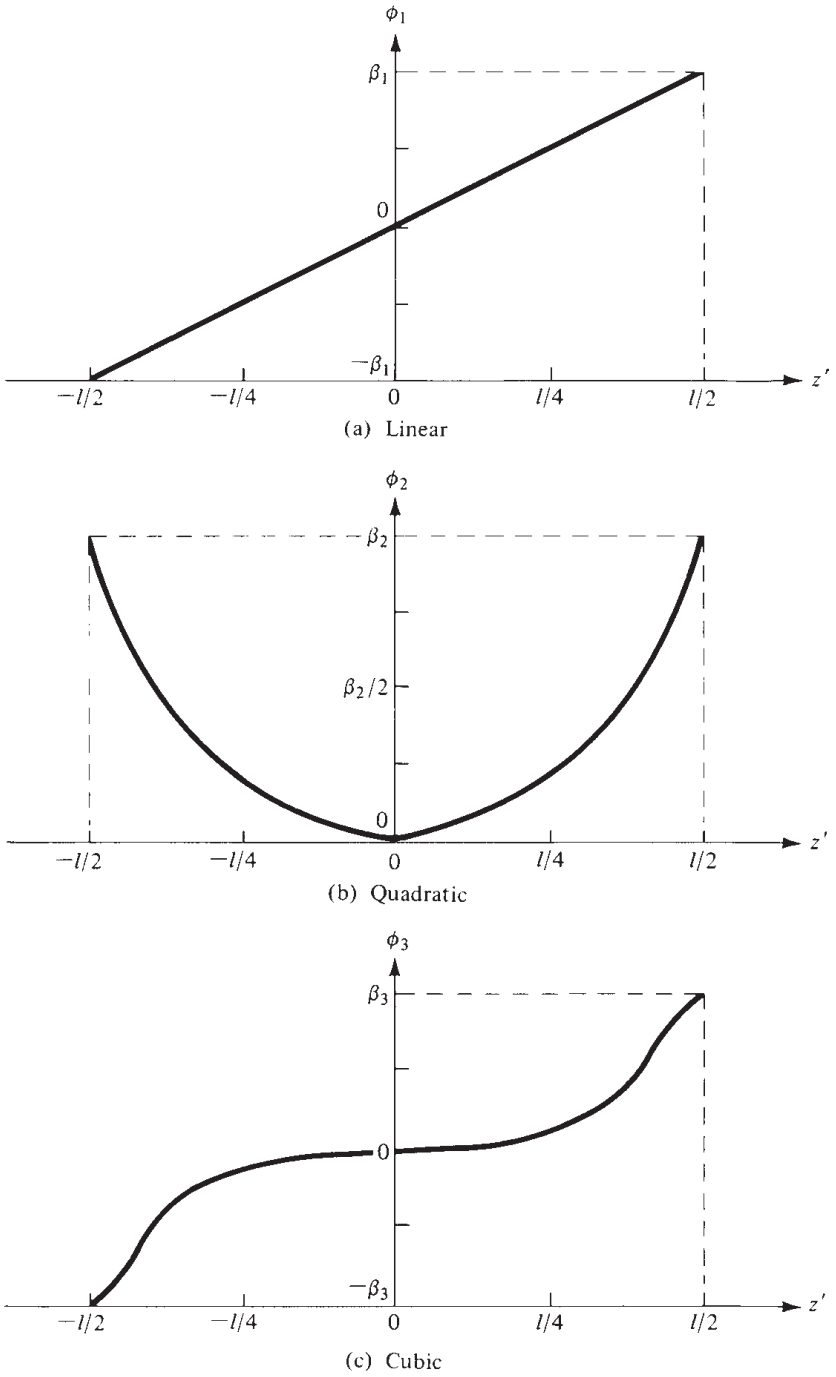


Figure 7.13 Linear, quadratic, and cubic phase variations.

7.10.1 Rectangular Aperture

Referring to the geometry of Figure 6.28(b), the space factor for a two-dimensional rectangular distribution along the x-y plane is given by

$$\text{SF} = \int_{-l_y/2}^{l_y/2} \int_{-l_x/2}^{l_x/2} A_n(x', y') e^{j[kx' \sin\theta \cos\phi + ky' \sin\theta \sin\phi + \phi_n(x', y')]} \, dx' \, dy' \tag{7-42}$$

EX2042
Page 381 of 1072

where l_x and l_y are, respectively, the linear dimensions of the rectangular aperture along the x and y axes. $A_n(x', y')$ and $\phi_n(x', y')$ represent, respectively, the amplitude and phase distributions on the aperture.

For many practical antennas (such as waveguides, horns, etc.) the aperture distribution (amplitude and phase) is separable. That is,

$$A_n(x', y') = I_x(x')I_y(y') \tag{7-42a}$$

$$\phi_n(x', y') = \phi_x(x') + \phi_y(y') \tag{7-42b}$$

so that (7-42) can be written as

$$\text{SF} = S_x S_y \tag{7-43}$$

where

$$S_x = \int_{-l_x/2}^{l_x/2} I_x(x') e^{j[kx' \sin\theta \cos\phi + \phi_x(x')]}\, dx' \tag{7-43a}$$

$$S_y = \int_{-l_y/2}^{l_y/2} I_y(y') e^{j[ky' \sin\theta \sin\phi + \phi_y(y')]}\, dy' \tag{7-43b}$$

which is analogous to the array factor of (6-85)–(6-85b) for discrete-element arrays.

The evaluation of (7-42) can be accomplished either analytically or graphically. If the distribution is separable, as in (7-42a) and (7-42b), the evaluation can be performed using the results of a line-source distribution.

The total field of the aperture antenna is equal to the product of the element and space factors. As for the line-sources, the element factor for apertures depends on the type of equivalent current density and its orientation.

7.10.2 Circular Aperture

The space factor for a circular aperture can be obtained in a similar manner as for the rectangular distribution. Referring to the geometry of Figure 6.37, the space factor for a circular aperture with radius a can be written as

$$\boxed{\text{SF}(\theta, \phi) = \int_0^{2\pi} \int_0^a A_n(\rho', \phi') e^{j[k\rho' \sin\theta \cos(\phi - \phi') + \zeta_n(\rho', \phi')]} \rho'\, d\rho'\, d\phi'} \tag{7-44}$$

where ρ' is the radial distance ($0 \le \rho' \le a$), ϕ' is the azimuthal angle over the aperture ($0 \le \phi' \le 2\pi$ for $0 \le \rho' \le a$), and $A_n(\rho', \phi')$ and $\zeta_n(\rho', \phi')$ represent, respectively, the amplitude and phase distributions over the aperture. Equation (7-44) is analogous to the array factor of (6-112a) for discrete elements.

If the aperture distribution has uniform phase [$\zeta_n(\rho', \phi') = \zeta_0 = 0$] and azimuthal amplitude symmetry [$A_n(\rho', \phi') = A_n(\rho')$], (7-44) reduces, by using (5-48), to

$$\text{SF}(\theta) = 2\pi \int_0^a A_n(\rho') J_0(k\rho' \sin\theta) \rho'\, d\rho' \tag{7-45}$$

where $J_0(x)$ is the Bessel function of the first kind and of order zero.

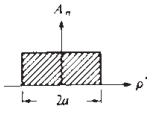
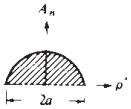
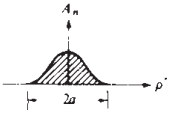
Many practical antennas, such as a parabolic reflector, have distributions that taper toward the edges of the apertures. These distributions can be approximated reasonably well by functions of the form

$$A_n(\rho') = \begin{cases} \left[1 - \left(\dfrac{\rho'}{a}\right)^2\right]^n & 0 \le \rho' \le a, \quad n = 0, 1, 2, 3, \ldots \\ 0 & \text{elsewhere} \end{cases} \tag{7-46}$$

For $n = 0$, (7-46) reduces to a uniform distribution.

The radiation characteristics of circular apertures or planar circular arrays with distributions (7-46) with $n = 0$, 1, 2 are shown tabulated in Table 7.2 [19]. It is apparent, as before, that distributions with lower taper toward the edges (larger values of n) have smaller sidelobes but larger beamwidths. In design, a compromise between sidelobe level and beamwidth is necessary.

TABLE 7.2 Radiation Characteristics for Circular Apertures and Circular Planar Arrays with Circular Symmetry and Tapered Distribution

Distribution	Uniform	Radial Taper	Radial Taper Squared
Distribution (analytical)	$I_0\left[1 - \left(\dfrac{\rho'}{a}\right)^2\right]^0$	$I_1\left[1 - \left(\dfrac{\rho'}{a}\right)^2\right]^1$	$I_2\left[1 - \left(\dfrac{\rho'}{a}\right)^2\right]^2$
Distribution (graphical)			
Space factor (SF) $u = \left(2\pi\dfrac{a}{\lambda}\right)\sin\theta$	$I_0 2\pi a^2 \dfrac{J_1(u)}{u}$	$I_1 4\pi a^2 \dfrac{J_2(u)}{u}$	$I_2 16\pi a^2 \dfrac{J_3(u)}{u}$
Half-power beamwidth (degrees) $a \gg \lambda$	$\dfrac{29.2}{(a/\lambda)}$	$\dfrac{36.4}{(a/\lambda)}$	$\dfrac{42.1}{(a/\lambda)}$
First-null beamwidth (degrees) $a \gg \lambda$	$\dfrac{69.9}{(a/\lambda)}$	$\dfrac{93.4}{(a/\lambda)}$	$\dfrac{116.3}{(a/\lambda)}$
First sidelobe max. (to main max.) (dB)	-17.6	-24.6	-30.6
Directivity factor	$\left(\dfrac{2\pi a}{\lambda}\right)^2$	$0.75\left(\dfrac{2\pi a}{\lambda}\right)^2$	$0.56\left(\dfrac{2\pi a}{\lambda}\right)^2$

7.11 MULTIMEDIA

In the CD that is part of the book, the following multimedia resources are included for the review, understanding, and visualization of the material of this chapter:

a. **Java**-based **interactive questionnaire**, with answers.
b. **Java**-based **applet** for computing and displaying the synthesis characteristics of Schelkunoff, Woodward-Lawson and Tschebyscheff-error designs.
c. **Matlab** computer program, designated ***Synthesis***, for computing and displaying the radiation characteristics of
   - Schelkunoff
   - Fourier transform (line-source and linear array)
   - Woodward-Lawson (line-source and linear array)
   - Taylor (Tschebyscheff-error and One-parameter) synthesis designs.
d. **Power Point (PPT)** viewgraphs, in multicolor.

REFERENCES

1. S. A. Schelkunoff, "A Mathematical Theory of Linear Arrays," *Bell System Technical Journal*, Vol. 22, pp. 80–107, 1943.
2. H. G. Booker and P. C. Clemmow, "The Concept of an Angular Spectrum of Plane Waves, and Its Relation to That of Polar Diagram and Aperture Distribution," *Proc. IEE* (London), Paper No. 922, Radio Section, Vol. 97, pt. III, pp. 11–17, January 1950.
3. P. M. Woodward, "A Method for Calculating the Field over a Plane Aperture Required to Produce a Given Polar Diagram," *J. IEE*, Vol. 93, pt. IIIA, pp. 1554–1558, 1946.
4. P. M. Woodward and J. D. Lawson, "The Theoretical Precision with Which an Arbitrary Radiation-Pattern May be Obtained from a Source of a Finite Size," *J. IEE*, Vol. 95, pt. III, No. 37, pp. 363–370, September 1948.
5. T. T. Taylor, "Design of Line-Source Antennas for Narrow Beamwidth and Low Sidelobes," *IRE Trans. Antennas Propagat.*, Vol. AP-3, No. 1, pp. 16–28, January 1955.
6. T. T. Taylor, "One Parameter Family of Line-Sources Producing Modified $\text{Sin}(\pi u)/\pi u$ Patterns," Hughes Aircraft Co. Tech. Mem. 324, Culver City, Calif., Contract AF 19(604)-262-F-14, September 4, 1953.
7. R. S. Elliott, "On Discretizing Continuous Aperture Distributions," *IEEE Trans. Antennas Propagat.*, Vol. AP-25, No. 5, pp. 617–621, September 1977.
8. R. C. Hansen (ed.), *Microwave Scanning Antennas*, Vol. I, Academic Press, New York, 1964, p. 56.
9. J. Ruze, "Physical Limitations on Antennas," MIT Research Lab., Electronics Tech. Rept. 248, October 30, 1952.
10. M. I. Skolnik, *Introduction to Radar Systems*, McGraw-Hill, New York, 1962, pp. 320–330.
11. R. S. Elliott, "Criticisms of the Woodward-Lawson Method," *IEEE Antennas Propagation Society Newsletter*, Vol. 30, p. 43, June 1988.
12. H. Steyskal, "The Woodward-Lawson Method: A Second Opinion," *IEEE Antennas Propagation Society Newsletter*, Vol. 30, p. 48, October 1988.

13. R. S. Elliott, "More on the Woodward-Lawson Method," *IEEE Antennas Propagation Society Newsletter*, Vol. 30, pp. 28–29, December 1988.
14. H. Steyskal, "The Woodward-Lawson Method-To Bury or Not to Bury," *IEEE Antennas Propagation Society Newsletter*, Vol. 31, pp. 35–36, February 1989.
15. H. J. Orchard, R. S. Elliott, and G. J. Stern. "Optimizing the Synthesis of Shaped Beam Antenna Patterns," *IEE Proceedings*, Part H, pp. 63–68, 1985.
16. R. S. Elliott, "Design of Line-Source Antennas for Narrow Beamwidth and Asymmetric Low Sidelobes," *IEEE Trans. Antennas Propagat.*, Vol. AP-23, No. 1, pp. 100–107, January 1975.
17. G. N. Watson, *A Treatise on the Theory of Bessel Functions*, 2nd. Ed., Cambridge University Press, London, pp. 50 and 379, 1966.
18. S. Silver (ed.), *Microwave Antenna Theory and Design*, MIT Radiation Laboratory Series, Vol. 12, McGraw-Hill, New York, 1965, Chapter 6, pp. 169–199.
19. R. C. Johnson and H. Jasik (eds.), *Antenna Engineering Handbook*, 2nd. Ed., McGraw-Hill, New York, 1984, pp. 2–14 to 2-41.

PROBLEMS

7.1. A three-element array is placed along the z-axis. Assuming the spacing between the elements is $d = \lambda/4$ and the relative amplitude excitation is equal to $a_1 = 1, a_2 = 2, a_3 = 1$,

(a) find the angles where the array factor vanishes when $\beta = 0, \pi/2, \pi$, and $3\pi/2$

(b) plot the relative pattern for each array factor

Use Schelkunoff's method.

7.2. Design a linear array of isotropic elements placed along the z-axis such that the zeros of the array factor occur at $\theta = 0^\circ, 60^\circ$, and 120°. Assume that the elements are spaced $\lambda/4$ apart and that the progressive phase shift between them is 0°.

(a) Find the required number of elements.

(b) Determine their excitation coefficients.

(c) Write the array factor.

(d) Plot the array factor pattern to verify the validity of the design.

Verify using the computer program ***Synthesis***.

7.3. To minimize interference between the operational system, whose antenna is a linear array with elements placed along the z-axis, and other undesired sources of radiation, it is required that nulls be placed at elevation angles of $\theta = 0^\circ, 60^\circ, 120^\circ$, and 180°. The elements will be separated with a uniform spacing of $\lambda/4$. Choose a synthesis method that will allow you to design such an array that will meet the requirements of the amplitude pattern of the array factor. To meet the requirements:

(a) Specify the synthesis method you will use.

(b) Determine the number of elements.

(c) Find the excitation coefficients.

7.4. It is desired to synthesize a discrete array of vertical infinitesimal dipoles placed along the z-axis with a spacing of $d = \lambda/2$ between the adjacent elements. It is

desired for the array factor to have nulls along $\theta = 60^\circ, 90^\circ$, and 120°. *Assume there is no initial progressive phase excitation between the elements*. To achieve this, determine:

(a) number of elements.

(b) excitation coefficients.

(c) angles (*in degrees*) of all the nulls of the entire array (*including of the actual elements*).

7.5. It is desired to synthesize a linear array of elements with spacing $d = 3\lambda/8$. It is important that the array factor (AF) exhibits nulls along $\theta = 0$, 90, and 180 *degrees*. Assume there is no initial progressive phase excitation between the elements (i.e., $\beta = 0$). To achieve this design, determine:

(a) The number of elements

(b) The excitation coefficients (amplitude and phase)
If the design allows the progressive phase shift (β) to change, while maintaining the spacing constant ($d = 3\lambda/8$),

(c) What would it be the range of possible values for the progressive phase shift to cause the null at $\theta = 90$ *degrees* disappear (to place its corresponding root outside the visible region)?

7.6. The z-plane array factor of an array of isotropic elements placed along the z-axis is given by

$$\text{AF} = z(z^4 - 1)$$

Determine the

(a) number of elements of the array. If there are any elements with zero excitation coefficients (null elements), so indicate

(b) position of each element (including that of null elements) along the z axis

(c) magnitude and phase (in degrees) excitation of each element

(d) angles where the pattern vanishes when the total array length (including null elements) is 2λ

Verify using the computer program ***Synthesis***.

7.7. Repeat Problem 7.6 when

$$\text{AF} = z(z^3 - 1)$$

7.8. The z-plane array factor of an array of isotropic elements placed along the z-axis is given by (assume $\beta = 0$)

$$\text{AF}(z) = (z + 1)^3$$

Determine the

(a) Number of elements of the discrete array to have such an array factor.

(b) *Normalized* excitation coefficients of each of the elements of the array (*the ones at the edges to be unity*).

(c) *Classical name* of the array design with these excitation coefficients.

(d) Angles in theta (θ *in degrees*) of *all the nulls* of the array factor when the spacing d between the elements is $d = \lambda/2$.

EX2042
Page 386 of 1072

(e) Half-power beamwidth (*in degrees*) of the array factor when $d = \lambda/2$.
(f) Maximum directivity (*dimensionless* and *in dB*) of the array factor when $d = \lambda/2$.

7.9. The z-plane array factor of an array of isotropic elements placed along the z-axis is given by (assume $\beta = 0$)

$$\text{AF}(z) = (z+1)^4$$

Determine the
(a) Number of elements of the discrete array to have such an array factor.
(b) *Normalized* excitation coefficients of each of the elements of the array (*the ones at the edges to be unity*).
(c) *Classical name* of the array design with these excitation coefficients.
(d) Angles in theta (θ *in degrees*) of *all the nulls* of the array factor when the spacing d between the elements is
  1. $d = \lambda_0/4$
  2. $d = \lambda_0/2$
(e) Half-power beamwidth (*in degrees*) of the array factor when $d = \lambda_0/2$.
(f) Maximum directivity (*dimensionless* and *in dB*) of the array factor when $d = \lambda_0/2$.

7.10. The desired array factor in complex form (z-plane) of an array, with the elements along the z-axis, is given by

$$\begin{aligned}\text{AF}(z) &= (z^4 - \sqrt{2}z^3 + 2z^2 - \sqrt{2}z + 1) = (z^2+1)(z^2 - \sqrt{2}z + 1) \\ &= (z^2+1)\left[\left(z^2 - \sqrt{2}z + \frac{1}{2}\right) + \frac{1}{2}\right] = (z^2+1)\left[\left(z - \frac{1}{\sqrt{2}}\right)^2 + \frac{1}{2}\right]\end{aligned}$$

where $z = x + jy$ in the complex z-plane.
(a) Determine the *number of elements* that you will need to realize this array factor.
(b) Determine *all the roots* of this array factor *on the unity circle* of the complex plane.
(c) For a spacing of $d = \lambda/4$ and zero initial phase ($\beta = 0$), determine *all the angles* θ (*in degrees*) where *this pattern possesses nulls*.

7.11. The z-plane ($z = x + jy$) array factor of a linear array of elements placed along the z-axis, with a uniform spacing d between them and with $\beta = 0$, is given by

$$\text{AF} = z(z^2+1)$$

Determine, analytically, the
(a) number of elements of the array;
(b) excitation coefficients;
(c) *all* the roots of the array factor in the *visible region only* ($0 \le \theta \le 180^\circ$) when $d = \lambda/4$;

(d) *all* the nulls of the array factor (*in degrees*) in the *visible region only* ($0 \le \theta \le 180^\circ$) when $d = \lambda/4$.

Verify using the computer program ***Synthesis***.

7.12. Repeat Example 7.2 when

$$\mathrm{SF}(\theta) = \begin{cases} 1 & 40^\circ \le \theta \le 140^\circ \\ 0 & \text{elsewhere} \end{cases}$$

Verify using the computer program ***Synthesis***.

7.13. Repeat the Fourier transform design of Example 7.2 for a line-source along the z-axis whose sectoral pattern is given by

$$\mathrm{SF}(\theta) = \begin{cases} 1 & 60^\circ \le \theta \le 120^\circ \\ 0 & \text{elsewhere} \end{cases}$$

Use $l = 5\lambda$ and 10λ. Compare the reconstructed patterns with the desired one. Verify using the computer program ***Synthesis***.

7.14. Repeat the Fourier transform design of Problem 7.13 for a linear array with a spacing of $d = \lambda/2$ between the elements and

(a) $N = 11$ elements

(b) $N = 21$ elements

7.15. Repeat the design of Problem 7.13 using the Woodward-Lawson method for line sources.

7.16. Repeat the design of Problem 7.14 using the Woodward-Lawson method for linear arrays for $N = 10, 20$.

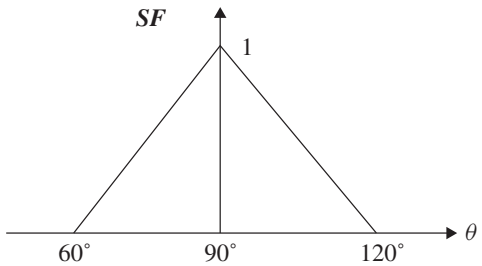
7.17. Design, using the Woodward-Lawson method, a line-source of $l = 5\lambda$ whose space factor pattern is given by

$$\mathrm{SF}(\theta) = \sin^3(\theta) \qquad 0^\circ \le \theta \le 180^\circ$$

Determine the current distribution and compare the reconstructed pattern with the desired pattern. Verify using the computer program ***Synthesis***.

7.18. The desired Space Factor SF of a *line-source* of $\ell = 3\lambda$ is the sectoral pattern of

$$\mathrm{SF} = \begin{cases} \dfrac{1}{30}\theta - 2, & 60^\circ \le \theta \le 90^\circ \\ -\dfrac{1}{30}\theta + 4, & 90^\circ \le \theta \le 120^\circ \quad (\theta \text{ is in degrees}) \\ 0 & \text{elsewhere} \end{cases}$$



It is required to synthesize the desired pattern using the *Woodward–Lawson method with odd samples*. To accomplish this, determine *analytically* when $\ell = 3\lambda$, the

(a) number of samples;

(b) *all* the angles (*in degrees*) where the SF is sampled;

(c) *all* the excitation coefficients b_m at the sampling points.

Verify using the computer program ***Synthesis***.

7.19. Repeat Problem 7.18 using the *Woodward-Lawson method with even* samples.

7.20. Repeat the design of Problem 7.17 for a linear array of $N = 10$ elements with a spacing of $d = \lambda/2$ between them.

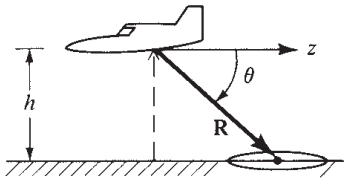
7.21. In target-search, grounding-mapping radars, and in airport beacons it is desirable to have the echo power received from a target, of constant cross section, to be independent of its range R.

Generally, the far-zone field radiated by an antenna is given by

$$|E(R, \theta, \phi)| = C_0 \frac{|F(\theta, \phi)|}{R}$$

where C_0 is a constant. According to the geometry of the figure

$$R = h/\sin(\theta) = h \csc(\theta)$$



For a constant value of ϕ, the radiated field expression reduces to

$$|E(R, \theta, \phi = \phi_0)| = C_0 \frac{|F(\theta, \phi = \phi_0)|}{R} = C_1 \frac{|f(\theta)|}{R}$$

A constant value of field strength can be maintained provided the radar is flying at a constant altitude h and the far-field antenna pattern is equal to

$$f(\theta) = C_2 \csc(\theta)$$

This is referred to as a cosecant pattern, and it is used to compensate for the range variations. For very narrow beam antennas, the total pattern is approximately equal to the space or array factor. Design a line-source, using the Woodward-Lawson method, whose space factor is given by

$$\mathrm{SF}(\theta) = \begin{cases} 0.342 \csc(\theta), & 20^\circ \le \theta \le 60^\circ \\ 0 & \text{elsewhere} \end{cases}$$

Plot the synthesized pattern for $l = 20\lambda$, and compare it with the desired pattern. Verify using the computer program ***Synthesis***.

7.22. Repeat the design of Problem 7.21 for a linear array of $N = 41$ elements with a spacing of $d = \lambda/2$ between them.

EX2042
Page 389 of 1072

7.23. For some radar search applications, it is more desirable to have an antenna which has a square beam for $0 \leq \theta \leq \theta_0$, a cosecant pattern for $\theta_0 \leq \theta \leq \theta_m$, and it is zero elsewhere. Design a line-source, using the Woodward-Lawson method, with a space factor of

$$\text{SF}(\theta) = \begin{cases} 1 & 15^\circ \leq \theta < 20^\circ \\ 0.342 \csc(\theta) & 20^\circ \leq \theta \leq 60^\circ \\ 0 & \text{elsewhere} \end{cases}$$

Plot the reconstructed pattern for $l = 20\lambda$, and compare it with the desired pattern.

7.24. Repeat the design of Problem 7.23, using the Woodward-Lawson method, for a linear array of 41 elements with a spacing of $d = \lambda/2$ between them.

7.25. Repeat Problem 7.18 for a linear array of $\ell = 3\lambda$ with a spacing of $d = 0.5\lambda$ between the elements. Replacing the space factor (SF) of Problem 7.18 with an array factor (AF) and using the *Woodward-Lawson method with odd samples*, determine analytically the

(a) number of elements;
(b) number of samples;
(c) angles (*in degrees*) where the AF is sampled;
(d) *all* the excitation coefficients b_m at the sampling points.
(e) *all* the normalized excitation coefficients a_n of the elements.
Verify using the computer program ***Synthesis***.

7.26. Repeat Problem 7.25 using the *Woodward-Lawson method with even samples*.

7.27. Design a Taylor (Tschebyscheff-error) line-source with a

(a) -25 dB sidelobe level and $\overline{n} = 5$
(b) -20 dB sidelobe level and $\overline{n} = 10$

For each, find the half-power beamwidth and plot the normalized current distribution and the reconstructed pattern when $l = 10\lambda$. Verify using the computer program ***Synthesis***.

7.28. Derive (7-33) using (7-1), (7-32), and Gegenbauer's finite integral and polynomials.

7.29. Repeat the design of Example 7.7 for an array with $l = 4\lambda$, $d = \lambda/2$, $N = 9$.

7.30. Using a spacing of $d = \lambda/4$ between the elements, determine for a Taylor Line-Source (Tschebyscheff-error) of -30 dB, for $\overline{n} = 4$ and an *equivalent length* equal to that of *20 discrete elements:*

(a) The half-power beamwidth (*in degrees*).
(b) State whether the half-power beamwidth in *Part a* is larger or smaller than that of an equivalent design for a Dolph-Tschebyscheff array with the same sidelobe level. *Explain as to why one is larger or smaller than the other.*
(c) The number of complete *innermost minor lobes* that would have *approximately equal sidelobe level.*

7.31. Design a broadside five-element, -40 dB sidelobe level Taylor (one-parameter) distribution array of isotropic sources. The elements are placed along the x-axis with a spacing of $\lambda/4$ between them. Determine the

EX2042
Page 390 of 1072

(a) normalized excitation coefficients (amplitude and phase) of each element
(b) array factor

Verify using the computer program ***Synthesis***.

7.32. Given a continuous line-source, whose total length is 4λ, design a *symmetrical Taylor One-Parameter* distribution array whose sidelobe is 35 dB down from the maximum of the major lobe.

(a) Find the constant B.
(b) For a spacing of λ between the elements, find the number of discrete elements needed to approximate the continuous source. *Assume that the two extreme elements are placed at the edges of the continuous line source*.
(c) Find the total normalized coefficients (edge elements to be unity) of the discrete array of part (c). Identify the position of the corresponding elements.
(d) Write the array factor of the discrete array of parts (c) and (d).

Verify using the computer program ***Synthesis***.

7.33. Derive the space factors for uniform, triangular, cosine, and cosine-squared line-source continuous distributions. Compare with the results in Table 7.1.

7.34. Compute the half-power beamwidth, first-null beamwidth, first sidelobe level (in dB), and directivity of a linear array of closely spaced elements with overall length of 4λ when its amplitude distribution is

(a) uniform (b) triangular
(c) cosine (d) cosine-squared

7.35. A nonuniform linear array with *a triangular symmetrical distribution* consists of seven discrete elements placed $\lambda/2$ *apart*. The *total length (edge-to-edge with elements at the edges)* of the array is $l = 3\lambda$. Determine the following:

(a) *Normalized amplitude* excitation coefficients (*maximum is unity*).
(b) Half-power beamwidth (*in degrees*).
(c) Maximum directivity (*dimensionless* and in *dB*) for the triangular distribution.
(d) Maximum directivity (*dimensionless* and in *dB*) *if the distribution were uniform*. How does it compare with that of Part c? Is it smaller or larger, and *by how many dB?*
(e) Maximum effective length (*assuming that the distribution of the discrete array is the same as that of a continuous line-source*) *compared to physical length l*:
    1. If the distribution *is triangular.*
    2. If the distribution *is uniform.*

7.36. Synthesize a 7-element nonuniform array *with symmetrical amplitude excitation and with uniform spacing between the elements*. The desired amplitude distribution across the elements (*relative to the center of the array*) is $\cos^2$ [i.e., $\cos^2(\pi x'/L)$] where L is the total length of the array (*the end elements are at the edges of the array length*) and x' is the position of each element *relative to the center* of the array. *The overall length L of the array is* 3λ. The end elements are at the edges of the array length. Determine the:

(a) Spacing between the elements (*in* λ).

(b) Normalized *total* amplitude coefficients of each of the elements (*normalize them so that the amplitude of the center element is unity*). Identify each of the element position and its corresponding normalized amplitude coefficient.

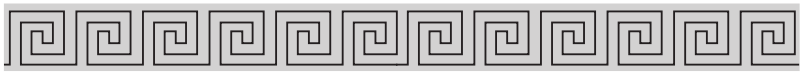
(c) Approximate half-power beamwidth (*in degrees*).

(d) Approximate maximum directivity (*in dB*).

7.37. Derive the space factors for the uniform radial taper, and radial taper-squared circular aperture continuous distributions. Compare with the results in Table 7.2.

7.38. Compute the half-power beamwidth, first-null beamwidth, first sidelobe level (in dB), and gain factor of a circular planar array of closely spaced elements, with radius of 2λ when its amplitude distribution is
(a) uniform (b) radial taper (c) radial taper-squared.

CHAPTER 8



Integral Equations, Moment Method, and Self and Mutual Impedances

8.1 INTRODUCTION

In Chapter 2 it was shown, by the Thévenin and Norton equivalent circuits of Figures 2.27 and 2.28, that an antenna can be represented by an equivalent impedance $Z_A[Z_A = (R_r + R_L) + jX_A]$. The equivalent impedance is attached across two terminals (terminals $a - b$ in Figures 2.27 and 2.28) which are used to connect the antenna to a generator, receiver, or transmission line. In general, this impedance is called the *driving-point* impedance. However, when the antenna is radiating in an unbounded medium, in the absence of any other interfering elements or objects, the driving-point impedance is the same as the *self-impedance* of the antenna. In practice, however, there is always the ground whose presence must be taken into account in determining the antenna driving-point impedance. The self- and driving-point impedances each have, in general, a real and an imaginary part. The real part is designated as the resistance and the imaginary part is called the reactance.

The impedance of an antenna depends on many factors including its frequency of operation, its geometry, its method of excitation, and its proximity to the surrounding objects. Because of their complex geometries, only a limited number of practical antennas have been investigated analytically. For many others, the input impedance has been determined experimentally.

The impedance of an antenna at a point is defined as the ratio of the electric to the magnetic fields at that point; alternatively, at a pair of terminals, it is defined as the ratio of the voltage to the current across those terminals. There are many methods that can be used to calculate the impedance of an antenna [1]. Generally, these can be classified into three categories: (1) the boundary-value method, (2) the transmission-line method, and (3) the Poynting vector method. Extensive and brief discussions and comparisons of these methods have been reported [1], [2].

The boundary-value approach is the most basic, and it treats the antenna as a boundary-value problem. The solution to this is obtained by enforcing the boundary conditions (usually that the tangential electric-field components vanish at the conducting surface). In turn, the current distribution and finally the impedance (ratio of applied

Antenna Theory: Analysis Design, Third Edition, by Constantine A. Balanis
ISBN 0-471-66782-X Copyright © 2005 John Wiley & Sons, Inc.

EX2042
Page 393 of 1072

emf to current) are determined, with no assumptions as to their distribution, as solutions to the problem. The principal disadvantage of this method is that it has limited applications. It can only be applied and solved exactly on simplified geometrical shapes where the scalar wave equation is separable.

The transmission-line method, which has been used extensively by Schelkunoff [3], treats the antenna as a transmission line, and it is most convenient for the biconical antenna. Since it utilizes tangential electric-field boundary conditions for its solution, this technique may also be classified as a boundary-value method.

The basic approach to the Poynting vector method is to integrate the Poynting vector (power density) over a closed surface. The closed surface chosen is usually either a sphere of a very large radius r ($r \geq 2D^2/\lambda$ where D is the largest dimension of the antenna) or a surface that coincides with the surface of the antenna. The large sphere closed surface method has been introduced in Chapters 4 and 5, but it lends itself to calculations only of the real part of the antenna impedance (radiation resistance). The method that utilizes the antenna surface has been designated as the induced emf method, and it has been utilized [4]–[6] for the calculation of antenna impedances.

The impedance of an antenna can also be found using an integral equation with a numerical technique solution, which is widely referred to as the *Integral Equation Method of Moments* [7]–[14]. This method, which in the late 1960s was extended to include electromagnetic problems, is analytically simple, it is versatile, but it requires large amounts of computation. The limitation of this technique is usually the speed and storage capacity of the computer.

In this chapter the integral equation method, with a Moment Method numerical solution, will be introduced and used first to find the self- and driving-point impedances, and mutual impedance of wire type of antennas. This method casts the solution for the induced current in the form of an integral (hence its name) where the unknown induced current density is part of the integrand. Numerical techniques, such as the *Moment Method* [7]–[14], can then be used to solve the current density. In particular two classical integral equations for linear elements, *Pocklington's and Hallén's Integral Equations*, will be introduced. This approach is very general, and it can be used with today's modern computational methods and equipment to compute the characteristics of complex configurations of antenna elements, including skewed arrangements. For special cases, closed-form expressions for the self, driving-point, and mutual impedances will be presented using the induced emf method. This method is limited to classical geometries, such as straight wires and arrays of collinear and parallel straight wires.

8.2 INTEGRAL EQUATION METHOD

The objective of the Integral Equation (IE) method for radiation or scattering is to cast the solution for the unknown current density, which is induced on the surface of the radiator/scatterer, in the form of an integral equation where the unknown induced current density is part of the integrand. The integral equation is then solved for the unknown induced current density using numerical techniques such as the *Moment Method* (MM). To demonstrate this technique, we will initially consider some specific problems. For introduction, we will start with an electrostatics problem and follow it with time-harmonic problems.

8.2.1 Electrostatic Charge Distribution

In electrostatics, the problem of finding the potential that is due to a given charge distribution is often considered. In physical situations, however, it is seldom possible to specify a charge distribution. Whereas we may connect a conducting body to a voltage source, and thus specify the potential throughout the body, the distribution of charge is obvious only for a few rotationally symmetric geometries. In this section we will consider an integral equation approach to solve for the electric charge distribution once the electric potential is specified. Some of the material here and in other sections is drawn from [15], [16].

From statics we know that a linear electric charge distribution $\rho(r')$ creates an electric potential, $V(r)$, according to [17]

$$V(r) = \frac{1}{4\pi\epsilon_0} \int_{\substack{\text{source} \\ \text{(charge)}}} \frac{\rho(r')}{R} dl' \tag{8-1}$$

where $r'(x', y', z')$ denotes the source coordinates, $r(x, y, z)$ denotes the observation coordinates, dl' is the path of integration, and R is the distance from any one point on the source to the observation point, which is generally represented by

$$R(r, r') = |\mathbf{r} - \mathbf{r}'| = \sqrt{(x - x')^2 + (y - y')^2 + (z - z')^2} \tag{8-1a}$$

We see that (8-1) may be used to calculate the potentials that are due to any known line charge density. However, the charge distribution on most configurations of practical interest, i.e., complex geometries, is not usually known, even when the potential on the source is given. It is the nontrivial problem of determining the charge distribution, for a specified potential, that is to be solved here using an integral equation-numerical solution approach.

A. Finite Straight Wire

Consider a straight wire of length l and radius a, placed along the y axis, as shown in Figure 8-1(a). The wire is given a normalized constant electric potential of 1 V.

Note that (8-1) is valid everywhere, including on the wire itself ($V_{\text{wire}} = 1$ V). Thus, choosing the observation along the wire axis ($x = z = 0$) and representing the charge density on the surface of the wire, (8-1) can be expressed as

$$1 = \frac{1}{4\pi\epsilon_0} \int_0^1 \frac{\rho(y')}{R(y, y')} dy', \quad 0 \le y \le l \tag{8-2}$$

where

$$\begin{aligned} R(y, y') = R(r, r')|_{x=z=0} &= \sqrt{(y - y')^2 + [(x')^2 + (z')^2]} \\ &= \sqrt{(y - y')^2 + a^2} \end{aligned} \tag{8-2a}$$

The observation point is chosen along the wire axis and the charge density is represented along the surface of the wire to avoid $R(y, y') = 0$, which would introduce a singularity in the integrand of (8-2).

EX2042
Page 395 of 1072

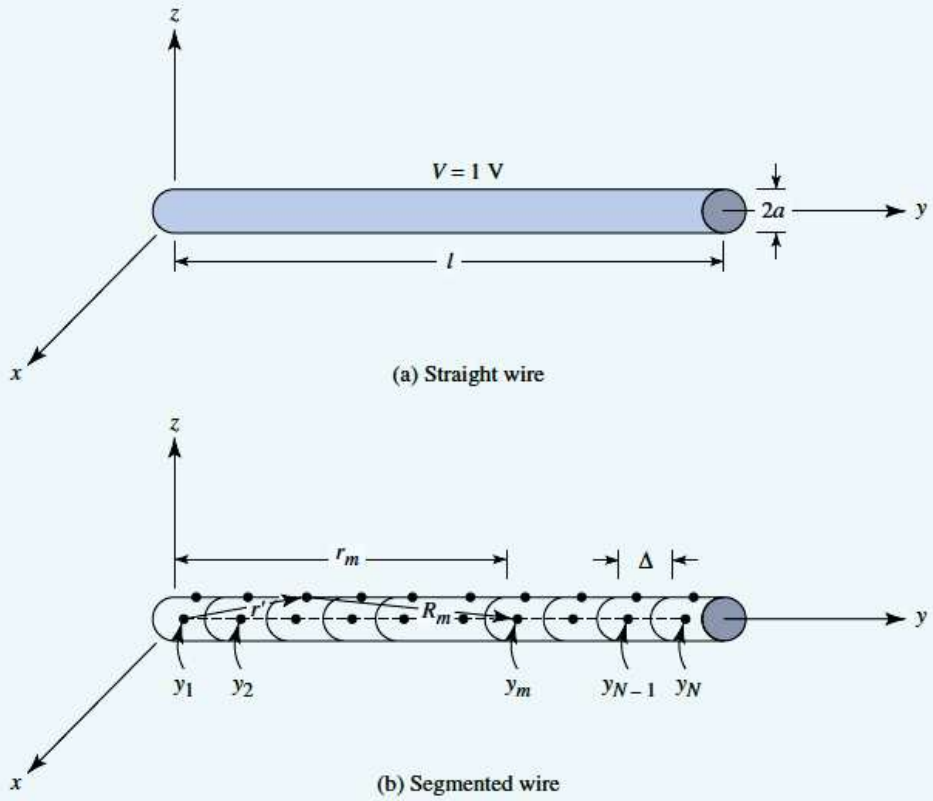


Figure 8.1 Straight wire of constant potential and its segmentation.

It is necessary to solve (8-2) for the unknown $\rho(y')$ (an inversion problem). Equation (8-2) is an integral equation that can be used to find the charge density $\rho(y')$ based on the 1-V potential. The solution may be reached numerically by reducing (8-2) to a series of linear algebraic equations that may be solved by conventional matrix equation techniques. To facilitate this, let us approximate the unknown charge distribution $\rho(y')$ by an expansion of N known terms with constant, but unknown, coefficients, that is,

$$\rho(y') = \sum_{n=1}^{N} a_n g_n(y') \tag{8-3}$$

Thus, (8-2) may be written, using (8-3), as

$$4\pi\epsilon_0 = \int_0^l \frac{1}{R(y, y')} \left[\sum_{n=1}^{N} a_n g_n(y') \right] dy' \tag{8-4}$$

Because (8-4) is a nonsingular integral, its integration and summation can be interchanged, and it can be written as

$$4\pi\epsilon_0 = \sum_{n=1}^{N} a_n \int_0^l \frac{g_n(y')}{\sqrt{(y - y')^2 + a^2}} dy' \tag{8-4a}$$

The wire is now divided into N uniform segments, each of length $\Delta = l/N$, as illustrated in Figure 8.1(b). The $g_n(y')$ functions in the expansion (8-3) are chosen for their ability to accurately model the unknown quantity, while minimizing computation. They are often referred to as *basis* (or expansion) functions, and they will be discussed further in Section 8.4.1. To avoid complexity in this solution, subdomain piecewise constant (or "pulse") functions will be used. These functions, shown in Figure 8.8, are defined to be of a constant value over one segment and zero elsewhere, or

$$g_n(y') = \begin{cases} 0 & y' < (n-1)\Delta \\ 1 & (n-1)\Delta \le y' \le n\Delta \\ 0 & n\Delta < y' \end{cases} \tag{8-5}$$

Many other basis functions are possible, some of which will be introduced later in Section 8.4.1.

Replacing y in (8-4) by a fixed point such as y_m, results in an integrand that is solely a function of y', so the integral may be evaluated. Obviously, (8-4) leads to one equation with N unknowns a_n written as

$$\begin{aligned} 4\pi\epsilon_0 = a_1 \int_0^{\Delta} \frac{g_1(y')}{R(y_m, y')}\, dy' + a_2 \int_{\Delta}^{2\Delta} \frac{g_2(y')}{R(y_m, y')}\, dy' + \dots \\ + a_n \int_{(n-1)\Delta}^{n\Delta} \frac{g_n(y')}{R(y_m, y')}\, dy' + \cdots + a_N \int_{(N-1)\Delta}^{l} \frac{g_N(y')}{R(y_m, y')}\, dy' \end{aligned} \tag{8-6}$$

In order to obtain a solution for these N amplitude constants, N linearly independent equations are necessary. These equations may be produced by choosing N observation points y_m each at the center of each Δ length element as shown in Figure 8.1(b). This results in one equation of the form of (8-6) corresponding to each observation point. For N such points, we can reduce (8-6) to

$$\begin{aligned} 4\pi\epsilon_0 &= a_1 \int_0^{\Delta} \frac{g_1(y')}{R(y_1, y')}\, dy' + \cdots + a_N \int_{(N-1)\Delta}^{l} \frac{g_N(y')}{R(y_1, y')}\, dy' \\ &\vdots \\ 4\pi\epsilon_0 &= a_1 \int_0^{\Delta} \frac{g_1(y')}{R(y_N, y')}\, dy' + \cdots + a_N \int_{(N-1)\Delta}^{l} \frac{g_N(y')}{R(y_N, y')}\, dy' \end{aligned} \tag{8-6a}$$

We may write (8-6a) more concisely using matrix notation as

$$[V_m] = [Z_{mn}][I_n] \tag{8-7}$$

where each Z_{mn} term is equal to

$$\begin{aligned} Z_{mn} &= \int_0^{l} \frac{g_n(y')}{\sqrt{(y_m - y')^2 + a^2}}\, dy' \\ &= \int_{(n-1)\Delta}^{n\Delta} \frac{1}{\sqrt{(y_m - y')^2 + a^2}}\, dy' \end{aligned} \tag{8-7a}$$

EX2042
Page 397 of 1072

and

$$[I_n] = [a_n] \tag{8-7b}$$

$$[V_m] = [4\pi\epsilon_0]. \tag{8-7c}$$

The V_m column matrix has all terms equal to $4\pi\epsilon_0$, and the $I_n = a_n$ values are the unknown charge distribution coefficients. Solving (8-7) for $[I_n]$ gives

$$[I_n] = [a_n] = [Z_{mn}]^{-1}[V_m] \tag{8-8}$$

Either (8-7) or (8-8) may readily be solved on a digital computer by using any of a number of matrix inversion or equation solving routines. Whereas the integral involved here may be evaluated in closed form by making appropriate approximations, this is not usually possible with more complicated problems. Efficient numerical integral computer subroutines are commonly available in easy-to-use forms.

One closed-form evaluation of (8-7a) is to reduce the integral and represent it by

$$Z_{mn} = \begin{cases} 2\ln\left(\dfrac{\dfrac{\Delta}{2} + \sqrt{a^2 + \left(\dfrac{\Delta}{2}\right)^2}}{a}\right) & m = n \qquad (8\text{-}9a) \\ \ln\left\{\dfrac{d_{mn}^+ + [(d_{mn}^+)^2 + a^2]^{1/2}}{d_{mn}^- + [(d_{mn}^-)^2 + a^2]^{1/2}}\right\} & m \neq n \text{ but } |m-n| \leq 2 \qquad (8\text{-}9b) \\ \ln\left(\dfrac{d_{mn}^+}{d_{mn}^-}\right) & |m-n| > 2 \qquad (8\text{-}9c) \end{cases}$$

where

$$d_{mn}^+ = l_m + \frac{\Delta}{2} \tag{8-9d}$$

$$d_{mn}^- = l_m - \frac{\Delta}{2} \tag{8-9e}$$

l_m is the distance between the mth matching point and the center of the nth source point.

In summary, the solution of (8-2) for the charge distribution on a wire has been accomplished by approximating the unknown with some basis functions, dividing the wire into segments, and then sequentially enforcing (8-2) at the center of each segment to form a set of linear equations.

Even for the relatively simple straight wire geometry we have discussed, the exact form of the charge distribution is not intuitively apparent. To illustrate the principles of the numerical solution, an example is now presented.

Example 8.1

A 1-m long straight wire of radius $a = 0.001$ m is maintained at a constant potential of 1 V. Determine the linear charge distribution on the wire by dividing the length into 5 and 20 uniform segments. Assume subdomain pulse basis functions.

EX2042
Page 398 of 1072

Solution:

1. $N = 5$. When the 1-m long wire is divided into five uniform segments each of length $\Delta = 0.2$ m, (8-7) reduces to

$$\begin{bmatrix} 10.60 & 1.10 & 0.51 & 0.34 & 0.25 \\ 1.10 & 10.60 & 1.10 & 0.51 & 0.34 \\ 0.51 & 1.10 & 10.60 & 1.10 & 0.51 \\ 0.34 & 0.51 & 1.10 & 10.60 & 1.10 \\ 0.25 & 0.34 & 0.51 & 1.10 & 10.60 \end{bmatrix} \begin{bmatrix} a_1 \\ a_2 \\ a_3 \\ a_4 \\ a_5 \end{bmatrix} = \begin{bmatrix} 1.11 \times 10^{-10} \\ 1.11 \times 10^{-10} \\ \vdots \\ 1.11 \times 10^{-10} \end{bmatrix}$$

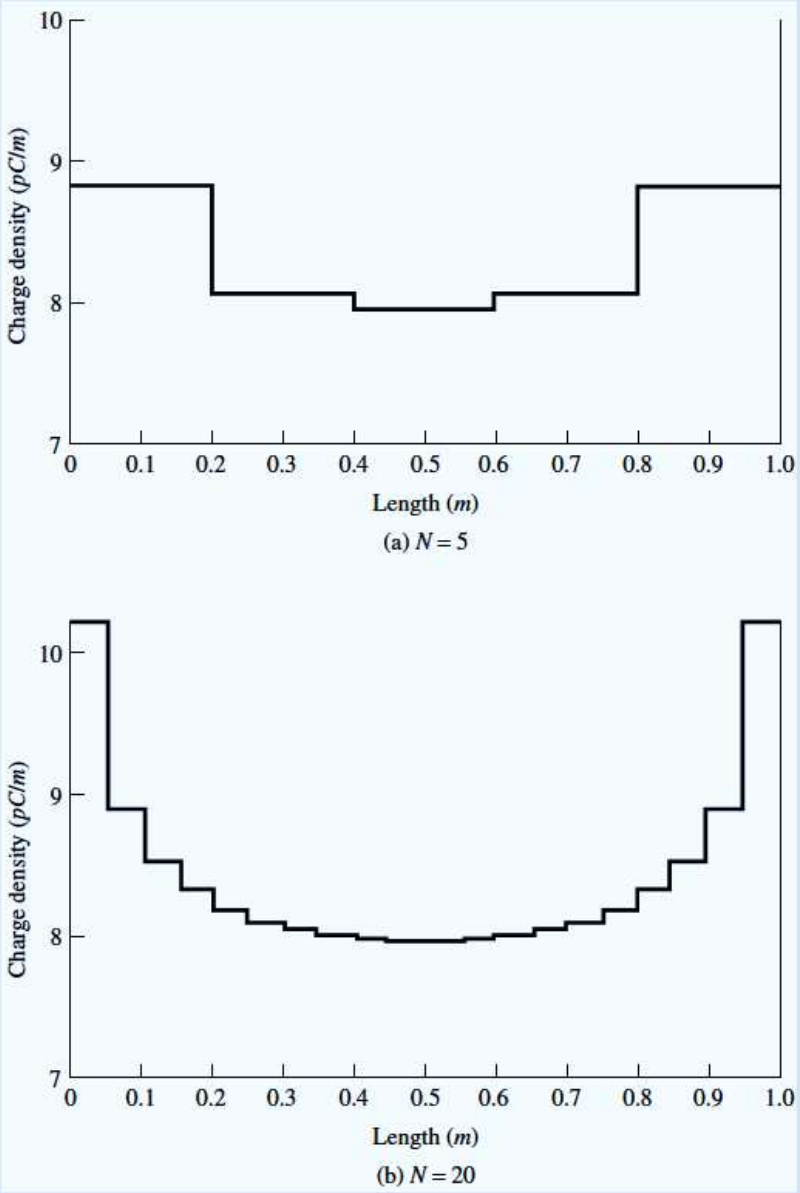


Figure 8.2 Charge distribution on a 1-m straight wire at 1 V.

Inverting this matrix leads to the amplitude coefficients and subsequent charge distribution of

$$a_1 = 8.81 pC/m$$
$$a_2 = 8.09 pC/m$$
$$a_3 = 7.97 pC/m$$
$$a_4 = 8.09 pC/m$$
$$a_5 = 8.81 pC/m$$

The charge distribution is shown in Figure 8.2(a).

2. $N = 20$. Increasing the number of segments to 20 results in a much smoother distribution, as shown plotted in Figure 8.2(b). As more segments are used, a better approximation of the actual charge distribution is attained, which has smaller discontinuities over the length of the wire.

B. Bent Wire

In order to illustrate the solution of a more complex structure, let us analyze a body composed of two noncollinear straight wires; that is, a bent wire. If a straight wire is bent, the charge distribution will be altered, although the solution to find it will differ only slightly from the straight wire case. We will assume a bend of angle α, which remains on the yz-plane, as shown in Figure 8.3.

For the first segment l_1 of the wire, the distance R can be represented by (8-2a). However, for the second segment l_2 we can express the distance as

$$R = \sqrt{(y - y')^2 + (z - z')^2} \tag{8-10}$$

Also because of the bend, the integral in (8-7a) must be separated into two parts of

$$Z_{mn} = \int_0^{l_1} \frac{\rho_n(l_1')}{R} dl_1' + \int_0^{l_2} \frac{\rho_n(l_2')}{R} dl_2' \tag{8-11}$$

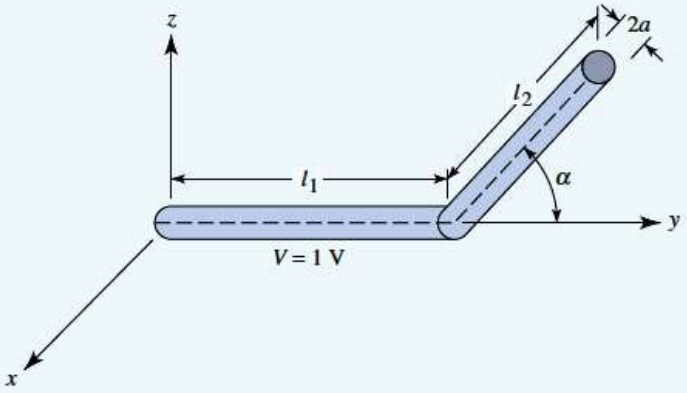


Figure 8.3 Geometry for bent wire.

EX2042
Page 400 of 1072

where l_1 and l_2 are measured along the corresponding straight sections from their left ends.

Example 8.2

Repeat Example 8.1 assuming that the wire has been bent 90° at its midpoint. Subdivide the wire into 20 uniform segments.

Solution: The charge distribution for this case, calculated using (8-10) and (8-11), is plotted in Figure 8.4 for $N = 20$ segments. Note that the charge is relatively more concentrated near the ends of this structure than was the case for a straight wire of Figure 8.2(b). Further, the overall density, and thus capacitance, on the structure has decreased.

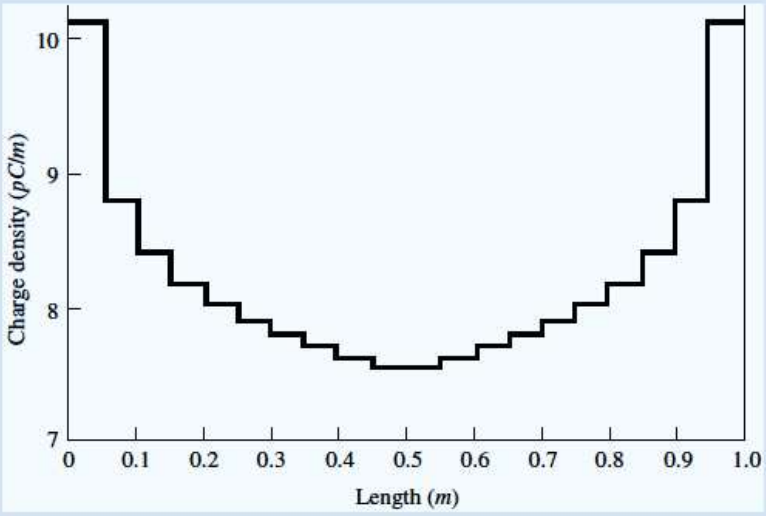


Figure 8.4 Charge distribution on a 1-m bent wire ($\alpha = 90°$, $N = 20$).

Arbitrary wire configurations, including numerous ends and even curved sections, may be analyzed by the methods already outlined here. As with the simple bent wire, the only alterations generally necessary are those required to describe the geometry analytically.

8.2.2 Integral Equation

Equation (8-2) for the 1-V potential on a wire of length l is an integral equation, which can be used to solve for the charge distribution. Numerically this is accomplished using a method, which is usually referred to as *Moment Method* or *Method of Moments* [7]–[14]. To solve (8-2) numerically the unknown charge density $\rho(y')$ is represented by N terms, as given by (8-3). In (8-3) $g_n(y')$ are a set of N known functions, usually referred to as *basis* or *expansion* functions, while a_n represents a set of N constant, but unknown, coefficients. The basis or expansion functions are chosen to best represent the unknown charge distribution.

Equation (8-2) is valid at every point on the wire. By enforcing (8-2) at N discrete but different points on the wire, the integral equation of (8-2) is reduced to a set of N

linearly independent algebraic equations, as given by (8-6a). This set is generalized by (8-7)–(8-7c), which is solved for the unknown coefficients a_n by (8-8) using matrix inversion techniques. Since the system of N linear equations each with N unknowns, as given by (8-6a)–(8-8), was derived by applying the boundary condition (constant 1-V potential) at N discrete points on the wire, the technique is referred to as *point-matching* (or *collocation*) method [7], [8]. Thus, by finding the elements of the $[V]$ and $[Z]$, and then the inverse $[Z]^{-1}$ matrices, we can then determine the coefficients a_n of the $[I]$ matrix using (8-8). This in turn allows us to approximate the charge distribution $\rho(y')$ using (8-3). This was demonstrated by Examples 8.1 and 8.2 for the straight and bent wires, respectively.

In general, there are many forms of integral equations. For time-harmonic electromagnetics, two of the most popular integral equations are the *electric-field integral equation* (EFIE) and the *magnetic field integral equation* (MFIE) [14]. The EFIE enforces the boundary condition on the tangential electric field while the MFIE enforces the boundary condition on the tangential components of the magnetic field. The EFIE is valid for both closed or open surfaces while the MFIE is valid for closed surfaces. These integral equations can be used for both radiation and scattering problems. Two- and three-dimensional EFIE and MFIE equations for TE and TM polarizations are derived and demonstrated in [14]. For radiation problems, especially wire antennas, two popular EFIEs are the *Pocklington Integral Equation* and the *Hallén Integral Equation*. Both of these will be discussed and demonstrated in the section that follows.

8.3 FINITE DIAMETER WIRES

In this section we want to derive and apply two classic three-dimensional integral equations, referred to as *Pocklington's integrodifferential equation* and *Hallén's integral equation* [18]–[26], that can be used most conveniently to find the current distribution on conducting wires. Hallén's equation is usually restricted to the use of a *delta-gap* voltage source model at the feed of a wire antenna. Pocklington's equation, however, is more general and it is adaptable to many types of feed sources (through alteration of its excitation function or excitation matrix), including a magnetic frill [27]. In addition, Hallén's equation requires the inversion of an $N + 1$ order matrix (where N is the number of divisions of the wire) while Pocklington's equation requires the inversion of an N order matrix.

For very thin wires, the current distribution is usually assumed to be of sinusoidal form as given by (4-56). For finite diameter wires (usually diameters d of $d > 0.05\lambda$), the sinusoidal current distribution is representative but not accurate. To find a more accurate current distribution on a cylindrical wire, an integral equation is usually derived and solved. Previously, solutions to the integral equation were obtained using iterative methods [20]; presently, it is most convenient to use moment method techniques [7]–[9].

If we know the voltage at the feed terminals of a wire antenna and find the current distribution, the input impedance and radiation pattern can then be obtained. Similarly, if a wave impinges upon the surface of a wire scatterer, it induces a current density that in turn is used to find the scattered field. Whereas the linear wire is simple, most of the information presented here can be readily extended to more complicated structures.

8.3.1 Pocklington's Integral Equation

To derive Pocklington's integral equation, refer to Figure 8.5. Although this derivation is general, it can be used either when the wire is a scatterer or an antenna. Let us assume that an incident wave impinges on the surface of a conducting wire, as shown in Figure 8.5(a), and it is referred to as the *incident electric field* $\mathbf{E}^i(\mathbf{r})$. When the wire is an antenna, the incident field is produced by the feed source at the gap, as shown in Figure 8.7. Part of the incident field impinges on the wire and induces on its surface a linear current density $\mathbf{J}_s$ (amperes per meter). The induced current density $\mathbf{J}_s$ reradiates and produces an electric field that is referred to as the *scattered electric field* $\mathbf{E}^s(\mathbf{r})$. Therefore, at any point in space the total electric field $\mathbf{E}^t(\mathbf{r})$ is the sum of the incident and scattered fields, or

$$\mathbf{E}^t(\mathbf{r}) = \mathbf{E}^i(\mathbf{r}) + \mathbf{E}^s(\mathbf{r}) \tag{8-12}$$

where

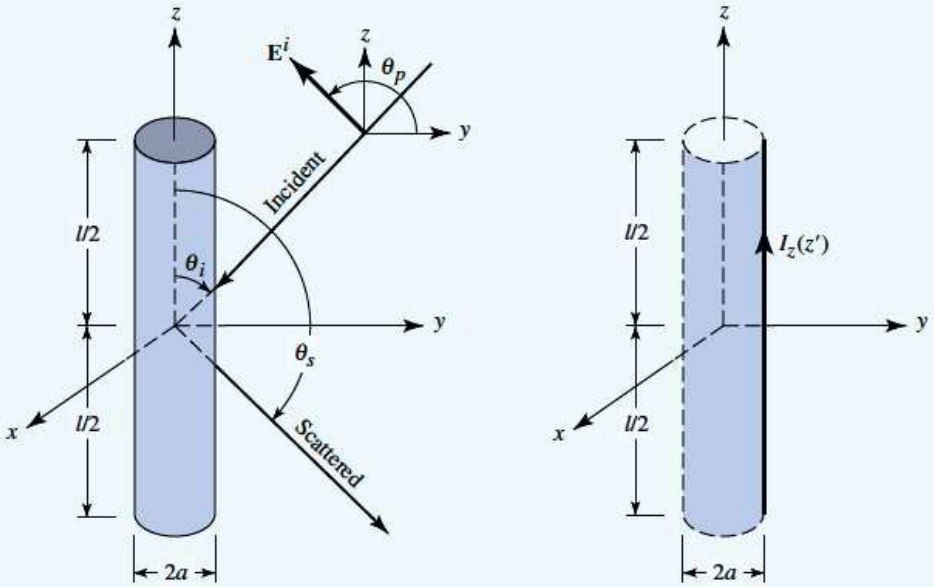
$\mathbf{E}^t(\mathbf{r})$ = total electric field
$\mathbf{E}^i(\mathbf{r})$ = incident electric field
$\mathbf{E}^s(\mathbf{r})$ = scattered electric field

When the observation point is moved to the surface of the wire ($r = r_s$) and the wire is perfectly conducting, the total tangential electric field vanishes. In cylindrical coordinates, the electric field radiated by the dipole has a radial component (E_ρ) and a tangential component (E_z). These are represented by (8-55a) and (8-55b). Therefore on the surface of the wire the tangential component of (8-12) reduces to

$$E_z^t(r = r_s) = E_z^i(r = r_s) + E_z^s(r = r_s) = 0 \tag{8-13}$$

or

$$E_z^s(r = r_s) = -E_z^i(r = r_s) \tag{8-13a}$$



(a) Geometry (b) Equivalent current

Figure 8.5 Uniform plane wave obliquely incident on a conducting wire.

In general, the scattered electric field generated by the induced current density $\mathbf{J_s}$ is given by (3-15), or

$$\mathbf{E^s}(\mathbf{r}) = -j\omega\mathbf{A} - j\frac{1}{\omega\mu\epsilon}\nabla(\nabla\cdot\mathbf{A})$$
$$= -j\frac{1}{\omega\mu\epsilon}[k^2\mathbf{A} + \nabla(\nabla\cdot\mathbf{A})] \tag{8-14}$$

However, for observations at the wire surface only the z component of (8-14) is needed, and we can write it as

$$E_z^s(r) = -j\frac{1}{\omega\mu\epsilon}\left(k^2A_z + \frac{\partial^2 A_z}{\partial z^2}\right) \tag{8-15}$$

According to (3-51) and neglecting edge effects

$$A_z = \frac{\mu}{4\pi}\iint_S J_z\frac{e^{-jkR}}{R}\,ds' = \frac{\mu}{4\pi}\int_{-l/2}^{+l/2}\int_0^{2\pi} J_z\frac{e^{-jkR}}{R}a\,d\phi'\,dz' \tag{8-16}$$

If the wire is very thin, the current density J_z is not a function of the azimuthal angle ϕ, and we can write it as

$$2\pi a J_z = I_z(z') \Rightarrow J_z = \frac{1}{2\pi a}I_z(z') \tag{8-17}$$

where $I_z(z')$ is assumed to be an equivalent filament line-source current located a radial distance $\rho = a$ from the z axis, as shown in Figure 8.6(a). Thus (8-16) reduces to

$$A_z = \frac{\mu}{4\pi}\int_{-l/2}^{+l/2}\left[\frac{1}{2\pi a}\int_0^{2\pi} I_z(z')\frac{e^{-jkR}}{R}a\,d\phi'\right]dz' \tag{8-18}$$

$$R = \sqrt{(x-x')^2 + (y-y')^2 + (z-z')^2}$$
$$= \sqrt{(\rho^2 + a^2 - 2\rho a\cos(\phi-\phi') + (z-z')^2} \tag{8-18a}$$

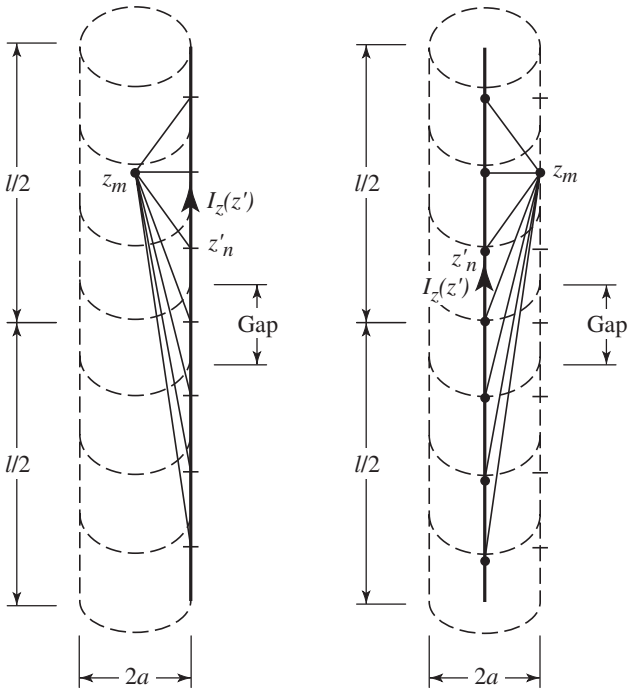
where ρ is the radial distance to the observation point and a is the radius.

Because of the symmetry of the scatterer, the observations are not a function of ϕ. For simplicity, let us then choose $\phi = 0$. For observations on the surface $\rho = a$ of the scatterer (8-18) and (8-18a) reduce to

$$A_z(\rho = a) = \mu\int_{-l/2}^{+l/2} I_z(z')\left(\frac{1}{2\pi}\int_0^{2\pi}\frac{e^{-jkR}}{4\pi R}\,d\phi'\right)dz'$$
$$= \mu\int_{-l/2}^{+l/2} I_z(z')G(z,z')\,dz' \tag{8-19}$$

$$G(z,z') = \frac{1}{2\pi}\int_0^{2\pi}\frac{e^{-jkR}}{4\pi R}\,d\phi' \tag{8-19a}$$

$$R(\rho = a) = \sqrt{4a^2\sin^2\left(\frac{\phi'}{2}\right) + (z-z')^2} \tag{8-19b}$$



(a) On the surface (b) Along the center

Figure 8.6 Dipole segmentation and its equivalent current.

Thus for observations at the surface $\rho = a$ of the scatterer, the z component of the scattered electric field can be expressed as

$$E_z^s(\rho = a) = -j\frac{1}{\omega\epsilon}\left(k^2 + \frac{d^2}{dz^2}\right)\int_{-l/2}^{+l/2} I_z(z')G(z, z')\,dz' \tag{8-20}$$

which by using (8-13a) reduces to

$$-j\frac{1}{\omega\epsilon}\left(\frac{d^2}{dz^2} + k^2\right)\int_{-l/2}^{+l/2} I_z(z')G(z, z')\,dz' = -E_z^i(\rho = a) \tag{8-21}$$

or

$$\left(\frac{d^2}{dz^2} + k^2\right)\int_{-l/2}^{+l/2} I_z(z')G(z, z')\,dz' = -j\omega\epsilon E_z^i(\rho = a) \tag{8-21a}$$

Interchanging integration with differentiation, we can rewrite (8-21a) as

$$\boxed{\int_{-l/2}^{+l/2} I_z(z')\left[\left(\frac{\partial^2}{\partial z^2} + k^2\right)G(z, z')\right]dz' = -j\omega\epsilon E_z^i(\rho = a)} \tag{8-22}$$

where $G(z, z')$ is given by (8-19a).

Equation (8-22) is referred to as *Pocklington's integral equation* [1], and it can be used to determine the equivalent filamentary line-source current of the wire, and thus current density on the wire, by knowing the incident field on the surface of the wire.

If we assume that the wire is very thin ($a \ll \lambda$) such that (8-19a) reduces to

$$G(z, z') = G(R) = \frac{e^{-jkR}}{4\pi R} \tag{8-23}$$

(8-22) can also be expressed in a more convenient form as [22]

$$\boxed{\int_{-l/2}^{+l/2} I_z(z') \frac{e^{-jkR}}{4\pi R^5} [(1 + jkR)(2R^2 - 3a^2) + (kaR)^2]\, dz' = -j\omega\epsilon E_z^i(\rho = a)} \tag{8-24}$$

where for observations along the center of the wire ($\rho = 0$)

$$R = \sqrt{a^2 + (z - z')^2} \tag{8-24a}$$

In (8-22) or (8-24), $I_z(z')$ represents the equivalent filamentary line-source current located on the surface of the wire, as shown in Figure 8.5(b), and it is obtained by knowing the incident electric field on the surface of the wire. By point-matching techniques, this is solved by matching the boundary conditions at discrete points on the surface of the wire. Often it is easier to choose the matching points to be at the interior of the wire, especially along the axis as shown in Figure 8.6(a), where $I_z(z')$ is located on the surface of the wire. By reciprocity, the configuration of Figure 8.6(a) is analogous to that of Figure 8.6(b) where the equivalent filamentary line-source current is assumed to be located along the center axis of the wire and the matching points are selected on the surface of the wire. Either of the two configurations can be used to determine the equivalent filamentary line-source current $I_z(z')$; the choice is left to the individual.

8.3.2 Hallén's Integral Equation

Referring again to Figure 8.5(a), let us assume that the length of the cylinder is much larger than its radius ($l \gg a$) and its radius is much smaller than the wavelength ($a \ll \lambda$) so that the effects of the end faces of the cylinder can be neglected. Therefore the boundary conditions for a wire with infinite conductivity are those of vanishing total tangential **E** fields on the surface of the cylinder and vanishing current at the ends of the cylinder [$I_z(z' = \pm l/2) = 0$].

Since only an electric current density flows on the cylinder and it is directed along the z axis ($\mathbf{J} = \hat{\mathbf{a}}_z J_z$), then according to (3-14) and (3-51) $\mathbf{A} = \hat{\mathbf{a}}_z A_z(z')$, which for small radii is assumed to be only a function of z'. Thus (3-15) reduces to

$$E_z^t = -j\omega A_z - j\frac{1}{\omega\mu\epsilon}\frac{\partial^2 A_z}{\partial z^2} = -j\frac{1}{\omega\mu\epsilon}\left[\frac{d^2 A_z}{dz^2} + \omega^2\mu\epsilon A_z\right] \tag{8-25}$$

Since the total tangential electric field E_z^t vanishes on the surface of the cylinder, (8-25) reduces to

$$\frac{d^2 A_z}{dz^2} + k^2 A_z = 0 \tag{8-25a}$$

EX2042
Page 406 of 1072

Because the current density on the cylinder is symmetrical [$J_z(z') = J_z(-z')$], the potential A_z is also symmetrical (i.e., $A_z(z') = A_z(-z')$]. Thus the solution of (8-25a) is given by

$$A_z(z) = -j\sqrt{\mu\epsilon}[B_1 \cos(kz) + C_1 \sin(k|z|)] \tag{8-26}$$

where B_1 and C_1 are constants. For a current-carrying wire, its potential is also given by (3-53). Equating (8-26) to (3-53) leads to

$$\boxed{\int_{-l/2}^{+l/2} I_z(z') \frac{e^{-jkR}}{4\pi R}\, dz' = -j\sqrt{\frac{\epsilon}{\mu}}[B_1 \cos(kz) + C_1 \sin(k|z|)]} \tag{8-27}$$

If a voltage V_i is applied at the input terminals of the wire, it can be shown that the constant $C_1 = V_i/2$. The constant B_1 is determined from the boundary condition that requires the current to vanish at the end points of the wire.

Equation (8-27) is referred to as *Hallén's integral equation* for a perfectly conducting wire. It was derived by solving the differential equation (3-15) or (8-25a) with the enforcement of the appropriate boundary conditions.

8.3.3 Source Modeling

Let us assume that the wire of Figure 8.5 is symmetrically fed by a voltage source, as shown in Figure 8.7(a), and the element is acting as a dipole antenna. To use, for example, Pocklington's integrodifferential equation (8-22) or (8-24) we need to know how to express $E_z^i(\rho = a)$. Traditionally there have been two methods used to model the excitation to represent $E_z^i(\rho = a, 0 \le \phi \le 2\pi, -l/2 \le z \le +l/2)$ at all points on the surface of the dipole: One is referred to as the *delta-gap* excitation and the other as the *equivalent magnetic ring current* (better known as *magnetic-frill generator*) [27].

A. Delta Gap

The delta-gap source modeling is the simplest and most widely used of the two, but it is also the least accurate, especially for impedances. Usually it is most accurate for smaller width gaps. Using the delta gap, it is assumed that the excitation voltage at the feed terminals is of a constant V_i value and zero elsewhere. Therefore the incident electric field $E_z^i(\rho = a, 0 \le \phi \le 2\pi, -l/2 \le z \le +l/2)$ is also a constant (V_s/Δ where Δ is the gap width) over the feed gap and zero elsewhere, hence the name delta gap. For the delta-gap model, the feed gap Δ of Figure 8.7(a) is replaced by a narrow band of strips of equivalent magnetic current density of

$$\mathbf{M}_g = -\hat{\mathbf{n}} \times \mathbf{E}^i = -\hat{\mathbf{a}}_\rho \times \hat{\mathbf{a}}_z \frac{V_s}{\Delta} = \hat{\mathbf{a}}_\phi \frac{V_s}{\Delta} \qquad -\frac{\Delta}{2} \le z' \le \frac{\Delta}{2} \tag{8-28}$$

The magnetic current density $\mathbf{M}_g$ is sketched in Figure 8.7(a).

B. Magnetic-Frill Generator

The magnetic-frill generator was introduced to calculate the near- as well as the far-zone fields from coaxial apertures [27]. To use this model, the feed gap is replaced

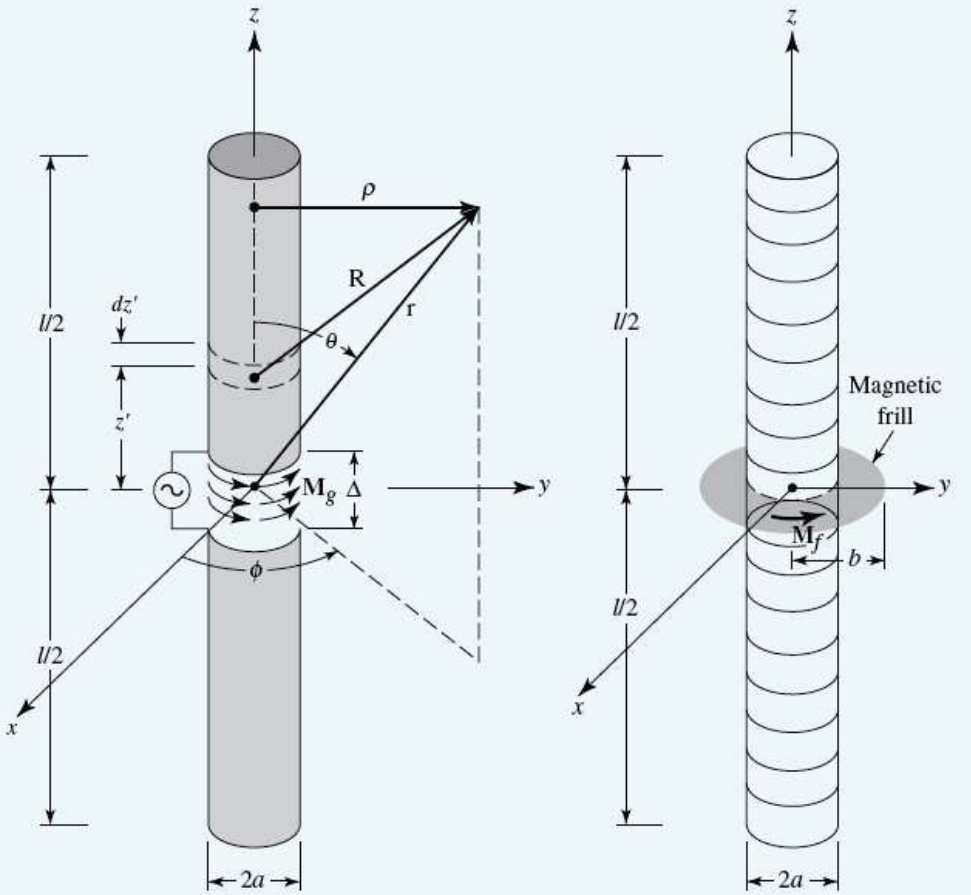


Figure 8.7 Cylindrical dipole, its segmentation, and gap modeling.

with a circumferentially directed magnetic current density that exists over an annular aperture with inner radius a, which is usually chosen to be the radius of the wire, and an outer radius b, as shown in Figure 8.7(b). Since the dipole is usually fed by transmission lines, the outer radius b of the equivalent annular aperture of the magnetic-frill generator is found using the expression for the characteristic impedance of the transmission line.

Over the annular aperture of the magnetic-frill generator, the electric field is represented by the TEM mode field distribution of a coaxial transmission line given by

$$\mathbf{E}_f = \hat{\mathbf{a}}_\rho \frac{V_s}{2\rho' \ln(b/a)} \quad a \le \rho' \le b \tag{8-29}$$

where V_s is the voltage supplied by the source. *The 1/2 factor is used because it is assumed that the source impedance is matched to the input impedance of the antenna. The 1/2 should be replaced by unity if the voltage V_i present at the input connection to the antenna is used, instead of the voltage V_s supplied by the source.*

Therefore the corresponding equivalent magnetic current density $\mathbf{M}_f$ for the magnetic-frill generator used to represent the aperture is equal to

$$\mathbf{M}_f = -2\hat{\mathbf{n}} \times \mathbf{E}_f = -2\hat{\mathbf{a}}_z \times \hat{\mathbf{a}}_\rho E_\rho = -\hat{\mathbf{a}}_\phi \frac{V_s}{\rho' \ln(b/a)} \quad a \le \rho' \le b \tag{8-30}$$

EX2042
Page 408 of 1072

The fields generated by the magnetic-frill generator of (8-30) on the surface of the wire are found by using [27]

$$E_z^i\left(\rho = a,\, 0 \le \phi \le 2\pi,\, -\frac{l}{2} \le z \le \frac{l}{2}\right)$$
$$\simeq -V_s\left(\frac{k(b^2-a^2)e^{-jkR_0}}{8\ln(b/a)R_0^2}\left\{2\left[\frac{1}{kR_0}+j\left(1-\frac{b^2-a^2}{2R_0^2}\right)\right]\right.\right.$$
$$+\frac{a^2}{R_0}\left[\left(\frac{1}{kR_0}+j\left(1-\frac{(b^2+a^2)}{2R_0^2}\right)\right)\left(-jk-\frac{2}{R_0}\right)\right.$$
$$\left.\left.\left.+\left(-\frac{1}{kR_0^2}+j\frac{b^2+a^2}{R_0^3}\right)\right]\right\}\right) \tag{8-31}$$

where

$$R_0 = \sqrt{z^2+a^2} \tag{8-31a}$$

The fields generated on the surface of the wire computed using (8-31) can be approximated by those found along the axis ($\rho = 0$). Doing this leads to a simpler expression of the form [27]

$$E_z^i\left(\rho = 0, -\frac{l}{2} \le z \le \frac{l}{2}\right) = -\frac{V_s}{2\ln(b/a)}\left[\frac{e^{-jkR_1}}{R_1}-\frac{e^{-jkR_2}}{R_2}\right] \tag{8-32}$$

where

$$R_1 = \sqrt{z^2+a^2} \tag{8-32a}$$

$$R_2 = \sqrt{z^2+b^2} \tag{8-32b}$$

To compare the results using the two-source modelings (delta-gap and magnetic-frill generator), an example is performed.

Example 8.3

For a center-fed linear dipole of $l = 0.47\lambda$ and $a = 0.005\lambda$, determine the induced voltage along the length of the dipole based on the incident electric field of the magnetic frill of (8-32). Subdivide the wire into 21 segments ($N = 21$). Compare the induced voltage distribution based on the magnetic frill to that of the delta gap. Assume a 50-ohm characteristic impedance with free-space between the conductors for the annular feed.

Solution: Since the characteristic impedance of the annular aperture is 50 ohms, then

$$Z_c = \sqrt{\frac{\mu_0}{\epsilon_0}}\frac{\ln(b/a)}{2\pi} = 50 \;\Rightarrow\; \frac{b}{a} = 2.3$$

Subdividing the total length ($l = 0.47\lambda$) of the dipole to 21 segments makes

$$\Delta = \frac{0.47\lambda}{21} = 0.0224\lambda$$

Using (8-32) to compute E_z^i, the corresponding induced voltages obtained by multiplying the value of $-E_z^i$ at each segment by the length of the segment are listed in Table 8.1, where they are compared with those of the delta gap. In Table 8.1 $n = 1$ represents the outermost segment and $n = 11$ represents the center segment. Because of the symmetry, only values for the center segment and half of the other segments are shown. Although the two distributions are not identical, the magnetic-frill distribution voltages decay quite rapidly away from the center segment and they very quickly reach almost vanishing values.

TABLE 8.1 Unnormalized and Normalized Dipole Induced Voltage† Differences for Delta-Gap and Magnetic-Frill Generator ($l = 0.47\lambda, a = 0.005\lambda, N = 21$)

Segment Number n	Delta-Gap Voltage		Magnetic-Frill Generator Voltage			
	Unnormalized	Normalized	Unnormalized		Normalized	
1	0	0	1.11×10^{-4}	-26.03°	7.30×10^{-5}	-26.03°
2	0	0	1.42×10^{-4}	-20.87°	9.34×10^{-5}	-20.87°
3	0	0	1.89×10^{-4}	-16.13°	1.24×10^{-4}	-16.13°
4	0	0	2.62×10^{-4}	-11.90°	1.72×10^{-4}	-11.90°
5	0	0	3.88×10^{-4}	-8.23°	2.55×10^{-4}	-8.23°
6	0	0	6.23×10^{-4}	-5.22°	4.10×10^{-4}	-5.22°
7	0	0	1.14×10^{-3}	-2.91°	7.50×10^{-4}	-2.91°
8	0	0	2.52×10^{-3}	-1.33°	1.66×10^{-3}	-1.33°
9	0	0	7.89×10^{-3}	-0.43°	5.19×10^{-3}	-0.43°
10	0	0	5.25×10^{-2}	-0.06°	3.46×10^{-2}	-0.06°
11	1	1	1.52	0°	1.0	0°

†Voltage differences as defined here represent the product of the incident electric field at the center of each segment and the corresponding segment length.

8.4 MOMENT METHOD SOLUTION

Equations (8-22), (8-24), and (8-27) each has the form of

$$F(g) = h \tag{8-33}$$

where F is a known linear operator, h is a known excitation function, and g is the response function. For (8-22) F is an integrodifferential operator while for (8-24) and (8-27) it is an integral operator. The objective here is to determine g once F and h are specified.

While the inverse problem is often intractable in closed form, the linearity of the operator F makes a numerical solution possible. One technique, known as the Moment Method [7]–[14] requires that the unknown response function be expanded as a linear

combination of N terms and written as

$$g(z') \simeq a_1 g_1(z') + a_2 g_2(z') + \cdots + a_N g_N(z') = \sum_{n=1}^{N} a_n g_n(z') \tag{8-34}$$

Each a_n is an unknown constant and each $g_n(z')$ is a known function usually referred to as a *basis* or *expansion* function. The domain of the $g_n(z')$ functions is the same as that of $g(z')$. Substituting (8-34) into (8-33) and using the linearity of the F operator reduces (8-33) to

$$\sum_{n=1}^{N} a_n F(g_n) = h \tag{8-35}$$

The basis functions g_n are chosen so that each $F(g_n)$ in (8-35) can be evaluated conveniently, preferably in closed form or at the very least numerically. The only task remaining then is to find the a_n unknown constants.

Expansion of (8-35) leads to one equation with N unknowns. It alone is not sufficient to determine the N unknown a_n $(n = 1, 2, \ldots, N)$ constants. To resolve the N constants, it is necessary to have N linearly independent equations. This can be accomplished by evaluating (8-35) (e.g., applying boundary conditions) at N different points. This is referred to as *point-matching* (or *collocation*). Doing this, (8-35) takes the form of

$$\sum_{n=1}^{N} I_n F(g_n) = h_m, \quad m = 1, 2, \ldots, N \tag{8-36}$$

In matrix form, (8-36) can be expressed as

$$[Z_{mn}][I_n] = [V_m] \tag{8-37}$$

where

$$Z_{mn} = F(g_n) \tag{8-37a}$$

$$I_n = a_n \tag{8-37b}$$

$$V_m = h_m \tag{8-37c}$$

The unknown coefficients a_n can be found by solving (8-37) using matrix inversion techniques, or

$$[I_n] = [Z_{mn}]^{-1}[V_m] \tag{8-38}$$

8.4.1 Basis Functions

One very important step in any numerical solution is the choice of basis functions. In general, one chooses as basis functions the set that has the ability to accurately represent and resemble the anticipated unknown function, while minimizing the computational effort required to employ it [28]–[30]. Do not choose basis functions with smoother properties than the unknown being represented.

Theoretically, there are many possible basis sets. However, only a limited number are used in practice. These sets may be divided into two general classes. The first class

consists of subdomain functions, which are nonzero only over a part of the domain of the function $g(x')$; its domain is the surface of the structure. The second class contains entire-domain functions that exist over the entire domain of the unknown function. The entire-domain basis function expansion is analogous to the well-known Fourier series expansion method.

A. Subdomain Functions

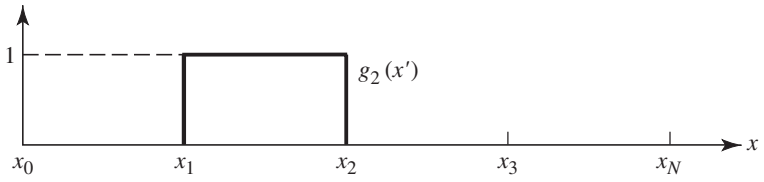
Of the two types of basis functions, subdomain functions are the most common. Unlike entire-domain bases, they may be used without prior knowledge of the nature of the function that they must represent.

The subdomain approach involves subdivision of the structure into N nonoverlapping segments, as illustrated on the axis in Figure 8.8(a). For clarity, the segments are shown here to be collinear and of equal length, although neither condition is necessary. The basis functions are defined in conjunction with the limits of one or more of the segments.

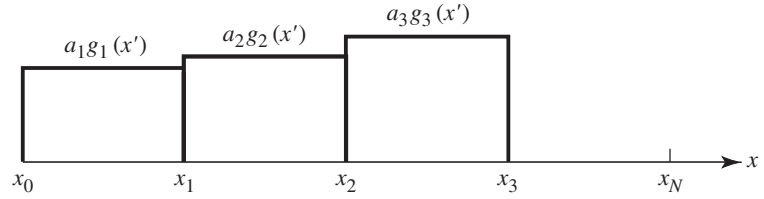
Perhaps the most common of these basis functions is the conceptually simple piecewise constant, or "pulse" function, shown in Figure 8.8(a). It is defined by

Piecewise Constant

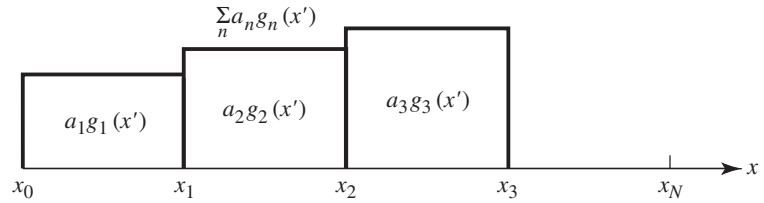
$$g_n(x') = \begin{cases} 1 & x'_{n-1} \le x' \le x'_n \\ 0 & \text{elsewhere} \end{cases} \tag{8-39}$$



(a) Single



(b) Multiple



(c) Function representation

Figure 8.8 Piecewise constant subdomain functions.

EX2042
Page 412 of 1072

Once the associated coefficients are determined, this function will produce a staircase representation of the unknown function, similar to that in Figures 8.8(b) and (c).

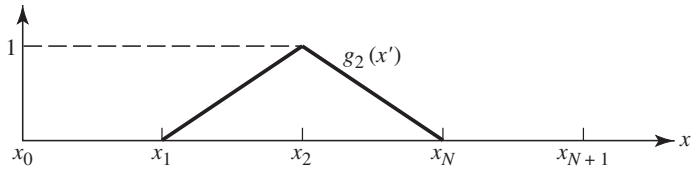
Another common basis set is the piecewise linear, or "triangle," functions seen in Figure 8.9(a). These are defined by

Piecewise Linear

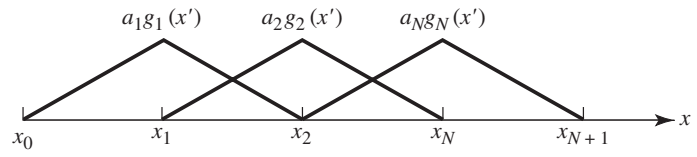
$$g_n(x') = \begin{cases} \dfrac{x' - x'_{n-1}}{x'_n - x'_{n-1}} & x'_{n-1} \le x' \le x'_n \\ \dfrac{x'_{n+1} - x'}{x'_{n+1} - x'_n} & x'_n \le x' \le x'_{n+1} \\ 0 & \text{elsewhere} \end{cases} \tag{8-40}$$

and are seen to cover two segments, and overlap adjacent functions [Figure 8.9(b)]. The resulting representation [Figure 8.9(c)] is smoother than that for "pulses," but at the cost of increased computational complexity.

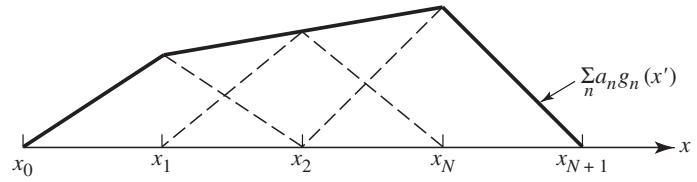
Increasing the sophistication of subdomain basis functions beyond the level of the "triangle" may not be warranted by the possible improvement in accuracy. However, there are cases where more specialized functions are useful for other reasons. For example, some integral operators may be evaluated without numerical integration when their integrands are multiplied by a $\sin(kx')$ or $\cos(kx')$ function, where x' is the variable of integration. In such examples, considerable advantages in computation time and resistance to errors can be gained by using basis functions like the piecewise sinusoid of Figure 8.10 or truncated cosine of Figure 8.11. These functions are defined by



(a) Single



(b) Multiple



(c) Function representation

Figure 8.9 Piecewise linear subdomain functions.

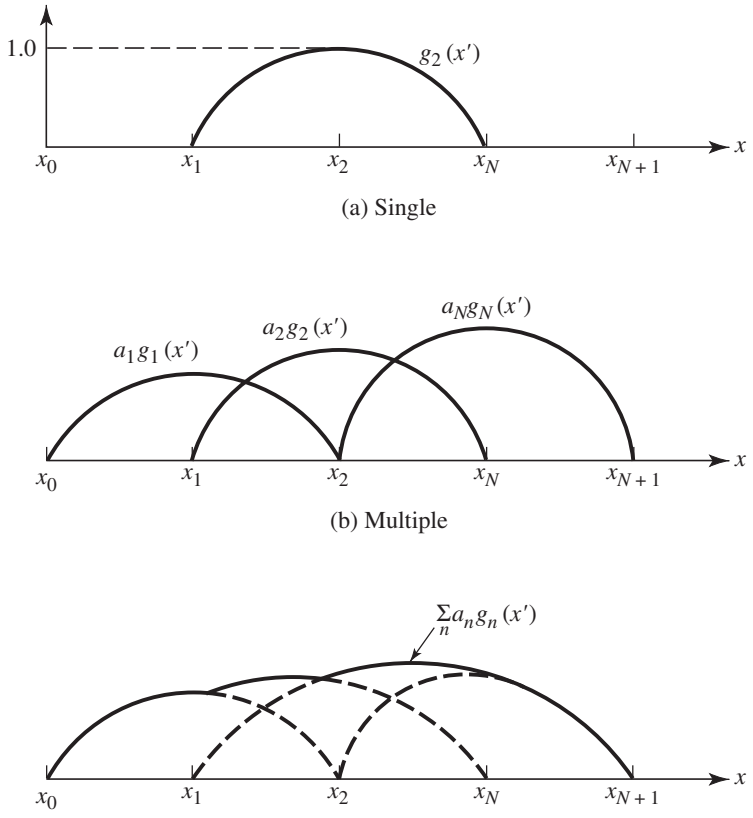


Figure 8.10 Piecewise sinusoids subdomain functions.

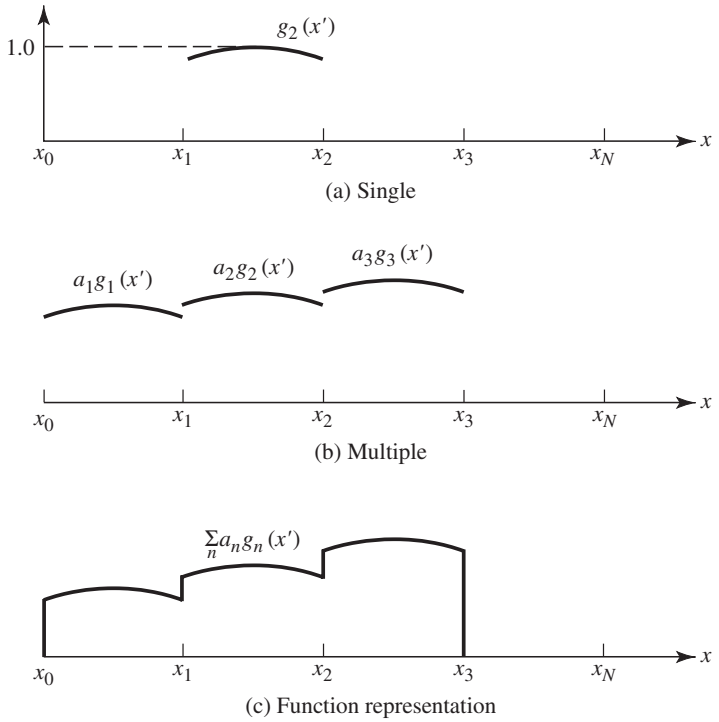


Figure 8.11 Truncated cosines subdomain functions.

EX2042
Page 414 of 1072

Piecewise Sinusoid

$$g_n(x') = \begin{cases} \dfrac{\sin[k(x' - x'_{n-1})]}{\sin[k(x'_n - x'_{n-1})]} & x'_{n-1} \le x' \le x'_n \\ \dfrac{\sin[k(x'_{n+1} - x')]}{\sin[k(x'_{n+1} - x'_n)]} & x'_n \le x' \le x'_{n+1} \\ 0 & \text{elsewhere} \end{cases} \tag{8-41}$$

Truncated Cosine

$$g_n(x') = \begin{cases} \cos\left[k\left(x' - \dfrac{x'_n - x'_{n-1}}{2}\right)\right] & x'_{n-1} \le x' \le x'_n \\ 0 & \text{elsewhere} \end{cases} \tag{8-42}$$

B. Entire-Domain Functions

Entire-domain basis functions, as their name implies, are defined and are nonzero over the entire length of the structure being considered. Thus no segmentation is involved in their use.

A common entire-domain basis set is that of sinusoidal functions, where

Entire Domain

$$g_n(x') = \cos\left[\frac{(2n-1)\pi x'}{l}\right] \quad -\frac{l}{2} \le x' \le \frac{l}{2} \tag{8-43}$$

Note that this basis set would be particularly useful for modeling the current distribution on a wire dipole, which is known to have primarily sinusoidal distribution. The main advantage of entire-domain basis functions lies in problems where the unknown function is assumed *a priori* to follow a known pattern. Such entire-domain functions may render an acceptable representation of the unknown while using far fewer terms in the expansion of (8-34) than would be necessary for subdomain bases. Representation of a function by entire-domain cosine and/or sine functions is similar to the Fourier series expansion of arbitrary functions.

Because we are constrained to use a finite number of functions (or modes, as they are sometimes called), entire-domain basis functions usually have difficulty in modeling arbitrary or complicated unknown functions.

Entire-domain basis functions, sets like (8-43), can be generated using Tschebyscheff, Maclaurin, Legendre, and Hermite polynomials, or other convenient functions.

8.4.2 Weighting (Testing) Functions

To improve the point-matching solution of (8-36), (8-37), or (8-38) an inner product $\langle w, g \rangle$ can be defined which is a scalar operation satisfying the laws of

$$\langle w, g \rangle = \langle g, w \rangle \tag{8-44a}$$

$$\langle bf + cg, w \rangle = b\langle f, w \rangle + c\langle g, w \rangle \tag{8-44b}$$

$$\langle g^*, g \rangle > 0 \quad \text{if } g \neq 0 \tag{8-44c}$$

$$\langle g^*, g \rangle = 0 \quad \text{if } g = 0 \tag{8-44d}$$

where b and c are scalars and the asterisk (*) indicates complex conjugation. A typical, but not unique, inner product is

$$\langle \mathbf{w}, \mathbf{g} \rangle = \iint_s \mathbf{w}^* \cdot \mathbf{g}\, ds \tag{8-45}$$

where the w's are the *weighting* (*testing*) functions and S is the surface of the structure being analyzed. Note that the functions w and g can be vectors. This technique is better known as the *Moment Method* or *Method of Moments* (MM) [7], [8].

The collocation (point-matching) method is a numerical technique whose solutions satisfy the electromagnetic boundary conditions (e.g., vanishing tangential electric fields on the surface of an electric conductor) only at discrete points. Between these points the boundary conditions may not be satisfied, and we define the deviation as a *residual* (e.g., residual $= \Delta E|_{\tan} = E(\text{scattered})|_{\tan} + E(\text{incident})|_{\tan} \neq 0$ on the surface of an electric conductor). For a half-wavelength dipole, a typical residual is shown in Figure 8.12(a) for pulse basis functions and point-matching and Figure 8.12(b) exhibits the residual for piecewise sinusoids-Galerkin method [31]. As expected, the pulse basis point-matching exhibits the most ill-behaved residual and the piecewise sinusoids-Galerkin method indicates an improved residual. To minimize the residual in such a way that its overall average over the entire structure approaches zero, the method of *weighted residuals* is utilized in conjunction with the inner product of (8-45). This technique, referred to as the *Moment Method* (MM), does not lead to a vanishing residual at every point on the surface of a conductor, but it forces the boundary conditions to be satisfied in an average sense over the entire surface.

To accomplish this, we define a set of N *weighting* (or testing) functions $\{w_m\} = w_1, w_2, \ldots, w_N$ in the domain of the operator F. Forming the inner product between each of these functions, (8-35) results in

$$\sum_{n=1}^{N} a_n \langle w_m, F(g_n) \rangle = \langle w_m, h \rangle \qquad m = 1, 2, \ldots, N \tag{8-46}$$

This set of N equations may be written in matrix form as

$$[F_{mn}][a_n] = [h_m] \tag{8-47}$$

where

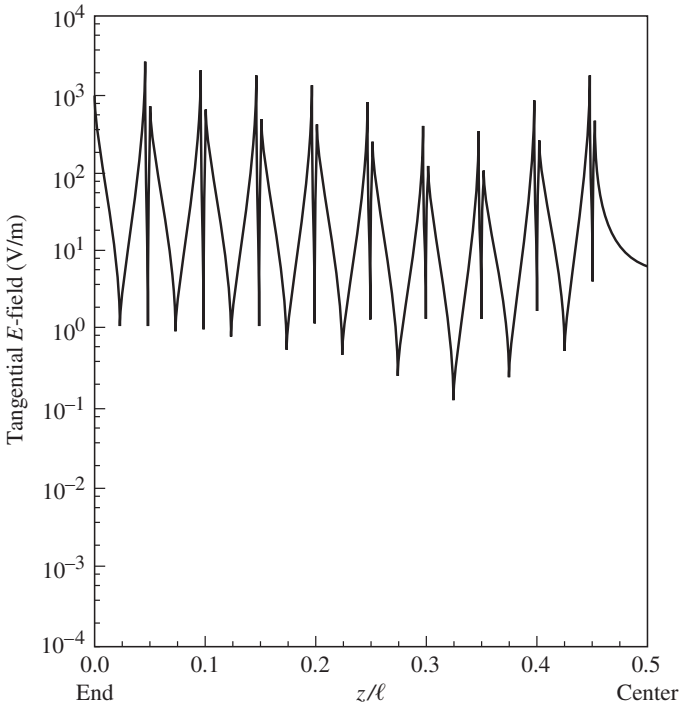
$$[F_{mn}] = \begin{bmatrix} \langle w_1, F(g_1) \rangle & \langle w_1, F(g_2) \rangle & \cdots \\ \langle w_2, F(g_1) \rangle & \langle w_2, F(g_2) \rangle & \\ \vdots & & \vdots \end{bmatrix} \tag{8-47a}$$

$$[a_n] = \begin{bmatrix} a_1 \\ a_2 \\ \vdots \\ a_N \end{bmatrix} \quad [h_m] = \begin{bmatrix} \langle w_1, h \rangle \\ \langle w_2, h \rangle \\ \vdots \\ \langle w_N, h \rangle \end{bmatrix} \tag{8-47b}$$

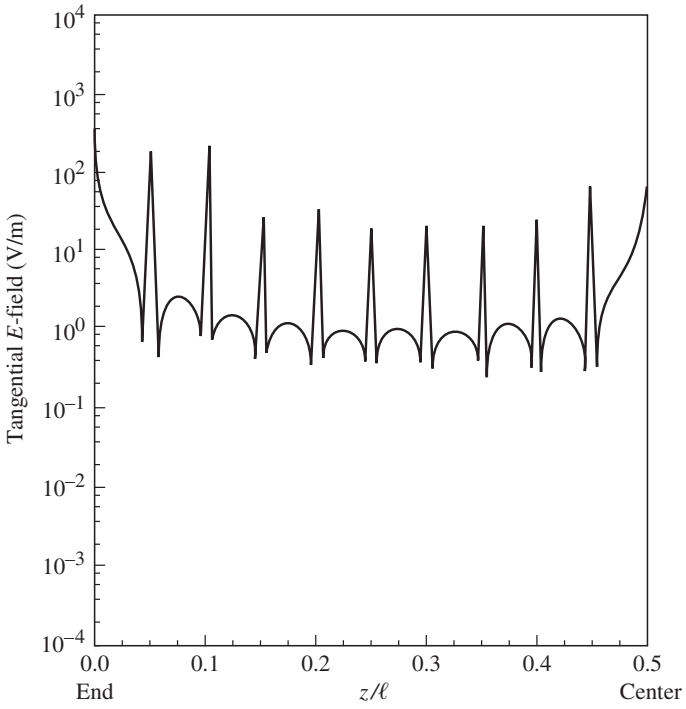
The matrix of (8-47) may be solved for the a_n by inversion, and it can be written as

$$[a_n] = [F_{mn}]^{-1}[h_m] \tag{8-48}$$

EX2042
Page 416 of 1072



(a) Pulse point-matching



(b) Piecewise sinusoids-Galerkin

Figure 8.12 Tangential electric field on the conducting surface of a $\lambda/2$ dipole. (SOURCE: E. K. Miller and F. J. Deadrick, "Some computational aspects of thin-wire modeling" in *Numerical and Asymptotic Techniques in Electromagnetics*, 1975, Springer-Verlag).

EX2042
Page 417 of 1072

The choice of weighting functions is important in that the elements of $\{w_n\}$ must be linearly independent, so that the N equations in (8-46) will be linearly independent [7]–[9], [29], [30]. Further, it will generally be advantageous to choose weighting functions that minimize the computations required to evaluate the inner product.

The condition of linear independence between elements and the advantage of computational simplicity are also important characteristics of basis functions. Because of this, similar types of functions are often used for both weighting and expansion. A particular choice of functions may be to let the weighting and basis function be the same, that is, $w_n = g_n$. This technique is known as *Galerkin's method* [32].

It should be noted that there are N^2 terms to be evaluated in (8-47a). Each term usually requires two or more integrations; at least one to evaluate each $F(g_n)$ and one to perform the inner products of (8-45). When these integrations are to be done numerically, as is often the case, vast amounts of computation time may be necessary. There is, however, a unique set of weighting functions that reduce the number of required integrations. This is the set of Dirac delta weighting functions

$$[w_m] = [\delta(p - p_m)] = [\delta(p - p_1), \delta(p - p_2), \ldots] \tag{8-49}$$

where p specifies a position with respect to some reference (origin) and p_m represents a point at which the boundary condition is enforced. Using (8-45) and (8-49) reduces (8-46) to

$$\begin{aligned} \langle \delta(p - p_m), h \rangle &= \sum_n a_n \langle \delta(p - p_m), F(g_n) \rangle \quad m = 1, 2, \ldots, N \\ \iint_s \delta(p - p_m) h \, ds &= \sum_n a_n \iint_s \delta(p - p_m) F(g_n) \, ds \quad m = 1, 2, \ldots, N \\ h|_{p=p_m} &= \sum_n a_n F(g_n)|_{p=p_m} \quad m = 1, 2, \ldots, N \end{aligned} \tag{8-50}$$

Hence, the only remaining integrations are those specified by $F(g_n)$. This simplification may lead to solutions that would be impractical if other weighting functions were used. Physically, the use of Dirac delta weighting functions is seen as the relaxation of boundary conditions so that they are enforced only at discrete points on the surface of the structure, hence the name point-matching.

An important consideration when using point-matching is the positioning of the N points (p_m). While equally-spaced points often yield good results, much depends on the basis functions used. When using subsectional basis functions in conjunction with point-matching, one match point should be placed on each segment (to maintain linear independence). Placing the points at the center of the segments usually produces the best results. It is important that a match point does not coincide with the "peak" of a triangle or a similar discontinuous function, where the basis function is not differentiably continuous. This may cause errors in some situations.

8.5 SELF-IMPEDANCE

The input impedance of an antenna is a very important parameter, and it is used to determine the efficiency of the antenna. In Section 4.5 the real part of the impedance

(referred either to the current at the feed terminals or to the current maximum) was found. At that time, because of mathematical complexities, no attempt was made to find the imaginary part (reactance) of the impedance. In this section the self-impedance of a linear element will be examined using both the Integral Equation-Moment Method and the induced emf method. The real and imaginary parts of the impedance will be found using both methods.

8.5.1 Integral Equation-Moment Method

To use this method to find the self-impedance of a dipole, the first thing to do is to solve the integral equation for the current distribution. This is accomplished using either Pocklington's Integral equation of (8-22) or (8-24) or Hallén's integral equation of (8-27). For Pocklington's integral equation you can use either the delta-gap voltage excitation of (8-28) or the magnetic-frill model of (8-31) or (8-32). Hallén's integral equation is based on the delta-gap model of (8-28).

Once the current distribution is found, using either or both of the integral equations, then the self (input) impedance is determined using the ratio of the voltage to current, or

$$Z_{in} = \frac{V_{in}}{I_{in}} \tag{8-51}$$

A computer program ***Moment Method*** has been developed based on Pocklington's and Hallén's integral equations, and it is found in the CD attached to the book. Pocklington's uses both the delta-gap and magnetic-frill models while Hallén's uses only the delta-gap feed model. Both, however, use piecewise constant subdomain functions and point-matching. The program computes the current distribution, normalized amplitude radiation pattern, and input impedance. The user must specify the length of the wire, its radius (both in wavelengths), and the type of feed modeling (delta-gap or magnetic-frill) and the number of segments.

To demonstrate the procedure and compare the results using the two-source modelings (delta-gap and magnetic-frill generator) for Pocklington's integral equation, an example is performed.

Example 8.4

Assume a center-fed linear dipole of $l = 0.47\lambda$ and $a = 0.005\lambda$. This is the same element of Example 8.3.

1. Determine the normalized current distribution over the length of the dipole using $N = 21$ segments to subdivide the length. Plot the current distribution.
2. Determine the input impedance using segments of $N = 7$, 11, 21, 29, 41, 51, 61, 71, and 79.

Use Pocklington's integrodifferential equation (8-24) with piecewise constant subdomain basis functions and point-matching to solve the problem, model the gap with one segment, and use both the delta-gap and magnetic-frill generator to model the excitation. Use (8-32)

for the magnetic-frill generator. Because the current at the ends of the wire vanishes, the piecewise constant subdomain basis functions are not the most judicious choice. However, because of their simplicity, they are chosen here to illustrate the principles even though the results are not the most accurate. Assume that the characteristic impedance of the annular aperture is 50 ohms and the excitation voltage V_i is 1 V.

Solution:

1. The voltage distribution was found in Example 8.3, and it is listed in Table 8.1. The corresponding normalized currents obtained using (8-24) with

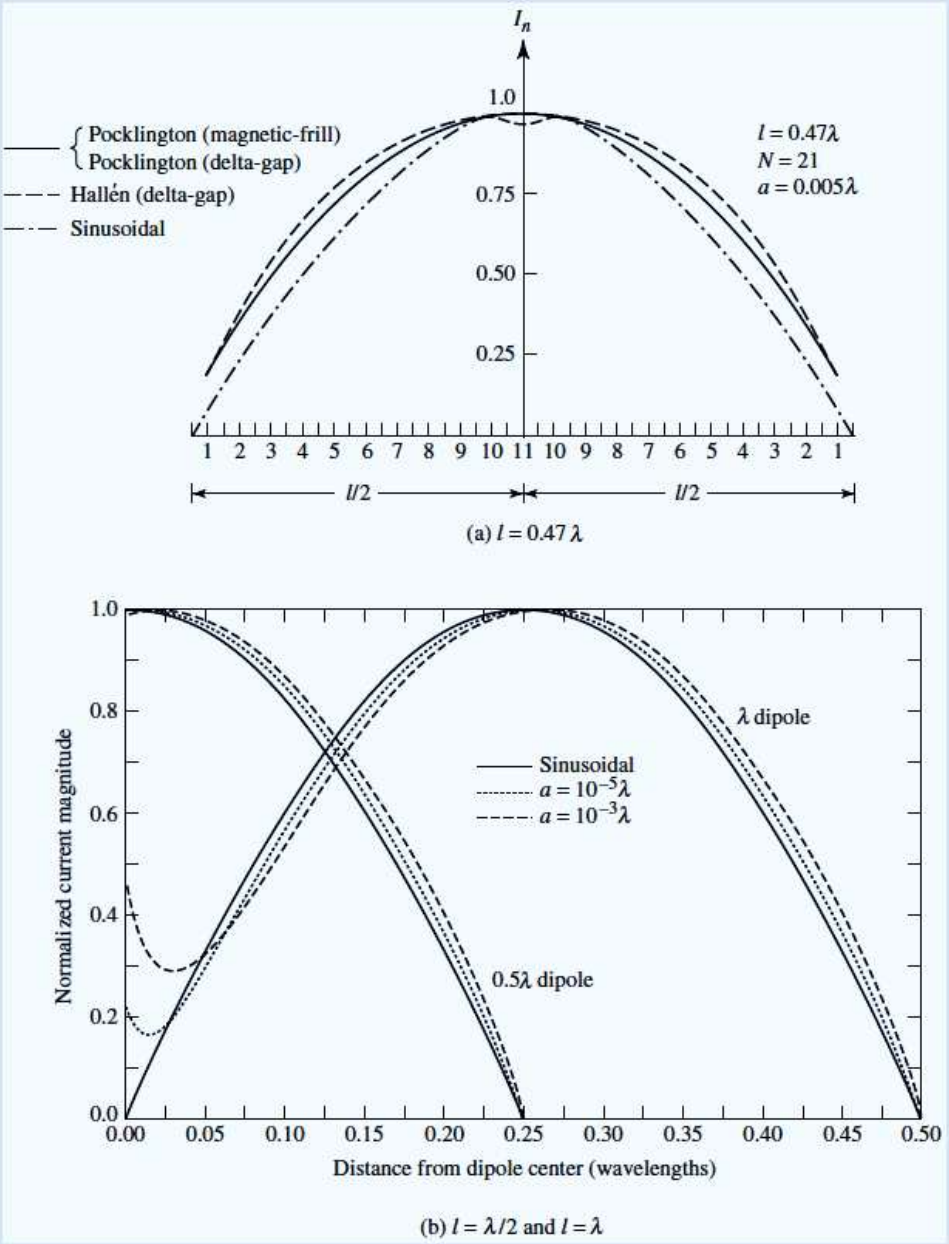


Figure 8.13 Current distribution on a dipole antenna.

piecewise constant pulse functions and point-matching technique for both the delta-gap and magnetic-frill generator are shown plotted in Figure 8.13(a). It is apparent that the two distributions are almost identical in shape, and they resemble that of the ideal sinusoidal current distribution which is more valid for very thin wires and very small gaps. The distributions obtained using Pocklington's integral equation do not vanish at the ends because of the use of piecewise constant subdomain basis functions.

2. The input impedances using both the delta-gap and the magnetic-frill generator are shown listed in Table 8.2. It is evident that the values begin to stabilize and compare favorably to each other once 61 or more segments are used.

TABLE 8.2 Dipole Input Impedance for Delta-Gap and Magnetic-Frill Generator Using Pocklington's Integral Equation ($l = 0.47\lambda, a = 0.005\lambda$)

N	Delta Gap	Magnetic Frill
7	$122.8 + j113.9$	$26.8 + j24.9$
11	$94.2 + j49.0$	$32.0 + j16.7$
21	$77.7 - j0.8$	$47.1 - j0.2$
29	$75.4 - j6.6$	$57.4 - j4.5$
41	$75.9 - j2.4$	$68.0 - j1.0$
51	$77.2 + j2.4$	$73.1 + j4.0$
61	$78.6 + j6.1$	$76.2 + j8.5$
71	$79.9 + j7.9$	$77.9 + j11.2$
79	$80.4 + j8.8$	$78.8 + j12.9$

To further illustrate the point on the variation of the current distribution on a dipole, it has been computed by Moment Method and plotted in Figure 8.13(b) for $l = \lambda/2$ and $l = \lambda$ for wire radii of $a = 10^{-5}\lambda$ and $10^{-3}\lambda$ where it is compared with that based on the sinusoidal distribution. It is apparent that the radius of the wire does not influence to a large extent the distribution of the $l = \lambda/2$ dipole. However it has a profound effect on the current distribution of the $l = \lambda$ dipole at and near the feed point. Therefore the input impedance of the $l = \lambda$ dipole is quite different for the three cases of Figure 8.13(b), since the zero current at the center of the sinusoidal distribution predicts an infinite impedance. In practice, the impedance is not infinite but is very large.

8.5.2 Induced EMF Method

The induced emf method is a classical method to compute the self and mutual impedances [1]–[6], [33]. The method is basically limited to straight, parallel, and in echelon elements, and it is more difficult to account accurately for the radius of the wires as well as the gaps at the feeds. However it leads to closed-form solutions which provide very good design data. From the analysis of the infinitesimal dipole

in Section 4.2, it was shown that the imaginary part of the power density, which contributes to the imaginary power, is dominant in the near-zone of the element and becomes negligible in the far-field. Thus, near-fields of an antenna are required to find its input reactance.

A. Near-Field of Dipole

In Chapter 4 the far-zone electric and magnetic fields radiated by a finite length dipole with a sinusoidal current distribution were found. The observations were restricted in the far-field in order to reduce the mathematical complexities. The expressions of these fields were used to derive the radiation resistance and the input resistance of the dipole. However, when the input reactance and/or the mutual impedance between elements are desired, the near-fields of the element must be known. It is the intent here to highlight the derivation.

The fields are derived based on the geometry of Figure 8.14. The procedure is identical to that used in Section 4.2.1 for the infinitesimal dipole. The major difference is that the integrations are much more difficult. To minimize long derivations involving

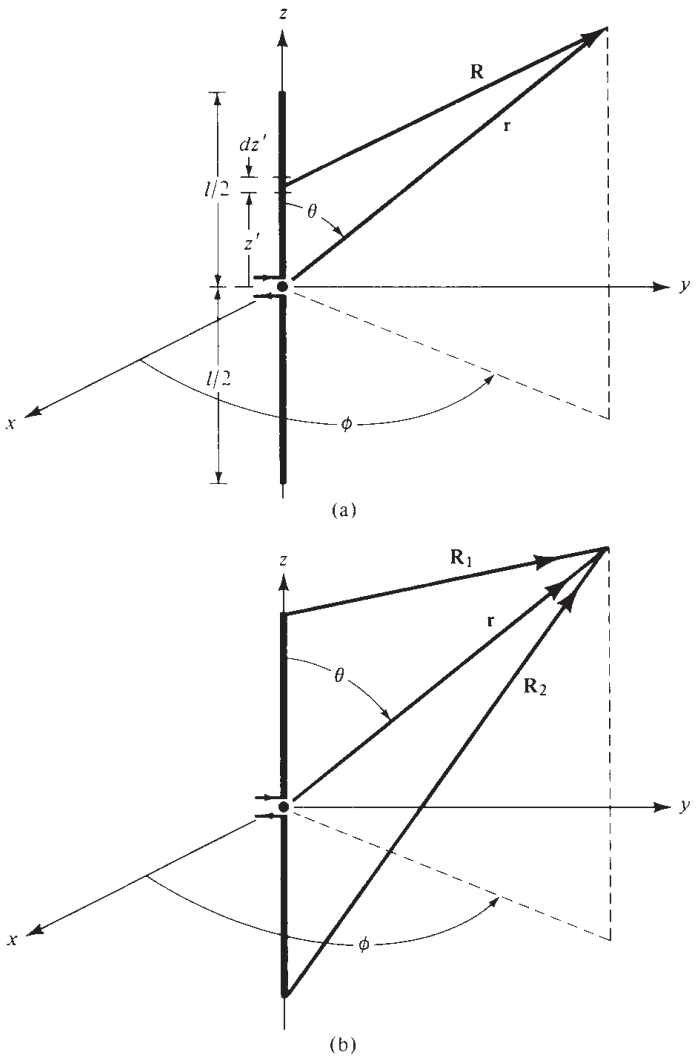


Figure 8.14 Dipole geometry for near-field analysis.

complex integrations, only the procedure will be outlined and the final results will be given. The derivation is left as an end of the chapter problems. The details can also be found in the first edition of this book.

To derive the fields, the first thing is to specify the sinusoidal current distribution for a finite dipole which is that of (4-56). Once that is done, then the vector potential **A** of (4-2) is determined. Then the magnetic field is determined using (3-2a), or

$$\mathbf{H} = \frac{1}{\mu}\nabla \times \mathbf{A} = -\hat{\mathbf{a}}_\phi \frac{1}{\mu}\frac{\partial A_z}{\partial \rho} \tag{8-52}$$

It is recommended that cylindrical coordinates are used. By following this procedure and after some lengthy analytical details, it can be shown by referring to Figure 8.14(b) that the magnetic field radiated by the dipole is

$$\mathbf{H} = \hat{\mathbf{a}}_\phi H_\phi = -\hat{\mathbf{a}}_\phi \frac{I_0}{4\pi j}\frac{1}{y}\left[e^{-jkR_1} + e^{-jkR_2} - 2\cos\left(\frac{kl}{2}\right)e^{-jkr}\right] \tag{8-53}$$

where

$$r = \sqrt{x^2 + y^2 + z^2} = \sqrt{\rho^2 + z^2} \tag{8-53a}$$

$$R_1 = \sqrt{x^2 + y^2 + \left(z - \frac{l}{2}\right)^2} = \sqrt{\rho^2 + \left(z - \frac{l}{2}\right)^2} \tag{8-53b}$$

$$R_2 = \sqrt{x^2 + y^2 + \left(z + \frac{l}{2}\right)^2} = \sqrt{\rho^2 + \left(z + \frac{l}{2}\right)^2} \tag{8-53c}$$

The corresponding electric field is found using Maxwell's equation of

$$\mathbf{E} = \frac{1}{j\omega\epsilon}\nabla \times \mathbf{H} \tag{8-54}$$

Once this is done, it can be shown that the electric field radiated by the dipole is

$$\mathbf{E} = \hat{\mathbf{a}}_\rho E_\rho + \hat{\mathbf{a}}_z E_z = -\hat{\mathbf{a}}_\rho \frac{1}{j\omega\epsilon}\frac{\partial H_\phi}{\partial z} + \hat{\mathbf{a}}_z \frac{1}{j\omega\epsilon}\frac{1}{\rho}\frac{\partial}{\partial \rho}(\rho H_\phi) \tag{8-55}$$

where

$$E_\rho = E_y = j\frac{\eta I_0}{4\pi y}\left[\left(z - \frac{l}{2}\right)\frac{e^{-jkR_1}}{R_1} + \left(z + \frac{l}{2}\right)\frac{e^{-jkR_2}}{R_2} - 2z\cos\left(\frac{kl}{2}\right)\frac{e^{-jkr}}{r}\right] \tag{8-55a}$$

$$E_z = -j\frac{\eta I_0}{4\pi}\left[\frac{e^{-jkR_1}}{R_1} + \frac{e^{-jkR_2}}{R_2} - 2\cos\left(\frac{kl}{2}\right)\frac{e^{-jkr}}{r}\right] \tag{8-55b}$$

It should be noted that the last term in (8-53), (8-55a), and (8-55b) vanishes when the overall length of the element is an integral number of odd half-wavelengths ($l = n\lambda/2, n = 1, 3, 5, \ldots$) because $\cos(kl/2) = \cos(n\pi/2) = 0$ for $n = 1, 3, 5, \ldots$.

The fields of (8-53), (8-55a), and (8-55b) were derived assuming a zero radius wire. In practice all wire antennas have a finite radius which in most cases is very small

EX2042
Page 423 of 1072

electrically (typically less than $\lambda/200$). Therefore the fields of (8-53), (8-55a), and (8-55b) are good approximations for finite, but small, radius dipoles.

B. Self-Impedance

The technique, which is used in this chapter to derived closed-form expressions for the self- and driving-point impedances of finite linear dipoles, is known as the *induced emf method*. The general approach of this method is to form the Poynting vector using (8-53), (8-55a), and (8-55b), and to integrate it over the surface that coincides with the surface of the antenna (linear dipole) itself. However, the same results can be obtained using a slightly different approach, as will be demonstrated here. The expressions derived using this method are more valid for small radii dipoles. Expressions, which are more accurate for larger radii dipoles, were derived in the previous section based on the Integral Equation-Moment Method.

To find the input impedance of a linear dipole of finite length and radius, shown in Figure 8.15, the tangential electric-field component on the surface of the wire is needed. This was derived previously and is represented by (8-55b). Based on the current distribution and tangential electric field along the surface of the wire, the induced potential developed at the terminals of the dipole based on the maximum current is given by

$$\begin{aligned} V_m &= \int_{-\ell/2}^{+\ell/2} dV_m \\ &= -\frac{1}{I_m}\int_{-\ell/2}^{+\ell/2} I_z(\rho = a, z = z')E_z(\rho = a, z = z')\,dz' \end{aligned} \tag{8-56}$$

where I_m is the maximum current. The input impedance (*referred to at the current maximum* I_m) is defined as

$$Z_m = \frac{V_m}{I_m} \tag{8-57}$$

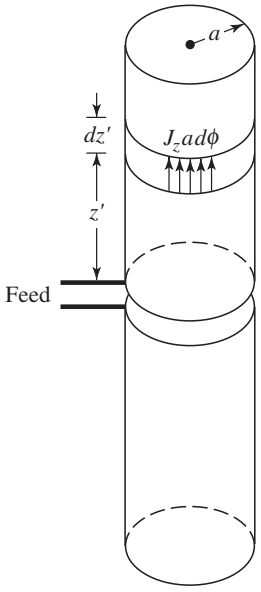


Figure 8.15 Uniform linear current density over cylindrical surface of wire.

EX2042
Page 424 of 1072

and can be expressed using (8-56) as

$$Z_m = -\frac{1}{I_m^2}\int_{-\ell/2}^{\ell/2} I_z(\rho = a, z = z')E_z(\rho = a, z = z')\,dz' \tag{8-57a}$$

Equation (8-57a) can also be obtained by forming the complex power density, integrating it over the surface of the antenna, and then relating the complex power to the terminal and induced voltages [2]. The integration can be performed either over the gap at the terminals or over the surface of the conducting wire.

For a wire dipole, the total current I_z is uniformly distributed around the surface of the wire, and it forms a linear current sheet J_z. The current is concentrated primarily over a very small thickness of the conductor, as shown in Figure 8.15, and it is given, based on (4-56), by

$$I_z = 2\pi a J_z = I_m \sin\left[k\left(\frac{l}{2} - |z'|\right)\right] \tag{8-58}$$

Therefore (8-57a) can be written as

$$Z_m = -\frac{1}{I_m}\int_{-\ell/2}^{\ell/2} \sin\left[k\left(\frac{l}{2} - |z'|\right)\right] E_z(\rho = a, z = z')\,dz' \tag{8-59}$$

For simplicity, it is assumed that the E-field produced on the surface of the wire by a current sheet is the same as if the current were concentrated along a filament placed along the axis of the wire. Then the E-field used in (8-59) is the one obtained along a line parallel to the wire at a distance $\rho = a$ from the filament.

Letting $I_m = I_o$ and substituting (8-55b) into (8-59) it can be shown, after some lengthy but straightforward manipulations, that the real and imaginary parts of the input impedance (referred to at the *current maximum*) can be expressed as

$$\begin{aligned} R_r = R_m = \frac{\eta}{2\pi}\Bigg\{ & C + \ln(kl) - C_i(kl) + \frac{1}{2}\sin(kl)[S_i(2kl) - 2S_i(kl)] \\ & + \frac{1}{2}\cos(kl)[C + \ln(kl/2) + C_i(2kl) - 2C_i(kl)]\Bigg\} \end{aligned} \tag{8-60a}$$

$$\begin{aligned} X_m = \frac{\eta}{4\pi}\Bigg\{ & 2S_i(kl) + \cos(kl)[2S_i(kl) - S_i(2kl)] \\ & - \sin(kl)\left[2C_i(kl) - C_i(2kl) - C_i\left(\frac{2ka^2}{l}\right)\right]\Bigg\} \end{aligned} \tag{8-60b}$$

where $S_i(x)$ and $C_i(x)$ are the sine and cosine integrals of Appendix III. Equation (8-60a) is identical to (4-70). In deriving (8-60a) it was assumed that the radius of the wire is negligible (in this case set to zero), and it has little effect on the overall answer. This is a valid assumption provided $l \gg a$, and it has been confirmed by other methods.

The input resistance and input reactance (*referred to at the current at the input terminals*) can be obtained by a transfer relation given by (4-79), or

$$R_{in} = \left(\frac{I_0}{I_{in}}\right)^2 R_r = \frac{R_r}{\sin^2(kl/2)} \tag{8-61a}$$

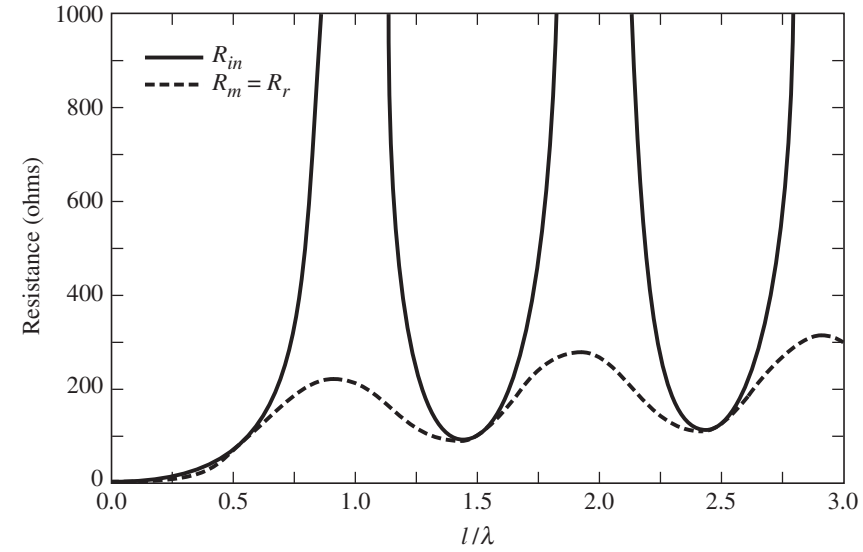
EX2042
Page 425 of 1072

$$X_{in} = \left(\frac{I_0}{I_{in}}\right)^2 X_m = \frac{X_m}{\sin^2(kl/2)} \tag{8-61b}$$

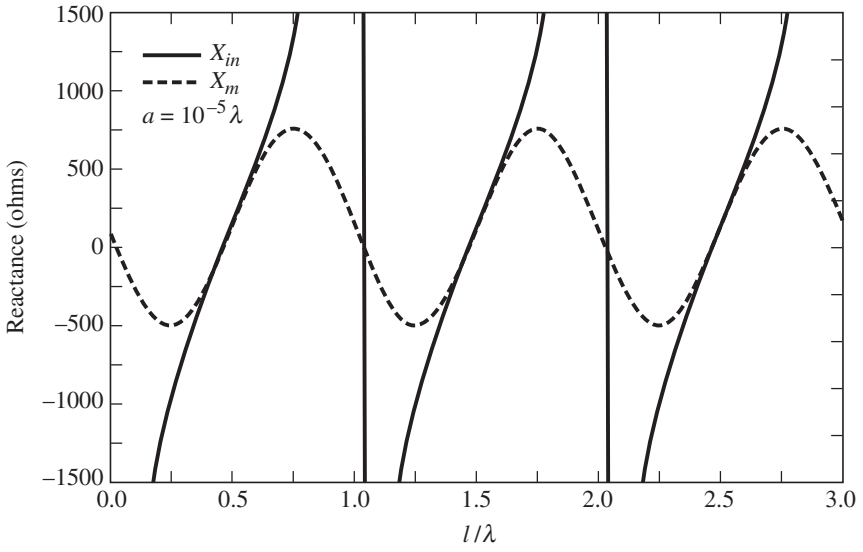
For a small dipole the input reactance is given by [34]

$$X_{in} = X_m = -120\frac{[\ln(l/2a) - 1]}{\tan(kl/2)} \tag{8-62}$$

while its input resistance and radiation resistance are given by (4-37). Plots of the self-impedance, both resistance and reactance, based on (8-60a), (8-60b) and (8-61a), (8-61b) for $0 \le l \le 3\lambda$ are shown in Figures 8.16(a,b). The radius of the wire is $10^{-5}\lambda$.



(a) Resistance



(b) Reactance

Figure 8.16 Self-resistance and self-reactance of dipole antenna with wire radius of 10^{-5} λ.

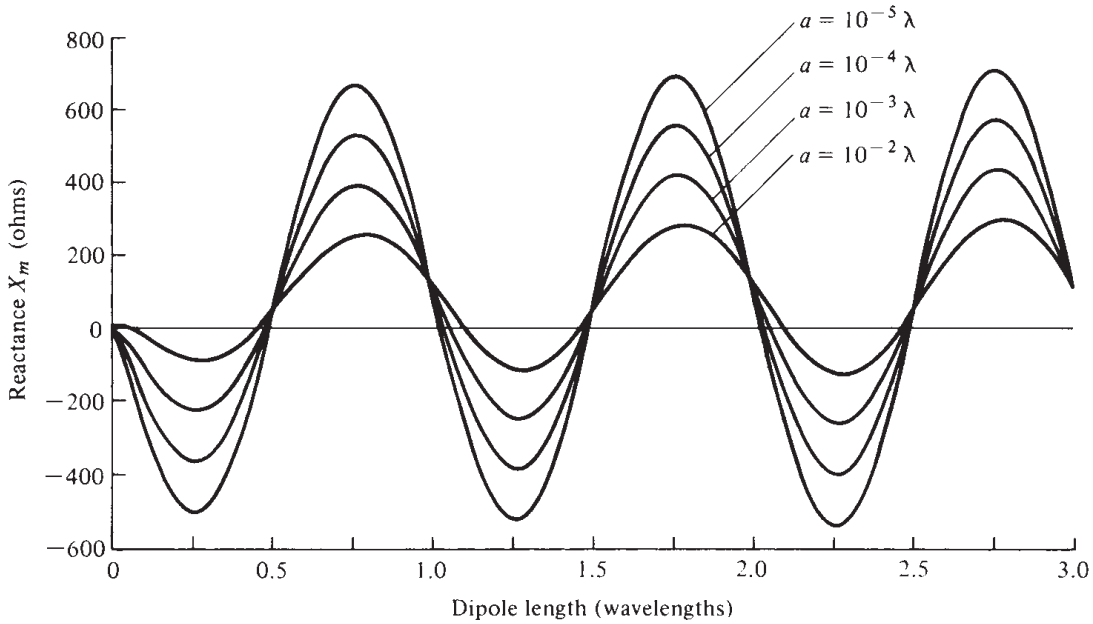


Figure 8.17 Reactance (referred to the current maximum) of linear dipole with sinusoidal current distribution for different wire radii.

It is evident that when the length of the wire is multiples of a wavelength the resistances and reactances become infinite; in practice they are large.

Ideally the radius of the wire does not affect the input resistance, as is indicated by (8-60a). However in practice it does have an effect, although it is not as significant as it is for the input reactance. To examine the effect the radius has on the values of the reactance, its values as given by (8-60b) have been plotted in Figure 8.17 for $a = 10^{-5}\lambda, 10^{-4}\lambda, 10^{-3}\lambda$, and $10^{-2}\lambda$. The overall length of the wire is taken to be $0 < l \leq 3\lambda$. It is apparent that the reactance can be reduced to zero provided the overall length is slightly less than $n\lambda/2, n = 1, 3, \ldots$, or slightly greater than $n\lambda/2, n = 2, 4, \ldots$. This is commonly done in practice for $l \simeq \lambda/2$ because the input resistance is close to 50 ohms, an almost ideal match for the widely used 50-ohm lines. For small radii, the reactance for $l = \lambda/2$ is equal to 42.5 ohms.

From (8-60b) it is also evident that when $l = n\lambda/2, n = 1, 2, 3, \ldots$, the terms within the last bracket do not contribute because $\sin(kl) = \sin(n\pi) = 0$. Thus for dipoles whose overall length is an integral number of half-wavelengths, the radius has no effect on the antenna reactance. This is illustrated in Figure 8.17 by the intersection points of the curves.

Example 8.5

Using the induced emf method, compute the input reactance for a linear dipole whose lengths are $n\lambda/2$, where $n = 1 - 6$.

Solution: The input reactance for a linear dipole based on the induced emf method is given by (8-60b) whose values are equal to 42.5 for $\lambda/2$, 125.4 for λ, 45.5 for $3\lambda/2$, 133.1 for 2λ, 46.2 for $5\lambda/2$, and 135.8 for 3λ.

8.6 MUTUAL IMPEDANCE BETWEEN LINEAR ELEMENTS

In the previous section, the input impedance of a linear dipole was derived when the element was radiating into an unbounded medium. The presence of an obstacle, which could be another element, would alter the current distribution, the field radiated, and in turn the input impedance of the antenna. Thus the antenna performance depends not only on its own current but also on the current of neighboring elements. For resonant elements with no current excitation of their own, there could be a substantial current induced by radiation from another source. These are known as parasitic elements, as in the case of a Yagi-Uda antenna (see Section 10.3.3), and play an important role in the overall performance of the entire antenna system. The antenna designer, therefore, must take into account the interaction and mutual effects between elements. The input impedance of the antenna in the presence of the other elements or obstacles, which will be referred to as *driving-point impedance*, depends upon the self-impedance (input impedance in the absence of any obstacle or other element) and the mutual impedance between the driven element and the other obstacles or elements.

To simplify the analysis, it is assumed that the antenna system consists of two elements. The system can be represented by a two-port (four-terminal) network, as shown in Figure 8.18, and by the voltage-current relations

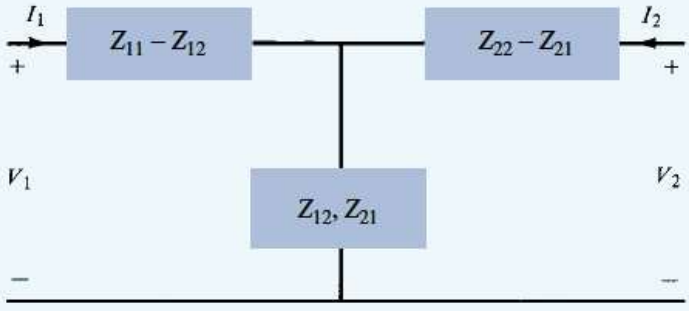
$$\left.\begin{aligned} V_1 &= Z_{11}I_1 + Z_{12}I_2 \\ V_2 &= Z_{21}I_1 + Z_{22}I_2 \end{aligned}\right\} \tag{8-63}$$

where

$$Z_{11} = \left.\frac{V_1}{I_1}\right|_{I_2=0} \tag{8-63a}$$



(a) Two-port network



(b) T-network equivalent

Figure 8.18 Two-port network and its T-equivalent.

is the input impedance at port #1 with port #2 open-circuited,

$$Z_{12} = \left.\frac{V_1}{I_2}\right|_{I_1=0} \tag{8-63b}$$

is the mutual impedance at port #1 due to a current at port #2 (with port #1 open-circuited),

$$Z_{21} = \left.\frac{V_2}{I_1}\right|_{I_2=0} \tag{8-63c}$$

is the mutual impedance at port #2 due to a current in port #1 (with port #2 open-circuited),

$$Z_{22} = \left.\frac{V_2}{I_2}\right|_{I_1=0} \tag{8-63d}$$

is the input impedance at port #2 with port #1 open-circuited. For a reciprocal network, $Z_{12} = Z_{21}$.

The impedances Z_{11} and Z_{22} are the input impedances of antennas 1 and 2, respectively, when each is radiating in an unbounded medium. The presence of another element modifies the input impedance and the extent and nature of the effects depends upon (1) the antenna type, (2) the relative placement of the elements, and (3) the type of feed used to excite the elements.

Equation (8-63) can also be written as

$$Z_{1d} = \frac{V_1}{I_1} = Z_{11} + Z_{12}\left(\frac{I_2}{I_1}\right) \tag{8-64a}$$

$$Z_{2d} = \frac{V_2}{I_2} = Z_{22} + Z_{21}\left(\frac{I_1}{I_2}\right) \tag{8-64b}$$

Z_{1d} and Z_{2d} represent the driving-point impedances of antennas 1 and 2, respectively. Each driving-point impedance depends upon the current ratio I_1/I_2, the mutual impedance, and the self-input impedance (when radiating into an unbounded medium). When attempting to match any antenna, it is the driving-point impedance that must be matched. It is, therefore, apparent that the mutual impedance plays an important role in the performance of an antenna and should be investigated. However, the analysis associated with it is usually quite complex and only simplified models can be examined with the induced emf method. Integral Equation-Moment Method techniques can be used for more complex geometries, including skewed arrangements of elements.

Referring to Figure 8.19, the induced open-circuit voltage in antenna 2, *referred to its current at the input terminals*, due to radiation from antenna 1 is given by

$$V_{21} = -\frac{1}{I_{2i}}\int_{-l_2/2}^{l_2/2} E_{z21}(z')I_2(z')\,dz' \tag{8-65}$$

where

$E_{z21}(z') = E$-field component radiated by antenna 1, which is parallel to antenna 2
$I_2(z') =$ current distribution along antenna 2

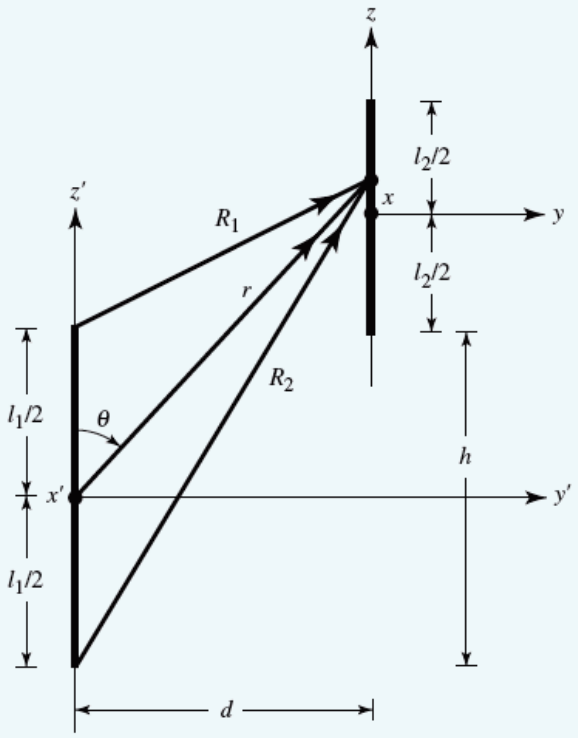


Figure 8.19 Dipole positioning for mutual coupling.

Therefore the mutual impedance of (8-63c), (referred to at the *input current* I_{1i} *of antenna 1*), is expressed as

$$Z_{21i} = \frac{V_{21}}{I_{1i}} = -\frac{1}{I_{1i}I_{2i}} \int_{-l_2/2}^{l_2/2} E_{z21}(z')I_2(z')\,dz' \tag{8-66}$$

8.6.1 Integral Equation-Moment Method

To use this method to find the mutual impedance based on (8-66), an integral equation must be formed to find E_{z21}, which is the field radiated by antenna 1 at any point on antenna 2. This integral equation must be a function of the unknown current on antenna 1, and it can be derived using a procedure similar to that used to form Pocklington's Integral Equation of (8-22) or (8-24), or Hallén's Integral Equation of (8-27). The unknown current of antenna 1 can be represented by a series of finite number of terms with N unknown coefficients and a set of known (chosen) basis functions. The current $I_2(z)$ must also be expanded into a finite series of N terms with N unknown coefficients and a set of N chosen basis functions. Once each of them is formulated, then they can be used interactively to reduce (8-66) into an $N \times N$ set of linearly independent equations to find the mutual impedance.

To accomplish this requires a lengthy formulation, computer programming, and usually a digital computer. The process usually requires numerical integrations or special functions for the evaluation of the impedance matrices of E_{z21} and the integral of (8-66). There are national computer codes, such as the Numerical Electromagnetics Code (NEC) and the simplified version Mini Numerical Electromagnetics Code (MININEC),

EX2042
Page 430 of 1072

for the evaluation of the radiation characteristics, including impedances, of wire antennas [35]–[37]. Both of these are based on an Integral Equation-Moment Method formulation. Information concerning these two codes follows. There are other codes; however, these two seem to be popular, especially for wire type antennas.

Another procedure that has been suggested to include mutual effects in arrays of linear elements is to use a convergent iterative algorithm [38], [39]. This method can be used in conjunction with a calculator [38], and it has been used to calculate impedances, patterns, and directivities of arrays of dipoles [39].

A. Numerical Electromagnetics Code (NEC)

The Numerical Electromagnetics Code (NEC) is a user-oriented program developed at Lawrence Livermore National Laboratory. It is a moment method code for analyzing the interaction of electromagnetic waves with arbitrary structures consisting of conducting wires and surfaces. It combines an integral equation for smooth surfaces with one for wires to provide convenient and accurate modeling for a wide range of applications. The code can model nonradiating networks and transmission lines, perfect and imperfect conductors, lumped element loading, and perfect and imperfect conducting ground planes. It uses the electric-field integral equation (EFIE) for thin wires and the magnetic field integral equation (MFIE) for surfaces. The excitation can be either an applied voltage source or an incident plane wave. The program computes induced currents and charges, near- and far-zone electric and magnetic fields, radar cross section, impedances or admittances, gain and directivity, power budget, and antenna-to-antenna coupling.

B. Mini-Numerical Electromagnetics Code (MININEC)

The Mini-Numerical Electromagnetics Code (MININEC) [36], [37] is a user-oriented compact version of the NEC developed at the Naval Ocean Systems Center (NOSC). It is also a moment method code, but coded in BASIC, and has retained the most frequently used options of the NEC. It is intended to be used in mini, micro, and personal computers, as well as work stations, and it is most convenient to analyze wire antennas. It computes currents, and near- and far-field patterns. It also optimizes the feed excitation voltages that yield desired radiation patterns.

Information concerning the NEC and MININEC, and their availability, can be directed to:

G. J. Burke, L-156
Lawrence Livermore National Laboratory
P.O. Box 5504
Livermore, CA 94550

8.6.2 Induced EMF Method

The induced emf method is also based on (8-66) except that $I_2(z')$ is assumed to be the ideal current distribution of (4-56) or (8-58) while $E_{z21}(z')$ is the electric field of (8-55b). Using (8-58) and (8-55b), we can express (8-66) as

$$Z_{21i} = \frac{V_{21}}{I_{1i}} = j\frac{\eta I_{1m} I_{2m}}{4\pi I_{1i} I_{2i}} \int_{-l_2/2}^{l_2/2} \sin\left[k\left(\frac{l_2}{2} - |z'|\right)\right] \left[\frac{e^{-jkR_1}}{R_1} + \frac{e^{-jkR_2}}{R_2} - 2\cos\left(k\frac{l_1}{2}\right)\frac{e^{-jkr}}{r}\right] dz' \tag{8-67}$$

where r, R_1, and R_2 are given, respectively, by (8-53a), (8-53b) and (8-53c) but with $y = d$ and $l = l_1$. I_{1m}, I_{2m} and I_{1i}, I_{2i} represent, respectively, the maximum and input currents for antennas 1 and 2. By referring each of the maximum currents to those at the input using (4-78) and assuming free-space, we can write (8-67) as

$$Z_{21i} = j\frac{30}{\sin\left(\frac{kl_1}{2}\right)\sin\left(\frac{kl_2}{2}\right)}\int_{-l_2/2}^{l_2/2}\sin\left[k\left(\frac{l_2}{2}-|z'|\right)\right]\left[\frac{e^{-jkR_1}}{R_1}+\frac{e^{-jkR_2}}{R_2}-2\cos\left(k\frac{l_1}{2}\right)\frac{e^{-jkr}}{r}\right]dz' \tag{8-68}$$

The mutual impedance referred to the current maxima is related to that at the input of (8-68) by

$$Z_{21m} = Z_{21i}\sin\left(\frac{kl_1}{2}\right)\sin\left(\frac{kl_2}{2}\right) \tag{8-69}$$

which for identical elements ($l_1 = l_2 = l$) reduces to

$$Z_{21m} = Z_{21i}\sin^2\left(\frac{kl}{2}\right) \tag{8-70}$$

whose real and imaginary parts are related by

$$R_{21m} = R_{21i}\sin^2\left(\frac{kl}{2}\right) \tag{8-70a}$$

$$X_{21m} = X_{21i}\sin^2\left(\frac{kl}{2}\right) \tag{8-70b}$$

For a two-element array of linear dipoles, there are three classic configurations for which closed-form solutions for (8-68), in terms of sine and cosine integrals, are obtained [33]. These are shown in Figure 8.20, and they are referred to as the *side-by-side* [Figure 8.20(a)], *collinear* [Figure 8.20(b)], and *parallel-in-echelon* [Figure 8.20(c)]. For two identical elements (each with *odd* multiples of $\lambda/2$, $l = n\lambda/2$, $n = 1, 3, 5, \ldots$) (8-70) reduces for each arrangement to the expressions that follow. Expressions for linear elements of any length are much more complex and can be found in [33].

A MATLAB and FORTRAN computer program referred to as ***Self And Mutual Impedances***, based on (8-71a)–(8-73i), is included in the CD attached to the book.

Side-by-Side Configuration [Figure 8.20(a)]

$$R_{21m} = \frac{\eta}{4\pi}[2C_i(u_0) - C_i(u_1) - C_i(u_2)] \tag{8-71a}$$

$$X_{21m} = -\frac{\eta}{4\pi}[2S_i(u_0) - S_i(u_1) - S_i(u_2)] \tag{8-71b}$$

$$u_0 = kd \tag{8-71c}$$

$$u_1 = k(\sqrt{d^2 + l^2} + l) \tag{8-71d}$$

$$u_2 = k(\sqrt{d^2 + l^2} - l) \tag{8-71e}$$

EX2042
Page 432 of 1072

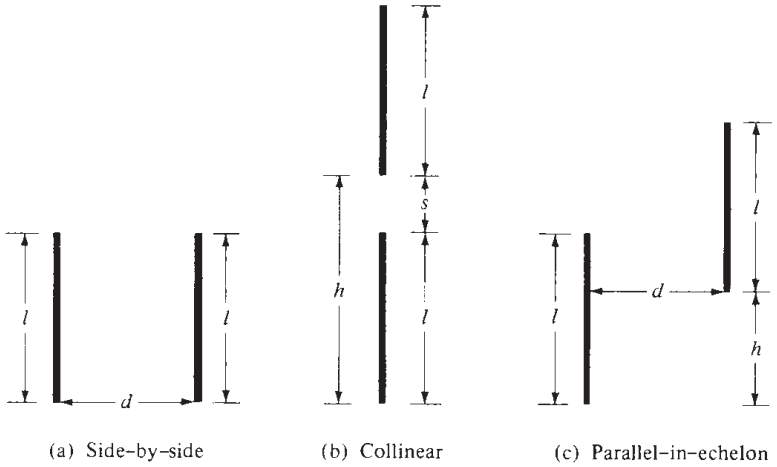


Figure 8.20 Dipole configuration of two identical elements for mutual impedance computations.

Collinear Configuration [Figure 8-20(b)]

$$R_{21m} = -\frac{\eta}{8\pi}\cos(v_0)[-2C_i(2v_0) + C_i(v_2) + C_i(v_1) - \ln(v_3)] + \frac{\eta}{8\pi}\sin(v_0)[2S_i(2v_0) - S_i(v_2) - S_i(v_1)] \tag{8-72a}$$

$$X_{21m} = -\frac{\eta}{8\pi}\cos(v_0)[2S_i(2v_0) - S_i(v_2) - S_i(v_1)] + \frac{\eta}{8\pi}\sin(v_0)[2C_i(2v_0) - C_i(v_2) - C_i(v_1) - \ln(v_3)] \tag{8-72b}$$

$$v_0 = kh \tag{8-72c}$$

$$v_1 = 2k(h + l) \tag{8-72d}$$

$$v_2 = 2k(h - l) \tag{8-72e}$$

$$v_3 = (h^2 - l^2)/h^2 \tag{8-72f}$$

Parallel-in-Echelon Configuration [Figure 8.20(c)]

$$\begin{aligned} R_{21m} = -\frac{\eta}{8\pi}\cos(w_0)[&-2C_i(w_1) - 2C_i(w_1') + C_i(w_2) \\ &+ C_i(w_2') + C_i(w_3) + C_i(w_3')] \\ &+ \frac{\eta}{8\pi}\sin(w_0)[2S_i(w_1) - 2S_i(w_1') - S_i(w_2) \\ &+ S_i(w_2') - S_i(w_3) + S_i(w_3')] \end{aligned} \tag{8-73a}$$

$$\begin{aligned} X_{21m} = -\frac{\eta}{8\pi}\cos(w_0)[&2S_i(w_1) + 2S_i(w_1') - S_i(w_2) \\ &- S_i(w_2') - S_i(w_3) - S_i(w_3')] \\ &+ \frac{\eta}{8\pi}\sin(w_0)[2C_i(w_1) - 2C_i(w_1') - C_i(w_2) + C_i(w_2') \\ &- C_i(w_3) + C_i(w_3')] \end{aligned} \tag{8-73b}$$

$$w_0 = kh \tag{8-73c}$$

$$w_1 = k(\sqrt{d^2 + h^2} + h) \tag{8-73d}$$

$$w_1' = k(\sqrt{d^2 + h^2} - h) \tag{8-73e}$$

$$w_2 = k[\sqrt{d^2 + (h-l)^2} + (h-l)] \tag{8-73f}$$

$$w_2' = k[\sqrt{d^2 + (h-l)^2} - (h-l)] \tag{8-73g}$$

$$w_3 = k[\sqrt{d^2 + (h+l)^2} + (h+l)] \tag{8-73h}$$

$$w_3' = k[\sqrt{d^2 + (h+l)^2} - (h+l)] \tag{8-73i}$$

The mutual impedance, referred to the current maximum, based on the induced emf method of a side-by-side and a collinear arrangement of two half-wavelength dipoles is shown plotted in Figure 8.21. It is apparent that the side-by-side arrangement exhibits larger mutual effects since the antennas are placed in the direction of maximum radiation. The data is compared with those based on the Moment Method/NEC [35] using a wire with a radius of $10^{-5}\lambda$. A very good agreement is indicated between the two sets because a wire with a radius of $10^{-5}\lambda$ for the MM/NEC is considered very thin. Variations as a function of the radius of the wire for both the side-by-side and collinear arrangements using the MM/NEC are shown, respectively, in Figures 8.22(a,b). Similar sets of data were computed for the parallel-in-echelon arrangement of Figure 8.20(c), and they are shown, respectively, in Figures 8.23(a) and 8.23(b) for $d = \lambda/2$, $0 \le h \le \lambda$ and $h = \lambda/2$, $0 < d < \lambda$ for wire radii of $10^{-5}\lambda$. Again a very good agreement between the induced emf and Moment Method/NEC data is indicated.

Example 8.6

Two identical linear half-wavelength dipoles are placed in a side-by-side arrangement, as shown in Figure 8.20(a). Assuming that the separation between the elements is $d = 0.35\lambda$, find the driving-point impedance of each.

Solution: Using (8-64a)

$$Z_{1d} = \frac{V_1}{I_1} = Z_{11} + Z_{12}\left(\frac{I_2}{I_1}\right)$$

Since the dipoles are identical, $I_1 = I_2$. Thus

$$Z_{1d} = Z_{11} + Z_{12}$$

From Figure 8.21(a)

$$Z_{12} \simeq 25 - j38$$

Since

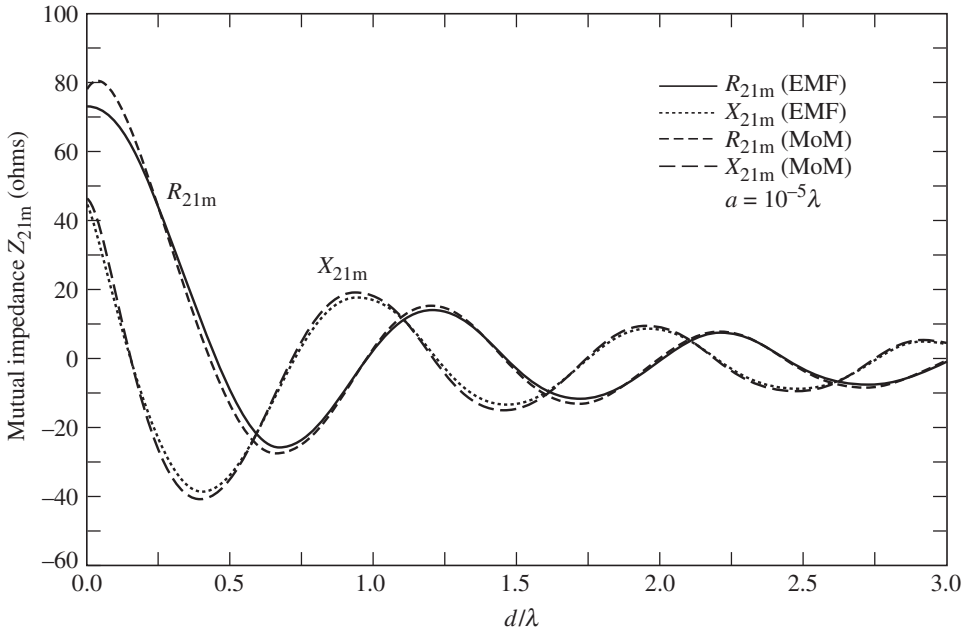
$$Z_{11} = 73 + j42.5$$

EX2042
Page 434 of 1072

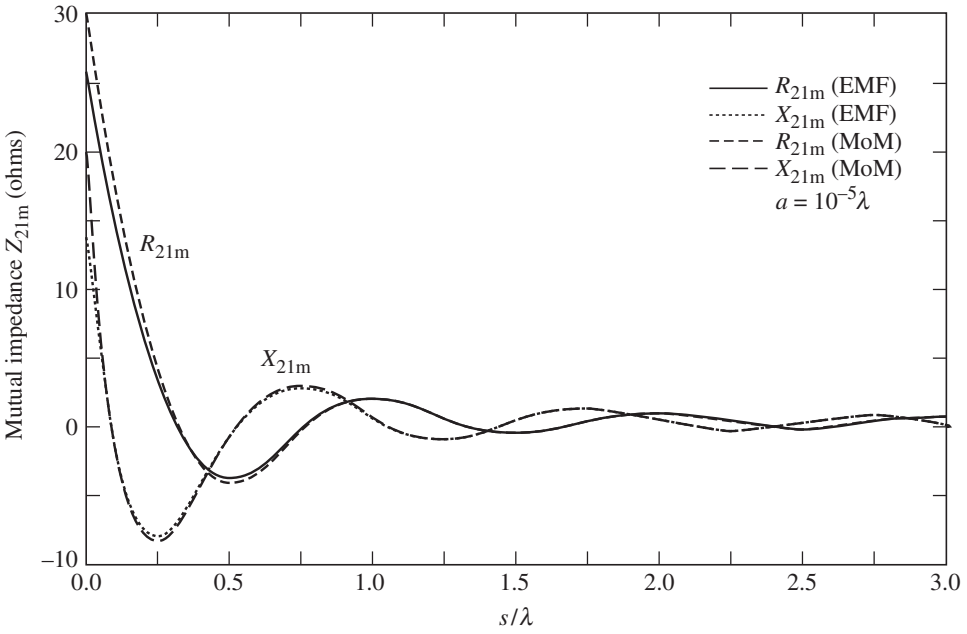
Z_{1d} reduces to

$$Z_{1d} \simeq 98 + j4.5$$

which is also equal to Z_{2d} of (8-64b).

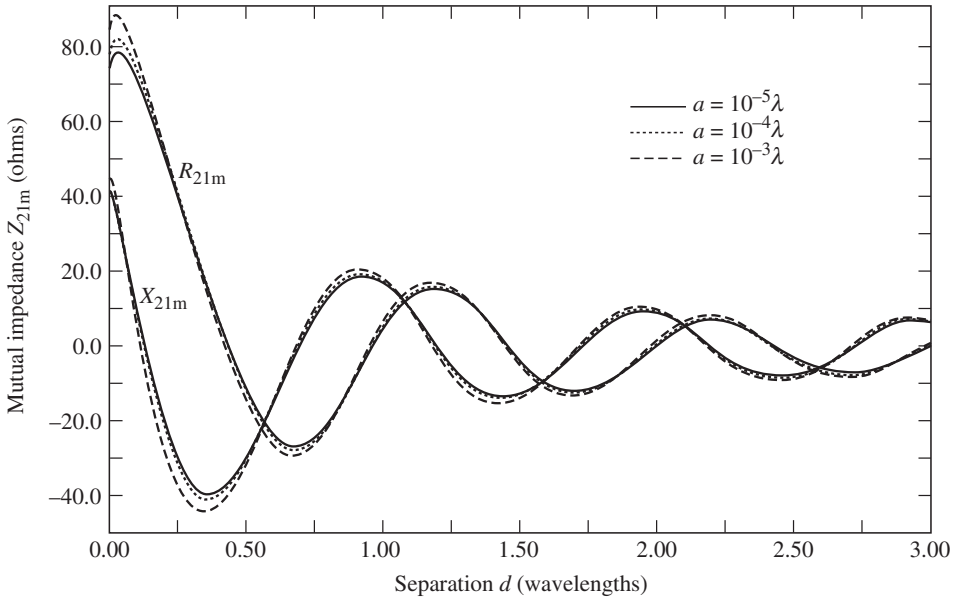


(a) Side-by-side

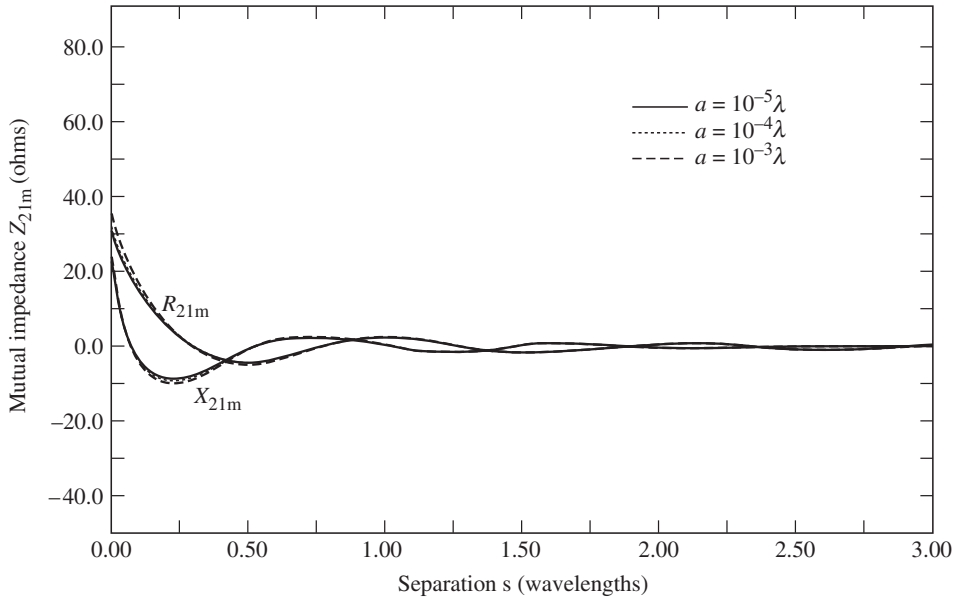


(b) Collinear

Figure 8.21 Mutual impedance of two side-by-side and collinear $\lambda/2$ dipoles using the moment method and induced emf method.



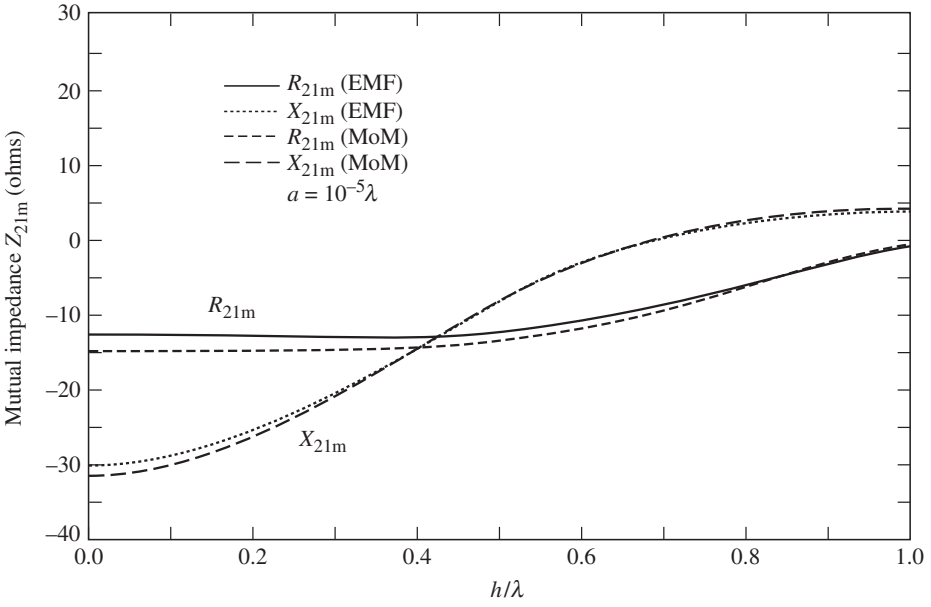
(a) Side-by-side



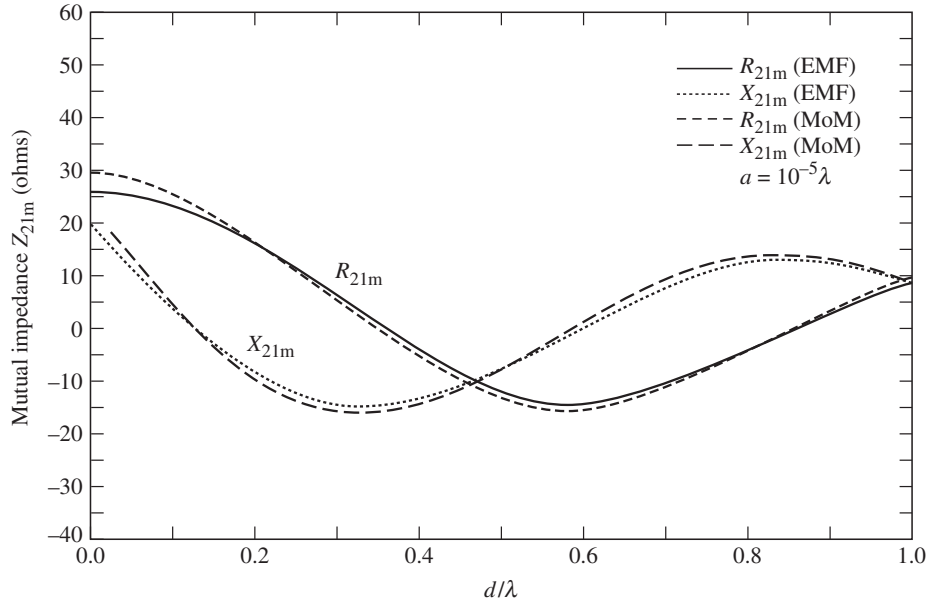
(b) Collinear

Figure 8.22 Variations of mutual impedance as a function of wire radius for side-by-side and collinear $\lambda/2$ dipole arrangements.

As discussed in Chapter 2, Section 2.13, maximum power transfer between the generator and the transmitting antenna occurs when their impedances are conjugate-matched. The same is necessary for the receiver and receiving antenna. This ensures maximum power transfer between the transmitter and receiver, when there is no interaction between the antennas. In practice, the input impedance of one antenna depends on the load connected to the other antenna. Under those conditions, the matched loads and maximum coupling can be computed using the Linville method [40], which is used in rf amplifier design. This technique has been incorporated into the NEC [35]. Using



(a) $d = 0.5\lambda$



(b) $h = 0.5\lambda$

Figure 8.23 Mutual impedance for two parallel-in-echelon $\lambda/2$ dipoles with wire radii of 10^{-5} λ.

this method, maximum coupling is computed using [35]

$$C_{\max} = \frac{1}{L}[1 - (1 - L^2)^{1/2}] \tag{8-74}$$

where

$$L = \frac{|Y_{12}Y_{21}|}{2\mathrm{Re}(Y_{11})\mathrm{Re}(Y_{22}) - \mathrm{Re}(Y_{12}Y_{21})} \tag{8-74a}$$

EX2042
Page 437 of 1072

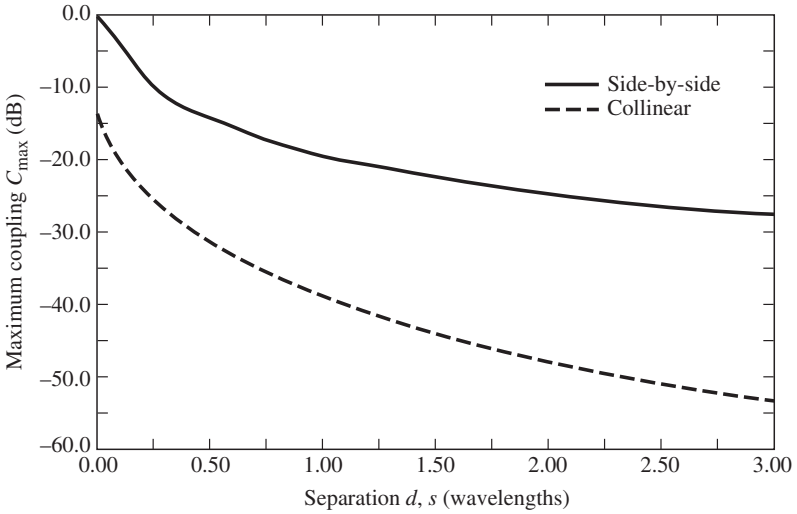


Figure 8.24 Maximum coupling for the two $\lambda/2$ dipoles in side-by-side and collinear arrangements as a function of separation.

To ensure maximum coupling, the admittance of the matched load on the receiving antenna should be [35]

$$Y_L = \left[\frac{1-\rho}{1+\rho} + 1\right] \mathrm{Re}(Y_{22}) - Y_{22} \tag{8-75}$$

where

$$\rho = \frac{G_{\mathrm{MAX}}(Y_{12}Y_{21})^*}{|Y_{12}Y_{21}|} \tag{8-75a}$$

The corresponding input admittance of the transmitting antenna is

$$Y_{in} = Y_{11} - \frac{Y_{21}Y_{12}}{Y_L + Y_{22}} \tag{8-76}$$

Based on (8-74)–(8-76), maximum coupling for two half-wavelength dipoles in side-by-side and collinear arrangements as a function of the element separation (d for side-by-side and s for collinear) was computed using the NEC, and it is shown in Figure 8.24. As expected, the side-by-side arrangement exhibits much stronger coupling, since the elements are placed along the direction of their respective maximum radiation. Similar curves can be computed for the parallel-in-echelon arrangement.

8.7 MUTUAL COUPLING IN ARRAYS

When two antennas are near each other, whether one and/or both are transmitting or receiving, some of the energy that is primarily intended for one ends up at the other. The amount depends primarily on the

a. radiation characteristics of each
b. relative separation between them
c. relative orientation of each

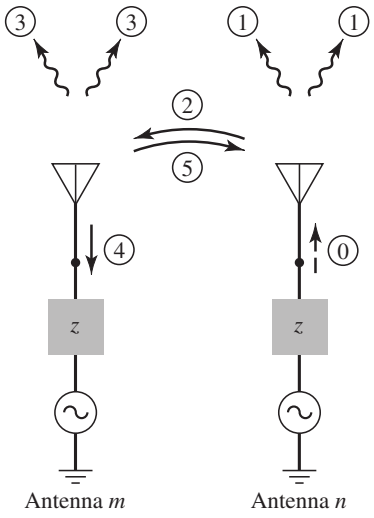
There are many different mechanisms that can cause this interchange of energy. For example, even if both antennas are transmitting, some of the energy radiated from each will be received by the other because of the nonideal directional characteristics of practical antennas. Part of the incident energy on one or both antennas may be rescattered in different directions allowing them to behave as secondary transmitters. This interchange of energy is known as "mutual coupling," and in many cases it complicates the analysis and design of an antenna. Furthermore, for most practical configurations, mutual coupling is difficult to predict analytically but must be taken into account because of its significant contribution. Because the mutual effects of any antenna configuration cannot be generalized, in this section we want first to briefly introduce them in a qualitative manner and then examine their general influence on the behavior of the radiation characteristics of the antenna. Most of the material and presentation in this section is followed from a well-written document on this subject [41].

8.7.1 Coupling in the Transmitting Mode

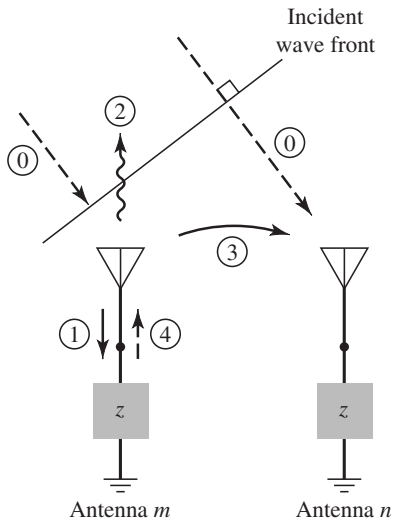
To simplify the discussion, let us assume that two antennas m and n of an array are positioned relative to each other as shown in Figure 8.25(a). The procedure can be extended to a number of elements. If a source is attached to antenna n, the generated energy traveling toward the antenna labeled as (0) will be radiated into space (1) and toward the mth antenna (2). The energy incident on the mth antenna sets up currents which have a tendency to rescatter some of the energy (3) and allow the remaining to travel toward the generator of m (4). Some of the rescattered energy (3) may be redirected back toward antenna n (5). This process can continue indefinitely. The same process would take place if antenna m is excited and antenna n is the parasitic element. If both antennas, m and n, are excited simultaneously, the radiated and rescattered fields by and from each must be added vectorially to arrive at the total field at any observation point. Thus, "*the total contribution to the far-field pattern of a particular element in the array depends not only upon the excitation furnished by its own generator (the direct excitation) but upon the total parasitic excitation as well, which depends upon the couplings from and the excitation of the other generators* [41]."

The wave directed from the n to the m antenna and finally toward its generator (4) adds vectorially to the incident and reflected waves of the m antenna itself, thus enhancing the existing standing wave pattern within m. For coherent excitations, the coupled wave (4) due to source n differs from the reflected one in m only in phase and amplitude. The manner in which these two waves interact depends on the coupling between them and the excitation of each. It is evident then that the vector sum of these two waves will influence the input impedance looking in at the terminals of antenna m and will be a function of the position and excitation of antenna n. This coupling effect is commonly modeled as a change in the apparent driving impedance of the elements and it is usually referred to as *mutual impedance variation*.

To demonstrate the usefulness of the driving impedance variation, let us assume that a set of elements in an array are excited. For a given element in the array, the generator impedance that is optimum in the sense of maximizing the radiated power for that element is that which would be a conjugate impedance match at the element terminals. This is accomplished by setting a reflected wave which is equal in amplitude and phase to the backwards traveling waves induced due to the coupling. Even though this is not the generator impedance which is a match to a given element when all other elements are not excited, it does achieve maximum power transfer.



(a) Transmitting



(b) Receiving

Figure 8.25 Transmitting and receiving mode coupling paths between antennas m and n. (Reprinted with permission of MIT Lincoln Laboratory, Lexington, MA.)

To minimize confusion, let us adopt the following terminology [41]:

1. *Antenna impedance*: The impedance looking into a single isolated element.
2. *Passive driving impedance*: The impedance looking into a single element of an array with all other elements of the array passively terminated in their normal generator impedance unless otherwise specified.
3. *Active driving impedance*: The impedance looking into a single element of an array with all other elements of the array excited.

Since the passive driving impedance is of minor practical importance and differs only slightly from the antenna impedance, the term *driving impedance* will be used to indicate *active* driving impedance, unless otherwise specified.

EX2042
Page 440 of 1072

Since the driving impedance for a given element is a function of the placement and excitation of the other elements, then *optimum generator impedance that maximizes array radiation efficiency (gain) varies with array excitation*. These changes, with element excitation variations, constitute one of the principal aggravations in electronic scanning arrays.

8.7.2 Coupling in the Receiving Mode

To illustrate the coupling mechanism in the receiving mode, let us again assume that the antenna system consists of two passively loaded elements of a large number, as shown in Figure 8.25(b). Assume that a plane wave (0) is incident, and it strikes antenna *m* first where it causes current flow. Part of the incident wave will be rescattered into space as (2), the other will be directed toward antenna *n* as (3) where it will add vectorially with the incident wave (0), and part will travel into its feed as (1). It is then evident that the amount of energy received by each element of an antenna array is the vector sum of the direct waves and those that are coupled to it parasitically from the other elements.

The amount of energy that is absorbed and reradiated by each element depends on its match to its terminating impedance. Thus, the amount of energy received by any element depends upon its terminating impedance as well as that of the other elements. In order to maximize the amount of energy extracted from an incident wave, we like to minimize the total backscattered (2) energy into space by properly choosing the terminating impedance. This actually can be accomplished by mismatching the receiver itself relative to the antenna so that the reflected wave back to the antenna (4) is cancelled by the rescattered wave, had the receiver been matched to the actual impedance of each antenna.

As a result of the previous discussion, it is evident that mutual coupling plays an important role in the performance of an antenna. However, the analysis and understanding of it may not be that simple.

8.7.3 Mutual Coupling on Array Performance

The effects of the mutual coupling on the performance of an array depends upon the

a. antenna type and its design parameters
b. relative positioning of the elements in the array
c. feed of the array elements
d. scan volume of the array

These design parameters influence the performance of the antenna array by varying its element impedance, reflection coefficients, and overall antenna pattern. In a finite-element array, the multipath routes the energy follows because of mutual coupling will alter the pattern in the absence of these interactions. However, for a very large regular array (array with elements placed at regular intervals on a grid and of sufficient numbers so that edge effects can be ignored), the relative shape of the pattern will be the same with and without coupling interactions. It will only require a scaling up or down in amplitude while preserving the shape. This, however, is not true for irregular placed elements or for small regular arrays where edge effects become dominant.

8.7.4 Coupling in an Infinite Regular Array

The analysis and understanding of coupling can be considerably simplified by considering an infinite regular array. Although such an array is not physically realizable, it does provide an insight and in many cases answers of practical importance. For the infinite regular array we assume that

a. all the elements are placed at regular intervals
b. all the elements are identical
c. all the elements have uniform (equal) amplitude excitation
d. there can be a linear relative phasing between the elements in the two orthogonal directions

The geometry of such an array is shown in Figure 6.28 with its array factor given by (6-87) or (6-88). This simplified model will be used to analyze the coupling and describes fairly accurately the behavior of most elements in arrays of modest to large size placed on flat or slowly curve surfaces with smoothly varying amplitude and phase taper.

To assess the behavior of the element driving impedance as a function of scan angle, we can write the terminal voltage of any one element in terms of the currents flowing in the others, assuming a single-mode operation, as

$$V_{mn} = \sum_{p} \sum_{q} Z_{mn,pq} I_{pq} \tag{8-77}$$

where $Z_{mn,pq}$ defines the terminal voltage at antenna mn due to a unity current in element pq when the current in all the other elements is zero. Thus the $Z_{mn,pq}$ terms represent the *mutual impedances* when the indices mn and pq are not identical. The *driving impedance* of the mnth element is defined as

$$Z_{Dmn} = \frac{V_{mn}}{I_{mn}} = \sum_{p} \sum_{q} Z_{mn,pq} \frac{I_{pq}}{I_{mn}} \tag{8-78}$$

Since we assumed that the amplitude excitation of the elements of the array was uniform and the phase linear, we can write that

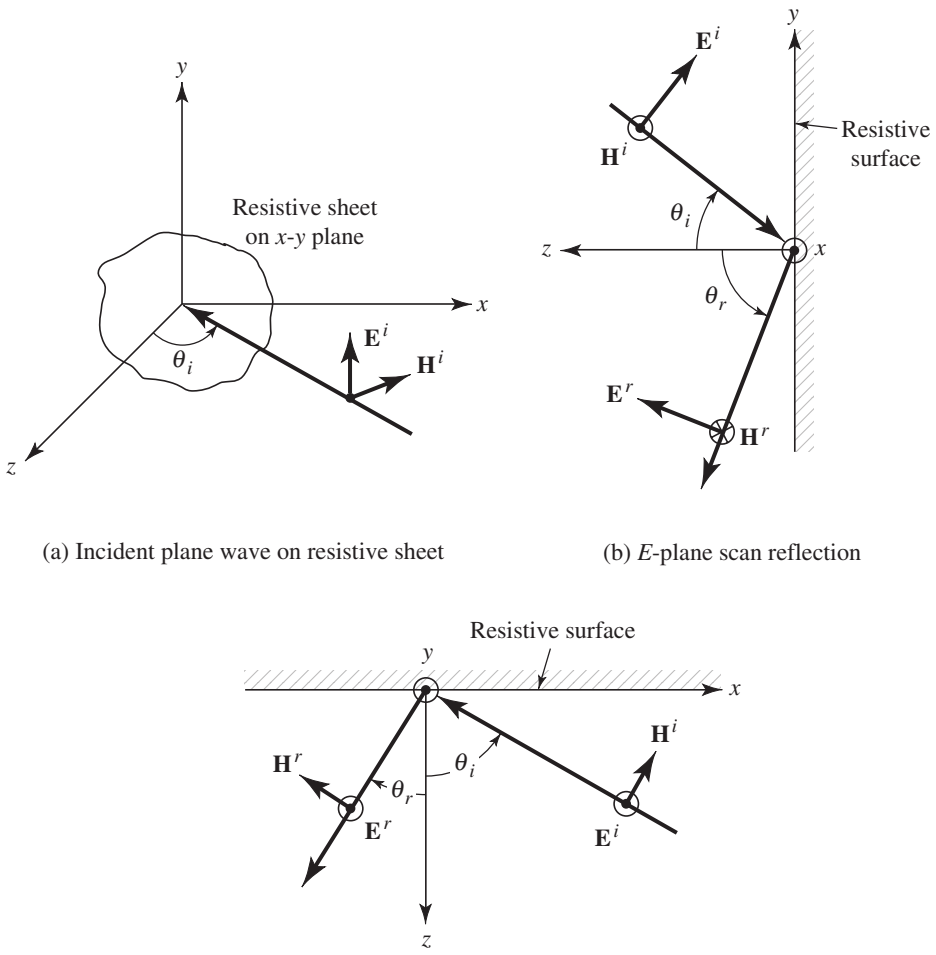
$$I_{pq} = I_{00} e^{j(p\beta_x + q\beta_y)} \tag{8-79a}$$

$$I_{mn} = I_{00} e^{j(m\beta_x + n\beta_y)} \tag{8-79b}$$

Thus, (8-78) reduces to

$$Z_{Dmn} = \sum_{p} \sum_{q} Z_{mn,pq} e^{j(p-m)\beta_x} e^{j(q-n)\beta_y} \tag{8-80}$$

It is evident that the driving-point impedance of mn element is equal to the vector sum of the element self impedance ($mn = pq$) and the phased mutual impedances between it and the other elements ($mn \neq pq$). The element self-impedance ($mn = pq$) is obtained when all other elements are open-circuited so that the current at their feed points is zero



(a) Incident plane wave on resistive sheet

(b) *E*-plane scan reflection

(c) *H*-plane scan reflection

Figure 8.26 Geometry for plane wave reflection from resistive sheet. (Reprinted with permission of MIT Lincoln Laboratory, Lexington, MA.)

$[I_{pq}(pq \neq mn) = 0]$. For most practical antennas, physically this is almost equivalent to removing the pq elements and finding the impedance of a single isolated element.

A consequence of the mutual coupling problem is the change of the array impedance with scan angle. In order not to obscure the basic principle with the complexity of the problem, this can best be illustrated by examining the behavior of the reflection coefficient of a uniform plane wave in free-space incident on a resistive sheet of infinite extent backed by an open circuit so that there are no transmitted fields through the sheet, as shown in Figure 8.26(a). Although the open circuit is not physically realizable, nevertheless the model is useful. This is accomplished by choosing the surface resistivity of the sheet to be that of free-space ($\eta_0 = 120\pi$) so that the sheet is an exact match for a normally incident wave. Referring to Figure 8.26(b) for an E-plane scan and Figure 8.26(c) for an H-plane scan, we impose that at the boundary ($z = 0$ for all x and y) the ratio of the total tangential electric field to the total tangential magnetic field is equal to the surface impedance of the sheet. The same procedure is used in electromagnetics to derive the Fresnel reflection and transmission coefficients from planar interfaces for vertical and horizontal polarizations [14].

EX2042
Page 443 of 1072

Referring to Figure 8.26(b), we can write that the incident and reflected waves for the **E**- and **H**-fields as

$$\mathbf{E}^i = E_0^i(\hat{\mathbf{a}}_y \cos\theta_i - \hat{\mathbf{a}}_z \sin\theta_i)e^{+jk_0(y\sin\theta_i + z\cos\theta_i)} \tag{8-81a}$$

$$\mathbf{H}^i = \hat{\mathbf{a}}_x H_0^i e^{+jk_0(y\sin\theta_i + z\cos\theta_i)} \tag{8-81b}$$

$$\mathbf{E}^r = E_0^r(\hat{\mathbf{a}}_y \cos\theta_r + \hat{\mathbf{a}}_z \sin\theta_r)e^{-jk_0(-y\sin\theta_r + z\cos\theta_r)} \tag{8-81c}$$

$$\mathbf{H}^r = -\hat{\mathbf{a}}_x H_0^r e^{-jk_0(-y\sin\theta_r + z\cos\theta_r)} \tag{8-81d}$$

Applying boundary conditions on the tangential components of the electric and magnetic field of (8-81a)–(8-81d) gives

$$\eta_0 = \frac{E_{\tan}}{H_{\tan}} = \frac{E_0^i \cos\theta_i e^{jk_0 y\sin\theta_i} + E_0^r \cos\theta_r e^{jk_0 y\sin\theta_r}}{H_0^i e^{jk_0 y\sin\theta_i} - H_0^r e^{jk_0 y\sin\theta_r}} \tag{8-82}$$

Since

$$H_0^i = \frac{E_0^i}{\eta_0} \tag{8-82a}$$

$$H_0^r = \frac{E_0^r}{\eta_0} \tag{8-82b}$$

we can write (8-82) as

$$E_0^i(\cos\theta_i - 1)e^{jk_0 y\sin\theta_i} = -E_0^r(\cos\theta_r + 1)e^{jk_0 y\sin\theta_r} \tag{8-83}$$

whose only solution independent of y occurs when $\theta_r = \theta_i$. Thus,

$$\Gamma_e = \frac{E_0^r}{E_0^i} = \frac{1-\cos\theta_i}{1+\cos\theta_i} = \tan^2\left(\frac{\theta_i}{2}\right) \tag{8-84}$$

which can also be written as

$$\Gamma_e = \frac{E_0^r}{E_0^i} = \frac{1-\cos\theta_i}{1+\cos\theta_i} = \frac{\frac{1}{\cos\theta_i} - 1}{\frac{1}{\cos\theta_i} + 1} = \frac{Z_e - 1}{Z_e + 1} \tag{8-85}$$

By comparison with the reflection coefficient Γ of a transmission line with a normalized load $\overline{Z}_L$

$$\Gamma = \frac{\overline{Z}_L - 1}{\overline{Z}_L + 1} \tag{8-86}$$

the sheet represents an impedance to the wave that varies as

$$Z_e = \frac{1}{\cos\theta_i} \tag{8-87}$$

This is usually referred to as a *normalized directional impedance* [14].

Referring to Figure 8.26(c), it can be shown that for the H-plane scan the reflection coefficient is

$$\Gamma_h = -\frac{1-\cos\theta_i}{1+\cos\theta_i} = -\tan^2\left(\frac{\theta_i}{2}\right) \tag{8-88}$$

and the sheet represents to the wave a directional impedance that varies as

$$Z_h = \cos\theta_i \tag{8-89}$$

It is clear that even for such a simple problem of a plane wave impinging on a resistive sheet, there is a change, as a function of the scan angle, of the apparent impedance that the resistive sheet represents to the wave.

To illustrate the practical importance of the resistive sheet problem, the computed reflection coefficient magnitude for the E- and H-plane scans for arrays of half-wavelength dipoles for various spacings $d(d = d_x = d_y)$ and height h above a ground plane are shown in Figures 8.27 (a,b) [41]. The height h was chosen to minimize the mismatch in the principal planes of scan. The curves are discontinued at the angles where major lobes are equally disposed about broadside and retrace themselves beyond that point. The angles of discontinuity become smaller for wider spacings. It is also evident that the reflection coefficient for a given scan angle in the principal plane becomes smaller as the elements are brought closer together. In the same figures and indicated by small x's is the reflection coefficient of the central element of a large

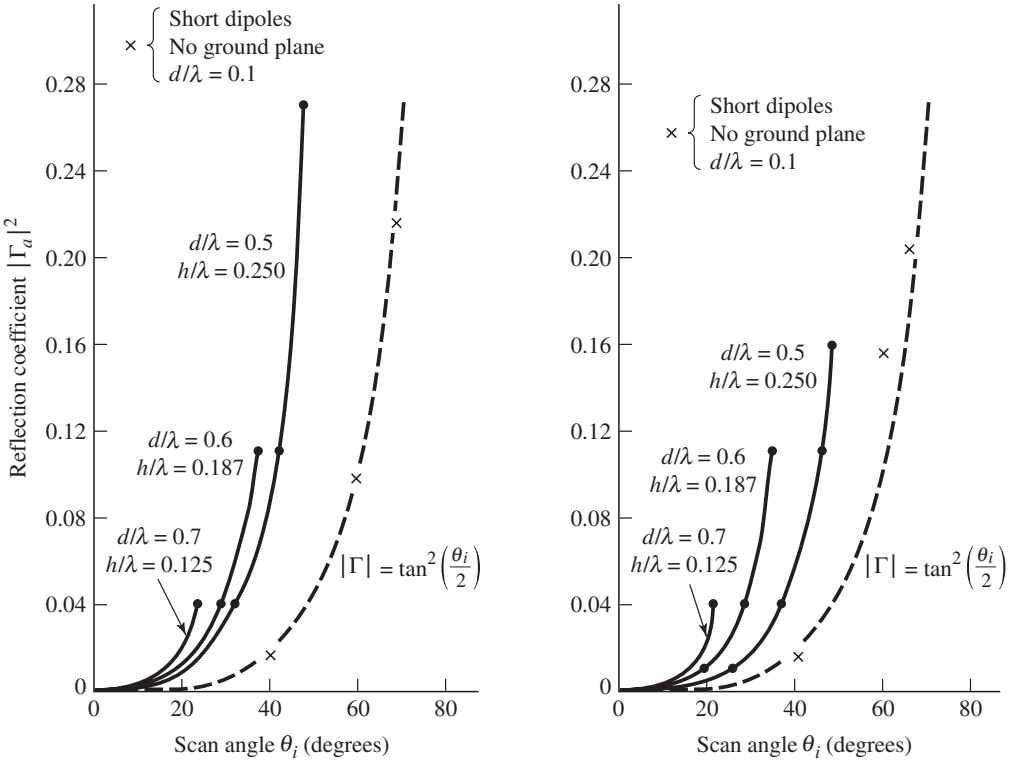


Figure 8.27 Magnitude of reflection coefficient as a function of principal-plane scan angle. (Reprinted with permission of MIT Lincoln Laboratory, Lexington, MA.)

array of short dipoles with a spacing of $d_x = d_y = 0.1\lambda$ but without a ground plane. The resistive sheet reflection coefficient is also plotted for comparison purposes. It should be noted that the results of Figure 8.27 were computed assuming the generator impedance is matched to the element driving impedance when the array's major lobe was toward broadside. This requires the tuning of the driving reactance for broadside conditions, which for small spacings is exceedingly large.

8.7.5 Grating Lobes Considerations

Because of the periodic nature of an infinite array, the impedance behavior as a function of scan volume for different elements and interelement spacing can be described in the form of an infinite series. This is accomplished by expressing the radiated and stored (real and reactive) powers in the vicinity of the array in terms of the current, field distribution, or pattern, of a typical element. The analysis, which was pioneered by Wheeler [42]; Edelberg and Oliner [43], [44]; and Stark [45] is straightforward, but it will not be included here because it requires a knowledge of Fourier transforms, and it is beyond the scope of the book at this point. However, some qualitative results will be briefly discussed.

It was shown in Section 6.10.1 that *grating lobes* in an array can be formed provided (6-89a) and (6-89b) are satisfied. This was illustrated by the three-dimensional pattern of Figure 6.34. It was indicated there that additional grating lobes can be formed by increasing the interelement spacing. The grating lobes disappear as the spacing recedes toward zero. In general, grating lobes can be moved into and out of the visible region by controlling the spacing and/or relative phase between the elements.

The dependence of the element driving impedance $Z_D(\beta_x, \beta_y)$ on the pointing direction (scan) of the main beam of the array is demonstrated by examining it for different elements, spacings, and the presence of a ground plane. The discussion is restricted to planar arrays and the impedance variations are illustrated for the E-, H-, and D-planes. We define D- as the diagonal plane (45° from the E- and H-planes) and θ_e, θ_h, and θ_d as the angles of the main beam from broadside for the E-, H- and D-planes, respectively.

If the elements are polarized in the y-direction, then according to (6-90a) and (6-90b) the progressive phase shifts between the elements must be

$$\begin{aligned} \beta_x &= 0 \\ \beta_y &= -kd_y \sin\theta_e \end{aligned} \qquad E\text{-plane scan } (\phi_0 = 90^\circ, \theta_0 = \theta_e) \tag{8-90}$$

$$\begin{aligned} \beta_x &= -kd_x \sin\theta_h \\ \beta_y &= 0 \end{aligned} \qquad H\text{-plane scan } (\phi_0 = 0^\circ, \theta_0 = \theta_h) \tag{8-91}$$

$$\left(\frac{\beta_x}{d_x}\right)^2 + \left(\frac{\beta_y}{d_y}\right)^2 = k \sin\theta_d \qquad D\text{-plane scan } (\phi_0 = 45^\circ, \theta_0 = \theta_d) \tag{8-92}$$

To make the presentation of the results more uniform, the element driving impedance $Z_D(\theta)$ is displayed on a Smith chart in a normalized form

$$Z_D(\theta)_{\text{norm}} = \frac{Z_D(\theta) - jX_D(0)}{R_D(0)} \tag{8-93}$$

where

$$Z_D(\theta) = R_D(\theta) + jX_D(\theta) \tag{8-93a}$$

$$\left.\begin{aligned} R_D(0) &= R_D(\theta = 0^\circ) \\ X_D(0) &= X_D(\theta = 0^\circ) \end{aligned}\right\} \quad \text{beam pointed at broadside} \tag{8-93b}$$

In Figure 8.28, we display the normalized driving impedance in the E-, H- and D-planes for a planar array of half-wavelength dipoles ($l = 0.5\lambda$) spaced $d_x = d_y = 0.55\lambda$ [41]. The E- and H-planes are discontinued at 65°. Physically that angle corresponds to a grating lobe at −65°, symmetrically disposed relative to the main beam. Scanning beyond that point is equivalent to moving the main beam in from 65° or retracing the curve.

For a VSWR of 3:1, the half-wavelength dipole array of Figure 8.28 can be scanned up to 45° in the H-plane, 79° in the D-plane, and anywhere in the E-plane; for a VSWR of 2:1, then the maximum scan angles are 50° in the E-plane, 40° in the H-plane, and 77° in the D-plane. For a small dipole ($l = 0.1\lambda$) the maximum scans are 47° in the H-plane, 79° in the D-plane, and anywhere for the E-plane for a 3:1 VSWR; maximum scans of 40° in the H-plane, 76° in the D-plane, and anywhere in the E-plane for a 2:1 VSWR. The results are summarized in Table 8.3 [41].

To demonstrate the effects of a ground plane on the element driving impedance, the normalized impedance of the half-wavelength ($l = 0.5\lambda$) dipole arrays, when placed

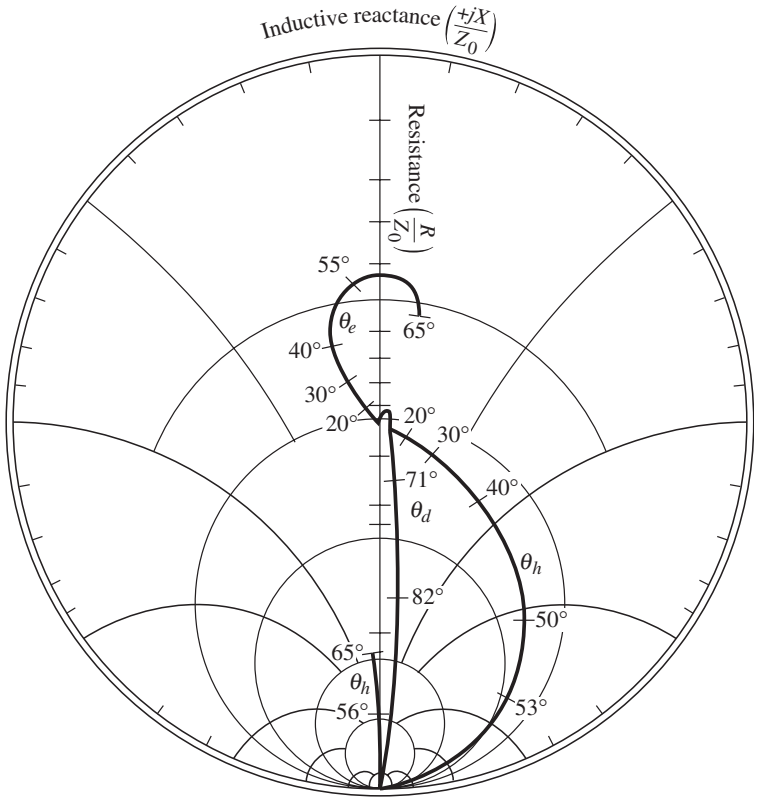


Figure 8.28 Normalized element impedance versus scan angle on the E-, H-, and D-planes for a planar array of half-wavelength dipoles ($\ell = 0.5\lambda$) with $d_x = d_y = 0.55\lambda$ and with no ground plane. (Reprinted with permission of MIT Lincoln Laboratory, Lexington, MA.)

TABLE 8.3 Maximum Scan Volume of Short and Half-Wavelength Dipole Planar Array with $d_x = d_y = 0.55\lambda$ and without Ground Plane for VSWRs of 3:1 and 2:1

		Maximum Scan Angle	
VSWR	Scan Plane	Short Dipole ($l = 0.1\lambda$)	Half-Wavelength Dipole ($l = 0.5\lambda$)
3:1	E-plane	—	—
	H-plane	47°	45°
	D-plane	79°	79°
2:1	E-plane	—	50°
	H-plane	40°	40°
	D-plane	76°	77°

[Reprinted with permission of MIT Lincoln Laboratory, Lexington, MA]

horizontally a height $h = 0.25\lambda$ above an infinite electric ground plane, are displayed in Figure 8.29. Physically, the introduction of the ground plane below the horizontal electric dipoles prevents them from radiating along the ground plane, so the impedance is continuous when a grating lobe moves into the visible region. The maximum scan angles for VSWR's of 3:1 and 2:1 are shown listed in Table 8.4 [41].

The impedances of a short dipole ($\ell = 0.1\lambda$) are similar to those of the half-wavelength dipole shown in Figures 8.28 and 8.29. The most striking variation in impedance of a given array of dipoles is accomplished by the introduction of the ground plane particularly for scan angles near grating-lobe formation.

By comparing the results of Tables 8.3 and 8.4 it is evident that if for dipole arrays the element spacing for allowing grating lobes to appear marginally is used as a design criterion, placing the arrays above a ground plane would give vastly better (but still poor) VSWR performance at extreme scans. If, however, the element spacing is chosen to maintain the maximum VSWR below a given value, there appears little difference between the elements but results in a smaller maximum scan for a given element spacing.

To examine the effect the height h above the ground plane has on the maximum VSWR (within a specified scan volume), the maximum VSWR as a function of the height for E- and H-plane scans of two large square arrays of half-wavelength dipoles with $d_x = d_y = 0.5\lambda$ and $d_x = d_y = 0.6\lambda$ spacing between the elements are displayed in Figure 8.30. The maximum scan angle is 40° and the arrays are assumed to be matched at broadside. It is evident from the results that as the height is decreased the maximum E-plane mismatch becomes very large while that of the H-plane decreases monotonically. The optimum height which leads to equal maximum mismatches in the E- and H-planes of scan for a given scan volume is determined by the spacing between the elements. The optimum heights for the two arrays are indicated in Figure 8.30.

It can be concluded that when an array is placed at its optimum height above the ground plane for a given scan volume and the spacing between the elements of the array is smaller than that required by the grating lobes, that array will exhibit

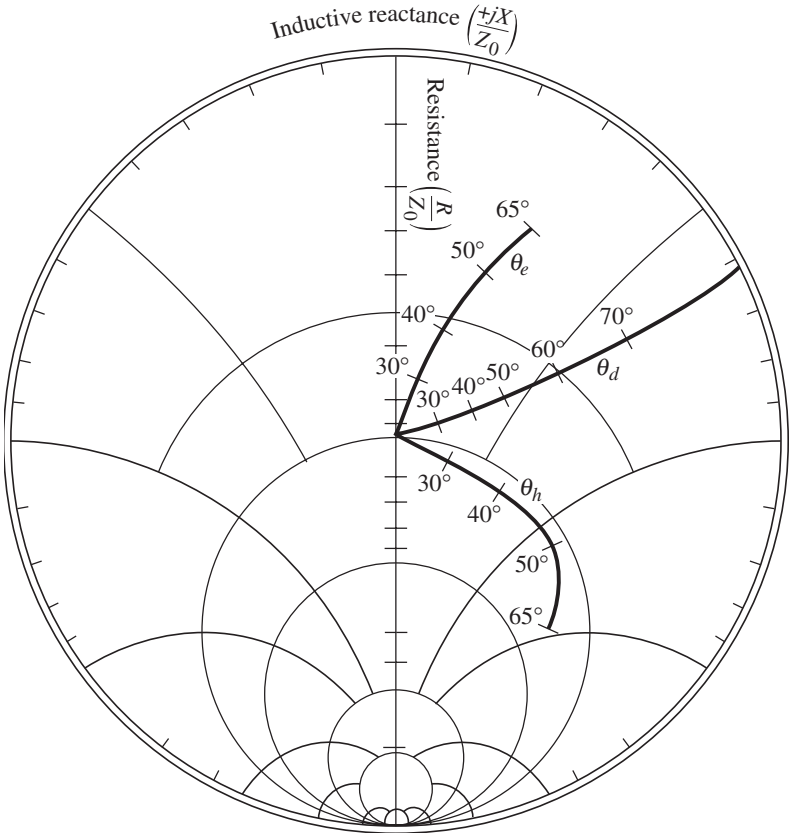


Figure 8.29 Normalized element impedance versus scan angle on the E-, H-, and D-planes for a planar array of half-wavelength ($\ell = 0.5\lambda$) dipoles with $d_x = d_y = 0.55\lambda$ and placed $h = 0.25\lambda$ above a ground plane. (Reprinted with permission of MIT Lincoln Laboratory, Lexington, MA.)

TABLE 8.4 Maximum Scan Volume of Short and Half-Wavelength Dipole Planar Array with $d_x = d_y = 0.55\lambda$ and with Ground Plane ($h = 0.25\lambda$) for VSWRs of 3:1 and 2:1

		Maximum Scan Angle	
VSWR	**Scan Plane**	**Short Dipole ($l = 0.1\lambda$)**	**Half-Wavelength Dipole ($l = 0.5\lambda$)**
3:1	E-plane	55°	50°
	H-plane	50°	50°
	D-plane	62°	62°
2:1	E-plane	45°	40°
	H-plane	40°	40°
	D-plane	52°	50°

[Reprinted with permission of MIT Lincoln Laboratory, Lexington, MA]

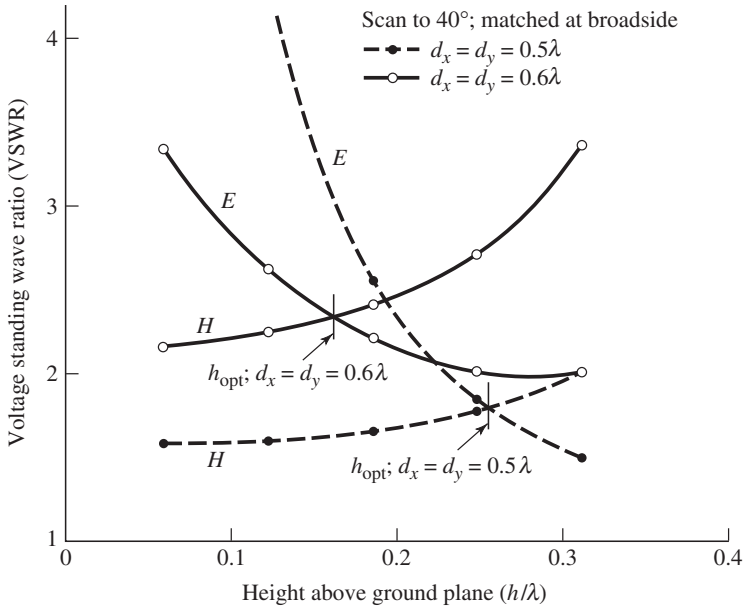


Figure 8.30 VSWR at θ_{max} versus height above ground plane for two large planar square arrays of half-wavelength ($\ell = 0.5\lambda$) dipoles. (Reprinted with permission of MIT Lincoln Laboratory, Lexington, MA.)

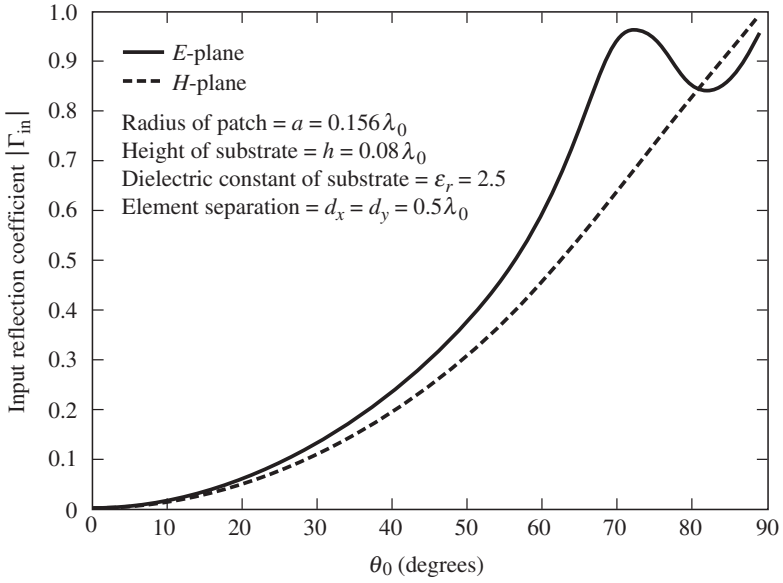


Figure 8.31 Typical magnitude of input reflection coefficient versus scan angle in E- and H-planes for infinite array of microstrip patches (courtesy J. T. Aberle and F. Zavosh).

less impedance variations than the one which just satisfies the scan volume requirement.

To demonstrate the variations of the input reflection coefficient, and thus of the input impedance, of an infinite array as a function of scan angle, the input reflection coefficient of an infinite array of circular microstrip patches matched at broadside is shown in Figure 8.31 for the E-plane and H-plane [46]. The variations are due mainly

to coupling between the elements. The variations are more pronounced for the E-plane than for the H-plane. For microstrip patches, coupling is attributed to space waves (with $1/r$ radial variations), higher order waves (with $1/\rho^2$ radial variations), surface waves (with $1/\rho^2$ radial variations), and leaky waves [with $\exp(-\lambda\rho)/\rho^{1/2}$ radial variations]. As is shown in Chapter 14 and Figures 14.39, 14.40, the variations of the reflection coefficient can be reduced by suppressing the surface waves supported by the substrate using cavities to back the patches [46]. The variations of the reflection coefficient as a function of scan angle can lead, due to large values of the reflection coefficient (ideally unity), to what is usually referred as *array scan blindness* [47]–[50]. This is evident for the E-plane near 72°–73° and is due to excitation in that plane of a leaky-wave mode, which is not as strongly excited as the scan angle increases beyond those values. Scan blindness is reached at a scan angle of 90°. Also there can be degradation of side lobe level and main beam shape due to the large variations of the reflection coefficient.

Scan blindness is attributed to slow waves which are supported by the structure of the antenna array. These structures may take the form of dielectric layers (such as radomes, superstrates, and substrates) over the face of the array, or metallic grids or fence structures. The scan blindness has been referred to as a "forced surface wave" [47], [48], or a "leaky wave" [49], resonant response of the slow wave structure by the phased array. For the microstrip arrays, the substrate layer supports a slow surface wave which contributes to scan blindness [50].

8.8 MULTIMEDIA

In the CD, that is part of the book, the following multimedia resources are included for the review, understanding, and visualization of the material of this chapter:

a. **Java**-based **interactive questionnaire**, with answers.
b. **Matlab** and **Fortran** Method of Moment computer program, designated ***MoM***, for computing and displaying the radiation characteristics of dipoles, using Hallén's and Pocklington's integral equations.
c. **Matlab** and **Fortran** computer program, designated ***Impedance***, for computing the self and mutual impedance of linear elements.
d. **Power Point (PPT)** viewgraphs, in multicolor.

REFERENCES

1. R. E. Burgess, "Aerial Characteristics," *Wireless Engr.*, Vol. 21, pp. 154–160, April 1944.
2. J. D. Kraus, *Antennas*, McGraw-Hill, New York, 1988, Chapters 9, 10, pp. 359–434.
3. S. A. Schelkunoff and H. T. Friis, *Antennas: Theory and Practice*, Wiley, New York, 1952, pp. 213–242.
4. A. A. Pistolkors, "The Radiation Resistance of Beam Antennas," *Proc. IRE*, Vol. 17, pp. 562–579, March 1929.
5. R. Bechmann, "On the Calculation of Radiation Resistance of Antennas and Antenna Combinations," *Proc. IRE*, Vol. 19. pp. 461–466, March 1931.
6. P. S. Carter, "Circuit Relations in Radiation Systems and Applications to Antenna Problems," *Proc. IRE*, Vol. 20, pp. 1004–1041, June 1932.

7. R. F. Harrington, "Matrix Methods for Field Problems," *Proc. IEEE*, Vol. 55, No. 2, pp. 136–149, February 1967.
8. R. F. Harrington, *Field Computation by Moment Methods*, Macmillan, New York, 1968.
9. J. H. Richmond, "Digital Computer Solutions of the Rigorous Equations for Scattering Problems," *Proc. IEEE*, Vol. 53, pp. 796–804, August 1965.
10. L. L. Tsai, "Moment Methods in Electromagnetics for Undergraduates," *IEEE Trans. Educ.*, Vol. E–21, No. 1, pp. 14–22, February 1978.
11. R. Mittra (Ed.), *Computer Techniques for Electromagnetics*, Pergamon, New York, 1973.
12. J. Moore and R. Pizer, *Moment Methods in Electromagnetics*, John Wiley and Sons, New York, 1984.
13. J. J. H. Wang, *Generalized Moment Methods in Electromagnetics*, John Wiley and Sons, New York, 1991.
14. C. A. Balanis, *Advanced Engineering Electromagnetics*, John Wiley and Sons, New York, 1989.
15. J. D. Lilly, "Application of The Moment Method to Antenna Analysis," MSEE Thesis, Department of Electrical Engineering, West Virginia University, 1980.
16. J. D. Lilly and C. A. Balanis, "Current Distributions, Input Impedances, and Radiation Patterns of Wire Antennas," North American Radio Science Meeting of URSI, Université Laval, Quebec, Canada, June 2–6, 1980.
17. D. K. Cheng, *Field and Wave Electromagnetics*, Addison-Wesley, Reading, MA, 1989, p. 97.
18. H. C. Pocklington, "Electrical Oscillations in Wire," *Cambridge Philos. Soc. Proc.*, Vol. 9, pp. 324–332, 1897.
19. E. Hallén, "Theoretical investigations into the transmitting and receiving qualities of antennae," *Nova Acta Regiae Soc. Sci. Upsaliensis*, Ser. IV, No. 4, pp. 1–44, 1938.
20. R. King and C. W. Harrison, Jr., "The distribution of current along a symmetric center-driven antenna," *Proc. IRE*, Vol. 31, pp. 548–567, October 1943.
21. J. H. Richmond, "A Wire-Grid Model for Scattering by Conducting Bodies," *IEEE Trans. Antennas Propagat.*, Vol. AP–14, No. 6, pp. 782–786, November 1966.
22. G. A. Thiele, "Wire Antennas," in *Computer Techniques for Electromagnetics*, R. Mittra (Ed.), Pergamon, New York, Chapter 2, pp. 7–70, 1973.
23. C. M. Butler and D. R. Wilton, "Evaluation of Potential Integral at Singularity of Exact Kernel in Thin-Wire Calculations," *IEEE Trans. Antennas Propagat.*, Vol. AP-23, No. 2, pp. 293–295, March 1975.
24. L. W. Pearson and C. M. Butler, "Inadequacies of Collocation Solutions to Pocklington-Type Models of Thin-Wire Structures," *IEEE Trans. Antennas Propagat.*, Vol. AP-23, No. 2, pp. 293–298, March 1975.
25. C. M. Butler and D. R. Wilton, "Analysis of Various Numerical Techniques Applied to Thin-Wire Scatterers," *IEEE Trans. Antennas Propagat.*, Vol. AP-23, No. 4, pp. 534–540, July 1975.
26. D. R. Wilton and C. M. Butler, "Efficient Numerical Techniques for Solving Pocklington's Equation and their Relationships to Other Methods," *IEEE Trans. Antennas Propagat.*, Vol. AP-24, No. 1, pp. 83–86, January 1976.
27. L. L. Tsai, "A Numerical Solution for the Near and Far Fields of an Annular Ring of Magnetic Current," *IEEE Trans. Antennas Propagat.*, Vol. AP-20, No. 5, pp. 569–576, September 1972.
28. R. Mittra and C. A. Klein, "Stability and Convergence of Moment Method Solutions," in *Numerical and Asymptotic Techniques in Electromagnetics*, R. Mittra (Ed.), Springer-Verlag, New York, 1975, Chapter 5, pp. 129–163.

29. T. K. Sarkar, "A Note on the Choice Weighting Functions in the Method of Moments," *IEEE Trans. Antennas Propagat.*, Vol. AP-33, No. 4, pp. 436–441, April 1985.
30. T. K. Sarkar, A. R. Djordjević and E. Arvas, "On the Choice of Expansion and Weighting Functions in the Numerical Solution of Operator Equations," *IEEE Trans. Antennas Propagat.*, Vol. AP-33, No. 9, pp. 988–996, September 1985.
31. E. K. Miller and F. J. Deadrick, "Some Computational Aspects of Thin-Wire Modeling," in *Numerical and Asymptotic Techniques in Electromagnetics*, R. Mittra (Ed.), Springer-Verlag, New York, 1975, Chapter 4, pp. 89–127.
32. L. Kantorovich and G. Akilov, *Functional Analysis in Normed Spaces*, Pergamon, Oxford, pp. 586–587, 1964.
33. H. E. King, "Mutual Impedance of Unequal Length Antennas in Echelon," *IRE Trans. Antennas Propagat.*, Vol. AP-5, pp. 306–313, July 1957.
34. R. C. Hansen, "Fundamental Limitations in Antennas," *Proc. IEEE*, Vol. 69, No. 2, pp. 170–182, February 1981.
35. G. J. Burke and A. J. Poggio, "Numerical Electromagnetics Code (NEC)-Method of Moments," Technical Document 11, Naval Ocean Systems Center, San Diego, Calif., January 1981.
36. A. J. Julian, J. M. Logan, and J. W. Rockway, "MININEC: A Mini-Numerical Electromagnetics Code," Technical Document 516, Naval Ocean Systems Center, San Diego, Calif, September 6, 1982.
37. J. Rockway, J. Logan, D. Tam, and S. Li, *The MININEC SYSTEM: Microcomputer Analysis of Wire Antennas*, Artech House, 1988.
38. J. A. G. Malherbe, "Calculator Program for Mutual Impedance," *Microwave Journal*, (Euro-Global Ed.), pp. 82-H–82-M, February 1984.
39. J. A. G. Malherbe, "Analysis of a Linear Antenna Array Including the Effects of Mutual Coupling," *IEEE Trans. Educ.*, Vol. 32, No. 1, pp. 29–34, February 1989.
40. D. Rubin, The Linville Method of High Frequency Transistor Amplifier Design, Naval Weapons Center, NWCCL TP 845, Corona Labs., Corona, CA, March 1969.
41. J. L. Allen and B. L. Diamond, "Mutual Coupling in Array Antennas," Technical Report EDS-66–443, Lincoln Lab., MIT, October 4, 1966.
42. H. A. Wheeler, "The Radiation Resistance of an Antenna in an Infinite Array or Waveguide," *Proc. IRE*, Vol. 48, pp. 478–487, April 1948.
43. S. Edelberg and A. A. Oliner, "Mutual Coupling Effects in Large Antenna Arrays, Part I," *IRE Trans. Antennas Propagat.*, Vol. AP-8, No. 3, pp. 286–297, May 1960.
44. S. Edelberg and A. A. Oliner, "Mutual Coupling Effects in Large Antenna Arrays," Part II," *IRE Trans. Antennas Propagat.*, Vol. AP-8, No. 4, pp. 360–367, July 1960.
45. L. Stark, "Radiation Impedance of a Dipole in an Infinite Planar Phased Array," *Radio Sci.*, Vol. 3, pp. 361–375, 1966.
46. F. Zavosh and J. T. Aberle, "Infinite Phased Arrays of Cavity-Backed Patches," *IEEE Trans. Antennas Propagat.*, Vol. 42, No. 3, pp. 390–394, March 1994.
47. N. Amitay, V. Galindo, and C. P. Wu, *Theory and Analysis of Phased Array Antennas*, John Wiley and Sons, New York, 1972.
48. L. Stark, "Microwave Theory of Phased-Array Antennas—A Review," *Proc. IEEE*, Vol. 62, pp. 1661–1701, December 1974.
49. G. H. Knittel, A. Hessel and A. A. Oliner, "Element Pattern Nulls in Phased Arrays and Their Relation to Guided Waves," *Proc. IEEE*, Vol. 56, pp. 1822–1836, November 1968.
50. D. M. Pozar and D. H. Schaubert, "Scan Blindness in Infinite Phased Arrays of Printed Dipoles," *IEEE Trans. Antennas Propagat.*, Vol. AP-32, No. 6, pp. 602–610, June 1984.

EX2042
Page 453 of 1072

PROBLEMS

8.1. Derive Pocklington's integral equation 8–24 using (8–22) and (8–23).

8.2. Derive the solution of (8–26) to the differential equation of (8–25a). Show that Hallén's integral equation can be written as (8–27).

8.3. Show that the incident tangential electric field (E_z^i) generated on the surface of a wire of radius a by a magnetic field generator of (8–30) is given by (8–31).

8.4. Reduce (8–31) to (8–32) valid only along the z axis ($\rho = 0$).

8.5. For the center-fed dipole of Example 8.3 write the $[Z]$ matrix for $N = 21$ using for the gap the delta-gap generator and the magnetic-frill generator. Use the computer program ***Moment Method*** (Pocklington) of this chapter.

8.6. For an infinitesimal center-fed dipole of $\ell = \lambda/50$ and radius $a = 0.005\lambda$, derive the input impedance using Pocklington's integral equation with piecewise constant subdomain basis functions and point-matching. Use $N = 21$ and model the gap as a delta-gap generator and as a magnetic-frill generator. Use the ***Moment Method*** (Pocklington) computer program of this chapter.

8.7. Using the ***Moment Method*** (Hallén) computer program at the end of the chapter, compute the input impedance of a $\lambda/4$ and $3\lambda/4$ dipole with an l/d ratio of $l/d = 50$ and 25. Use 20 subsections. Compare the results with the impedances of a dipole with $l/d = 10^9$. Plot the current distribution and the far-field pattern of each dipole.

8.8. Derive (8-53)–(8-55b) using (8-52), (3-2a), and (4-56).

8.9. For a linear dipole with sinusoidal current distribution, radiating in free-space, find the radiation Z_{im} and the input Z_{in} impedances when $a = \lambda/20$. Verify using the computer program ***Self And Mutual Impedances*** of this chapter.
(a) $l = \lambda/4$ (b) $l = \lambda/2$
(c) $l = 3\lambda/4$ (d) $l = \lambda$

8.10. A $\lambda/2$ dipole of finite radius is not self-resonant. However, if the dipole is somewhat less than $\lambda/2$, it becomes self-resonant. For a dipole with radius of $a = \lambda/200$ radiating in free-space, find the
(a) nearest length by which the $\lambda/2$ dipole becomes self-resonant
(b) radiation resistance (referred to the current maximum) of the new resonant dipole
(c) input resistance
(d) VSWR when the dipole is connected to a 50-ohm line

8.11. Find the length, at the first resonance, of linear dipoles with wire radii of
(a) $10^{-5}\lambda$ (b) $10^{-4}\lambda$
(c) $10^{-3}\lambda$ (d) $10^{-2}\lambda$
Compute the radiation resistance of each.

8.12. A quarter-wavelength monopole of radius $a = 10^{-2}\lambda$ is placed upon an infinite ground plane. Determine the

(a) impedance of the monopole

(b) length by which it must be shortened to become self-resonant (first resonance)

(c) impedance of the monopole when its length is that given in part b.

(d) VSWR when the monopole of part b is connected to a 50-ohm line.

8.13. For two half-wavelength dipoles radiating in free-space, compute (using equations, *not* curves) the mutual impedance Z_{21m} referred to the current maximum for

(a) side-by-side arrangement with $d = \lambda/4$

(b) collinear configuration with $s = \lambda/4$

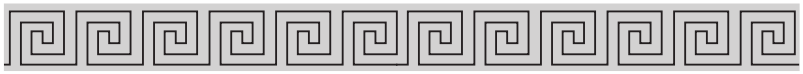
Verify using the computer program ***Self And Mutual Impedances*** of this chapter.

8.14. Two identical linear $\lambda/2$ dipoles are placed in a collinear arrangement a distance $s = 0.35\lambda$ apart. Find the driving-point impedance of each. Verify using the computer program ***Self And Mutual Impedances*** of this chapter.

8.15. Two identical linear $\lambda/2$ dipoles are placed in a collinear arrangement. Find the spacings between them so that the driving-point impedance of each has the smallest reactive part.

EX2042
Page 455 of 1072

CHAPTER 9



Broadband Dipoles and Matching Techniques

9.1 INTRODUCTION

In Chapter 4 the radiation properties (pattern, directivity, input impedance, mutual impedance, etc.) of very thin-wire antennas were investigated by assuming that the current distribution, which in most cases is nearly sinusoidal, is known. In practice, infinitely thin (electrically) wires are not realizable but can be approximated. In addition, their radiation characteristics (such as pattern, impedance, gain, etc.) are very sensitive to frequency. The degree to which they change as a function of frequency depends on the antenna bandwidth. For applications that require coverage over a broad range of frequencies, such as television reception of all channels, wide-band antennas are needed. There are numerous antenna configurations, especially of arrays, that can be used to produce wide bandwidths. Some simple and inexpensive dipole configurations, including the conical and cylindrical dipoles, can be used to accomplish this to some degree.

For a finite diameter wire (usually $d > 0.05\lambda$) the current distribution may not be sinusoidal and its effect on the radiation pattern of the antenna is usually negligible. However, it has been shown that the current distribution has a pronounced effect on the input impedance of the wire antenna, especially when its length is such that a near null in current occurs at its input terminals. The effects are much less severe when a near current maximum occurs at the input terminals.

Historically there have been three methods that have been used to take into account the finite conductor thickness. The first method treats the problem as boundary-value problem [1], the second as a tapered transmission line or electromagnetic horn [2], and the third finds the current distribution on the wire from an integral equation [3]. The boundary-value approach is well suited for idealistic symmetrical geometries (e.g., ellipsoids, prolate spheroids) which cannot be used effectively to approximate more practical geometries such as the cylinder. The method expresses the fields in terms of an infinite series of free oscillations or natural modes whose coefficients are chosen to satisfy the conditions of the driving source. For the assumed idealized configurations, the method does lead to very reliable data, but it is very difficult to know how to

Antenna Theory: Analysis Design, Third Edition, by Constantine A. Balanis
ISBN 0-471-66782-X Copyright © 2005 John Wiley & Sons, Inc.

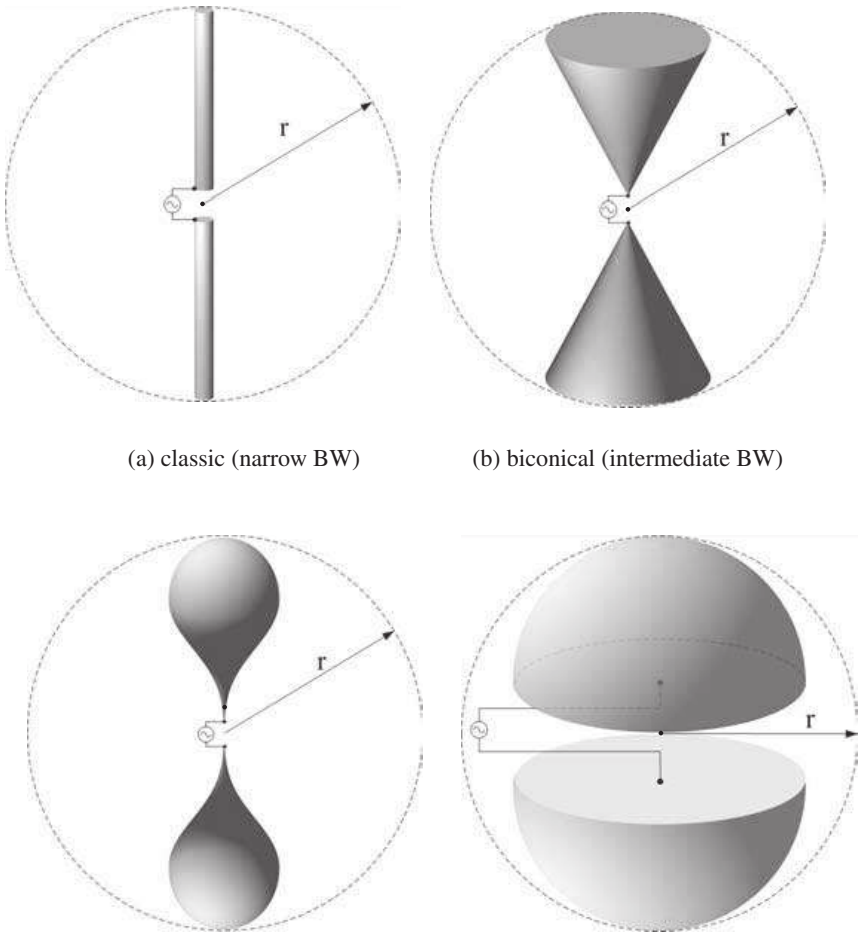
EX2042
Page 456 of 1072

approximate more practical geometries (such as a cylinder) by the more idealized configurations (such as the prolate spheroid). For these reasons the boundary-value method is not very practical and will not be pursued any further in this text.

In the second method Schelkunoff represents the antenna as a two-wire uniformly tapered transmission line, each wire of conical geometry, to form a biconical antenna. Its solution is obtained by applying transmission-line theory (incident and reflected waves), so well known to the average engineer. The analysis begins by first finding the radiated fields which in turn are used, in conjunction with transmission-line theory, to find the input impedance.

For the third technique, the main objectives are to find the current distribution on the antenna and in turn the input impedance. These were accomplished by Hallén by deriving an integral equation for the current distribution whose approximate solution, of different orders, was obtained by iteration and application of boundary conditions. Once a solution for the current is formed, the input impedance is determined by knowing the applied voltage at the feed terminals.

The details of the second method will follow in summary form. The integral equation technique of Hallén, along with that of Pocklington, form the basis of Moment Method techniques which were discussed in Chapter 8.



(a) classic (narrow BW) (b) biconical (intermediate BW)

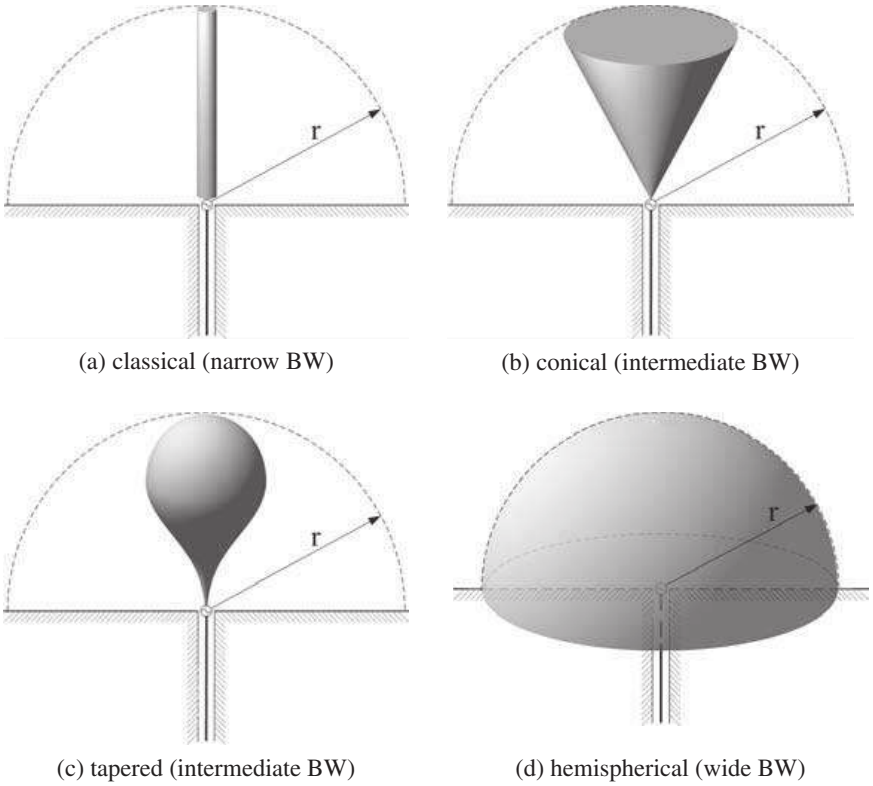
(c) tapered (intermediate BW) (d) hemispherical (wide BW)

Figure 9.1 Dipole configurations and associated qualitative bandwidths (BW).

EX2042
Page 457 of 1072

One of the main objectives in the design of an antenna is to broadband its characteristics—increase its bandwidth. Usually, this is a daunting task, especially if the specifications are quite ambitious. Typically, the response of each antenna, versus frequency, can be classified qualitatively into four categories: *narrowband, intermediate band*, and *wide band*. In Chapter 11, Section 11.5, it is pointed out that *the bandwidth of an antenna (which can be enclosed within a sphere of radius r) can be improved only if the antenna utilizes efficiently, with its geometrical configuration, the available volume within the sphere*. In Figure 9.1, we exhibit four different dipole configurations, starting with the classic dipole in Figure 9.1(a) and concluding with the hemispherical dipole of Figure 9.1(d). If we were to examine the frequency characteristics of a dipole on the basis of this fundamental principle, we can qualitatively categorize the frequency response of the different dipole configurations of Figure 9.1 into three groups; *narrowband, intermediate band*, and *wide band*. The same can be concluded for the geometries of the four monopole geometries of Figure 9.2. It should be pointed out that the third configuration (*tapered*) in each figure will provide the best reflection (matching) efficiency when fed from traditional transmission lines. Although in each of the previous two figures, Figures 9.1 and 9.2, the last two configurations (*d* and *e* in each) exhibit the most broadband characteristics, usually these geometries are not as convenient and economical for practical implementation. However, any derivatives of these geometries, especially two-dimensional simulations, are configurations that may be used to broadband the frequency characteristics.

Since the biconical antenna of Figure 9.1(b) and derivatives of it are classic configurations with practical applications, they will be examined in some detail in the section that follows.



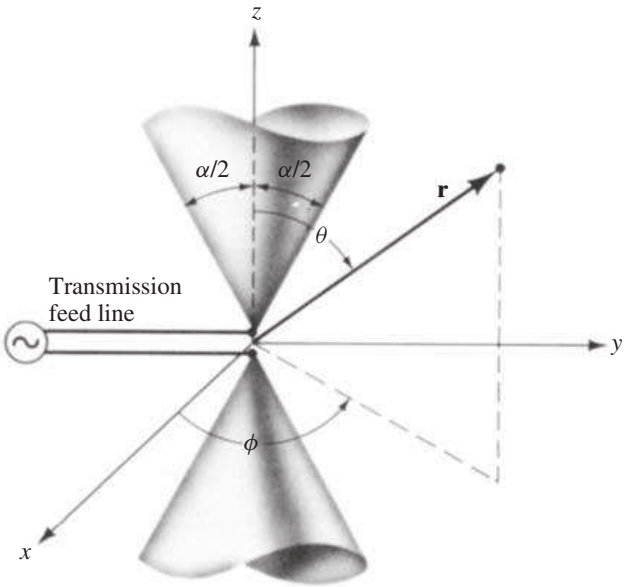
(a) classical (narrow BW) (b) conical (intermediate BW)

(c) tapered (intermediate BW) (d) hemispherical (wide BW)

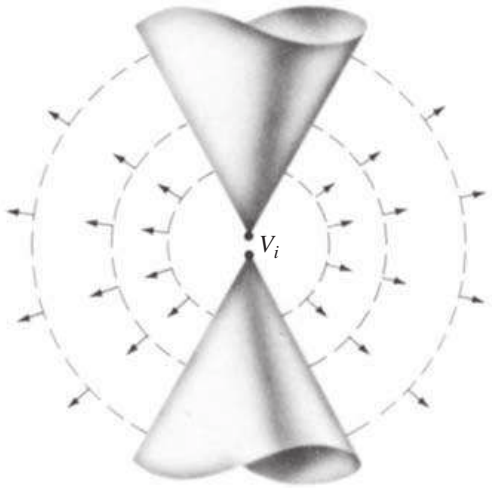
Figure 9.2 Monopole configurations and associated qualitative bandwidths (BW).

9.2 BICONICAL ANTENNA

One simple configuration that can be used to achieve broadband characteristics is the biconical antenna formed by placing two cones of infinite extent together, as shown in Figure 9.3(a). This can be thought to represent a uniformly tapered transmission line. The application of a voltage V_i at the input terminals will produce outgoing spherical waves, as shown in Figure 9.3(b), which in turn produce at any point $(r, \theta = \theta_c, \phi)$ a current I along the surface of the cone and voltage V between the cones (Figure 9.4). These can then be used to find the characteristic impedance of the transmission line, which is also equal to the input impedance of an infinite geometry. Modifications to this expression, to take into account the finite lengths of the cones, will be made using transmission-line analogy.



(a) Biconical geometry



(b) Spherical waves

Figure 9.3 Biconical antenna geometry and radiated spherical waves.

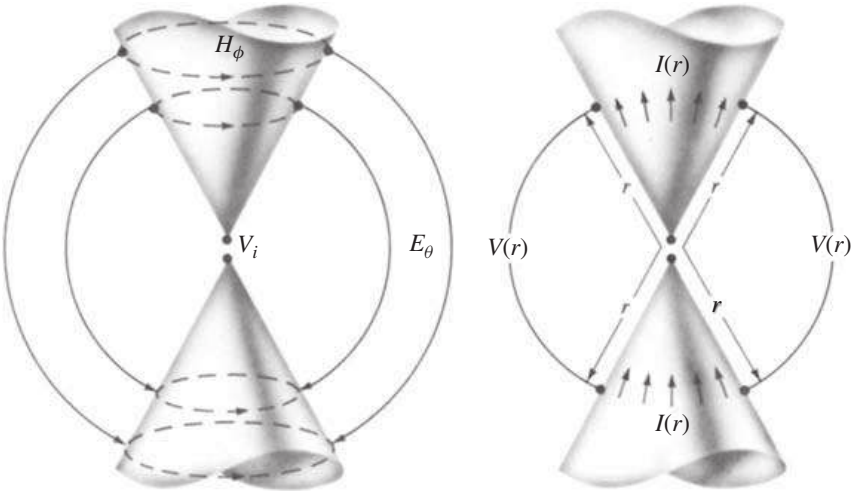


Figure 9.4 Electric and magnetic fields, and associated voltages and currents, for a biconical antenna.

9.2.1 Radiated Fields

The analysis begins by first finding the radiated **E**- and **H**-fields between the cones, assuming dominant TEM mode excitation (**E** and **H** are transverse to the direction of propagation). Once these are determined for any point (r, θ, ϕ), the voltage V and current I at any point on the surface of the cone $(r, \theta = \theta_c, \phi)$ will be formed. From Faraday's law we can write that

$$\nabla \times \mathbf{E} = -j\omega\mu\mathbf{H} \tag{9-1}$$

which when expanded in spherical coordinates and assuming that the **E**-field has only an E_θ component independent of ϕ, reduces to

$$\nabla \times \mathbf{E} = \hat{\mathbf{a}}_\phi \frac{1}{r}\frac{\partial}{\partial r}(rE_\theta) = -j\omega\mu(\hat{\mathbf{a}}_r H_r + \hat{\mathbf{a}}_\theta H_\theta + \hat{\mathbf{a}}_\phi H_\phi) \tag{9-2}$$

Since **H** only has an H_ϕ component, necessary to form the TEM mode with E_θ, (9-2) can be written as

$$\frac{1}{r}\frac{\partial}{\partial r}(rE_\theta) = -j\omega\mu H_\phi \tag{9-2a}$$

From Ampere's law we have that

$$\nabla \times \mathbf{H} = +j\omega\epsilon\mathbf{E} \tag{9-3}$$

which when expanded in spherical coordinates, and assuming only E_θ and H_ϕ components independent of ϕ, reduces to

$$\hat{\mathbf{a}}_r \frac{1}{r^2 \sin\theta}\left[\frac{\partial}{\partial\theta}(r\sin\theta H_\phi)\right] - \hat{\mathbf{a}}_\theta \frac{1}{r\sin\theta}\left[\frac{\partial}{\partial r}(r\sin\theta H_\phi)\right] = +j\omega\epsilon(\hat{\mathbf{a}}_\theta E_\theta) \tag{9-4}$$

EX2042
Page 460 of 1072

which can also be written as

$$\frac{\partial}{\partial\theta}(r\sin\theta H_\phi) = 0 \tag{9-4a}$$

$$\frac{1}{r\sin\theta}\frac{\partial}{\partial r}(r\sin\theta H_\phi) = -j\omega\epsilon E_\theta \tag{9-4b}$$

Rewriting (9-4b) as

$$\frac{1}{r}\frac{\partial}{\partial r}(rH_\phi) = -j\omega\epsilon E_\theta \tag{9-5}$$

and substituting it into (9-2a) we form a differential equation for H_ϕ as

$$-\frac{1}{j\omega\epsilon r}\frac{\partial}{\partial r}\left[\frac{\partial}{\partial r}(rH_\phi)\right] = -j\omega\mu H_\phi \tag{9-6}$$

or

$$\frac{\partial^2}{\partial r^2}(rH_\phi) = -\omega^2\mu\epsilon(rH_\phi) = -k^2(rH_\phi) \tag{9-6a}$$

A solution for (9-6a) must be obtained to satisfy (9-4a). To meet the condition of (9-4a), the θ variations of H_ϕ must be of the form

$$H_\phi = \frac{f(r)}{\sin\theta} \tag{9-7}$$

A solution of (9-6a), which also meets the requirements of (9-7) and represents an outward traveling wave, is

$$H_\phi = \frac{H_0}{\sin\theta}\frac{e^{-jkr}}{r} \tag{9-8}$$

where

$$f(r) = H_0\frac{e^{-jkr}}{r} \tag{9-8a}$$

An inward traveling wave is also a solution but does not apply to the infinitely long structure.

Since the field is of TEM mode, the electric field is related to the magnetic field by the intrinsic impedance, and we can write it as

$$E_\theta = \eta H_\phi = \eta\frac{H_0}{\sin\theta}\frac{e^{-jkr}}{r} \tag{9-9}$$

In Figure 9.4(a) we have sketched the electric and magnetic field lines in the space between the two conical structures. The voltage produced between two corresponding points on the cones, a distance r from the origin, is found by

$$V(r) = \int_{\alpha/2}^{\pi-\alpha/2}\mathbf{E}\cdot d\mathbf{l} = \int_{\alpha/2}^{\pi-\alpha/2}(\hat{\mathbf{a}}_\theta E_\theta)\cdot(\hat{\mathbf{a}}_\theta r\,d\theta) = \int_{\alpha/2}^{\pi-\alpha/2}E_\theta r\,d\theta \tag{9-10}$$

EX2042
Page 461 of 1072

or by using (9-9)

$$V(r) = \eta H_0 e^{-jkr} \int_{\alpha/2}^{\pi-\alpha/2} \frac{d\theta}{\sin\theta} = \eta H_0 e^{-jkr} \ln\left[\frac{\cot(\alpha/4)}{\tan(\alpha/4)}\right]$$

$$V(r) = 2\eta H_0 e^{-jkr} \ln\left[\cot\left(\frac{\alpha}{4}\right)\right] \tag{9-10a}$$

The current on the surface of the cones, a distance r from the origin, is found by using (9-8) as

$$I(r) = \int_0^{2\pi} H_\phi r \sin\theta \, d\phi = H_0 e^{-jkr} \int_0^{2\pi} d\phi = 2\pi H_0 e^{-jkr} \tag{9-11}$$

In Figure 9.4(b) we have sketched the voltage and current at a distance r from the origin.

9.2.2 Input Impedance

A. Infinite Cones

Using the voltage of (9-10a) and the current of (9-11), we can write the characteristic impedance as

$$Z_c = \frac{V(r)}{I(r)} = \frac{\eta}{\pi} \ln\left[\cot\left(\frac{\alpha}{4}\right)\right] \tag{9-12}$$

Since the characteristic impedance is not a function of the radial distance r, it also represents the input impedance at the antenna feed terminals of the infinite structure. For a free-space medium, (9-12) reduces to

$$\boxed{Z_c = Z_{in} = 120 \ln\left[\cot\left(\frac{\alpha}{4}\right)\right]} \tag{9-12a}$$

which is a pure resistance. For small cone angles

$$Z_{in} = \frac{\eta}{\pi} \ln\left[\cot\left(\frac{\alpha}{4}\right)\right] = \frac{\eta}{\pi} \ln\left[\frac{1}{\tan(\alpha/4)}\right] \simeq \frac{\eta}{\pi} \ln\left(\frac{4}{\alpha}\right) \tag{9-12b}$$

Variations of Z_{in} as a function of the half-cone angle $\alpha/2$ are shown plotted in Figure 9.5(a) for $0^\circ < \alpha/2 \leq 90^\circ$ and in Figure 9.5(b) in an expanded scale for $0^\circ < \alpha/2 \leq 2^\circ$. Although the half-cone angle is not very critical in the design, it is usually chosen so that the characteristic impedance of the biconical configuration is nearly the same as that of the transmission line to which it will be attached. Small angle biconical antennas are not very practical but wide-angle configurations ($30^\circ < \alpha/2 < 60^\circ$) are frequently used as broadband antennas.

The radiation resistance of (9-12) can also be obtained by first finding the total radiated power

$$P_{\text{rad}} = \oiint_S \mathbf{W}_{\text{av}} \cdot d\mathbf{s} = \int_0^{2\pi} \int_{\alpha/2}^{\pi-\alpha/2} \frac{|E|^2}{2\eta} r^2 \sin\theta \, d\theta \, d\phi = \pi\eta |H_0|^2 \int_0^{\pi-\alpha/2} \frac{d\theta}{\sin\theta}$$

$$P_{\text{rad}} = 2\pi\eta |H_0|^2 \ln\left[\cot\left(\frac{\alpha}{4}\right)\right] \tag{9-13}$$

EX2042
Page 462 of 1072

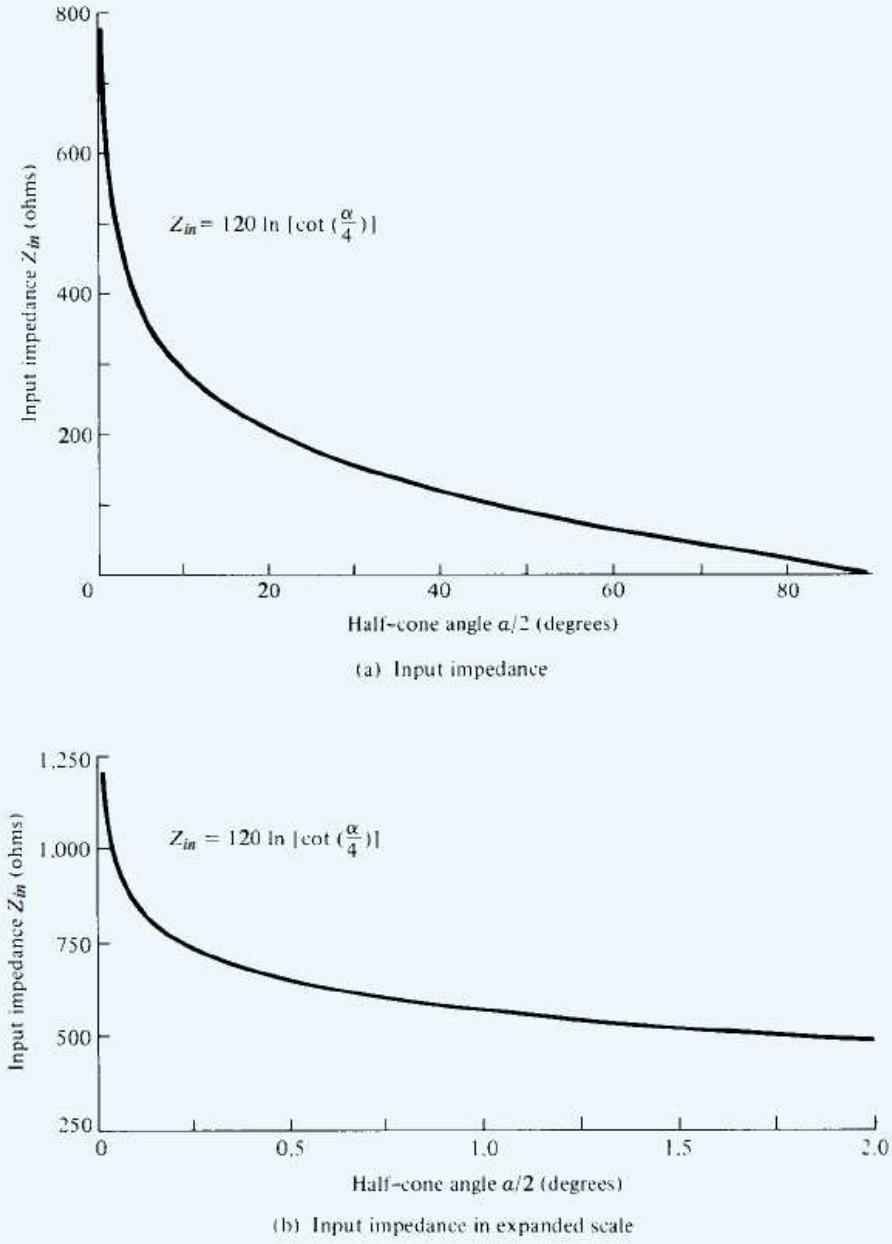


Figure 9.5 Input impedance of an infinitely long biconical antenna radiating in free-space.

and by using (9-11) evaluated at $r = 0$ we form

$$R_r = \frac{2P_{\text{rad}}}{[I(0)]^2} = \frac{\eta}{\pi} \ln\left[\cot\left(\frac{\alpha}{4}\right)\right] \tag{9-14}$$

which is identical to (9-12).

B. Finite Cones

The input impedance of (9-12) or (9-14) is for an infinitely long structure. To take into account the finite dimensions in determining the input impedance, Schelkunoff [2] has devised an ingenious method where he assumes that for a finite length cone ($r = l/2$)

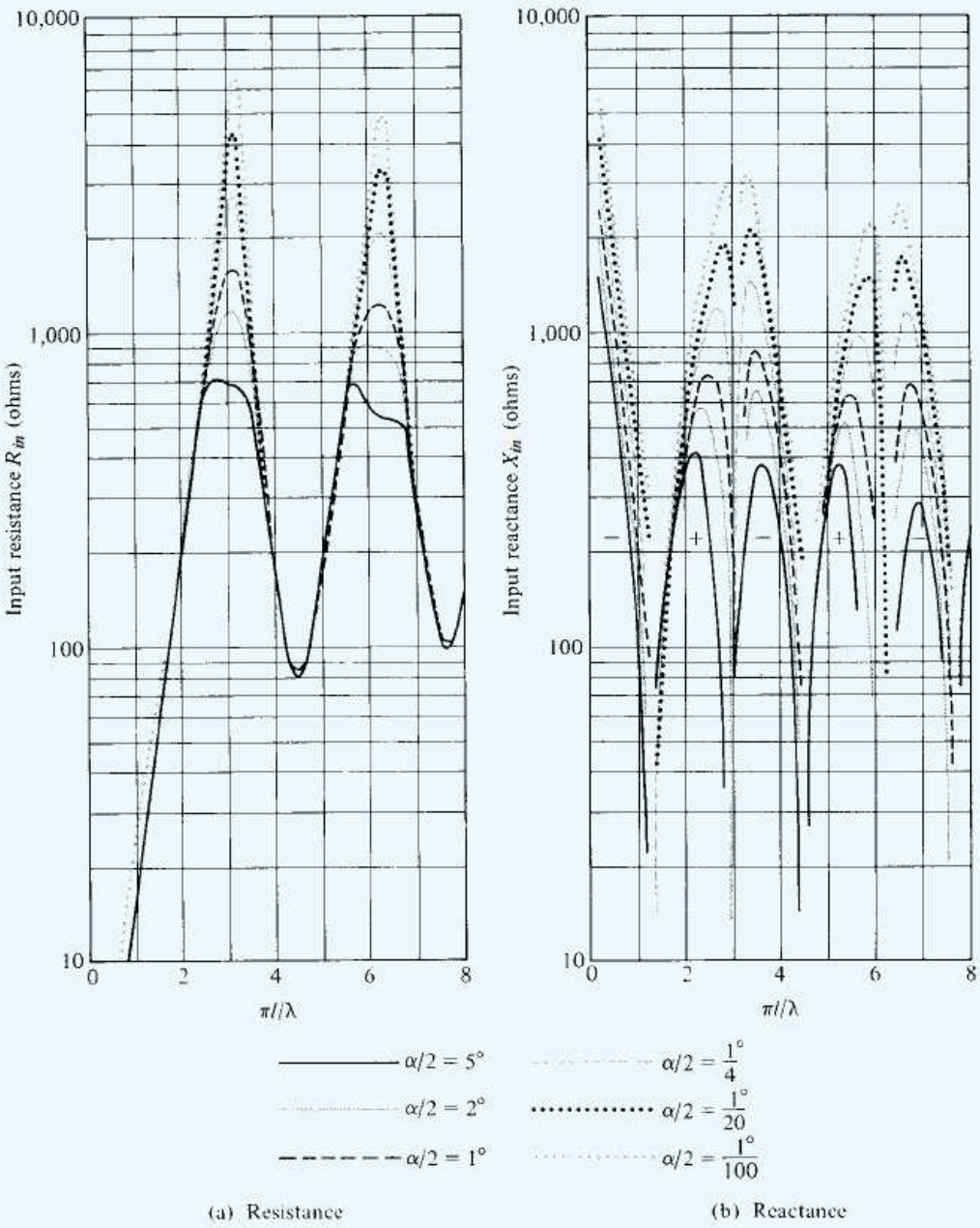


Figure 9.6 Input impedance (at feed terminals) of finite length biconical antenna. (SOURCE: H. Jasik (ed.), *Antenna Engineering Handbook*, McGraw-Hill, New York, 1961, Chapter 3).

some of the energy along the surface of the cone is reflected while the remaining is radiated. Near the equator most of the energy is radiated. This can be viewed as a load impedance connected across the ends of the cones. The electrical equivalent is a transmission line of characteristic impedance Z_c terminated in a load impedance Z_L. Computed values [4] for the input resistance and reactance of small angle cones are shown in Figure 9.6. It is apparent that the antenna becomes more broadband (its resistance and reactance variations are less severe) as the cone angle increases.

The biconical antenna represents one of the canonical problems in antenna theory, and its model is well suited for examining general characteristics of dipole-type antennas.

C. Unipole

Whenever one of the cones is mounted on an infinite plane conductor (i.e., the lower cone is replaced by a ground plane), it forms a unipole and its input impedance is one-half of the two-cone structure. Input impedances for unipoles of various cone angles as a function of the antenna length l have been measured [5]. Radiation patterns of biconical dipoles fed by coaxial lines have been computed by Papas and King [6].

9.3 TRIANGULAR SHEET, BOW-TIE, AND WIRE SIMULATION

Because of their broadband characteristics, biconical antennas have been employed for many years in the VHF and UHF frequency ranges. However, the solid or shell biconical structure is so massive for most frequencies of operation that it is impractical to use. Because of its attractive radiation characteristics, compared to those of other single antennas, realistic variations to its mechanical structure have been sought while retaining as many of the desired electrical features as possible.

Geometrical approximations to the solid or shell conical unipole or biconical antenna are the triangular sheet and bow-tie antennas shown in Figures 9.7(a) and (b), respectively, each fabricated from sheet metal. The triangular sheet has been investigated experimentally by Brown and Woodward [5]. Each of these antennas can also be simulated by a wire along the periphery of its surface which reduces significantly the weight and wind resistance of the structure. The computed input impedances and radiation patterns of wire bow-tie antennas, when mounted above a ground plane, have been computed using the Moment Method [7]. The impedance is shown plotted in Figure 9.8. A comparison of the results of Figure 9.8 with those of reference [5] reveals that the bow-tie antenna does not exhibit as broadband characteristics (i.e., nearly constant resistance and essentially zero reactance over a large frequency range) as the corresponding solid biconical antenna for $30^\circ < \alpha < 90^\circ$. Also for a given flare angle the resistance and reactance of the bow-tie wire structure fluctuate more than for a triangular sheet antenna. Thus the wire bow-tie is very narrowband as compared to the biconical surface of revolution or triangular sheet antenna.

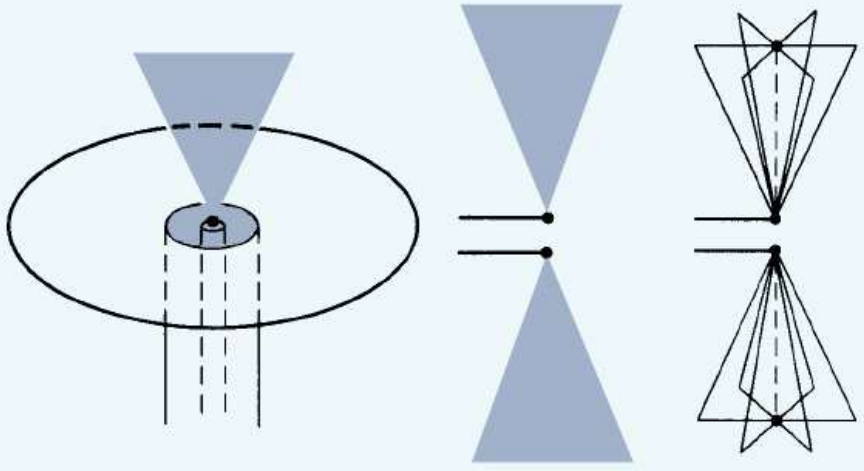
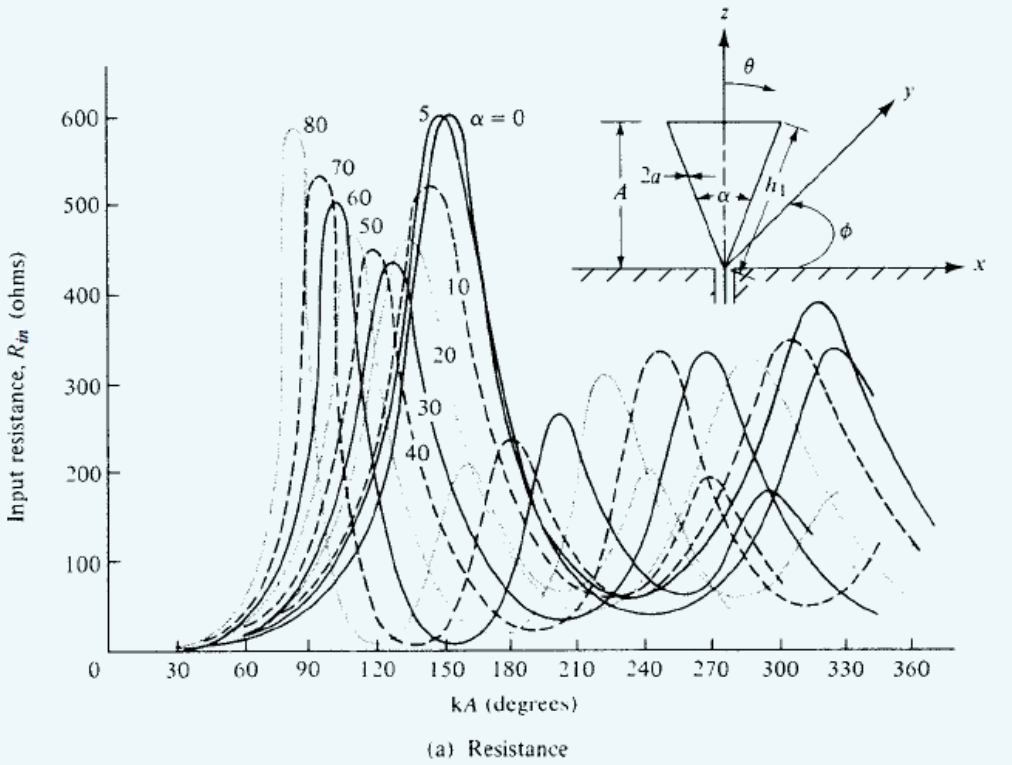
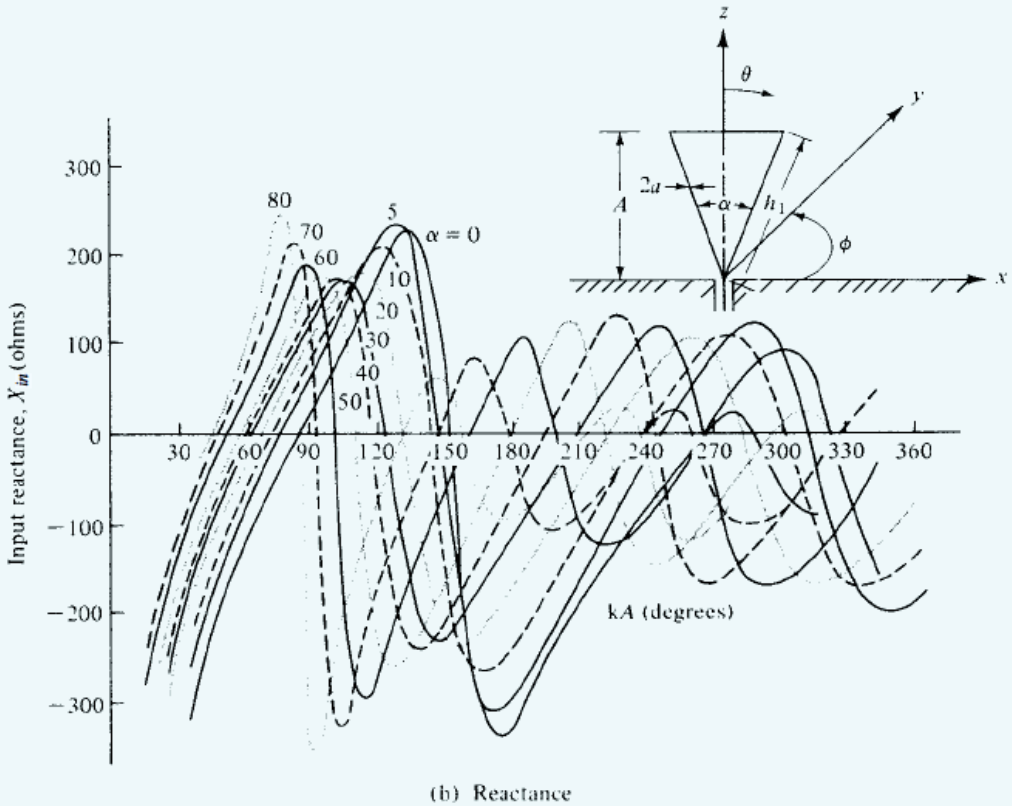


Figure 9.7 Triangular sheet, bow-tie, and wire simulation of biconical antenna.



(a) Resistance



(b) Reactance

Figure 9.8 Computed impedance of wire bow-tie (or wire unipole) as a function of length for various included angles. (SOURCE: C. E. Smith, C. M. Butler, and K. R. Umashankar, "Characteristics of Wire Biconical Antenna," *Microwave Journal*, pp. 37–40, September 1979).

In order to simulate better the attractive surface of revolution of a biconical antenna by low-mass structures, multielement intersecting wire bow-ties were employed as shown in Figure 9.7(c). It has been shown that eight or more intersecting wire-constructed bow-ties can approximate reasonably well the radiation characteristics of a conical body-of-revolution antenna.

9.4 CYLINDRICAL DIPOLE

Another simple and inexpensive antenna whose radiation characteristics are frequency dependent is a cylindrical dipole (i.e., a wire of finite diameter and length) of the form shown in Figure 9.9. Thick dipoles are considered broadband while thin dipoles are more narrowband. This geometry can be considered to be a special form of the biconical antenna when $\alpha = 0^\circ$. A thorough analysis of the current, impedance, pattern, and other radiation characteristics can be performed using the Moment Method. With that technique the antenna is analyzed in terms of integral formulations of the Hallén and Pocklington type which can be evaluated quite efficiently by the Moment Method. The analytical formulation of the Moment Method has been presented in Chapter 8. In this section we want to present, in summary form, some of its performance characteristics.

9.4.1 Bandwidth

As has been pointed out previously, a very thin linear dipole has very narrowband input impedance characteristics. Any small perturbations in the operating frequency will result in large changes in its operational behavior. One method by which its acceptable operational bandwidth can be enlarged will be to decrease the l/d ratio.

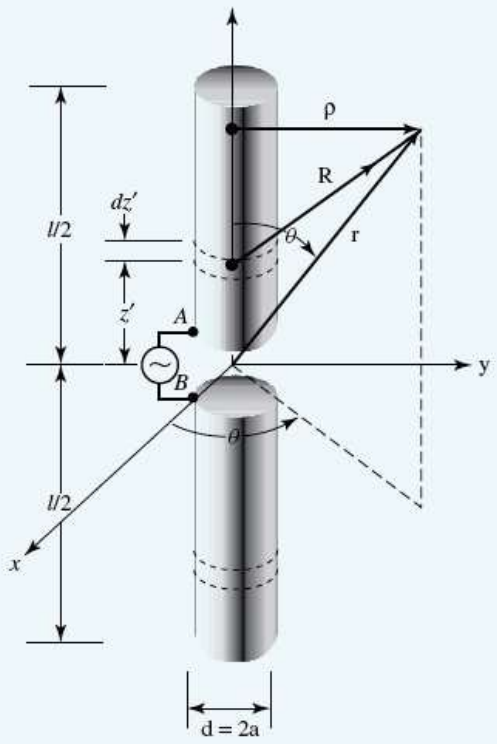
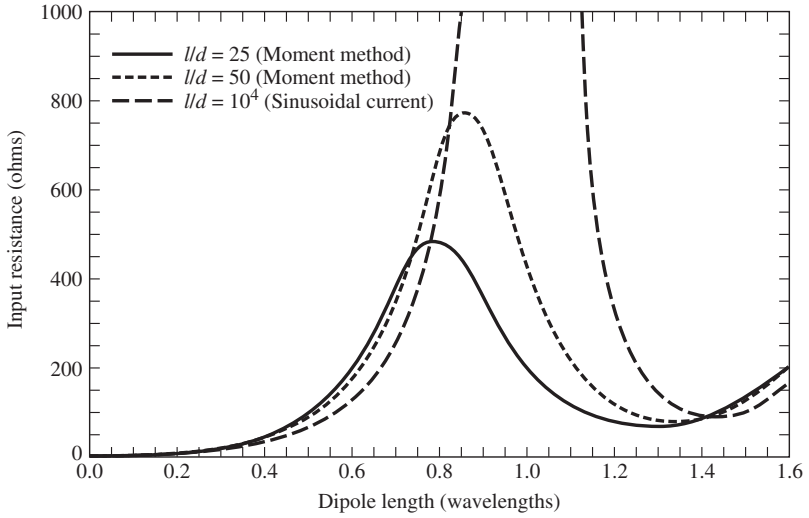


Figure 9.9 Center-fed cylindrical antenna configuration.

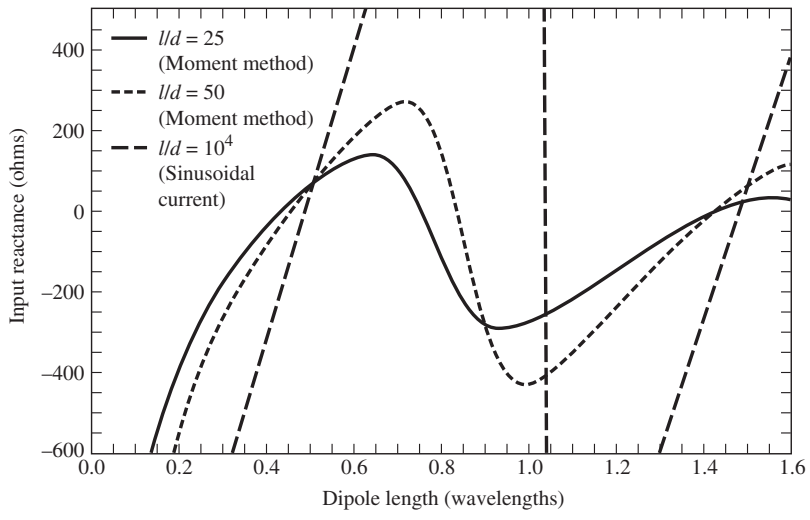
For a given antenna, this can be accomplished by holding the length the same and increasing the diameter of the wire. For example, an antenna with a $l/d \simeq 5{,}000$ has an acceptable bandwidth of about 3%, which is a small fraction of the center frequency. An antenna of the same length but with a $l/d \simeq 260$ has a bandwidth of about 30%.

9.4.2 Input Impedance

The input impedance (resistance and reactance) of a very thin dipole of length l and diameter d can be computed using (8-60a)–(8-61b). As the radius of the wire increases, these equations become inaccurate. However, using integral equation analyses along with the Moment Method of Chapter 8, input impedances can be computed for wires with different l/d ratios. In general, it has been observed that for a given length wire its impedance variations become less sensitive as a function of frequency as the l/d ratio decreases. Thus more broadband characteristics can be obtained by increasing the diameter of a given wire. To demonstrate this, in Figures 9.10(a) and (b) we have



(a) Input resistance



(b) Input reactance

Figure 9.10 (a) Input resistance and (b) reactance of wire dipoles.

plotted, as a function of electrical length (as a function of frequency for a constant physical length), the input resistance and reactance of dipoles with $l/d = 10^4 (\Omega = 19.81)$, $50 (\Omega = 9.21)$, and $25 (\Omega = 6.44)$ where $\Omega = 2\ln(2l/d)$. For $l/d = 10^4$ the values were computed using (8-60a) and (8-61a) and then transferred to the input terminals by (8-60b) and (8-61b), respectively. The others were computed using the Moment Method techniques of Chapter 8. It is noted that the variations of each are less pronounced as the l/d ratio decreases, thus providing greater bandwidth.

Measured input resistances and reactances for a wide range of constant l/d ratios have been reported [8]. These curves are for a cylindrical antenna driven by a coaxial cable mounted on a large ground plane on the earth's surface. Thus they represent half of the input impedance of a center-fed cylindrical dipole radiating in free-space. The variations of the antenna's electrical length were obtained by varying the frequency while the length-to-diameter (l/d) ratio was held constant.

9.4.3 Resonance and Ground Plane Simulation

The imaginary part of the input impedance of a linear dipole can be eliminated by making the total length, l, of the wire slightly less than an integral number of half-wavelengths (i.e., l slight less than $n\lambda/2, n = 1, 3, \ldots$) or slightly greater than an integral number of wavelengths (i.e., l slightly greater than $n\lambda$, $n = 1, 2, \ldots$). The amount of reduction or increase in length, is a function of the radius of the wire, and it can be determined for thin wires iteratively using (8-60b) and (8-61b). At the resonance length, the resistance can then be determined using (8-60a) and (8-61a). Empirical equations for approximating the length, impedance, and the order of resonance of the

TABLE 9.1 Cylindrical Dipole Resonances

	First Resonance	Second Resonance	Third Resonance	Fourth Resonance
LENGTH	$0.48\lambda F$	$0.96\lambda F$	$1.44\lambda F$	$1.92\lambda F$
RESISTANCE (ohms)	67	$\frac{R_n^2}{67}$	95	$\frac{R_n^2}{95}$
$F = \frac{l/2a}{1 + l/2a}; R_n = 150\log_{10}(l/2a)$				

TABLE 9.2 Cylindrical Stub Resonances

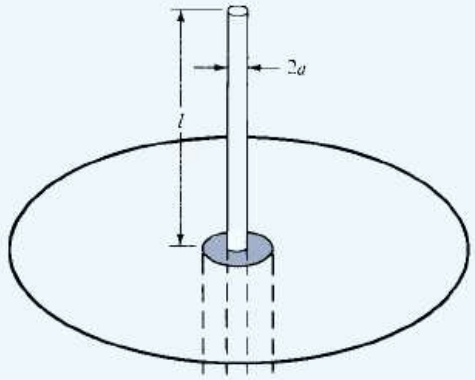
	First Resonance	Second Resonance	Third Resonance	Fourth Resonance
LENGTH	$0.24\lambda F'$	$0.48\lambda F'$	$0.72\lambda F'$	$0.96\lambda F'$
RESISTANCE (ohms)	34	$\frac{(R_n')^2}{34}$	48	$\frac{(R_n')^2}{48}$
$F' = \frac{l/a}{1 + l/a}; R_n' = 75\log_{10}(l/a)$				

cylindrical dipoles are found in Table 9.1 [9]. R_n is called the natural resistance and represents the geometric mean resistance at an odd resonance and at the next higher even resonance. For a cylindrical stub above a ground plane, as shown in Figure 9.11, the corresponding values are listed in Table 9.2 [9].

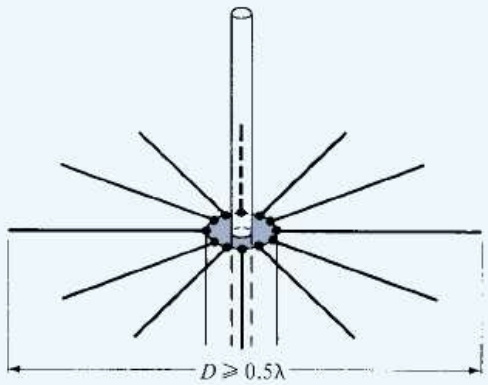
To reduce the wind resistance, to simplify the design, and to minimize the costs, a ground plane is often simulated, especially at low frequencies, by crossed wires as shown in Figure 9.11(b). Usually only two crossed wires (four radials) are employed. A larger number of radials results in a better simulation of the ground plane. Ground planes are also simulated by wire mesh. The spacing between the wires is usually selected to be equal or smaller than $\lambda/10$. The flat or shaped reflecting surfaces for UHF educational TV are usually realized approximately by using wire mesh.

9.4.4 Radiation Patterns

The theory for the patterns of infinitesimally thin wires was developed in Chapter 4. Although accurate patterns for finite diameter wires can be computed using current distributions obtained by the Moment Method of Chapter 8, the patterns calculated using ideal sinusoidal current distributions, valid for infinitely small diameters, provide a good first-order approximation even for relatively thick cylinders. To illustrate this, in Figure 9.12 we have plotted the relative patterns for $l = 3\lambda/2$ with $l/d = 10^4(\Omega = 19.81), 50(\Omega = 9.21), 25(\Omega = 6.44)$, and $8.7(\Omega = 5.71)$, where $\Omega = 2\ln(2l/d)$. For $l/d = 10^4$ the current distribution was assumed to be purely sinusoidal, as given by (4-56); for the others, the Moment Method techniques of Chapter 8



(a) Cylindrical monopole



(b) Wire simulation of ground plane

Figure 9.11 Cylindrical monopole above circular solid and wire-simulated ground planes.

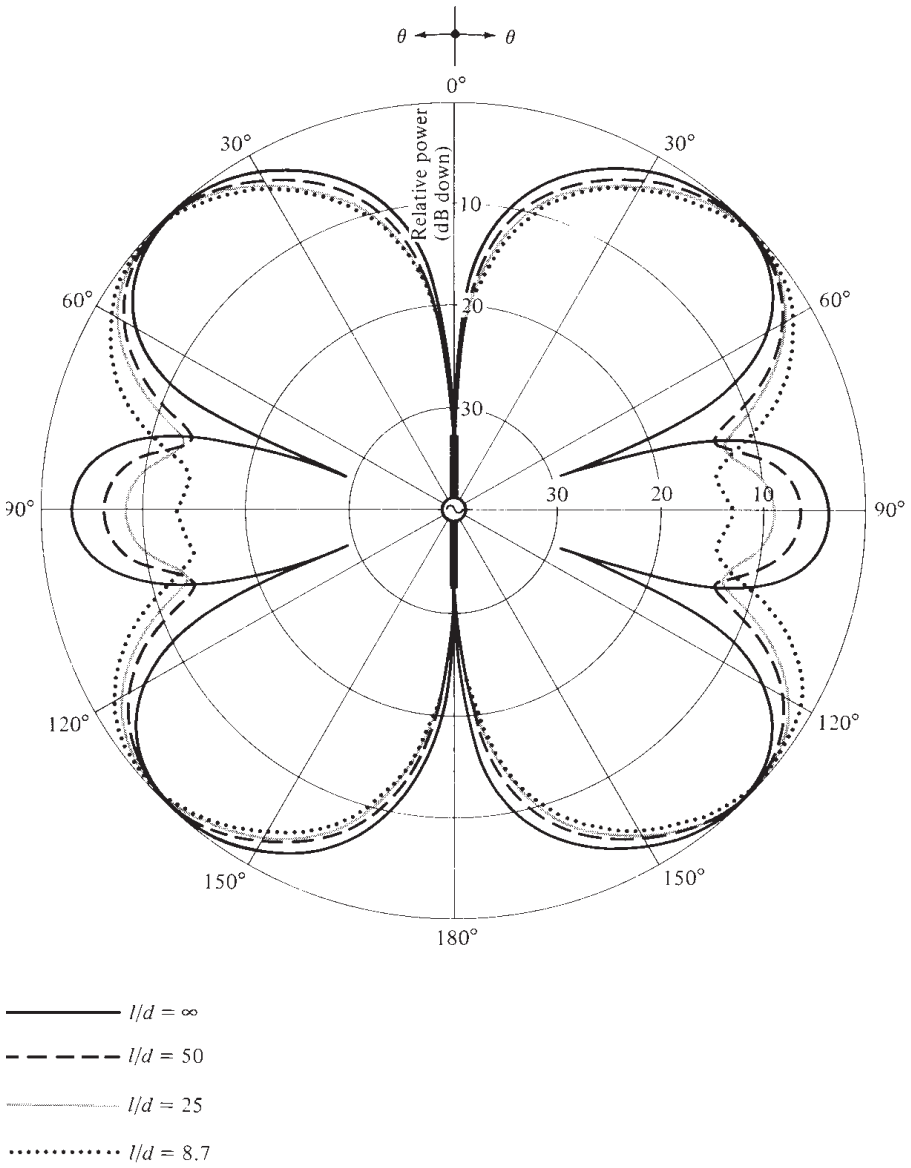


Figure 9.12 Amplitude radiation patterns of a $3\lambda/2$ dipole of various thicknesses.

were used. The patterns were computed using the Moment Method formulations outlined in Section 8.4. It is noted that the pattern is essentially unaffected by the thickness of the wire in regions of intense radiation. However, as the radius of the wire increases, the minor lobes diminish in intensity and the nulls are filled by low-level radiation. The same characteristics have been observed for other length dipoles such as $l = \lambda/2, \lambda$ and 2λ. The input impedance for the $l = \lambda/2$ and $l = 3\lambda/2$ dipoles, with $l/d = 10^4$, 50, and 25, is equal to

$l = \lambda/2$	$l = 3\lambda/2$	
$Z_{in}(l/d = 10^4) = 73 + j42.5$	$Z_{in}(l/d = 10^4) = 105.49 + j45.54$	
$Z_{in}(l/d = 50) = 85.8 + j54.9$	$Z_{in}(l/d = 50) = 103.3 + j9.2$	(9-15)
$Z_{in}(l/d = 25) = 88.4 + j27.5$	$Z_{in}(l/d = 25) = 106.8 + j4.9$	

9.4.5 Equivalent Radii

Up to now, the formulations for the current distribution and the input impedance assume that the cross section of the wire is constant and of radius a. An electrical equivalent radius can be obtained for some uniform wires of noncircular cross section. This is demonstrated in Table 9.3 where the actual cross sections and their equivalent radii are illustrated.

The equivalent radius concept can be used to approximate the antenna or scattering characteristics of electrically small wires of arbitrary cross sections. It is accomplished by replacing the noncircular cross-section wire with a circular wire whose radius is the "equivalent" radius of the noncircular cross section. In electrostatics, the equivalent radius represents the radius of a circular wire whose capacitance is equal to that of the noncircular geometry. This definition can be used at all frequencies provided the wire remains electrically small. The circle with equivalent radius lies between the circles which circumscribe and inscribe the geometry and which together bound the noncircular cross section.

9.4.6 Dielectric Coating

Up to now it has been assumed that the wire antennas are radiating into free-space. The radiation characteristics of a wire antenna (current distribution, far-field pattern, input impedance, bandwidth, radiation efficiency, and effective length) coated with a layer of electrically and magnetically lossless [10] or lossy [11] medium, as shown in Figure 9.13, will be affected unless the layer is very thin compared to the radius and the wavelength. The problem was investigated analytically by the Moment Method and the effects on the radiation characteristics can be presented by defining the two parameters

$$P = \left(\frac{\dot{\epsilon}_r - 1}{\dot{\epsilon}_r}\right) \ln\left(\frac{b}{a}\right) \tag{9-16}$$

$$Q = (\dot{\mu}_r - 1) \ln\left(\frac{b}{a}\right) \tag{9-17}$$

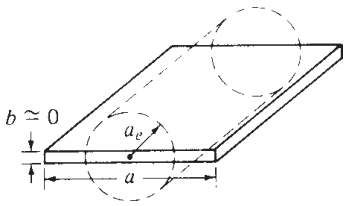
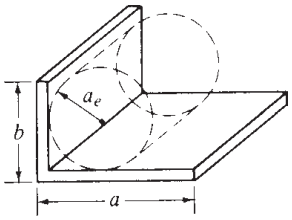
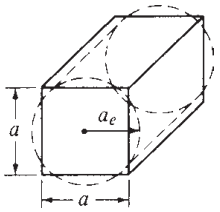
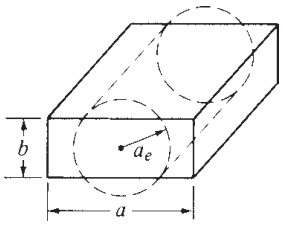
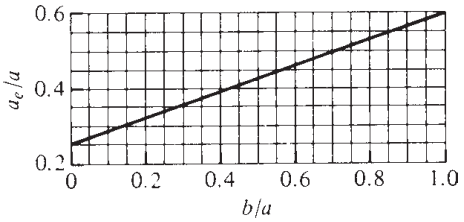
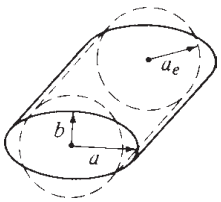
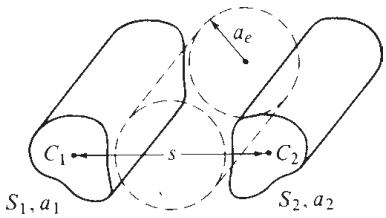
where

$\dot{\epsilon}_r$ = relative (to the ambient medium) complex permittivity
$\dot{\mu}_r$ = relative (to the ambient medium) complex permeability
a = radius of the conducting wire
$b - a$ = thickness of coating

In general:

1. Increasing the real part of either P or Q
   a. increases the peak input admittance
   b. increases the electrical length (lowers the resonant frequency)
   c. narrows the bandwidth
2. Increasing the imaginary part of P or Q
   a. decreases the peak input admittance
   b. decreases the electrical length (increases the resonant frequency)
   c. increases the bandwidth
   d. accentuates the power dissipated (decreases the radiation efficiency)
   e. accentuates the traveling wave component of the current distribution

TABLE 9.3 Conductor Geometrical Shapes and their Equivalent Circular Cylinder Radii

Geometrical Shape	Electrical Equivalent Radius
	$a_e = 0.25a$
	$a_e \simeq 0.2(a + b)$
	$a_e = 0.59a$
	
	$a_e = \frac{1}{2}(a + b)$
	$\ln a_e \simeq \frac{1}{(S_1 + S_2)^2}$ $\times [S_1^2 \ln a_1 + S_2^2 \ln a_2 + 2S_1 S_2 \ln s]$ S_1, S_2 = peripheries of conductors C_1, C_2 a_1, a_2 = equivalent radii of conductors C_1, C_2

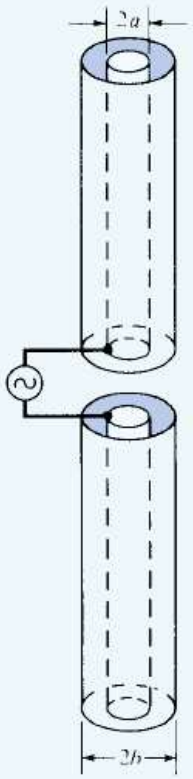


Figure 9.13 Coated linear dipole.

Thus the optimum bandwidth of the antenna can be achieved by choosing a lossy dielectric material with maximum imaginary parts of P and Q and minimum real parts. However, doing this decreases the radiation efficiency. In practice, a trade-off between bandwidth and efficiency is usually required. This is not a very efficient technique to broadband the antenna.

9.5 FOLDED DIPOLE

To achieve good directional pattern characteristics and at the same time provide good matching to practical coaxial lines with 50- or 75-ohm characteristic impedances, the length of a single wire element is usually chosen to be $\lambda/4 \leq l < \lambda$. The most widely used dipole is that whose overall length is $l \simeq \lambda/2$, and which has an input impedance of $Z_{in} \simeq 73 + j42.5$ and directivity of $D_0 \simeq 1.643$. In practice, there are other very common transmission lines whose characteristic impedance is much higher than 50 or 75 ohms. For example, a "twin-lead" transmission line (usually two parallel wires separated by about $\frac{5}{16}$ in. and embedded in a low-loss plastic material used for support and spacing) is widely used for TV applications and has a characteristic impedance of about 300 ohms.

In order to provide good matching characteristics, variations of the single dipole element must be used. One simple geometry that can achieve this is a folded wire which forms a very thin ($s \ll \lambda$) rectangular loop as shown in Figure 9.14(a). This antenna, when the spacing between the two larger sides is very small (usually $s < 0.05\lambda$), is known as a *folded dipole* and it serves as a step-up impedance transformer (approximately by a factor of 4 when $l = \lambda/2$) of the single-element impedance. Thus

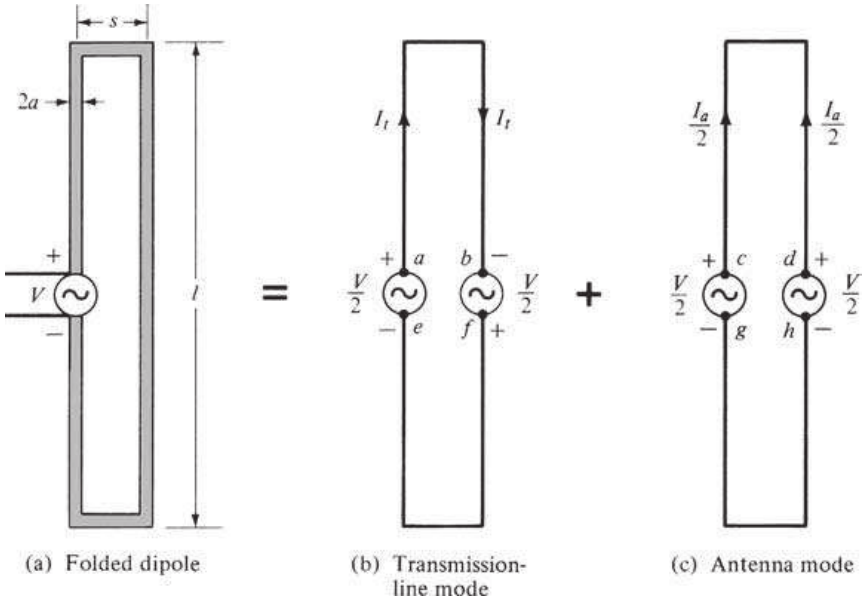


Figure 9.14 Folded dipole and its equivalent transmission-line and antenna mode models. (SOURCE: G. A. Thiele, E. P. Ekelman, Jr., and L. W. Henderson, "On the Accuracy of the Transmission Line Model for Folded Dipole," *IEEE Trans. Antennas Propagat.*, Vol. AP-28, No. 5, pp. 700–703, September 1980. © (1980) IEEE).

when $l = \lambda/2$ and the antenna is resonant, impedances on the order of about 300 ohms can be achieved, and it would be ideal for connections to "twin-lead" transmission lines.

A folded dipole operates basically as a balanced system, and it can be analyzed by assuming that its current is decomposed into two distinct modes: a transmission-line mode [Figure 9.14(b)] and an antenna mode [Figure 9.14(c)]. This type of an analytic model can be used to predict accurately the input impedance provided the longer parallel wires are close together electrically ($s \ll \lambda$).

To derive an equation for the input impedance, let us refer to the modeling of Figure 9.14. For the transmission-line mode of Figure 9.14(b), the input impedance at the terminals $a - b$ or $e - f$, looking toward the shorted ends, is obtained from the impedance transfer equation

$$Z_t = Z_0 \left[\frac{Z_L + jZ_0 \tan(kl')}{Z_0 + jZ_L \tan(kl')} \right]_{\substack{l'=l/2 \\ Z_L=0}} = jZ_0 \tan\left(k\frac{l}{2}\right) \tag{9-18}$$

where Z_0 is the characteristic impedance of a two-wire transmission line

$$Z_0 = \frac{\eta}{\pi} \cosh^{-1}\left(\frac{s/2}{a}\right) = \frac{\eta}{\pi} \ln\left[\frac{s/2 + \sqrt{(s/2)^2 - a^2}}{a}\right] \tag{9-19}$$

which can be approximated for $s/2 \gg a$ by

$$Z_0 = \frac{\eta}{\pi} \ln\left[\frac{s/2 + \sqrt{(s/2)^2 - a^2}}{a}\right] \simeq \frac{\eta}{\pi} \ln\left(\frac{s}{a}\right) = 0.733\eta \log_{10}\left(\frac{s}{a}\right) \tag{9-19a}$$

Since the voltage between the points a and b is $V/2$, and it is applied to a transmission line of length $l/2$, the transmission-line current is given by

$$I_t = \frac{V/2}{Z_t} \tag{9-20}$$

For the antenna mode of Figure 9.14(c), the generator points $c-d$ and $g-h$ are each at the same potential and can be connected, without loss of generality, to form a dipole. Each leg of the dipole is formed by a pair of closely spaced wires ($s \ll \lambda$) extending from the feed ($c-d$ or $g-h$) to the shorted end. Thus the current for the antenna mode is given by

$$I_a = \frac{V/2}{Z_d} \tag{9-21}$$

where Z_d is the input impedance of a linear dipole of length l and diameter d computed using (8-60a)–(8-61b). For the configuration of Figure 9.14(c), the radius that is used to compute Z_d for the dipole can be either the half-spacing between the wires ($s/2$) or an equivalent radius a_e. The equivalent radius a_e is related to the actual wire radius a by (from Table 9.3)

$$\ln(a_e) = \frac{1}{2}\ln(a) + \frac{1}{2}\ln(s) = \ln(a) + \frac{1}{2}\ln\left(\frac{s}{a}\right) = \ln\sqrt{as} \tag{9-22}$$

or

$$a_e = \sqrt{as} \tag{9-22a}$$

It should be expected that the equivalent radius yields the most accurate results.

The total current on the feed leg (left side) of the folded dipole of Figure 9.12(a) is given by

$$I_{in} = I_t + \frac{I_a}{2} = \frac{V}{2Z_t} + \frac{V}{4Z_d} = \frac{V(2Z_d + Z_t)}{4Z_t Z_d} \tag{9-23}$$

1 and the input impedance at the feed by

$$\boxed{Z_{in} = \frac{V}{I_{in}} = \frac{2Z_t(4Z_d)}{2Z_t + 4Z_d} = \frac{4Z_t Z_d}{2Z_d + Z_t}} \tag{9-24}$$

Based on (9-24), the folded dipole behaves as the equivalent of Figure 9.15(a) in which the antenna mode impedance is stepped up by a ratio of four. The transformed impedance is then placed in shunt with twice the impedance of the nonradiating (transmission-line) mode to result in the input impedance.

When $l = \lambda/2$, it can be shown that (9-24) reduces to

$$\boxed{Z_{in} = 4Z_d} \tag{9-25}$$

or that the impedance of the folded dipole is four times greater than that of an isolated dipole of the same length as one of its sides. This is left as an exercise for the reader (Prob. 9.9).

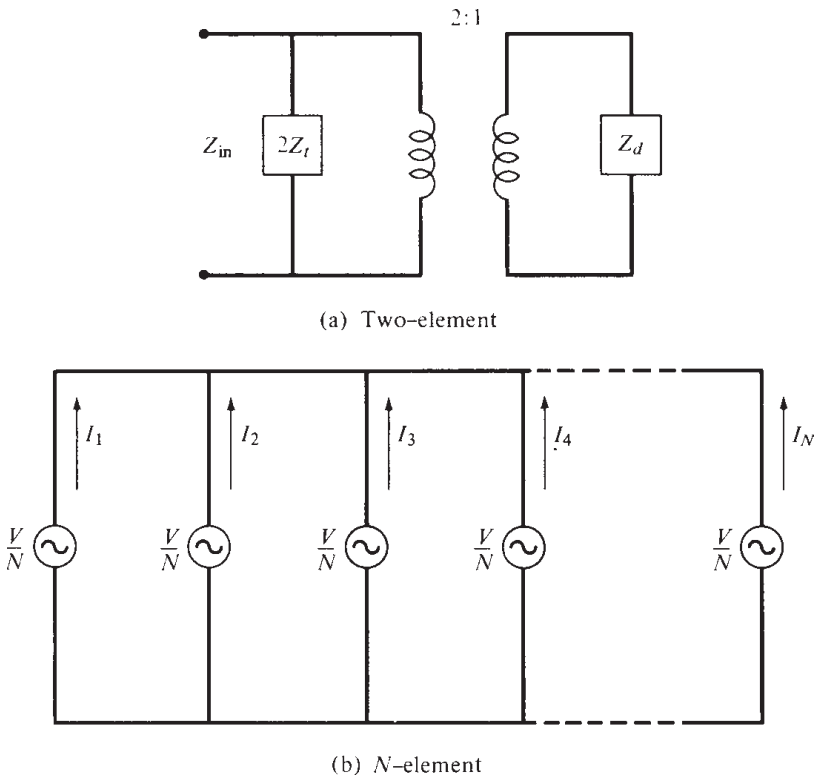


Figure 9.15 Equivalent circuits for two-element and N-element (with equal radii elements) folded dipoles.

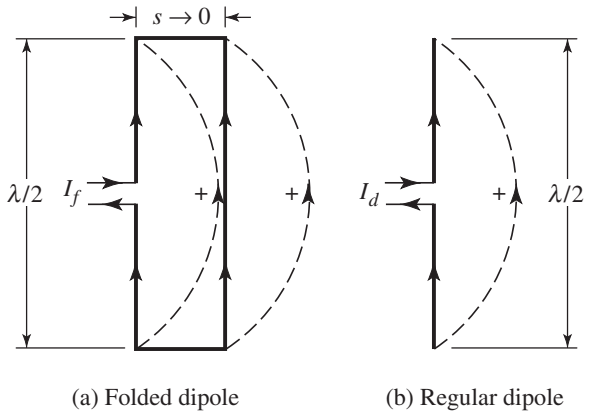


Figure 9.16 Folded dipole and equivalent regular dipole.

The impedance relation of (9-25) for the $l = \lambda/2$ can also be derived by referring to Figure 9.16. Since for a folded dipole the two vertical arms are closely spaced ($s \ll \lambda$), the current distribution in each is identical as shown in Figure 9.16(a). The equivalent of the folded dipole of Figure 9.16(a) is the ordinary dipole of Figure 9.16(b). Comparing the folded dipole to the ordinary dipole, it is apparent that the currents of the two closely spaced and identical arms of the folded dipole are equal to the one current of the ordinary dipole, or

$$2I_f = I_d \tag{9-26}$$

EX2042
Page 477 of 1072

where I_f is the current of the folded dipole and I_d is the current of the ordinary dipole. Also the input power of the two dipoles are identical, or

$$P_f \equiv \frac{1}{2} I_f^2 Z_f = P_d \equiv \frac{1}{2} I_d^2 Z_d \tag{9-27}$$

Substituting (9-26) into (9-27) leads to

$$Z_f = 4Z_d \tag{9-28}$$

where Z_f is the impedance of the folded dipole while Z_d is the impedance of the ordinary dipole. Equation (9-28) is identical to (9-25).

To better understand the impedance transformation of closely spaced conductors (of equal diameter) and forming a multielement folded dipole, let us refer to its equivalent circuit in Figure 9.15(b). For N elements, the equivalent voltage at the center of each conductor is V/N and the current in each is $I_n, n = 1, 2, 3, \ldots, N$. Thus the voltage across the first conductor can be represented by

$$\frac{V}{N} = \sum_{n=1}^{N} I_n Z_{1n} \tag{9-29}$$

where Z_{1n} represents the self or mutual impedance between the first and nth element. Because the elements are closely spaced

$$I_n \simeq I_1 \quad \text{and} \quad Z_{1n} \simeq Z_{11} \tag{9-30}$$

for all values of $n = 1, 2, \ldots, N$. Using (9-30), we can write (9-29) as

$$\frac{V}{N} = \sum_{n=1}^{N} I_n Z_{1n} \simeq I_1 \sum_{n=1}^{N} Z_{1n} \simeq N I_1 Z_{11} \tag{9-31}$$

or

$$\boxed{Z_{in} = \frac{V}{I_1} \simeq N^2 Z_{11} = N^2 Z_r} \tag{9-31a}$$

since the self-impedance Z_{11} of the first element is the same as its impedance Z_r in the absence of the other elements. Additional impedance step-up of a single dipole can be obtained by introducing more elements. For a three-element folded dipole with elements of identical diameters and of $l \simeq \lambda/2$, the input impedance would be about nine times greater than that of an isolated element or about 650 ohms. Greater step-up transformations can be obtained by adding more elements; in practice, they are seldom needed. Many other geometrical configurations of a folded dipole can be obtained which would contribute different values of input impedances. Small variations in impedance can be obtained by using elements of slightly different diameters and/or lengths.

To test the validity of the transmission-line model for the folded dipole, a number of computations were made [12] and compared with data obtained by the Moment

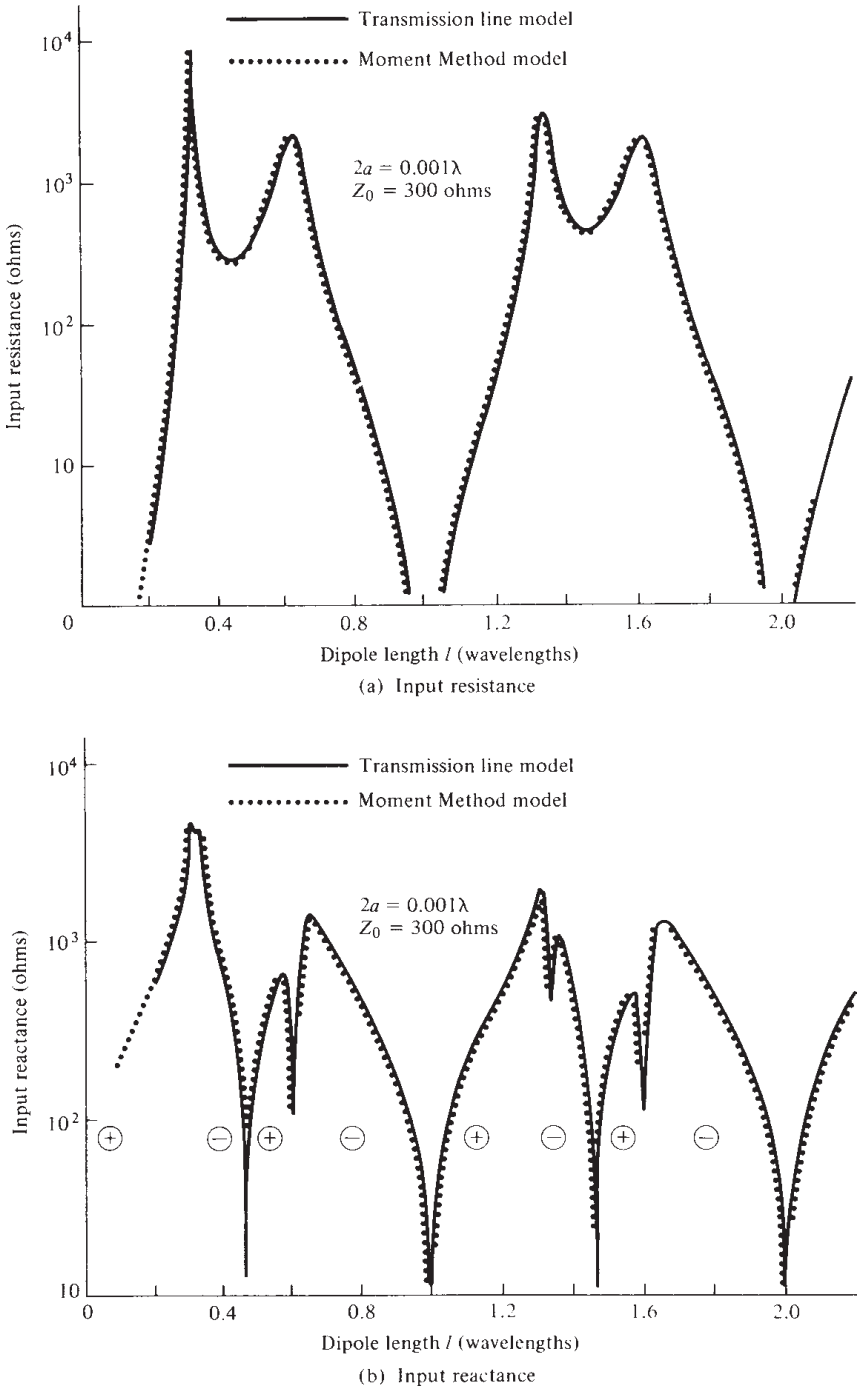


Figure 9.17 Input resistance and reactance of folded dipole. (SOURCE: G. A. Thiele, E. P. Ekelman, Jr., and L. W. Henderson, "On the Accuracy of the Transmission Line Model for Folded Dipole," *IEEE Trans. Antennas Propagat.*, Vol. AP-28, No. 5, pp. 700–703, September 1980. © (1980) IEEE).

Method, which is considered to be more accurate. In Figures 9.17(a) and (b) the input resistance and reactance for a two-element folded dipole is plotted as a function of l/λ when the diameter of each wire is $d = 2a = 0.001\lambda$ and the spacing between the elements is $s = 0.00613\lambda$. The characteristic impedance of such a transmission line is 300 ohms. The equivalent radius was used in the calculations of Z_d. An

excellent agreement is indicated between the results of the transmission-line model and the Moment Method. Computations and comparisons for other spacings ($s = 0.0213\lambda$, $Z_0 = 450$ ohms and $s = 0.0742\lambda$, $Z_0 = 600$ ohms) but with elements of the same diameter ($d = 0.001\lambda$) have been made [12]. It has been shown that as the spacing between the wires increased, the results of the transmission-line mode began to disagree with those of the Moment Method. For a given spacing, the accuracy for the characteristic impedance, and in turn for the input impedance, can be improved by increasing the diameter of the wires. The characteristic impedance of a transmission line, as given by (9-19) or (9-19a), depends not on the spacing but on the spacing-to-diameter (*s/d*) ratio, which is more accurate for smaller *s/d*. Computations were also made whereby the equivalent radius was not used. The comparisons of these results indicated larger disagreements, thus concluding the necessity of the equivalent radius, especially for the larger wire-to-wire spacings.

A two-element folded dipole is widely used, along with "twin-lead" line, as feed element of TV antennas such as Yagi-Uda antennas. Although the impedance of an isolated folded dipole may be around 300 ohms, its value will be somewhat different when it is used as an element in an array or with a reflector. The folded dipole has better bandwidth characteristics than a single dipole of the same size. Its geometrical arrangement tends to behave as a short parallel stub line which attempts to cancel the off resonance reactance of a single dipole. The folded dipole can be thought to have a bandwidth which is the same as that of a single dipole but with an equivalent radius ($a < a_e < s/2$).

Symmetrical and asymmetrical planar folded dipoles can also be designed and constructed using strips which can be fabricated using printed-circuit technology [13]. The input impedance can be varied over a wide range of values by adjusting the width of the strips. In addition, the impedance can be adjusted to match the characteristic impedance of printed-circuit transmission lines with four-to-one impedance ratios.

A MATLAB computer program, entitled ***Folded***, has been developed to perform the design of a folded dipole. The description of the program is found in the corresponding READ ME file included in the CD attached to the book.

9.6 DISCONE AND CONICAL SKIRT MONOPOLE

There are innumerable variations to the basic geometrical configurations of cones and dipoles, some of which have already been discussed, to obtain broadband characteristics. Two other common radiators that meet this characteristic are the conical skirt monopole and the discone antenna [14] shown in Figures 9.18(a) and (b), respectively.

For each antenna, the overall pattern is essentially the same as that of a linear dipole of length $l < \lambda$ (i.e., a solid of revolution formed by the rotation of a figure-eight) whereas in the horizontal (azimuthal) plane it is nearly omnidirectional. The polarization of each is vertical. Each antenna because of its simple mechanical design, ease of installation, and attractive broadband characteristics has wide applications in the VHF (30–300 MHz) and UHF (300 MHz–3 GHz) spectrum for broadcast, television, and communication applications.

The discone antenna is formed by a disk and a cone. The disk is attached to the center conductor of the coaxial feed line, and it is perpendicular to its axis. The cone is connected at its apex to the outer shield of the coaxial line. The geometrical dimensions and the frequency of operation of two designs [14] are shown in Table 9.4.

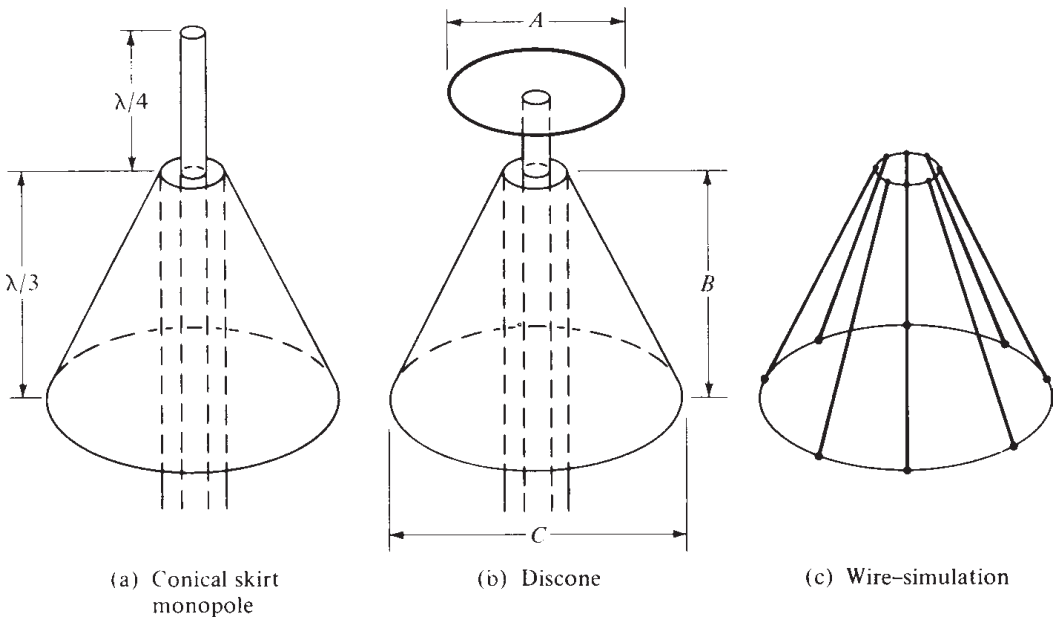


Figure 9.18 Conical skirt monopole, discone, and wire-simulated cone surface.

TABLE 9.4 Frequency and Dimensions of Two Designs

Frequency (MHz)	*A* (cm)	*B* (cm)	*C* (cm)
90	45.72	60.96	50.80
200	22.86	31.75	35.56

In general, the impedance and pattern variations of a discone as a function of frequency are much less severe than those of a dipole of fixed length l. The performance of this antenna as a function of frequency is similar to a high-pass filter. Below an effective cutoff frequency it becomes inefficient, and it produces severe standing waves in the feed line. At cutoff, the slant height of the cone is approximately $\lambda/4$.

Measured elevation (vertical) plane radiation patterns from 250 to 650 MHz, at 50-MHz intervals, have been published [14] for a discone with a cutoff frequency of 200 MHz. No major changes in the "figure-eight" shape of the patterns were evident other than at the high-frequency range where the pattern began to turn downward somewhat.

The conical skirt monopole is similar to the discone except that the disk is replaced by a monopole of length usually $\lambda/4$. Its general behavior also resembles that of the discone. Another way to view the conical skirt monopole is with a $\lambda/4$ monopole mounted above a finite ground plane. The plane has been tilted downward to allow more radiation toward and below the horizontal plane.

To reduce the weight and wind resistance of the cone, its solid surface can be simulated by radial wires, as shown in Figure 9.18(c). This is a usual practice in the simulation of finite size ground planes for monopole antennas. The lengths of the wires used to simulate the ground plane are on the order of about $\lambda/4$ or greater.

EX2042
Page 481 of 1072

9.7 MATCHING TECHNIQUES

The operation of an antenna system over a frequency range is not completely dependent upon the frequency response of the antenna element itself but rather on the frequency characteristics of the transmission line–antenna element combination. In practice, the characteristic impedance of the transmission line is usually real whereas that of the antenna element is complex. Also the variation of each as a function of frequency is not the same. Thus efficient coupling-matching networks must be designed which attempt to couple-match the characteristics of the two devices over the desired frequency range.

There are many coupling-matching networks that can be used to connect the transmission line to the antenna element and which can be designed to provide acceptable frequency characteristics. Only a limited number will be introduced here.

9.7.1 Stub-Matching

Ideal matching at a given frequency can be accomplished by placing a short- or open-circuited shunt stub a distance s from the transmission-line–antenna element connection, as shown in Figure 9.19(a). Assuming a real characteristic impedance, the length s is controlled so as to make the real part of the antenna element impedance equal to the characteristic impedance. The length l of the shunt line is varied until the susceptance of the stub is equal in magnitude but opposite in phase to the line input susceptance at the point of the transmission line–shunt element connection. The matching procedure is illustrated best graphically with the use of a Smith chart. Analytical methods, on which the Smith chart graphical solution is based, can also be used. The short-circuited stub is more practical because an equivalent short can be created by a pin connection in a coaxial cable or a slider in a waveguide. This preserves the overall length of the stub line for matchings which may require longer length stubs.

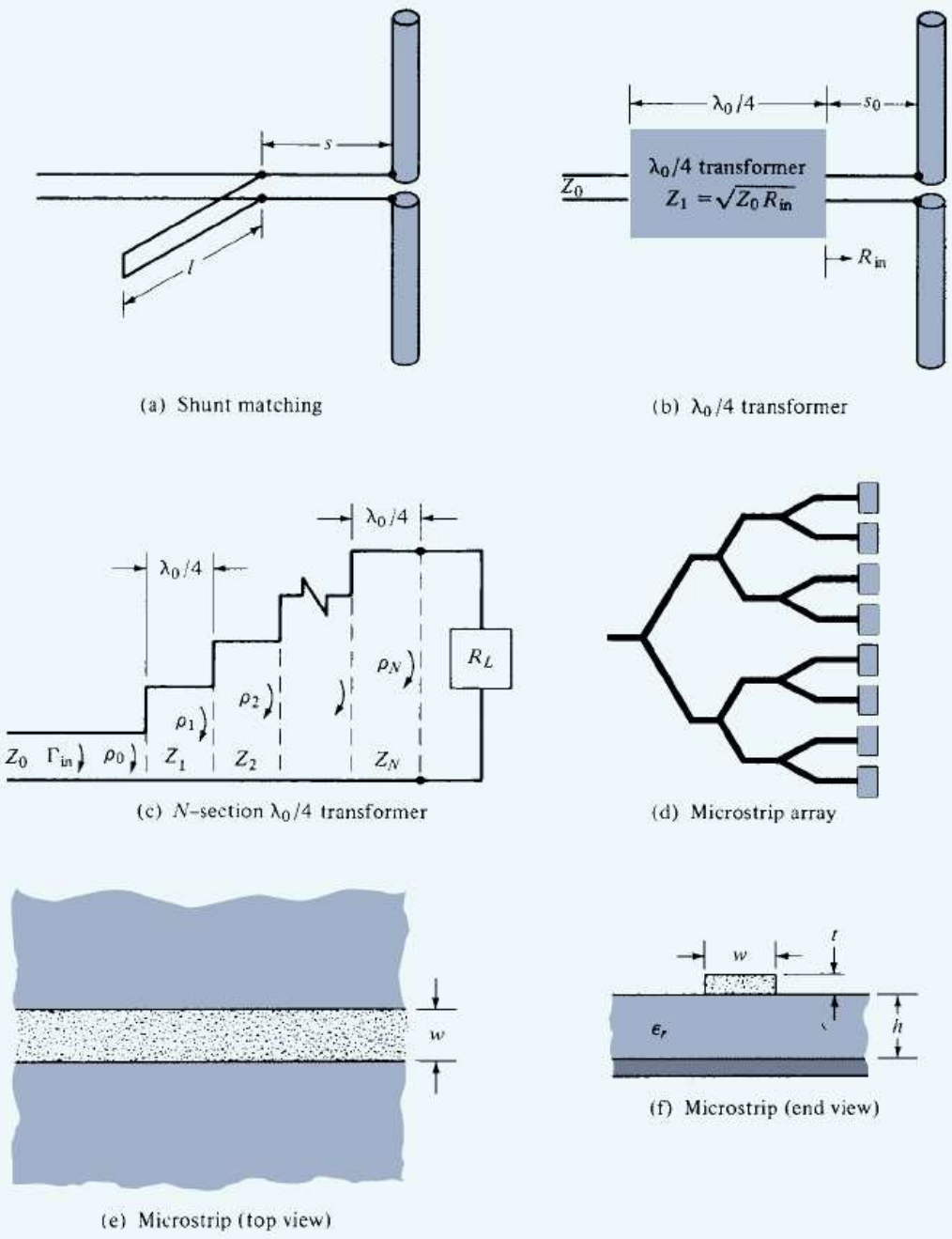
A single stub with a variable length l cannot always match all antenna (load) impedances. A double-stub arrangement positioned a fixed distance s from the load, with the length of each stub variable and separated by a constant length d, will match a greater range of antenna impedances. However, a triple-stub configuration will always match all loads.

Excellent treatments of the analytical and graphical methods for the single-, double-, triple-stub, and other matching techniques are presented in [15] and [16]. The higher-order stub arrangements provide more broad and less sensitive matchings (to frequency variations) but are more complex to implement. Usually a compromise is chosen, such as the double-stub.

9.7.2 Quarter-Wavelength Transformer

A. Single Section

Another technique that can be used to match the antenna to the transmission line is to use a $\lambda/4$ transformer. If the impedance of the antenna is real, the transformer is attached directly to the load. However if the antenna impedance is complex, the transformer is placed a distance s_0 away from the antenna, as shown in Figure 9.19(b). The distance s_0 is chosen so that the input impedance toward the load at s_0 is real and designated as R_{in}. To provide a match, the transformer characteristic impedance Z_1 should be $Z_1 = \sqrt{R_{in} Z_0}$, where Z_0 is the characteristic impedance (real) of the input



(a) Shunt matching

(b) $\lambda_0/4$ transformer

(c) N-section $\lambda_0/4$ transformer

(d) Microstrip array

(e) Microstrip (top view)

(f) Microstrip (end view)

Figure 9.19 Matching and microstrip techniques.

transmission line. The transformer is usually another transmission line with the desired characteristic impedance.

Because the characteristic impedances of most off-the-shelf transmission lines are limited in range and values, the quarter-wavelength transformer technique is most suitable when used with microstrip transmission lines. In microstrips, the characteristic impedance can be changed by simply varying the width of the center conductor.

B. Multiple Sections

Matchings that are less sensitive to frequency variations and that provide broader bandwidths, require multiple $\lambda/4$ sections. In fact the number and characteristic impedance

of each section can be designed so that the reflection coefficient follows, within the desired frequency bandwidth, prescribed variations which are symmetrical about the center frequency. The antenna (load) impedance will again be assumed to be real; if not, the antenna element must be connected to the transformer at a point s_0 along the transmission line where the input impedance is real.

Referring to Figure 9.19(c), the total input reflection coefficient Γ_{in} for an N-section quarter-wavelength transformer with $R_L > Z_0$ can be written approximately as [15]

$$\begin{aligned}\Gamma_{in}(f) &\simeq \rho_0 + \rho_1 e^{-j2\theta} + \rho_2 e^{-j4\theta} + \cdots + \rho_N e^{-j2N\theta} \\ &= \sum_{n=0}^{N} \rho_n e^{-j2n\theta}\end{aligned} \tag{9-32}$$

where

$$\rho_n = \frac{Z_{n+1} - Z_n}{Z_{n+1} + Z_n} \tag{9-32a}$$

$$\theta = k\Delta l = \frac{2\pi}{\lambda}\left(\frac{\lambda_0}{4}\right) = \frac{\pi}{2}\left(\frac{f}{f_0}\right) \tag{9-32b}$$

In (9-32), ρ_n represents the reflection coefficient at the junction of two infinite lines with characteristic impedances Z_n and Z_{n+1}, f_0 represents the designed center frequency, and f the operating frequency. Equation (9-32) is valid provided the ρ_n's at each junction are small ($R_L \simeq Z_0$). If $R_L < Z_0$, the ρ_n's should be replaced by $-\rho_n$'s. For a real load impedance, the ρ_n's and Z_n's will also be real.

For a symmetrical transformer ($\rho_0 = \rho_N$, $\rho_1 = \rho_{N-1}$, etc.), (9-32) reduces to

$$\Gamma_{in}(f) \simeq 2e^{-jN\theta}[\rho_0 \cos N\theta + \rho_1 \cos(N-2)\theta + \rho_2 \cos(N-4)\theta + \cdots] \tag{9-33}$$

The last term in (9-33) should be

$$\rho_{[(N-1)/2]} \cos\theta \quad \text{for } N = \text{odd integer} \tag{9-33a}$$

$$\tfrac{1}{2}\rho_{(N/2)} \quad \text{for } N = \text{even integer} \tag{9-33b}$$

C. Binomial Design

One technique, used to design an N-section $\lambda/4$ transformer, requires that the input reflection coefficient of (9-32) have maximally flat passband characteristics. For this method, the junction reflection coefficients (ρ_n's) are derived using the binomial expansion. Doing this, we can equate (9-32) to

$$\begin{aligned}\Gamma_{in}(f) &= \sum_{n=0}^{N} \rho_n e^{-j2n\theta} = e^{-jN\theta}\frac{R_L - Z_0}{R_L + Z_0}\cos^N(\theta) \\ &= 2^{-N}\frac{R_L - Z_0}{R_L + Z_0}\sum_{n=0}^{N} C_n^N e^{-j2n\theta}\end{aligned} \tag{9-34}$$

where

$$C_n^N = \frac{N!}{(N-n)!n!}, \quad n = 0, 1, 2, \ldots, N \tag{9-34a}$$

From (9-32)

$$\boxed{\rho_n = 2^{-N} \frac{R_L - Z_0}{R_L + Z_0} C_n{}^N} \tag{9-35}$$

For this type of design, the fractional bandwidth $\Delta f/f_0$ is given by

$$\boxed{\frac{\Delta f}{f_0} = 2\frac{(f_0 - f_m)}{f_0} = 2\left(1 - \frac{f_m}{f_0}\right) = 2\left(1 - \frac{2}{\pi}\theta_m\right)} \tag{9-36}$$

Since

$$\theta_m = \frac{2\pi}{\lambda_m}\left(\frac{\lambda_0}{4}\right) = \frac{\pi}{2}\left(\frac{f_m}{f_0}\right) \tag{9-37}$$

(9-36) reduces using (9-34) to

$$\boxed{\frac{\Delta f}{f_0} = 2 - \frac{4}{\pi}\cos^{-1}\left[\frac{\rho_m}{(R_L - Z_0)/(R_L + Z_0)}\right]^{1/N}} \tag{9-38}$$

where ρ_m is the maximum value of reflection coefficient which can be tolerated within the bandwidth.

The usual design procedure is to specify the

1. load impedance (R_L)
2. input characteristic impedance (Z_0)
3. number of sections (N)
4. maximum tolerable reflection coefficient (ρ_m) [or fractional bandwidth ($\Delta f/f_0$)]

and to find the

1. characteristic impedance of each section
2. fractional bandwidth [or maximum tolerable reflection coefficient (ρ_m)]

To illustrate the principle, let us consider an example.

Example 9.1

A linear dipole with an input impedance of $70 + j37$ is connected to a 50-ohm line. Design a two-section $\lambda/4$ binomial transformer by specifying the characteristic impedance of each section to match the antenna to the line at $f = f_0$. If the input impedance (at the point the transformer is connected) is assumed to remain constant as a function of frequency, determine the maximum reflection coefficient and VSWR within a fractional bandwidth of 0.375.

Solution: Since the antenna impedance is not real, the antenna must be connected to the transformer through a transmission line of length s_0. Assuming a 50-ohm characteristic impedance for that section of the transmission line, the input impedance at $s_0 = 0.062\lambda$ is real and equal to 100 ohms. Using (9-34a) and (9-35)

$$\rho_n = 2^{-N}\frac{R_L - Z_0}{R_L + Z_0}C_n{}^N = 2^{-N}\frac{R_L - Z_0}{R_L + Z_0}\frac{N!}{(N-n)!n!}$$

which for $N = 2$, $R_L = 100$, $Z_0 = 50$

$$n = 0: \quad \rho_0 = \frac{Z_1 - Z_0}{Z_1 + Z_0} = \frac{1}{12} \Rightarrow Z_1 = 1.182Z_0 = 59.09$$

$$n = 1: \quad \rho_1 = \frac{Z_2 - Z_1}{Z_2 + Z_1} = \frac{1}{6} \Rightarrow Z_2 = 1.399Z_1 = 82.73$$

For a fractional bandwidth of 0.375 ($\theta_m = 1.276$ rad $= 73.12°$) we can write, using (9-38)

$$\frac{\Delta f}{f_0} = 0.375 = 2 - \frac{4}{\pi}\cos^{-1}\left[\frac{\rho_m}{(R_L - Z_0)/(R_L + Z_0)}\right]^{1/2}$$

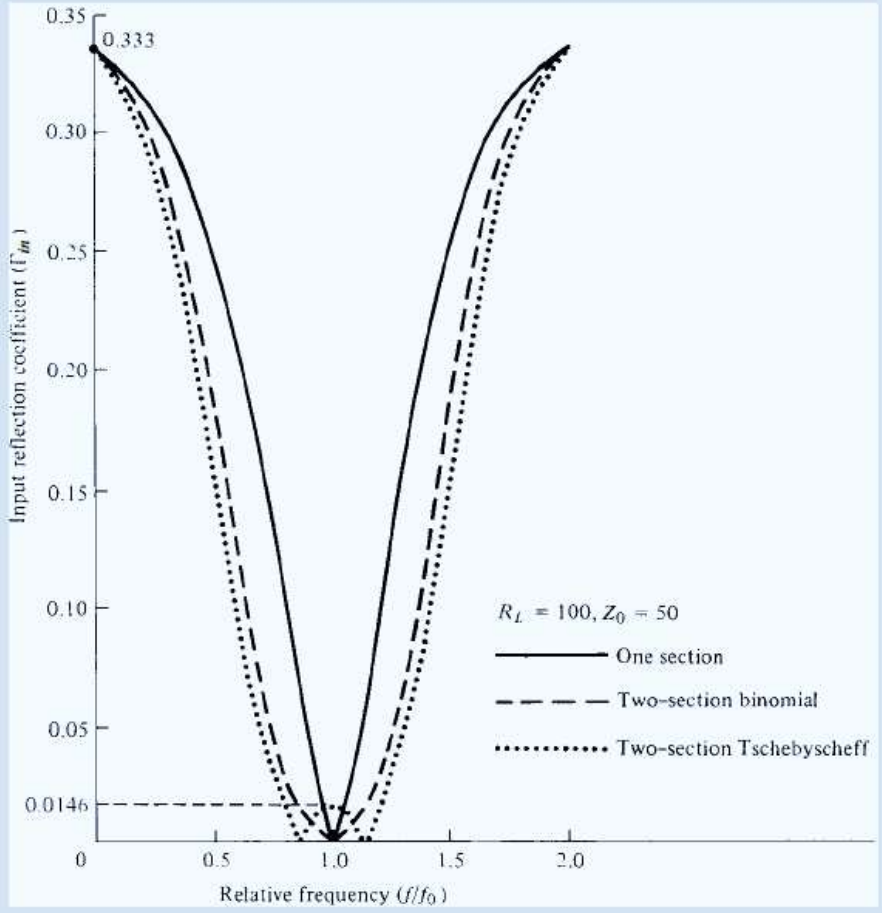


Figure 9.20 Responses of single-section, and two-section binomial and Tschebyscheff quarter-wavelength transformers.

which for $R_L = 100$ and $Z_0 = 50$ gives

$$\rho_m = 0.028$$

The maximum voltage standing wave ratio is

$$\text{VSWR}_m = \frac{1+\rho_m}{1-\rho_m} = 1.058$$

The magnitude of the reflection coefficient is given by (9-34) as

$$|\Gamma_{in}| = \rho_{in} = \left|\frac{R_L - Z_0}{R_L + Z_0}\right| \cos^2\theta = \frac{1}{3}\cos^2\left[\frac{2\pi}{\lambda}\left(\frac{\lambda_0}{4}\right)\right] = \frac{1}{3}\cos^2\left[\frac{\pi}{2}\left(\frac{f}{f_0}\right)\right]$$

which is shown plotted in Figure 9.20, and it is compared with the response of a single-section $\lambda/4$ transformer.

Microstrip designs are ideally suited for antenna arrays, as shown in Figure 9.19(d). In general the characteristic impedance of a microstrip line, whose top and end views are shown in Figures 9.19(e) and (f), respectively, is given by [17].

$$Z_c = \frac{87}{\sqrt{\epsilon_r + 1.41}} \ln\left(\frac{5.98h}{0.8w + t}\right) \qquad \text{for } h < 0.8w \tag{9-39}$$

where

ϵ_r = dielectric constant of dielectric substrate (board material)
h = height of substrate
w = width of microstrip center conductor
t = thickness of microstrip center conductor

Thus for constant values of ϵ_r, h, and t, the characteristic impedance can be changed by simply varying the width (w) of the center conductor.

D. Tschebyscheff Design

The reflection coefficient can be made to vary within the bandwidth in an oscillatory manner and have equal-ripple characteristics. This can be accomplished by making Γ_{in} behave according to a Tschebyscheff polynomial. For the Tschebyscheff design, the equation that corresponds to (9-34) is

$$\Gamma_{in}(f) = e^{-jN\theta} \frac{R_L - Z_0}{R_L + Z_0} \frac{T_N(\sec\theta_m \cos\theta)}{T_N(\sec\theta_m)} \tag{9-40}$$

where $T_N(x)$ is the Tschebyscheff polynomial of order N.

The maximum allowable reflection coefficient occurs at the edges of the passband where $\theta = \theta_m$ and $T_N(\sec\theta_m \cos\theta)|_{\theta=\theta_m} = 1$. Thus

$$\rho_m = \left|\frac{R_L - Z_0}{R_L + Z_0} \frac{1}{T_N(\sec\theta_m)}\right| \tag{9-41}$$

or

$$|T_N(\sec\theta_m)| = \left|\frac{1}{\rho_m}\frac{R_L - Z_0}{R_L + Z_0}\right| \tag{9-41a}$$

Using (9-41), we can write (9-40) as

$$\Gamma_{in}(f) = e^{-jN\theta}\rho_m T_N(\sec\theta_m \cos\theta) \tag{9-42}$$

and its magnitude as

$$|\Gamma_{in}(f)| = |\rho_m T_N(\sec\theta_m \cos\theta)| \tag{9-42a}$$

For this type of design, the fractional bandwidth $\Delta f/f_o$ is also given by (9-36).

To be physical, ρ_m is chosen to be

$$\rho_m < \left|\frac{R_L - Z_0}{R_L + Z_0}\right| \Rightarrow |T_N(\sec\theta_m)| > 1 \tag{9-43}$$

The Tschebyscheff polynomial can be represented by either (6-71a) or (6-71b). Since $|T_N(\sec\theta_m)| > 1$, then using (6-71b) we can express it as

$$T_N(\sec\theta_m) = \cosh[N\cosh^{-1}(\sec\theta_m)] \tag{9-44}$$

or using (9-41a) as

$$|T_N(\sec\theta_m)| = |\cosh[N\cosh^{-1}(\sec\theta_m)]| = \left|\frac{1}{\rho_m}\frac{R_L - Z_0}{R_L + Z_0}\right| \tag{9-44a}$$

Thus

$$\sec\theta_m = \cosh\left[\frac{1}{N}\cosh^{-1}\left(\left|\frac{1}{\rho_m}\frac{R_L - Z_0}{R_L + Z_0}\right|\right)\right] \tag{9-45}$$

or

$$\boxed{\theta_m = \sec^{-1}\left\{\cosh\left[\frac{1}{N}\cosh^{-1}\left(\left|\frac{1}{\rho_m}\frac{R_L - Z_0}{R_L + Z_0}\right|\right)\right]\right\}} \tag{9-45a}$$

Using (9-42) we can write the reflection coefficient of (9-33) as

$$\boxed{\begin{aligned}\Gamma_{in}(\theta) &= 2e^{-jN\theta}[\rho_0\cos(N\theta) + \rho_1\cos(N-2)\theta + \cdots] \\ &= e^{-jN\theta}\rho_m T_N(\sec\theta_m\cos\theta)\end{aligned}} \tag{9-46}$$

For a given N, replace $T_N(\sec\theta_m\cos\theta)$ *by its polynomial series expansion of* (6-69) *and then match terms*. The usual procedure for the Tschebyscheff design is the same as that of the binomial as outlined previously.

The first few Tschebyscheff polynomials are given by (6-69). For $z = \sec\theta_m\cos\theta$, the first three polynomials reduce to

$$\begin{aligned}T_1(\sec\theta_m\cos\theta) &= \sec\theta_m\cos\theta \\ T_2(\sec\theta_m\cos\theta) &= 2(\sec\theta_m\cos\theta)^2 - 1 = \sec^2\theta_m\cos 2\theta + (\sec^2\theta_m - 1) \\ T_3(\sec\theta_m\cos\theta) &= 4(\sec\theta_m\cos\theta)^3 - 3(\sec\theta_m\cos\theta) \\ &= \sec^3\theta_m\cos 3\theta + 3(\sec^3\theta_m - \sec\theta_m)\cos\theta\end{aligned} \tag{9-47}$$

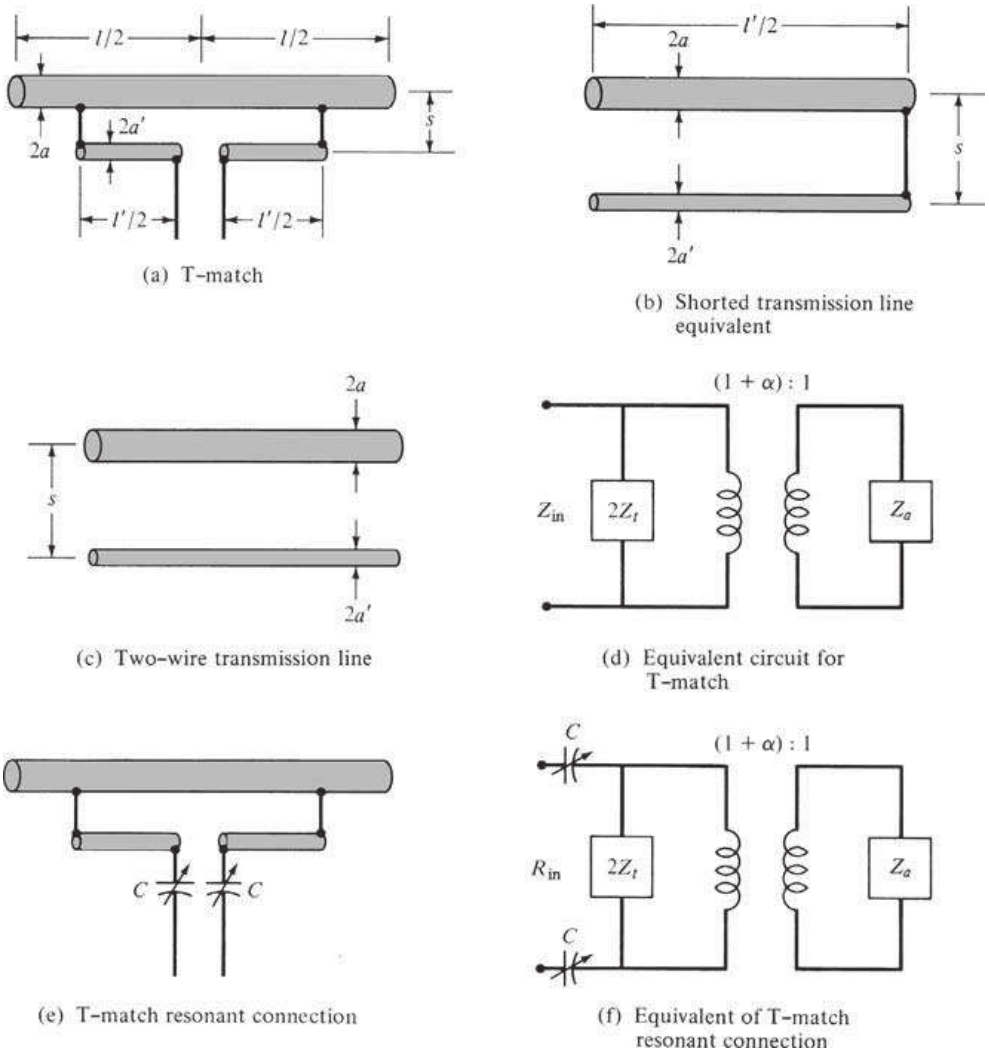


Figure 9.21 T-match and its associated equivalents.

The design of Example 9.1 using a Tschebyscheff transformer is assigned as an exercise to the reader (Prob. 9.19). However its response is shown plotted in Figure 9.20 for comparison.

In general, the multiple sections (either binomial or Tschebyscheff) provide greater bandwidths than a single section. As the number of sections increases, the bandwidth also increases. The advantage of the binomial design is that the reflection coefficient values within the bandwidth monotonically decrease from both ends toward the center. Thus the values are always smaller than an acceptable and designed value that occurs at the "skirts" of the bandwidth. For the Tschebyscheff design, the reflection coefficient values within the designed bandwidth are equal or smaller than an acceptable and designed value. The number of times the reflection coefficient reaches the maximum ripple value within the bandwidth is determined by the number of sections. In fact, for an even number of sections the reflection coefficient at the designed center frequency is equal to its maximum allowable value, while for an odd number of sections it is zero. For a maximum tolerable reflection coefficient, the N-section Tschebyscheff transformer provides a larger bandwidth than a corresponding N-section binomial design,

EX2042
Page 489 of 1072

or for a given bandwidth the maximum tolerable reflection coefficient is smaller for a Tschebyscheff design.

A MATLAB computer program, entitled ***Quarterwave***, has been developed to perform the design of binomial and Tschebyscheff quarter-wavelength impedance transformer designs. The description of the program is found in the corresponding READ ME file included in the CD attached to the book.

9.7.3 T-Match

Another effective shunt-matching technique is the T-match connection shown in Figure 9.21(a). With this method the dipole of length l and radius a is connected to the transmission line by another dipole of length $l'(l' < l)$ and radius a'. The smaller dipole is "tapped" to the larger one at distances $l'/2$ from the center and the two are separated by a small distance s. The transmission line is connected to the smaller dipole at its center. The T-match connection is a general form of a folded dipole since the two legs are usually not of the same length or diameter. Since the T-match is a symmetrical and balanced system, it is well suited for use with parallel-conductor transmission lines such as the "twin lead." Coaxial lines, which are unsymmetrical and unbalanced lines, should be connected to dipoles using the gamma match.

The design procedure for the T-match is developed similarly to that of the folded dipole. The T-match is also modeled by transmission line and antenna modes, as shown in Figure 9.14 for the folded dipole. The total current at the input terminals is divided between the two conductors in a way that depends on the relative radii of the two conductors and the spacing between them. Since the two conductors are not in general of the same radius, the antenna mode current division is not unity. Instead, a current division factor is assigned which also applies to the voltage division of the transmission-line mode.

Instead of including all the details of the analysis, only the steps that are applicable to a T-match design will be included.

A. Design Procedure

1. Calculate the current division factor α by

$$\alpha = \frac{\cosh^{-1}\left(\dfrac{v^2 - u^2 + 1}{2v}\right)}{\cosh^{-1}\left(\dfrac{v^2 + u^2 - 1}{2vu}\right)} \simeq \frac{\ln(v)}{\ln(v) - \ln(u)} \tag{9-48}$$

$$u = \frac{a}{a'} \tag{9-48a}$$

$$v = \frac{s}{a'} \tag{9-48b}$$

2. From Table 9.3, the "equivalent" radius of the two-wire arrangement can be written as

$$\ln(a_e) \simeq \frac{1}{(a' + a)^2}[a'^2 \ln a' + a^2 \ln a + 2a'a \ln s] \tag{9-49}$$

since $S_1 = 2\pi a'$, $S_2 = 2\pi a$. It can be shown that (9-49) reduces to

$$\ln(a_e) \simeq \ln a' + \frac{1}{(1+u)^2}(u^2 \ln u + 2u \ln v) \tag{9-49a}$$

3. Calculate the impedance at the input terminals for the transmission line mode [i.e., two-wire shorted transmission line of length $l'/2$ with radii a, a' and separation s shown in Figure 9.21(b)]

$$Z_t = jZ_0 \tan\left(k\frac{l'}{2}\right) \tag{9-50}$$

where

$$Z_0 = 60 \cosh^{-1}\left(\frac{s^2 - a^2 - a'^2}{2aa'}\right) \simeq 276 \log_{10}\left(\frac{s}{\sqrt{aa'}}\right) \tag{9-50a}$$

Z_0 is the characteristic impedance of the two-wire transmission line with radii a, a' and separation s, as shown in Figure 9.21(c).

4. The total input impedance, which is a combination of the antenna (radiating) and the transmission (nonradiating) modes, can be written as

$$\boxed{Z_{in} = R_{in} + jX_{in} = \frac{2Z_t[(1+\alpha)^2 Z_a]}{2Z_t + (1+\alpha)^2 Z_a}} \tag{9-51}$$

and the input admittance as

$$\boxed{Y_{in} = \frac{1}{Z_{in}} = \frac{Y_a}{(1+\alpha)^2} + \frac{1}{2Z_t}} \tag{9-52}$$

$Z_a = 1/Y_a$ is the center-point free-space input impedance of the antenna in the absence of the T-match connection.

B. Equivalent Circuit

Based upon (9-51) or (9-52), the T-match behaves as the equivalent circuit of Figure 9.21(d) in which the antenna impedance is stepped up by a ratio of $1 + \alpha$, and it is placed in shunt with twice the impedance of the nonradiating mode (transmission line) to result in the input impedance. When the current division factor is unity ($\alpha = 1$), the T-match equivalent of Figure 9.21(d) reduces to that of Figure 9.16(a) for the folded dipole.

For $l' \simeq \lambda/2$, the transmission-line impedance Z_t is much greater than $(1+\alpha)^2 Z_a$ and the input impedance of (9-51) reduces to

$$\boxed{Z_{in} \simeq (1+\alpha)^2 Z_a} \tag{9-53}$$

For two equal radii conductors, the current division factor is unity and (9-53) becomes

$$\boxed{Z_{in} \simeq 4Z_a} \tag{9-54}$$

a relation obtained previously and represented by (9-25).

The impedance of (9-51) is generally complex. Because each of the lengths $(l'/2)$ of the T-match rods are usually selected to be very small (0.03 to 0.06λ), Z_{in} is inductive. To eliminate the reactance (resonate the antenna) at a given center frequency and keep a balanced system, two variable series capacitors are usually used, as shown in Figure 9.21(e). The value of each capacitor is selected so that Z_{in} of (9-51) is equal to $R_{in}(Z_{in} = R_{in})$. To accomplish this

$$\boxed{C = 2C_{in} = \frac{1}{\pi f X_{in}}} \tag{9-55}$$

where f is the center frequency, and C_{in} is the series combination of the two C capacitors. The resonant circuit equivalent is shown in Figure 9.21(f).

The T-match connection of Figure 9.21(e) is used not only to resonate the circuit, but also to make the total input impedance equal to the characteristic impedance of the feed transmission line. This is accomplished by properly selecting the values of $l'/2$ and C (s is not usually varied because the impedance is not very sensitive to it). In most cases, a trial and error procedure is followed. An orderly graphical method using the Smith chart is usually more convenient, and it is demonstrated in the following section for the gamma match.

A MATLAB computer program, entitled ***Tee***, has been developed to perform the design of a T-Match. The description of the program and its contents are found in the corresponding READ ME file in the CD attached to the book.

9.7.4 Gamma Match

Frequently dipole antennas are fed by coaxial cables which are unbalanced transmission lines. A convenient method to connect the dipole or other antennas (Yagi-Uda, log-periodic, etc.) to 50- or 75-ohm "coaxs" and to obtain a match is to use the gamma match arrangement shown in Figure 9.22.

A. Equivalent Circuit

The gamma match is equivalent to half of the T-match, and it also requires a capacitor in series with the gamma rod. The equivalent is shown in Figure 9.22(b), and its input impedance is equal to

$$\boxed{Z_{in} = -jX_c + \frac{Z_g[(1+\alpha)^2 Z_a]}{2Z_g + (1+\alpha)^2 Z_a}} \tag{9-56}$$

where Z_a is the center-point free-space impedance of the antenna in the absence of the gamma match connection. The second term of (9-56) is similar in form to that of (9-51).

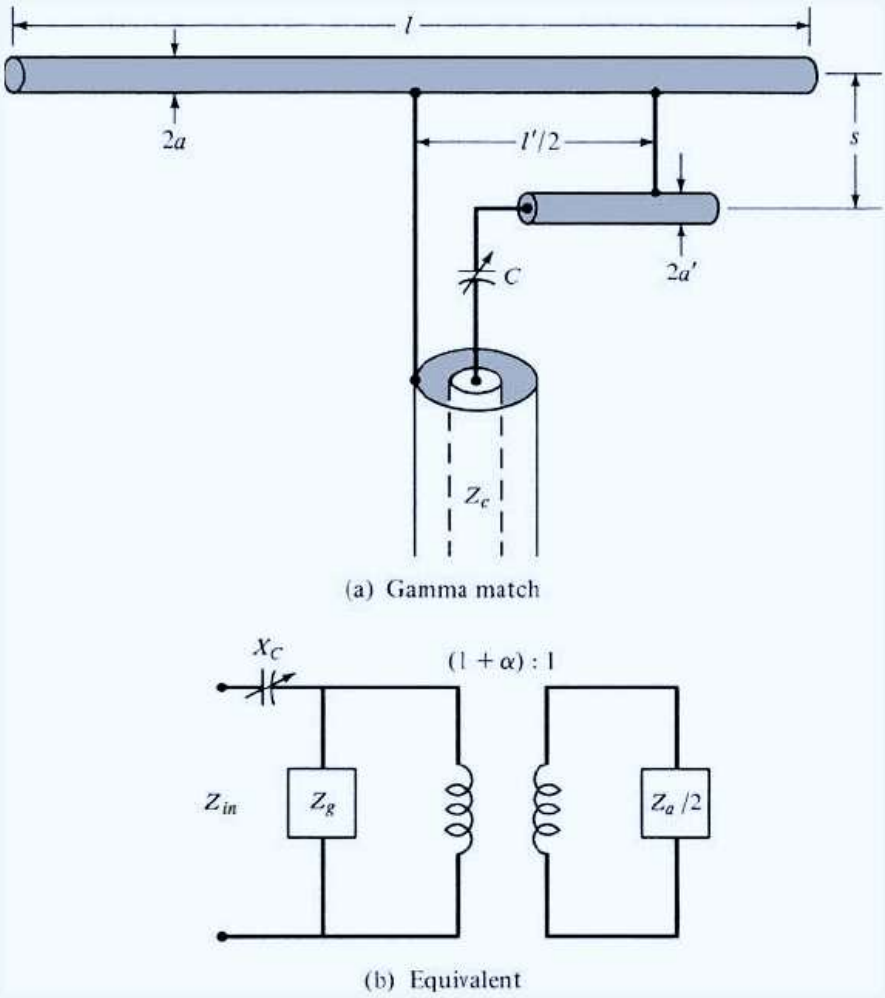


Figure 9.22 Gamma match and its equivalent.

The usual problem encountered is that the length of the wire antenna (l) and the characteristic impedance of the feed coax (Z_c) are known. What is required are the values of the radii a and a', the length $l'/2$, and the capacitance C which will achieve a match. Since the arrangement is similar to the T-match or folded dipole, its analysis is based on the same theory.

To accomplish the match, a graphical design technique, which is different from that reported in [18] and [19], will be demonstrated. This procedure utilizes the Smith chart, and it is based on the equivalent of Figure 9.22(b). A purely mathematical procedure is also available [20], but it will not be included here.

Because the input impedance is not very sensitive to a, a', and s, the usual procedure is to select their values and keep them fixed. The parameters that are usually varied are then $l'/2$ and C. In practice, $l'/2$ is varied by simply using a sliding clamp to perform the shorted connection at the end of the gamma rod.

The graphical design method assumes that $l'/2$ is given, and C that resonates the circuit is found. If the input resistance is not equal to the characteristic impedance Z_c of the feed line, another value of $l'/2$ is selected, and the procedure is repeated until $R_{in} = Z_c$. The graphical method is suggestive as to how the length $l'/2$ should be changed (smaller or larger) to accomplish the match.

B. Design Procedure

1. Determine the current division factor α by using (9-48)–(9-48b).
2. Find the free-space impedance (in the absence of the gamma match) of the driven element at the center point. Designate it as Z_a.
3. Divide Z_a by 2 and multiply it by the step-up ratio $(1+\alpha)^2$. Designate the result as Z_2.

$$Z_2 = R_2 + jX_2 = (1+\alpha)^2 \frac{Z_a}{2} \tag{9-57}$$

4. Determine the characteristic impedance Z_0 of the transmission line formed by the driven element and the gamma rod using (9-50a).
5. Normalize Z_2 of (9-57) by Z_0 and designate it as z_2.

$$z_2 = \frac{Z_2}{Z_0} = \frac{R_2 + jX_2}{Z_0} = r_2 + jx_2 \tag{9-58}$$

and enter on the Smith chart.

6. Invert z_2 of (9-58) and obtain its equivalent admittance $y_2 = g_2 + jb_2$. On the Smith chart this is accomplished by moving z_2 diagonally across from its position.
7. In shunt with the admittance y_2 from step 6 is an inductive reactance due to the short-circuited transmission line formed by the antenna element and the gamma rod. This is an inductive reactance because the length of the gamma rod is very small (usually 0.03 to 0.06λ), but always much smaller than $\lambda/2$. Obtain its normalized value using

$$z_g = j \tan\left(k\frac{l'}{2}\right) \tag{9-59}$$

and place it on the Smith chart. The impedance z_g of (9-59) can also be obtained by using exclusively the Smith chart. You begin by locating the short-circuited load at $Z_s = 0 + j0$. Then you move this point a distance $l'/2$ toward the generator, along the outside perimeter of the Smith chart. The new point represents the normalized impedance z_g of (9-59).

8. Invert the impedance from step 7 (z_g) to obtain its equivalent admittance $y_g = g_g + jb_g$. On the Smith chart this is accomplished by moving z_g diagonally across from its position.
9. Add the two parallel admittances (from steps 6 and 8) to obtain the total input admittance at the gamma feed. That is,

$$y_{in} = y_2 + y_g = (g_2 + g_g) + j(b_2 + b_g) \tag{9-60}$$

and locate it on the Smith chart.

10. Invert the normalized input admittance y_{in} of (9-60) to obtain the equivalent normalized input impedance

$$z_{in} = r_{in} + jx_{in} \tag{9-61}$$

11. Obtain the unnormalized input impedance by multiplying z_{in} by Z_0.

$$Z_{in} = R_{in} + jX_{in} = Z_0 z_{in} \tag{9-62}$$

12. Select the capacitor C so that its reactance is equal in magnitude to X_{in}.

$$\frac{1}{\omega C} = \frac{1}{2\pi f_0 C} = X_{in} \tag{9-63}$$

If all the dimensions were chosen properly for a perfect match, the real part R_{in} of (9-62) should be equal to Z_c. If not, change one or more of the dimensions (usually the length of the rod) and repeat the procedure until $R_{in} = Z_c$. Practically the capacitor C is chosen to be variable so adjustments can be made with ease to obtain the best possible match.

Example 9.2

The driven element impedance of a 20-m ($f \simeq 15$ MHz; see Appendix IX.3) Yagi-Uda antenna has a free-space impedance at its center point of $30.44(1 - j)$ ohms [19]. It is desired to connect it to a 50-ohm coaxial line using a gamma match. The driven element and the gamma rod are made of tubing with diameters of $0.95\times10^{-3}\lambda$(0.75 in. = 1.905 cm) and $3.175\times10^{-4}\lambda$(0.25 in. = 0.635 cm), respectively. The center-to-center separation between the driven element and the rod is $3.81\times10^{-3}\lambda$(3 in. = 7.62 cm). Determine the required capacitance to achieve a match. Begin with a gamma rod length of 0.036λ(28.35 in. = 72.01 cm).

Solution:

1. Using (9-48)–(9-48b)

$$u = \frac{a}{a'} = 3 \qquad v = \frac{s}{a'} = \frac{3.81}{0.15875} = 24$$

$$\alpha \simeq \frac{\ln(24)}{\ln(24) - \ln(3)} = 1.528$$

and the step-up ratio

$$(1 + \alpha)^2 = (1 + 1.528)^2 = 6.39$$

2. $Z_a = 30.44(1 - j)$, as given.
3. Using (9-57)

$$Z_2 = (1 + 1.528)^2 \frac{30.44(1 - j)}{2} = 97.25(1 - j)$$

4. $Z_0 = 276 \log_{10}\left[\dfrac{2(3.81)}{\sqrt{0.95(0.3175)}}\right] = 315.25 \simeq 315$

5. $z_2 = \dfrac{97.25}{315}(1 - j) = 0.31(1 - j)$
6. On the Smith chart in Figure 9.23 locate z_2 and invert it to y_2. It leads to

$$y_2 = \frac{1}{z_2} = 1.6(1 + j)$$

7. On the Smith chart locate $z_s = 0 + j0$ and advance it toward the generator a distance 0.036λ to obtain

$$z_g = 0 + j0.23$$

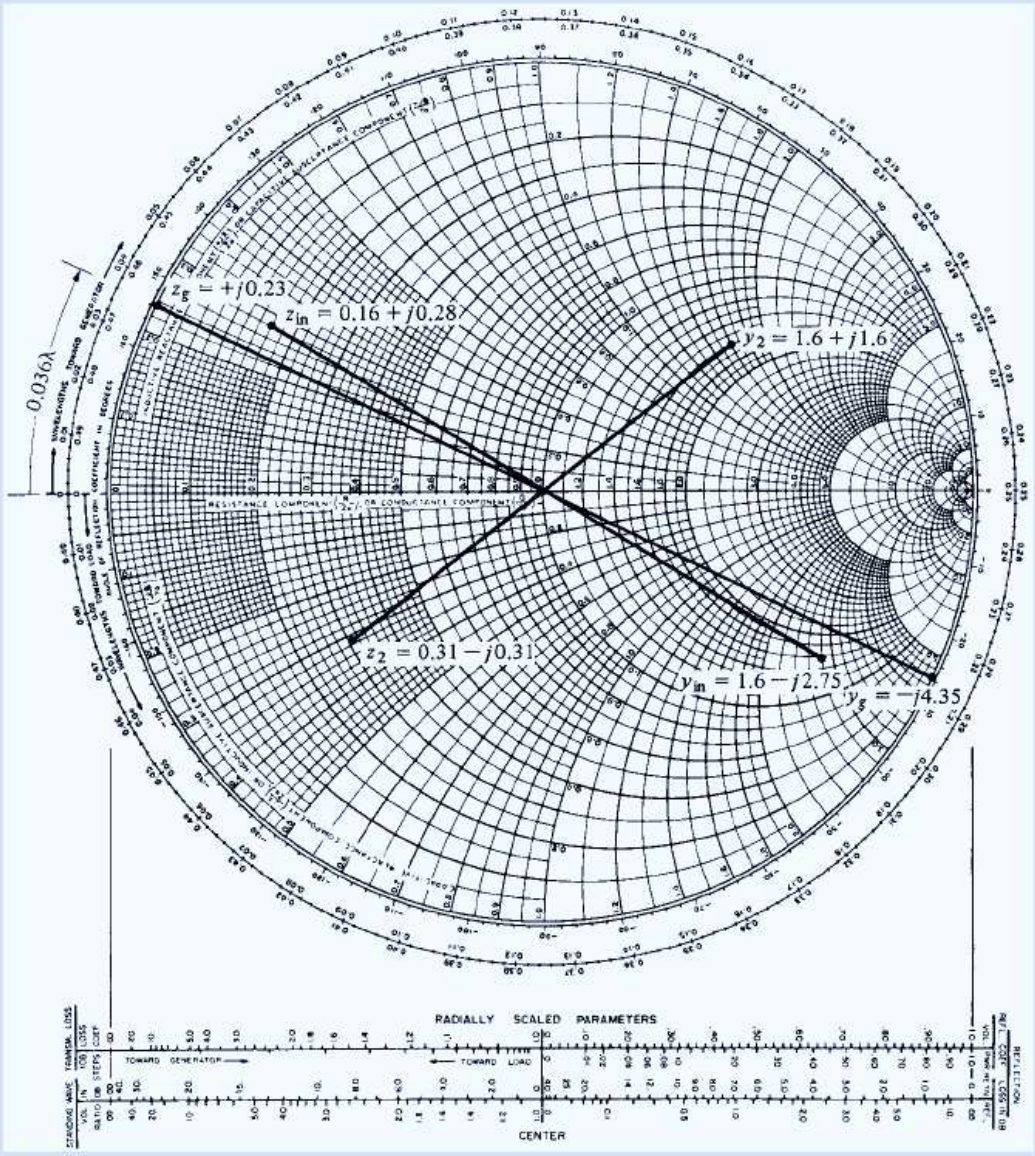


Figure 9.23 Smith chart for Example 9.2. Copyright renewal 1976 by P. H. Smith, Murray Hill, N.J.

8. From the Smith chart
$$y_g = \frac{1}{z_g} = -j4.35$$
9. Add y_2 and y_g
$$y_{in} = y_2 + y_g = 1.6 - j2.75$$
which is located on the Smith chart.
10. Inverting y_{in} on the Smith chart to z_{in} gives
$$z_{in} = 0.16 + j0.28$$
11. Unnormalizing z_{in} by $Z_0 = 315$, reduces it to
$$Z_{in} = 50.4 + j88.2$$
12. The capacitance should be
$$C = \frac{1}{2\pi f_0(88.2)} = \frac{1}{2\pi(15\times10^6)(88.2)}$$
$$= 120.3\times10^{-12} \simeq 120 \text{ pF}$$

Since $R_{in} = 50.4$ ohms is not exactly equal to $Z_0 = 50$ ohms, one of the physical dimensions (usually the length of the rod) can be changed slightly and then the process can be repeated. However in this case they are so close that for practical purposes this is not required.

A MATLAB computer program, entitled ***Gamma***, has been developed to perform the design of a folded dipole. The description of the program is found in the corresponding READ ME file included in the CD attached to the book.

9.7.5 Omega Match

A slightly modified version of the gamma match is the omega match shown in Figure 9.24. The only difference between the two is that in addition to the series capacitor C_1 there is one in shunt C_2 which can aid in achieving the match. Usually the presence of C_2 makes it possible to use a shorter rod or makes it easier to match a resonant driven element. The primary function of C_2 is to change y_{in} in step 9 of the design procedure so that when it is inverted its unnormalized real part is equal to the characteristic impedance of the input transmission line. This will possibly eliminate the need of changing the dimensions of the matching elements, if a match is not achieved.

9.7.6 Baluns and Transformers

A twin-lead transmission line (two parallel-conductor line) is a symmetrical line whereas a coaxial cable is inherently unbalanced. Because the inner and outer (inside

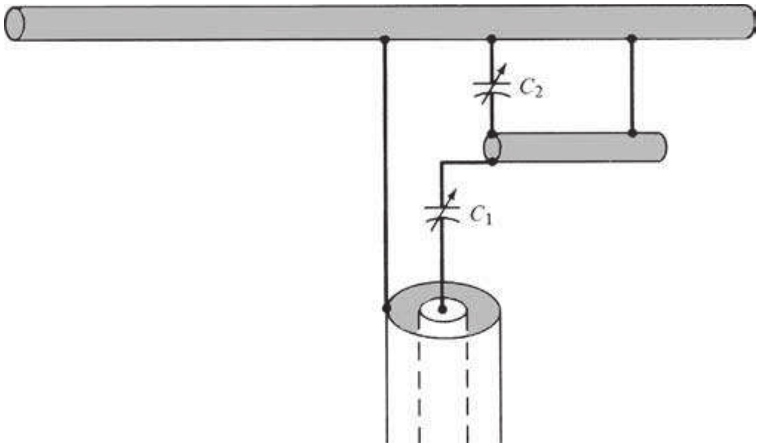


Figure 9.24 Omega match arrangement.

and outside parts of it) conductors of the coax are not coupled to the antenna in the same way, they provide the unbalance. The result is a net current flow to ground on the outside part of the outer conductor. This is shown in Figure 9.25(a) where an electrical equivalent is also indicated. The amount of current flow I_3 on the outside surface of the outer conductor is determined by the impedance Z_g from the outer shield to ground. If Z_g can be made very large, I_3 can be reduced significantly. Devices that can be used to balance inherently unbalanced systems, by canceling or choking the outside current, are known as *baluns* (*bal*ance to *un*balance).

One type of a balun is that shown in Figure 9.25(b), referred to usually as a *bazooka* balun. Mechanically it requires that a $\lambda/4$ in length metal sleeve, and shorted at its one end, encapsulates the coaxial line. Electrically the input impedance at the open end of this $\lambda/4$ shorted transmission line, which is equivalent to Z_g, will be very large (ideally infinity). Thus the current I_3 will be choked, if not completely eliminated, and the system will be nearly balanced.

Another type of a balun is that shown in Figure 9.25(c). It requires that one end of a $\lambda/4$ section of a transmission line be connected to the outside shield of the main coaxial line while the other is connected to the side of the dipole which is attached to the center conductor. This balun is used to cancel the flow of I_3. The operation of it can be explained as follows: In Figure 9.25(a) the voltages between each side of the dipole and the ground are equal in magnitude but 180° out of phase, thus producing a current flow on the outside of the coaxial line. If the two currents I_1 and I_2 are equal in magnitude, I_3 would be zero. Since arm #2 of the dipole is connected directly to the shield of the coax while arm #1 is weakly coupled to it, it produces a much larger current I_2. Thus there is relatively little cancellation in the two currents.

The two currents, I_1 and I_2, can be made equal in magnitude if the center conductor of the coax is connected directly to the outer shield. If this connection is made directly at the antenna terminals, the transmission line and the antenna would be short-circuited, thus eliminating any radiation. However, the indirect parallel-conductor connection of Figure 9.25(c) provides the desired current cancellation without eliminating the radiation. The current flow on the outer shield of the main line is canceled at the bottom end of the $\lambda/4$ section (where the two join together) by the equal in magnitude, but opposite in phase, current in the $\lambda/4$ section of the auxiliary line. Ideally then there is no current flow in the outer surface of the outer shield of the remaining part of the

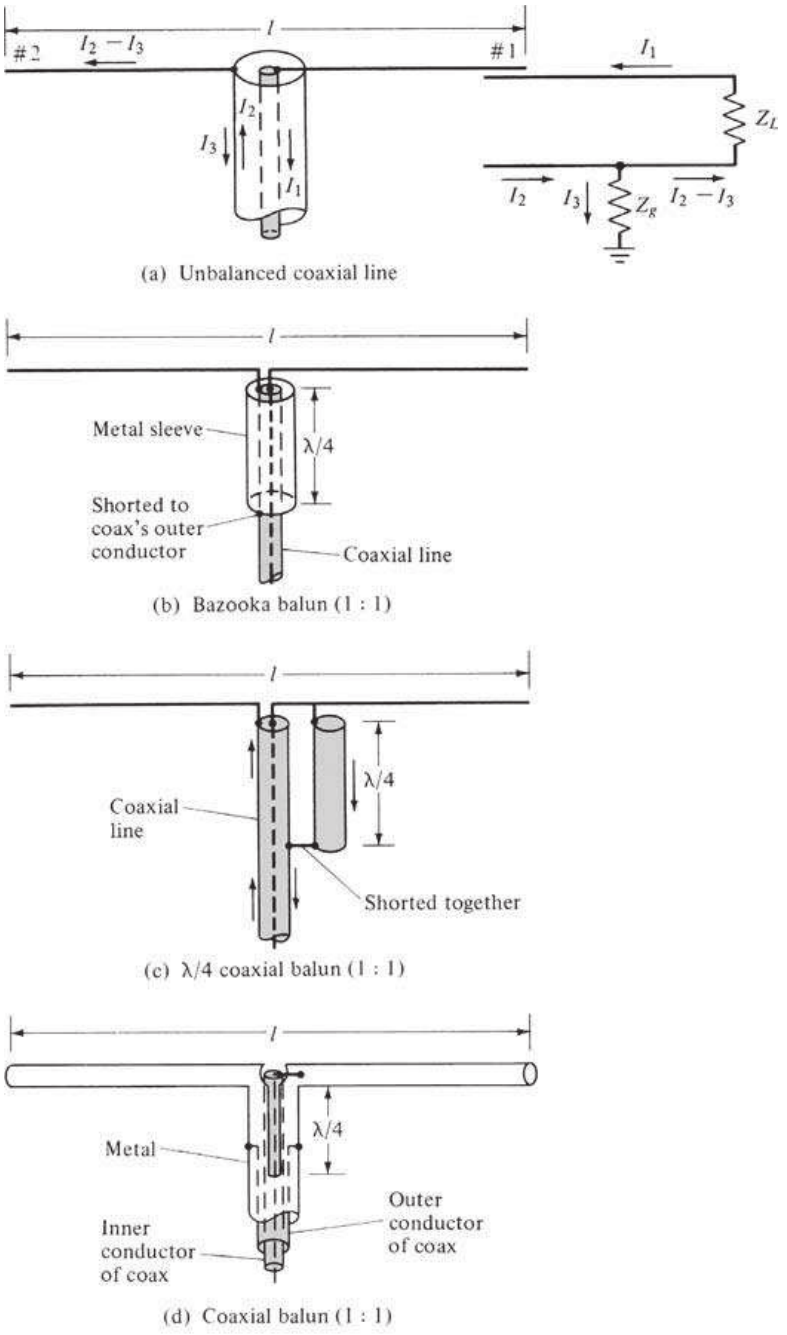


Figure 9.25 Balun configurations.

main coaxial line. It should be stated that the parallel auxiliary line need not be made $\lambda/4$ in length to achieve the balance. It is made $\lambda/4$ to prevent the upsetting of the normal operation of the antenna.

A compact construction of the balun in Figure 9.25(c) is that in Figure 9.25(d). The outside metal sleeve is split and a portion of it is removed on opposite sides. The remaining opposite parts of the outer sleeve represent electrically the two shorted $\lambda/4$ parallel transmission lines of Figure 9.25(c). All of the baluns shown in Figure 9.25 are narrowband devices.

EX2042
Page 499 of 1072

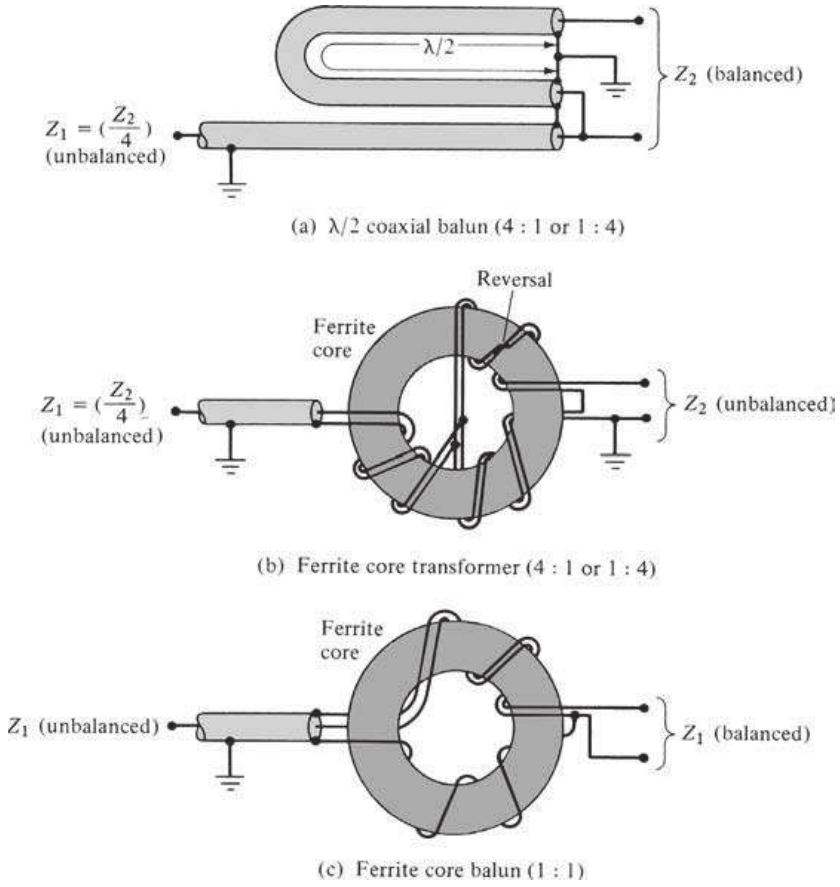


Figure 9.26 Balun and ferrite core transformers.

Devices can be constructed which provide not only balancing but also step-up impedance transformations. One such device is the $\lambda/4$ coaxial balun, with a 4:1 impedance transformation, of Figure 9.26(a). The U-shaped section of the coaxial line must be $\lambda/2$ long [21].

Because all the baluns-impedance transformers that were discussed so far are narrowband devices, the bandwidth can be increased by employing ferrite cores in their construction [22]. Two such designs, one a 4:1 or 1:4 transformer and the other a 1:1 balun, are shown in Figures 9.26(b) and (c). The ferrite core has a tendency to maintain high impedance levels over a wide frequency range [23]. A good design and construction can provide bandwidths of 8 or even 10 to 1. Coil coaxial baluns, constructed by coiling the coaxial line itself to form a balun [23], can provide bandwidths of 2 or 3 to 1.

9.8 MULTIMEDIA

In the CD that is part of the book the following multimedia resources are included for the review, understanding, and visualization of the material of this chapter:

a. **Java**-based **interactive questionnaire**, with answers.
b. **Matlab** computer program, designated ***Quarterwave***, for computing and displaying the characteristics of binomial and Tschebyscheff quarter-wavelength impedance matching designs.

c. **Matlab** computer programs, designated
   - ***Folded***
   - ***Tee***
   - ***Gamma***

   for computing the characteristics of a folded dipole, and tee and gamma impedance matches.

d. **Power Point (PPT)** viewgraphs, in multicolor.

REFERENCES

1. M. Abraham, "Die electrischen Schwingungen um einen stabformingen Leiter, behandelt nach der Maxwelleschen Theorie," *Ann. Phys.*, Vol. 66, pp. 435–472, 1898.
2. S. A. Schelkunoff, *Electromagnetic Waves*, Van Nostrand, New York, 1943, Chapter 11.
3. E. Hallén, "Theoretical Investigations into the Transmitting and Receiving Qualities of Antennae," *Nova Acta Reg. Soc. Sci. Upsaliensis*, Ser. IV, Vol. 11, No. 4, pp. 1–44, 1938.
4. R. C. Johnson and H. Jasik (eds.), *Antenna Engineering Handbook*, McGraw-Hill, New York, 1984, Chapter 4.
5. G. H. Brown and O. M. Woodward Jr., "Experimentally Determined Radiation Characteristics of Conical and Triangular Antennas," *RCA Rev.*, Vol. 13, No. 4, p. 425, December 1952.
6. C. H. Papas and R. King, "Radiation from Wide-Angle Conical Antennas Fed by a Coaxial Line," *Proc. IRE*, Vol. 39, p. 1269, November 1949.
7. C. E. Smith, C. M. Butler, and K. R. Umashankar, "Characteristics of a Wire Biconical Antenna," *Microwave J.*, pp. 37–40, September 1979.
8. G. H. Brown and O. M. Woodward Jr., "Experimentally Determined Impedance Characteristics of Cylindrical Antennas," *Proc. IRE*, Vol. 33, pp. 257–262, 1945.
9. J. D. Kraus, *Antennas*, McGraw-Hill, New York, 1950, pp. 276–278.
10. J. H. Richmond and E. H. Newman, "Dielectric Coated Wire Antennas," *Radio Sci.*, Vol. 11, No. 1, pp. 13–20, January 1976.
11. J. Y. P. Lee and K. G. Balmain, "Wire Antennas Coated with Magnetically and Electrically Lossy Material," *Radio Sci.*, Vol. 14, No. 3, pp. 437–445, May-June 1979.
12. G. A. Thiele, E. P. Ekelman Jr., and L. W. Henderson, "On the Accuracy of the Transmission Line Model for Folded Dipole," *IEEE Trans. Antennas Propagat.*, Vol. AP-28, No. 5, pp. 700–703, September 1980.
13. R. W. Lampe, "Design Formulas for an Asymmetric Coplanar Strip Folded Dipole," *IEEE Trans. Antennas Propagat.*, Vol. AP-33, No. 9, pp. 1028–1031, September 1985.
14. A. G. Kandoian, "Three New Antenna Types and Their Applications," *Proc. IRE*, Vol. 34, pp. 70W–75W, February 1946.
15. R. E. Collin, *Foundations for Microwave Engineering*, McGraw-Hill, New York, 1992, Chapter 5, pp. 303–386.
16. D. M. Pozar, *Microwave Engineering*, John Wiley & Sons, Inc., NJ, 2004.
17. S. Y. Liao, *Microwave Devices and Circuits*, Prentice-Hall, Englewood Cliffs, N.J., 1980, pp. 418–422.
18. D. J. Healey, III, "An Examination of the Gamma Match," *QST*, pp. 11–15, April 1969.
19. *The ARRL Antenna Book*, American Radio Relay League, Inc., Newington, Conn., 1974, pp. 118–121.

20. H. T. Tolles, "How To Design Gamma-Matching Networks," *Ham Radio*, pp. 46–55, May 1973.
21. O. M. Woodward Jr., "Balance Measurements on Balun Transformers," *Electronics*, Vol. 26, No. 9, pp. 188–191, September 1953.
22. C. L. Ruthroff, "Some Broad-Band Transformers," *Proc. IRE*, Vol. 47, pp. 1337–1342, August 1959.
23. W. L. Weeks, *Antenna Engineering*, McGraw-Hill, New York, 1968, pp. 161–180.

PROBLEMS

9.1. A 300-ohm "twin-lead" transmission line is attached to a biconical antenna.
(a) Determine the cone angle that will match the line to an infinite length biconical antenna.
(b) For the cone angle of part (a), determine the two smallest cone lengths that will resonate the antenna.
(c) For the cone angle and cone lengths from part (b), what is the input VSWR?

9.2. Determine the first two resonant lengths, and the corresponding diameters and input resistances, for dipoles with $l/d = 25$, 50, and 10^4 using
(a) the data in Figures 9.10(a) and 9.10(b)
(b) Table 9.1

9.3. Design a resonant cylindrical stub monopole of length l, diameter d, and l/d of 50. Find the length (in λ), diameter (in λ), and the input resistance (in ohms) at the first four resonances.

9.4. A linear dipole of $l/d = 25$, 50, and 10^4 is attached to a 50-ohm line. Determine the VSWR of each l/d when
(a) $l = \lambda/2$ (b) $l = \lambda$ (c) $l = 3\lambda/2$

9.5. Find the equivalent circular radius a_e for a
(a) very thin flat plate of width $\lambda/10$
(b) square wire with sides of $\lambda/10$
(c) rectangular wire with sides of $\lambda/10$ and $\lambda/100$
(d) elliptical wire with major and minor axes of $\lambda/10$ and $\lambda/20$
(e) twin-lead transmission line with wire radii of 1.466×10^{-2} cm and separation of 0.8 cm

9.6. Compute the characteristic impedance of a two-wire transmission line with wire diameter of $d = 10^{-3}\lambda$ and center-to-center spacings of
(a) $6.13\times10^{-3}\lambda$ (b) $2.13\times10^{-2}\lambda$ (c) $7.42\times10^{-2}\lambda$

9.7. Verify (9-49) from the expressions listed in Table 9.3.

9.8. To increase its bandwidth, a $\lambda/4$ monopole antenna operating at 1 GHz is made of two side-by-side copper wires ($\sigma = 5.7\times10^7$ S/m) of circular cross section. The wires at each end of the arm are connected (shorted) electrically together. The radius of each wire is $\lambda/200$ and the separation between them is $\lambda/50$.

(a) What is the effective radius (in meters) of the two wires? Compare with the physical radius of each wire (in meters).

(b) What is the high-frequency loss resistance of each wire? What is the total loss resistance of the two together in a side-by-side shorted at the ends arrangement? What is the loss resistance based on the effective radius?

(c) What is the radiation efficiency of one wire by itself? Compare with that of the two together in a side-by-side arrangement. What is the radiation efficiency based on the loss resistance of the effective radius?

9.9. Show that the input impedance of a two-element folded dipole of $l = \lambda/2$ is four times greater than that of an isolated element of the same length.

9.10. Design a two-element folded dipole with wire diameter of $10^{-3}\lambda$ and center-to-center spacing of $6.13\times10^{-3}\lambda$.

(a) Determine its shortest length for resonance.

(b) Compute the VSWR at the first resonance when it is attached to a 300-ohm line.

9.11. A two-element folded dipole of identical wires has an $l/d = 500$ and a center-to-center spacing of $6.13\times10^{-3}\lambda$ between the wires. Compute the

(a) approximate length of a single wire at its first resonance

(b) diameter of the wire at the first resonance

(c) characteristic impedance of the folded dipole transmission line

(d) input impedance of the transmission line mode model

(e) input impedance of the folded dipole using as the radius of the antenna mode (1) the radius of the wire a, (2) the equivalent radius a_e of the wires, (3) half of the center-to-center spacing ($s/2$). Compare the results.

9.12. The input impedance of a 0.47λ folded dipole operating at 10 MHz is

$$Z_{in} = 306 + j75.3$$

To resonate the element, it is proposed to place a lumped element in shunt (parallel) at the input terminals where the impedance is measured.

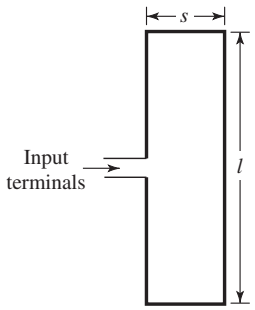
(a) What kind of an element (capacitor or inductor) should be used to accomplish the requirement?

(b) What is the value of the element (in farads or henries)?

(c) What is the new value of the input impedance?

(d) What is the VSWR when the resonant antenna is connected to a 300-ohm line?

Verify using the computer program ***Folded***.



9.13. A half-wavelength, two-element symmetrical folded dipole is connected to a 300-ohm "twin-lead" transmission line. In order for the input impedance of the dipole to be real, an energy storage lumped element is placed across its input terminals. Determine, assuming $f = 100$ MHz, the

(a) capacitance or inductance of the element that must be placed across the terminals.

(b) VSWR at the terminals of the transmission line taking into account the dipole and the energy storage element.

Verify using the computer program ***Folded***.

9.14. A half-wavelength, two-element symmetrical folded dipole whose each wire has a radius of $10^{-3}\lambda$ is connected to a 300-ohm "twin-lead" transmission line. The center-to-center spacing of the two wires is $4\times10^{-3}\lambda$. In order for the input impedance of the dipole to be real, determine, assuming $f = 100$ MHz, the

(a) total capacitance C_T that must be placed in series at the input terminals.

(b) capacitance C (two of them) that must be placed in series at each of the input terminals of the dipole in order to keep the antenna symmetrical.

(c) VSWR at the terminals of the transmission line connected to the dipole through the two capacitances.

Verify using the computer program ***Folded***.

9.15. An $l = 0.47\lambda$ folded dipole, whose wire radius is $5\times10^{-3}\lambda$, is fed by a "twin lead" transmission line with a 300-ohm characteristic impedance. The center-to-center spacing of the two side-by-side wires of the dipole is $s = 0.025\lambda$. The dipole is operating at $f = 10$ MHz. The input impedance of the "regular" dipole of $l = 0.47\lambda$ is $Z_d = 79 + j13$.

(a) Determine the

i. Input impedance of the folded dipole.

ii. Amplification factor of the input impedance of the folded dipole, compared to the corresponding value of the regular dipole.

iii. Input reflection coefficient.

iv. Input VSWR.

(b) To resonate the folded dipole and keep the system balanced, two capacitors (each C) are connected each symmetrically in series at the input terminals of the folded dipole.

i. What should C be to resonate the dipole?

ii. What is the new reflection coefficient at the input terminals of the "twin-lead" line?

iii. What is the new VSWR?

9.16. A folded dipole of length $\lambda_0/2$ is composed of two wires, each of radii $\lambda_0/200$ and $\lambda_0/300$, respectively, and separated by a distance of $\lambda_0/100$. The folded dipole is connected to a 300-ohm transmission line. Determine the following:

(a) Input impedance of the dipole.

(b) What *capacitance or inductance* must be placed in *series* to the transmission line at the feed point so that the *dipole is resonant at* $f_o = 600$ *MHz*.

(c) Input reflection coefficient, assuming the resonant dipole is connected to a 300-ohm transmission line.

(d) Input VSWR of the resonant dipole when connected to the 300-ohm transmission line.

9.17. A folded dipole antenna operating at 100 MHz with identical wires in both arms, and with overall length of each arm being 0.48λ, is connected to a 300-ohm *twin-lead* line. The radius of each wire is $a = 5\times10^{-4}\lambda$ while the center-to-center separation is $s = 5\times10^{-3}\lambda$. Determine the

(a) Approximate length (*in* λ) of the regular dipole, *at the first resonance*, in the absence of the other wire.

(b) Input impedance of the single wire *resonant regular* dipole.

(c) Input impedance of the folded dipole at the length of the first resonance of the single element.

(d) Capacitance (*in f/m*) or inductance (*in h/m*), whichever is appropriate, that must be placed in series with the element at the feed to *resonate the folded dipole*. To keep the element balanced, place two elements, one in each arm.

(e) VSWR of the resonant folded dipole.

9.18. A $\lambda/2$ folded dipole is used as the feed element for a Yagi-Uda array whose input impedance, *when the array is fed by a regular dipole*, is $30 + j3$. The folded dipole used is *not symmetrical* (i.e., the two wires are not of the same radius). One of the wires has a radius of $10^{-4}\lambda$ and the other (*the one that is connected to the feed*) has a radius of $0.5\times10^{-4}\lambda$. The center-to-center spacing between the two dipoles is $2\times10^{-4}\lambda$. Determine the

(a) *turns ratio* of the *equivalent-circuit impedance transformer*

(b) *effective impedance* of the regular dipole when it is transferred from the *secondary* to the *primary* of the *equivalent-circuit impedance transformer*

(c) *input impedance* of the folded dipole.

9.19. Repeat the design of Example 9.1 using a Tschebyscheff transformer.

9.20. Repeat the design of Example 9.1 for a three-section

(a) binomial transformer

(b) Tschebyscheff transformer

Verify using the computer program ***Quarterwave***.

9.21. A self-resonant (*first resonance*) half-wavelength dipole of radius $a = 10^{-3}\lambda$ is connected to a 300-ohm "twin-lead" line through a three-section binomial impedance transformer. Determine the impedances of the three-section binomial transformer required to match the resonant dipole to the "twin-lead" line.
Verify using the computer program ***Quarterwave***.

9.22. Consider a center-fed thin-wire dipole with wire radius $a = 0.005\lambda$.

(a) Determine the shortest resonant length l (in wavelengths) and corresponding input resistance R_{in} of the antenna using assumed sinusoidal current distribution.

(b) Design a two-section Tschebyscheff quarter-wavelength transformer to match the antenna to a 75-ohm transmission line. Design the transformer to achieve an equal-ripple response to R_{in} over a fractional bandwidth of 0.25.

(c) Compare the performance of the matching network in part (b) to an ideal transformer by plotting the input reflection coefficient magnitude versus normalized frequency for $0 \leq f/f_0 \leq 2$ for both cases.

Verify using the computer program ***Quarterwave***.

9.23. The free-space impedance at the center point of the driven element of a 15-MHz Yagi-Uda array is $25 - j25$. Assuming the diameters of the wires of a T-match are $1.9\times10^{-3}\lambda$(3.8 cm) and $6.35\times10^{-4}\lambda$(1.27 cm), the center-to-center spacing between the wires is $7.62\times10^{-3}\lambda$(15.24 cm), and the length $l'/2$ of each T-match rod is 0.0285λ (57 cm), find the

(a) input impedance of the T-match

(b) input capacitance C_{in} that will resonate the antenna

(c) capacitance C that must be used in each leg to resonate the antenna

Verify using the computer program ***Tee***.

9.24. The input impedance of a 145.4 MHz Yagi-Uda antenna is $14 + j3$. Design a gamma match using diameters of 0.9525 cm (for the antenna) and 0.2052 cm (for the rod), and center-to-center spacing between the wires of 1.5316 cm. The match is for a 50-ohm input coaxial line. Find the shortest gamma rod length and the required capacitance. First, do the problem analytically. The design must be such that the real part of the designed input impedance is *within 1 ohm* of the required 50 ohms. Second, check your answers with the Smith chart.
Verify using the computer program ***Gamma***.

9.25. Repeat Problem 9.24 for an input impedance of $14 - j3$.

9.26. A $\lambda/4$ monopole is mounted on a ground plane and has an input impedance of $34 + j17$ at $f = 145.4$ MHz. Design a gamma match to match the monopole to a 50-ohm coaxial line. The wire diameters are identical (0.9525 cm) and the center-to-center spacing is 3.1496 cm. Find the required capacitance and the shortest gamma rod length. First, do the problem analytically. The design must be such that the real part of the designed input impedance is *within 1 ohm* of the required 50 ohms. Second, check your answers with the Smith chart.
Verify using the computer program ***Gamma***.

9.27. Using a gamma match, a $\lambda/2$ dipole is connected to an amateur 425 MHz radio receiver using a 78-ohm coaxial line. The length of the gamma match is $\lambda/4$ and its wire radius is identical to that of the dipole.

(a) What is the input impedance of the antenna-gamma match arrangement at the input terminals in the absence of a matching capacitor?

(b) To resonate the antenna, a capacitor is placed in series to the arm that is connected to the center conductor of the coaxial line. What is the value of the capacitor?

(c) When the resonant antenna is connected to a 78-ohm coaxial line, what is the magnitude of the reflection coefficient? What is the VSWR?

Verify using the computer program ***Gamma***.

9.28. A 300 MHz resonant $\lambda/2$ dipole with an input impedance of 67 ohms is connected to a coaxial line through a gamma match. The radii of the wires for the dipole and gamma match, and the spacing between them, are such that

the turns ratio of the transformer is 3:1. The characteristic impedance of the transmission line that the dipole and gamma match part form is 250 ohms. The overall length of the gamma match is 0.1λ.

(a) What is the total input impedance at the input terminals of the gamma match?

(b) What value of capacitor placed in series shall be selected so that the new input impedance is real (resonate the load)?

9.29. A T-match is connected to the antennas of Problems 9.24 and 9.25. Assuming that the wire diameters and lengths for each leg of the T-match are those derived for each gamma match, find the

(a) input impedance of the T-match

(b) capacitance C in each leg to make the antenna system resonant

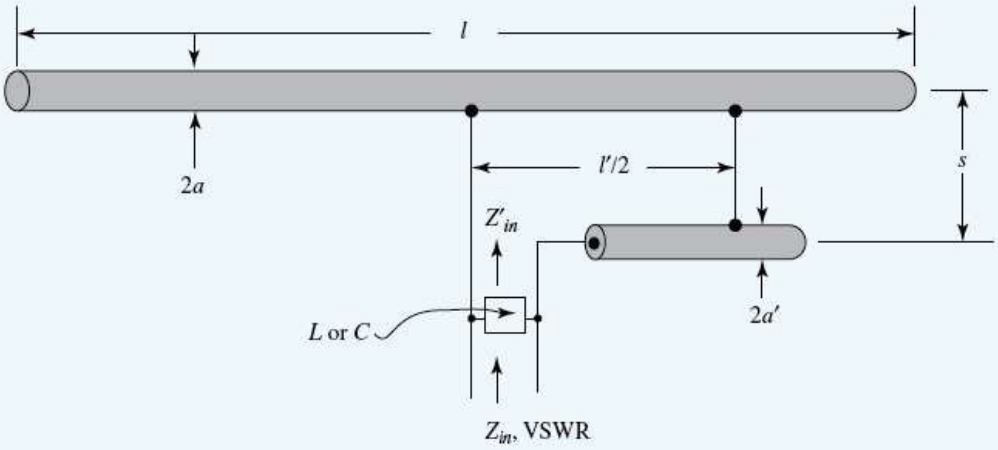
9.30. Repeat Problem 9.29 but select the lengths $l'/2$ of the T-match rods so that the input resistance is 300 ohms. Use diameters of 0.1026 cm (for the rod), 0.9525 cm (for the antenna), and center-to-center spacing of 0.7658 cm. This connection is ideal for use with a 300-ohm "twin-lead" line.

9.31. A *half-wavelength linear dipole* ($l = \lambda/2$), with an *ideal sinusoidal current distribution*, is connected to a Gamma Match whose length is $l'/2 = \lambda/4$. The radius of the wire of the dipole is $\lambda/200$, the radius of the wire of the Gamma Match is $\lambda/400$, and the center-to-center separation of the two wires is $\lambda/100$.

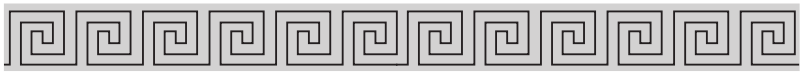
(a) Determine the input impedance Z'_{in}.

(b) *Instead of using a series capacitance*, as is shown in the book to tune-out the reactance of the Gamma Match, *a parallel inductor L or capacitor C, is used to accomplish the same purpose*, as shown in the figure below. What is the value of the *parallel inductance (in henries) or capacitance (in farads)* that is needed at a frequency of 500 MHz?

(c) *After tuning-out the reactance*, as done in Part b of this problem, what is the input impedance Z_{in} *and VSWR* of the antenna with the Gamma Match when they are connected to a 50-ohm coaxial transmission line?



CHAPTER 10



Traveling Wave and Broadband Antennas

10.1 INTRODUCTION

In the previous chapters we have presented the details of classical methods that are used to analyze the radiation characteristics of some of the simplest and most common forms of antennas (i.e., infinitely thin linear and circular wires, broadband dipoles, and arrays). In practice there is a myriad of antenna configurations, and it would be almost impossible to consider all of them in this book. In addition, many of these antennas have bizarre types of geometries and it would be almost impractical, if not even impossible, to investigate each in detail. However, the general performance behavior of some of them will be presented in this chapter with a minimum of analytical formulations. Today, comprehensive analytical formulations are available for most of them, but they would require so much space that it would be impractical to include them in this book.

10.2 TRAVELING WAVE ANTENNAS

In Chapter 4, center-fed linear wire antennas were discussed whose amplitude current distribution was

1. constant for infinitesimal dipoles ($l \leq \lambda/50$)
2. linear (triangular) for short dipoles ($\lambda/50 < l \leq \lambda/10$)
3. sinusoidal for long dipoles ($l > \lambda/10$)

In all cases the phase distribution was assumed to be constant. The sinusoidal current distribution of long open-ended linear antennas is a standing wave constructed by two waves of equal amplitude and 180° phase difference at the open end traveling in opposite directions along its length. The voltage distribution has also a standing wave pattern except that it has maxima (loops) at the end of the line instead of nulls (nodes) as the current. In each pattern, the maxima and minima repeat every integral number of half wavelengths. There is also a $\lambda/4$ spacing between a null and a maximum in each of the wave patterns. The current and voltage distributions on open-ended wire antennas

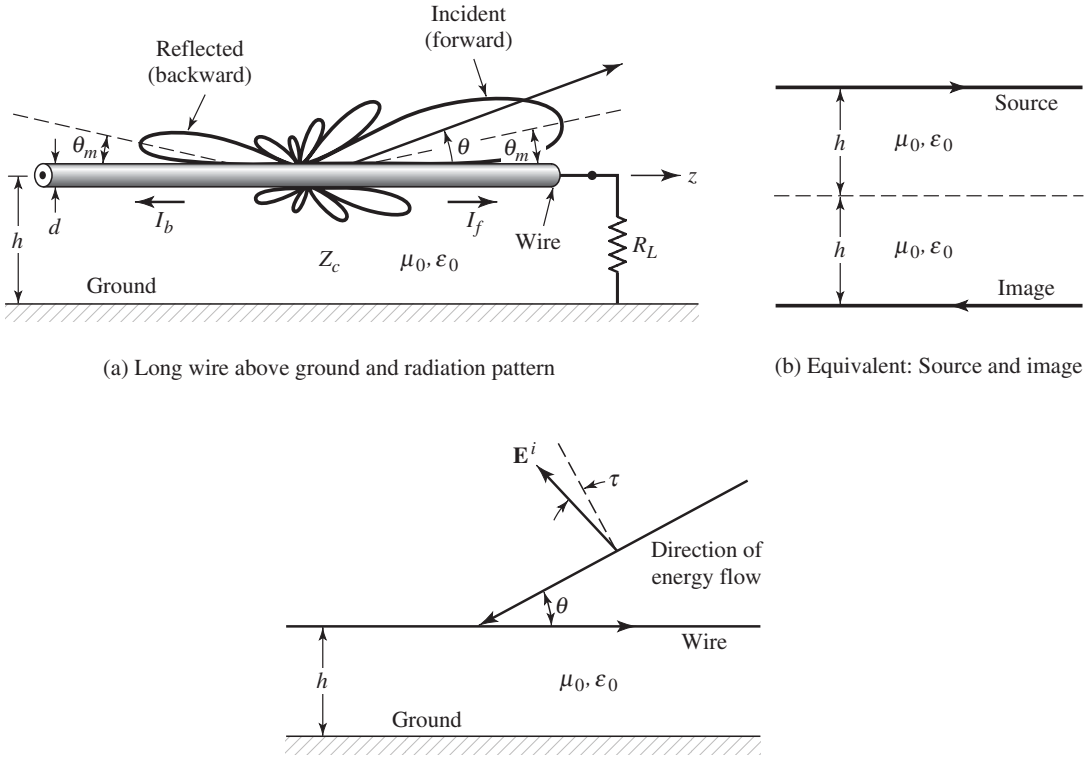
Antenna Theory: Analysis Design, Third Edition, by Constantine A. Balanis
ISBN 0-471-66782-X Copyright © 2005 John Wiley & Sons, Inc.

EX2042
Page 508 of 1072

are similar to the standing wave patterns on open-ended transmission lines. Linear antennas that exhibit current and voltage standing wave patterns formed by reflections from the open end of the wire are referred to as *standing wave* or *resonant* antennas.

Antennas can be designed which have traveling wave (uniform) patterns in current and voltage. This can be achieved by properly terminating the antenna wire so that the reflections are minimized if not completely eliminated. An example of such an antenna is a long wire that runs horizontal to the earth, as shown in Figure 10.1. The input terminals consist of the ground and one end of the wire. This configuration is known as *Beverage or wave antenna*. There are many other configurations of traveling wave antennas. In general, all antennas whose current and voltage distributions can be represented by one or more traveling waves, usually in the same direction, are referred to as *traveling wave* or *nonresonant* antennas. A progressive phase pattern is usually associated with the current and voltage distributions.

Standing wave antennas, such as the dipole, can be analyzed as traveling wave antennas with waves propagating in opposite directions (forward and backward) and represented by traveling wave currents I_f and I_b in Figure 10.1(a). Besides the long-wire antenna there are many examples of traveling wave antennas such as dielectric rod (polyrod), helix, and various surface wave antennas. Aperture antennas, such as reflectors and horns, can also be treated as traveling wave antennas. In addition, arrays of closely spaced radiators (usually less than $\lambda/2$ apart) can also be analyzed as traveling wave antennas by approximating their current or field distribution by a continuous traveling wave. Yagi-Uda, log-periodic, and slots and holes in a waveguide are some examples of discrete-element traveling wave antennas. In general, a traveling wave



(a) Long wire above ground and radiation pattern

(b) Equivalent: Source and image

(c) Wave tilt

Figure 10.1 Beverage (long-wire) antenna above ground.

EX2042
Page 509 of 1072

antenna is usually one that is associated with radiation from a continuous source. An excellent book on traveling wave antennas is one by C. H. Walter [1].

A traveling wave may be classified as a *slow* wave if its phase velocity v_p($v_p = \omega/k$, $\omega =$ wave angular frequency, $k =$ wave phase constant) is equal or smaller than the velocity of light c in free-space ($v_p/c \leq 1$). A fast wave is one whose phase velocity is greater than the speed of light ($v_p/c > 1$).

In general, there are two types of traveling wave antennas. One is the *surface wave* antenna defined as "an antenna which radiates power flow from discontinuities in the structure that interrupt a bound wave on the antenna surface."* A surface wave antenna is, in general, a slow wave structure whose phase velocity of the traveling wave is equal to or less than the speed of light in free-space ($v_p/c \leq 1$).

For slow wave structures radiation takes place only at nonuniformities, curvatures, and discontinuities (see Figure 1.10). Discontinuities can be either discrete or distributed. One type of discrete discontinuity on a surface wave antenna is a transmission line terminated in an unmatched load, as shown in Figure 10.1(a). A distributed surface wave antenna can be analyzed in terms of the variation of the amplitude and phase of the current along its structure. In general, power flows parallel to the structure, except when losses are present, and for plane structures the fields decay exponentially away from the antenna. Most of the surface wave antennas are end-fire or near-end-fire radiators. Practical configurations include line, planar surface, curved, and modulated structures.

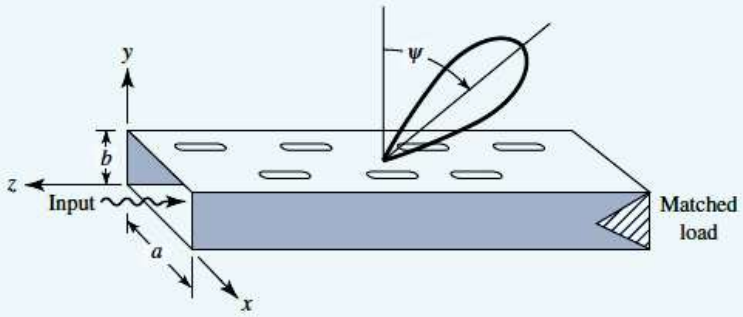
Another traveling wave antenna is a *leaky-wave* antenna defined as "an antenna that couples power in small increments per unit length, either continuously or discretely, from a traveling wave structure to free-space"† Leaky-wave antennas continuously lose energy due to radiation, as shown in Figure 10.2 by a slotted rectangular waveguide. The fields decay along the structure in the direction of wave travel and increase in others. Most of them are fast wave structures.

10.2.1 Long Wire

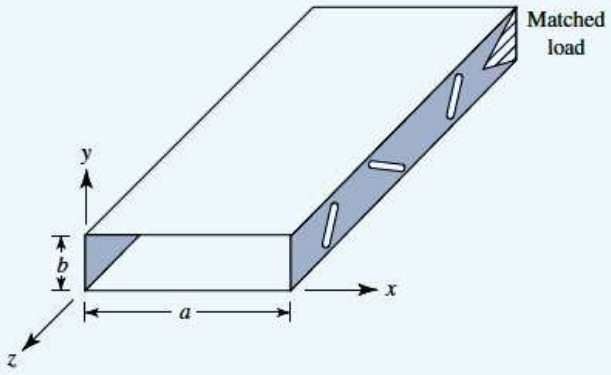
An example of a slow wave traveling antenna is a long wire, as shown in Figure 10.1. An antenna is usually classified as a *long* wire antenna if it is a straight conductor with a length from one to many wavelengths. A long wire antenna has the distinction of being the first traveling wave antenna.

The long wire of Figure 10.1(a), in the presence of the ground, can be analyzed approximately using the equivalent of Figure 10.1(b) where an image is introduced to take into account the presence of the ground. The magnitude and phase of the image are determined using the reflection coefficient for horizontal polarization as given by (4-128). The height h of the antenna above the ground must be chosen so that the reflected wave (or wave from the image), which includes the phase due to reflection is in phase with the direct wave at the angles of desired maximum radiation. However, for typical electrical constitutive parameters of the earth, and especially for observation angles near grazing, the reflection coefficient for horizontal polarization is approximately -1. Therefore the total field radiated by the wire in the presence of the ground can be

*"IEEE Standard Definitions of Terms for Antennas" (IEEE Std 145-1983), *IEEE Trans. Antennas and Propagat.*, Vol. AP-31, No. 6, Part II, Nov. 1983.
†Ibid.



(a) Upper wall—longitudinal



(b) Sidewall—inclined

Figure 10.2 Leaky-wave waveguide slots; upper (broad) and side (narrow) walls.

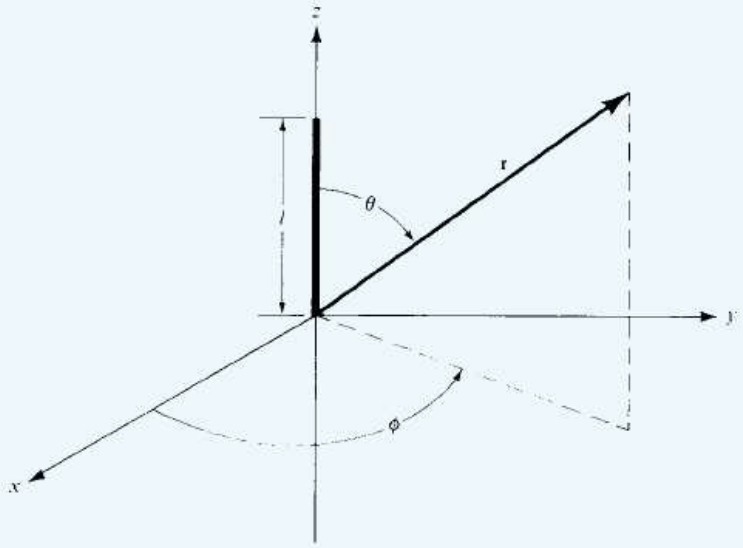


Figure 10.3 Long-wire antenna.

found by multiplying the field radiated by the wire in free space by the array factor of a two-element array, as was done in Section 4.8.2 and represented by (4-129).

The objective now is to find the field radiated by the long wire in free space. This is accomplished by referring to Figure 10.3. As the wave travels along the wire from the source toward the load, it continuously leaks energy. This can be represented by

an attenuation coefficient. Therefore the current distribution of the forward traveling wave along the structure can be represented by

$$\mathbf{I}_f = \hat{\mathbf{a}}_z I_z(z') e^{-\gamma(z')z'} = \hat{\mathbf{a}}_z I_0 e^{-[\alpha(z')+jk_z(z')]z'} \tag{10-1}$$

where $\gamma(z')$ is the propagation coefficient [$\gamma(z') = \alpha(z') + jk_z(z')$ where $\alpha(z')$ is the attenuation constant (nepers/meter) while $k_z(z')$ is the phase constant (radians/meter) associated with the traveling wave]. In addition to the losses due to leakage, there are wire and ground losses. The attenuation factor $\alpha(z')$ can also be used to take into account the ohmic losses of the wire as well as ground losses. However, these, especially the ohmic losses, are usually very small and for simplicity are neglected. In addition, when the radiating medium is air, the loss of energy in a long wire ($l \gg \lambda$) due to leakage is also usually very small, and it can also be neglected. Therefore the current distribution of (10-1) can be approximated by

$$\mathbf{I} = \hat{\mathbf{a}}_z I(z') e^{-jk_z z'} = \hat{\mathbf{a}}_z I_0 e^{-jk_z z'} \tag{10-1a}$$

where $I(z') = I_0$ is assumed to be constant. Using techniques outlined and used in Chapter 4, it can be easily shown that in the far field

$$E_r \simeq E_\phi = H_r = H_\theta = 0 \tag{10-2a}$$

$$E_\theta \simeq j\eta \frac{klI_0 e^{-jkr}}{4\pi r} e^{-j(kl/2)(K-\cos\theta)} \sin\theta \frac{\sin[(kl/2)(\cos\theta - K)]}{(kl/2)(\cos\theta - K)} \tag{10-2b}$$

$$H_\phi \simeq \frac{E_\theta}{\eta} \tag{10-2c}$$

where K is used to represent the ratio of the phase constant of the wave along the transmission line (k_z) to that of free-space (k), or

$$K = \frac{k_z}{k} = \frac{\lambda}{\lambda_g} \tag{10-3}$$

λ_g = wavelength of the wave along the transmission line

Assuming a perfect electric conductor for the ground, the total field for Figure 10.1(a) is obtained by multiplying each of (10-2a)–(10-2c) by the array factor $\sin(kh\sin\theta)$.

For $k_z = k(K = 1)$ the time-average power density can be written as

$$\mathbf{W}_{\text{av}} = \mathbf{W}_{\text{rad}} = \hat{\mathbf{a}}_r \eta \frac{|I_0|^2}{8\pi^2 r^2} \frac{\sin^2\theta}{(\cos\theta - 1)^2} \sin^2\left[\frac{kl}{2}(\cos\theta - 1)\right] \tag{10-4}$$

which reduces to

$$\mathbf{W}_{\text{av}} = \mathbf{W}_{\text{rad}} = \hat{\mathbf{a}}_r \eta \frac{|I_0|^2}{8\pi^2 r^2} \cot^2\left(\frac{\theta}{2}\right) \sin^2\left[\frac{kl}{2}(\cos\theta - 1)\right] \tag{10-5}$$

From (10-5) it is evident that the power distribution of a wire antenna of length l is a multilobe pattern whose number of lobes depends upon its length. Assuming that l is

very large such that the variations in the sine function of (10-5) are more rapid than those of the cotangent, the peaks of the lobes occur approximately when

$$\sin^2\left[\frac{kl}{2}(\cos\theta - 1)\right]_{\theta=\theta_m} = 1 \tag{10-6}$$

or

$$\frac{kl}{2}(\cos\theta_m - 1) = \pm\left(\frac{2m+1}{2}\right)\pi, \quad m = 0, 1, 2, 3, \ldots \tag{10-6a}$$

The angles where the peaks occur are given by

$$\theta_m = \cos^{-1}\left[1 \pm \frac{\lambda}{2l}(2m+1)\right], \quad m = 0, 1, 2, 3, \ldots \tag{10-7}$$

The angle where the maximum of the major lobe occurs is given by $m = 0$ (or $2m + 1 = 1$). As l becomes very large ($l \gg \lambda$), the angle of the maximum of the major lobe approaches zero degrees and the structure becomes a near-end-fire array.

In finding the values of the maxima, the variations of the cotangent term in (10-5) were assumed to be negligible (as compared to those of the sine term). If the effects of the cotangent term were to be included, then the values of the $2m + 1$ term in (10-7) should be

$$2m + 1 = 0.742, 2.93, 4.96, 6.97, 8.99, 11, 13, \ldots \tag{10-8}$$

(instead of $1, 3, 5, 7, 9, \ldots$) for the first, second, third, and so forth maxima. The approximate values approach those of the exact for the higher order lobes.

In a similar manner, the nulls of the pattern can be found and occur when

$$\sin^2\left[\frac{kl}{2}(\cos\theta - 1)\right]_{\theta=\theta_n} = 0 \tag{10-9}$$

or

$$\frac{kl}{2}(\cos\theta_n - 1) = \pm n\pi, \quad n = 1, 2, 3, 4, \ldots \tag{10-9a}$$

The angles where the nulls occur are given by

$$\theta_n = \cos^{-1}\left(1 \pm n\frac{\lambda}{l}\right), \quad n = 1, 2, 3, 4, \ldots \tag{10-10}$$

for the first, second, third, and so forth nulls.

The total radiated power can be found by integrating (10-5) over a closed sphere of radius r and reduces to

$$P_{\text{rad}} = \oiint_S \mathbf{W}_{\text{rad}} \cdot d\mathbf{s} = \frac{\eta}{4\pi}|I_0|^2\left[1.415 + \ln\left(\frac{kl}{\pi}\right) - C_i(2kl) + \frac{\sin(2kl)}{2kl}\right] \tag{10-11}$$

where $C_i(x)$ is the cosine integral of (4-68a). The radiation resistance is then found to be

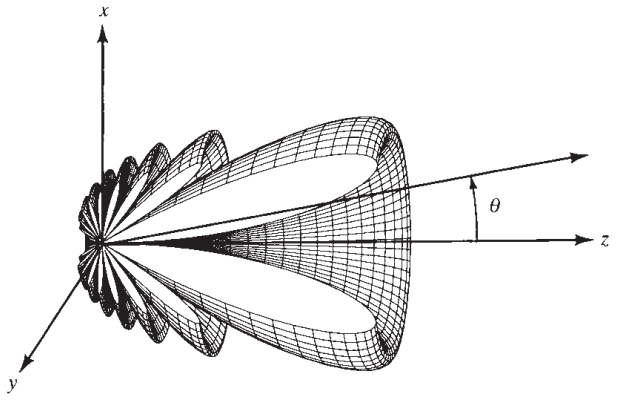
$$R_r = \frac{2P_{\text{rad}}}{|I_0|^2} = \frac{\eta}{2\pi}\left[1.415 + \ln\left(\frac{kl}{\pi}\right) - C_i(2kl) + \frac{\sin(2kl)}{2kl}\right] \tag{10-12}$$

Using (10-5) and (10-11) the directivity can be written as

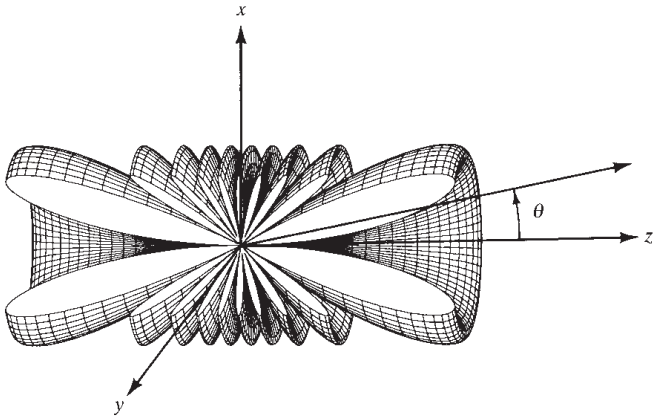
$$D_0 = \frac{4\pi U_{\max}}{P_{\text{rad}}} = \frac{2\cot^2\left[\frac{1}{2}\cos^{-1}\left(1 - \frac{0.371\lambda}{l}\right)\right]}{1.415 + \ln\left(\frac{2l}{\lambda}\right) - C_i(2kl) + \frac{\sin(2kl)}{2kl}} \tag{10-13}$$

A. Amplitude Patterns, Maxima, and Nulls

To verify some of the derivations and illustrate some of the principles, a number of computations were made. Shown in Figure 10.4(a) is the three-dimensional pattern of a traveling wire antenna with length $l = 5\lambda$ while in Figure 10.4(b) is the three-dimensional



(a) Traveling wave



(b) Standing wave

Figure 10.4 Three-dimensional free-space amplitude pattern for traveling and standing wave wire antennas of $l = 5\lambda$.

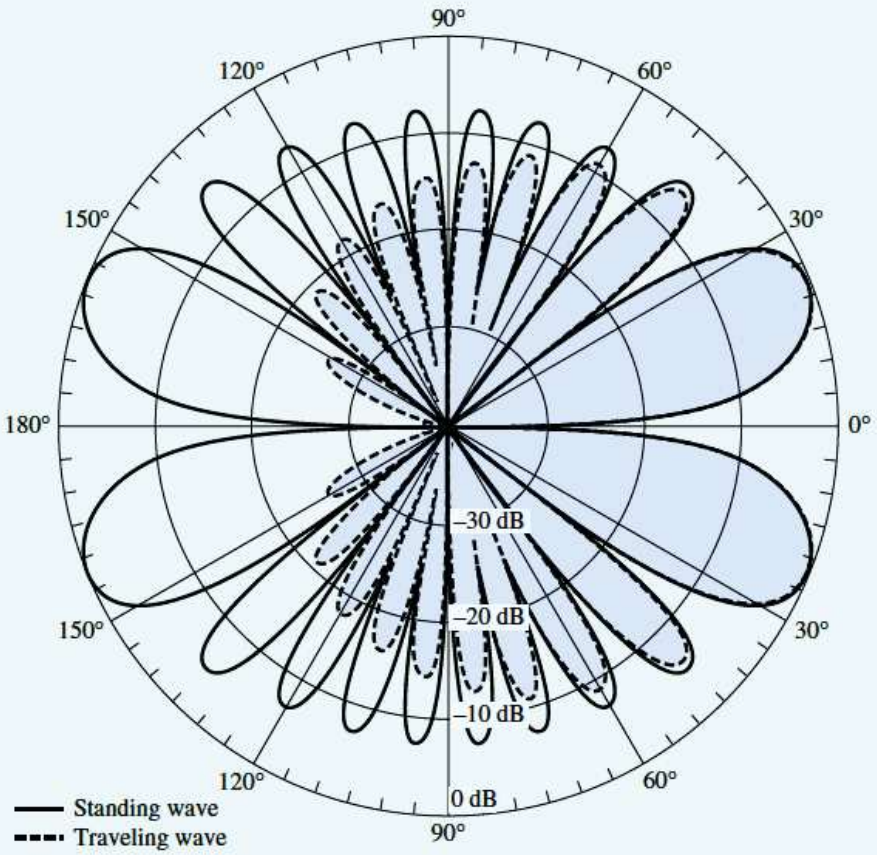


Figure 10.5 Two-dimensional free-space amplitude pattern for traveling and standing wave wire antennas of $l = 5\lambda$.

pattern for a standing wave wire antenna with length $l = 5\lambda$. The corresponding two-dimensional patterns are shown in Figure 10.5. The pattern of Figure 10.4(a) is formed by the forward traveling wave current $I_f = I_1 e^{-jkz}$ of Figure 10.1(a) while that of Figure 10.4(b) is formed by the forward I_f plus backward I_b traveling wave currents of Figure 10.1(a). The two currents I_f and I_b together form a standing wave; that is, $I_s = I_f + I_b = I_1 e^{-jkz} - I_2 e^{+jkz} = -2jI_0 \sin(kz)$ when $I_2 = I_1 = I_0$. As expected, for the traveling wave antenna of Figure 10.4(a) there is maximum radiation in the forward direction while for the standing wave antenna of Figure 10.4(b) there is maximum radiation in the forward and backward directions. The lobe near the axis of the wire in the directions of travel is the largest. The magnitudes of the other lobes from the main decrease progressively, with an envelope proportional to $\cot^2(\theta/2)$, toward the other direction. The traveling wave antenna is used when it is desired to radiate or receive predominantly from one direction. As the length of the wire increases, the maximum of the main lobe shifts closer toward the axis and the number of lobes increase. This is illustrated in Figure 10.6 for a traveling wave wire antenna with $l = 5\lambda$ and 10λ. The angles of the maxima of the first four lobes, computed using (10-8), are plotted in Figure 10.7(a) for $0.5\lambda \leq l \leq 10\lambda$. The corresponding angles of the first four nulls, computed using (10-10), are shown in Figure 10.7(b) for $0.5\lambda \leq l \leq 10\lambda$. These curves can be used effectively to design long wires when the direction of the maximum or null is desired.

EX2042
Page 515 of 1072

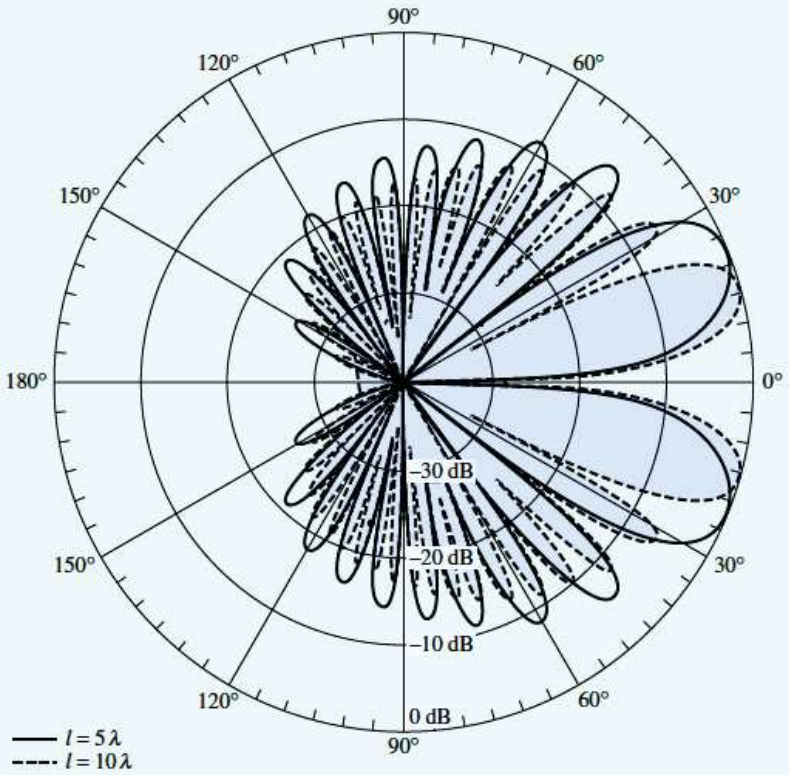


Figure 10.6 Two-dimensional free-space amplitude pattern for traveling wave wire antenna of $l = 5\lambda$ and 10λ.

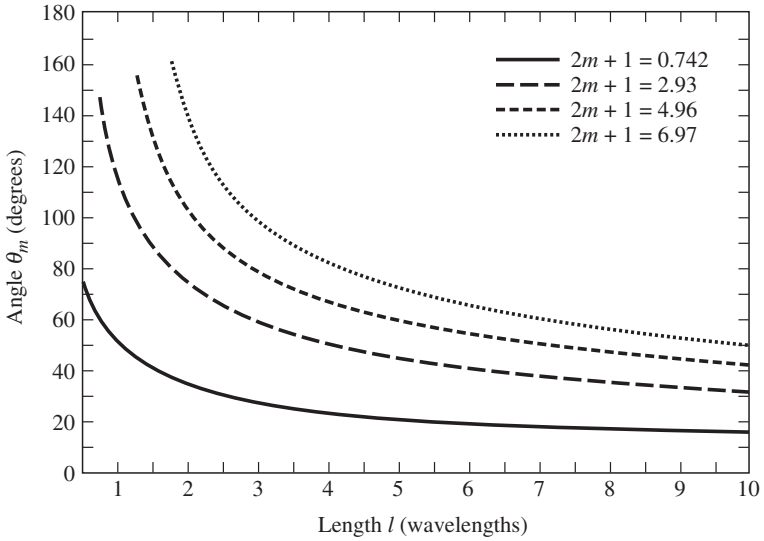
B. Input Impedance

For traveling wave wire antennas the radiation in the opposite direction from the maximum is suppressed by reducing, if not completely eliminating, the current reflected from the end of the wire. This is accomplished by increasing the diameter of the wire or more successfully by properly terminating it to the ground, as shown in Figure 10.1. Ideally a complete elimination of the reflections (perfect match) can only be accomplished if the antenna is elevated only at small heights (compared to the wavelength) above the ground, and it is terminated by a resistive load. The value of the load resistor, to achieve the impedance match, is equal to the characteristic impedance of the wire near the ground (which is found using image theory). For a wire with diameter d and height h above the ground, an approximate value of the termination resistance is obtained from

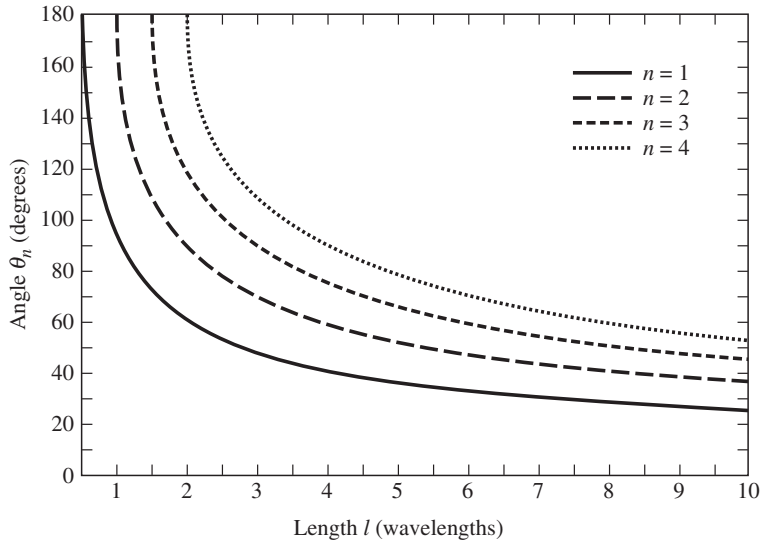
$$R_L = 138 \log_{10}\left(4\frac{h}{d}\right) \tag{10-14}$$

To achieve a reflection-free termination, the load resistor can be adjusted about this value (usually about 200–300 ohms) until there is no standing wave on the antenna wire. Therefore the input impedance is the same as the load impedance or the characteristic impedance of the line, as given by (10-14).

If the antenna is not properly terminated, waves reflected from the load traveling in the opposite direction from the incident waves create a standing wave pattern. Therefore



(a) Maxima



(b) Nulls

Figure 10.7 Angles versus length of wire antenna where maxima and nulls occur.

the input impedance of the line is not equal to the load impedance. To find the input impedance, the transmission line impedance transfer equation of (9-18) can be used. Doing this we can write that the impedance at the input terminals of Figure 10.1(a) is

$$Z_{in}(l) = Z_c \left[\frac{R_L + jZ_c \tan(\beta l)}{Z_c + jR_L \tan(\beta l)} \right] \tag{10-15}$$

C. Polarization

A long-wire antenna is linearly polarized, and it is always parallel to the plane formed by the wire and radial vector from the center of the wire to the observation point. The direction of the linear polarization is not the same in all parts of the pattern, but it is perpendicular to the radial vector (and parallel to the plane formed by it and

the wire). Thus the wire antenna of Figure 10.1, when its height above the ground is small compared to the wavelength and its main beam is near the ground, is not an effective element for horizontal polarization. Instead it is usually used to transmit or receive waves that have an appreciable vector component in the vertical plane. This is what is known as a *Beverage antenna* which is used more as a receiving rather than a transmitting element because of its poor radiation efficiency due to power absorbed in the load resistor.

When a TEM wave travels parallel to an air-conductor interface, it creates a forward wave tilt [2] which is determined by applying the boundary conditions on the tangential fields along the interface. The amount of tilt is a function of the constitutive parameters of the ground. If the conductor is a perfect electric conductor (PEC), then the wave tilt is zero because the tangential electric field vanishes along the PEC. The wave tilt increases with frequency and with ground resistivity. Therefore, for a Beverage wire antenna, shown in Figure 10.1(c) in the receiving mode, reception is influenced by the tilt angle of the incident vertically polarized wavefront, which is formed by the losses of the local ground. The electric-field vector of the incident wavefront produces an electric force that is parallel to the wire, which in turn induces a current in the wire. The current flows in the wire toward the receiver, and it is reinforced up to a certain point along the wire by the advancing wavefront. The wave along the wire is transverse magnetic.

D. Resonant Wires

Resonant wire antennas are formed when the load impedance of Figure 10.1(a) is not matched to the characteristic impedance of the line. This causes reflections which with the incident wave form a standing wave. Resonant antennas, including the dipole, were examined in detail in Chapter 4, and the electric and magnetic field components of a center-fed wire of total length l are given, respectively, by (4-62a) and (4-62b). Other radiation characteristics (including directivity, radiation resistance, maximum effective area, etc.) are found in Chapter 4.

Resonant antennas can also be formed using long wires. It can be shown that for *resonant* long wires with lengths odd multiple of half wavelength ($l = n\lambda/2$, $n = 1, 3, 5, \ldots$), the radiation resistance is given approximately (within 0.5 ohms) by [3], [4]

$$R_r = 73 + 69\log_{10}(n) \tag{10-16}$$

This expression gives a very good answer even for $n = 1$. For the same elements, the angle of maximum radiation is given by

$$\theta_{\max} = \cos^{-1}\left(\frac{n-1}{n}\right) \tag{10-17}$$

This formula is more accurate for small values of n, although it gives good results even for large values of n. It can also be shown that the maximum directivity is related to the radiation resistance by

$$D_0 = \frac{120}{R_r \sin^2\theta_{\max}} \tag{10-18}$$

The values based on (10-18) are within 0.5 dB from those based on (4-75). It is apparent that all three expressions, (10-16)–(10-18), lead to very good results for the half-wavelength dipole ($n = 1$).

Long-wire antennas (both resonant and nonresonant) are very simple, economical, and effective directional antennas with many uses for transmitting and receiving waves in the MF (300 KHz–3 MHz) and HF (3–30 MHz) ranges. Their properties can be enhanced when used in arrays.

A MATLAB computer program, entitled ***Beverage***, has been developed to analyze the radiation characteristics of a long-wire antenna. The description of the program is found in the corresponding READ ME file included in the CD attached to the book.

10.2.2 V Antenna

For some applications a single long-wire antenna is not very practical because (1) its directivity may be low, (2) its side lobes may be high, and (3) its main beam is inclined at an angle, which is controlled by its length. These and other drawbacks of single long-wire antennas can be overcome by utilizing an array of wires.

One very practical array of long wires is the V antenna formed by using two wires each with one of its ends connected to a feed line as shown in Figure 10.8(a). In most applications, the plane formed by the legs of the V is parallel to the ground leading to a horizontal V array whose principal polarization is parallel to the ground and the plane of the V. Because of increased sidelobes, the directivity of ordinary linear dipoles begins to diminish for lengths greater than about 1.25λ, as shown in Figure 4.9. However by adjusting the included angle of a V-dipole, its directivity can be made greater and its side lobes smaller than those of a corresponding linear dipole. Designs for maximum directivity usually require smaller included angles for longer V's.

Most V antennas are symmetrical ($\theta_1 = \theta_2 = \theta_0$ and $l_1 = l_2 = l$). Also V antennas can be designed to have unidirectional or bidirectional radiation patterns, as shown in Figures 10.8(b) and (c), respectively. To achieve the unidirectional characteristics, the wires of the V antenna must be nonresonant which can be accomplished by minimizing if not completely eliminating reflections from the ends of the wire. The reflected waves can be reduced by making the inclined wires of the V relatively thick. In theory, the reflections can even be eliminated by properly terminating the open ends of the V leading to a purely traveling wave antenna. One way of terminating the V antenna will be to attach a load, usually a resistor equal in value to the open end characteristic impedance of the V-wire transmission line, as shown in Figure 10.9(a). The terminating resistance can also be divided in half and each half connected to the ground leading to the termination of Figure 10.9(b). If the length of each leg of the V is very long (typically $l > 5\lambda$), there will be sufficient leakage of the field along each leg that when the wave reaches the end of the V it will be sufficiently reduced that there will not necessarily be a need for a termination. Of course, termination with a load is not possible without a ground plane.

The patterns of the individual wires of the V antenna are conical in form and are inclined at an angle from their corresponding axes. The angle of inclination is determined by the length of each wire. For the patterns of each leg of a symmetrical V antenna to add in the direction of the line bisecting the angle of the V and to form one major lobe, the total included angle $2\theta_0$ of the V should be equal to $2\theta_m$, which is twice the angle that the cone of maximum radiation of each wire makes with its axis. When this is done, beams 2 and 3 of Figure 10.8(b) are aligned and add constructively. Similarly for Figure 10.8(c), beams 2 and 3 are aligned and add constructively in the forward direction, while beams 5 and 8 are aligned and add constructively in the

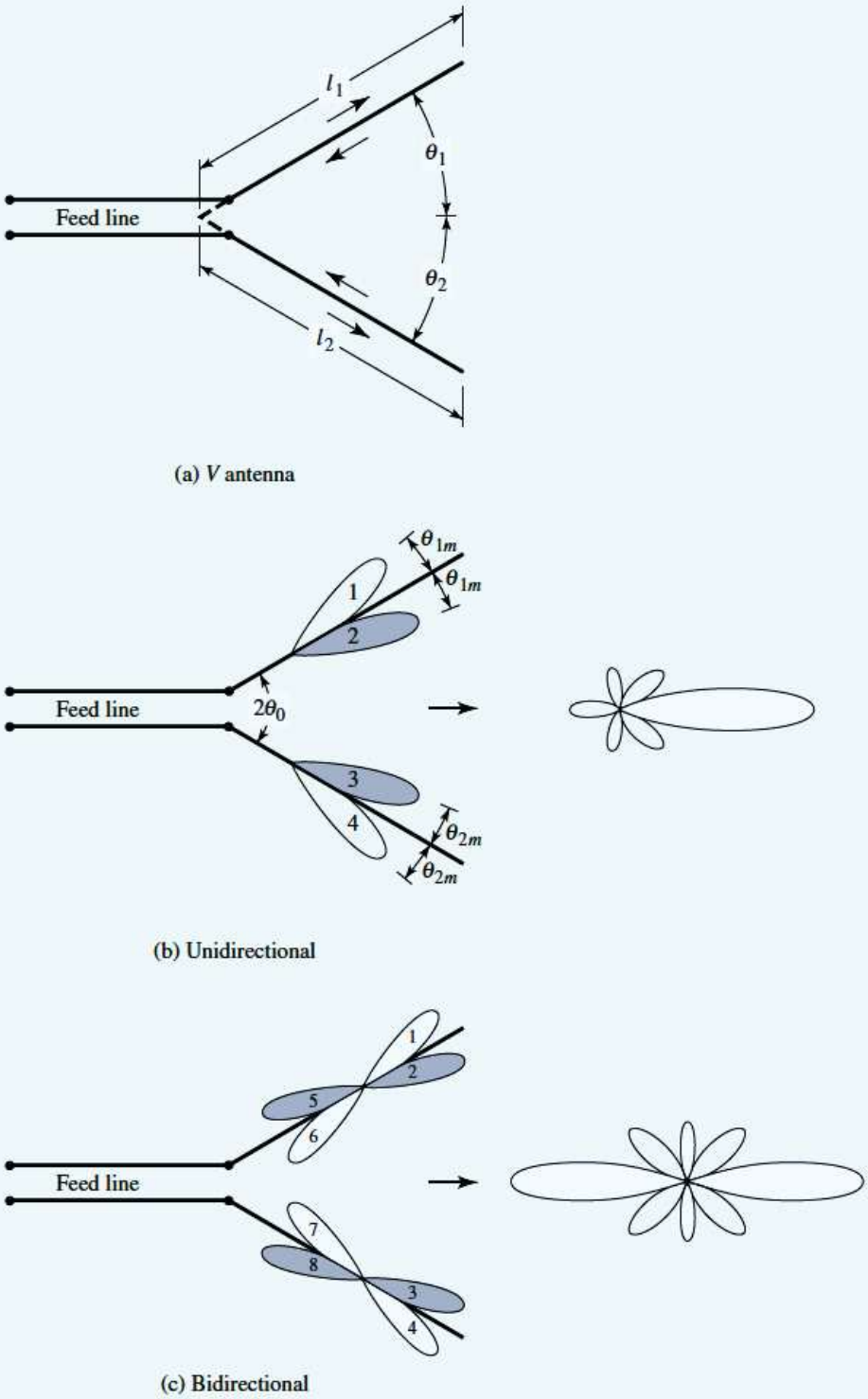


Figure 10.8 Unidirectional and bidirectional V antennas.

backward direction. If the total included angle of the V is greater than $2\theta_m (2\theta_0 > 2\theta_m)$ the main lobe is split into two distinct beams. However, if $2\theta_0 < 2\theta_m$, then the maximum of the single major lobe is still along the plane that bisects the V but it is tilted upward from the plane of the V. This may be a desired designed characteristic when the antenna is required to transmit waves upward toward the ionosphere for optimum

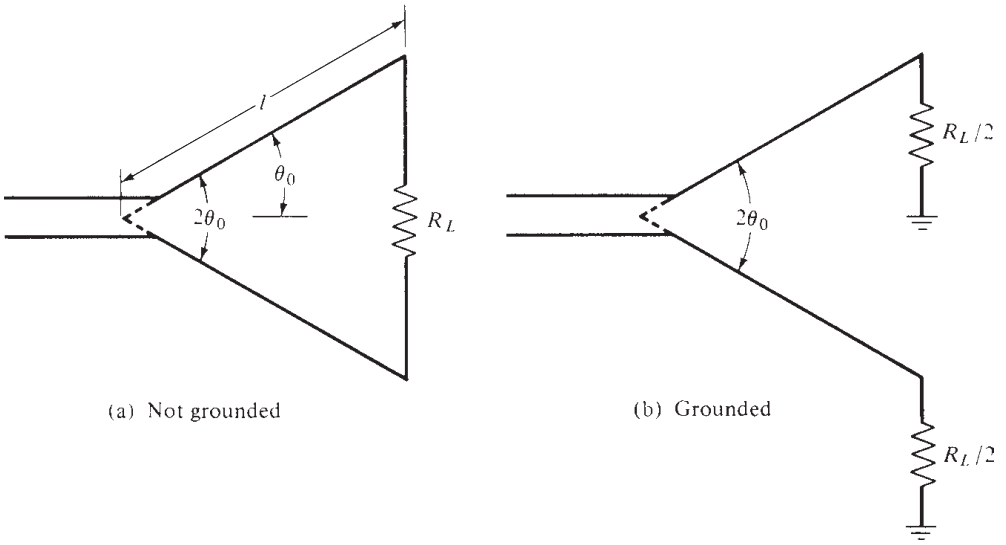


Figure 10.9 Terminated V antennas.

reflection or to receive signals reflected downward by the ionosphere. For optimum operation, typically the included angle is chosen to be approximately $\theta_0 \simeq 0.8\theta_m$. When this is done, the reinforcement of the fields from the two legs of the V lead to a total directivity for the V of approximately twice the directivity of one leg of the V.

For a symmetrical V antenna with legs each of length l, there is an optimum included angle which leads to the largest directivity. Design data for optimum included angles of V dipoles were computed [5] using Moment Method techniques and are shown in Figure 10.10(a). The corresponding directivities are shown in Figure 10.10(b). In each figure the dots (·) represent values computed using the Moment Method while the solid curves represent second- or third-order polynomials fitted through the computed data. The polynomials for optimum included angles and maximum directivities are given by

$$2\theta_0 = \begin{cases} -149.3\left(\dfrac{l}{\lambda}\right)^3 + 603.4\left(\dfrac{l}{\lambda}\right)^2 - 809.5\left(\dfrac{l}{\lambda}\right) + 443.6 & \text{(10-19a)} \\ \quad \text{for } 0.5 \le l/\lambda \le 1.5 & \\ 13.39\left(\dfrac{l}{\lambda}\right)^2 - 78.27\left(\dfrac{l}{\lambda}\right) + 169.77 & \text{(10-19b)} \\ \quad \text{for } 1.5 \le l/\lambda \le 3 & \end{cases}$$

$$D_0 = 2.94\left(\frac{l}{\lambda}\right) + 1.15 \quad \text{for } 0.5 \le l/\lambda \le 3 \qquad \text{(10-20)}$$

The dashed curves represent data obtained from empirical formulas [6]. The corresponding input impedances of the V's are slightly smaller than those of straight dipoles.

Another form of a V antenna is shown in the insert of Figure 10.11(a). The V is formed by a monopole wire, bent at an angle over a ground plane, and by its image shown dashed. The included angle of the V as well as the length can be used to

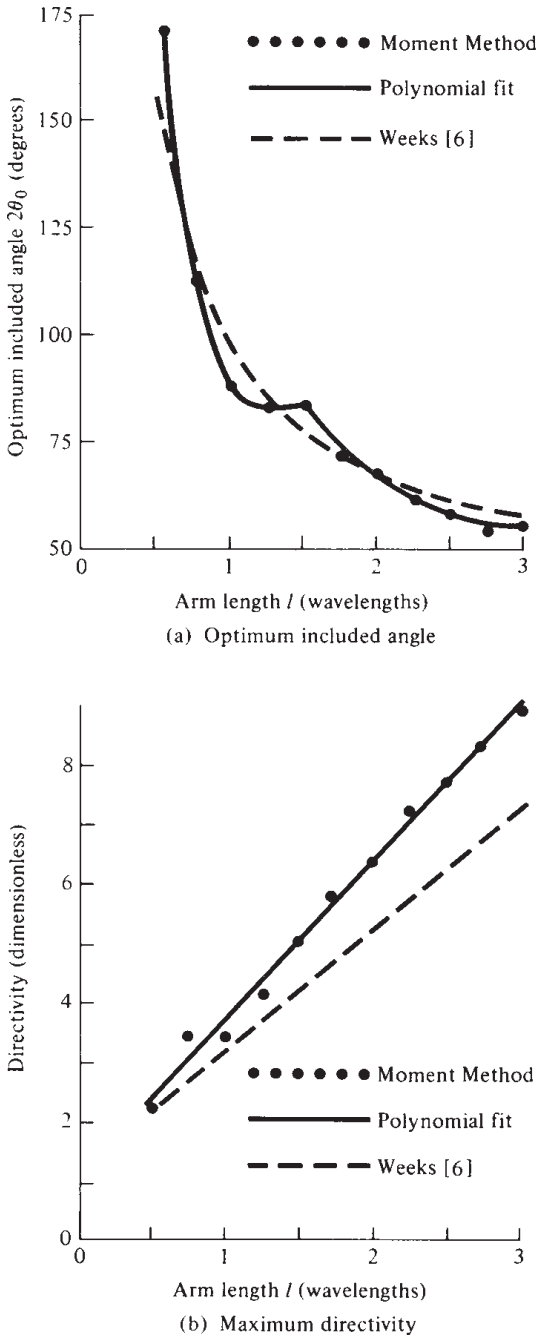
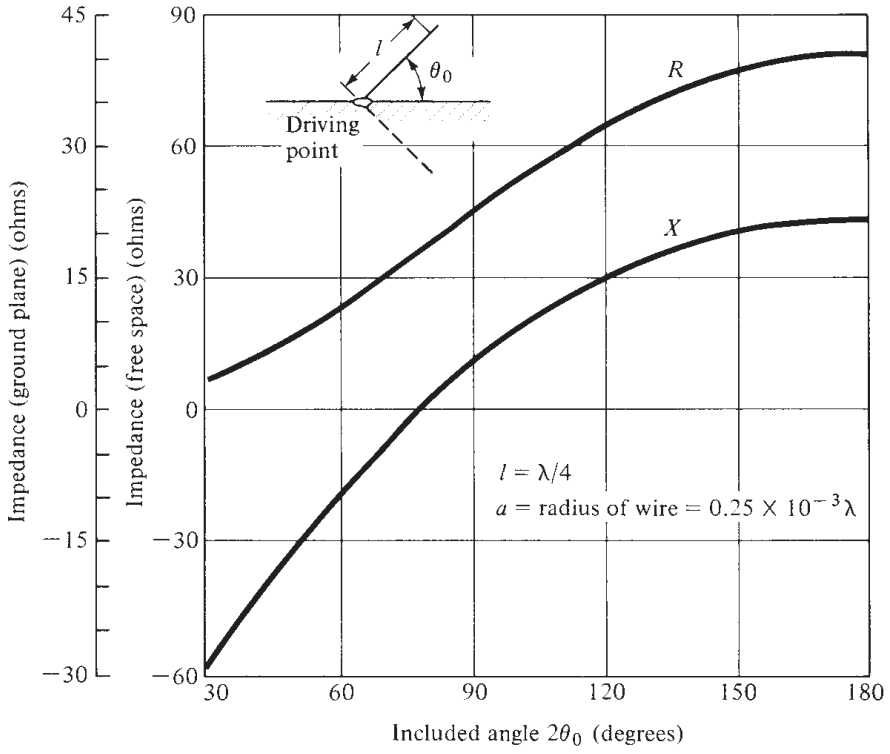


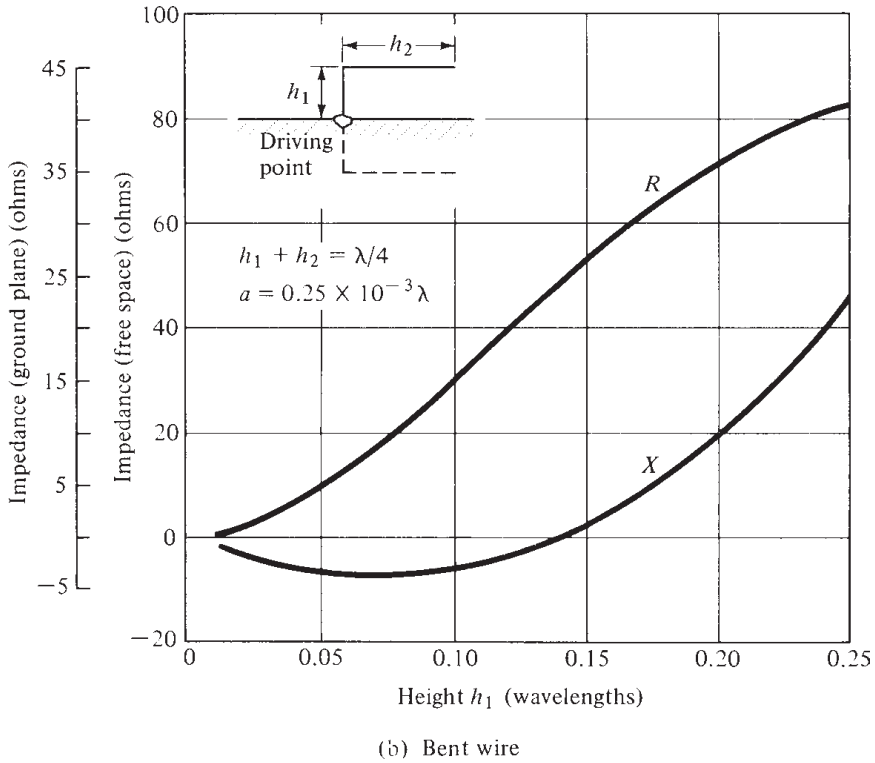
Figure 10.10 Optimum included angle for maximum directivity as a function of arm length for V dipoles. (SOURCE: G. A. Thiele and E. P. Ekelman, Jr., "Design Formulas for Vee Dipoles," *IEEE Trans. Antennas Propagat.*, Vol. AP-28, pp. 588–590, July 1980. © (1980) IEEE).

tune the antenna. For included angles greater than 120° ($2\theta_0 > 120°$), the antenna exhibits primarily vertical polarization with radiation patterns almost identical to those of straight dipoles. As the included angle becomes smaller than about 120°, a horizontally polarized field component is excited which tends to fill the pattern toward the horizontal direction, making it a very attractive communication antenna for aircraft. The computed impedance of the ground plane and free-space V configurations obtained by the Moment Method [7] is shown plotted in Figure 10.11(a).

EX2042
Page 522 of 1072



(a) V antenna



(b) Bent wire

Figure 10.11 Computed impedance $(R + jX)$ of V and bent wire antennas above ground. (SOURCE: D. G. Fink (ed.), *Electronics Engineer's Handbook*, Chapter 18 (by W. F. Croswell), McGraw-Hill, New York, 1975).

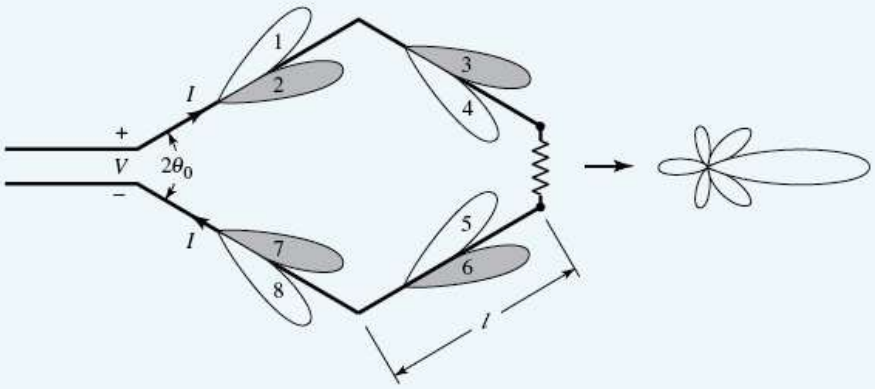
EX2042
Page 523 of 1072

Another practical form of a dipole antenna, particularly useful for airplane or ground-plane applications, is the 90° bent wire configuration of Figure 10.11(b). The computed impedance of the antenna, obtained also by the Moment Method [7], is shown plotted in Figure 10.11(b). This antenna can be tuned by adjusting its perpendicular and parallel lengths h_1 and h_2. The radiation pattern in the plane of the antenna is nearly omnidirectional for $h_1 \leq 0.1\lambda$. For $h_1 > 0.1\lambda$ the pattern approaches that of vertical $\lambda/2$ dipole.

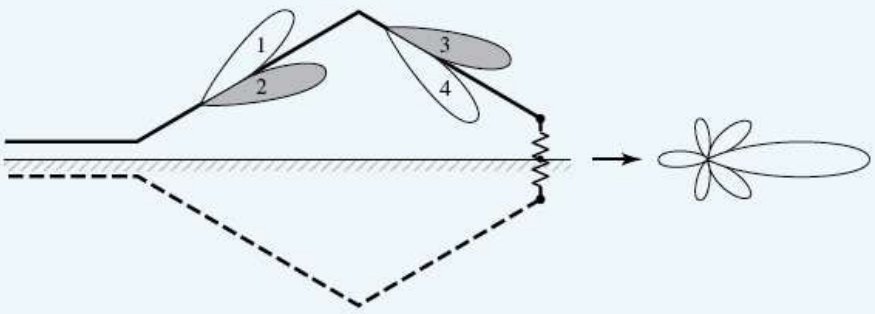
10.2.3 Rhombic Antenna

A. Geometry and Radiation Characteristics

Two V antennas can be connected at their open ends to form a diamond or rhombic antenna, as shown in Figure 10.12(a). The antenna is usually terminated at one end in a resistor, usually about 600–800 ohms, in order to reduce if not eliminate reflections. However, if each leg is long enough (typically greater than 5λ) sufficient leakage occurs along each leg that the wave that reaches the far end of the rhombus is sufficiently reduced that it may not be necessary to terminate the rhombus. To achieve the single main lobe, beams 2, 3, 6, and 7 are aligned and add constructively. The other end is used to feed the antenna. Another configuration of a rhombus is that of Figure 10.12(b) which is formed by an inverted V and its image (shown dashed). The inverted V is connected to the ground through a resistor. As with the V antennas, the pattern of rhombic antennas can be controlled by varying the element lengths, angles



(a) Rhombus formed by 2 V's



(b) Rhombus formed by inverted vertical V over ground

Figure 10.12 Rhombic antenna configurations.

between elements, and the plane of the rhombus. Rhombic antennas are usually preferred over V's for nonresonant and unidirectional pattern applications because they are less difficult to terminate. Additional directivity and reduction in side lobes can be obtained by stacking, vertically or horizontally, a number of rhombic and/or V antennas to form arrays.

The field radiated by a rhombus can be found by adding the fields radiated by its four legs. For a symmetrical rhombus with equal legs, this can be accomplished using array theory and pattern multiplication. When this is done, a number of design equations can be derived [8]–[11]. For this design, the plane formed by the rhombus is placed parallel and a height h above a perfect electric conductor.

B. Design Equations

Let us assume that it is desired to design a rhombus such that the maximum of the main lobe of the pattern, in a plane which bisects the V of the rhombus, is directed at an angle ψ_0 above the ground plane. The design can be optimized if the height h is selected according to

$$\frac{h_m}{\lambda_0} = \frac{m}{4\cos(90^\circ - \psi_0)}, \quad m = 1, 3, 5, \ldots \tag{10-21}$$

with $m = 1$ representing the minimum height.

The minimum optimum length of each leg of a symmetrical rhombus must be selected according to

$$\frac{l}{\lambda_0} = \frac{0.371}{1 - \sin(90^\circ - \psi_0)\cos\theta_0} \tag{10-22}$$

The best choice for the included angle of the rhombus is selected to satisfy

$$\theta_0 = \cos^{-1}[\sin(90^\circ - \psi_0)] \tag{10-23}$$

10.3 BROADBAND ANTENNAS

In Chapter 9 broadband dipole antennas were discussed. There are numerous other antenna designs that exhibit greater broadband characteristics than those of the dipoles. Some of these antenna can also provide circular polarization, a desired extra feature for many applications. In this section we want to discuss briefly some of the most popular broadband antennas.

10.3.1 Helical Antenna

Another basic, simple, and practical configuration of an electromagnetic radiator is that of a conducting wire wound in the form of a screw thread forming a helix, as shown in Figure 10.13. In most cases the helix is used with a ground plane. The ground plane can take different forms. One is for the ground to be flat, as shown in Figure 10.13. Typically the diameter of the ground plane should be at least $3\lambda/4$. However, the ground plane can also be cupped in the form of a cylindrical cavity (see Figure 10.17) or in the form of a frustrum cavity [8]. In addition, the helix is usually connected to the center conductor of a coaxial transmission line at the feed point with the outer conductor of the line attached to the ground plane.

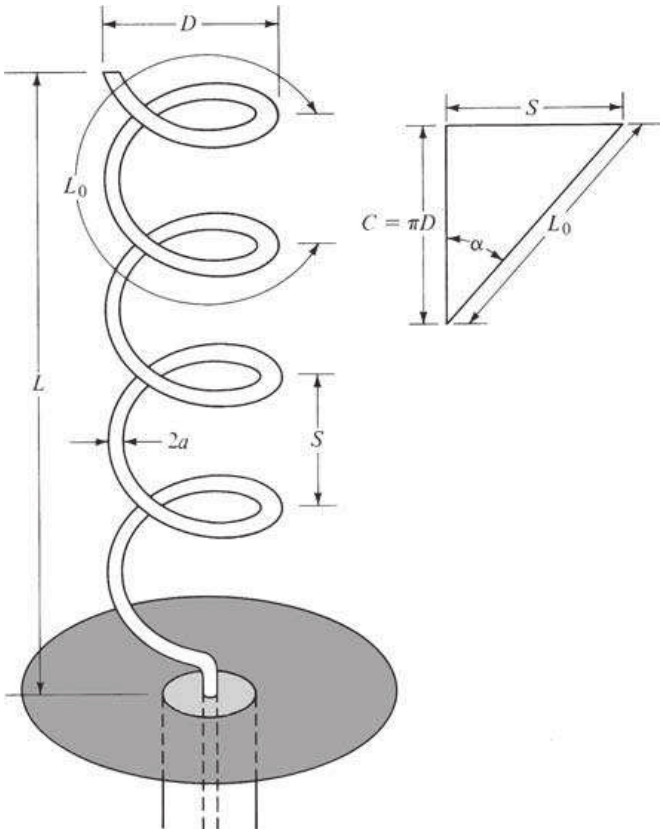


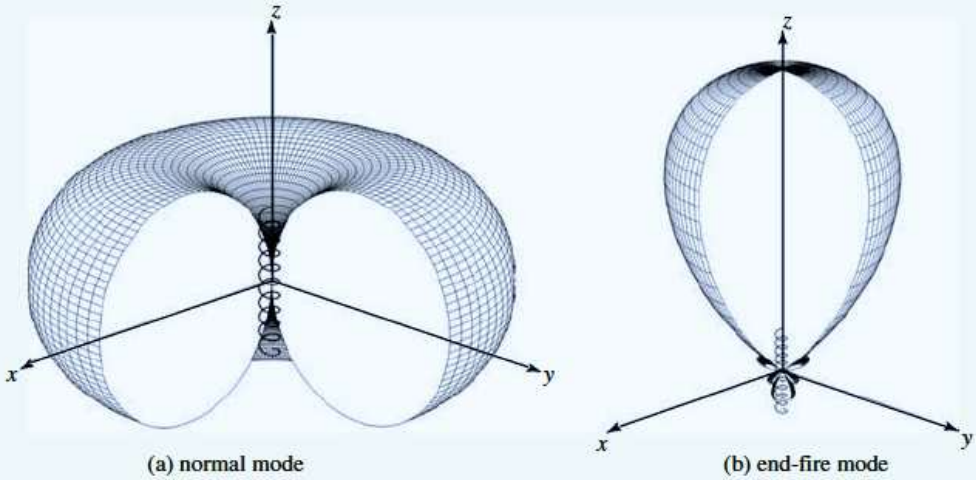
Figure 10.13 Helical antenna with ground plane.

The geometrical configuration of a helix consists usually of N turns, diameter D and spacing S between each turn. The total length of the antenna is $L = NS$ while the total length of the wire is $L_n = NL_0 = N\sqrt{S^2 + C^2}$ where $L_0 = \sqrt{S^2 + C^2}$ is the length of the wire between each turn and $C = \pi D$ is the circumference of the helix. Another important parameter is the pitch angle α which is the angle formed by a line tangent to the helix wire and a plane perpendicular to the helix axis. The pitch angle is defined by

$$\boxed{\alpha = \tan^{-1}\left(\frac{S}{\pi D}\right) = \tan^{-1}\left(\frac{S}{C}\right)} \tag{10-24}$$

When $\alpha = 0^\circ$, then the winding is flattened and the helix reduces to a loop antenna of N turns. On the other hand, when $\alpha = 90^\circ$ then the helix reduces to a linear wire. When $0^\circ < \alpha < 90^\circ$, then a true helix is formed with a circumference greater than zero but less than the circumference when the helix is reduced to a loop ($\alpha = 0^\circ$).

The radiation characteristics of the antenna can be varied by controlling the size of its geometrical properties compared to the wavelength. The input impedance is critically dependent upon the pitch angle and the size of the conducting wire, especially near the feed point, and it can be adjusted by controlling their values. The general polarization of the antenna is elliptical. However circular and linear polarizations can be achieved over different frequency ranges.



(a) normal mode (b) end-fire mode

Figure 10.14 Three-dimensional normalized amplitude linear power patterns for *normal* and *end-fire* modes helical designs.

The helical antenna can operate in many modes; however the two principal ones are the *normal* (*broadside*) and the *axial* (*end-fire*) modes. The three-dimensional amplitude patterns representative of a helix operating, respectively, in the normal (broadside) and axial (end-fire) modes are shown in Figure 10.14. The one representing the normal mode, Figure 10.14(a), has its maximum in a plane normal to the axis and is nearly null along the axis. The pattern is similar in shape to that of a small dipole or circular loop. The pattern representative of the axial mode, Figure 10.14(b), has its maximum along the axis of the helix, and it is similar to that of an end-fire array. More details are in the sections that follow. The axial (end-fire) mode is usually the most practical because it can achieve circular polarization over a wider bandwidth (usually 2:1) and it is more efficient.

Because an elliptically polarized antenna can be represented as the sum of two orthogonal linear components in time-phase quadrature, a helix can always receive a signal transmitted from a rotating linearly polarized antenna. Therefore helices are usually positioned on the ground for space telemetry applications of satellites, space probes, and ballistic missiles to transmit or receive signals that have undergone Faraday rotation by traveling through the ionosphere.

A. Normal Mode

In the normal mode of operation the field radiated by the antenna is maximum in a plane normal to the helix axis and minimum along its axis, as shown sketched in Figure 10.14(a), which is a figure-eight rotated about its axis similar to that of a linear dipole of $l < \lambda_0$ or a small loop ($a \ll \lambda_0$). To achieve the normal mode of operation, the dimensions of the helix are usually small compared to the wavelength (i.e., $NL_0 \ll \lambda_0$).

The geometry of the helix reduces to a loop of diameter D when the pitch angle approaches zero and to a linear wire of length S when it approaches 90°. Since the limiting geometries of the helix are a loop and a dipole, the far field radiated by a small helix in the normal mode can be described in terms of E_θ and E_ϕ components of the dipole and loop, respectively. In the normal mode, the helix of Figure 10.15(a) can

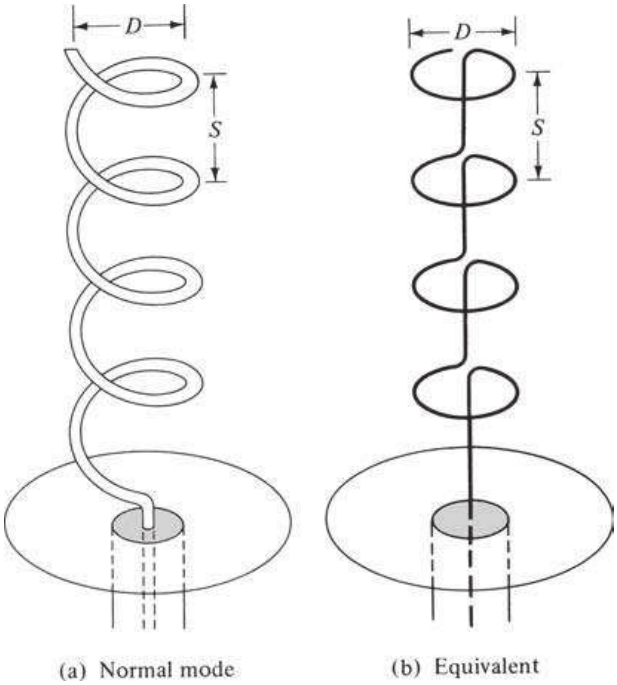


Figure 10.15 Normal (broadside) mode for helical antenna and its equivalent.

be simulated approximately by N small loops and N short dipoles connected together in series as shown in Figure 10.14(b). The fields are obtained by superposition of the fields from these elemental radiators. The planes of the loops are parallel to each other and perpendicular to the axes of the vertical dipoles. The axes of the loops and dipoles coincide with the axis of the helix.

Since in the normal mode the helix dimensions are small, the current throughout its length can be assumed to be constant and its relative far-field pattern to be independent of the number of loops and short dipoles. Thus its operation can be described accurately by the sum of the fields radiated by a small loop of radius D and a short dipole of length S, with its axis perpendicular to the plane of the loop, and each with the same constant current distribution.

The far-zone electric field radiated by a short dipole of length S and constant current I_0 is E_θ, and it is given by (4-26a) as

$$E_\theta = j\eta \frac{kI_0 S e^{-jkr}}{4\pi r} \sin\theta \tag{10-25}$$

where l is being replaced by S. In addition the electric field radiated by a loop is E_ϕ, and it is given by (5-27b) as

$$E_\phi = \eta \frac{k^2 (D/2)^2 I_0 e^{-jkr}}{4r} \sin\theta \tag{10-26}$$

where $D/2$ is substituted for a. A comparison of (10-25) and (10-26) indicates that the two components are in time-phase quadrature, a necessary but not sufficient condition for circular or elliptical polarization.

The ratio of the magnitudes of the E_θ and E_ϕ components is defined here as the axial ratio (AR), and it is given by

$$\boxed{\text{AR} = \frac{|E_\theta|}{|E_\phi|} = \frac{4S}{\pi k D^2} = \frac{2\lambda S}{(\pi D)^2}} \tag{10-27}$$

By varying the D and/or S the axial ratio attains values of $0 \le \text{AR} \le \infty$. The value of $\text{AR} = 0$ is a special case and occurs when $E_\theta = 0$ leading to a linearly polarized wave of horizontal polarization (the helix is a loop). When $\text{AR} = \infty$, $E_\phi = 0$ and the radiated wave is linearly polarized with vertical polarization (the helix is a vertical dipole). Another special case is the one when AR is unity ($\text{AR} = 1$) and occurs when

$$\frac{2\lambda_0 S}{(\pi D)^2} = 1 \tag{10-28}$$

or

$$\boxed{C = \pi D = \sqrt{2S\lambda_0}} \tag{10-28a}$$

for which

$$\boxed{\tan\alpha = \frac{S}{\pi D} = \frac{\pi D}{2\lambda_0}} \tag{10-29}$$

When the dimensional parameters of the helix satisfy the above relation, the radiated field is circularly polarized in *all directions* other than $\theta = 0^\circ$ where the fields vanish.

When the dimensions of the helix do not satisfy any of the above special cases, the field radiated by the antenna is not circularly polarized. The progression of polarization change can be described geometrically by beginning with the pitch angle of zero degrees ($\alpha = 0^\circ$), which reduces the helix to a loop with linear horizontal polarization. As α increases, the polarization becomes elliptical with the major axis being horizontally polarized. When α, is such that $C/\lambda_0 = \sqrt{2S/\lambda_0}$, $\text{AR} = 1$ and we have circular polarization. For greater values of α, the polarization again becomes elliptical but with the major axis vertically polarized. Finally when $\alpha = 90^\circ$ the helix reduces to a linearly polarized vertical dipole.

To achieve the normal mode of operation, it has been assumed that the current throughout the length of the helix is of constant magnitude and phase. This is satisfied to a large extent provided the total length of the helix wire NL_0 is very small compared to the wavelength ($L_n \ll \lambda_0$) and its end is terminated properly to reduce multiple reflections. Because of the critical dependence of its radiation characteristics on its geometrical dimensions, which must be very small compared to the wavelength, this mode of operation is very narrow in bandwidth and its radiation efficiency is very small. Practically this mode of operation is limited, and it is seldom utilized.

B. Axial Mode

A more practical mode of operation, which can be generated with great ease, is the axial or end-fire mode. In this mode of operation, there is only one major lobe and its

maximum radiation intensity is along the axis of the helix, as shown in Figure 10.14(b). The minor lobes are at oblique angles to the axis.

To excite this mode, the diameter D and spacing S must be large fractions of the wavelength. To achieve circular polarization, primarily in the major lobe, the circumference of the helix must be in the $\frac{3}{4} < C/\lambda_0 < \frac{4}{3}$ range (with $C/\lambda_0 = 1$ near optimum), and the spacing about $S \simeq \lambda_0/4$. The pitch angle is usually $12^\circ \leq \alpha \leq 14^\circ$. Most often the antenna is used in conjunction with a ground plane, whose diameter is at least $\lambda_0/2$, and it is fed by a coaxial line. However, other types of feeds (such as waveguides and dielectric rods) are possible, especially at microwave frequencies. The dimensions of the helix for this mode of operation are not as critical, thus resulting in a greater bandwidth.

C. Design Procedure

The terminal impedance of a helix radiating in the axial mode is nearly resistive with values between 100 and 200 ohms. Smaller values, even near 50 ohms, can be obtained by properly designing the feed. Empirical expressions, based on a large number of measurements, have been derived [8], and they are used to determine a number of parameters. The input impedance (purely resistive) is obtained by

$$R \simeq 140\left(\frac{C}{\lambda_0}\right) \tag{10-30}$$

which is accurate to about ±20%, the half-power beamwidth by

$$\text{HPBW (degrees)} \simeq \frac{52\lambda_0^{3/2}}{C\sqrt{NS}} \tag{10-31}$$

the beamwidth between nulls by

$$\text{FNBW (degrees)} \simeq \frac{115\lambda_0^{3/2}}{C\sqrt{NS}} \tag{10-32}$$

the directivity by

$$D_0 \text{ (dimensionless)} \simeq 15N\frac{C^2S}{\lambda_0^3} \tag{10-33}$$

the axial ratio (for the condition of increased directivity) by

$$\text{AR} = \frac{2N+1}{2N} \tag{10-34}$$

and the normalized far-field pattern by

$$E = \sin\left(\frac{\pi}{2N}\right)\cos\theta\frac{\sin[(N/2)\psi]}{\sin[\psi/2]} \tag{10-35}$$

where

$$\psi = k_0\left(S\cos\theta - \frac{L_0}{p}\right) \tag{10-35a}$$

$$p = \frac{L_0/\lambda_0}{S/\lambda_0 + 1} \qquad \text{For ordinary end-fire radiation} \tag{10-35b}$$

$$p = \frac{L_0/\lambda_0}{S/\lambda_0 + \left(\dfrac{2N+1}{2N}\right)} \qquad \text{For Hansen-Woodyard end-fire radiation} \tag{10-35c}$$

All these relations are approximately valid provided $12^\circ < \alpha < 14^\circ$, $\frac{3}{4} < C/\lambda_0 < \frac{4}{3}$, and $N > 3$.

The far-field pattern of the helix, as given by (10-35), has been developed by assuming that the helix consists of an array of N identical turns (each of nonuniform current and identical to that of the others), a uniform spacing S between them, and the elements are placed along the z-axis. The $\cos\theta$ term in (10-35) represents the field pattern of a single turn, and the last term in (10-35) is the array factor of a uniform array of N elements. The total field is obtained by multiplying the field from one turn with the array factor (pattern multiplication).

The value of p in (10-35a) is the ratio of the velocity with which the wave travels along the helix wire to that in free space, and it is selected according to (10-35b) for ordinary end-fire radiation or (10-35c) for Hansen-Woodyard end-fire radiation. These are derived as follows.

For ordinary end-fire the relative phase ψ among the various turns of the helix (elements of the array) is given by (6-7a), or

$$\psi = k_0 S\cos\theta + \beta \tag{10-36}$$

where $d = S$ is the spacing between the turns of the helix. For an end-fire design, the radiation from each one of the turns along $\theta = 0^\circ$ must be in phase. Since the wave along the helix wire between turns travels a distance L_0 with a wave velocity $v = pv_0$ ($p < 1$ where v_0 is the wave velocity in free space) and the desired maximum radiation is along $\theta = 0^\circ$, then (10-36) for *ordinary end-fire* radiation is equal to

$$\psi = (k_0 S\cos\theta - kL_0)_{\theta=0^\circ} = k_0\left(S - \frac{L_0}{p}\right) = -2\pi m, \quad m = 0, 1, 2, \ldots \tag{10-37}$$

Solving (10-37) for p leads to

$$p = \frac{L_0/\lambda_0}{S/\lambda_0 + m} \tag{10-38}$$

For $m = 0$ and $p = 1$, $L_0 = S$. This corresponds to a straight wire ($\alpha = 90^\circ$), and not a helix. Therefore the next value is $m = 1$, and it corresponds to the first transmission mode for a helix. Substituting $m = 1$ in (10-38) leads to

$$p = \frac{L_0/\lambda_0}{S/\lambda_0 + 1} \tag{10-38a}$$

which is that of (10-35b).

In a similar manner, it can be shown that for Hansen-Woodyard end-fire radiation (10-37) is equal to

$$\psi = (k_0 S \cos\theta - kL_0)_{\theta=0^\circ} = k_0\left(S - \frac{L_0}{p}\right) = -\left(2\pi m + \frac{\pi}{N}\right), \quad m = 0, 1, 2, \ldots \tag{10-39}$$

which when solved for p leads to

$$p = \frac{L_0/\lambda_0}{S/\lambda_0 + \left(\dfrac{2mN + 1}{2N}\right)} \tag{10-40}$$

For $m = 1$, (10-40) reduces to

$$p = \frac{L_0/\lambda_0}{S/\lambda_0 + \left(\dfrac{2N + 1}{2N}\right)} \tag{10-40a}$$

which is identical to (10-35c).

Example 10.1

Design a 10-turn helix to operate in the axial mode. For an optimum design,

1. Determine the:
   a. Circumference (in λ_o), pitch angle (*in degrees*), and separation between turns (in λ_o)
   b. Relative (to free space) wave velocity along the wire of the helix for:
      i. Ordinary end-fire design
      ii. Hansen-Woodyard end-fire design
   c. Half-power beamwidth of the main lobe (*in degrees*)
   d. Directivity (in dB) using:
      i. A formula
      ii. The computer program ***Directivity*** of Chapter 2
   e. Axial ratio (*dimensionless* and in *dB*)
2. Plot the normalized three-dimensional linear power pattern for the ordinary and Hansen-Woodyard designs.

EX2042
Page 532 of 1072

Solution:

1. a. For an optimum design

$$C \simeq \lambda_o, \alpha \simeq 13^\circ \Rightarrow S = C\tan\alpha = \lambda_o \tan(13^\circ) = 0.231\lambda_o$$

b. The length of a single turn is

$$L_o = \sqrt{S^2 + C^2} = \lambda_o\sqrt{(0.231)^2 + (1)^2} = 1.0263\lambda_o$$

Therefore the relative wave velocity is:

i. Ordinary end-fire:

$$p = \frac{v_h}{v_o} = \frac{L_o/\lambda_o}{S_o/\lambda_o + 1} = \frac{1.0263}{0.231 + 1} = 0.8337$$

ii. Hansen-Woodyard end-fire:

$$p = \frac{v_h}{v_o} = \frac{L_o/\lambda_o}{S_o/\lambda_o + \left(\dfrac{2N+1}{2N}\right)} = \frac{1.0263}{0.231 + 21/20} = 0.8012$$

c. The half-power beamwidth according to (10-31) is

$$\text{HPBW} \simeq \frac{52\lambda_o^{3/2}}{C\sqrt{NS}} = \frac{52}{1\sqrt{10(0.231)}} = 34.2135^\circ$$

d. The directivity is:

i. Using (10-33):

$$D_o \simeq 15N\frac{C^2S}{\lambda_o^3} = 15(10)(1)^2(0.231) = 34.65\ (\textit{dimensionless})$$

$$= 15.397\ \text{dB}$$

ii. Using the computer program ***Directivity*** and (10-35):

a. ordinary end-fire ($p = 0.8337$): $D_o = 12.678\ (\textit{dimensionless})$

$$= 11.03\ \text{dB}$$

b. H-W end-fire ($p = 0.8012$): $D_o = 26.36\ (\textit{dimensionless}) = 14.21\ \text{dB}$

e. The axial ratio according to (10-34) is:

$$\text{AR} = \frac{2N+1}{2N} = \frac{20+1}{20} = 1.05\ (\textit{dimensionless}) = 0.21\ \text{dB}$$

2. The three-dimensional linear power patterns for the two end-fire designs, *ordinary* and *Hansen-Woodyard*, are shown in Figure 10.16.

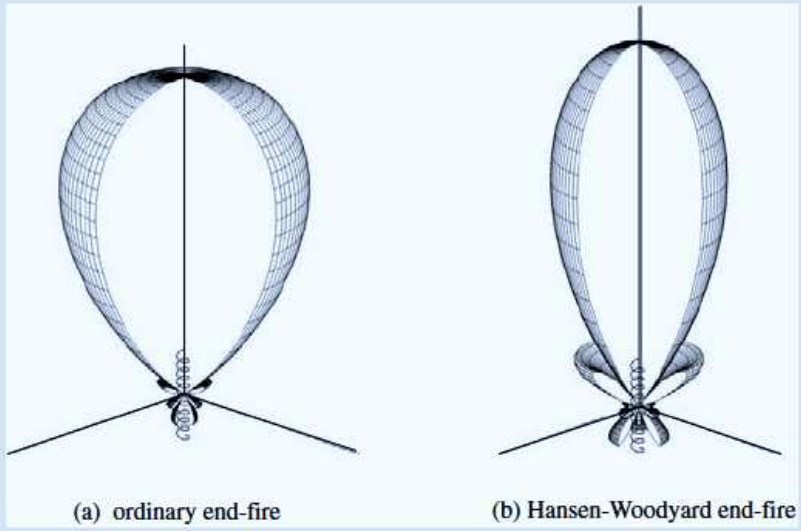


Figure 10.16 Three-dimensional normalized amplitude linear power patterns for helical *ordinary* ($p = 0.8337$) and *Hansen-Woodyard* ($p = 0.8012$) end-fire designs.

D. Feed Design

The nominal impedance of a helical antenna operating in the axial mode, computed using (10-30), is 100–200 ohms. However, many practical transmission lines (such as a coax) have characteristic impedance of about 50 ohms. In order to provide a better match, the input impedance of the helix must be reduced to near that value. There may be a number of ways by which this can be accomplished. One way to effectively control the input impedance of the helix is to properly design the first 1/4 turn of the helix which is next to the feed [8], [12]. To bring the input impedance of the helix from nearly 150 ohms down to 50 ohms, the wire of the first 1/4 turn should be flat in the form of a strip and the transition into a helix should be very gradual. This is accomplished by making the wire from the feed, at the beginning of the formation of the helix, in the form of a strip of width w by flattening it and nearly touching the ground plane which is covered with a dielectric slab of height [2]

$$h = \frac{w}{\dfrac{377}{\sqrt{\epsilon_r} Z_0} - 2} \tag{10-41}$$

where

w = width of strip conductor of the helix starting at the feed
ϵ_r = dielectric constant of the dielectric slab covering the ground plane
Z_0 = characteristic impedance of the input transmission line

Typically the strip configuration of the helix transitions from the strip to the regular circular wire and the designed pitch angle of the helix very gradually within the first 1/4–1/2 turn.

This modification decreases the characteristic impedance of the conductor-ground plane effective transmission line, and it provides a lower impedance over a substantial

but reduced bandwidth. For example, a 50-ohm helix has a VSWR of less than 2:1 over a 40% bandwidth compared to a 70% bandwidth for a 140-ohm helix. In addition, the 50-ohm helix has a VSWR of less than 1.2:1 over a 12% bandwidth as contrasted to a 20% bandwidth for one of 140 ohms.

A simple and effective way of increasing the thickness of the conductor near the feed point will be to bond a thin metal strip to the helix conductor [12]. For example, a metal strip 70-mm wide was used to provide a 50-ohm impedance in a helix whose conducting wire was 13-mm in diameter and it was operating at 230.77 MHz.

A commercially available helix with a cupped ground plane is shown in Figure 10.17. It is right-hand circularly-polarized (RHCP) operating between 100–160 MHz with a gain of about 6 dB at 100 MHz and 12.8 dB at 160 MHz. The right-hand winding of the wire is clearly shown in the photo. The axial ratio is about 8 dB at 100 MHz and 2 dB at 160 MHz. The maximum VSWR in the stated operating frequency, relative to a 50-ohm line, does not exceed 3:1.

A MATLAB computer program, entitled ***Helix***, has been developed to analyze and design a helical antenna. The description of the program is found in the corresponding READ ME file included in the CD attached to the book.

10.3.2 Electric-Magnetic Dipole

It has been shown in the previous section that the circular polarization of a helical antenna operating in the normal mode was achieved by assuming that the geometry of the helix is represented by a number of horizontal small loops and vertical infinitesimal dipoles. It would then seem reasonable that an antenna with only one loop and a single vertical dipole would, in theory, represent a radiator with an elliptical polarization. Ideally circular polarization, in all space, can be achieved if the current in each element can be controlled, by dividing the available power between the dipole and the loop, so that the magnitude of the field intensity radiated by each is equal.

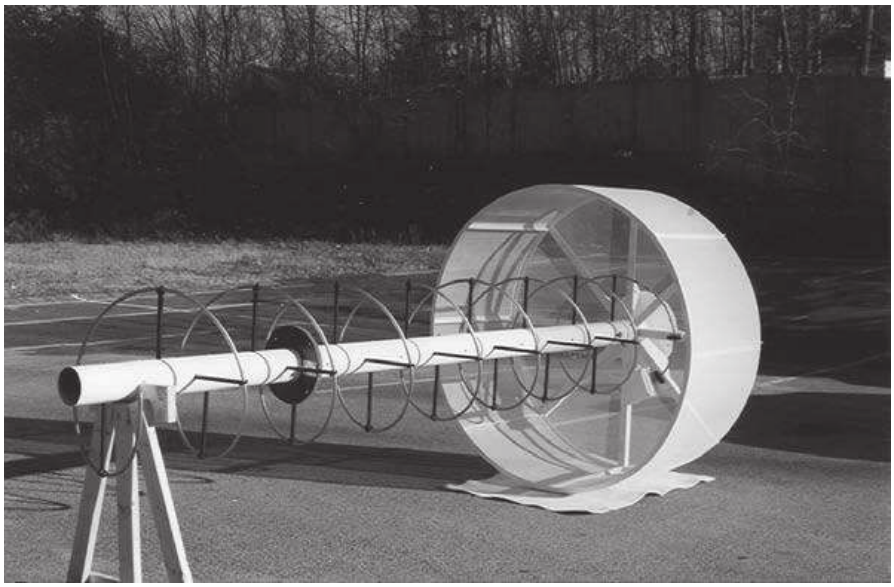


Figure 10.17 Commercial helix with a cupped ground plane. (Courtesy: Seavey Engineering Associates, Inc, Pembroke, MA).

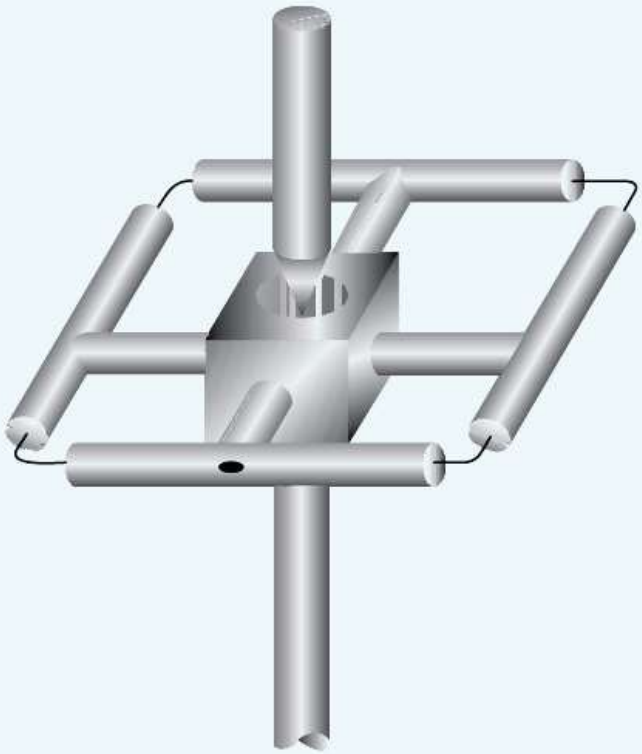


Figure 10.18 Electric-magnetic dipole configuration. (SOURCE: A. G. Kandoian, "Three New Antenna Types and Their Applications," *Proc. IRE*, Vol. 34, pp. 70W–75W, February 1946. © (1946) IEEE).

Experimental models of such an antenna were designed and built [13] one operating around 350 MHz and the other near 1.2 GHz. A sketch of one of them is shown in Figure 10.18. The measured VSWR in the 1.15–1.32 GHz frequency range was less than 2:1.

This type of an antenna is very useful in UHF communication networks where considerable amount of fading may exist. In such cases the fading of the horizontal and vertical components are affected differently and will not vary in the same manner. Hopefully, even in severe cases, there will always be one component all the time which is being affected less than the other, thus providing continuous communication. The same results would apply in VHF and/or UHF broadcasting. In addition, a transmitting antenna of this type would also provide the versatility to receive with horizontally or vertically polarized elements, providing a convenience in the architectural design of the receiving station.

10.3.3 Yagi-Uda Array of Linear Elements

Another very practical radiator in the HF (3–30 MHz), VHF (30–300 MHz), and UHF (300–3,000 MHz) ranges is the Yagi-Uda antenna. This antenna consists of a number of linear dipole elements, as shown in Figure 10.19, one of which is energized directly by a feed transmission line while the others act as parasitic radiators whose currents are induced by mutual coupling. A common feed element for a Yagi-Uda antenna is a folded dipole. This radiator is exclusively designed to operate as an end-fire array, and it is accomplished by having the parasitic elements in the forward beam act as